

## CD26 分子に基づく悪性中皮腫への新治療法開発

森本 幾夫 大沼 圭\*

[*Jpn J Cancer Chemother* 43(7): 855-862, July, 2016]

Development of New Therapy for Malignant Mesothelioma Based on CD26 Molecule: Chikao Morimoto and Kei Ohnuma (Dept. of Therapy Development and Innovation for Immune Disorders and Cancers, Graduate School of Medicine, Juntendo University)

## Summary

CD26 is a 110 kDa, type II transmembrane glycoprotein with dipeptidyl peptidase IV activity and is capable of cleaving N-terminal dipeptides with either L-proline or L-alanine at the penultimate position. Malignant mesothelioma (MM) is an aggressive malignancy arising from the mesothelial cells. It is generally associated with a history of asbestos exposure and has a very poor prognosis. Due to lack of efficacy of conventional treatments, novel therapeutic strategies are urgently needed to improve outcomes. Recently we showed that CD26 is preferentially expressed on epithelial type of MM cells but not on normal mesothelial cells. We have developed a highly biological active humanized anti-CD26 monoclonal antibody (mAb) and have published previously extensive *in vivo* data demonstrating the anti-tumor activity of humanized anti-CD26 mAb (YS110) in mouse xenograft models. The use of a humanized anti-CD26 mAb may therefore be a rational therapy for patients with MM. The first-in-human (FIH) phase I study performed in France demonstrates that humanized anti-CD26 therapy is generally well-tolerated with preliminary evidence of activity in patients with advanced/refractory CD26-expressing cancers, particularly refractory malignant mesothelioma. From the above results, the phase I clinical trial for malignant mesothelioma in Japan is to be started in the very near future. **Key words:** CD26, DPPIV, Malignant mesothelioma

**要旨** CD26 分子は 110 kDa の膜蛋白質で dipeptidyl peptidase IV (DPPIV) 酵素活性をもち、N 末端から二つ目のプロリンやアラニンを切断する酵素である。悪性中皮腫 (MM) は胸膜中皮細胞から発生する非常に攻撃的な腫瘍で一般的にはアスベスト曝露により発生し、非常に予後が悪い。有効な標準治療法は存在しないことから、新規かつ有効な治療法開発は急務とされている。最近われわれは、CD26 分子は正常中皮細胞には発現しないが、上皮型中皮腫の約 80% に発現することを報告した。さらに、非常に生物学的活性の強い良質なヒト化 CD26 抗体を開発してヒト癌細胞移植モデルマウスを用いて本抗体が強い抗腫瘍効果を有するという広範なデータを示してきた。本結果から、ヒト化 CD26 抗体は悪性中皮腫の新規治療法として臨床応用できる有望な可能性を強く示唆した。本抗体を用いて初めてヒトに投与する (first-in-human: FIH) 第 I 相臨床試験をフランスにて行い、ヒト化 CD26 抗体は良好な耐容性および CD26 陽性腫瘍、特に治療抵抗性悪性中皮腫に対して有効性を示す予備的な証拠も得ることができた。これらの結果を踏まえて、日本でも悪性中皮腫をターゲットとして第 I 相臨床試験が近々開始される予定である。

## はじめに

CD26 分子は dipeptidyl peptidase IV (DPPIV) 酵素を含む T 細胞活性化分子で、われわれは単クローン CD26 抗体の開発、CD26 cDNA の単離を世界に先駆けて行い、当分野の研究では世界の最先端にいる<sup>1)</sup>。この研究過程で悪性中皮腫細胞株 JMN が CD26 を発現していること

を発見し<sup>2)</sup>、高親和性、高生物学活性の高いヒト化 CD26 抗体を開発した。本抗体は *in vitro* で中皮腫細胞株の増殖および浸潤を抑制し、中皮腫株移植マウスで腫瘍縮小、生存延長を来し、正常中皮では発現のない CD26 が悪性中皮腫、特に上皮型では 80% 以上に発現していることを見いだした<sup>3)</sup>。CD26 は悪性中皮腫の増殖、浸潤に重要な役割を果たし、本抗体がその機能を抑制することから悪

\* 順天堂大学大学院医学研究科・免疫病・がん先端治療学講座

連絡先: 〒113-8421 東京都文京区本郷 2-1-1 順天堂大学大学院医学研究科・免疫病・がん先端治療学講座  
森本 幾夫

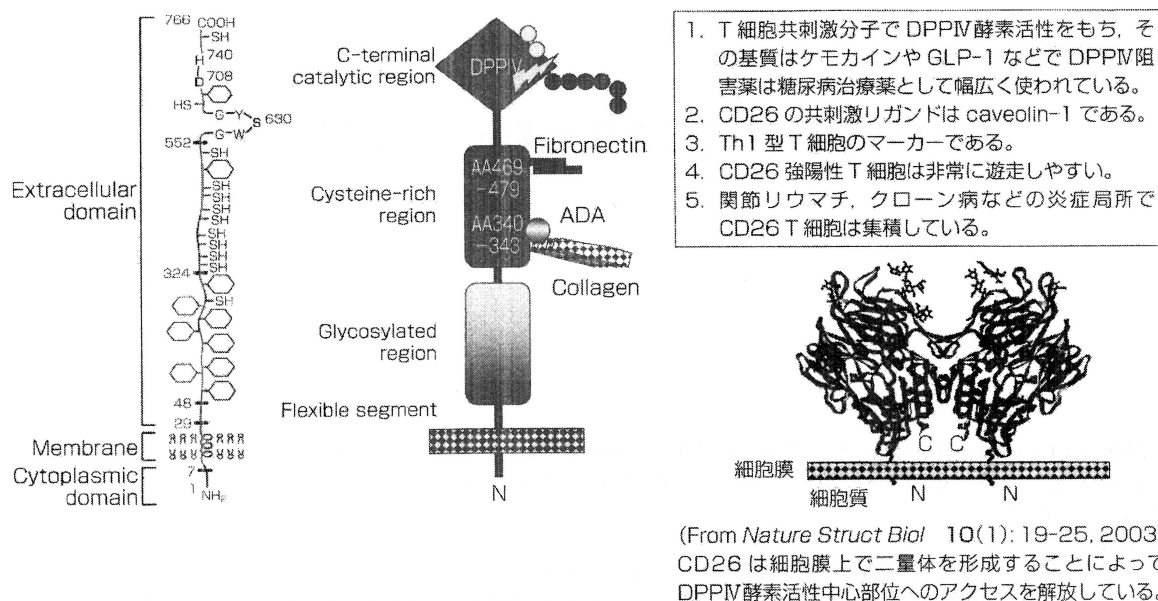


図 1 CD26 分子の構造と機能

性中皮腫の新規治療法として有望な可能性が強く示唆された<sup>4,5)</sup>。

アスベストは潜伏期 20~40 年を経て悪性中皮腫を引き起こすため、今後ますます患者数が増加し 2030 年にピークを迎え、死亡者数も 2013 年には 1,425 人に上り、東日本大震災のがれきにもアスベストが混入しているといわれ、大きな社会問題となっている。多くの患者は最初の症状発現から 10~17 か月以内に死亡している。現時点では悪性中皮腫に対する有効な治療法はなく、新規かつ有効な治療法開発は急務である。

本稿では CD26 分子について概説して、ヒト化 CD26 抗体の悪性中皮腫移植マウスでの成績、作用機序および first-in-human (FIH) 第 I 相臨床試験の成績について紹介したい。

### I. CD26 分子の構造と機能

CD26 は 110 kDa の膜糖蛋白で Tal という単クローン抗体と反応するヒト T 細胞表面抗原分子として報告され、活性化 T 細胞に強発現することから T 細胞活性化抗原として確立された<sup>6,7)</sup>。一方、以前から肝臓や腸管粘膜表面にペプチダーゼ酵素活性が存在することが知られており DPPIV として研究されていたが、1992 年われわれによる遺伝子クローニングにより、DPPIV 酵素と CD26 分子が同一のものであることが明らかとなった<sup>8,9)</sup>。図 1 に示すように CD26 は 766 個のアミノ酸よりなり、N 末端が細胞質内、C 末端が細胞外に存在する II 型膜蛋白質である。細胞質部分は六つのアミノ酸からなり、既存のシグナル関連モチーフ構造は存在しない。

アミノ酸配列から予想される CD26 の平均分子量は

88 kDa であるが、48~324 番目の残基領域は糖鎖修飾を受けるため、生体では 110 kDa の糖蛋白として検出される<sup>1)</sup>。さらに、630 番目のセリン残基を中心としてセリンプロテアーゼである DPPIV 酵素活性をもっている<sup>1)</sup>。CD26 の構造は種を越えて強く保存されており、種の間で高いホモロジーを示す<sup>10)</sup>。ヒト CD26 とラット DPP IV およびマウス CD26 との相同性はそれぞれ 85%, 86% である<sup>9,11)</sup>。しかし、ヒト CD26 はアデノシンデアミナーゼ (adenosine deaminase: ADA) の結合蛋白であるがラット、マウス CD26 は ADA に結合しない<sup>10,11)</sup>。

### II. CD26 陽性 T 細胞の生物学的機能

末梢血リンパ球における CD26 を静止 T 細胞での flow cytometry で検討すると 3 相性のパターンを示す<sup>6,7)</sup>。CD26 強陽性の T 細胞集団 (CD26<sup>bright</sup> T 細胞) は CD45RO 陽性メモリー T 細胞サブセットである<sup>6)</sup>。CD26<sup>bright</sup> T 細胞は IL-2 や IFN- $\gamma$  などのサイトカインを分泌する Th1 型のリンパ球とされている<sup>6)</sup>。最近になり Th17 T 細胞に CD26 は強く発現しているという報告もある<sup>12)</sup>。このように CD26<sup>bright</sup> T 細胞は炎症のエフェクター細胞として関節リウマチやバセドウ病などの自己免疫疾患の末梢血 T 細胞でその発現が増加し、これら疾患の炎症局所でも CD26<sup>bright</sup> T 細胞の集簇が認められる<sup>13)</sup>。一方、マウス CD26 分子は当初 thymocyte activating molecule (THAM) として報告され、胸腺細胞の CD4<sup>-</sup>CD8<sup>-</sup> double negative 細胞に強発現しており、静止期、活性化 T 細胞、B 細胞、NK 細胞はともに弱陽性である<sup>11)</sup>。ヒト CD26 は胸腺においてはマウスと異なり、medullary thymocyte (髄質胸腺) から発現し、活性化さ



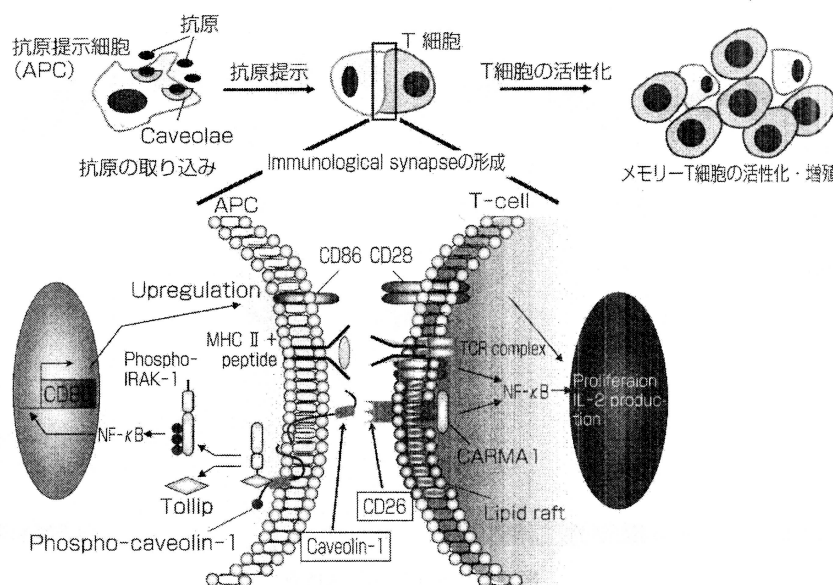


図2 CD26 共刺激シグナルについて

れると末梢T細胞はその発現は上昇し、また共刺激分子である<sup>6)</sup>。しかし、マウスCD26にはこの機能はなく、ヒトCD26とマウスCD26の免疫系での役割は異なっている。C57BL/6バックグラウンドをもつCD26ノックアウトマウス(CD26<sup>-/-</sup> KOマウス)は正常表現型で生存するが脾臓ではCD4T細胞の減少とNK細胞の増加を認め、末梢血中ではCD4陽性NKT細胞が著明に減少し、IL-2、IFN- $\gamma$ の産生減少が認められる<sup>14)</sup>。

### Ⅲ. CD26 共刺激シグナル伝達機構

図2にCD26共刺激シグナルについて模式図を示した。われわれは、長らく不明であったT細胞上CD26共刺激シグナル伝達の分子メカニズムを解明した。また、CD26陽性T細胞のメモリー応答における共刺激リガンドとして抗原提示細胞(antigen presenting cell: APC)上のcaveolin-1を同定し、CD26およびcaveolin直下のシグナル分子を解明しCD26-caveolin系がT細胞のメモリー応答において新たな共刺激系であることを提示した<sup>15)</sup>。すなわち、CD26が抗原を取り込んだAPC上のcaveolin-1と結合してcaveolin-1がリン酸化され、APC上のCD28リガンドであるCD86の発現を誘導する<sup>15)</sup>。この際、caveolin-1の82~101番目のアミノ酸残基がCD26のDPP IV酵素活性中心(DPP IVポケット構造)との結合に関与している<sup>15)</sup>。CD26のDPP IV酵素活性部位の630番目のセリン残基をアラニンに置換して酵素活性を失活させると、caveolin-1はCD26に結合できなくなる<sup>15)</sup>。T細胞のCD26のメモリー抗原に曝露されたAPCのcaveolin-1が互いに接触してimmunological synapseを形成し、メモリーT細胞に対する増殖反応がもたら

される。CD26によってAPC内で惹起されるcaveolin-1下流のシグナル伝達機構としてcaveolin-1、Tollip、IRAK-1複合体がNF- $\kappa$ Bを活性化してCD86の発現増強が誘発されるというCD26-caveolinという新たな免疫活性化経路を解明した<sup>16)</sup>。さらにcaveolin-1がT細胞上のCD26と結合し、CD26の細胞質ドメインに結合するCARMA1がscaffolding proteinとして刺激シグナル伝達をつかさどり、T細胞増殖やIFN- $\gamma$ 産生などが誘導されることも明らかとなった<sup>17)</sup>。

CD26とcaveolin-1の免疫病態での意義を解明するため、関節リウマチ患者の罹患関節から得られた増殖滑膜の手術検体を病理組織学的に検討したところ、滑膜炎部位に集積するリンパ球はCD26を強く発現しており、これらのリンパ球に隣接した胚中心を形成するAPCや増殖滑膜細胞、血管内皮細胞にcaveolin-1が強く発現していることが連続切片による解析で明らかとなった<sup>18)</sup>。

### Ⅳ. CD26分子と悪性中皮腫

CD26陽性T細胞腫瘍株やヒト細胞クローンを用いて*in vitro*でCD26抗体で処理すると細胞増殖を抑制し、この時にcyclin dependent kinase inhibitor (CDKI)のp21が誘導され細胞周期を止めることを見いだした<sup>19)</sup>。

さらに、T細胞腫瘍株を用いた系でも*in vitro*でCD26抗体で処理するとp21が誘導され細胞増殖を抑制し、この細胞株を移植した免疫不全マウスの系でもCD26抗体の*in vivo*投与で腫瘍細胞は壊死に陥り、抗体投与マウスは長期生存した<sup>20)</sup>。この結果より、CD26抗体はT細胞異常を示す免疫病やCD26陽性T細胞リンパ腫などの治療に有効な可能性を示した。そこで、自ら

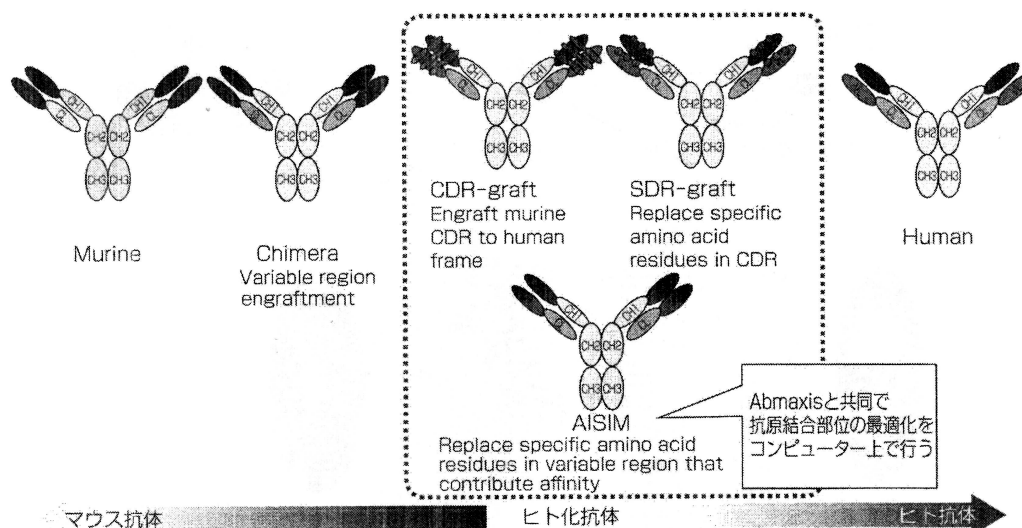


図3 ヒト化抗体作製技術

開発したマウス由来 CD26 抗体から最も活性が強いと思われるものを選択して CD26 抗体の抗原結合部位のアミノ酸および遺伝子配列解析を施行し、米国アプマキシス社と共同でインシリコ法にて良質なヒト化 CD26 抗体を開発した (図3)。

また、このヒト化抗体はもとのマウス型抗体と比しても親和性も高く、生物学活性はより強く、ヒトに用いる前に前臨床毒性試験を行うサル組織とも交叉反応性を示し良好な生産性も示した。

本ヒト抗体を開発した 2005 年にクボタショックという事件が話題に上った。つまりクボタショックとは、2005 年 6 月 29 日に毎日新聞が兵庫県尼崎市の大手機械メーカー・クボタの旧工場の周辺住民にアスベスト疾患が発生していると報告したのを契機として、社会的なアスベスト健康被害の問題が急浮上してきた現象をいい、その後連日のようにマスメディアにアスベストと中皮腫などアスベスト疾患の記事が報道された。

CD26 はコラーゲンの結合蛋白であり、われわれは T 細胞上の CD26 とコラーゲンの相互作用の研究を行っていたが、上皮型の細胞においてもその相互作用の解析を行う目的で種々癌細胞株の CD26 発現をスクリーニングする過程で偶然悪性中皮腫由来株である JMN が CD26 陽性であることを同定した<sup>2)</sup>。

CD26 が特殊な JMN という悪性中皮腫細胞株にのみ発現している可能性があるため、慶應義塾大学医学部病理学 山田健人准教授 (現埼玉医大病理学教授) に予備的に中皮腫患者の病理組織での CD26 発現を解析していただいたところ、反応性中皮では CD26 は発現していないのに悪性中皮腫では 9 例中 7 例に強発現することを見いだした。

さらに *in vivo* でヒト化 CD26 抗体は JMN 細胞株の増殖を抑制し、移植した免疫不全マウスの系においてもヒト化 CD26 抗体投与により、腫瘍縮小、生存延長、肺への転移抑制などをもたらすことを見だし、CD26 分子が悪性中皮腫の治療ターゲットになる可能性が示唆された<sup>4)</sup>。

## V. CD26 の悪性中皮腫における発現およびその機能とヒト化 CD26 抗体の有効性について

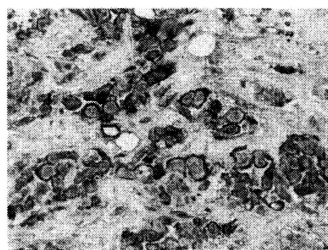
悪性中皮腫はその病理組織型により上皮型、混合型、肉腫型の三つに分けることができる<sup>21)</sup>。広島大学医学部病理学 井内康輝教授との共同研究で 152 症例の悪性中皮腫患者病理組織での CD26 発現を検討したところ、正常中皮ではまったく発現せず、上皮型では約 80% が陽性、混合型では約 40% が陽性、肉腫型ではほとんど発現せず、上皮型悪性中皮腫に有意に CD26 が発現することが明らかとなった<sup>3)</sup> (図4)。

JMN 以外の悪性中皮腫細胞株において CD26 の発現を検討したところ、9 種類の中皮腫株中 1 種類の MSTO 株のみが CD26 陰性で、他はすべて陽性であった。

この陰性株の MSTO 株に CD26 遺伝子を導入して CD26 を発現させたところ *in vitro* で親株に比して、ラミニン、IV型コラーゲン、フィブロネクチンをコートしたプレートに対して細胞遊走能、浸潤能ともに亢進が認められた<sup>22,23)</sup>。

さらに、CD26 発現 MSTO 細胞株を免疫不全マウスへの胸腔内投与により、胸腔内でびまん性に中皮腫細胞が進展し、胸壁に浸潤するとともに心臓や対側胸壁にも転移浸潤するヒト中皮腫浸潤・増殖モデルマウスの作製に成功した。このモデルマウスにヒト化 CD26 抗体を週 2

Membranous expression		Total No. of cases	(+)	(-)
Epithelioid mesothelioma	Well differentiated	48	40 (84%)	8
	Less differentiated	32	23 (72%)	9
Biphasic mesothelioma	Epithelioid component	21	16 (76%)	5
	Sarcomatoid component	21	0	21
Sarcomatoid mesothelioma		30	1 (3%)	29
Non-neoplastic mesothelial cells		32	0	32



(広島大学 井内康輝教授グループ)

CD26 expressed on the mesothelioma cells

図4 悪性中皮腫のCD26分子の免疫組織染色

回、4週間腹腔内投与したところ、コントロールIgG投与群と比して、心外膜、対側胸壁への転移浸潤が著明に抑制され、さらに原発腫瘍そのものもほとんど消失した。このようにヒト化CD26抗体は本モデルにおいても有効性を示したことから、悪性中皮腫での新規治療法として臨床応用できる可能性を強く示唆した。

また、CD26分子と悪性中皮腫患者の予後との関係について解析したところ、悪性中皮腫組織のCD26発現そのものは予後との関係は認められなかったが、悪性中皮腫組織上のCD26発現をベメトレキセド、シスプラチンなど現行の悪性中皮腫の化学療法施行症例に限ると、その有効率と予後に有意な関連が認められた<sup>24)</sup>。すなわち、CD26陽性発現度が高いほど化学療法の奏効率が高い傾向にあった。このように、CD26は化学療法剤治療反応性予測のバイオマーカーとなる可能性も示唆され、CD26陽発現性中皮腫症例には積極的に化学療法を施行すべきであると考えられた。

## VI. ヒト化CD26抗体のFIH第I相臨床試験

ヒト化CD26抗体のFIH第I相臨床試験をスタートにするに当たって、サルを用いた前臨床毒性試験を行う必要がある。カニクイザルを用いて10~100 mg/kgの単回静脈内点滴投与において特記すべき副作用と思われる変化は認められず、さらに毎週1回3か月間に及ぶ反復投与長期毒性試験においてもその安全性が確認された。

そこで、フランスのGustave-Roussy Institute Hospital, Cochin Hospital, Lyon Hospital, Caen Hospital, Dijon Hospitalの5施設で、化学療法抵抗性の悪性中皮

腫およびその他CD26陽性悪性腫瘍をターゲットにした第I相臨床試験がスタートした。0.1 mg/kg, 0.4 mg/kg, 1.0 mg/kg, 2.0 mg/kg, 4.0 mg/kg, 6.0 mg/kgの6用量・3例または6例/コホートからなり、第4コホートの途中までは隔週投与で1か月間計3回の投与、その後ヒト化CD26抗体の血中濃度をさらに上げるためプロトコルを変更して1か月間ごと週計5回投与を行い、投与終了2週後にmodified RECISTにてその有効性を評価した。

化学療法剤抵抗性悪性腫瘍141症例のCD26発現をスクリーニングして、20%以上病理組織標本においてCD26陽性の場合にその対象症例とした。総計33例の化学療法抵抗性の固形癌で、22例が進行性悪性中皮腫、10例が腎癌および1例が尿路上皮癌であった。ヒト化CD26抗体投与の成績であるが、13例がprogressive disease (PD)、13例がstabilized disease (SD)、7例が評価できずであった。さらに、悪性中皮腫の評価可能例19例中10例がSDと評価され、5例が6か月以上SDを継続し、1例が3か月以上SDが継続し、有効性を示唆するデータも得られた。安全性に関して注射後反応が認められるcaseはあったが、免疫不全をはじめとして特記すべき有害事象は認められず、安全性も確認できた<sup>25)</sup>。フランスのGustave-Roussy Institute Hospitalは悪性中皮腫をターゲットにして様々な抗体を含む薬剤の第I臨床試験を行っていたが、*Lung Cancer*という雑誌にこのグループが悪性中皮腫の第I相臨床試験に使用された薬剤25種類についてその評価を報告し、そのなかで本抗体は三つの有望な薬剤の一つに選ばれた(後の二つとしては、FAK inhibitor および ckit inhibitor である)<sup>5)</sup>。

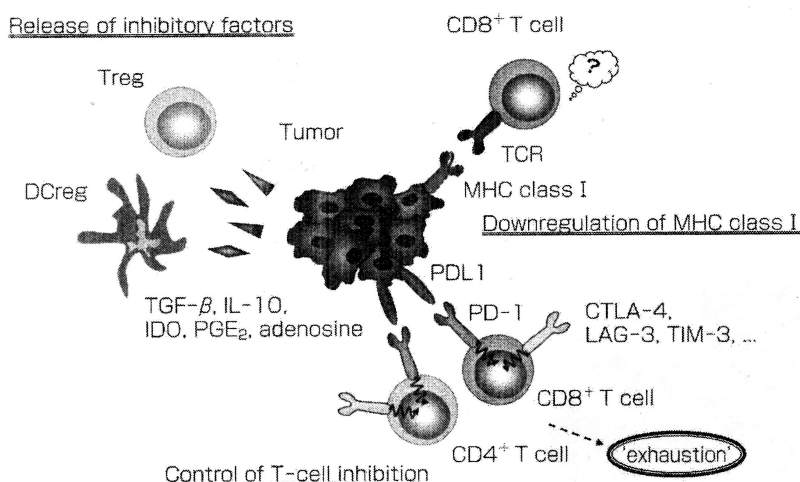


図5 癌細胞の免疫系からの攻撃を逃れる様々な機構について  
IDO: indoleamine-2,3-dioxygenase, PGE<sub>2</sub>: prostaglandin E<sub>2</sub>

## VII. ヒト化 CD26 抗体の作用機構

われわれはこれまでにヒト化 CD26 抗体の抗腫瘍作用メカニズムとして、本抗体は IgG1 であるので NK 細胞や macrophage の FcR 受容体に抗体が結合することで抗体医薬特有の抗体依存性細胞傷害 (ADCC) 活性などの間接的作用に加えて、CD26 陽性腫瘍に抗体が結合することによる直接的な作用があることを明らかにしてきた<sup>4)</sup>。癌細胞の細胞膜上の CD26 にヒト化 CD26 抗体が結合すると、CDKI である p21 や p27 の発現が上昇し、S 期の細胞を減少させるとともに G<sub>2</sub>/M 期で細胞周期を遅延させることが明らかになっている<sup>4,19,20)</sup>。さらに、CD26 抗体と CD26 の複合体が膜から細胞質、さらに核内へと移行し、RNA polymerase である POLR2A 遺伝子の転写領域下流に結合することで POLR2A の転写を抑制し増殖を抑制する<sup>26)</sup>。このように、細胞増殖や生存プログラムに重要な役割を果たす POLR2A 遺伝子機能を抑制することで、細胞増殖を抑制することを明らかにした。また、CD26 は collagen や fibronectin との結合蛋白であるが、CD26 抗体が結合することでそれらの蛋白への接着が阻害され<sup>4)</sup>、このことから CD26 抗体が CD26<sup>+</sup>腫瘍の浸潤・転移の抑制にも働くことが示唆された。

CD26 はヒト T 細胞に活性化シグナルを伝達する T 細胞共刺激分子であり、CD26 抗体は CD26 のリガンドである caveolin-1 の CD26 への結合をブロックする<sup>15,17,27)</sup>。また、CD26 の機能の一つに DPPIV 酵素活性があり、N 末端から 2 番目にプロリンまたはアラニンを有するペプチドの 2 アミノ酸を切断する<sup>8)</sup>。生体内で様々な生理活性物質がその基質となることが知られているが、いくつかのケモカインも DPPIV による切断を受

けその細胞遊走活性が不活性化される<sup>10,13)</sup>。最近担癌マウスに DPPIV 阻害薬のシタグリプチンを混ぜたエサを食べさせることにより、ケモカイン CXCL10 の DPPIV 酵素による分解を抑えることにより CXCR3 陽性 T 細胞の腫瘍微小環境への遊走を促進し、その結果腫瘍の増殖抑制をもたらすことが報告されている<sup>28)</sup>。CD26 抗体は DPPIV 酵素活性自体に直接は影響しないが、フランスでの第 I 相臨床試験の結果から、ヒト化 CD26 抗体の投与により血中の可溶性 CD26 の量が顕著に低下し、DPPIV 酵素活性も同様に低下することが示されている。DPPIV 酵素活性の低下により CXCL10 のケモカインの切断と不活性化が抑えられ、特に CXCR3 陽性細胞が腫瘍組織に遊走しやすくなり、腫瘍細胞を破壊する可能性が考えられる<sup>29)</sup>。これらの知見から、CD26 抗体は免疫系にも影響する可能性が強く示唆される。

## VIII. CD26 と免疫チェックポイント機構

さて、癌細胞には免疫系からの攻撃を逃れる様々な機構が備わっている (図 5)。たとえば Treg 細胞, regulatory dendritic cells などから TGF-β, IL-10 産生がされて免疫系を抑制したり、腫瘍細胞上の MHC クラス I の発現低下が生じて腫瘍特異的キラー T 細胞機能が発揮できなかつたり、さらに CTLA-4, PD-1, LAG-3 などの分子が T 細胞表面に発現誘導され、その結果 T 細胞機能が抑制されるというものである<sup>30)</sup>。

現在臨床現場では、特にメラノーマや非小細胞性肺癌の領域で CTLA-4 抗体や PD-1/PDL1 抗体を投与して免疫チェックポイント阻害により抗腫瘍免疫効果を亢進させ、ある患者集団ではとても有効であるとの報告がある<sup>31)</sup>。

現在、腫瘍免疫エスケープを改善させるため様々な種

類の癌に対して CTLA-4, PD-1/PDL1 抗体, さらに LAG-3 抗体およびそれら抗体の組み合わせなどの臨床試験が行われており<sup>32)</sup>,すでに CTLA-4 抗体や PD-1/PDL1 抗体はメラノーマや肺癌において臨床現場に届いている<sup>33)</sup>。

CD26 分子と免疫チェックポイント機構について, われわれはヒト CD4 T 細胞を CD3 と CD26 抗体および CD3 と CD28 抗体で刺激して様々なサイトカイン産生および細胞表面分子の発現を検討した。その結果, CD26 刺激では IL-10 および LAG-3 分子の発現上昇が認められた<sup>34)</sup>。しかし, CD28 刺激では認められなかった。また, IL-10 および LAG-3 とともに CD26 刺激の強さが増加するにつれ, その産生量および発現もますます高くなったが CD28 刺激ではこれらは認められなかった<sup>34)</sup>。しかし, CTLA-4 や FOXP3 の発現は CD26, CD28 刺激ともに差は認められなかった<sup>34)</sup>。

最近, 他のグループもヒト CD4 regulatory T 細胞における CD26 陽性サブセットは CD3 刺激において最も IL-10 を強産生する細胞集団であることを報告し, われわれの結果を支持するデータをだしている<sup>35)</sup>。このように, ヒト CD4 T 細胞に強い CD26 共刺激シグナルが伝達すると代表的抑制性サイトカインの IL-10 の強産生および免疫チェックポイント分子の LAG-3 分子の発現が誘導されることが明らかとなり, 癌微小環境において CD26 分子は, IL-10 高産生, LAG-3 分子の高発現を通じて免疫チェックポイントとして機能している可能性が示唆され, ヒト化 CD26 抗体の投与によりこれら免疫チェックポイントが阻害され腫瘍免疫を亢進している可能性が考えられる<sup>29,31)</sup>。

## おわりに

CD26 分子の免疫系および癌, 特に悪性中皮腫での機能, さらにヒト化 CD26 抗体の前臨床でのデータおよびフランスでの第 I 相臨床試験の結果を説明した。本抗体は本邦でも近々, 治療抵抗性の悪性中皮腫を対象として第 I 相臨床試験がスタートされる予定である。

CD26 分子は悪性中皮腫以外にも非小細胞性肺癌, 肝癌, 大腸癌, 腎癌など幅広く発現しており, これらの細胞株においても担癌マウスの系でヒト化抗体の有効性を確認しており, さらに化学療法剤との相乗作用の結果も得ている。

CD26 抗体は直接的な抗癌作用以外にも免疫チェックポイント阻害など非常にユニークな機能を有しており, 今後その対象を拡大させていく予定で癌に苦しむ患者に少しでも役立つことを願っている。

## 文 献

- Ohnuma K, Dang NH and Morimoto C: Revisiting an old acquaintance: CD26 and its molecular mechanisms in T cell function. *Trends Immunol* 29(5): 295-301, 2008.
- Dang NH, Torimoto Y, Schlossman SF, *et al*: Human CD4 helper T cell activation: functional involvement of two distinct collagen receptors, 1F7 and VLA integrin family. *J Exp Med* 172(2): 649-652, 1990.
- Amatya VJ, Takeshima Y, Kushitani K, *et al*: Overexpression of CD26/DPP4 in mesothelioma tissue and mesothelioma cell lines. *Oncol Rep* 26(6): 1369-1375, 2011.
- Inamoto T, Yamada T, Ohnuma K, *et al*: Humanized anti-CD26 monoclonal antibody as a treatment for malignant mesothelioma tumors. *Clin Cancer Res* 13(14): 4191-4200, 2007.
- Raphael J, Le Teuff G, Hollebecque A, *et al*: Efficacy of phase I trials in malignant pleural mesothelioma: description of a series of patients at a single institution. *Lung Cancer* 85(2): 251-257, 2014.
- Morimoto C and Schlossman SF: The structure and function of CD26 in the T-cell immune response. *Immunol Rev* 161(1): 55-70, 1998.
- Morimoto C, Torimoto Y, Levinson G, *et al*: 1F7, a novel cell surface molecule, involved in helper function of CD4 cells. *J Immunol* 143(11): 3430-3439, 1989.
- Hopsu-Havu VK and Glenner GG: A new dipeptide naphthylamidase hydrolyzing glycyl-prolyl-beta-naphthylamide. *Histochemie* 7(3): 197-201, 1966.
- Tanaka T, Camerini D, Seed B, *et al*: Cloning and functional expression of the T cell activation antigen CD26. *J Immunol* 149(2): 481-486, 1992.
- Ohnuma K and Morimoto C: DPP4 (dipeptidyl-peptidase 4). *Atlas Genet Cytogenet Oncol Haematol* 17(5): 301-312, 2013.
- Marguet D, Bernard AM, Vivier I, *et al*: cDNA cloning for mouse thymocyte-activating molecule. A multifunctional ecto-dipeptidyl peptidase IV (CD26) included in a subgroup of serine proteases. *J Biol Chem* 267(4): 2200-2208, 1992.
- Bengsch B, Seigel B, Flecken T, *et al*: Human Th17 cells express high levels of enzymatically active dipeptidyl-peptidase IV (CD26). *J Immunol* 188(11): 5438-5447, 2012.
- Ohnuma K, Hosono O, Dang NH, *et al*: Dipeptidyl peptidase in autoimmune pathophysiology. *Adv Clin Chem* 53: 51-84, 2011.
- Yan S, Marguet D, Dobers J, *et al*: Deficiency of CD26 results in a change of cytokine and immunoglobulin secretion after stimulation by pokeweed mitogen. *Eur J Immunol* 33(6): 1519-1527, 2003.
- Ohnuma K, Yamochi T, Uchiyama M, *et al*: CD26 up-regulates expression of CD86 on antigen-presenting cells by means of caveolin-1. *Proc Natl Acad Sci USA* 101(39): 14186-14191, 2004.
- Ohnuma K, Yamochi T, Uchiyama M, *et al*: CD26 mediates dissociation of Tollip and IRAK-1 from caveolin-1 and induces upregulation of CD86 on antigen-presenting cells. *Mol Cell Biol* 25(17): 7743-7757, 2005.
- Ohnuma K, Uchiyama M, Yamochi T, *et al*: Caveolin-1 triggers T-cell activation via CD26 in association with CARMA1. *J Biol Chem* 282(13): 10117-10131, 2007.
- Ohnuma K, Inoue H, Uchiyama M, *et al*: T-cell activation via CD26 and caveolin-1 in rheumatoid synovium. *Mod Rheumatol* 16(1): 3-13, 2006.
- Ohnuma K, Ishii T, Iwata S, *et al*: G1/S cell cycle arrest provoked in human T cells by antibody to CD26. *Immunology* 107(3): 325-333, 2002.

- 20) Ho L, Aytac U, Stephens LC, *et al*: *In vitro* and *in vivo* antitumor effect of the anti-CD26 monoclonal antibody 1F7 on human CD30+ anaplastic large cell T-cell lymphoma Karpas 299. *Clin Cancer Res* 7(7): 2031-2040, 2001.
- 21) Ismail-Khan R, Robinson LA, Williams CC, *et al*: Malignant pleural mesothelioma: a comprehensive review. *Cancer Control* 13(4): 255-263, 2006.
- 22) Okamoto T, Iwata S, Yamazaki H, *et al*: CD9 negatively regulates CD26 expression and inhibits CD26-mediated enhancement of invasive potential of malignant mesothelioma cells. *PLoS One* 9(1): e86671, 2014.
- 23) Yamamoto J, Ohnuma K, Hatano R, *et al*: Regulation of somatostatin receptor 4-mediated cytostatic effects by CD26 in malignant pleural mesothelioma. *Br J Cancer* 110(9): 2232-2245, 2014.
- 24) Aoe K, Amatya VJ, Fujimoto N, *et al*: CD26 overexpression is associated with prolonged survival and enhanced chemosensitivity in malignant pleural mesothelioma. *Clin Cancer Res* 18(5): 1447-1456, 2012.
- 25) Angevin E, Isambert N, Trillet-Lenoir VN, *et al*: First-in-human phase I administration of YS 110, a monoclonal antibody directed against CD26 immunostimulatory molecule in advanced cancer patients. *J Clin Oncol* 33(15): abstr 2519, 2015.
- 26) Yamada K, Hayashi M, Du W, *et al*: Localization of CD26/DPP4 in nucleus and its nuclear translocation enhanced by anti-CD26 monoclonal antibody with anti-tumor effect. *Cancer Cell Int* 9: 17, 2009.
- 27) Ohnuma K, Uchiyama M, Hatano R, *et al*: Blockade of CD26-mediated T cell costimulation with soluble caveolin-1-Ig fusion protein induces anergy in CD4<sup>+</sup> T cells. *Biochem Biophys Res Commun* 386(2): 327-332, 2009.
- 28) Barreira da Silva R, Laird ME, Yatim N, *et al*: Dipeptidyl-peptidase 4 inhibition enhances lymphocyte trafficking, improving both naturally occurring tumor immunity and immunotherapy. *Nat Immunol* 16(8): 850-858, 2015.
- 29) Ohnuma K, Hatano R and Morimoto C: DPP4 in anti-tumor immunity: going beyond the enzyme. *Nat Immunol* 16(8): 791-792, 2015.
- 30) Palucka AK and Coussens LM: The basis of oncoimmunology. *Cell* 164(6): 1233-1247, 2016.
- 31) Hamanishi J, Mandai M, Matsumura N, *et al*: PD-1/PD-L1 blockade in cancer treatment: perspectives and issues. *Int J Clin Oncol*: 2016. [Epub ahead of print]
- 32) Spranger S: Mechanisms of tumor escape in the context of the T cell-inflamed and the non-T-cell-inflamed tumor microenvironment. *Int Immunol*: 2016. [Epub ahead of print].
- 33) Nguyen LT and Ohashi PS: Clinical blockade of PD1 and LAG3—potential mechanisms of action. *Nat Rev Immunol* 15(1): 45-56, 2015.
- 34) Hatano R, Ohnuma K, Otsuka H, *et al*: CD26-mediated induction of EGR2 and IL-10 as potential regulatory mechanism for CD26 costimulatory pathway. *J Immunol* 194(3): 960-972, 2015.
- 35) Hua J, Davis SP, Hill JA, *et al*: Diverse gene expression in human regulatory T cell subsets uncovers connection between regulatory T cell genes and suppressive function. *J Immunol* 195(8): 3642-3653, 2015.



## 特集

## 分子標的治療薬

# 標的別分子標的薬

## 6) モノクローナル抗体\*

大 沼 圭\*\*  
森 本 幾 夫\*\*

**Key Words :** monoclonal antibody, CD26, dipeptidyl peptidase IV, YS110, renal cell carcinoma

### はじめに

2015年のノーベル生理学・医学賞が北里研究所の大村智氏に授与された。トランスレーショナルリサーチを実践する日本人のサムライスピリットを世界中が賞賛した。北里研究所を創立した北里柴三郎は、当時蔓延していた伝染病を撲滅するため医学研究と診療に一生を捧げ、破傷風菌の血清療法を開発し多くの伝染病患者を救った。これこそが現代の抗体療法の原点であり、そのスピリットはわれわれ日本人医学者に脈々と受け継がれている。現在、多くの抗体医薬が当局の認可を受け、日常診療で使用可能となっており、さらに、数百を超える抗体医薬品の臨床試験が世界各国で行われている。本稿では、抗体療法の基礎となっているモノクローナル抗体について概説し、われわれの研究室が世界に向けて発信している抗CD26モノクローナル抗体による、腎がんを含む難治性悪性腫瘍の治療について説明する。

### ヒト抗体分子の基礎

1938年、TiseliusとKabatは血清療法の本体である「抗体」の活性を持つ物質がγグロブリン画分に存在することを証明した<sup>1)</sup>。現在では、こ

の「抗体」とよばれるヒト生体内のタンパク質は免疫グロブリン(immunoglobulin; Ig)であり、IgG, IgA, IgM, IgE, IgDの5つのクラスがあることがわかっている。免疫グロブリンの基本構造を図1に、また、各クラスの相違を表1に示した。この中でIgG型抗体は分子量、生体内での安定性、エフェクター機能、産生・精製の簡便さなどから、抗体医薬の主流となっている。IgGはFc領域のアミノ酸配列の違いにより、IgG1, IgG2, IgG3, IgG4の4つのサブクラス(アイソタイプ)に分けられる。これらのアイソタイプにおける相違を表2にまとめた。IgG1はエフェクター機能の強さと生体内での半減期のバランスが良く、抗体医薬に最も適したアイソタイプである。最近話題のIgG4はユニークなIgGアイソタイプで、持続する抗原刺激に反応して産生されるアイソタイプと考えられている。生体内において「最も持続する抗原刺激」とは自己抗原によるものであるが、IgG4の半分子とハイブリッド分子は自己反応性抗体のクリアランスに関与しており、自己反応性IgG4の増加はIgG4関連疾患として知られている<sup>2)</sup>。また、抗体医薬としては、免疫チェックポイント阻害薬である抗PD-1抗体のnivolumabが完全ヒト型IgG4抗体である。

抗体はB細胞で産生されるが、B細胞は抗原刺激を受容するとプラズマ細胞に分化し、抗原特異的な抗体を大量に産生・分泌する。また、

\* Monoclonal antibody.

\*\* Kei OHNUMA, M.D., Ph.D. & Chikao MORIMOTO, M.D., Ph.D.: 順天堂大学大学院医学研究科免疫病・がん先端治療学講座[〒113-8421 東京都文京区本郷2-1-1]; Department of Therapy Development and Innovation for Immune Disorders and Cancers, Graduate School of Medicine, Juntendo University, Tokyo 113-8421, JAPAN

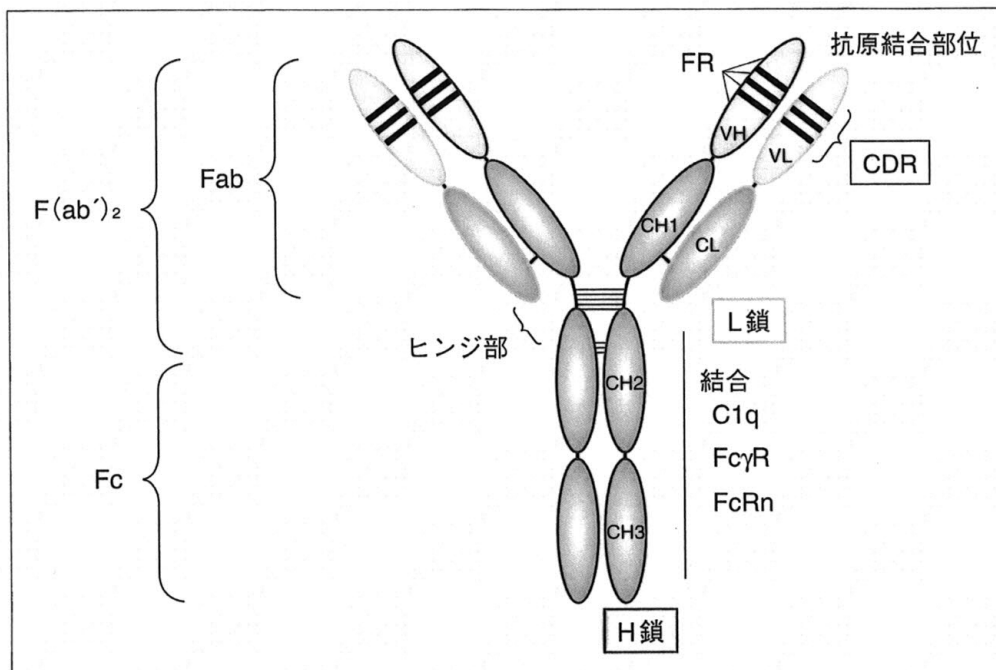


図1 免疫グロブリン(Ig)の基本構造

免疫グロブリンの基本構造は、分子量約25 kDaの軽鎖(light chain; L鎖)と分子量約50～77 kDaの重鎖(heavy chain; H鎖)のポリペプチドがそれぞれ2本ずつ、合計4本のポリペプチドがジスルフィド結合したヘテロ4量体で、Y字型の模式図で表される。4本のポリペプチドは、アミノ酸配列の類似性が低く変化に富む抗原結合領域(antigen binding fragment; Fab領域)とアミノ酸配列が非常に高い類似性を示す定常領域(constant fragment; Fc領域)よりなっている。Fab領域のうちアミノ酸配列に多彩な変化がみられる可変領域をV領域(variable region)といい、L鎖の可変領域をVL領域、重鎖の可変領域をVH領域と呼ぶ。V領域以外のFab領域とFc領域は、比較的变化の少ない領域で、L鎖の定常領域をCL領域、H鎖の定常領域をCH領域と呼ぶ。CH領域はさらにCH1～CH3の3つのドメインから構成されている。H鎖のFab領域とFc領域をつなぐ部分はヒンジ部とよばれており、左右のH鎖はこのヒンジ部がジスルフィド結合しており、抗原結合部位Fab領域の可動性を維持する。ヒンジ部のジスルフィド結合のFc側で切断してできたFab領域が2つ結合した断片をF(ab')<sub>2</sub>と呼び、ヒンジ部より可変領域側を切断してできた断片をFabと呼ぶ。したがって、F(ab')<sub>2</sub>は2価(bivalent)、Fabは1価(monovalent)の抗原結合能を有する。Fc領域は抗体がエフェクター機能を発揮するために重要な部分であり、医薬品としての抗体を決定づける重要な要素である。抗体のFc領域を介したエフェクター機能としては、抗体依存性細胞傷害活性(antibody-dependent cell-mediated cytotoxicity; ADCC)、補体依存性細胞傷害活性(complement-dependent cytotoxicity; CDC)、オプソニン作用、補体活性化機能、中和作用がある。V領域の中で、抗原と直接結合する部位は、約10アミノ酸残基よりなる超可変領域と呼ばれ、抗体によってアミノ酸配列の変化が非常に大きく、抗原に対する特異性を決定する領域であるため相補性決定領域(complementarity-determining region; CDR)と呼び、それ以外の可変領域の部分はこのCDRを支えるフレームワーク領域(frame work region; FR)と呼ぶ。L鎖とH鎖の可変領域に、それぞれ3つのCDR(CDR1～CDR3)と、3つのCDRを取り囲む4つのFR(FR1～FR4)が存在する。VLの3つのCDRとVHの3つのCDRの合計6つのCDRが1つの抗原と結合する、すなわち、1つのFabは1つの抗原と結合するため、抗体1分子は2か所の抗原結合部位を有している。

一部はメモリーB細胞となって体内で維持され、次の抗原侵入時に即応する準備を整える。1975年、KöhlerとMilsteinはマウスB細胞由来のハイブリドーマを用いてマウスモノクローナル抗体をより簡便に作製する技術を開発し、その結果、抗体療法への道が大きく開けることとなっ

た<sup>3)</sup>。その後、Schlossmanらにより開発されたヒトリンパ球抗原に対するマウスモノクローナル抗体OKT3が臓器移植後の拒絶反応に対して投与された<sup>4)</sup>。しかし、投与された抗体そのものがマウス由来のタンパクであったため、人体に繰り返し投与すると、ヒト抗マウス抗体(human anti-

表1 ヒト免疫グロブリン各クラスの相違

	IgG	IgA	IgM	IgD	IgE
H鎖クラス	$\gamma$	$\alpha$	$\mu$	$\delta$	$\epsilon$
L鎖クラス	$\lambda$ または $\kappa$	$\lambda$ または $\kappa$	$\lambda$ または $\kappa$	$\lambda$ または $\kappa$	$\lambda$ または $\kappa$
分子構造	単量体	単または二量体	五量体	単量体	単量体
分子量(kDa)	150	160(単量体) 400(分泌型)	900	184	188
抗原結合価	2価	2価(単量体) 4価(分泌型)	10価	2価	2価
血清中濃度(mg/dl)	800~1,600	140~400	50~200	0~10	1~45
総Igに対する割合(%)	80	13	6	1	0.002
生体内産生速度(mg/kg/日)	33	24	6.7	0.4	0.02
血中半減期(日)	21	5.8	10	2.8	2.3
マクロファージ結合	+	—	+	—	—
体外分泌	—	+	—	—	—
マスト細胞結合	—	—	—	—	+
組織間質移行	+	—	—	—	—
胎児移行	+	—	—	—	—
ADCC活性	+	—	—	—	—
補体結合	+	—	+	—	—

表2 各IgGアイソタイプの性質

	IgG1	IgG2	IgG3	IgG4
機能的分子構造	単量体	二量体	単量体	半量体
抗原結合価	2価	4価	2価	1価
抗原	タンパク抗原	糖タンパク抗原	タンパク抗原	持続刺激抗原
総IgGに対する割合	60%	25%	10%	5%
血中半減期	21日	20日	7日	21日
ヒンジ部のアミノ酸	15残基	12残基	62残基	12残基
Fc $\gamma$ RI(CD64)結合	++++	—	++	+
Fc $\gamma$ RII(CD32)結合	+++	±	+	+
Fc $\gamma$ RIII(CD16)結合	+	—	+	—
FcRn結合	+	+	+	+
ADCC活性	+	—	+	—
補体C1結合	++	±	+++	—

mouse antibody ; HAMA) が高頻度に出現し、アナフィラキシーなどの重篤な副作用が認められ、さらに、治療用抗体が体内から急速に消失してしまうなどの問題点が明らかとなった。その後、遺伝子組み換え技術が著しい進歩を遂げ、モノクローナル抗体の持つ抗原特異性と異種タンパクの抗原性とを分離して大量生産することが可能となり、多くの治療用抗体が臨床現場に届けられている(図2)。

#### 新しいモノクローナル抗体YS110 (抗CD26ヒト化抗体)の臨床開発について

CD26分子はリンパ球のほか、腎尿細管、前立

腺、腸粘膜等に出現しており、細胞膜上のシグナル分子および dipeptidyl peptidase IV (DPPIV) というペプチダーゼ酵素として機能している<sup>5)6)</sup>。当初、このCD26分子はTa1というマウスモノクローナル抗体と反応するヒト末梢血T細胞表面抗原として報告され、その後、活性化T細胞に強く発現することから、T細胞活性化抗原として確立された<sup>7)8)</sup>。CD26陽性T細胞は炎症部位に集まるエフェクター細胞であり、特にCD4<sup>+</sup>CD26<sup>high</sup>T細胞はヒトメモリーT細胞で、最も遊走しやすいリンパ球サブセットである<sup>9)</sup>。ヒトCD4T細胞における抗原特異的活性化機構については、われわれの研究により、T細胞共刺激

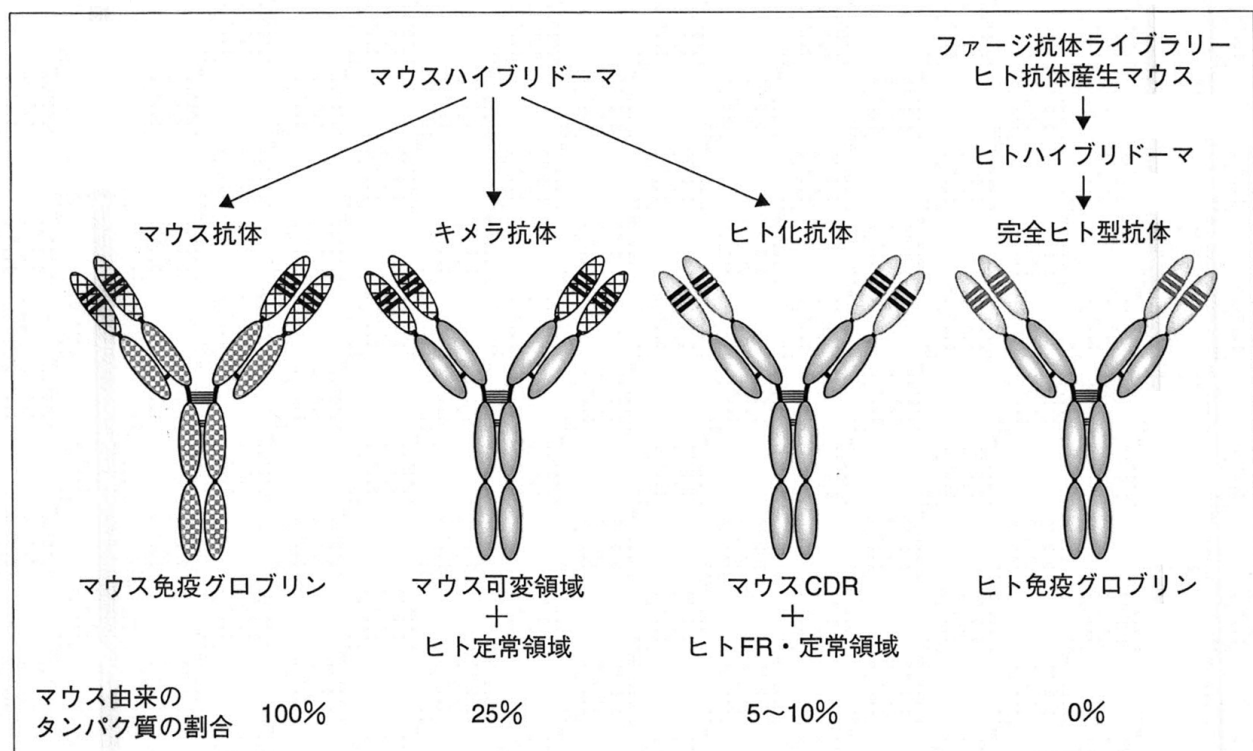


図2 治療用抗体の種類

ヒトに投与可能な治療用抗体としては、マウスモノクローナル抗体(一般名の末尾は~omab)のほか、ヒト・マウスキメラ抗体(chimeric monoclonal antibody; 一般名の末尾は~ximab)、ヒト化抗体(humanized monoclonal antibody; 一般名の末尾は~zumab)、完全ヒト型抗体(fully human monoclonal antibody; 一般名の末尾は~mumab)が作製されている。キメラ抗体は、マウスのモノクローナル抗体の抗原認識部位である可変領域(VLとVH)とヒト抗体の定常領域を融合した抗体である(CD20抗体のrituximabやTNF $\alpha$ 抗体のinfliximab等)。ヒト化抗体は、マウスモノクローナル抗体の抗原結合部位である超可変領域のみを残し、他の部分にヒト由来のIgGを用いたものである。すなわち、ヒト化抗体は抗体1分子につき、Fabにあるマウス由来の12か所のCDRをヒト抗体のFRおよび定常領域に移植(CDRグラフト技術)した抗体である(抗HER2抗体のtrastuzumabや抗VEGF抗体のbevacizumab等)。完全ヒト型抗体は、100%ヒトアミノ酸配列の抗体で、ヒトB細胞由来cDNAライブラリーやヒト免疫グロブリン遺伝子を組み込んだトランスジェニックマウスにより作製する(抗EGFR抗体のpanitumumabや抗CTLA4抗体のipilimumab等)。

分子としてのCD26分子のシグナル伝達の詳細が明らかになっている(図3)<sup>10)~12)</sup>。その結果、CD26を標的とした抗体療法は、難治性免疫病の新規治療法として注目されている<sup>13)~15)</sup>。

一方、がん細胞においてもCD26分子は細胞増殖や遊走・浸潤・転移に深く関与している。前立腺がん組織においては、前立腺肥大症に比べて、CD26/DPP-IVの発現が2倍増加している<sup>16)</sup>。また、前立腺がんの肺転移巣においては、転移していない前立腺がん組織に比べて、CD26/DPP-IVの発現が著明に増加している<sup>16)</sup>。さらに、われわれは、CD26陽性腎細胞がん株を移植した担がんマウスモデルを作製し、抗CD26モノクローナル抗体の治療効果を検討したところ、腎細胞がんの増殖および転移を抑制し、生存率が延長することを報告した<sup>17)</sup>。同様に、難治性のため

に画期的な治療法の開発が待ち望まれている悪性中皮腫においても、われわれは、CD26分子が増殖・浸潤・転移の重要な分子であり、抗CD26モノクローナル抗体が悪性中皮腫の革新的な治療薬になることを明らかにしてきた<sup>16)18)</sup>。臨床検体を用いたCD26発現解析では、前立腺がん107例中88例、腎細胞がん124例中106例、悪性中皮腫100例中85例といずれも80%以上がCD26陽性症例であった(未発表データ)。図4に、その一例を提示した。

これらの基礎研究の成果を臨床現場に届けるため、われわれは、ヒト化CD26抗体を作製した。実験室で用いたCD26マウスモノクローナル抗体のCDRのアミノ酸配列をもとに、親和性の高いヒト化抗体の作製に必要なCDRおよびFRのアミノ酸配列をコンピュータ上で予測し



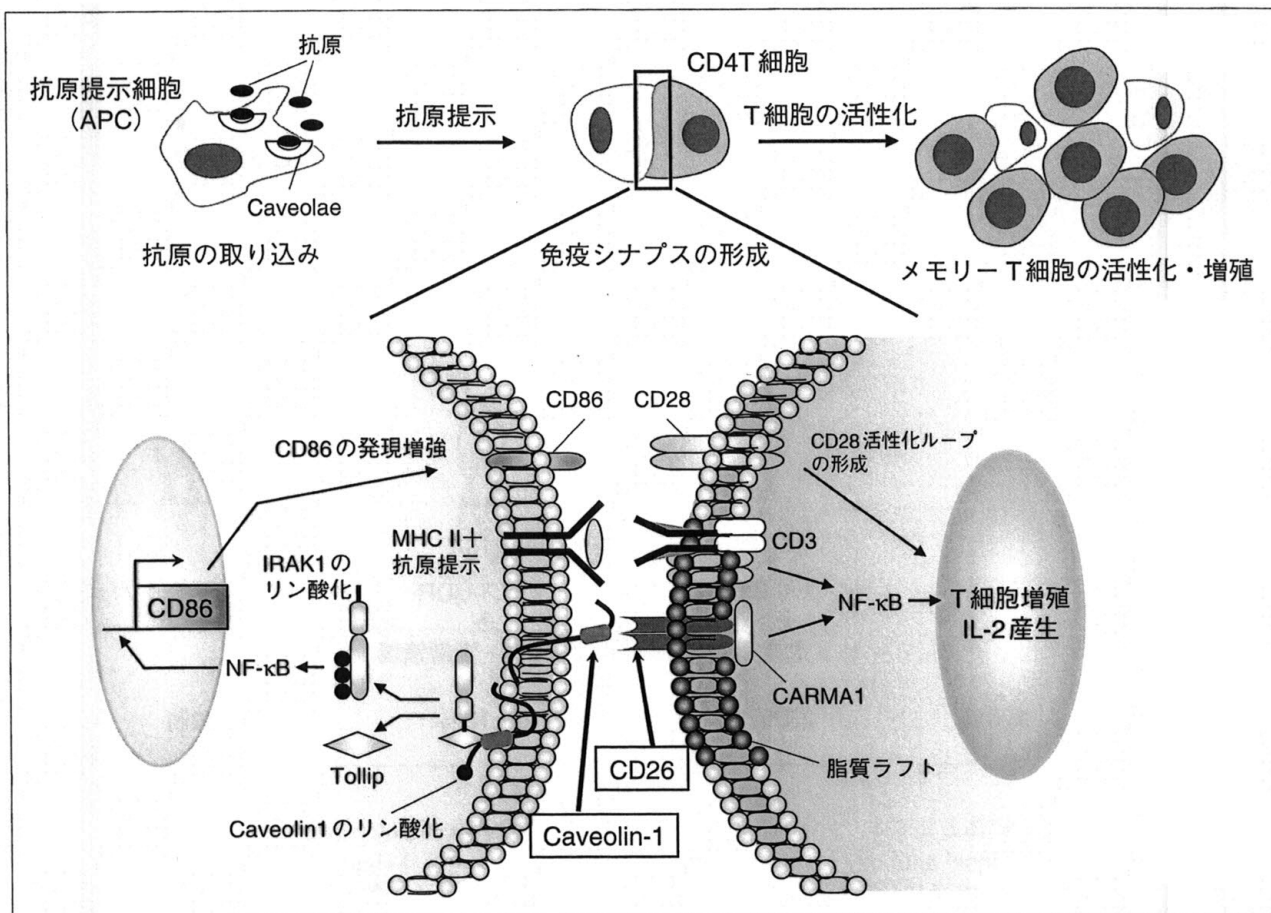


図3 ヒトT細胞におけるCD26分子のシグナル経路

T細胞のCD26のメモリー抗原に曝露された抗原提示細胞(APC)のCaveolin-1が互いに接触して immunological synapse を形成し、メモリーT細胞に対する増殖反応がもたらされる。T細胞表面のCD26は、抗原を取り込んだAPC上のCaveolin-1と結合すると、Caveolin-1がリン酸化され下流のシグナルが活性化(IRA K1のリン酸化、NF-κBの活性化)。その結果、強力なT細胞共刺激分子CD28のリガンドであるCD86がAPC上に発現する。さらに、Caveolin-1と結合したT細胞上のCD26は、CD26の細胞質ドメインに結合するCARMA1を足場分子としてT細胞内のシグナルが活性化され、抗原特異的なT細胞クローンの増殖やIL-2産生が亢進する結果、抗原特異的T細胞性免疫が働くことになる。

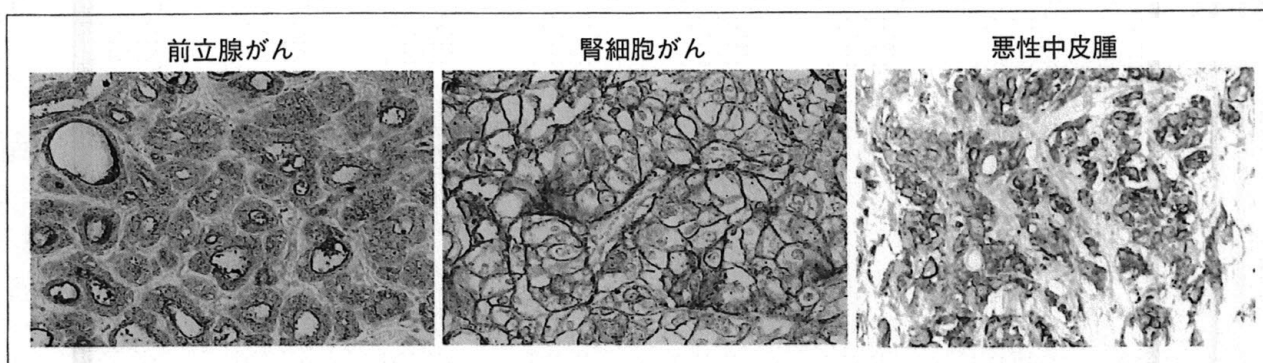


図4 腫瘍組織病理標本のCD26免疫染色

前立腺がん、腎細胞がん、胸膜悪性中皮腫の手術検体からパラフィン固定病理組織標本を作製し、CD26抗体で免疫染色を行った。それぞれ代表的な症例の写真を提示した。CD26陽性細胞が茶色に染まっている。

て、高親和性で生物学的活性が高いIgG1型ヒト化CD26抗体を複数クローン作製した。さらに、毒性試験で使用するカニクイザルの組織における

CD26との交叉反応性、および、良好なヒト化抗体生産細胞株の構築などの観点からYS110というクローンを樹立し、量産体制を整えた。

薬理効果を実証するため、CD26陽性腎がん、白血病、悪性中皮腫細胞株を移植した担がんマウスで検討を行ったところ、CD26抗体は著明な腫瘍抑制効果を示した<sup>17)~19)</sup>。その作用機序として、まず、Fc領域のエフェクター機能であるADCC活性等の間接的作用があることを証明した<sup>18)</sup>。次に、CD26陽性腫瘍細胞に抗体が結合することによる直接的な作用があることを明らかにした<sup>13)17)~19)</sup>。すなわち、CD26抗体ががん細胞に結合すると、サイクリン依存性キナーゼ阻害因子であるp21<sup>Cip1</sup>やp27<sup>Kip1</sup>の発現が上昇するため細胞周期が停止して腫瘍増殖が抑制されることを明らかにした<sup>13)17)~19)</sup>。さらに、CD26抗体とCD26分子の複合体が細胞膜から核内へと移行し、RNAポリメラーゼであるPOLR2Aの転写領域下流に結合することでPOLR2Aの転写を阻害し、細胞増殖を抑制することを見出した<sup>20)</sup>。また、CD26はコラゲンやフィブロネクチン等の細胞外マトリックスとも結合してがん細胞の浸潤・転移を促進しているが、CD26抗体により細胞外マトリックスとの接着が阻害され、腫瘍の浸潤・転移の抑制にも作用していることが明らかとなった<sup>17)</sup>。

一方、カニクイザルを用いてYS110の安全性試験を実施した(YS110はカニクイザルのCD26分子にも交叉反応するエピトープを持っている)。カニクイザルを用いた10~100 mg/kgの単回静脈内点滴投与において特記すべき副反応は認められず、さらに毎週1回3か月間に及ぶ反復投与長期毒性試験においてもその安全性が確認された。また、投与期間中および投与後56日間の試験期間中、いずれの投与群においても、CD3, CD4, CD8, CD25, CD26陽性リンパ球に変化は認められなかった。

以上の成果をもとに、われわれは、化学療法抵抗性の腎細胞がん、悪性中皮腫およびその他CD26陽性悪性腫瘍患者を対象にfirst-in-human (FIH) 第I相臨床試験をフランスで実施した<sup>21)</sup>。試験プロトコルは、0.1~6.0 mg/kgの6用量・各コホート3例または6例で、第4コホートの途中までは隔週投与で1か月間計3回の投与、その後、より高い薬剤血中濃度を維持する目的で1か月間毎週計5回投与を行った。いずれのコホート

も投与終了2週後にmodified RECISTに準じて有効性を評価した。投与症例は化学療法抵抗性悪性腫瘍141症例から選択され、採取された病理組織のパラフィン固定標本を免疫組織化学法で評価し、がん組織の20%以上がCD26陽性の症例を投与対象とした。最終的な投与症例は33例で、22例が悪性中皮腫、10例が腎細胞がん、1例が尿路上皮がんであった。試験中の重篤な有害事象として、注射後反応が2例に発現したが、ステロイドの前投薬で予防することが可能となり、試験は計画どおり完遂した。また、免疫不全をはじめとして特記すべき有害事象は認められず、安全性が実証された<sup>21)</sup>。有効性の評価では、13例がprogressive disease (PD)、13例がstabilized disease (SD)、評価不能が7例であった。さらに、悪性中皮腫の評価可能症例19例中10例がSD、このうち5例が6か月以上SDを継続し、1例が3か月以上SDを継続する結果となった<sup>21)</sup>。これは、既存の化学療法で抵抗性となった悪性中皮腫に対する治療効果としては、きわめて画期的な結果となった。

さらに、われわれは臨床試験と並行して、YS110のエピトープとは交叉しない新たな抗ヒトCD26モノクローナル抗体を樹立し、パラフィン固定病理組織標本やフローサイトメトリー、ELISA等の検査できわめて良好な性能を示すコンパニオン診断薬を開発した<sup>6)</sup>。このコンパニオン診断薬の開発により、YS110治療中あるいは治療後においても標的分子の精密なモニタリングが可能となり、薬効と副反応の監視を厳密に行える基盤が整った。

## CD26抗体療法の新たな展開

CD26分子の機能の一つにDPPIV酵素活性があり、生体内でさまざまな生理活性物質がその基質となることが知られている<sup>5)</sup>。たとえば、血糖コントロールにかかわるインクレチンはDPPIVの基質であり、DPPIV阻害薬は経口血糖降下薬として臨床で使用されている。免疫系では、CXCL10等のケモカインもDPPIVによるペプチダーゼ分解を受け、細胞遊走活性が不活性化される<sup>5)22)</sup>。最近、経口血糖降下薬として使用されているDPPIV阻害薬が、抗腫瘍免疫を活性



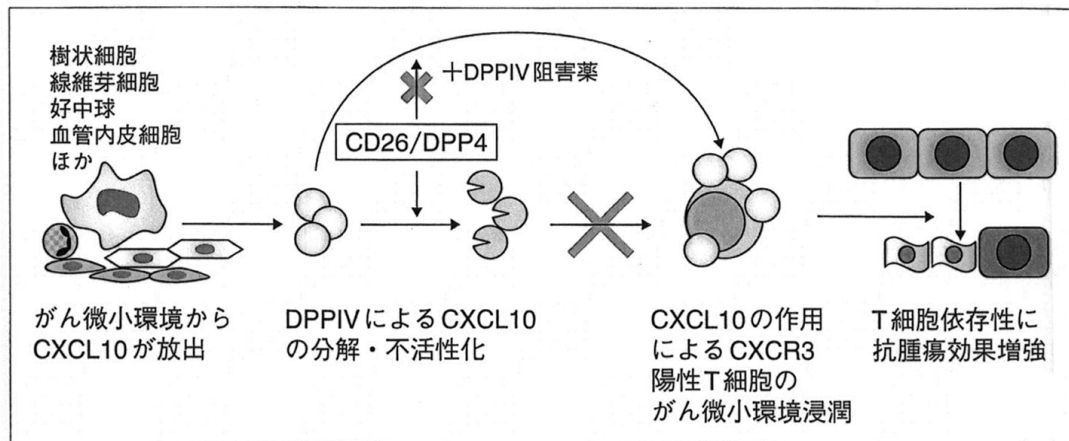


図5 DPPIV阻害薬によるT細胞依存性抗腫瘍免疫の活性化のメカニズム  
詳細は本文記載参照。

化して腫瘍抑制効果を惹起することが報告された<sup>23)</sup>。すなわち、DPPIV阻害薬がCXCL10の分解・不活性化を抑制した結果、CXCL10の受容体であるCXCR3を発現した腫瘍特異的活性リンパ球が腫瘍周囲に集簇し、これにより、腫瘍の増殖抑制をもたらすことが、担がんマウスモデルによって示された<sup>23)</sup>。われわれが開発したヒト化CD26抗体YS110はDPPIV酵素活性自体に直接は影響しないが、治療量のYS110投与によって、DPPIV阻害薬の内服と同程度に血中DPPIV活性が低下することが明らかとなっている<sup>15)21)</sup>。この事実より、YS110投与によって体内のDPPIV酵素活性が低下してCXCL10の分解・不活性化が抑制され、その結果、CXCR3陽性抗腫瘍T細胞を介した抗腫瘍効果が発現されると考えられる(図5)<sup>24)</sup>。

ところで、過剰な免疫反応を監視し免疫にブレーキをかける機能を免疫チェックポイント機能という。がん細胞はCD8T細胞などの免疫的な攻撃によって排除される一方で、免疫チェックポイント機能を獲得し、免疫的排除機構からエスケープして増殖・浸潤する<sup>25)</sup>。すなわち、がん微小環境においては、IL-10やTGF- $\beta$ 等の免疫抑制因子が発現し、PD-1(programmed cell death protein 1: CD279), CTLA-4(cytotoxic T-lymphocyte-associated protein 4: CD152), LAG-3(lymphocyte activation gene 3: CD223), BTLA(B- and T-lymphocyte attenuator: CD272)等の免疫チェックポイント分子を介して免疫抑制細胞が増加することにより、がん細胞の生存に

とって好都合な環境が作り出されている<sup>25)</sup>。そこで、CTLA-4抗体やPD-1/PD-L1抗体による免疫チェックポイント阻害療法が開発され、種々のがん腫に対して著明な効果を上げている<sup>26)</sup>。一方、われわれは、CD26分子シグナルによりIL-10およびLAG-3分子の発現が上昇するCD4T細胞サブセットを同定し、CD26分子が免疫チェックポイント分子としても機能していることを発見した(図6)<sup>27)</sup>。さらに、米国のグループも、ヒトCD26陽性制御性T細胞はIL-10を最も強く産生する制御性T細胞サブセットであることを見出し、われわれの結果を支持するデータを報告している<sup>28)</sup>。このように、がん微小環境においてCD26分子は、IL-10高産生、LAG-3分子の高発現を通じて免疫チェックポイント分子として機能している可能性が示された。すなわち、CD26抗体はこれら免疫チェックポイントを阻害し抗腫瘍免疫を亢進するものと考えられる<sup>27)</sup>(図6)。このことは、YS110はCD26陰性悪性腫瘍においても抗腫瘍効果を発揮することが期待できる抗がんモノクローナル抗体といえる。

## おわりに

フランスでのFIH第I相試験の結果を受けて、YS110は、悪性中皮腫の第I臨床試験に使用された薬剤25種類のうち、FAK阻害薬、c-KIT阻害薬に並び最も有望な新規薬剤に選ばれた<sup>29)</sup>。そして、本邦でも、治療抵抗性の悪性中皮腫を対象とした第I相臨床試験を近々に開始する予定である。

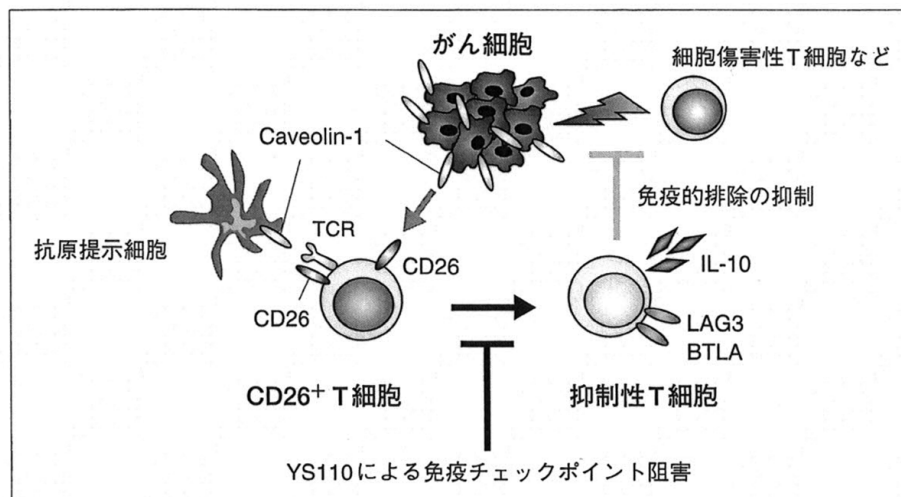


図6 CD26抗体の免疫チェックポイント阻害作用による腫瘍増殖抑制  
がん微小環境に存在する抗原提示細胞やがん細胞に発現した Caveolin-1 からの刺激を受容した CD26 陽性 T 細胞は、抑制性サイトカインの IL-10 を産生し、また、免疫チェックポイント分子の LAG-3 や BTLA を発現して抑制性 T 細胞に分化する。その結果、がん微小環境において抑制性細胞が増加して抗腫瘍免疫細胞を抑制し、がん細胞が免疫的排除からエスケープするため、がん細胞の増殖・浸潤・転移が促進される。しかし、このような免疫チェックポイントを抗 CD26 抗体 YS110 が阻害することにより免疫抑制が解除されるため、免疫的排除機構が増強し、腫瘍増殖が抑制される。

CD26 分子は悪性中皮腫以外にも腎細胞がん、前立腺がん、非小細胞性肺がん、肝細胞がん、大腸がんなど幅広く発現しており、これらががん腫の担がんマウスモデルを用いた検討において、YS110 の有効性および化学療法剤との併用効果に関する前臨床データを取得している。さらに、YS110 は直接的な抗がん作用以外にも免疫チェックポイント阻害など非常にユニークな機能を有しており、今後、バスケット試験として CD26 陰性の進行がんにもその治療対象を拡大させていく予定である。

われわれは誇り高き日本人医学者としてサムライスピリットを忘れず、メスでは切れないがんに対してモノクローナル抗体という刀で挑み、1人でも多くの患者さんを苦しみから解放する努力を続けていきたい。

## 文 献

- 1) Tiselius A, Kabat EA. Electrophoresis of immune serum. *Science* 1938 ; 87 : 416.
- 2) van der Neut Kofschoten M, Schuurman J, Losen M, et al. Anti-inflammatory activity of human IgG4 antibodies by dynamic Fab arm exchange. *Science* 2007 ; 317 : 1554.
- 3) Köhler G, Milstein C. Continuous cultures of fused cells secreting antibody of predefined specificity. *Nature* 1975 ; 256 : 495.
- 4) Kung P, Goldstein G, Reinherz EL, Schlossman SF. Monoclonal antibodies defining distinctive human T cell surface antigens. *Science* 1979 ; 206 : 347.
- 5) Ohnuma K, Hosono O, Dang NH, Morimoto C. Dipeptidyl peptidase in autoimmune pathophysiology. *Adv Clin Chem* 2011 ; 53 : 51.
- 6) Hatano R, Yamada T, Matsuoka S, et al. Establishment of monoclonal anti-human CD26 antibodies suitable for immunostaining of formalin-fixed tissue. *Diagn Pathol* 2014 ; 9 : 30.
- 7) Eguchi K, Ueki Y, Shimomura C, et al. Increment in the  $Ta1^{+}$  cells in the peripheral blood and thyroid tissue of patients with Graves' disease. *J Immunol* 1989 ; 142 : 4233.
- 8) Morimoto C, Torimoto Y, Levinson G, et al. 1F7, a novel cell surface molecule, involved in helper function of CD4 cells. *J Immunol* 1989 ; 143 : 3430.
- 9) Morimoto C, Schlossman SF. The structure and function of CD26 in the T-cell immune response. *Immunol Rev* 1998 ; 161 : 55.
- 10) Ohnuma K, Dang NH, Morimoto C. Revisiting an

- old acquaintance : CD26 and its molecular mechanisms in T cell function. *Trends Immunol* 2008 ; 29 : 295.
- 11) Ohnuma K, Uchiyama M, Yamochi T, et al. Caveolin-1 triggers T-cell activation via CD26 in association with CARMA1. *J Biol Chem* 2007 ; 282 : 10117.
  - 12) Ohnuma K, Yamochi T, Uchiyama M, et al. CD26 up-regulates expression of CD86 on antigen-presenting cells by means of caveolin-1. *Proc Natl Acad Sci USA* 2004 ; 101 : 14186.
  - 13) Ohnuma K, Ishii T, Iwata S, et al. G1/S cell cycle arrest provoked in human T cells by antibody to CD26. *Immunology* 2002 ; 107 : 325.
  - 14) Hatano R, Ohnuma K, Yamamoto J, et al. Prevention of acute graft-versus-host disease by humanized anti-CD26 monoclonal antibody. *Br J Haematol* 2013 ; 162 : 263.
  - 15) Ohnuma K, Hatano R, Aune TM, et al. Regulation of pulmonary graft-versus-host disease by IL-26<sup>+</sup> CD26<sup>+</sup> CD4 T lymphocytes. *J Immunol* 2015 ; 194 : 3697.
  - 16) Havre PA, Abe M, Urasaki Y, et al. The role of CD26/dipeptidyl peptidase IV in cancer. *Front Biosci* 2008 ; 13 : 1634.
  - 17) Inamoto T, Yamochi T, Ohnuma K, et al. Anti-CD26 monoclonal antibody-mediated G1-S arrest of human renal clear cell carcinoma Caki-2 is associated with retinoblastoma substrate dephosphorylation, cyclin-dependent kinase 2 reduction, p27<sup>kip1</sup> enhancement, and disruption of binding to the extracellular matrix. *Clin Cancer Res* 2006 ; 12 : 3470.
  - 18) Inamoto T, Yamada T, Ohnuma K, et al. Humanized anti-CD26 monoclonal antibody as a treatment for malignant mesothelioma tumors. *Clin Cancer Res* 2007 ; 13 : 4191.
  - 19) Ho L, Aytac U, Stephens LC, et al. In vitro and in vivo antitumor effect of the anti-CD26 monoclonal antibody 1F7 on human CD30<sup>+</sup> anaplastic large cell T-cell lymphoma Karpas 299. *Clin Cancer Res* 2001 ; 7 : 2031.
  - 20) Yamada K, Hayashi M, Du W, et al. Localization of CD26/DPPIV in nucleus and its nuclear translocation enhanced by anti-CD26 monoclonal antibody with anti-tumor effect. *Cancer Cell Int* 2009 ; 9 : 17.
  - 21) Angevin E, Isambert N, Trillet-Lenoir VT, et al. First-in-human phase I administration of YS110, a monoclonal antibody directed against the CD26 immunostimulatory molecule in advanced cancer patients[abstract]. *J Clin Oncol* 2015 ; 33 Suppl. Abstract No. 2519.
  - 22) Ohnuma K, Morimoto C. DPP4 (dipeptidyl-peptidase 4). *Atlas Genet Cytogenet Oncol Haematol* 2013 ; 17 : 301.
  - 23) Barreira da Silva R, Laird ME, Yatim N, et al. Dipeptidylpeptidase 4 inhibition enhances lymphocyte trafficking, improving both naturally occurring tumor immunity and immunotherapy. *Nat Immunol* 2015 ; 16 : 850.
  - 24) Ohnuma K, Hatano R, Morimoto C. DPP4 in anti-tumor immunity : going beyond the enzyme. *Nat Immunol* 2015 ; 16 : 791.
  - 25) Joyce JA, Fearon DT. T cell exclusion, immune privilege, and the tumor microenvironment. *Science* 2015 ; 348 : 74.
  - 26) Sharma P, Allison JP. The future of immune checkpoint therapy. *Science* 2015 ; 348 : 56.
  - 27) Hatano R, Ohnuma K, Otsuka H, et al. CD26-mediated induction of EGR2 and IL-10 as potential regulatory mechanism for CD26 costimulatory pathway. *J Immunol* 2015 ; 194 : 960.
  - 28) Hua J, Davis SP, Hill JA, Yamagata T. Diverse gene expression in human regulatory T cell subsets uncovers connection between regulatory T cell genes and suppressive function. *J Immunol* 2015 ; 195 : 3642.
  - 29) Raphael J, Le Teuff G, Hollebecque A, et al. Efficacy of phase 1 trials in malignant pleural mesothelioma : description of a series of patients at a single institution. *Lung Cancer* 2014 ; 85 : 251.

\*

\*

\*



## 胸膜中皮腫の病理と診断 (治療)

岸本 卓巳 藤本 伸一 西 英行\*

[Jpn J Cancer Chemother 43(5):513-517, May, 2016]

Clinical Pathological Diagnosis, and Treatment for Pleural Mesothelioma: Takumi Kishimoto, Nobukazu Fujimoto and Hideyuki Nishi (Research Center for Asbestos-Related Diseases, Okayama Rosai Hospital)

## Summary

For the differential diagnosis between fibrous pleuritis and other malignancies such as lung cancer, multiple immunostaining is essential to diagnose pleural mesothelioma. For cytological diagnosis of pleural effusions, differentiation between mesothelioma cells and reactive mesothelial cells is very difficult. Therefore, histological diagnoses of tumor tissues obtained via biopsy are essential. To diagnose epithelioid mesothelioma, more than 2 positive and negative markers must be consistent with those known for mesothelioma. To diagnose sarcomatoid mesothelioma, keratin is usually positive, differentiating the diagnosis from that for real sarcoma. For surgical treatment for pleural mesothelioma, extrapleural pneumonectomy (EPP) and pleurectomy/decortication (P/D) are usually performed. The proportion of P/D increases because of the low death rates with surgery and similar survivals. However, a trimodal approach, such as EPP with chemotherapy and radiotherapy, is best for longer survival and expected to be curative. For chemotherapy, only cisplatin (CDDP) combined with pemetrexed (PEM) is effective, and no other agents have been identified for this disease. Nowadays, clinical immunotherapy trials start with phase II study. **Key words:** Pleural mesothelioma, Asbestos exposure, Immunostaining, **Corresponding author:** Takumi Kishimoto, Research Center for Asbestos-Related Diseases, Okayama Rosai Hospital, 1-10-25 Chikko midori-machi, Minami-ku, Okayama 702-8055, Japan

**要旨** 中皮腫の病理診断では、細胞診における中皮腫細胞と反応性中皮細胞の鑑別が難しいため腫瘍組織生検による鑑別が必須である。確定診断のためには複数の免疫染色を行い、線維性胸膜炎や肺癌との鑑別を行う。上皮型中皮腫の診断には陽性、陰性抗体が各2種類以上中皮腫に一致する必要がある。また、肉腫型中皮腫では真の肉腫との鑑別でケラチン陽性が重要である。中皮腫の治療法では外科手術として extrapleural pneumonectomy (EPP) と pleurectomy/decortication (P/D) が行われるが、周術期の死亡率が高い EPP に対して P/D は比較的低く、生存期間がほぼ同様であるため P/D の施行頻度が増加している。しかし、治癒をめざすためには、EPP に化学療法と放射線療法を加えた trimodality が望まれる。化学療法としては cisplatin (CDDP) + pemetrexed (PEM) のみが有効であり、その他の治療法として免疫療法が試みられるようになってきた。

## はじめに

胸膜中皮腫は壁側胸膜の中皮細胞が腫瘍性増殖する疾病で、ほとんどが悪性腫瘍である。欧米では本疾患の約80%以上がアスベスト曝露によるが、日本においても73.7%が職業性アスベスト曝露により、その他環境曝露などを加えると約80%であることが明らかとなった<sup>1)</sup>。また、日本における中皮腫による死亡者数は1995年に500人であったものが増加傾向を示し、2013年には

1,410人となった。そのうち増加しているのは男性の胸膜中皮腫であり、女性の胸膜中皮腫と腹膜中皮腫には増加傾向はみられない。一方、その診断は難しく、厚生労働省人口動態統計上中皮腫であると診断された症例において、男性の胸膜中皮腫のうち26%が中皮腫以外の疾患であったことも報告<sup>2)</sup>されている。

## I. 画像診断

進行期胸膜中皮腫の特徴像は胸膜がびまん性に不整な

\* 岡山労災病院・アスベスト研究センター



肥厚を示す環状胸膜肥厚像 (pleural rind) を呈するが、早期病変では胸膜肥厚をまったく呈さず胸水貯留のみのこともある。また、縦隔側胸膜肥厚のみや、胸膜炎の際に認められる不整のない軽度胸膜肥厚像を呈することも少なくない。肺癌と鑑別を要する胸膜上の単発腫瘤形成像や転移性腫瘍を示唆する多発腫瘤形成型もあることから、胸膜上に腫瘍性病変が存在する場合には鑑別診断として胸膜中皮腫を念頭に置く必要がある。

## II. 血清あるいは胸水補助診断

胸膜中皮腫の血液マーカーとして、米国の FDA や日本の厚生労働省に認可されているのは soluble mesothelin related peptides (SMRP) のみである。本マーカーは治療経過のマーカーとしては有用であるが、Helsinki Criteria 2014<sup>3)</sup>では中皮腫診断上推奨される血液マーカーはないとしており、血清 SMRP も必ずしも有用な診断マーカーであるとはいえない。

一方、胸水マーカーとして胸水ヒアルロン酸値が 100,000 ng/mL 以上であれば中皮腫の可能性が高いとする報告があり、有用性が高い。しかし、中皮腫のうち約半数以上は 100,000 ng/mL 未満である<sup>4)</sup>。これを補完するマーカーとして前述の SMRP が 8 ng/mL 以上であれば、ヒアルロン酸に近い有用性がある<sup>5)</sup>。

また、胸膜中皮腫の除外マーカーとして結核性胸膜炎の際に高値を示す adenosine deaminase (ADA) があるが、胸膜中皮腫の際にも高値を示すので注意を要する。肺癌や癌性胸膜炎において増加するマーカーとして CEA, CYFRA21-1 があげられる。CYFRA21-1 はサイトケラチン中間径フィラメントの可溶性フラグメントであり、胸膜中皮腫でも増加するが、肺癌でも増加するので特異的ではない。

## III. 病理診断

### 1. 胸水細胞診

胸膜中皮腫では、その 80% 以上で胸水を伴うので胸水細胞診が有用であることもある。しかし、胸水に中皮腫細胞が認められるのは初回胸水貯留から間もない時期であり、腫瘍細胞が認められないことも少なくない。また、中皮細胞が出現していても中皮腫細胞ではなく、胸膜炎の際に増加する反応性中皮細胞であることも多く、この両者の鑑別が極めて難しい。

中皮腫細胞の特徴は、通常 long slender microvilli を有することから細胞辺縁の輪部がぼやけ、核が大型で核小体が目立ち、2 核以上の多核細胞、相互封入像や hump 様細胞質突起が認められることである<sup>6)</sup>。反応性中皮細胞と比較すると、中皮腫細胞では EMA が膜表間に染色

表 1 中皮腫組織型別の抗体選択

	上皮型	肉腫型
陽性マーカー	Calretinin	CK (AE1/AE3)
	WT1	CAM5.2
	D2-40	D2-40
	Thrombomodulin	WT1
	Mesothelin	EMA
陰性マーカー	CEA	S-100
	TTF-1	Desmin
	BerEP-4	CD34
	MOC31	
	ER, PgR, etc	

されるとともに GLUT-1, insulin-like growth factor II mRNA-binding protein 3 (IMP3), CD146 が陽性を示し、desmin が陰性を示すことが鑑別に有用である<sup>7)</sup>。

しかし WHO 第 4 版には、両者の鑑別は難しく不可能であると記載されている<sup>8)</sup>。一方、原発性あるいは転移性肺癌や胸膜あるいは胸壁原発の肉腫などとの鑑別には、以下に述べる病理組織におけるマーカーを使用する<sup>8)</sup>。

### 2. 病理組織診断

病理診断のためには胸腔鏡下生検が望ましく、脂肪織も含めた十分な大きさの組織を複数箇所から採取することが推奨される。

WHO 第 4 版は、中皮腫をびまん性悪性中皮腫、限局性中皮腫、高分化型乳頭状中皮腫、アデノマトイド腫瘍に分類した。アデノマトイド腫瘍は良性腫瘍であるが、その他は悪性で、大半はびまん性である。びまん性悪性中皮腫は上皮型、肉腫型、二相型に分類され、豊富な膠原線維を伴う線維形成型中皮腫は肉腫型の亜型とされる。組織型別では上皮型が約 60%、二相型が約 25%、肉腫型が約 15% である。

上皮型で最も多いパターンは solid type, tubulo-papillary type, trabecular type であり、特殊型として pleomorphic type, clear cell type, deciduoid type, lymphohistiocytoid type などのパターンや、細胞形成態を呈する型も知られている<sup>8)</sup>。中皮腫の組織診断では中皮由来であることの確認が必要で、上皮型中皮腫の確定診断には主に腺癌との鑑別のため、表 1 にあげられる陽性マーカーが二つ以上、かつ陰性マーカーが二つ以上であることの確認が必要である (表 2)。扁平上皮癌ではカルレチニン (calretinin) の陽性率が比較的高いので、その鑑別には p40, p63 が陰性であることを確認する<sup>9)</sup>。さらに、claudin 4 は中皮腫と癌腫の鑑別に有用である。一方、肉腫型の診断では真の肉腫を否定するため、上皮由来であることを示すサイトケラチン (CK) (AE1/AE3, CAM 5.2 など) が陽性であることを確認する (表 2)。CK 陰性



表2 胸膜中皮腫の鑑別診断

鑑別要件	中皮腫	その他の疾患
中皮腫の陽性抗体, 陰性抗体	上皮型中皮腫	肺癌
CK (AE1/AE3, CAM5.2)	2種類以上中皮腫に一致	中皮腫に一致しない
	肉腫型中皮腫	肉腫
画像所見	陽性	陰性
	肉腫型中皮腫	肉腫様癌
	胸膜病変	肺内病変
FISH 法 (homozygous deletion)	線維形成型中皮腫	線維性胸膜炎
	陽性	陰性
融合遺伝子	二相型中皮腫	滑膜肉腫
	陰性	陽性

の肉腫型中皮腫の存在も報告されているが、肉腫との鑑別には画像の他に総合的な診断を必要とする。また、肉腫型中皮腫と肉腫様癌の鑑別には現在のところ鑑別マーカーがないことから、画像所見における腫瘍の首座が肺か胸膜かによって鑑別を行う。

肉腫型中皮腫、特に線維形成型中皮腫の診断では線維性胸膜炎（良性石綿胸水）との鑑別が重要である。線維形成型では組織学的に細胞配列の乱れや肥厚の程度に不均一性があり、FISH 法による p16 遺伝子の homozygous deletion が高頻度に認められる（表2）。一方、線維性胸膜炎では homozygous deletion はなく、胸膜表面から垂直に伸びる血管増生と胸膜表層から深部に向かうにつれて細胞密度や異型度が低下する（zonation）ことが特徴である。p16 遺伝子の homozygous deletion は良性病変との鑑別に有用で、その特異度は100%であるが他の悪性腫瘍との鑑別にはならない<sup>10)</sup>。

二相型中皮腫では、二相性を示す頻度の高い滑膜肉腫との鑑別が必要である。滑膜肉腫では転座 t (X;18) (p11;q11) に伴う融合遺伝子が必ず認められるので、最終診断はこの融合遺伝子の存在を確認する（表2）。

#### IV. 治療

米国の National Comprehensive Cancer Network (NCCN) のガイドライン<sup>11)</sup>では、その推奨グレードはカテゴリー 2A「比較的低レベルのエビデンスに基づく」推奨である。

##### 1. 外科治療法

外科治療の目的は肉眼的完全切除であるが、術後の局所再発が極めて高率である。そのため、化学療法あるいは放射線療法と組み合わせた集学治療が必要である。肉腫型では術後再発の頻度が極めて高く、予後不良であることから手術は避けるべきであるとされている。

##### 1) 胸膜肺全摘出術 (extrapleural pneumonectomy: EPP)

胸膜、肺、横隔膜、心膜を胸膜外側から一括して切除

する方法である。手術関連死亡が比較的多く、術後の QOL 低下などのリスクのある手術ではあるが、治療がうまくいけば生存期間の延長が期待される。IMIG 分類の stage I, II までの早期病変が適応となる。特に左胸膜原発はよい適応である。EPP を行う場合には、まず cisplatin (CDDP) + pemetrexed (PEM) による化学療法を2コース施行後に EPP を行い、術後に胸腔内に 60 Gy の放射線療法を行う (trimodality) ことが標準とされ、遂行可能例では予後良好で5年生存も認められている<sup>12)</sup>。

##### 2) 胸膜切除・肺剥皮術 (pleurectomy/decortication: P/D)

肺を温存する縮小手術であり、手術関連死亡率が低い。しかし術式は様々で、腫瘍を切除する目的の debulking P/D、壁側および臓側胸膜を広範囲に切除するいわゆる P/D、心膜・横隔膜の合併切除を行う extended P/D があるため一括した評価は難しいが、P/D と extended P/D には統計的に有意差があるという報告がある<sup>13)</sup>。肺が残存するため術後の管理が比較的容易であり、右胸膜原発、合併症のある症例などリスクをもつ症例に施行されている。

EPP の場合には高い合併症の発生があるため、化学療法単独との比較試験 (mesothelioma and radical surgery: MARS 試験) では EPP の MST 14.4 か月 vs 化学療法単独の MST 19.5 か月と、その有益性が証明されなかった<sup>14)</sup>。

また、これら手術に対するメタアナリシス<sup>15)</sup>から EPP の周術期死亡率は 2.9% で OS は 2~22 か月 (P/D: 6.8 %, 12~29 か月) であったことから、2014 年の NCCN のガイドライン<sup>11)</sup>あるいは The International Association for the Study of Lung Cancer (IASLC) の集計結果<sup>16)</sup>では、stage II 以上には治療関連死亡の少ない P/D を選択することを推奨している。しかし、P/D を行った場合には患者側に肺が残存するため、放射線療法により根治療法が行えないという欠点がある。現在、EPP と P/

表 3 胸膜中皮腫手術別治療成績 (prospective study)

EPP					
著者	年	症例数	併用療法	死亡率 (%)	OS (M)
Pagan	2006	44	術後 CT+RT	4.5	20
Rea	2007	17	導入 CT+RT	0	25.5
Weder	2007	45	CT+RT	2.2	23
de Perrot	2009	45	CT+RT	6.7	14
Krug	2009	54	CT+RT	3.7	21.9
Van Schil	2010	42	導入 CT+RT	6.5	18.4
P/D					
著者	年	症例数	併用療法	死亡率 (%)	OS (M)
Richards	2006	44	CT	11	13
Bölkbus	2011	35	CT, RT	0	25
Nakas	2012	67	CT	3	13.4
Laug-Lazdunski	2012	54	CT	0	23
Fiedberg	2012	38	CT	2.6	31.7

D の比較試験は施行されていないので、どちらの手術療法を選択するかについては病変が左右のどちらか、患者の stage, PS, 年齢や基礎疾患の有無などに応じて慎重に決定されるべきである<sup>17)</sup>(表 3)。

## 2. 化学療法

標準初回療法は CDDP と PEM 併用療法である。CD DP 単独投与を対象とした第Ⅲ相比較試験<sup>18)</sup>で奏効率 41.3%, PFS 5.7 か月, MST 12.1 か月であったことから米国の FDA で認可され、日本でも 2007 年 1 月に保険適応となった。carboplatin+PEM も無作為化比較試験はないが同様と評価されているため、CDDP が使用できない高齢者や腎機能障害のある症例に対して使用されている。second-line として vinorelbine や gemcitabine が用いられるが、有意な効果は認められておらず、現在その他にも治療効果が認められている薬剤はない。

最近の臨床第Ⅲ相試験において CDDP+PEM に bevacizumab を追加することにより、PFS 2 か月、OS は 2.75 か月の有意な延長が認められ、毒性は増加するものの管理可能であることが報告された<sup>19)</sup>。同じく最近の第Ⅱ相試験で、amatuximab (抗メソテリン・キメラ型抗体) の CDDP+PEM への上乗せ効果として PFS 6.1 か月、OS は 14.8 か月であったと報告されている<sup>20)</sup>。また、抗 cytotoxic T-lymphocyte antigen 4 (CTLA4) 抗体である tremelimumab を用いた第Ⅱ相試験が施行され、PFS 6.2 か月、OS が 10.7 か月と報告されている<sup>21)</sup>。これらの成績は有望であるが、治療効果の評価は今後の臨床試験にゆだねられている。また、抗 PD-1 抗体も効果があることが報告されており<sup>22)</sup>、今後の臨床試験が期待される。その他、抗 CD26 ヒト化抗体や遺伝子治療が開始されているが、まだ第Ⅰ相試験の段階である。

## 文 献

- 1) Gemba K, Fujimoto N, Kato K, *et al*: National survey of malignant mesothelioma and asbestos exposure in Japan. *Cancer Sci* 103(3): 483-490, 2012.
- 2) Takeshima Y, Inai K, Amatya VJ, *et al*: Accuracy of pathological diagnosis of mesothelioma cases in Japan: clinicopathological analysis of 382 cases. *Lung Cancer* 66(2): 191-197, 2009.
- 3) Wolff H, Vehmas T, Oksa P, *et al*: Asbestos, asbestosis, and cancer, the Helsinki criteria for diagnosis and attribution 2014: recommendations. *Scand J Work Environ Health* 41(1): 5-15, 2015.
- 4) 藤本伸一, 青江啓介, 大泉聡史・他: 胸膜中皮腫を中心とした胸水ヒアルロン酸に関する症例調査. 肺癌 54(6): 767-771, 2014.
- 5) Fujimoto N, Gemba K, Asano M, *et al*: Soluble mesothelin-related protein in pleural effusion from patients with malignant pleural mesothelioma. *Exp Ther Med* 1(2): 313-317, 2010.
- 6) 亀井敏昭: 石綿関連疾患での中皮腫診断への体腔液細胞診の意義と検証. 平成 24 年度石綿関連疾患に係る医学的所見の解析調査業務 (体腔液細胞診による中皮腫診断の在り方に関する調査編) 報告書, 2013, pp1-21.
- 7) 廣島健三: 悪性胸膜中皮腫～病理診断の困難さ～. 日職災医誌 63(4): 215-218, 2015.
- 8) Galateau-Salle F, Churg A, Roggli V, *et al*: Epithelioid mesothelioma. Pathology and Genetics, Tumours of the lung, pleura, thymus and heart (eds by Travis WD, Brambilla E, Müller-Hermelink K, *et al*), International Agency for Research on Cancer, Lyon, 2015, pp156-164.
- 9) Husain AN, Colby T, Ordonez N, *et al*: Guidelines for pathologic diagnosis of malignant mesothelioma: 2012 update of the consensus statement from the International Mesothelioma Interest Group. *Arch Pathol Lab Med* 137(5): 647-667, 2013.
- 10) 鍋島一樹, 濱崎 慎, 松本慎二・他: 中皮腫と p16 遺伝子の欠失. 呼吸 33(8): 754-761, 2014.
- 11) NCCN Clinical Practice Guidelines in Oncology (NCCN Guidelines), Malignant Pleural Mesothelioma, version 1, 2014.
- 12) Sugarbaker DJ, Flores RM, Jaklitsch MT, *et al*: Resection margins, extrapleural nodal status, and cell type determine postoperative long-term survival in trimodality therapy of malignant pleural mesothelioma: results in 183 patients. *J Thorac Cardiovasc Surg* 117(1): 54-63,

- 1999.
- 13) Bedirhan MA, Cansever L, Demir A, *et al*: Which type of surgery should become the preferred procedure for malignant pleural mesothelioma: extrapleural pneumonectomy or extended pleurectomy? *J Thorac Dis* 5(4): 446-454, 2013.
  - 14) Treasure T, Lang-Lazdunski L, Waller D, *et al*: Extra-pleural pneumonectomy versus no extra-pleural pneumonectomy for patients with malignant pleural mesothelioma: clinical outcomes of the Mesothelioma and Radical Surgery (MARS) randomised feasibility study. *Lancet Oncol* 12(8): 763-772, 2011.
  - 15) Cao C, Tian D, Park J, *et al*: A systematic review and meta-analysis of surgical treatments for malignant pleural mesothelioma. *Lung Cancer* 83(2): 240-245, 2014.
  - 16) Rusch VW, Giroux D, Kennedy C, *et al*: Initial analysis of the international association for the study of lung cancer mesothelioma database. *J Thorac Oncol* 7(11): 1631-1639, 2012.
  - 17) Opitz I: Management of malignant pleural mesothelioma—The European experience. *J Thorac Dis* 6(Suppl 2): S238-S252, 2014.
  - 18) Vogelzang NJ, Rusthoven JJ, Symanowski J, *et al*: Phase III study of pemetrexed in combination with cisplatin versus cisplatin alone in patients with malignant pleural mesothelioma. *J Clin Oncol* 21(14): 2636-2644, 2003.
  - 19) Zalcman G, Mazières J, Margery J, *et al*: Bevacizumab 15 mg/kg plus cisplatin-pemetrexed (CP) triplet versus CP doublet in malignant pleural mesothelioma (MPM): results of the IFCT-GFPC-0701 MAPS randomized phase 3 trial. *J Clin Oncol* 33(15s): abstr 7500, 2015.
  - 20) Hassan R, Kindler HL, Jahan T, *et al*: Phase II clinical trial of amatuximab, a chimeric antimesothelin antibody with pemetrexed and cisplatin in advanced unresectable pleural mesothelioma. *Clin Cancer Res* 20(23): 5927-5936, 2014.
  - 21) 中野孝司, 栗林康造: 胸膜中皮腫の治療. *臨と研* 92(7): 899-906, 2015.
  - 22) Alley EW, Molife LR, Santoro A, *et al*: Pembrolizumab safe, with signs of clinical benefit, for patients with malignant pleural mesothelioma. AACR annual meeting in Philadelphia, 2015.



## DPP4 in anti-tumor immunity: going beyond the enzyme

Kei Ohnuma, Ryo Hatano & Chikao Morimoto

**Effective anti-tumor immune therapy in solid tumors relies on the presence of effector T cells. Inhibition of the dipeptidylpeptidase DPP4 (CD26) enhances chemokine CXCL10-mediated infiltration of lymphocytes into the tumor parenchyma, which results in diminished tumor growth.**

The dipeptidylpeptidase DPP4 is a homodimeric type II transmembrane glycoprotein expressed in many cell types and is identical with the leukocyte surface antigen CD26 (ref. 1). It is also present in serum and other body fluids in a truncated form. It preferentially cleaves amino-terminal dipeptides from polypeptides with proline or alanine in the penultimate position and regulates the activities of various cytokines and chemokines. However, direct *in vivo* evidence of a role for DPP4 in tumor biology and its interaction with the tumor microenvironment (TME) has not yet been reported. In this issue of *Nature Immunology*, work by Barreira da Silva *et al.* highlights the interaction between DPP4 and its substrate, the chemokine CXCL10, to demonstrate the function of DPP4-mediated post-translational modification of chemokines in regulating tumor immunity<sup>2</sup>.

The TME consists of various cell types, along with the neoplastic cells themselves. Among these are effector lymphocytes that are able to infiltrate the tumor sites and are specifically required for the anti-cancer immune response<sup>3</sup>. Barreira da Silva *et al.* utilize a tumor-transplant model of the mouse melanoma cell line B16F10 to show that tumor growth is significantly delayed in *Dpp4*<sup>-/-</sup> mice relative to that in their heterozygous littermates. Moreover, their studies of wild type (*Dpp4*<sup>+/+</sup>) mice fed chow formulated to contain the DPP4-specific inhibitor sitagliptin demonstrate that inhibition of DPP4 results in diminished tumor growth (Fig. 1). In addition,

inhibition of DPP4 significantly reduces the number of lung metastases following intravenous injection of B16F10 cells. Although DPP4 is not expressed by B16F10 cells cultured *in vitro*, the authors detect high activity and expression of DPP4 in tumors resected from wild-type mice. However, they detect only a low level of tumor-associated DPP4 activity when they implant B16F10 cells into *Dpp4*<sup>-/-</sup> mice. These findings suggest that DPP4 has a role in regulating tumor growth and that the contribution of DPP4 activity *in vivo* is from both tumor-induced effects on the stroma as well as the tumor cells themselves.

CXCL10 is a chemoattractant for cells of the immune system, such as monocytes, T cells and natural killer cells, and is secreted from a variety of cells, including monocytes, neutrophils, eosinophils, epithelial cells, endothelial cells, fibroblasts and keratinocytes, in response to interferon- $\gamma$ <sup>4</sup>. Cellular analysis of tumor-infiltrating leukocytes shows that large amounts of CXCL10 correlate with a greater number of CD4<sup>+</sup> and CD8<sup>+</sup> T cells in wild-type mice given implantation of B16F10 cells and fed chow containing sitagliptin. Meanwhile, the authors observe no significant difference between mice fed chow containing sitagliptin and those fed control chow (lacking sitagliptin) in the number of tumor-infiltrating myeloid cells, natural killer cells, B cells or CD25<sup>hi</sup> regulatory T cells. The authors do not find the beneficial effect of the inhibition of DPP4 on the reduction in tumor growth in B cell- and T cell-deficient *Rag2*<sup>-/-</sup> mice fed sitagliptin-containing chow or control chow, which suggests that inhibition of DPP4 activates anti-tumor immunity via chemokine-mediated trafficking of T cells. Barreira da Silva *et al.* confirm this hypothesis by showing that mice deficient in the CXCL10 receptor CXCR3, mice deficient in CXCL10 and wild-type mice treated with a blocking antibody to CXCL10

(anti-CXCL10) fail to exhibit diminished melanoma growth following inhibition of DPP4. The authors extend their initial observation to other tumor models by implanting CT26 mouse colon carcinoma cells into BALB/c mice fed sitagliptin-containing chow. Inhibition of DPP4 results in a marked delay of CT26 tumor growth, which correlates with increased infiltration of T cells and natural killer cells. Meanwhile, treatment with blocking anti-CXCR3 abrogates the reduction in CT26 tumor growth mediated by inhibition of DPP4. These findings indicate that DPP4 in the TME acts to negatively regulate CXCR3-mediated anti-tumor immunity and effectively limit the infiltration of T cells into the tumor parenchyma.

Focusing on the anti-tumor response via TME-driven regulation of T cells provides scope for novel anti-cancer therapies; among these, adjuvant therapy, adoptive T cell-transfer therapy, and checkpoint-blockade therapy (with antibodies to the immunomodulatory receptors CTLA-4 (CD152) and PD-1) have led to important clinical advances. Barreira da Silva *et al.* demonstrate the efficacy of an anti-cancer treatment that combines inhibition of DPP4 with the adjuvant oligodeoxynucleotide CpG, which induces the production of bioactive CXCL10 in plasma. Notably, CpG-mediated tumor immunity is dependent on interferon signaling and CXCR3 expression. Inhibition of DPP4 stabilizes the biologically active form of CXCL10, which results in enhanced migration of T cells into the TME as a strategy for enhancing adjuvant-based tumor immunity. The use of ovalbumin-expressing B16F10 melanoma cells that are recognized by CD8<sup>+</sup> OT-I T cells (which transgenically express an ovalbumin-specific T cell antigen receptor) demonstrates a synergistic effect on the reduction in tumor size when adoptive transfer of OT-I cells is combined with sitagliptin treatment. The most

Kei Ohnuma, Ryo Hatano and Chikao Morimoto are in the Department of Therapy Development and Innovation for Immune Disorders and Cancers, Graduate School of Medicine, Juntendo University, Tokyo, Japan.  
e-mail: morimoto@ims.u-tokyo.ac.jp

striking effects are produced by a combination of inhibition of DPP4 and checkpoint blockade: a triple therapy involving sitagliptin, anti-CTLA-4 and anti-PD-1 results in rejection of CT26 tumors by 100% of mice, whereas double therapy of anti-CTLA-4 plus anti-PD-1 cures only 42% of the mice. Barreira da Silva *et al.* therefore provide direct evidence of DPP4 as an *in vivo* regulator of CXCL10-mediated T cell trafficking, with relevance for tumor immunity and immunotherapy.

CXCL10 seems to have a dual role in tumor growth, with its proliferative or anti-proliferative activity being dependent on the cell type as a result of differences in the subtype of its receptor, CXCR3 (ref. 4). Expression of CXCR3 is rapidly induced on naive T cells following activation, and high CXCR3 expression is retained 'preferentially' on CD4<sup>+</sup> cells of the T<sub>H</sub>1 subset of helper T cells and on CD8<sup>+</sup> cytotoxic T lymphocytes (CTLs), which results in enhancement of T cell migration to facilitate immunological responses to tumors<sup>5</sup>. Although strong T<sub>H</sub>1 and CTL responses in the TME are beneficial for tumor suppression, these responses are counterbalanced to prevent unwanted tissue damage and immunopathology by disruption of the proinflammatory loop; indeed, CXCR3<sup>+</sup> regulatory T cells have been identified that ameliorate just such harmful inflammation<sup>6</sup>. Such cells are generated by interferon- $\gamma$  signaling, which upregulates their expression of the T<sub>H</sub>1-related transcription factor T-bet and in turn promotes their expression of CXCR3 in the inflammatory sites. Moreover, CXCR3 is also a marker of CD8<sup>+</sup> cells that produce interleukin 10 and have suppressive activity in both mice and human<sup>7</sup>. The exact factors that determine whether CXCR3<sup>+</sup> effector T cells and CXCR3<sup>+</sup> regulatory lymphocytes oppose each other or act cooperatively with each other during the tumor growth process *in vivo* remain to be elucidated.

Direct biological effects of DPP4 on tumor cells are also relevant to the malignant activity of tumors. In several human malignancies, including colorectal cancer, chronic myeloid leukemia and malignant mesothelioma, DPP4 expression is reported to be a marker of cancer stem cells<sup>8</sup>. Interestingly, the enzyme activity of DPP4 is important for regulating the growth of leukemic stem cells in the CD34<sup>+</sup>CD38<sup>-</sup>Lin<sup>-</sup> fraction in chronic myeloid leukemia and is a potential therapeutic target<sup>9</sup>. Although a direct correlation between disease aggressiveness and DPP4 expression has been reported in human T cell malignancies, an inverse correlation between DPP4 expression and the degree of malignant activity has been shown in melanocytes<sup>10</sup>. In addition to differences among cell types, the expression and function of DPP4 in the

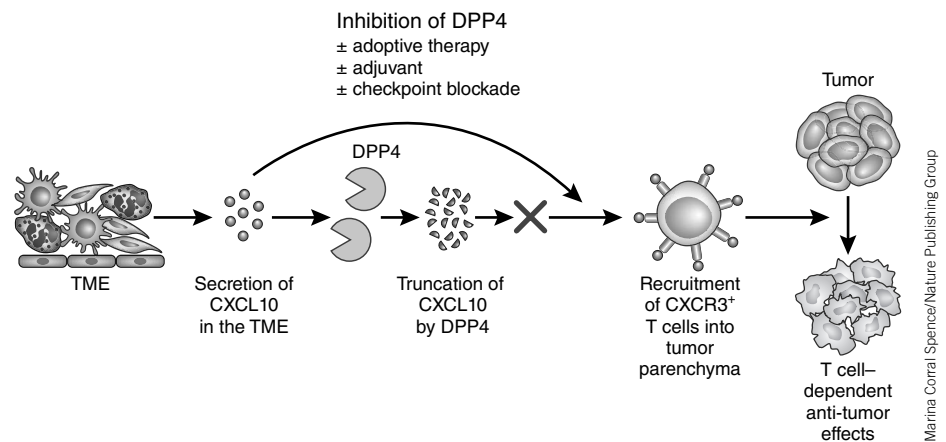


**Figure 1** Inhibition of DPP4 suppresses truncation of its ligand CXCL10, which leads to the recruitment of CXCR3<sup>+</sup> T cells into tumor parenchyma. Barreira da Silva *et al.* use *in vivo* tumor-transplant models to show that inhibition of DPP4 diminishes tumor growth through the preservation of bioactive CXCL10 in the TME. In the normal physiological state, CXCL10 is rapidly degraded by DPP4, which results in less recruitment and migration of CXCR3<sup>+</sup> T cells into the tumor parenchyma. In contrast, inhibition of DPP4 enhances tumor rejection by preserving the full-length biologically active form of CXCL10, which leads to increased trafficking of CXCR3<sup>+</sup> T cells into the tumor parenchyma. This anti-tumor response is potentiated in combination with other anti-tumor immunotherapeutic approaches, including CpG adjuvant therapy, adoptive T cell-transfer therapy and checkpoint-blockade therapy (anti-CTLA-4 and anti-PD-1). ±, with or without.

human immune system appears to differ from that in mice. Although the predicted amino acid sequence of human DPP4 shares approximately 85% homology with mouse DPP4, mouse DPP4 is neither a T cell-activation marker nor an adenosine deaminase-binding protein<sup>1</sup>. The differences between rodent DPP4 and human DPP4 therefore highlight the potentially limited utility of murine models for elucidating the function of human DPP4. Future work specifically focusing on the direct biological effects of DPP4 on human tumor cells will undoubtedly contribute to a more in-depth understanding of its role in various physiological states and as a possible anti-cancer therapeutic target.

Work on DPP4 in T cell immunity has reported that costimulation via the invariant signaling protein CD3 and CD26 (DPP4) induces the development of human type 1 regulatory T cells from CD4<sup>+</sup> T cells with substantial production of interleukin 10 and high expression of the coinhibitory receptor LAG-3 (ref. 11). Preclinical models have shown that antibody-mediated blockade of LAG-3 as a potential anti-cancer therapy leads to enhanced activation of antigen-specific T cells at tumor sites and disruption of tumor growth<sup>12</sup>. Moreover, dual-blockade therapy with anti-LAG-3 and anti-PD-1 cured most mice of established tumors that were largely resistant to single antibody treatment<sup>12</sup>. Thus, it is conceivable that DPP4 itself might function as an inhibitory molecule of an immunological-checkpoint system in certain disease conditions, similar to LAG-3 or PD-1.

In developing new assays for the intact form of CXCL10, Barreira da Silva *et al.* have also provided the first experimental evidence that amino-terminal truncation of post-translationally modified CXCL10 has an *in vivo* biological importance and that the regulation of this process through DPP4 affects lymphocyte migration and tumor immunity. Although DPP4 and CXCL10 have a plethora of biological functions in human tumor cells and the immune system, further detailed understanding of the role of these molecules in various clinical settings could lead potentially to novel therapeutic approaches. Indeed, DPP4-specific inhibitors already used as anti-diabetic drugs worldwide and could in theory be readily repurposed to enhance existing anti-tumor immunotherapies.

#### COMPETING FINANCIAL INTERESTS

The authors declare no competing financial interests.

- Ohnuma, K., Dang, N.H. & Morimoto, C. *Trends Immunol.* **29**, 295–301 (2008).
- Barreira da Silva, R. *et al.* *Nat. Immunol.* **16**, 850–858 (2015).
- van der Bruggen, P. *et al.* *Science* **254**, 1643–1647 (1991).
- Liu, M., Guo, S. & Stiles, J.K. *Oncol. Lett.* **2**, 583–589 (2011).
- Groom, J.R. & Luster, A.D. *Exp. Cell Res.* **317**, 620–631 (2011).
- Koch, M.A. *et al.* *Nat. Immunol.* **10**, 595–602 (2009).
- Shi, Z. *et al.* *Eur. J. Immunol.* **39**, 2106–2119 (2009).
- Davies, S., Beckenkamp, A. & Buffon, A. *Biomed. Pharmacother.* **71**, 135–138 (2015).
- Herrmann, H. *et al.* *Blood* **123**, 3951–3962 (2014).
- Havre, P.A. *et al.* *Front. Biosci.* **13**, 1634–1645 (2008).
- Hatano, R. *et al.* *J. Immunol.* **194**, 960–972 (2015).
- Nguyen, L.T. & Ohashi, P.S. *Nat. Rev. Immunol.* **15**, 45–56 (2015).



# Regulation of Pulmonary Graft-versus-Host Disease by IL-26<sup>+</sup>CD26<sup>+</sup>CD4 T Lymphocytes

Kei Ohnuma,\* Ryo Hatano,\* Thomas M. Aune,<sup>†</sup> Haruna Otsuka,\* Satoshi Iwata,\* Nam H. Dang,<sup>‡</sup> Taketo Yamada,<sup>§</sup> and Chikao Morimoto\*

Obliterative bronchiolitis is a potentially life-threatening noninfectious pulmonary complication after allogeneic hematopoietic stem cell transplantation and the only pathognomonic manifestation of pulmonary chronic graft-versus-host disease (cGVHD). In the current study, we identified a novel effect of IL-26 on transplant-related obliterative bronchiolitis. Sublethally irradiated NOD/Shi-*scid*IL2r $\gamma^{null}$  mice transplanted with human umbilical cord blood (HuCB mice) gradually developed clinical signs of graft-versus-host disease (GVHD) such as loss of weight, ruffled fur, and alopecia. Histologically, lung of HuCB mice exhibited obliterative bronchiolitis with increased collagen deposition and predominant infiltration with human IL-26<sup>+</sup>CD26<sup>+</sup>CD4 T cells. Concomitantly, skin manifested fat loss and sclerosis of the reticular dermis in the presence of apoptosis of the basilar keratinocytes, whereas the liver exhibited portal fibrosis and cholestasis. Moreover, although IL-26 is absent from rodents, we showed that IL-26 increased collagen synthesis in fibroblasts and promoted lung fibrosis in a murine GVHD model using *IL-26* transgenic mice. In vitro analysis demonstrated a significant increase in IL-26 production by HuCB CD4 T cells following CD26 costimulation, whereas Ig Fc domain fused with the N-terminal of caveolin-1 (Cav-Ig), the ligand for CD26, effectively inhibited production of IL-26. Administration of Cav-Ig before or after onset of GVHD impeded the development of clinical and histologic features of GVHD without interrupting engraftment of donor-derived human cells, with preservation of the graft-versus-leukemia effect. These results therefore provide proof of principle that cGVHD of the lungs is caused in part by IL-26<sup>+</sup>CD26<sup>+</sup>CD4 T cells, and that treatment with Cav-Ig could be beneficial for cGVHD prevention and therapy. *The Journal of Immunology*, 2015, 194: 3697–3712.

**A**llogeneic hematopoietic stem cell transplantation (alloHSCT) is a potentially curative treatment for many diseases arising from hematopoietic cells (1). However, chronic graft-versus-host disease (cGVHD) remains a significant barrier to successful alloHSCT (2). In particular, the lung damage in cGVHD causes potentially life-threatening complications (3). According to the National Institutes of Health consensus criteria,

obliterative bronchiolitis (historically named bronchiolitis obliterans by pathologists) is the only pathognomonic manifestation of pulmonary cGVHD (4). It is recognized that obliterative bronchiolitis has been associated with an increased risk of death, and patients diagnosed with obliterative bronchiolitis after alloHSCT have a 5-y survival rate of only 10% (5).

Although many preclinical models mimicking human cGVHD including obliterative bronchiolitis have been established (6), control of obliterative bronchiolitis after alloHSCT has not yet been achieved thoroughly (7). The clinical application of murine data is limited because multiple, yet limited schema have arisen to identify alloimmune reactions in cross-species comparisons. For instance, one extensively used model of cGVHD clearly exhibited immune-complex glomerulonephritis, which is rarely seen in human cGVHD (8). Moreover, transfer of autoantibodies from mice with GVHD to normal mice failed to cause autoimmune pathology (9). These limitations are based on preparative regimens, composition of donor graft, and genetic backgrounds of donor and recipient animals (6). In addition, recent work has demonstrated multiple differences in immunological functions between humans and mice (10, 11). In contrast, because in vivo T cell depletion is the only prophylactic measure that effectively decreases the incidence of cGVHD (2, 12), donor T cells clearly play an important role in the immune pathology of cGVHD. Taken together, to develop novel therapeutic strategies for use in the clinical setting, the establishment of a humanized murine model of cGVHD is urgently needed. We previously analyzed a humanized murine acute GVHD (aGVHD) model involving mice transplanted with human adult PBL, and showed that liver and skin were predominantly involved as target organs in this model of aGVHD, which was clearly impeded by the administration of anti-CD26 mAb (13). Our data suggest that CD26<sup>+</sup> T cells play an effector role in this aGVHD model. However, because the mice studied in our previous work succumbed to aGVHD ~4 wk

\*Department of Therapy Development and Innovation for Immune Disorders and Cancers, Graduate School of Medicine, Juntendo University, Tokyo 113-8421, Japan; <sup>†</sup>Department of Medicine, Vanderbilt University School of Medicine, Vanderbilt University Medical Center, Nashville, TN 37232; <sup>‡</sup>Division of Hematology and Oncology, University of Florida, Gainesville, FL 32610; and <sup>§</sup>Department of Pathology, Keio University School of Medicine, Tokyo, 160-8582, Japan

Received for publication November 4, 2014. Accepted for publication February 16, 2015.

This work was supported in part by a grant from the Ministry of Education, Science, Sports, and Culture, Japan (to K.O. and C.M.); a grant from the Ministry of Health, Labour, and Welfare, Japan (to C.M.); a grant-in-aid (S1311011) from the Foundation of Strategic Research Projects in Private Universities from the Ministry of Education, Culture, Sports, Science, and Technology, Japan (to K.O. and C.M.); and National Institutes of Health Grant RO1 AI044924 (to T.M.A.).

Address correspondence and reprint requests to Prof. Chikao Morimoto, Department of Therapy Development and Innovation for Immune Disorders and Cancers, Graduate School of Medicine, Juntendo University, 2-1-1, Hongo, Bunkyo-ku, Tokyo 113-8421, Japan. E-mail address: morimoto@ims.u-tokyo.ac.jp

The online version of this article contains supplemental material.

Abbreviations used in this article: aGVHD, acute GVHD; ALL, acute lymphoblastic leukemia; alloHSCT, allogeneic hematopoietic stem cell transplantation; alloPBSCT, allogeneic peripheral blood-stem cell transplant; B6, C57BL/6; BAC, bacterial artificial chromosome; Cav-Ig, Ig Fc domain fused with the N-terminal of caveolin-1; cGVHD, chronic GVHD; CNS, conserved noncoding sequence; DPP4, dipeptidyl peptidase IV; GVHD, graft-versus-host disease; GVL, graft-versus-leukemia; HPRT1, hypoxanthine phosphoribosyltransferase 1; HSC, hematopoietic stem cell; HuCB, human umbilical cord blood; MNC, mononuclear cell; NHLF, normal human lung fibroblast; pAb, polyclonal Ab; RA, rheumatoid arthritis; RIPA, radioimmuno-precipitation assay; Tg, transgenic.

Copyright © 2015 by The American Association of Immunologists, Inc. 0022-1767/15/\$25.00

after transplantation of human adult PBL, this early-onset model of aGVHD does not permit the assessment of longer-term consequences of interventional therapies such as the development of obliterative bronchiolitis, a form of cGVHD of the lung.

CD26 is associated with T cell signal transduction processes as a costimulatory molecule, as well as being a marker of T cell activation in human adult PBL (14–16). In fact, patients with autoimmune diseases such as multiple sclerosis and rheumatoid arthritis (RA) have been found to have increased numbers of CD26<sup>+</sup>CD4<sup>+</sup> T cells in both inflamed tissues and the peripheral blood, with enhancement of CD26 expression in these autoimmune diseases correlating with disease severity (17). Previously, we have demonstrated that caveolin-1 is a costimulatory ligand for human CD26, and that CD26 on activated memory T cells interacts with caveolin-1 on recall Ag-primed monocytes (18, 19). More recently, we demonstrated in *in vitro* experiments that blockade of CD26-mediated T cell costimulation by soluble Fc fusion proteins containing the N-terminal domain of caveolin-1 (Cav-Ig) diminished primary and secondary proliferative responses not only to recall Ag, but also to unrelated allogeneic APC (20). In contrast to adult PBL, the human umbilical cord blood (HuCB) lymphocytes have been reported to be immature, predominantly consisting of CD45RA<sup>+</sup> naive cells (21, 22). We previously showed that, although all HuCB CD4<sup>+</sup> T cells constitutively expressed CD26, CD26-mediated costimulation was considerably attenuated in HuCB CD4<sup>+</sup> T cells, compared with the robust activation via CD26 costimulation of adult PBL (21). Additionally, HuCB CD4<sup>+</sup> T cells exhibited only slight activation after long-sustained stimulation of CD26. These findings provided further insights into the cellular mechanisms of immature immune response in HuCB. Furthermore, it has been reported that humanized mice transplanted with human hematopoietic stem cell (HSC) isolated from HuCB exhibited human hematopoiesis reconstitution as well as B cell engraftment with a similar Ab repertoire as observed in B cells in human (23, 24). Based on these findings, we hypothesized that HuCB naive CD4<sup>+</sup> T cells gradually acquire a xenogeneic response via attenuated stimulatory signaling with indolent inflammation in the target organs, leading eventually to chronic inflammatory changes. We therefore sought to develop a humanized murine pulmonary cGVHD model utilizing HuCB donor cells, and to overcome the limitations seen in the humanized murine aGVHD model such as vigorous activation of all engrafted T cells and extensive loss of B cell maturation and activation (23).

In the current study, we established a xenogeneic pulmonary cGVHD murine model induced by transplantation of HuCB, which exhibited obliterative bronchiolitis as well as sclerodermatous skin and primary biliary cirrhosis-like liver. Moreover, we determined a novel effect of IL-26 produced by donor-derived human CD4<sup>+</sup> T cells on fibroproliferation of obliterative bronchiolitis, which was also shown in the murine alloHSCT model using human *IL26* transgenic mice. In addition, our findings indicated a decrease of collagen deposition in the lung of xenogeneic pulmonary cGVHD mice treated with anti-IL-26 neutralizing Ab. Our analysis of a patient specimen demonstrated the predominant infiltration of IL-26<sup>+</sup>CD26<sup>+</sup>CD4<sup>+</sup> T cells in the lung of obliterative bronchiolitis after alloHSCT. In *in vitro* experiments, we showed that IL-26 of HuCB CD4<sup>+</sup> T cells was produced via CD26 costimulation by its ligand caveolin-1, whereas CD28 costimulation did not generally enhance IL-26 production. Furthermore, abrogation of CD26 costimulation by Cav-Ig before or during early onset of GVHD impeded the development of pulmonary cGVHD. These results provide proof of principle that human IL-26<sup>+</sup>CD26<sup>+</sup>CD4<sup>+</sup> T cells are involved in the pathophysiology of pulmonary cGVHD, and

that blockade of CD26 costimulation by Cav-Ig appears to be a promising novel therapeutic strategy for the clinical control of cGVHD.

## Materials and Methods

### *Abs, reagents, and cells*

Mouse mAbs to human CD3 (OKT3, IgG2b), CD26 (1F7, IgG1), and CD28 (4B10, IgG1) for costimulation experiments were developed in our laboratory (25). Anti-IL-26 goat polyclonal Ab (pAb) (AF1375), which is available for neutralizing experiments (26), was obtained from R&D Systems (Minneapolis, MN). Human rIL-26 was purchased from R&D Systems and stocked at 1  $\mu\text{g ml}^{-1}$  in PBS. Cav-Ig and its control Fc protein were made in our laboratory, with previous references in the literature (27). Normal human lung fibroblast (NHLF) and the culture medium FGF-2 were purchased from LONZA (Walkersville, MD). Mouse fibroblast cell line NIH3T3 and mononuclear cells (MNCs) isolated from HuCB with Ficoll density gradient method were purchased from RIKEN BioResource Center (Tsukuba, Japan). T cell-depleted CD34<sup>+</sup> cells were purified from MNCs of HuCB using human CD34 MicroBead Kit (Miltenyi Biotec, Bergisch Gladbach, Germany).

### *Mice*

NOD/SCID/ $\gamma_c^{-/-}$  NOD.Cg-Prkdcscid Il2rgtm1Sug/Jic mice (NOG mice) (H-2<sup>d</sup>) were purchased from the Central Institute for Experimental Animals (Kawasaki, Japan). C57BL/6 (B6) mice (H-2<sup>b</sup>) were obtained from CLEA Japan (Tokyo, Japan). B6 mice carrying a 190-kb bacterial artificial chromosome (BAC) transgene with human *IFNG* and *IL26* gene (190-*IFNG* transgenic [Tg]) and a BAC Tg-deleting conserved noncoding sequence (CNS) positioned upstream of the *IFNG* transcription start site ( $\Delta\text{CNS-77 Tg}$ ) were developed in Thomas Aune's laboratory (28). All mice were housed in a specific pathogen-free facility in microisolator cages. Mice were used at 8–12 wk. Animal protocol was approved by the Institutional Animal Care and Use Committee.

### *Transplantation and assessment of GVHD*

On day  $-1$ , NOG mice received 200 cGy irradiation. On day 0, mice were injected *i.p.* with  $1 \times 10^7$  MNC (whole CB transplant) or  $1 \times 10^5$  CD34<sup>+</sup> cells (CD34<sup>+</sup> transplant) purified from HuCB. Mice were assessed for survival daily and weighed thrice weekly. In IL-26 blockade experiments, mice were treated with anti-IL-26 pAb or control goat IgG at 50  $\mu\text{g}$  per dose *i.p.* thrice per week from day +21 until day +32 (total six doses). In cGVHD prevention experiments, mice were given human Cav-Ig, or control human Fc at 100  $\mu\text{g}$  per dose *i.p.* thrice per week from day +1 until day +28 (total 12 doses). In cGVHD treatment experiments, at onset of first clinical signs of disease 28 d after HuCB transplantation, mice were given human Cav-Ig, or control human Fc at 100  $\mu\text{g}$  per dose *i.p.* thrice per week from day +29 until day +56 (total 12 doses) after confirmation of engraftment. Engraftment of HuCB was confirmed by quantification of human CD45<sup>+</sup> leukocytes in mouse peripheral blood using flow cytometry. The clinical GVHD score was assessed at least weekly according to the previous reference in the literature (29). For allogeneic bone marrow transplantation experiments using Tg mice, sublethally irradiated (200 cGy) NOG mice were transplanted with  $1 \times 10^7$  bone marrow and  $1 \times 10^6$  splenocytes isolated from 190-*IFNG* Tg,  $\Delta\text{CNS-77 Tg}$  or parental B6 (B6 wild-type) mice. Recipients were sacrificed at 4 wk posttransplantation, and the lungs were removed for histopathological evaluation.

### *Tissue histopathology and immunohistochemistry*

Skin from the upper back, the left lung, and liver specimens of recipients were fixed in 10% formalin, embedded in paraffin, sectioned, mounted on slides, and stained with H&E to determine pathology. The lung specimen of a patient undergoing an allogeneic peripheral blood-stem cell transplant (alloPBSCT) for acute lymphoblastic leukemia (ALL) was prepared for histopathologic and immunohistochemical studies by the same method as described above. Images were captured with an Olympus digital camera DP21 attached to an Olympus BX43 microscope using CellSens software (OLYMPUS, Tokyo, Japan). Slides were scored by a pathologist blinded to experimental groups. The GVHD pathology score was assessed according to the previous references in the literature (29–31). For detection of collagen, slides were stained with Azan-Mallory staining. Abs used in immunohistochemistry were anti-human CD4 mAb (4B12, mouse IgG1) and anti-human CD8 mAb (C8/144B, mouse IgG1) from Dako (Tokyo, Japan), anti-human CD26 goat pAb (AF1180) from R&D Systems, anti-IL-26 rabbit pAb (bs-2626R) from Bioss (Woburn, MA), and anti-IL-17A rab-

bit pAb (H-132) from Santa Cruz Biotechnology (Santa Cruz, CA). Immunohistochemical staining for CD4, CD8, CD26, or IL-26 was performed at the Department of Pathology, Keio University School of Medicine (Tokyo, Japan), as described previously (32). Immunohistochemical staining for IL-17A was conducted at the laboratory of MorphoTechnology (Sapporo, Japan).

#### Real-time quantitative RT-PCR

In experiments assessing expression of mRNA of effector molecules, a single-cell suspension was isolated from the lung of recipient mice using Lung Dissociation Kit (Miltenyi Biotec), followed by purification of human CD4 T cells using human CD4 MicroBeads (Miltenyi Biotec). Isolation and quantification of mRNA were performed, as described previously (33). Expression levels of mRNA were calculated on the basis of standard curves generated for each gene, and hypoxanthine phosphoribosyltransferase 1 (HPRT1) mRNA was used as an invariant control. Sequences of primers used in real-time RT-PCR analysis are as follows: human IL-2, forward 5'-AGAAGGCCACAGAACTGAAAC-3', reverse 5'-GCTGTCTCATCATATTCAC-3'; human IL-4, forward 5'-CAGTTCTACAGCCACCATGAGA-3', reverse 5'-CGTCTTTAGCCTTTCCAAGAAAG-3'; human IL-6, forward 5'-GCCAGAGCTGTGCAGATGAG-3', reverse 5'-TCAGCAGGCTGGCATTTG-3'; human IL-10, forward 5'-CTGGGGGAGAACTTGAAAGAC-3', reverse 5'-TGGCTTTGTAGATGCCTTTCTC-3'; human IL-17A, forward 5'-ACATCCATAACCGGAATACCAA-3', reverse 5'-ACATCCAT-AACCGGAATACCAA-3'; human IL-21, forward 5'-GACACTGGTCCACAAATCAAGTC-3', reverse 5'-TGCTGACTTTAGTTGGGCCTTC-3'; human IL-26, forward 5'-CAATTGCAAGGCTGCAAGAA-3', reverse 5'-TCTAGCTGATGAAGCACAGAA-3'; human IFN- $\gamma$ , forward 5'-GTGTG-GAGACCATCAAGGAAG-3', reverse 5'-ATGTATTGCTTTTTCGTTGGA-3'; human TNF- $\alpha$ , forward 5'-TCAGCCTCTTCTCCTTCCTG-3', reverse 5'-TT-TGCTACAACATGGGCTACA-3'; human CD26, forward 5'-GTACACAG-AACGTTACATGGGTCTC-3', reverse 5'-TCAGCTCTGCTCATGACTGTT-G-3'; and human HPRT1, forward 5'-CAGTCAACAGGGGACATAAAAG-3', reverse 5'-CCTGACCAAGGAAAGCAAG-3'.

#### Flow cytometry

The following Abs were from BD Biosciences (San Jose, CA): anti-human CD3 (UCHT1, mouse IgG1), anti-human CD4 (RPA-Ta, mouse IgG1), anti-human CD8 (HIT8a, mouse IgG1), anti-human CD14 (M5E2, mouse IgG1), anti-human CD19 (HIB19, mouse IgG1), anti-human CD26 (M-A261, mouse IgG1), anti-human CD45 (HI30, mouse IgG1), anti-human CD56 (B159, mouse IgG1), anti-human IFN- $\gamma$  (B27, mouse IgG1), anti-human IL-17A (N49-653, mouse IgG1) mAbs, and relevant control mAbs of the same Ig isotype. Fluorescent conjugates were FITC, PE, PerCP-Cy5.5, and allophycocyanin. Anti-IL-10RB rabbit pAb (bs-2602R) was purchased from Bioss, and anti-IL-20RA rabbit pAb (06-1073) from Millipore (Billerica, MA). Anti-IL-10RB and anti-IL-20RA pAbs recognize both human and murine Ags. mAb staining of intracellular IL-26 (clone 510414, mouse IgG1) was purchased from R&D Systems, being conjugated with Alexa Fluor 647 using Antibody Labeling Kit (Invitrogen, Carlsbad, CA). RBCs in samples of murine peripheral blood were lysed using BD FACS Lysing Solution (BD Biosciences). For analyzing lymphocytes infiltrated in the lung, a single-cell suspension was prepared using Lung Dissociation Kit, followed by purification with human CD45 MicroBeads (Miltenyi Biotec). For intracellular cytokine analysis, purified human CD45<sup>+</sup> cells were restimulated for 4 h with 25 ng ml<sup>-1</sup> PMA (Sigma-Aldrich, St. Louis, MO) plus 1  $\mu$ g ml<sup>-1</sup> ionomycin (Sigma-Aldrich) in the presence of BD GolgiPlug (BD Biosciences). Intracellular flow cytometry was performed according to the manufacturer's instructions using Human Intracellular Cytokine Staining Kit (BD Biosciences). Analysis was performed on two-laser FACSCalibur (BD Biosciences), and files were analyzed in CellQuest software (BD Biosciences).

#### Western blotting

To analyze expression of IL-20RA or IL-10RB, 10  $\mu$ g lysates of NHLF and NIH3T3 were prepared using radioimmunoprecipitation assay (RIPA) buffer, being resolved by SDS-PAGE in reducing condition and immunoblotted using anti-IL-20RA (ab25922; Abcam, Cambridge, MA) or anti-IL-10RB (bs-2602R; Bioss) rabbit pAbs recognizing both human and murine Ags. For analysis of phosphorylated STAT3 induced by exogenous IL-26, 1  $\times$  10<sup>5</sup> cells were seeded in 96-well flat-bottom plate, and the next day IL-26 (10 ng ml<sup>-1</sup> in PBS) was added to each well. Cells were harvested at each time point, and cell lysates were prepared in RIPA buffer containing Halt Protease and Phosphatase inhibitor mixture (Thermo Fisher Scientific, Waltham, MA). Each 10  $\mu$ g lysate was resolved by SDS-PAGE in reducing condition and immunoblotted with antiphosphorylated STAT3 (pY-STAT3) (#11045; SAB, Collage Park, MD) recognizing both

human and murine Ags, followed by stripping and reprobing with anti-STAT3 pAb (total STAT3) (GTX15523; GeneTex, Irvine, CA) recognizing both human and murine Ags.

#### Measurement of cytokines and soluble CD26/dipeptidyl peptidase IV

The collected sera were analyzed for inflammatory cytokines other than human IL-26 using Bio-Plex Pro Human Cytokine Assay (Bio-Rad Laboratories, Hercules, CA). IL-26 was assayed using Human IL-26 ELISA Kit (CUSABIO, Hubei, China). Assay for soluble CD26/dipeptidyl peptidase IV (DPP4) was developed in our laboratory (34). All samples were run in triplicates.

#### In vitro and in vivo collagen assay

NHLF or NIH3T3 cells were seeded in 96-well flat-bottom plate (1  $\times$  10<sup>5</sup> /well), and the next day IL-26 (0.1, 2.0, 5.0, or 10 ng ml<sup>-1</sup> in PBS) or PBS alone was added to each well. In neutralizing experiments, neutralizing anti-IL-20RA rabbit pAb (06-1073; R&D Systems) or control rabbit Ig (10  $\mu$ g ml<sup>-1</sup> each) was added to each well 1 h before exogenous IL-26 was added. The supernatants were harvested 48 h after IL-26 was added, followed by measuring soluble collagen using Sircol Collagen Assay Kit (Biocolor, County Antrim, U.K.). The total collagen of the left lung was extracted using acid-pepsin solution and measured according to the manufacturer's instructions of Sircol Collagen Assay Kit. All samples were examined in triplicates.

#### In vitro costimulation assay

For analysis of mRNA expression, CD4 T cells were purified isolated from HuCB MNCs, and 1  $\times$  10<sup>5</sup> cells/well were seeded in 96-well flat-bottom plate with immobilized anti-CD3 (0.05  $\mu$ g ml<sup>-1</sup>) plus anti-CD28 (10  $\mu$ g ml<sup>-1</sup>) or anti-CD26 (10  $\mu$ g ml<sup>-1</sup>) mAbs. After 7 d of stimulation, cell were harvested, mRNA was prepared, and transcript levels of human *IL2*, *IFNG*, *IL17A*, *IL26*, and *DPP4* were quantified by real-time RT-PCR. For IL-26 production analysis via costimulation, 1  $\times$  10<sup>5</sup> HuCB CD4 T cells were stimulated with plate-bound anti-CD3, anti-CD28, anti-CD26 mAbs, or Cav-Ig immobilized at the indicated concentration. The supernatants were harvested 7 or 14 d after stimulation. For inhibition assay, 1  $\times$  10<sup>5</sup> cells/well HuCB CD4 T cells were treated with blocking Cav-Ig or control Ig at the various concentrations (0, 1, 5, 10, 20, or 50  $\mu$ g ml<sup>-1</sup>) prior to stimulation. After 1-h blocking period, cells were stimulated with immobilized anti-CD3 (0.05  $\mu$ g ml<sup>-1</sup>) plus Cav-Ig (20  $\mu$ g ml<sup>-1</sup>), anti-CD28 (20  $\mu$ g ml<sup>-1</sup>), or anti-CD26 (20  $\mu$ g ml<sup>-1</sup>) mAbs. After 7 d of stimulation, the supernatants were harvested. HuCB CD4 T cells were cultured in AIM V serum-free medium (Invitrogen).

#### Graft-versus-leukemia and bioluminescence imaging

Firefly luciferase-transfected A20 murine lymphoma cells (A20-luc) of BALB/c background (H-2<sup>d</sup>) were provided by X. Chen (Medical College of Wisconsin, Milwaukee, WI) (35). NOG mice were irradiated at sublethal dose (200 cGy), inoculated the next day with 1  $\times$  10<sup>4</sup> A20-luc cells via tail vein, and then transplanted the following day with 1  $\times$  10<sup>7</sup> MNCs isolated from HuCB. Cav-Ig or control Ig (100  $\mu$ g/dose) was administered i.p. thrice per week, beginning at day +1 after transplantation until day +28 (total 12 doses). For other graft-versus-leukemia (GVL) experiments, NOG mice were irradiated at sublethal dose (200 cGy), and the next day were transplanted with 1  $\times$  10<sup>7</sup> MNCs isolated from HuCB. Cav-Ig or control Ig (100  $\mu$ g/dose) was administered i.p. thrice per week, beginning at day +1 after transplantation until day +28 (total 12 doses). A total of 1  $\times$  10<sup>5</sup> A20-luc cells was inoculated via tail vein on day +28 posttransplantation. Tumor dissemination was monitored every week using in vivo bioluminescence imaging, as previously described in the literature (36).

#### Statistics

Data were analyzed by two-tailed Student *t* test for two-group comparison or by ANOVA test for multiple comparison testing, followed by the Tukey-Kramer posthoc test. The *p* values  $\leq$  0.05 were considered statistically significant. Survival rates were analyzed by log-rank test using Kaplan-Meier method. Calculations were performed and graphed using GraphPad Prism 6 (GraphPad Software, La Jolla, CA).

#### Study approval

Human study protocols were approved by the Ethics Committees at Juntendo University (authorization number 2012077), and at Keio University (authorization number 20120206). Informed consent was obtained from a patient. Animal experiments were conducted following protocols approved by

the Animal Care and Use Committees at Juntendo University (authorization number 1082).

## Results

### *Establishment of obliterative bronchiolitis in mice transplanted with HuCB*

As described above, the establishment of a humanized murine model of pulmonary cGVHD is needed to better understand and treat this serious and often fatal complication of alloHSCT. To determine whether pulmonary cGVHD is induced by human immune cells in a murine model, we first attempted to establish a humanized murine model utilizing NOG mice as recipients and HuCB as donor cells. To establish a control that did not develop GVHD following hematopoietic reconstitution, we used T cell-depleted CD34<sup>+</sup> cells isolated from HuCB (37–39). As shown in Fig. 1A and Supplemental Fig. 1A, CD34<sup>+</sup> transplant mice survived for 5 mo without any sign or symptom of GVHD. Meanwhile, whole CB transplant mice exhibited clinical signs/symptoms of GVHD as early as 4 wk posttransplant (Fig. 1A), and demonstrated significantly decreased survival rate (Supplemental Fig. 1A). Human cells were engrafted similarly in both groups, as shown in Supplemental Fig. 1B. Previous work with other humanized murine models showed that reconstituted human CD45<sup>+</sup> cells were overcome by CD3<sup>+</sup> T cells posttransplantation due to reduced B cell development (23), which may impair the integrity of host immunity. In contrast, we confirmed that NOG mice transplanted with HuCB maintained a stable number of T and B cells (Supplemental Fig. 1C), consistent with previously reported results (24, 38–40). Therefore, the human immune system appeared to be effectively reconstituted in the present murine model involving whole CB as well as CD34<sup>+</sup> transplant. We next conducted histological studies of GVHD target organs. The lung of whole CB transplant mice showed perivascular and subepithelial inflammation and fibrotic narrowing of the bronchiole (Fig. 1B), whereas CD34<sup>+</sup> transplant control group displayed normal appearance of GVHD target organs such as the lung (Fig. 1C, *left panel*). For the diagnosis of pulmonary cGVHD, it is necessary to show concomitant active GVHD findings in other organs, including skin and liver (4). Skin of whole CB transplant mice manifested fat loss, follicular dropout, and sclerosis of the reticular dermis in the presence of apoptosis of the basilar keratinocytes, whereas the liver exhibited portal fibrosis and cholestasis (Supplemental Fig. 2). These findings indicate that whole CB transplant mice develop pulmonary cGVHD as well as concomitant active GVHD in skin and liver. Because obliterative bronchiolitis can be characterized as a fibroproliferative disease (7), we also performed Mallory staining and lung collagen assays to quantify collagen contents as a measurement of extent of disease. The lung of whole CB transplant mice displayed a significant increase in peribronchiolar and perivascular collagen deposition and in total lung collagen content, compared with CD34<sup>+</sup> transplant mice (Fig. 1C, 1D). Taken together, our data demonstrate that the lung of whole CB transplant mice exhibits obliterative bronchiolitis as manifestation of pulmonary GVHD.

To determine the potential cellular mechanisms involved in the pathogenesis of pulmonary GVHD, we next analyzed the composition of human lymphocytes in the GVHD lung. In contrast to data demonstrating that PBL contained human CD19<sup>+</sup>, CD33<sup>+</sup>, or CD56<sup>+</sup> as well as CD3<sup>+</sup> cells (Supplemental Fig. 1C), human CD3<sup>+</sup> cells were the predominant cell type observed in the lung of whole CB transplant mice, comprising >99% of the lymphocyte population (Fig. 1E). Moreover, human CD4 T cell subset was predominantly observed compared with CD8 T cells (Fig. 1F). These findings were also confirmed by immunohistochemistry studies of the lung specimens (Fig. 1G). These data suggest that

the development of obliterative bronchiolitis found in whole CB transplant mice involves donor-derived human CD3 lymphocytes, particularly CD4 T cells.

### *IL-26-producing CD4 T cell infiltration in the lung of mice with obliterative bronchiolitis*

We next analyzed the expression profile of mRNAs of various inflammatory cytokines in human CD4 T cells isolated from the lung of whole CB transplant mice. As shown in Fig. 2A, *IFNG*, *IL17A*, *IL21*, and *IL26* were significantly increased over the course of GVHD development following whole CB transplantation, whereas *IL2*, *TNF* (TNF- $\alpha$ ), *IL4*, *IL6*, and *IL10* were decreased. In addition, substantial increases were seen in levels of *IFNG* and *IL26*, with *IL17A* and *IL21* remaining at a low level. It has been reported that IFN- $\gamma$  and IL-26 are produced by Th1 cells (41), whereas IFN- $\gamma$ , IL-17A, and IL-26 are produced by Th17 cells (42). Because both Th1 and Th17 cells strongly express CD26 (15, 43), we next analyzed the expression level of CD26/DPP4. *DPP4* mRNA expression in human CD4 T cells infiltrating in the lung of mice with obliterative bronchiolitis was significantly increased (Fig. 2A).

To determine whether these cytokines were produced by the infiltrating human CD26<sup>+</sup>CD4 T cells, we next conducted flow cytometric analysis of lymphocytes isolated from the lung of whole CB or CD34<sup>+</sup> transplant control mice. As shown in Fig. 2B, levels of human IFN- $\gamma$ <sup>+</sup> or IL-26<sup>+</sup>CD26<sup>+</sup>CD4 T cells were significantly increased in whole CB transplant mice as compared with CD34<sup>+</sup> transplant control mice, whereas levels of IL-17A<sup>+</sup>CD26<sup>+</sup>CD4 T cells were similarly very low in both groups. These findings were also confirmed by immunohistochemistry studies of the lung specimens (Fig. 2C). To determine whether CD26<sup>+</sup>CD4 T cells produced IL-26, IFN- $\gamma$ , and/or IL-17A, multicolor-staining flow cytometric study was conducted. As shown in Fig. 2Di, CD26<sup>+</sup>CD4 T cells in the lung of whole CB transplant mice predominantly produced IL-26 rather than IFN- $\gamma$ . In addition, whereas CD26<sup>+</sup>IFN- $\gamma$ <sup>+</sup>CD4 cells exclusively expressed IL-26, CD26<sup>+</sup>IL-26<sup>+</sup>CD4 cells were predominantly IFN- $\gamma$ -negative cells, and IL-17A<sup>+</sup> cells were exclusively IL-26 negative (Fig. 2Dii). These data suggest that CD26<sup>+</sup>CD4 T cells in the lung of mice with obliterative bronchiolitis express IL-26 as well as IFN- $\gamma$ , but do not belong to the Th17 cell population.

To further confirm the above findings, we examined protein levels of the relevant cytokines. In addition, because soluble CD26/DPP4 level is correlated with T cell CD26 protein level and hematopoiesis (44, 45), we examined protein levels of human soluble CD26/DPP4 in murine sera. As shown in Fig. 2E, serum levels of human IFN- $\gamma$ , IL-26, and human soluble CD26/DPP4 were significantly increased in whole CB transplant mice as compared with CD34<sup>+</sup> transplant control mice. Meanwhile, serum levels of human IL-2, IL-4, IL-6, IL-10, IL-17A, and TNF- $\alpha$  were undetectable in both groups (data not shown). Taken together, these findings strongly suggest that IFN- $\gamma$ <sup>+</sup> and/or IL-26<sup>+</sup>CD26<sup>+</sup>CD4 T cells play an important role in the pathophysiology of obliterative bronchiolitis after HSCT.

To investigate the role of IL-26<sup>+</sup>CD26<sup>+</sup>CD4 T cells in humans, we conducted immunohistochemistry studies of a human lung specimen obtained from a patient with cGVHD. A 64-y-old woman underwent an alloPBSCT for ALL after being treated with busulfan, fludarabine, and melphalan as conditioning regimen. Tacrolimus was administered for the prevention of GVHD. The patient developed acute skin GVHD (stage 2 and grade I) on day +33 post-transplant. On day +95, the patient had dyspnea and the chest X-ray revealed ground glass opacity bilaterally. Transbronchial lung biopsy was performed on day +101. Histologic findings of the lung

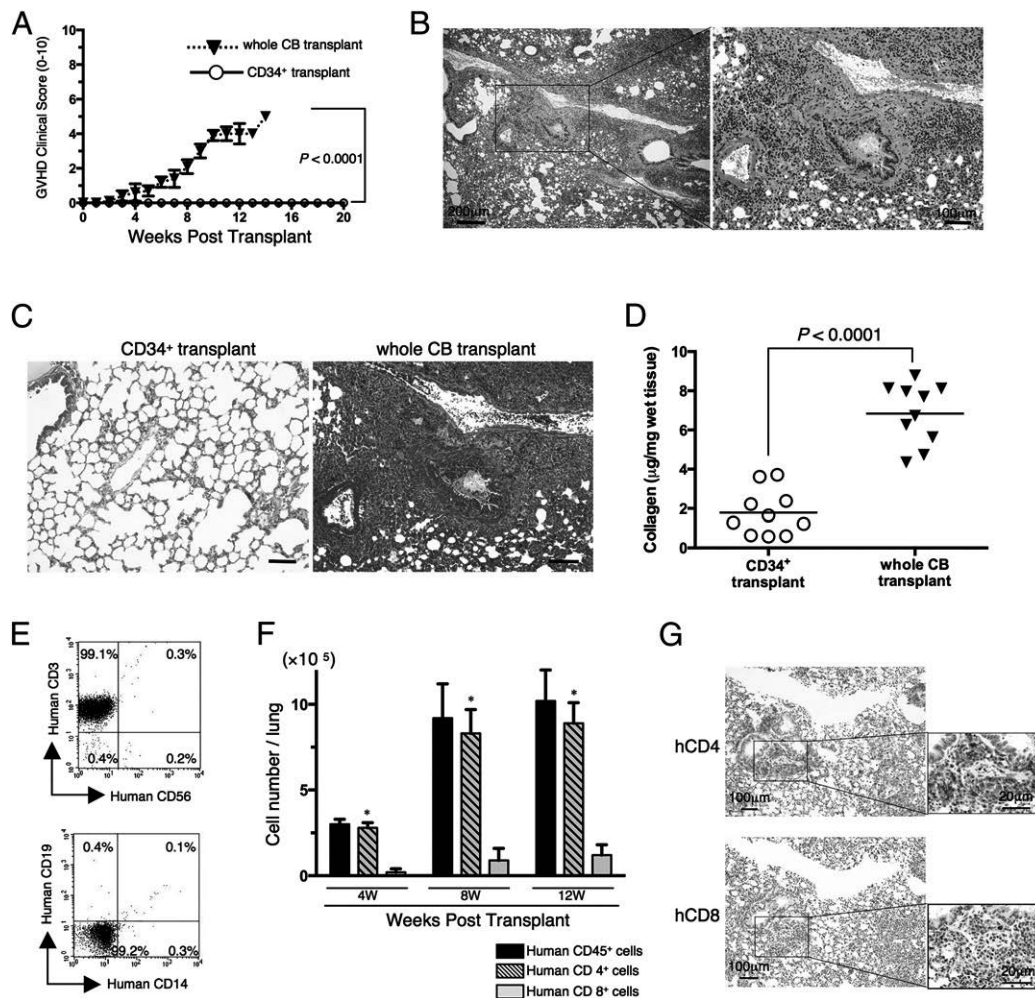


**FIGURE 1.** Obliterative bronchiolitis in sublethally irradiated NOG mice transplanted with HuCB cells. NOG mice were irradiated at sublethal dose (200 cGy) and the next day were transplanted with  $1 \times 10^5$  T cell–depleted  $CD34^+$  cells purified from HuCB ( $CD34^+$  transplant) or with  $1 \times 10^7$  MNCs isolated from HuCB (whole CB transplant). (**A**) Clinical GVHD score (mean  $\pm$  SEM). Data are cumulative results from three independent experiments (for each,  $n = 10$ ). The  $p$  value was calculated by log-rank test. (**B**) H&E staining of the lung of whole CB transplant (8 wk posttransplantation). The left panel shows lower original magnification ( $\times 40$ ) and the right panel shows higher original magnification ( $\times 100$ ). Representative histology is shown from three independent experiments (for each,  $n = 10$ ). (**C**) Collagen deposition was evaluated in the lung tissues of  $CD34^+$  or whole CB transplant (8 wk posttransplantation) with an Azan-Mallory staining. The histology shown in whole CB transplant mice is a sequential section of (B). Dark blue areas indicating collagen deposition are clearly observed in whole CB transplant mice, compared with those in  $CD34^+$  transplant mice. Representative histology is shown from three independent experiments (for each,  $n = 10$ ). Original magnification  $\times 100$ . Scale bars, 100  $\mu$ m. (**D**) Collagen contents in the lung were quantified by Sircol Collagen Assay. The mean number ( $\pm$  SEM) of total collagen contents ( $\mu$ g) per wet lung tissue weight (mg) was determined from three independent experiments (for each,  $n = 10$ ). Increased collagen contents were clearly observed in whole CB transplant mice, compared with those in  $CD34^+$  transplant mice. Each dot indicates individual value, and horizontal bars indicate mean value. (**E**) Representative two-dimensional dot plots of human lymphocyte composition in the lung of whole CB transplant mice (8 wk posttransplantation). Single-suspension cells isolated from the lung of whole CB transplant mice (8 wk posttransplantation) were sorted by human  $CD45^+$  cells and then analyzed using flow cytometry. The upper panel shows representative human CD3 and/or CD56 staining, and the lower panel shows representative human CD19 and/or CD14 staining. Numbers indicate relative percentages per quadrant. Similar results were observed in independent experiments ( $n = 8$ ). (**F**) Absolute cell numbers (mean  $\pm$  SEM) of human  $CD45^+$ ,  $CD4^+$ , or  $CD8^+$  cells per lung of whole CB transplant mice were quantified by flow cytometry.  $CD4^+$  T cells were predominantly observed in the lung of whole CB transplant mice. Data are cumulative results from three independent experiments ( $n = 10$  at 4 wk,  $n = 8$  at 8 wk, and  $n = 3$  at 12 wk).  $*p < 0.0001$  versus  $CD8^+$  cells. (**G**) Anti-human CD4 or CD8 immunohistochemistry of sequential sections of lung tissue of whole CB transplant mice (8 wk posttransplantation). Predominant infiltration of  $CD4^+$  cells was observed, with similar results to those obtained by flow cytometry, as shown in (F). Representative histology is shown from three independent experiments (for each,  $n = 10$ ). Original magnification  $\times 100$  or  $\times 400$  (inset in each panel).

specimen revealed perivascular and subepithelial inflammation and narrowing of the bronchiole with manifestation of peribronchiolar and perivascular collagen deposition (Fig. 2F). The patient was diagnosed as having pulmonary cGVHD with obliterative bronchiolitis. Immunohistochemistry studies showed predominant infiltration of  $IL-26^+CD26^+CD4$  T cells. These findings suggest that  $IL-26^+CD26^+CD4$  T cells play an important role in the pathophysiology of obliterative bronchiolitis after HSCT in human as well as humanized murine model.

#### Contribution of *IL-26* to collagen production in pulmonary GVHD

Because it has been reported that pulmonary GVHD development is independent of  $IFN-\gamma$  (46), we therefore focused on *IL-26* as a potential effector cytokine for pulmonary GVHD. As the *IL-26* gene is absent in rodents (41, 47), we cannot formally exclude the possibility that human *IL-26* activates murine cells. We therefore conducted in vitro assays to determine the effect of human *IL-26* on murine cells. In human cells, *IL-26* binds initially to *IL-20RA* to form the binary complex *IL-26* plus *IL-20RA*, followed by



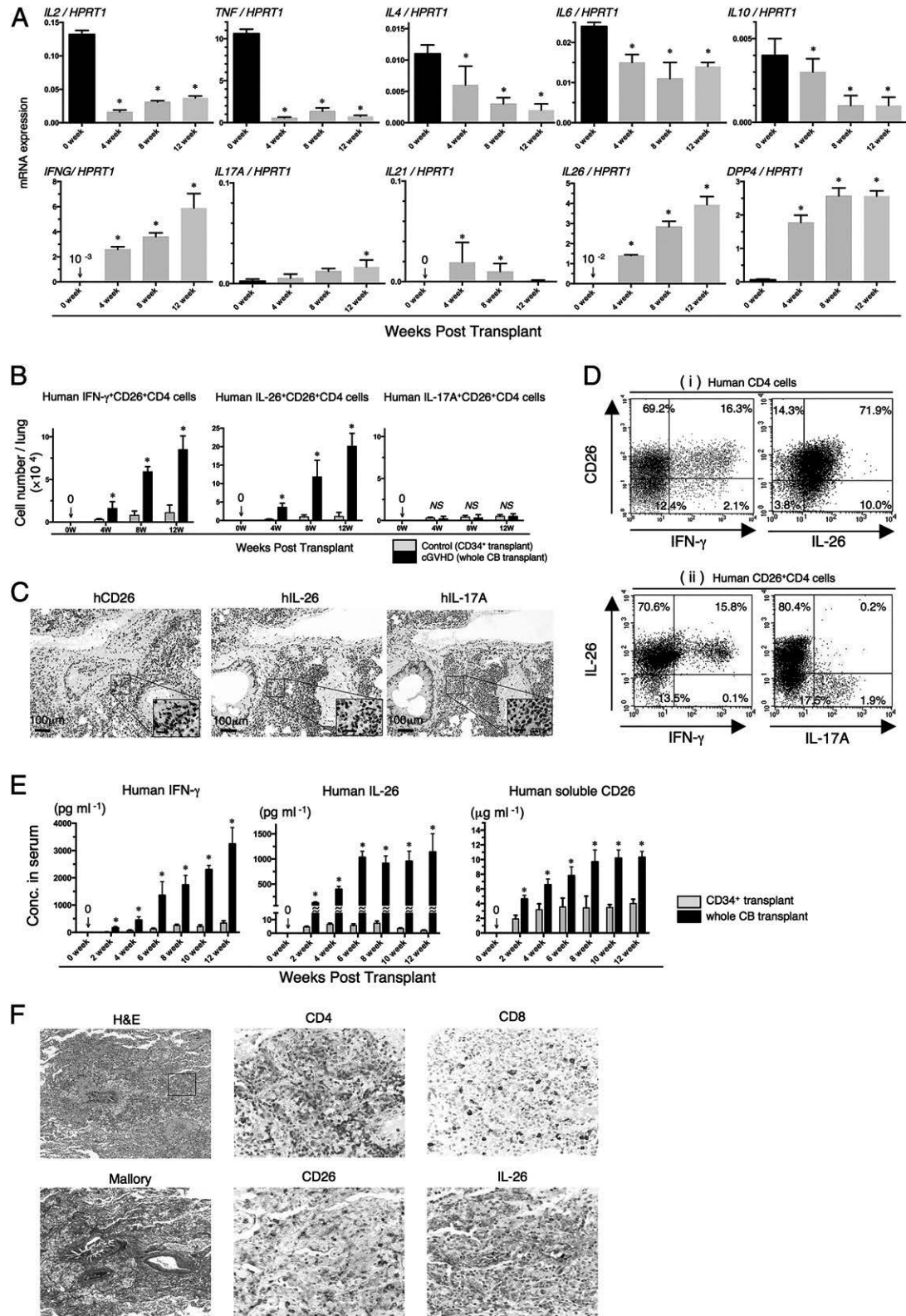


**FIGURE 2.** Predominant infiltration of IL-26<sup>+</sup>CD26<sup>+</sup>CD4 T cells in the lung of obliterative bronchiolitis. **(A)** Whole CB transplant mice were sacrificed at 4, 8, and 12 wk posttransplantation, and the lungs were removed, followed by isolation of human CD4<sup>+</sup> cells. mRNA expression of human cytokines or CD26/DPP4 was quantified by real-time RT-PCR. Each expression was normalized to HPRT1. Data at 0 wk were obtained using freshly isolated HuCB CD4 T cells of three different donors. Data are cumulative results from three independent experiments ( $n = 10$  at 4 wk,  $n = 8$  at 8 wk, and  $n = 3$  at 12 wk).  $*p < 0.0001$  versus each at 0 wk. **(B)** Absolute cell numbers of human IFN- $\gamma$ +CD26+CD4, IL-26+CD26+CD4, or IL-17A+CD26+CD4 cells in the lung of CD34<sup>+</sup> transplant or whole CB transplant mice were quantified by flow cytometry. Data are cumulative results from three independent experiments (for each,  $n = 10$  in CD34<sup>+</sup> transplant group, and  $n = 10$  at 4 wk,  $n = 8$  at 8 wk, and  $n = 3$  at 12 wk in whole CB transplant group).  $*p < 0.0001$  versus corresponding CD34<sup>+</sup> transplant group. **(C)** Anti-human CD26, IL-26, or IL-17A immunohistochemical staining of sequential sections of the lung from whole CB transplant mice (8 wk posttransplantation). The lung of whole CB transplant mice was clearly infiltrated with human CD26 or IL-26 (brown stained cells), but not with IL-17A-positive cells. Representative histology is shown from three independent experiments (*Figure legend continues*)

recruitment of the IL-10RB chain, leading to STAT3 phosphorylation (26). We thus confirmed that both IL-20RA and IL-10RB were expressed in murine fibroblast cell line NIH3T3 as well as NHLF (Fig. 3A, 3B). In both NHLF and NIH3T3, exogenous human rIL-26 induced phosphorylation of STAT3 (Fig. 3C), indicating that human IL-26 was active not only in NHLF, but also in murine fibroblast. To examine a functional effect of IL-26 on murine fibroblasts, we next conducted an in vitro assay for collagen production. As shown in Fig. 3D, increased levels of collagen production in NIH3T3 as well as in NHLF were observed in a dose-dependent manner following the addition of exogenous IL-26, and collagen production was inhibited by neutralizing anti-IL-20RA pAb. These results strongly suggest that human IL-26 activates both human and murine fibroblasts via IL-20RA, leading to increased collagen production.

To further extend the above in vitro results to an in vivo system, we analyzed the lung of murine alloreactive GVHD using human *IL26* Tg mice. For this purpose, we used mice carrying human *IFNG* and *IL26* transgene (190-*IFNG* Tg mice) or mice carrying human *IFNG* transgene with deleting *IL26* transcription ( $\Delta$ CNS-77 Tg mice). The 190-*IFNG* Tg mice exhibited production of IL-26 by CD4 T cells under Th1- or Th17-polarizing conditions, whereas expression of IL-26 was completely abrogated in  $\Delta$ CNS-77 Tg mice (41). In addition, production of IFN- $\gamma$  by T or NK cells was equivalent in both 190-*IFNG* Tg and  $\Delta$ CNS-77 Tg mice (28). As shown in Fig. 3E, lung histology of recipient NOG mice deriving from B6 wild-type or  $\Delta$ CNS-77 Tg mice showed peribronchial infiltration and cuffing denoting GVHD, whereas collagen deposit was not detected by Mallory staining, and IL-26<sup>+</sup> cells were not detected. In contrast, histology of recipient NOG mice deriving from 190-*IFNG* Tg mice showed peribronchial infiltration and cuffing denoting GVHD with collagen deposition and IL-26<sup>+</sup> cell infiltration. Significant increase in collagen contents of the lung of recipient NOG mice deriving from 190-*IFNG* Tg mice was noted (Fig. 3F). These results suggest that human IL-26, but not human IFN- $\gamma$ , plays a critical role in the pulmonary fibrosis associated with obliterative bronchiolitis after HSCT.

To further define the role of IL-26 in the pulmonary fibrosis associated with HSCT, we conducted studies to evaluate whether lung collagen contents were reduced by neutralizing IL-26 in whole CB transplant mice. For this purpose, anti-IL-26 pAb or control pAb was administered in sublethally irradiated NOG mice transplanted with whole CB on day +21 until day +32 thrice per week, followed by resection of the lung to measure total collagen content. As shown in Fig. 3G, a significant decrease in collagen contents of the lung of recipient NOG mice treated with anti-IL-

26 pAb was noted. Taken together, our data strongly suggest that IL-26 plays a critical role in the pulmonary fibrosis observed following HSCT.

#### *IL-26 production via CD26-mediated T cell costimulation*

IL-26 was preferentially expressed in CD26<sup>+</sup>CD4 T cells in the lung of whole CB transplant mice experiencing obliterative bronchiolitis (Fig. 2D), with increased expression of *DPP4* (Fig. 2A). Although upstream stimulation of IL-26 synthesis has not yet been determined, CD26/DPP4 as well as IFN- $\gamma$  is preferentially expressed on Th1 cells activated via CD26-mediated costimulation (15). We thus hypothesized that human CD4 T cells produce IL-26 following CD26 costimulation. To test this hypothesis, we conducted in vitro costimulatory experiments using HuCB CD4 T cells and analyzed expression of various inflammatory cytokines. As shown in Fig. 4A, although expression levels of *IL26* and *DPP4* were enhanced by CD28 (\*) or CD26 (\*\*) costimulation, significantly greater increase in levels of *IL26* and *DPP4* was observed following CD26 costimulation than CD28 costimulation (\*\*\*). In contrast, expression levels of *IL2*, *IFNG*, and *IL17A* were not increased following either CD26 costimulation or CD28 costimulation (Fig. 4A), due to the immaturity of HuCB T cells, as was previously reported (21, 48). We next conducted costimulatory experiments evaluating dose effect and time kinetics using the CD26 costimulatory ligand Cav-Ig as well as anti-CD26 or anti-CD28 mAbs, and assayed for secreted IL-26. As shown in Fig. 4B, production of IL-26 was increased following CD26 costimulation with Cav-Ig (\*) or anti-CD26 (\*\*) mAb in dose- and time-dependent manners, whereas a slight increase in IL-26 level was observed following CD28 costimulation only at higher doses of mAb and longer stimulation periods (\*\*\*). Blocking experiments were then performed for further confirmation, showing that IL-26 production induced by Cav-Ig or anti-CD26 mAb was clearly inhibited by treatment with soluble Cav-Ig in a dose-dependent manner (Fig. 4C), whereas no change was observed with CD28 costimulation (Fig. 4C). These findings strongly suggest that production of IL-26 by HuCB CD4 T cells is regulated via CD26-mediated costimulation. Moreover, because the functional sequences of the N-terminal of caveolin-1 are highly conserved between human and mouse (49), allowing for the capability to bind human CD26 as a costimulatory ligand, it is conceivable that donor HuCB T cells transferred into mice were activated via CD26 costimulation triggered by murine caveolin-1. Taken together, CD26-mediated IL-26 production triggered by caveolin-1 is identified as a possible therapeutic target in pulmonary cGVHD through the use of whole CB transplant mice.

( $n = 10$ ). Original magnification  $\times 100$  or  $\times 400$  (inset in each panel). Scale bars in the inset, 20  $\mu$ m. (D) Representative two-dimensional dot plots of human CD26 and IFN- $\gamma$  or IL-26 cells by gating for human CD4<sup>+</sup> cells (Di), and of human IFN- $\gamma$  or IL-17A among IL-26<sup>+</sup> cells by gating for human CD26<sup>+</sup>CD4<sup>+</sup> cells (Dii). Single-suspension cells isolated from the lung of whole CB transplant mice (8 wk posttransplantation) were sorted by human CD45<sup>+</sup> cells and then analyzed using flow cytometry. Numbers indicate relative percentages per quadrant. Similar results were observed in independent experiments ( $n = 10$ ). (E) Sera of CD34<sup>+</sup> transplant or whole CB transplant mice were collected at the indicated week posttransplantation, and serum levels of human IFN- $\gamma$ , IL-26, and soluble CD26/DPP4 were quantified. Data are cumulative results from three independent experiments (for each,  $n = 10$  in CD34<sup>+</sup> transplant group, and  $n = 10$  at 0–6 wk,  $n = 8$  at 8 wk,  $n = 7$  at 10 wk, and  $n = 3$  at 12 wk in whole CB transplant group). \* $p < 0.0001$  versus corresponding CD34<sup>+</sup> transplant group. (F) H&E, Azan-Mallory, anti-human CD4, CD8, CD26, or IL-26 immunohistochemical staining of sequential sections of the lung from a patient undergoing alloPBSCT for ALL. After having acute skin GVHD on day +33 posttransplant, the patient experienced dyspnea with ground glass opacity detected on the chest X-ray examination on day +95. The lung specimen was obtained by transbronchial lung biopsy on day +101, showing perivascular and subepithelial inflammation and narrowing of the bronchiole (H&E staining). Peribronchiolar and perivascular collagen deposition was detected by Azan-Mallory staining. The lung was clearly infiltrated with CD4<sup>+</sup>, CD26<sup>+</sup>, or IL-26<sup>+</sup> cells (brown stained cells), with CD8<sup>+</sup> cells found at a very low level. The histology shown in immunohistochemical staining is focused in the inset of the H&E staining panel. Original magnification  $\times 100$  (H&E and Azan-Mallory) or  $\times 400$  (anti-CD4, CD8, CD26, and IL-26 staining).

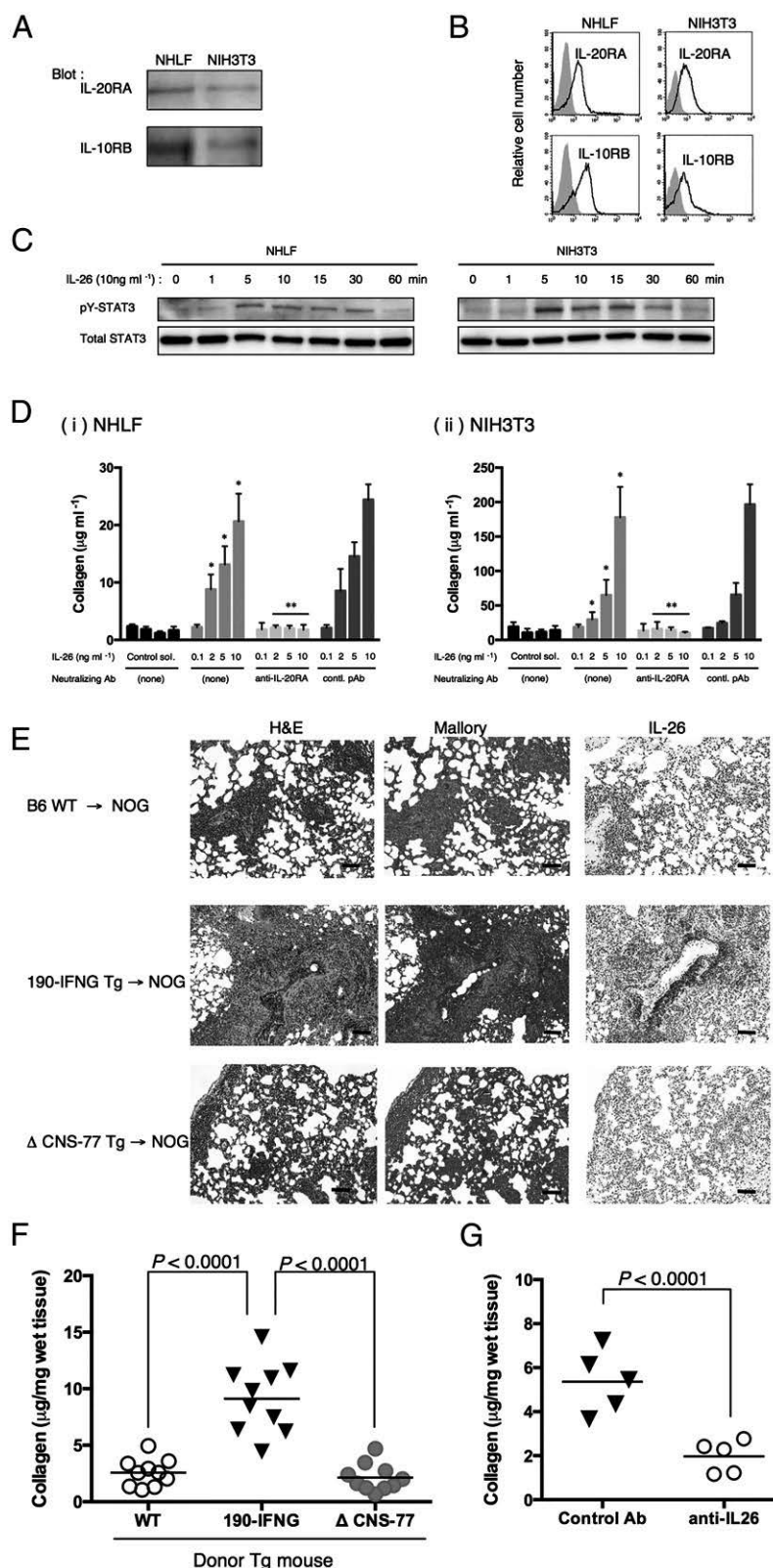


**FIGURE 3.** IL-26 stimulates fibroblast, and collagen deposition in the lung of obliterative bronchiolitis is induced in NOG mice receiving bone marrow cells and splenocytes of *IL26* Tg mice. **(A)** Western blot analysis of IL-20RA and IL-10RB in NHLF and NIH3T3 cells. Lysates (each, 10 μg) were prepared using RIPA buffer, being resolved by SDS-PAGE in reducing condition and immunoblotted using anti-IL-20RA or anti-IL-10RB pAbs recognizing both human and murine Ags. **(B)** Representative histogram of IL-20RA and IL-10RB of NHLF and NIH3T3 cells. Single-suspension cells were stained with anti-IL-20RA or anti-IL-10RB pAbs recognizing both human and murine Ags, and analyzed using flow cytometry (bold line). Gray histograms indicate isotype control (rabbit polyclonal IgG and anti-rabbit IgG-PE). **(C)** A total of  $1 \times 10^5$  cells of NHLF or NIH3T3 was seeded in 96-well flat-bottom plate, and the next day IL-26 (10 ng ml<sup>-1</sup> in PBS) was added to each well. Cells were harvested at each time point, and cell lysates were prepared in RIPA buffer containing Halt Protease and Phosphatase inhibitor mixture, and 10 μg each lysate was resolved by SDS-PAGE in reducing condition and immunoblotted with antiphosphorylated STAT3 (pY-STAT3) recognizing both human and murine Ags, followed (Figure legend continues)

### Prevention of obliterative bronchiolitis in whole CB transplant mice by Cav-Ig administration

Given the role of CD26 costimulation in IL-26 production and IL-26 regulation of collagen production, we therefore sought to determine whether disruption of CD26 costimulation by a blocking reagent, Cav-Ig, prolonged survival of the recipient mice associated with a reduction in the incidence of obliterative bronchiolitis. Recipients treated with Cav-Ig survived for 7 mo without any clinical findings of GVHD (Fig. 5A, 5B). Meanwhile, the survival rate of recipient mice treated with control Ig was significantly reduced (Fig. 5A), with clinical signs/symptoms of GVHD (Fig. 5B). Human cells were engrafted similarly in both groups, as shown in Supplemental Fig. 3A, 3B. Histologic findings of the lung showed the development of obliterative bronchiolitis in control Ig, while having normal appearances in Cav-Ig recipient mice, with none having positive pathology scores (Fig. 5C, 5D). These effects of Cav-Ig were also observed in other GVHD-target organs such as the skin and liver (Supplemental Fig. 3C). Moreover, IL-26<sup>+</sup>CD26<sup>+</sup>CD4 T cells in the lung and serum levels of human IL-26 and soluble CD26/DPP4 were significantly decreased in Cav-Ig-administered recipients than in control Ig (Fig. 5E, 5F). Furthermore, collagen contents in the lung were reduced in Cav-Ig-administered recipients (Fig. 5G, 5H). Taken together, the above results support the notion that Cav-Ig administration prevents the development of pulmonary GVHD in whole CB transplant mice by decreasing the number of IL-26<sup>+</sup>CD26<sup>+</sup>CD4 T cells.

### Effect of Cav-Ig administration after onset of GVHD

Because pulmonary GVHD progresses in an indolent manner over weeks and months, patients often are affected by the clinical findings prior to being diagnosed with cGVHD (50). We therefore sought to determine whether blockade of caveolin-1/CD26 interaction effectively suppresses obliterative bronchiolitis development following the appearance of clinical signs/symptoms. For this purpose, treatment began on day +29 following the appearance of an increase in GVHD scores, indicating the early stages of cGVHD development. Recipients treated with Cav-Ig survived for 7 mo with remission of GVHD symptoms (Fig. 6A, 6B). Meanwhile, the survival rate of recipients treated with control Ig was significantly decreased (Fig. 6A), with progression of clinical signs/symptoms of GVHD (Fig. 6B). Human cells were engrafted similarly in both groups (Supplemental Fig. 4A, 4B). In contrast to progressive obliterative bronchiolitis of control Ig-treated recipients, peribronchial inflammation shown at 5 wk posttransplantation was attenuated at 10 wk posttransplantation in Cav-Ig-treated recipients

(Fig. 6C). Correspondingly, the pathologic scores of control Ig-treated recipients were significantly increased at 10 wk, as compared with those at 5 wk (Fig. 6D). Meanwhile, the pathologic scores of Cav-Ig-treated recipients were significantly reduced at 10 wk, as compared with those at 5 wk (Fig. 6D), and were clearly decreased as compared with those of control Ig-treated recipients (Fig. 6D). These effects of Cav-Ig administration were observed in the skin and liver (Supplemental Fig. 4C–F). Moreover, levels of human IFN- $\gamma$ <sup>+</sup> and IL-26<sup>+</sup>CD26<sup>+</sup>CD4 T cells in the lung of control Ig-treated recipients were significantly increased at 10 wk, as compared with those at 5 wk (\* of Fig. 6E). In contrast, levels of human IFN- $\gamma$ <sup>+</sup> and IL-26<sup>+</sup>CD26<sup>+</sup>CD4 T cells in the lung of Cav-Ig-treated recipients were significantly reduced at 10 wk, as compared with those at 5 wk (\*\* of Fig. 6E), and were clearly decreased as compared with those of control Ig-treated recipients (\*\*\*) of Fig. 6E). Furthermore, total collagen contents in the lung were significantly lower in Cav-Ig-treated recipients than control Ig-treated recipients (Fig. 6F). Taken together, these data suggest that Cav-Ig administration not only prevents the development of cGVHD, but also provides a novel therapeutic approach for the early stages of cGVHD by regulating levels of IL-26<sup>+</sup>CD26<sup>+</sup>CD4 T cells.

### Treatment with Cav-Ig preserves GVL capability in recipient mice

Because GVHD and GVL effects are highly linked immune reactions (51), we evaluated the potential influence of Cav-Ig treatment on GVL effect. For this purpose, cohorts of Cav-Ig- or control Ig-treated recipient mice of whole CB transplant were irradiated at sublethal doses and then injected i.v. with luciferase-transfected A20 (A20-luc) cells 1 d prior to whole CB transplantation to allow for dissemination of tumor cells. The next day following transplantation, treatment with Cav-Ig or control Ig thrice per week began on day +1 until day +28. Mice inoculated with A20 cells alone all died of tumor progression within 6 wk (Fig. 7A, 7B). Recipients treated with control Ig exhibited clinical evidence of GVHD such as weight loss and ruffled fur and died of GVHD without tumor progression in 13 wk (Fig. 7A, 7B). In contrast, recipient mice treated with Cav-Ig displayed significantly prolonged survival (Fig. 7A) without involvement of A20-luc cells (Fig. 7B). To better characterize the potency of the GVL effect, we repeated these studies with injection of A20-luc cells on day +28 after whole CB transplantation to allow for acquisition of immunosuppression by Cav-Ig treatment. Mice inoculated with A20 cells alone all died of tumor progression within 2 wk after tumor inoculation (Fig. 7C, 7D). Recipient mice treated with control Ig

by stripping and reprobing with anti-STAT3 pAb (total STAT3) recognizing both human and murine Ags. Representative data are shown from three independent experiments with similar results. (D) Collagen production of NHLF (Di) or NIH3T3 (Dii) cells stimulated with exogenous IL-26 in the presence or absence of neutralizing anti-IL-20RA pAb or rabbit Ig (contl. pAb). Data are shown as mean  $\pm$  SEM, resulting from three independent experiments with triplicates. The amount of secreted soluble collagen increased with increasing level of exogenous IL-26 in a dose-dependent manner (\* $p$  < 0.0001 versus corresponding control solvent), and production of collagen was inhibited by the presence of neutralizing anti-IL-20RA pAb (\*\* $p$  < 0.0001 versus corresponding contl. pAb). (E) H&E, Azan-Mallory staining, and anti-IL-26 immunohistochemical staining of sequential sections of the lung from NOG mice at 4 wk after transplantation of BM and splenocytes isolated from parental B6 (B6 WT), 190-IFNG BAC Tg (190-IFNG Tg), or  $\Delta$ CNS-77 Tg mice. The lung of recipients of 190-IFNG Tg mice showed obliterative bronchiolitis with collagen deposition and IL-26<sup>+</sup> cell infiltration, whereas recipients of B6 WT or  $\Delta$ CNS-77 Tg mice showed peribronchial and septal infiltration without collagen deposition or IL-26<sup>+</sup> cells. Representative histology is shown from three independent experiments (for each,  $n$  = 6). Original magnification  $\times$ 100. Scale bars, 100  $\mu$ m. (F) Recipient mice were sacrificed at 4 wk posttransplantation, and the lungs were removed. Collagen contents in the lung were quantified by Sircol Collagen Assay. The mean number ( $\pm$ SEM) of total collagen contents ( $\mu$ g) per wet lung tissue weight (mg) was determined from three independent experiments (for each,  $n$  = 10). Increased collagen contents were clearly observed in recipients of 190-IFNG Tg mice, compared with those in recipients of B6 WT or  $\Delta$ CNS-77 Tg mice. Each dot indicates individual value, and horizontal bars indicate mean value. (G) Whole CB transplant mice were administered anti-IL-26 Ab or control Ab (each 50  $\mu$ g/dose) i.p. thrice per week, beginning at day +21 after transplantation until day +32. Recipient mice were sacrificed at 5 wk posttransplantation, and the lungs were removed. Collagen contents in the lung were quantified by Sircol Collagen Assay. The mean number ( $\pm$ SEM) of total collagen contents ( $\mu$ g) per wet lung tissue weight (mg) was determined from two independent experiments (for each,  $n$  = 5). Decreased collagen contents were clearly observed in the recipients of anti-IL-26 Ab. Each dot indicates individual value, and horizontal bars indicate mean value.

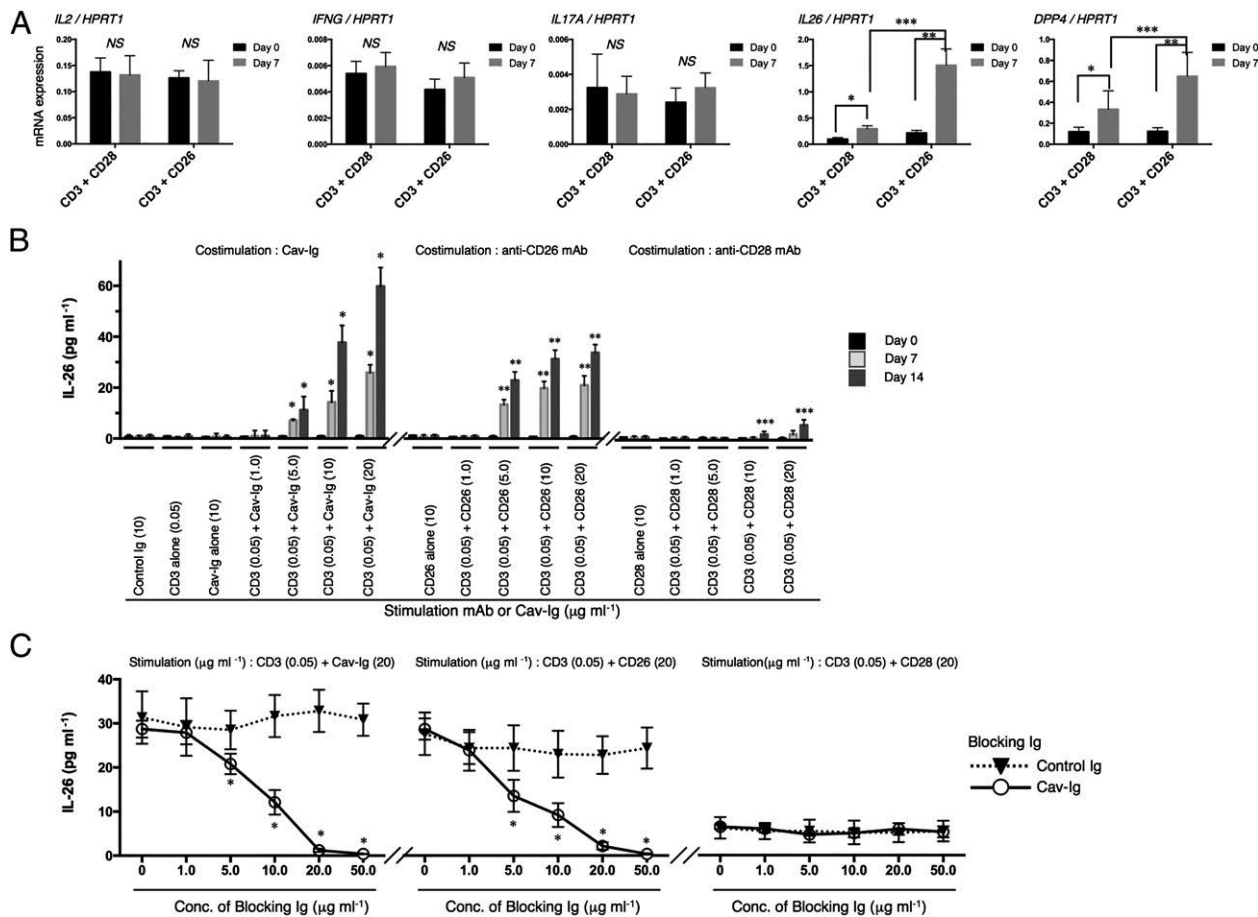


**FIGURE 4.** CD26 costimulation enhances IL-26 production in HuCB CD4 T cells, and blockade by the CD26 ligand caveolin-1 reduces production of IL-26. **(A)** HuCB CD4 T cells were stimulated with immobilized anti-CD3 (0.05  $\mu\text{g ml}^{-1}$ ) plus anti-CD28 (10  $\mu\text{g ml}^{-1}$ ) or anti-CD26 (10  $\mu\text{g ml}^{-1}$ ) mAbs. After 7 d of stimulation, mRNA levels of human *IL2*, *IFNG*, *IL17A*, *IL26*, and *DPP4* were quantified by real-time RT-PCR. Each expression was normalized to *HPRT1*. Data are shown as mean  $\pm$  SEM, resulting from three independent experiments with triplicates. \* $p < 0.05$ , \*\*\*\* $p < 0.0001$ . **(B)** HuCB CD4 T cells were stimulated with plate-bound anti-CD3, anti-CD28, anti-CD26 mAbs, or Cav-Ig immobilized at the indicated concentration. The supernatants were harvested 7 or 14 d after stimulation, and levels of human IL-26 were quantified. Data are shown as mean  $\pm$  SEM, resulting from three independent experiments with triplicates (\*\*\*\* $p < 0.0001$  or \*\*\* $p < 0.05$  versus corresponding samples at day 0). **(C)** HuCB CD4 T cells were treated with blocking Cav-Ig (solid line) or control Ig (dotted line) at the indicated concentration. After 1 h of incubation with blocking Cav-Ig or control Ig, cells were stimulated with immobilized anti-CD3 (0.05  $\mu\text{g ml}^{-1}$ ) plus Cav-Ig (20  $\mu\text{g ml}^{-1}$ ), anti-CD28 (20  $\mu\text{g ml}^{-1}$ ), or anti-CD26 (20  $\mu\text{g ml}^{-1}$ ) mAbs. After 7 d of stimulation, the supernatants were harvested and levels of human IL-26 were quantified. Data are shown as mean  $\pm$  SEM, resulting from three independent experiments with triplicates. \* $p < 0.0001$  versus corresponding control Ig.

demonstrated clinical evidence of GVHD such as weight loss and ruffled fur and died of GVHD without tumor progression within 13 wk after transplantation (Fig. 7C, 7D). In contrast, recipients treated with Cav-Ig exhibited significantly prolonged survival (Fig. 7C) without involvement of A20-luc cells (Fig. 7D). Collectively, these results demonstrate that Cav-Ig treatment of recipient mice of whole CB transplant was effective in reducing the symptoms of cGVHD without a concomitant loss of the GVL effect.

## Discussion

In the current study, we demonstrated that obliterative bronchiolitis developed in NOG mice transplanted with HuCB (whole CB transplant). Utilizing this humanized mouse model, we found that donor-derived CD4 T cells predominantly infiltrated in the lung of obliterative bronchiolitis, and that IL-26 as well as IFN- $\gamma$  levels were enhanced significantly in the infiltrating human CD26<sup>+</sup>CD4 T cells.

Originally discovered in *Herpesvirus saimiri*-transformed T cells (52), IL-26 is now classified as belonging to the IL-10 family of cytokines (42). IL-26 is a secreted protein produced

by T, NK cells, or synoviocytes (53, 54), and binding of IL-26 to a distinct cell surface receptor consisting of IL-20RA and IL-10RB results in functional activation via STAT3 phosphorylation (26). IL-26 gene expression or protein production has been analyzed in patients with RA, inflammatory bowel diseases, and hepatitis C virus infection (54–58). However, the effect of IL-26 on the pathophysiology of cGVHD has not yet been determined. Moreover, there has been little information available regarding the biological functions of IL-26 using animal models due to the absence of the IL-26 gene in mouse (41, 47). In this study, we described a novel effect of IL-26 on fibroproliferation in transplant-related obliterative bronchiolitis, using a humanized pulmonary cGVHD murine model. Moreover, we demonstrated that human IL-26, not IFN- $\gamma$ , induced collagen deposition in obliterative bronchiolitis of murine allogeneic transplantation model utilizing 190-*IFNG* Tg and  $\Delta$ CNS-77 Tg mice. In both 190-*IFNG* Tg and  $\Delta$ CNS-77 Tg mice, production of IFN- $\gamma$  by T or NK cells is equivalent in both tissue culture studies and analysis of basal levels in various tissues, including spleen, lymph node, and colon (28). In contrast, expression of IL-26 is observed in Th1- or Th17-polarizing CD4 cells of 190-*IFNG* Tg mice, whereas it is



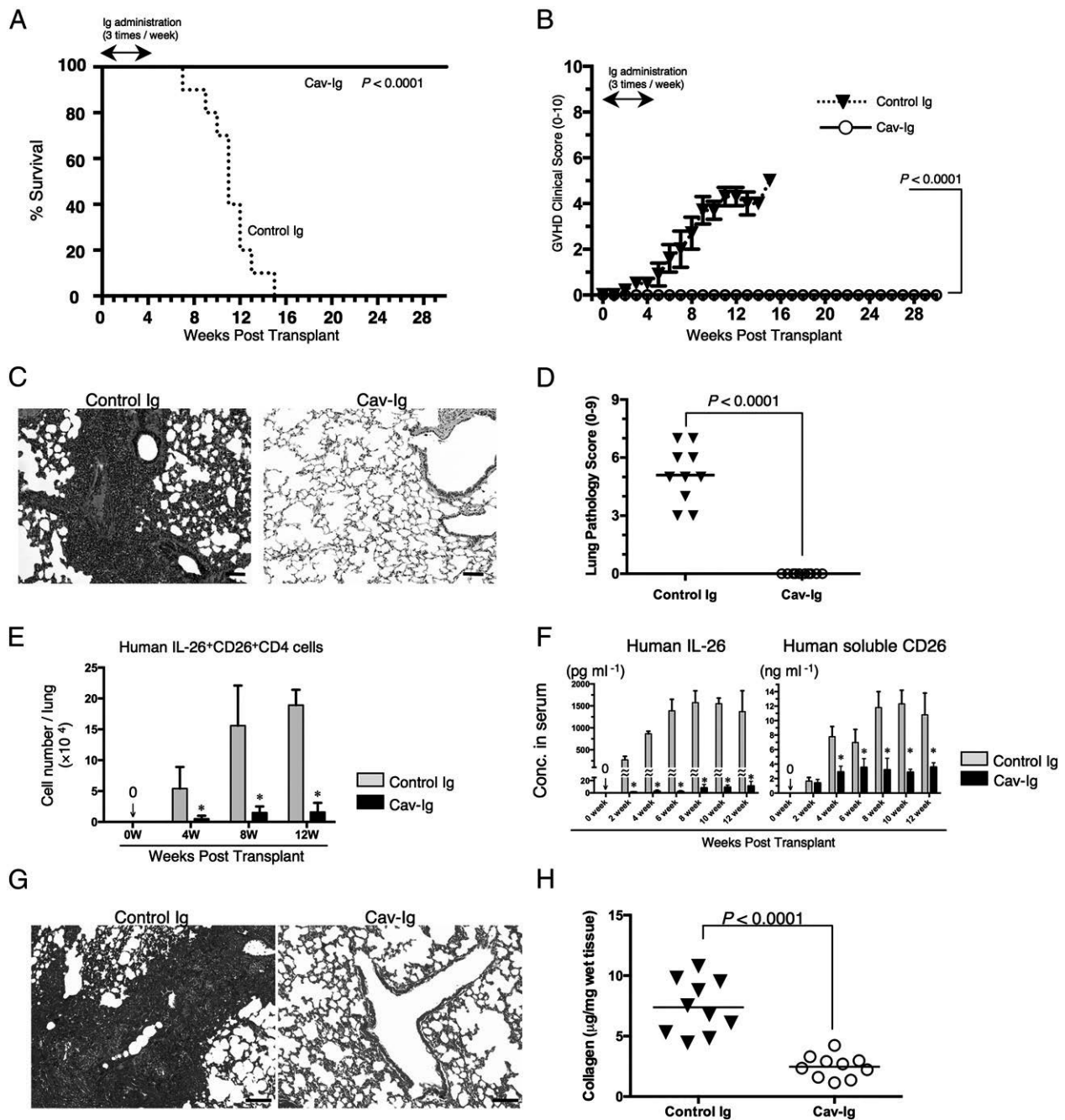


**FIGURE 5.** Administration of Cav-Ig prevents obliterative bronchiolitis by reducing level of IL-26<sup>+</sup>CD26<sup>+</sup>CD4 cells and collagen deposition. Sublethally irradiated NOG mice were transplanted with  $1 \times 10^7$  MNCs isolated from HuCB. Cav-Ig or control Ig (each 100  $\mu\text{g}/\text{dose}$ ) was administered i.p. thrice per week, beginning at day +1 after transplantation until day +28. **(A)** Overall survival and **(B)** clinical GVHD score (mean  $\pm$  SEM). Data are cumulative results from three independent experiments (for each,  $n = 10$ ). **(C)** H&E staining of the lung of recipients administered with control Ig or Cav-Ig group (6 wk posttransplantation). Representative histology is shown from three independent experiments (for each,  $n = 10$ ). Original magnification  $\times 100$ . Scale bars, 100  $\mu\text{m}$ . **(D)** Pathologic damage in the lung of recipients administered with Cav-Ig or control Ig was examined at 6 wk posttransplantation, using a semi-quantitative scoring system. Each dot indicates individual value, and horizontal bars indicate mean value. **(E)** Absolute cell number of human IL-26<sup>+</sup>CD26<sup>+</sup>CD4 cells in the lung of recipients of Cav-Ig or control Ig group. Data are cumulative results from three independent experiments (for each,  $n = 10$  in Cav-Ig group, and  $n = 10$  at 0–4 wk,  $n = 9$  at 8 wk, and  $n = 2$  at 12 wk in control Ig group).  $*p < 0.0001$  versus corresponding control Ig group. **(F)** Sera of recipients of Cav-Ig or control Ig group were collected at the indicated week posttransplantation, and serum levels of human IL-26 and soluble CD26/DPP4 were quantified. Data are cumulative results from three independent experiments (for each,  $n = 10$  in Cav-Ig group, and  $n = 10$  at 0–6 wk,  $n = 9$  at 8 wk,  $n = 7$  at 10 wk, and  $n = 2$  at 12 wk in control Ig group).  $*p < 0.0001$  versus corresponding control Ig group. **(G)** Collagen deposition was determined in the lung tissues of recipients of Cav-Ig or control Ig group (6 wk posttransplantation) with an Azan-Mallory staining. Representative histology is shown from three independent experiments (for each,  $n = 6$ ). Original magnification  $\times 100$ . Scale bars, 100  $\mu\text{m}$ . **(H)** Collagen contents in the lung of recipients of Cav-Ig or control Ig group (6 wk posttransplantation) were quantified by Sircol Collagen Assay. The mean number ( $\pm$ SEM) of total collagen contents ( $\mu\text{g}$ ) per wet lung tissue weight (mg) was determined from three independent experiments (for each,  $n = 10$ ). Decreased collagen contents were clearly observed in recipients of Cav-Ig group. Each dot indicates individual value, and horizontal bars indicate mean value.

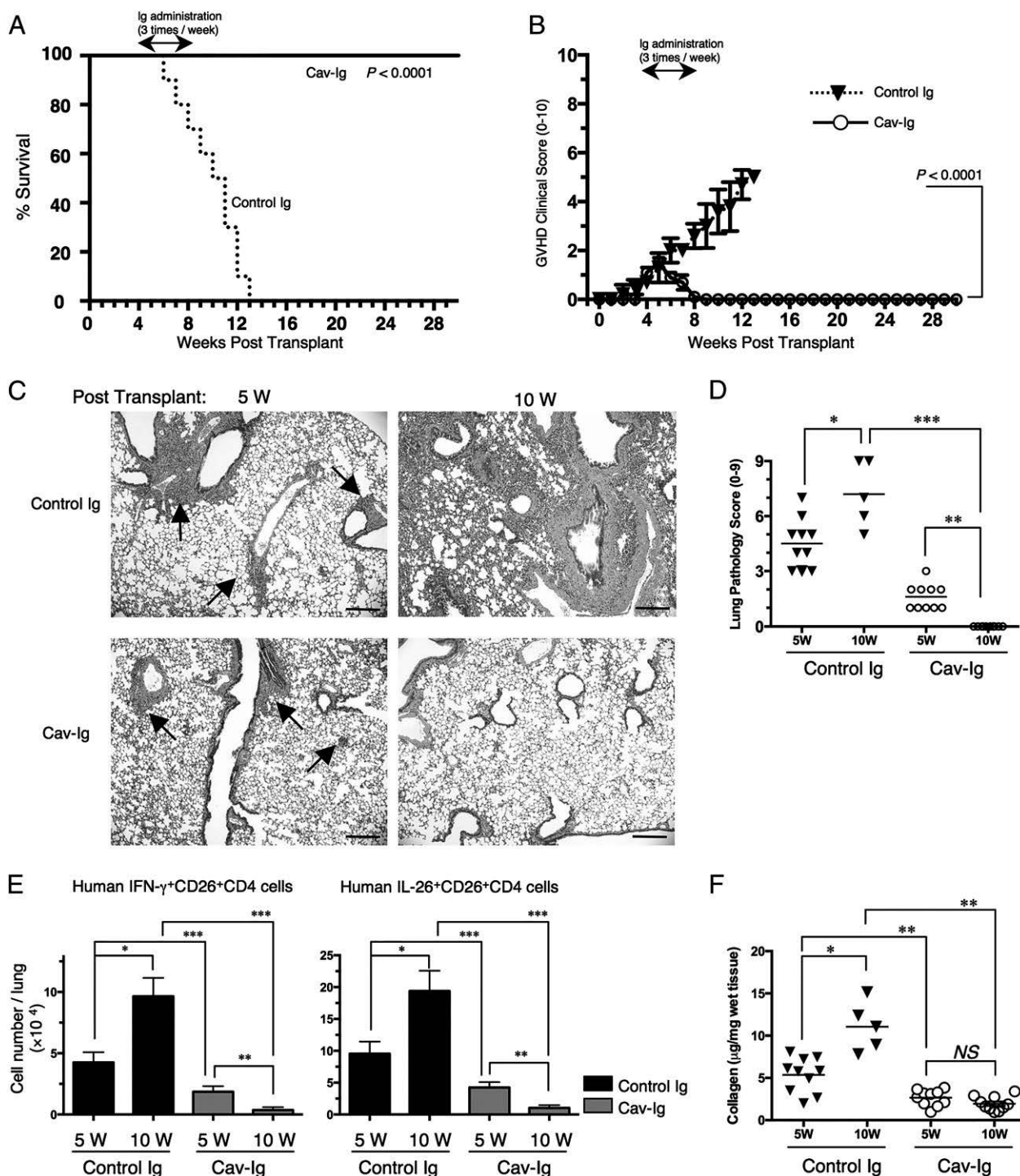


**FIGURE 6.** Administration of Cav-Ig during early GVHD development impedes lethal GVHD by reducing level of IL-26 $^+$ CD26 $^+$ CD4 cells and collagen deposition in the lung. Sublethally irradiated NOG mice were transplanted with  $1 \times 10^7$  MNCs isolated from HuCB. Cav-Ig or control Ig (each 100  $\mu$ g/dose) was administered i.p. thrice per week, beginning at day +29 after transplantation until day +56. **(A)** Overall survival and **(B)** clinical GVHD score (mean  $\pm$  SEM). Data are cumulative results from three independent experiments (for each,  $n = 10$ ). **(C)** H&E staining of the lung tissues of control Ig group and Cav-Ig group at 5 or 10 wk posttransplantation. Representative histology is shown from three independent experiments (for each,  $n = 10$  in Cav-Ig group, and  $n = 10$  at 5 wk and  $n = 5$  at 10 wk in control Ig group). Arrows indicate perivascular and peribronchial inflammation of the small airway. Original magnification  $\times 100$ . Scale bars, 100  $\mu$ m. **(D)** Pathologic damage in the lung of recipients administered with Cav-Ig or control Ig was examined at 5 and 10 wk posttransplantation using a semiquantitative scoring system. Each dot indicates individual value, and horizontal bars indicate mean value. Data are cumulative results from three independent experiments (for each,  $n = 10$  in Cav-Ig group, and  $n = 10$  at 5 wk and  $n = 5$  at 10 wk in control Ig group). \* $P < 0.01$ , \*\*\*\* $P < 0.0001$ . **(E)** Absolute cell number of human IFN- $\gamma^+$  or IL-26 $^+$ CD26 $^+$ CD4 cells in the lung of recipients of Cav-Ig or control Ig group. Data are cumulative results from three independent experiments (for each,  $n = 10$  in Cav-Ig group, and  $n = 10$  at 5 wk and  $n = 5$  at 10 wk in control Ig group). \*\*\*\* $P < 0.0001$ . **(F)** Collagen contents in the lung of recipients of Cav-Ig or control Ig group (5 and 10 wk posttransplantation) were quantified by Sircol Collagen Assay. The mean number ( $\pm$ SEM) of total collagen contents ( $\mu$ g) per wet lung tissue weight (mg) was determined from three independent experiments (for each,  $n = 10$  in Cav-Ig group, and  $n = 10$  at 5 wk and  $n = 5$  at 10 wk in control Ig group). Each dot indicates individual value, and horizontal bars indicate mean value. \*\*\* $P < 0.0001$ .

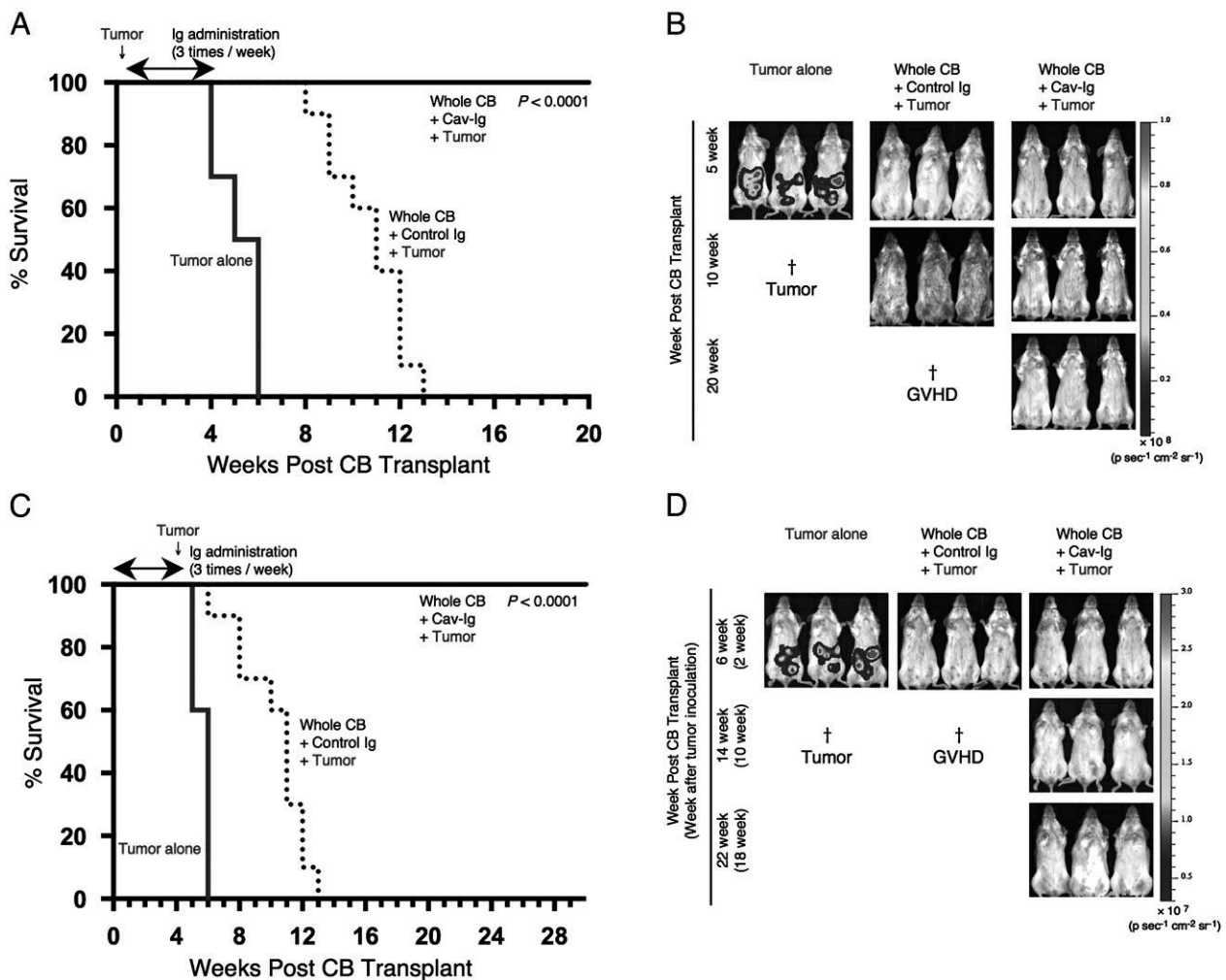


**FIGURE 7.** Cav-Ig preserves GVL effect. **(A)** NOG mice were irradiated at sublethal dose (200 cGy) and the next day were inoculated with  $1 \times 10^4$  A20-luc cells via tail vein, and then were transplanted the following day with  $1 \times 10^7$  MNCs isolated from HuCB. Cav-Ig or control Ig (each 100  $\mu$ g/dose) was administered i.p. thrice per week, beginning at day +1 after transplantation until day +28. Overall survival is depicted from cumulative results from three independent experiments (for each,  $n = 10$ ).  $p < 0.0001$  versus recipients of control Ig by log-rank test. **(B)** In vivo bioluminescence imaging was performed at the indicated time points after treatment, as described in (A). Representative mice are shown. Ruffled fur consistent with skin GVHD is shown in recipients of control Ig group at 10 wk posttransplant (middle panel). †Death of all mice in the group of tumor alone or control Ig groups. **(C)** Sublethally irradiated NOG mice were transplanted with MNCs isolated from HuCB. Cav-Ig or control Ig was administered i.p. thrice per week, beginning at day +1 after transplantation until day +28. A total of  $1 \times 10^5$  A20-luc cells was inoculated via tail vein on day +28 posttransplantation. Overall survival is depicted from cumulative results from three independent experiments (for each,  $n = 10$ ).  $p < 0.0001$  versus recipients of control Ig by log-rank test. **(D)** In vivo bioluminescence imaging was performed at the indicated time points after treatment, as described in (C). Representative mice are shown. Slightly ruffled fur consistent with skin GVHD is shown in recipients of control Ig group at 6 wk posttransplant (middle panel). †Death of all mice in the group of tumor alone or control Ig groups.

completely abrogated in  $\Delta$ CNS-77 Tg mice (41). Moreover, IFN- $\gamma$ <sup>+</sup>CD4<sup>+</sup> T cells infiltrating in the lung of obliterative bronchiolitis exclusively expressed IL-26, whereas IL-17A<sup>+</sup>CD4<sup>+</sup> T cells were negative for IL-26. To characterize the role of IL-26<sup>+</sup>CD26<sup>+</sup>CD4<sup>+</sup> T cells in patients with obliterative bronchiolitis, we analyzed the lung specimen of a patient with dyspnea and ground glass opacity detected on the chest X-ray examination on day +95 of alloPBSCT for ALL. Although a limited number of samples was obtained because invasive examinations including lung biopsy are not necessary to diagnose lung cGVHD (4), our data obtained from a human lung sample confirm the findings shown in the above murine model. Collectively, our data imply that IL-26<sup>+</sup>CD26<sup>+</sup> Th1 cells play an important role in the pathogenesis of obliterative bronchiolitis observed in a cGVHD patient as well as in whole CB transplant mice. Regarding its specific receptor, IL-26 primarily binds to IL-20RA, followed by recruitment of IL-

10RB (26). Although IL-10RB is broadly expressed on most cell types and tissues, IL-20RA is not expressed in lymphoid organs, but is expressed in the lung as well as skin (59). It is thus conceivable that IL-26-related fibroproliferation occurs in the lung and skin.

It has been reported that allogeneic Th17 cells could induce severe forms of acute GVHD associated with cutaneous and pulmonary pathologic manifestations (60). Moreover, in studies of lung transplant recipients using murine model and human samples, IL-17 was shown to be involved in the pathogenesis of obliterative bronchiolitis associated with chronic rejection (61, 62). In the current study, we demonstrated that levels of *IL17A* and IL-17-producing cells were slightly increased in CD4<sup>+</sup> T cells infiltrating the obliterative bronchiolitis lung. Although the role of IL-17 in cGVHD is still unclear (63), we could not exclude the possibility that small populations of IL-17<sup>+</sup>CD4<sup>+</sup> T cells are involved in

the pathogenesis of obliterative bronchiolitis in cGVHD. In addition, Th17 cells display a great degree of context-dependent plasticity, as they are capable of acquiring functional characteristics of Th1 cells (64). This late plasticity may play a role in the development of obliterative bronchiolitis regulated by CD26<sup>+</sup>CD4<sup>+</sup> Th1 cells, and may be associated with the emergence of IL-26<sup>+</sup>CD26<sup>+</sup> Th1 cells.

Several causes of obliterative bronchiolitis after alloHSCt have been proposed, including donor-derived T cell-mediated injury, several profibrotic factors, and autoantibody deposition (7). Recent report using a murine model showed that donor-derived B cell activation and maturation with the aid of T follicular helper cells were necessary for cGVHD, and bronchiolitis obliterans syndrome was reversed by the abrogation of IL-21 signaling (65). However, our present model using human donor cells did not demonstrate the presence of B cells in the lung of obliterative bronchiolitis, whereas a substantial B cell population was detected in the recipient PBL. In fact, no direct evidence for a causal relationship for autoantibodies or alloantibodies in the pathogenesis of organ manifestation of cGVHD has been observed in humans (9). Furthermore, cGVHD of the visceral organs seemed to respond poorly to B cell depletion therapy such as rituximab (7, 9). It is speculated that this observed discrepancy is due to differences in the B cell maturation process between mice and humans (11). Despite these limitations of murine or humanized murine models, targeting CD4 T cells to control cGVHD is a reasonable therapeutic approach because T cell help plays a pivotal role in B cell maturation and activation in cGVHD (66).

A related issue concerns the process of B cell development in humanized mice. Previous work has shown that reconstituted human CD45<sup>+</sup> cells in other models of humanized mice were overcome by CD3<sup>+</sup> T cells within several months of transplantation due to reduced B cell development (40). However, given the fact that HuCB contains ample HSC as well as naive lymphocytes, the use of HuCB as donor cells led to sustained recovery of lymphocytes in the recipient PBL, as had also been reported by other investigators (24, 38, 39, 67). In addition, it has been demonstrated that specific Abs in human B cells generated in the humanized mice transplanted with HSC isolated from HuCB are effectively synthesized (23, 24, 38, 40). A potential concern regarding the applicability of results obtained from our model is the lack of intestinal GVHD. Because recent work demonstrated that neutrophils play an important role in intestinal GVHD (68), one possible explanation for the lack of intestinal GVHD in our model is that achieving effective engraftment of neutrophils in our model is particularly difficult (40). Despite the limitations of cross-species comparisons, our study provides insights into the pathogenesis of clinical pulmonary cGVHD induced by human lymphocytes. Furthermore, data obtained from our study have identified potential novel therapeutic targets in the management of clinical cGVHD.

Because we previously showed an effectiveness of anti-CD26 mAb on an aGVHD model using adult PBL (13), we performed preliminary testing of anti-CD26 mAb effect on recipient mice of whole CB transplant, and found a high incidence of graft failure (data not shown). Our speculation of the reason for this failure is as follows: we previously reported that HuCB CD4 T cells broadly express CD26 (21), and other investigators observed that CD34<sup>+</sup>CD38<sup>low/-</sup> or CD34<sup>+</sup>CD38<sup>+</sup> hematopoietic stem/progenitor cells in HuCB preferentially express CD26 (69). These findings suggest that treatment with anti-CD26 mAb in a HuCB transplant model may reduce the levels of hematopoietic stem/progenitor and/or CD4 T cells in the graft of HuCB, resulting in increased graft failure. Meanwhile, it has been reported that endogenous CD26 expression on donor cells negatively regulates homing and engraftment (70), and that inhibition of DPP4 enzyme activity enhances engraftment of

hematopoietic cells in mice and humans (71, 72). In the current study, we observed no difference of engraftment between Cav-Ig- and control Ig-treated mice. It is conceivable that continuous inhibition of DPP4 enzyme activity was not achieved by the alternate-day schedule of administration of Cav-Ig used in the current study, with the resultant lack of continuous inhibition of related chemokines, cytokines, and CSFs (71).

In addition to issues involving the use of anti-CD26 mAb, it is important to point out that there may be potential adverse events such as off-target effects associated with the proposed use of Cav-Ig therapy. Although caveolin-1 exists in the inner surface of most cell types (49), its N terminus is detected on endothelial cells as well as APCs after activation (73). Therefore, it is possible that Cav-Ig binds to cell surface caveolin-1 and is consumed in such endothelial cells. Other issues relate to the GVL effects. Our data demonstrated that Cav-Ig clearly impeded GVHD in our model with preservation of GVL effects. We speculate that CD26-dependent xenogeneic priming of CD4 T cells is inhibited by Cav-Ig (13, 20), whereas CD28-dependent GVL effects are exerted after engraftment (74). However, studying GVHD and GVL effects that require similar CD4- or CD8-dependent pathways with the use of primary leukemic cells rather than cell lines should help to generate reliable models of GVL. Despite these concerns, our work revealed no abnormal findings in the vessels and organs of Cav-Ig-treated recipient mice with preservation of the GVL effect, hence suggesting a potentially promising novel therapeutic approach for controlling cGVHD.

The administration of Cav-Ig may potentially result in renal damage because CD26 is also expressed in the kidney (44, 45). However, we observed no pathological changes in the kidney in mice treated with Cav-Ig (data not shown). These findings may be partially due to the fact that CD26 in the kidney is mainly expressed in the proximal tubules (75), and that immune complex deposition of complexes consisting of Cav-Ig and membrane-bound CD26 did not occur in the glomeruli to cause renal injury.

In conclusion, our present work demonstrates that caveolin-1 blockade can control pulmonary GVHD by suppressing the immune functions of donor-derived T cells and decreasing IL-26 production. Moreover, IL-26<sup>+</sup>CD26<sup>+</sup>CD4 T cell infiltration appears to play a significant role in the lung of obliterative bronchiolitis. Although complete suppression of cGVHD with current interventional strategies represents a difficult challenge at the present time, our data demonstrate that control of cGVHD clinical findings can be achieved in a murine experimental system by regulating IL-26<sup>+</sup>CD26<sup>+</sup>CD4 T cells with Cav-Ig. Our work also suggests that Cav-Ig treatment may be a novel therapeutic approach for chronic inflammatory diseases, including RA and inflammatory bowel diseases, in which IL-26 plays an important role.

## Disclosures

The authors have no financial conflicts of interest.

## References

- Champlin, R. E., N. Schmitz, M. M. Horowitz, B. Chapuis, R. Chopra, J. J. Cornelissen, R. P. Gale, J. M. Goldman, F. R. Loberiza, Jr., B. Hertenstein, et al. 2000. Blood stem cells compared with bone marrow as a source of hematopoietic cells for allogeneic transplantation. *Blood* 95: 3702–3709.
- Socié, G., and J. Ritz. 2014. Current issues in chronic graft-versus-host disease. *Blood* 124: 374–384.
- Baird, K., and S. Z. Pavletic. 2006. Chronic graft versus host disease. *Curr. Opin. Hematol.* 13: 426–435.
- Filipovich, A. H., D. Weisdorf, S. Pavletic, G. Socié, J. R. Wingard, S. J. Lee, P. Martin, J. Chien, D. Przepiorka, D. Couriel, et al. 2005. National Institutes of Health consensus development project on criteria for clinical trials in chronic graft-versus-host disease: I. Diagnosis and staging working group report. *Biol. Blood Marrow Transplant.* 11: 945–956.

5. Bergeron, A., C. Godet, S. Chevet, G. Lorillon, R. Peffault de Latour, T. de Revel, M. Robin, P. Ribaud, G. Socié, and A. Tazi. 2013. Bronchiolitis obliterans syndrome after allogeneic hematopoietic SCT: phenotypes and prognosis. *Bone Marrow Transplant.* 48: 819–824.
6. Chu, Y. W., and R. E. Gress. 2008. Murine models of chronic graft-versus-host disease: insights and unresolved issues. *Biol. Blood Marrow Transplant.* 14: 365–378.
7. Barker, A. F., A. Bergeron, W. N. Rom, and M. I. Hertz. 2014. Obliterative bronchiolitis. *N. Engl. J. Med.* 370: 1820–1828.
8. Reddy, P., K. Johnson, J. P. Uberti, C. Reynolds, S. Silver, L. Ayash, T. M. Braun, and V. Ratanatharathorn. 2006. Nephrotic syndrome associated with chronic graft-versus-host disease after allogeneic hematopoietic stem cell transplantation. *Bone Marrow Transplant.* 38: 351–357.
9. Shimabukuro-Vornhagen, A., M. J. Hallek, R. F. Storb, and M. S. von Bergwelt-Baildon. 2009. The role of B cells in the pathogenesis of graft-versus-host disease. *Blood* 114: 4919–4927.
10. Seok, J., H. S. Warren, A. G. Cuenca, M. N. Mindrinos, H. V. Baker, W. Xu, D. R. Richards, G. P. McDonald-Smith, H. Gao, L. Hennessy, et al. 2013. Genomic responses in mouse models poorly mimic human inflammatory diseases. *Proc. Natl. Acad. Sci. USA* 110: 3507–3512.
11. Benítez, A., A. J. Weldon, L. Tatossyan, V. Velkuru, S. Lee, T. A. Milford, O. L. Francis, S. Hsu, K. Nazeri, C. M. Casiano, et al. 2014. Differences in mouse and human nonmemory B cell pools. *J. Immunol.* 192: 4610–4619.
12. Antin, J. H., B. E. Bierer, B. R. Smith, J. Ferrara, E. C. Guinan, C. Sieff, D. E. Golan, R. M. Macklis, N. J. Tarbell, E. Lynch, et al. 1991. Selective depletion of bone marrow T lymphocytes with anti-CD5 monoclonal antibodies: effective prophylaxis for graft-versus-host disease in patients with hematologic malignancies. *Blood* 78: 2139–2149.
13. Hatano, R., K. Ohnuma, J. Yamamoto, N. H. Dang, T. Yamada, and C. Morimoto. 2013. Prevention of acute graft-versus-host disease by humanized anti-CD26 monoclonal antibody. *Br. J. Haematol.* 162: 263–277.
14. Fox, D. A., R. E. Hussey, K. A. Fitzgerald, O. Acuto, C. Poole, L. Palley, J. F. Daley, S. F. Schlossman, and E. L. Reinherz. 1984. Ta1, a novel 105 KD human T cell activation antigen defined by a monoclonal antibody. *J. Immunol.* 133: 1250–1256.
15. Morimoto, C., and S. F. Schlossman. 1998. The structure and function of CD26 in the T-cell immune response. *Immunol. Rev.* 161: 55–70.
16. Ohnuma, K., N. H. Dang, and C. Morimoto. 2008. Revisiting an old acquaintance: CD26 and its molecular mechanisms in T cell function. *Trends Immunol.* 29: 295–301.
17. Ohnuma, K., O. Hosono, N. H. Dang, and C. Morimoto. 2011. Dipeptidyl peptidase in autoimmune pathophysiology. *Adv. Clin. Chem.* 53: 51–84.
18. Ohnuma, K., Y. Munakata, T. Ishii, S. Iwata, S. Kobayashi, O. Hosono, H. Kawasaki, N. H. Dang, and C. Morimoto. 2001. Soluble CD26/dipeptidyl peptidase IV induces T cell proliferation through CD86 up-regulation on APCs. *J. Immunol.* 167: 6745–6755.
19. Ohnuma, K., T. Yamochi, M. Uchiyama, K. Nishibashi, N. Yoshikawa, N. Shimizu, S. Iwata, H. Tanaka, N. H. Dang, and C. Morimoto. 2004. CD26 up-regulates expression of CD86 on antigen-presenting cells by means of caveolin-1. *Proc. Natl. Acad. Sci. USA* 101: 14186–14191.
20. Ohnuma, K., M. Uchiyama, R. Hatano, W. Takasawa, Y. Endo, N. H. Dang, and C. Morimoto. 2009. Blockade of CD26-mediated T cell costimulation with soluble caveolin-1-Ig fusion protein induces anergy in CD4<sup>+</sup>T cells. *Biochem. Biophys. Res. Commun.* 386: 327–332.
21. Kobayashi, S., K. Ohnuma, M. Uchiyama, K. Iino, S. Iwata, N. H. Dang, and C. Morimoto. 2004. Association of CD26 with CD45RA outside lipid rafts attenuates cord blood T-cell activation. *Blood* 103: 1002–1010.
22. Sato, K., H. Nagayama, and T. A. Takahashi. 1999. Aberrant CD3- and CD28-mediated signaling events in cord blood T cells are associated with dysfunctional regulation of Fas ligand-mediated cytotoxicity. *J. Immunol.* 162: 4464–4471.
23. Shultz, L. D., M. A. Brehm, J. V. Garcia-Martinez, and D. L. Greiner. 2012. Humanized mice for immune system investigation: progress, promise and challenges. *Nat. Rev. Immunol.* 12: 786–798.
24. Tezuka, K., R. Xun, M. Tei, T. Ueno, M. Tanaka, N. Takenouchi, and J. Fujisawa. 2014. An animal model of adult T-cell leukemia: humanized mice with HTLV-1-specific immunity. *Blood* 123: 346–355.
25. Morimoto, C., Y. Torimoto, G. Levinson, C. E. Rudd, M. Schrieber, N. H. Dang, N. L. Letvin, and S. F. Schlossman. 1989. IF7, a novel cell surface molecule, involved in helper function of CD4 cells. *J. Immunol.* 143: 3430–3439.
26. Hör, S., H. Pirzer, L. Dumoutier, F. Bauer, S. Wittmann, H. Sticht, J. C. Renauld, R. de Waal Malefyt, and H. Fickenscher. 2004. The T-cell lymphokine interleukin-26 targets epithelial cells through the interleukin-20 receptor 1 and interleukin-10 receptor 2 chains. *J. Biol. Chem.* 279: 33343–33351.
27. Ohnuma, K., M. Uchiyama, T. Yamochi, K. Nishibashi, O. Hosono, N. Takahashi, S. Kina, H. Tanaka, X. Lin, N. H. Dang, and C. Morimoto. 2007. Caveolin-1 triggers T-cell activation via CD26 in association with CARMA1. *J. Biol. Chem.* 282: 10117–10131.
28. Collins, P. L., S. Chang, M. Henderson, M. Soutto, G. M. Davis, A. G. McLeod, M. J. Townsend, L. H. Glimcher, D. P. Mortlock, and T. M. Aune. 2010. Distal regions of the human *IFNG* locus direct cell type-specific expression. *J. Immunol.* 185: 1492–1501.
29. Cooke, K. R., L. Kobzik, T. R. Martin, J. Brewer, J. Delmonte, Jr., J. M. Crawford, and J. L. Ferrara. 1996. An experimental model of idiopathic pneumonia syndrome after bone marrow transplantation: I. The roles of minor H antigens and endotoxin. *Blood* 88: 3230–3239.
30. Anderson, B. E., J. M. McNiff, C. Matte, I. Athanasiadis, W. D. Shlomchik, and M. J. Shlomchik. 2004. Recipient CD4<sup>+</sup> T cells that survive irradiation regulate chronic graft-versus-host disease. *Blood* 104: 1565–1573.
31. Kaplan, D. H., B. E. Anderson, J. M. McNiff, D. Jain, M. J. Shlomchik, and W. D. Shlomchik. 2004. Target antigens determine graft-versus-host disease phenotype. *J. Immunol.* 173: 5467–5475.
32. Aoe, K., V. J. Amatya, N. Fujimoto, K. Ohnuma, O. Hosono, A. Hiraki, M. Fujii, T. Yamada, N. H. Dang, Y. Takeshima, et al. 2012. CD26 overexpression is associated with prolonged survival and enhanced chemosensitivity in malignant pleural mesothelioma. *Clin. Cancer Res.* 18: 1447–1456.
33. Hatano, R., K. Ohnuma, J. Yamamoto, N. H. Dang, and C. Morimoto. 2013. CD26-mediated co-stimulation in human CD8<sup>+</sup> T cells provokes effector function via pro-inflammatory cytokine production. *Immunology* 138: 165–172.
34. Ohnuma, K., T. Saito, R. Hatano, O. Hosono, S. Iwata, N. H. Dang, H. Ninomiya, and C. Morimoto. 2014. Comparison of two commercial ELISAs against an in-house ELISA for measuring soluble CD26 in human serum. *J. Clin. Lab. Anal.* DOI: 10.1002/jcla.21736.
35. Chen, X., J. Dodge, R. Komorowski, and W. R. Drobyski. 2013. A critical role for the retinoic acid signaling pathway in the pathophysiology of gastrointestinal graft-versus-host disease. *Blood* 121: 3970–3980.
36. Yamamoto, J., K. Ohnuma, R. Hatano, T. Okamoto, E. Komiya, H. Yamazaki, S. Iwata, N. H. Dang, K. Aoe, T. Kishimoto, et al. 2014. Regulation of somatostatin receptor 4-mediated cytostatic effects by CD26 in malignant pleural mesothelioma. *Br. J. Cancer* 110: 2232–2245.
37. Ito, M., H. Hiramatsu, K. Kobayashi, K. Suzue, M. Kawahata, K. Hioki, Y. Ueyama, Y. Koyanagi, K. Sugamura, K. Tsuji, et al. 2002. NOD/SCID/ $\gamma^{\text{null}}$  mouse: an excellent recipient mouse model for engraftment of human cells. *Blood* 100: 3175–3182.
38. Matsumura, T., Y. Kametani, K. Ando, Y. Hirano, I. Katano, R. Ito, M. Shiina, H. Tsukamoto, Y. Saito, Y. Tokuda, et al. 2003. Functional CD5<sup>+</sup> B cells develop predominantly in the spleen of NOD/SCID/ $\gamma^{\text{null}}$  (NOD) mice transplanted either with human umbilical cord blood, bone marrow, or mobilized peripheral blood CD34<sup>+</sup> cells. *Exp. Hematol.* 31: 789–797.
39. Yahata, T., K. Ando, Y. Nakamura, Y. Ueyama, K. Shimamura, N. Tamaoki, S. Kato, and T. Hotta. 2002. Functional human T lymphocyte development from cord blood CD34<sup>+</sup> cells in nonobese diabetic/Shi-*scid*, IL-2 receptor  $\gamma$  null mice. *J. Immunol.* 169: 204–209.
40. Ito, R., T. Takahashi, I. Katano, and M. Ito. 2012. Current advances in humanized mouse models. *Cell. Mol. Immunol.* 9: 208–214.
41. Collins, P. L., M. A. Henderson, and T. M. Aune. 2012. Lineage-specific adjacent *IFNG* and *IL26* genes share a common distal enhancer element. *Genes Immun.* 13: 481–488.
42. Donnelly, R. P., F. Sheikh, H. Dickensheets, R. Savan, H. A. Young, and M. R. Walter. 2010. Interleukin-26: an IL-10-related cytokine produced by Th17 cells. *Cytokine Growth Factor Rev.* 21: 393–401.
43. Bengsch, B., B. Seigel, T. Flecken, J. Wolanski, H. E. Blum, and R. Thimme. 2012. Human Th17 cells express high levels of enzymatically active dipeptidylpeptidase IV (CD26). *J. Immunol.* 188: 5438–5447.
44. Gorrell, M. D., V. Gysbers, and G. W. McCaughan. 2001. CD26: a multifunctional integral membrane and secreted protein of activated lymphocytes. *Scand. J. Immunol.* 54: 249–264.
45. Wang, Z., C. Grigo, J. Steinbeck, S. von Hörsten, K. Amann, and C. Daniel. 2014. Soluble DPP4 originates in part from bone marrow cells and not from the kidney. *Peptides* 57: 109–117.
46. Yi, T., Y. Chen, L. Wang, G. Du, D. Huang, D. Zhao, H. Johnston, J. Young, I. Todorov, D. T. Umetsu, et al. 2009. Reciprocal differentiation and tissue-specific pathogenesis of Th1, Th2, and Th17 cells in graft-versus-host disease. *Blood* 114: 3101–3112.
47. Fickenscher, H., and H. Pirzer. 2004. Interleukin-26. *Int. Immunopharmacol.* 4: 609–613.
48. Kloosterboer, F. M., S. A. van Luxemburg-Heijs, R. Willemze, and J. H. Falkenburg. 2006. Similar potential to become activated and proliferate but differential kinetics and profiles of cytokine production of umbilical cord blood T cells and adult blood naive and memory T cells. *Hum. Immunol.* 67: 874–883.
49. Engelman, J. A., X. Zhang, F. Galbati, D. Volonte, F. Sotgia, R. G. Pestell, C. Minetti, P. E. Scherer, T. Okamoto, and M. P. Lisanti. 1998. Molecular genetics of the caveolin gene family: implications for human cancers, diabetes, Alzheimer disease, and muscular dystrophy. *Am. J. Hum. Genet.* 63: 1578–1587.
50. Soiffer, R. 2008. Immune modulation and chronic graft-versus-host disease. *Bone Marrow Transplant.* 42(Suppl. 1): S66–S69.
51. Wu, C. J., and J. Ritz. 2009. Revealing tumor immunity after hematopoietic stem cell transplantation. *Clin. Cancer Res.* 15: 4515–4517.
52. Knappe, A., S. Hör, S. Wittmann, and H. Fickenscher. 2000. Induction of a novel cellular homolog of interleukin-10, AK155, by transformation of T lymphocytes with herpesvirus saimiri. *J. Virol.* 74: 3881–3887.
53. Wilson, N. J., K. Boniface, J. R. Chan, B. S. McKenzie, W. M. Blumenschein, J. D. Mattson, B. Basham, K. Smith, T. Chen, F. Morel, et al. 2007. Development, cytokine profile and function of human interleukin 17-producing helper T cells. *Nat. Immunol.* 8: 950–957.
54. Corvaisier, M., Y. Delneste, H. Jeanvoine, L. Preisser, S. Blanchard, E. Garo, E. Hoppe, B. Barré, M. Audran, B. Bouvard, et al. 2012. IL-26 is overexpressed in rheumatoid arthritis and induces proinflammatory cytokine production and Th17 cell generation. *PLoS Biol.* 10: e1001395.
55. Goris, A., M. G. Marrosu, and K. Vandenbroeck. 2001. Novel polymorphisms in the IL-10 related AK155 gene (chromosome 12q15). *Genes Immun.* 2: 284–286.
56. Vandenbroeck, K., S. Cunningham, A. Goris, I. Alloza, S. Heggarty, C. Graham, A. Bell, and M. Rooney. 2003. Polymorphisms in the interferon-gamma/



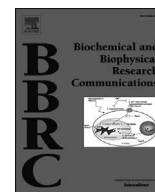
- interleukin-26 gene region contribute to sex bias in susceptibility to rheumatoid arthritis. *Arthritis Rheum.* 48: 2773–2778.
57. Silverberg, M. S., J. H. Cho, J. D. Rioux, D. P. McGovern, J. Wu, V. Annese, J. P. Achkar, P. Goyette, R. Scott, W. Xu, et al. 2009. Ulcerative colitis-risk loci on chromosomes 1p36 and 12q15 found by genome-wide association study. *Nat. Genet.* 41: 216–220.
  58. Miot, C., E. Beaumont, D. Duluc, H. Le Guillou-Guillemette, L. Preisser, E. Garo, S. Blanchard, I. Hubert Fouchard, C. Cr  minon, P. Lamourette, et al. 2014. IL-26 is overexpressed in chronically HCV-infected patients and enhances TRAIL-mediated cytotoxicity and interferon production by human NK cells. *Gut* DOI: 10.1136/gutjnl-2013-306604.
  59. Wolk, K., S. Kunz, K. Asadullah, and R. Sabat. 2002. Cutting edge: immune cells as sources and targets of the IL-10 family members? *J. Immunol.* 168: 5397–5402.
  60. Carlson, M. J., M. L. West, J. M. Coghill, A. Panoskaltsis-Mortari, B. R. Blazar, and J. S. Serody. 2009. In vitro-differentiated TH17 cells mediate lethal acute graft-versus-host disease with severe cutaneous and pulmonary pathologic manifestations. *Blood* 113: 1365–1374.
  61. Fan, L., H. L. Benson, R. Vittal, E. A. Mickler, R. Presson, A. J. Fisher, O. W. Cummings, K. M. Heidler, M. R. Keller, W. J. Burlingham, and D. S. Wilkes. 2011. Neutralizing IL-17 prevents obliterative bronchiolitis in murine orthotopic lung transplantation. *Am. J. Transplant.* 11: 911–922.
  62. Burlingham, W. J., R. B. Love, E. Jankowska-Gan, L. D. Haynes, Q. Xu, J. L. Bobadilla, K. C. Meyer, M. S. Hayney, R. K. Braun, D. S. Greenspan, et al. 2007. IL-17-dependent cellular immunity to collagen type V predisposes to obliterative bronchiolitis in human lung transplants. *J. Clin. Invest.* 117: 3498–3506.
  63. Serody, J. S., and G. R. Hill. 2012. The IL-17 differentiation pathway and its role in transplant outcome. *Biol. Blood Marrow Transplant.* 18: S56–S61.
  64. Muranski, P., and N. P. Restifo. 2013. Essentials of Th17 cell commitment and plasticity. *Blood* 121: 2402–2414.
  65. Flynn, R., J. Du, R. G. Veenstra, D. K. Reichenbach, A. Panoskaltsis-Mortari, P. A. Taylor, G. J. Freeman, J. S. Serody, W. J. Murphy, D. H. Munn, et al. 2014. Increased T follicular helper cells and germinal center B cells are required for cGVHD and bronchiolitis obliterans. *Blood* 123: 3988–3998.
  66. Zhang, C., I. Todorov, Z. Zhang, Y. Liu, F. Kandeel, S. Forman, S. Strober, and D. Zeng. 2006. Donor CD4<sup>+</sup> T and B cells in transplants induce chronic graft-versus-host disease with autoimmune manifestations. *Blood* 107: 2993–3001.
  67. Ishikawa, F., M. Yasukawa, B. Lyons, S. Yoshida, T. Miyamoto, G. Yoshimoto, T. Watanabe, K. Akashi, L. D. Shultz, and M. Harada. 2005. Development of functional human blood and immune systems in NOD/SCID/IL2 receptor  $\gamma$  chain<sup>null</sup> mice. *Blood* 106: 1565–1573.
  68. Schwab, L., L. Goroncy, S. Palaniyandi, S. Gautam, A. Triantafyllou, A. Mocsai, W. Reichardt, F. J. Karlsson, S. V. Radhakrishnan, K. Hanke, et al. 2014. Neutrophil granulocytes recruited upon translocation of intestinal bacteria enhance graft-versus-host disease via tissue damage. *Nat. Med.* 20: 648–654.
  69. Campbell, T. B., G. Hangoc, Y. Liu, K. Pollok, and H. E. Broxmeyer. 2007. Inhibition of CD26 in human cord blood CD34<sup>+</sup> cells enhances their engraftment of nonobese diabetic/severe combined immunodeficiency mice. *Stem Cells Dev.* 16: 347–354.
  70. Christopherson, K. W., II, G. Hangoc, C. R. Mantel, and H. E. Broxmeyer. 2004. Modulation of hematopoietic stem cell homing and engraftment by CD26. *Science* 305: 1000–1003.
  71. Broxmeyer, H. E., J. Hoggatt, H. A. O'Leary, C. Mantel, B. R. Chitteti, S. Cooper, S. Messina-Graham, G. Hangoc, S. Farag, S. L. Rohrabough, et al. 2012. Dipeptidylpeptidase 4 negatively regulates colony-stimulating factor activity and stress hematopoiesis. *Nat. Med.* 18: 1786–1796.
  72. Farag, S. S., S. Srivastava, S. Messina-Graham, J. Schwartz, M. J. Robertson, R. Abonour, K. Cornetta, L. Wood, A. Secrest, R. M. Strother, et al. 2013. In vivo DPP-4 inhibition to enhance engraftment of single-unit cord blood transplants in adults with hematological malignancies. *Stem Cells Dev.* 22: 1007–1015.
  73. Ohnuma, K., H. Inoue, M. Uchiyama, T. Yamochi, O. Hosono, N. H. Dang, and C. Morimoto. 2006. T-cell activation via CD26 and caveolin-1 in rheumatoid synovium. *Mod. Rheumatol.* 16: 3–13.
  74. Blazar, B. R., P. A. Taylor, M. W. Boyer, A. Panoskaltsis-Mortari, J. P. Allison, and D. A. Vallera. 1997. CD28/B7 interactions are required for sustaining the graft-versus-leukemia effect of delayed post-bone marrow transplantation splenocyte infusion in murine recipients of myeloid or lymphoid leukemia cells. *J. Immunol.* 159: 3460–3473.
  75. Hatano, R., T. Yamada, S. Matsuoka, S. Iwata, H. Yamazaki, E. Komiya, T. Okamoto, N. H. Dang, K. Ohnuma, and C. Morimoto. 2014. Establishment of monoclonal anti-human CD26 antibodies suitable for immunostaining of formalin-fixed tissue. *Diagn. Pathol.* 9: 30–42.



Contents lists available at ScienceDirect

Biochemical and Biophysical Research Communications

journal homepage: [www.elsevier.com/locate/ybbrc](http://www.elsevier.com/locate/ybbrc)



# The role of Cas-L/NEDD9 as a regulator of collagen-induced arthritis in a murine model



Tomoki Katayose<sup>a,1</sup>, Satoshi Iwata<sup>a,2</sup>, Naoki Oyaizu<sup>b</sup>, Osamu Hosono<sup>c</sup>,  
Taketo Yamada<sup>d,3</sup>, Nam H. Dang<sup>e</sup>, Ryo Hatano<sup>a,2</sup>, Hirotohi Tanaka<sup>a,c,4</sup>, Kei Ohnuma<sup>c,\*</sup>,  
Chikao Morimoto<sup>a,c,2</sup>

<sup>a</sup> Division of Clinical Immunology, Advanced Clinical Research Center, IMSUT Hospital, The Institute of Medical Science, The University of Tokyo, 4-6-1 Shirokanedai, Minato-ku, Tokyo 108-8639, Japan

<sup>b</sup> Department of Laboratory Medicine, IMSUT Hospital, The Institute of Medical Science, The University of Tokyo, 4-6-1 Shirokanedai, Minato-ku, Tokyo 108-8639, Japan

<sup>c</sup> Department of Rheumatology and Allergy, IMSUT Hospital, The Institute of Medical Science, The University of Tokyo, 4-6-1 Shirokanedai, Minato-ku, Tokyo 108-8639, Japan

<sup>d</sup> Department of Pathology, Keio University School of Medicine, 35 Shinanomachi, Shinjuku-ku, Tokyo, 160-8582, Japan

<sup>e</sup> Division of Hematology/Oncology, University of Florida, 1600 SW Archer Road, Box 100278, Room MSB M410A, Gainesville, FL 32610, USA

## ARTICLE INFO

### Article history:

Received 7 March 2015

Available online 3 April 2015

### Keywords:

Cas-L/NEDD9

Rheumatoid arthritis

Collagen-induced arthritis

IL-10

T cell

## ABSTRACT

Cas-L/NEDD9 is a cytoplasmic docking protein downstream of  $\beta 1$  integrin-mediated signaling pathway and is essential for cellular migration and  $\beta 1$  integrin-mediated costimulation of T cells. We previously found that increased number of Cas-L positive leukocytes migrated into the inflamed joints of HTLV-I tax transgenic mice which spontaneously develop polyarthritis, suggesting a role of Cas-L in rheumatoid arthritis (RA) pathophysiology. Our current study expanded these findings on the role of Cas-L/NEDD9 in the development of RA by analyzing the pathophysiological changes in a *Nedd9*<sup>−/−</sup> mouse collagen-induced arthritis (CIA) model. *Nedd9*<sup>−/−</sup> mice exhibited a decrease in arthritis severity as compared to *Nedd9*<sup>+/+</sup> mice. In addition, as being conducted bone marrow transplantation experiments with a CIA model, *Nedd9*<sup>−/−</sup> → *Nedd9*<sup>+/+</sup> transplant showed a decrease in the incidence and severity score of arthritis, compared to those of *Nedd9*<sup>+/+</sup> → *Nedd9*<sup>−/−</sup> transplant. For analysis of serum levels of various cytokines, IL-1 $\beta$ , IL-6, IL-17, TNF- $\alpha$ , IFN- $\gamma$  and anti-collagen antibody were decreased, while IL-4 and IL-10 levels were increased, in *Nedd9*<sup>−/−</sup> mice as compared to those in *Nedd9*<sup>+/+</sup> mice. Furthermore, collagen-mediated cellular responses of lymphocytes isolated from spleen or affected lymph nodes of *Nedd9*<sup>−/−</sup> mice were reduced. Our results strongly suggest that Cas-L/NEDD9 plays a pivotal role in the pathophysiology of CIA, and that Cas-L/NEDD9 may be a potential molecular target for the treatment of RA.

© 2015 Elsevier Inc. All rights reserved.

**Abbreviations:** BM, bone marrow; BMT, bone marrow transplantation; CII, chicken type II collagen; Cas-L, Crk-associated substrate lymphocyte type; CFA, complete Freund's adjuvant; CIA, collagen-induced arthritis; FCS, fetal calf serum; FN, fibronectin; HTLV-I, human T lymphotropic virus type I; IHC, immunohistochemistry; mAb, monoclonal antibody; LN, lymph node; NEDD9, neural precursor cell-expressed, developmentally downregulated 9; PMA, phorbol 12-myristate 13-acetate; RA, rheumatoid arthritis; TBI, total body irradiation; TCR, T cell receptor.

\* Corresponding author. Department of Therapy Development and Innovation for Immune Disorders and Cancers, Graduate School of Medicine, Juntendo University, 2-1-1, Hongo, Bunkyo-ku, Tokyo 113-8421, Japan. Fax: +81 3 3868 2310.

E-mail address: [kohnuma@juntendo.ac.jp](mailto:kohnuma@juntendo.ac.jp) (K. Ohnuma).

<sup>1</sup> Current affiliation: Department of Internal Medicine, National Hospital Organization Murayama Medical Center, 2-37-1, Gakuen, Musashimurayama, Tokyo 208-0011, Japan.

<sup>2</sup> Department of Therapy Development and Innovation for Immune Disorders and Cancers, Graduate School of Medicine, Juntendo University, 2-1-1, Hongo, Bunkyo-ku, Tokyo 113-8421, Japan.

<sup>3</sup> Department of Pathology Saitama Medical University, Morohongo 38, Moroyama-cho, Iruma-gun, Saitama 350-0459, Japan.

<sup>4</sup> Center for Antibody and Vaccine Therapy, IMSUT Hospital, The Institute of Medical Science, The University of Tokyo, 4-6-1 Shirokanedai, Minato-ku, Tokyo 108-8639, Japan.

<http://dx.doi.org/10.1016/j.bbrc.2015.03.156>

0006-291X/© 2015 Elsevier Inc. All rights reserved.

## 1. Introduction

$\beta 1$  integrins exhibit a variety of biological functions through specific interaction with their ligands including fibronectin (FN) [1]. We initially identified pp105 as the major phosphotyrosine-containing protein in H9 T-cell line stimulated with  $\beta 1$ -integrins [2,3]. Sequence analysis of isolated cDNA clone revealed homology with p130 Crk-associated substrate (Cas)/breast cancer anti-estrogen resistance 1 (BCAR1) which was identified as a tyrosine-phosphorylated protein in v-Crk and v-Src-transformed fibroblasts [4], thus designating pp105 as Crk-associated substrate lymphocyte type (Cas-L). Cas-L is identical to neural precursor cell-expressed, developmentally down-regulated 9 (NEDD9) [5] and human enhancer of filamentation 1 (HEF1) [6]. Cas-L/NEDD9/HEF1 is an integrin signaling adaptor or docking protein that consists of multiple preserved domains common to Cas family members [7]. Cas-L/NEDD9 is phosphorylated at its tyrosine residues by integrins and other stimuli. Ligation of T- and B-cell antigen receptors caused tyrosine phosphorylation of Cas-L/NEDD9, resulting in the association of Crk, Crk-L, and C3G [8]. Integrin- or integrin/T cell receptor (TCR)-elicited tyrosine phosphorylation of Cas-L/NEDD9 was mediated by focal adhesion kinase (FAK) and Src family tyrosine kinases [9]. Ectopic expression of Cas-L/NEDD9 conferred T cells with enhanced motility on the co-engagement of TCR/CD3 complex and  $\beta 1$ -integrins [10,11], suggesting a pivotal role of tyrosine-phosphorylated Cas-L/NEDD9 in TCR- and integrin-mediated cell motility.

We previously investigated the *in vivo* role of Cas-L/NEDD9 in the pathophysiology of rheumatoid arthritis (RA) in a mouse model of RA (using human T lymphotropic virus type I (HTLV-I) *tax* transgenic mice) as well as in RA patients [12]. HTLV-I transgenic mice that carry the *env*-pX gene developed high incidence of inflammatory arthropathy [13]. Our previous study demonstrated that Cas-L/NEDD9 involvement in the pathogenesis of RA-like disease in *tax* transgenic mice was mediated by its overexpression and hyperphosphorylation, resulting in markedly enhanced lymphocyte motility [12]. Moreover, we described the infiltration of Cas-L/NEDD9-positive, CD3-positive T cells into the affected joint lesion of RA patients [12]. These findings strongly suggest that Cas-L/NEDD9 plays a role in the pathophysiology of RA. However, it is unclear whether Cas-L/NEDD9 has a role in arthritis development in the absence of Tax since Cas-L/NEDD9 associates with Tax in HTLV-I-transformed cells [11]. To further characterize the role of Cas-L/NEDD9 in the pathogenesis of RA, our current work utilized a collagen-induced arthritis (CIA) model in *Nedd9*<sup>-/-</sup> mice to analyze the relevant clinical signs/symptoms, histopathology, serum levels of anti-collagen antibody and various cytokines, and lymphocytes characteristics.

## 2. Materials and methods

### 2.1. Mice

*Nedd9*<sup>-/-</sup> mice derived of C57BL/6J (B6) were generously provided by Dr. Seo from the Department of Hematology and Oncology, Graduate School of Medicine, University of Tokyo (Tokyo, Japan) [14]. Mice were used at 8–12 weeks. Animal experiments were conducted following protocols approved by the Animal Care and Use Committees at the Institute of Medical Science, University of Tokyo. All mice were housed in a specific pathogen-free facility in micro-isolator cages. All surgery was performed under sodium pentobarbital anesthesia, and all efforts were made to minimize suffering.

### 2.2. Induction of CIA and bone marrow transplantation (BMT)

CIA was induced as previously described with minor modifications [15]. Briefly, mice were injected intradermally at the base of tail with 200  $\mu$ g of chicken type II collagen (CII) (Sigma, USA) in 10 mM acetic acid, emulsified in complete Freund's adjuvant (CFA) (Difco Laboratories, USA). Twenty-one days after the first immunization, the mice were boosted by the same methods. Day of the first immunization was designated as day 0 for CIA induction. Arthritis clinical scores in CIA mice were evaluated as described in previously published literature [16]. For adoptive transfer experiments, after 6hrs of total body irradiation (TBI) at 950 cGy, *Nedd9*<sup>+/+</sup> or *Nedd9*<sup>-/-</sup> mice were injected intravenously with  $1 \times 10^6$  CD34<sup>+</sup> bone marrow (BM) cells isolated from *Nedd9*<sup>-/-</sup> (*Nedd9*<sup>-/-</sup>  $\rightarrow$  *Nedd9*<sup>+/+</sup>) or *Nedd9*<sup>+/+</sup> (*Nedd9*<sup>+/+</sup>  $\rightarrow$  *Nedd9*<sup>-/-</sup>), respectively. After 28 days and 49 days of transplantation, mice were immunized and evaluated by the same methods as described above.

### 2.3. Histopathology and immunohistochemistry (IHC)

Specimens of paw joints for histopathology and IHC were prepared by the same method as described in our previous report [12]. Antibodies used in IHC assays were anti-CD3 rabbit monoclonal antibody (mAb) (clone SP7) from Nichirei Bioscience (Japan), anti-mouse CD45R, B220 mAb (clone RA3-6B2) from BD Pharmingen (USA), and anti-Ly-6G/GR1 rat mAb (clone RB6-8C5) from Acris Antibodies (Germany).

### 2.4. Measurement of cytokines and anti-CII antibody

The collected sera were analyzed for various cytokines using Procarta Cytokine Assay (VERITAS, Tokyo, Japan) with Bio-Plex Suspension Array System (Bio-Rad Laboratories, USA). The serum antibody level to CII was evaluated using Mouse Anti-Chick Type II Collagen IgG Antibody Assay Kit (Chondrex, USA). All samples were run in triplicates.

### 2.5. Flow cytometry

The following antibodies were from BD Biosciences: Fluorescein isothiocyanate conjugated anti-mouse CD4 rat mAb (clone H129.19), phycoerythrin conjugated anti-mouse CD8 $\alpha$  rat mAb (clone 53-6.7), peridinin-chlorophyll-a Protein-Cy5.5 conjugated anti-mouse CD19 rat mAb (clone 1D3), and allophycocyanin conjugated anti-mouse TCR $\beta$  hamster mAb (clone H57-597). Analysis was performed on 2-laser FACSCalibur (BD Biosciences) and files were analyzed in FlowJo software (Tree Star, USA).

### 2.6. In vitro costimulation assay

For assay of proliferative responses to FN, CD4<sup>+</sup>T cells were purified from splenocytes isolated from *Nedd9*<sup>+/+</sup> or *Nedd9*<sup>-/-</sup> mice using mouse CD4<sup>+</sup>T cell Isolation Kit II (Miltenyi Biotec, Germany).  $1 \times 10^5$  cells per well were seeded in 96-well flat bottom plate with immobilized 0.5  $\mu$ g/ml of anti-mouse CD3 $\epsilon$  hamster mAb (clone 145-2C11, BD Pharmingen) and/or 1.0  $\mu$ g/ml of FN (BIOPUR, Switzerland). The cells were cultured for 72hrs, and pulsed with [<sup>3</sup>H]-thymidine (1 $\mu$ Ci/well; Perkin-Elmer, USA) for the last 6hrs. The incorporated radioactivity was measured using a microplate beta counter (Micro Beta Plus; Wallac, USA). For assay of proliferative responses to CII, mononuclear cells were isolated from brachial, axillary, inguinal and popliteal lymph nodes (LNs) of *Nedd9*<sup>+/+</sup> or *Nedd9*<sup>-/-</sup> mice after 6 days of CIA immunization. Single suspension cells were prepared from LN lymphocytes using Spleen

Dissociation Kit, mouse (Miltenyi Biotec).  $2 \times 10^5$  cells per well were cultured in the presence of 100 or 200  $\mu\text{g/ml}$  of CII. Cell proliferation was evaluated by the same [ $^3\text{H}$ ]-thymidine uptake assay as described above.

### 2.7. Statistical analysis

All experiments were performed in triplicates and repeated at least 3 times. Data were analyzed by two-tailed Student's *t* test for two group comparison or by ANOVA test for multiple comparison testing followed by the Tukey–Kramer *post-hoc* test. *P* values  $\leq 0.05$  were considered statistically significant. The calculations were conducted using SPSS Statistics software (IBM, USA).

## 3. Results and discussion

### 3.1. Reduced severity of CIA in *Nedd9*<sup>−/−</sup> mice

We first compared clinical signs/symptoms of arthritis between *Nedd9*<sup>+/+</sup> and *Nedd9*<sup>−/−</sup> mice following induction of CIA. The incidence of onset of arthritis in *Nedd9*<sup>−/−</sup> CIA mice was significantly decreased compared to that in *Nedd9*<sup>+/+</sup> CIA mice (Fig. 1A). Moreover, *Nedd9*<sup>−/−</sup> CIA mice exhibited decreased arthritis score compared to *Nedd9*<sup>+/+</sup> CIA mice (Fig. 1B). In addition, the severity and incidence of arthritis in *Nedd9* hetero knockout *Nedd9*<sup>+/-</sup> CIA mice were in-between those of *Nedd9*<sup>+/+</sup> and *Nedd9*<sup>−/−</sup> CIA mice (Fig. 1A and B). These data suggest that expression levels of Cas-L/NEDD9 affect induction of CIA.

To further characterize the clinical picture of the arthritis induced in this mouse model, we analyzed affected joints using planar X-ray examination. In *Nedd9*<sup>−/−</sup> CIA mice, metatarsal and tarsal bones at day 56 following the first immunization showed no significant changes as compared to findings seen in non-immunized mice (crucies in panels b and c of Fig. 1C), while metatarsal and tarsal joints of *Nedd9*<sup>+/+</sup> CIA mice exhibited narrowing, deformation and synostosis (circle in panel a of Fig. 1C). For additional analysis of the extent of arthritis, we conducted histopathologic examination using specimens of affected joints obtained at day 56 following the first immunization. As shown in Fig. 1D, *Nedd9*<sup>+/+</sup> CIA mice showed obvious thinning of articular cartilage and hyperplasia of synovium with infiltration of inflammatory cells (panels a and b), in contrast to the normal structure found in non-immunized mice (panel c). Meanwhile, the affected joint in *Nedd9*<sup>−/−</sup> CIA mice exhibited few signs of inflammation with slight thinning of articular cartilage and synovitis (panel d of Fig. 1D). To characterize the subsets of inflammatory cells found in the affected joints, we performed IHC using specimens of affected joints obtained at day 56 following the first immunization. In the affected joint of *Nedd9*<sup>+/+</sup> CIA mice, Ly-6G-positive granulocytes were predominantly found (panel a of Fig. 1E), while CD3-positive T and B220-positive B cells were at undetectable levels (panels b and c of Fig. 1E). On the other hand, in *Nedd9*<sup>−/−</sup> CIA mice, inflammatory cells were not detected by IHC in the affected joint (panels d–f of Fig. 1E). Taken together, these results suggest that Cas-L/NEDD9 has an important role in the development of inflammatory arthral changes in CIA.

To define the role of Cas-L/NEDD9 in leukocytes in the development of CIA, we next conducted adoptive transfer experiments. For this purpose, BM cells were harvested from *Nedd9*<sup>+/+</sup> or *Nedd9*<sup>−/−</sup> mice, and transplanted into the opposite recipient mice after TBI. Recipients *Nedd9*<sup>+/+</sup> mice of *Nedd9*<sup>−/−</sup> BM cells (*Nedd9*<sup>−/−</sup> → *Nedd9*<sup>+/+</sup>) showed a decrease in the incidence and severity score of arthritis, compared to those seen in recipients *Nedd9*<sup>−/−</sup> mice of *Nedd9*<sup>+/+</sup> BM cells (*Nedd9*<sup>+/+</sup> → *Nedd9*<sup>−/−</sup>) (Fig. 1F and G). Meanwhile, CIA in *Nedd9*<sup>+/+</sup> → *Nedd9*<sup>+/+</sup> BMT recipients was induced at a similar level to that seen in *Nedd9*<sup>+/+</sup> CIA mice

as shown in Fig. 1 (data not shown), while CIA was induced in *Nedd9*<sup>−/−</sup> → *Nedd9*<sup>−/−</sup> BMT recipients at lower levels than *Nedd9*<sup>+/+</sup> → *Nedd9*<sup>+/+</sup> BMT recipients, which were similar to that seen in *Nedd9*<sup>−/−</sup> CIA mice as shown in Fig. 1 (data not shown). These data strongly suggest that the presence of Cas-L/NEDD9 in leukocytes, but not in joint organs, is associated with the development of CIA, and that the development of CIA is not affected by BMT with TBI.

### 3.2. Decreased level of splenic lymphocytes in *Nedd9*<sup>−/−</sup> CIA mice

Since Cas-L/NEDD9 is involved in lymphocyte function [14,17], we next analyzed the lymphocytes in spleen and LN of *Nedd9*<sup>−/−</sup> CIA mice. For this purpose, spleen and LN cells were isolated from *Nedd9*<sup>+/+</sup> and *Nedd9*<sup>−/−</sup> mice before and after immunization, and we evaluated the cell numbers of each lymphocyte subset of spleen and LN cells. In spleen cells of *Nedd9*<sup>−/−</sup> mice, decreased levels of CD4<sup>+</sup>T, CD8<sup>+</sup>T and CD19<sup>+</sup>B cells were observed after immunization (Table 1). On the other hand, in spleen cells of *Nedd9*<sup>+/+</sup> mice, increased level of CD19<sup>+</sup>B cells was detected, while the levels of CD4<sup>+</sup>T and CD8<sup>+</sup>T cells were almost similar before and after immunization (Table 1). Moreover, among the LN lymphocytes of *Nedd9*<sup>−/−</sup> mice, increased level of CD19<sup>+</sup>B cells was observed after immunization, while the levels of CD4<sup>+</sup>T and CD8<sup>+</sup>T cells were almost similar before and after immunization (Table 1). Among the LN lymphocytes of *Nedd9*<sup>+/+</sup> mice, level of CD19<sup>+</sup>B cells was almost similar before and after immunization, and the levels of CD4<sup>+</sup>T and CD8<sup>+</sup>T cells were reduced after immunization (Table 1). Collectively, these data suggest that both T and B cells are involved in CIA of *Nedd9*<sup>−/−</sup> mice.

### 3.3. Decreased T and B cell functions in *Nedd9*<sup>−/−</sup> CIA mice

Given our previous findings that Cas-L/NEDD9 is involved in costimulatory signaling to CD3/TCR pathway associated with engagement of  $\beta 1$  integrins in T cells [2,9,18,19], we next examined T cell responses in *Nedd9*<sup>−/−</sup> or *Nedd9*<sup>+/+</sup> CIA mice. For this purpose, *in vitro* costimulation experiments using CD4<sup>+</sup>T cells purified from spleen were conducted. As shown in Fig. 2A, CD4<sup>+</sup>T cells from spleen of immunized or non-immunized *Nedd9*<sup>−/−</sup> mice exhibited decreased cellular proliferation following TCR plus FN (a ligand for  $\beta 1$  integrin) costimulation, compared to those from *Nedd9*<sup>+/+</sup> mice. Meanwhile, proliferative responses to PMA plus ionomycin were at similar levels of full activation for CD4<sup>+</sup>T cells from both *Nedd9*<sup>+/+</sup> and *Nedd9*<sup>−/−</sup> CIA mice, with or without immunization (Fig. 2A). These data suggest that Cas-L/NEDD9 is involved in T cell activation through TCR and engagement of  $\beta 1$  integrin. To further characterize the role of Cas-L/NEDD9 in cell proliferation, we examined proliferative response of lymphocytes to CII. As shown in Fig. 2B, LN mononuclear cells isolated from *Nedd9*<sup>−/−</sup> CIA mice exhibited decreased CII-mediated cell proliferation, compared to those from *Nedd9*<sup>+/+</sup> CIA mice. Meanwhile, proliferative responses to PMA plus ionomycin were at similar levels of full activation in both *Nedd9*<sup>+/+</sup> and *Nedd9*<sup>−/−</sup> CIA mice (Fig. 2B).

Migration and adhesion of B cells in *Nedd9*<sup>−/−</sup> mice have been shown previously to be impaired [14]. To further define the role of Cas-L/NEDD9 on the humoral response in CIA, we analyzed the immunologic response to CII in *Nedd9*<sup>−/−</sup> CIA mice. For this purpose, serum levels of anti-CII antibody were assayed. As shown in Fig. 2C, serum levels of anti-CII antibody in *Nedd9*<sup>−/−</sup> CIA mice were significantly decreased as compared to those in *Nedd9*<sup>+/+</sup> CIA mice, data which are consistent with the findings regarding the incidence and severity of clinical signs/symptoms of arthritis. Taken together, our data strongly suggest that Cas-L/NEDD9 in T cells as well as in B cells plays an important role in the development of arthritis in a CIA model.

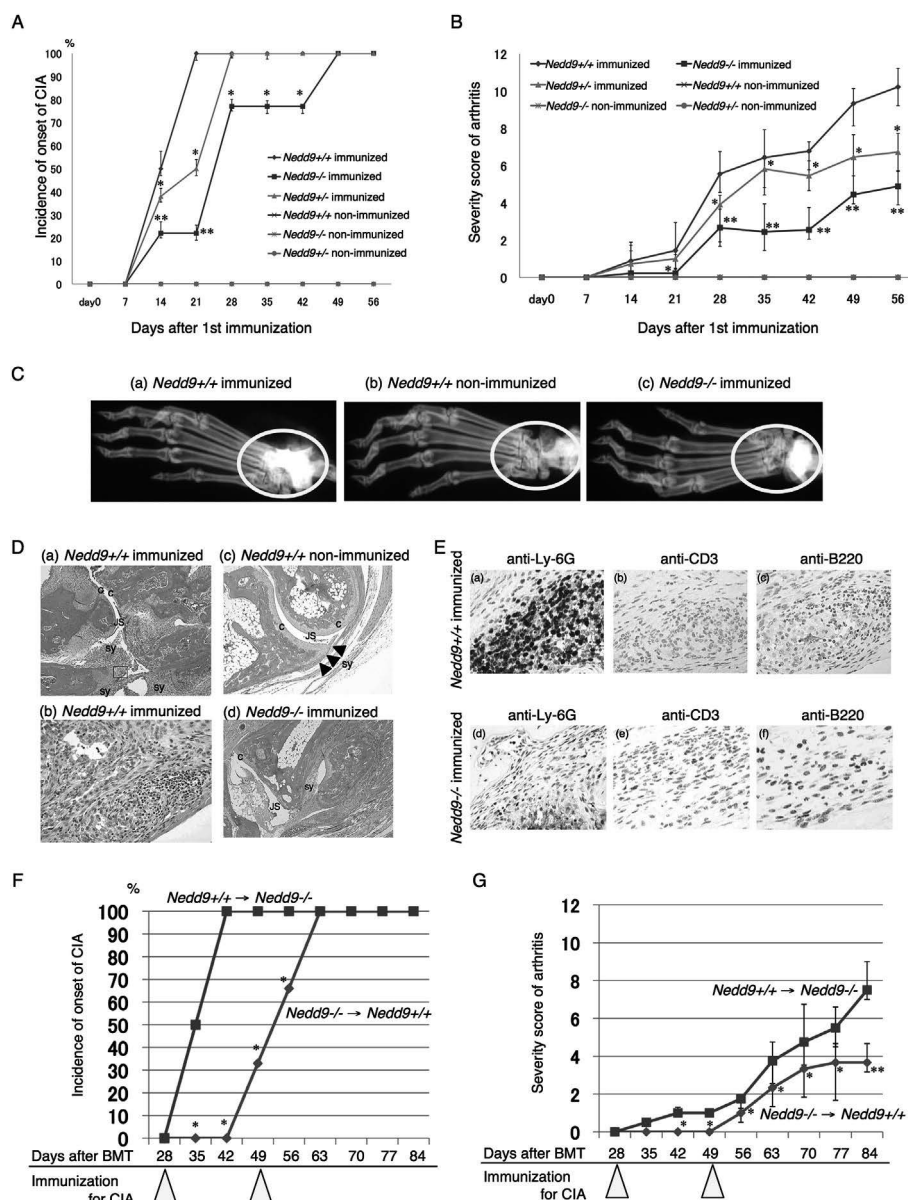


**Fig. 1.** Reduced incidence and severity of CIA in  $Nedd9^{-/-}$  mice. **A.** The incidence of mice developing CIA was calculated as % ratio of mice with severity score  $\geq 1$  to total in each cohort (each,  $n = 9$ ). Incidence of CIA decreased in  $Nedd9^{-/-}$  cohort, compared to that in  $Nedd9^{+/+}$  mice. Incidence of CIA in immunized  $Nedd9^{+/+}$  subset (green line) was in-between that found in  $Nedd9^{+/+}$  (blue line) and  $Nedd9^{-/-}$  (red line) cohorts. None of the non-immunized  $Nedd9^{+/+}$  (purple line),  $Nedd9^{-/-}$  (orange line) or  $Nedd9^{+/-}$  (light blue line) mice developed CIA. \* indicates  $P < 0.05$  vs. immunized  $Nedd9^{+/+}$  CIA cohort, and \*\* indicates  $P < 0.01$  vs. immunized  $Nedd9^{+/+}$  or  $Nedd9^{-/-}$  CIA cohort. **B.** The arthritis severity score was evaluated as described in Materials and methods. Severity of CIA decreased in  $Nedd9^{-/-}$  cohort, compared to that in  $Nedd9^{+/+}$  mice. Level of arthritis severity score of immunized  $Nedd9^{+/+}$  CIA cohort (green line) was in-between that of immunized  $Nedd9^{+/+}$  (blue line) and  $Nedd9^{-/-}$  (red line) CIA cohorts. None of the non-immunized  $Nedd9^{+/+}$  (purple line),  $Nedd9^{-/-}$  (orange line) or  $Nedd9^{+/-}$  (light blue line) mice developed CIA. \* indicates  $P < 0.05$  vs. immunized  $Nedd9^{+/+}$  CIA cohort, and \*\* indicates  $P < 0.01$  vs. immunized  $Nedd9^{+/+}$  or  $Nedd9^{-/-}$  CIA cohort. Data were shown as mean  $\pm$  standard deviation. **C.** Representative planar X-ray images of the upper limbs of  $Nedd9^{+/+}$  mice with or without CIA immunization (panels a or b, respectively), and immunized  $Nedd9^{-/-}$  CIA mice (panel c) on day 56 after the first immunization. **D.** H&E staining of the upper limbs of  $Nedd9^{+/+}$  mice with or without CIA immunization (panels a, b, respectively), and immunized  $Nedd9^{-/-}$  CIA mice (panel d). The specimens were resected on day 56 after the first immunization. Representative histology is shown from 3 independent experiments (each,  $n = 6$ ). **E.** Representative immunohistochemical images of the upper limbs of immunized  $Nedd9^{+/+}$  or  $Nedd9^{-/-}$  CIA mice. Representative histology is shown from 3 independent experiments (each,  $n = 6$ ). Original magnification  $\times 20$  for panels a, c, d, and  $\times 100$  for panel b. **F.** After total body irradiation,  $Nedd9^{+/+}$  or  $Nedd9^{-/-}$  mice received BM cells of  $Nedd9^{-/-}$  ( $Nedd9^{-/-} \rightarrow Nedd9^{+/+}$ ) or  $Nedd9^{+/+}$  ( $Nedd9^{+/+} \rightarrow Nedd9^{-/-}$ ) mice, respectively (each,  $n = 6$ ). Recipient mice were immunized for CIA after 28 and 49 days of BM transplantation (indicated in yellow triangles). The incidence of mice developing CIA was calculated as % ratio of mice with severity score  $\geq 1$  to total in each cohort. Incidence of CIA decreased in  $Nedd9^{-/-} \rightarrow Nedd9^{+/+}$  cohort (blue line), compared to that seen in the  $Nedd9^{+/+} \rightarrow Nedd9^{-/-}$  group (red line). \* indicates  $P < 0.01$  vs.  $Nedd9^{+/+} \rightarrow Nedd9^{-/-}$  cohort. **G.** Mice were treated by the same method as described in F. The arthritis severity score was evaluated as described in Materials and methods. Severity of CIA decreased in  $Nedd9^{-/-} \rightarrow Nedd9^{+/+}$  cohort (blue line), compared to that seen in the  $Nedd9^{+/+} \rightarrow Nedd9^{-/-}$  group (red line). \* or \*\* indicates  $P < 0.05$  or  $P < 0.001$  vs.  $Nedd9^{+/+} \rightarrow Nedd9^{-/-}$  cohort, respectively. Data were shown as mean  $\pm$  standard deviation. (For interpretation of the references to colour in this figure legend, the reader is referred to the web version of this article.)



**Table 1**Number of CD19<sup>+</sup> B, CD4<sup>+</sup> and CD8<sup>+</sup> T cells in spleen or lymph nodes of *Nedd9*<sup>+/+</sup> or *Nedd9*<sup>-/-</sup> mice before and after CIA immunization.

(Organ)	(Subset)	<i>Nedd9</i> <sup>+/+</sup>		<i>Nedd9</i> <sup>-/-</sup>	
		Non-immunized	Immunized	Non-immunized	Immunized
Spleen ( × 10 <sup>7</sup> /ml)	CD19 <sup>+</sup> B cell	2.60 ± 0.9	3.40 ± 1.4*	2.20 ± 0.7	1.20 ± 0.4**
	CD4 <sup>+</sup> T cell	0.90 ± 0.3	1.00 ± 0.4	1.00 ± 0.3	0.50 ± 0.1**
	CD8 <sup>+</sup> T cell	1.20 ± 0.4	1.40 ± 0.6	0.60 ± 0.2	0.35 ± 0.1**
Lymph node ( × 10 <sup>7</sup> /ml)	CD19 <sup>+</sup> B cell	0.17 ± 0.1	0.11 ± 0.0	0.10 ± 0.0	0.40 ± 0.1**
	CD4 <sup>+</sup> T cell	0.35 ± 0.2	0.15 ± 0.0**	0.21 ± 0.1	0.20 ± 0.0
	CD8 <sup>+</sup> T cell	0.34 ± 0.2	0.17 ± 0.0*	0.18 ± 0.1	0.19 ± 0.0

CIA was induced in *Nedd9*<sup>+/+</sup> or *Nedd9*<sup>-/-</sup> mice as described in Materials and methods. Spleen and regional lymph nodes of the affected joints were resected on day 56 following the first immunization. Cells were subjected to flow cytometric analysis as shown in Supplemental Figure. Data were shown as mean of absolute cell number ± standard errors, of cumulative results from 3 independent experiments (each, n = 9). \* or \*\* indicates  $P < 0.05$  or  $P < 0.01$  vs. those in each non-immunized cohort, respectively.

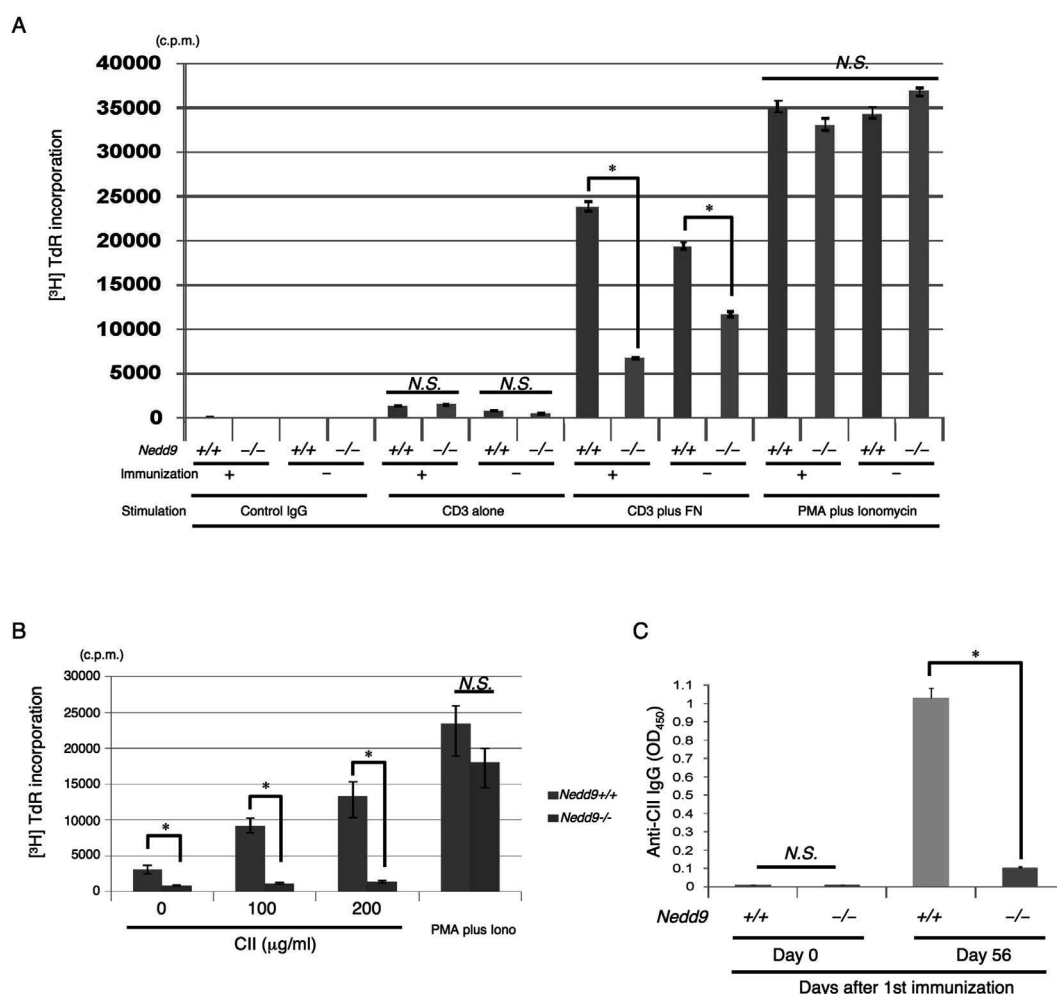


**Fig. 2.** Decreased proliferation of CD4<sup>+</sup>T cells and anti-collagen antibody levels in *Nedd9*<sup>-/-</sup> CIA mice. A. CD4<sup>+</sup>T cells were purified from spleen cells of *Nedd9*<sup>+/+</sup> or *Nedd9*<sup>-/-</sup> mice before and after immunization. Cells were stimulated with plate-bound anti-CD3 monoclonal antibody (mAb) and/or fibronectin (FN) at indicated concentrations, and assayed for cell proliferation by [<sup>3</sup>H]-thymidine (TdR) incorporation. Data were shown as mean ± standard errors (each, n = 6). \* indicates  $P < 0.001$ , and N.S., not significant. B. Lymph node (LN) mononuclear cells were isolated from the regional LNs of *Nedd9*<sup>+/+</sup> or *Nedd9*<sup>-/-</sup> mice after immunization. Cells were stimulated with type II collagen (CII) at indicated concentrations, and assayed for cell proliferation by [<sup>3</sup>H]-thymidine (TdR) incorporation. Cell proliferation by CII stimulation was significantly enhanced in *Nedd9*<sup>+/+</sup> mice (\*). Data were shown as mean ± standard errors (each, n = 6). \* indicates  $P < 0.001$ , and N.S., not significant. C. Serum levels of anti-CII IgG antibody in *Nedd9*<sup>+/+</sup> or *Nedd9*<sup>-/-</sup> mice on day 0 and day 56 after immunization were measured using ELISA. Data were shown as mean ± standard errors with triplicates (each, n = 9). \* indicates  $P < 0.001$ .

### 3.4. Decrease of proinflammatory cytokines and increase of anti-inflammatory cytokines in *Nedd9*<sup>-/-</sup> CIA mice

We previously reported that Cas-L/NEDD9 is involved in TGF-β-related cell regulation [20]. However, it has been unclear whether production of other cytokines is associated with Cas-L/

NEDD9. To examine whether Cas-L/NEDD9 has an effect on cytokine production in CIA, we assayed for serum levels of various cytokines in *Nedd9*<sup>+/+</sup> and *Nedd9*<sup>-/-</sup> CIA mice. As shown in Fig. 3A, levels of proinflammatory cytokines such as IL-1β (panel a), IL-6 (panel b), IL-17 (panel c), IFN-γ (panel d), and TNF-α (panel e) were significantly decreased in sera of *Nedd9*<sup>-/-</sup> CIA

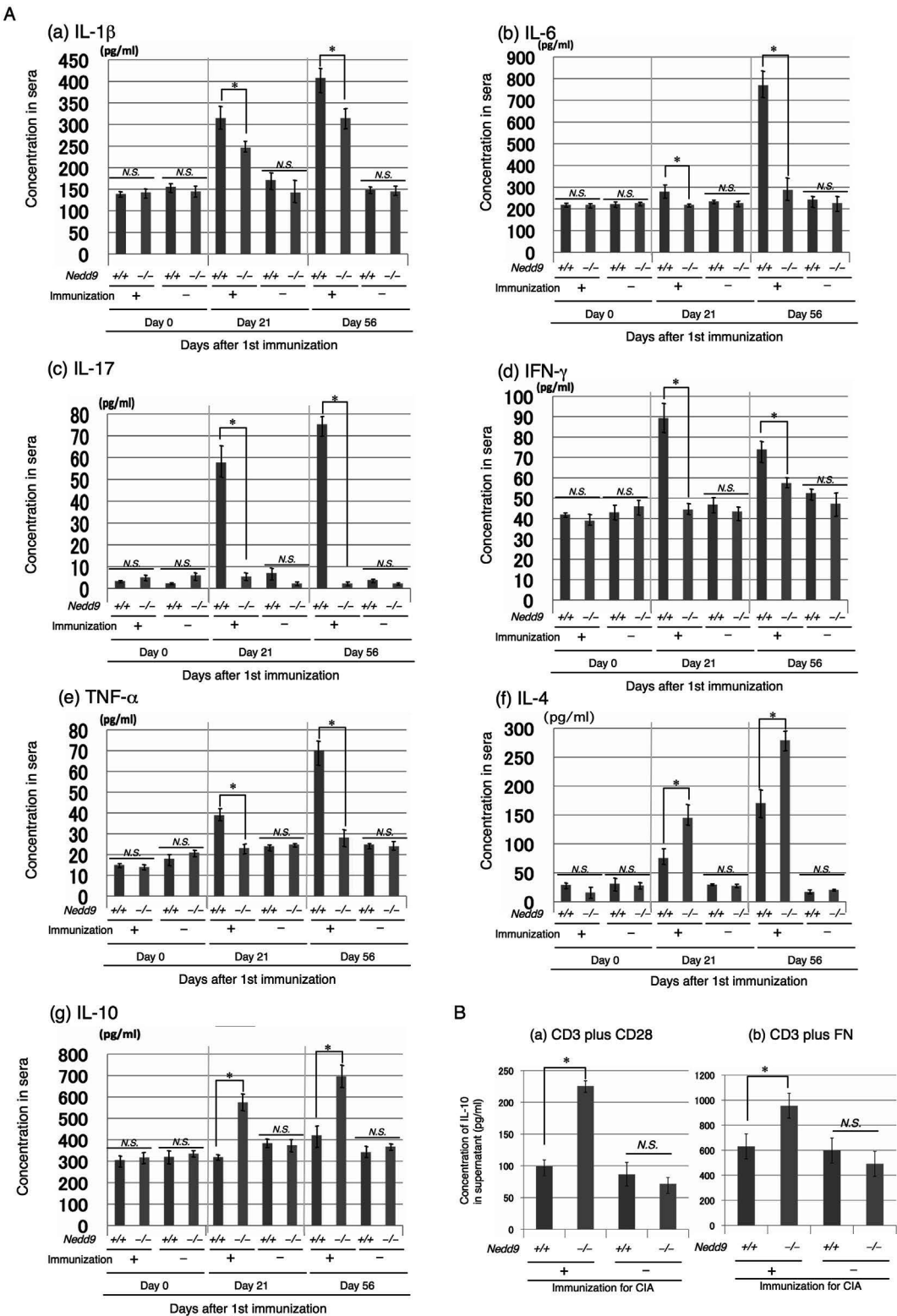


**Fig. 3.** Increase of IL-10 level in *Nedd9*<sup>-/-</sup> CIA mice. A. Sera of *Nedd9*<sup>+/+</sup> or *Nedd9*<sup>-/-</sup> mice were collected at the indicated day after CIA immunization, and serum levels of IL-1 $\beta$  (panel a), IL-6 (panel b), IL-17 (panel c), IFN- $\gamma$  (panel d), TNF- $\alpha$  (panel e), IL-4 (panel f) and IL-10 (panel g) were quantified. Data are shown as mean $\pm$ standard errors of cumulative results from 3 independent experiments (each, n = 9). \* indicates  $P < 0.001$ , and N.S., not significant. B. CD4<sup>+</sup>T cells were purified from spleen cells of *Nedd9*<sup>+/+</sup> or *Nedd9*<sup>-/-</sup> mice before and after immunization. Cells were stimulated with plate-bound anti-CD3 mAb plus anti-CD28 mAb (panel a), or anti-CD3 mAb plus fibronectin (FN). After 72 h, the supernatants were harvested, and subjected to IL-10 assay. Data are shown as mean $\pm$ standard errors with triplicates (each, n = 6). \* indicates  $P < 0.001$ , and N.S., not significant.

mice as compared to *Nedd9*<sup>+/+</sup> CIA mice. Meanwhile, levels of anti-inflammatory cytokines such as IL-4 and IL-10 were significantly increased in sera of *Nedd9*<sup>-/-</sup> CIA mice as compared to *Nedd9*<sup>+/+</sup> CIA mice (panels f and g of Fig. 3A). These data suggest that the decrease in T cell responses seen in *Nedd9*<sup>-/-</sup> mice is mediated at least partly by increased production of the anti-inflammatory cytokine IL-10.

To further evaluate this possibility, we conducted *in vitro* cytokine production assay using CD4<sup>+</sup>T cells isolated from *Nedd9*<sup>-/-</sup> and *Nedd9*<sup>+/+</sup> CIA mice. As shown in Fig. 3B, production of IL-10 by CD3 plus CD28 costimulation was significantly enhanced in CD4<sup>+</sup>T cells from *Nedd9*<sup>-/-</sup> CIA mice, compared to that of non-immunized *Nedd9*<sup>-/-</sup> or *Nedd9*<sup>+/+</sup> mice and *Nedd9*<sup>+/+</sup> CIA mice (panel a). Similarly, production of IL-10 by CD3 plus FN costimulation was significantly enhanced in CD4<sup>+</sup>T cells from *Nedd9*<sup>-/-</sup> CIA mice, compared to that of non-immunized *Nedd9*<sup>-/-</sup> or *Nedd9*<sup>+/+</sup> mice and *Nedd9*<sup>+/+</sup> CIA mice (panel b of Fig. 3B). These results suggest that the decreased incidence and severity of CIA seen in *Nedd9*<sup>-/-</sup> mice are partly associated with an increase in IL-10 production by T cells as well as a decrease in inflammatory T cell responses.

Collectively, our present results strongly suggest that Cas-L/NEDD9 in lymphocytes plays a pivotal role in the pathogenesis of CIA, and that targeting Cas-L/NEDD9 may be an effective novel therapeutic approach for autoimmune diseases including RA.

## Conflict of interest

The authors declare no conflict of interest.

## Acknowledgments

This study was supported in part by a grant of the Ministry of Education, Science, Sports and Culture, Japan (K.O. and C.M.), a grant of the Ministry of Health, Labour, and Welfare, Japan (C.M.) and a Grant-in-Aid (S1311011) from the Foundation of Strategic Research Projects in Private Universities from the Ministry of Education, Culture, Sports, Science, and Technology, Japan (K.O. and C.M.).

T.K. and S.I. contributed to the conception and design of the study, or acquisition of data, O.N., O.S., R.H., T.Y. and H.T. contributed to analysis and interpretation of data, K.O. and C.M. designed the research, interpreted the data and wrote the paper, N.H.D. interpreted the data, assisted with the paper, and proofread the manuscript. All authors showed final approval of the version to be submitted.

## Appendix A. Supplementary data

Supplementary data related to this article can be found at <http://dx.doi.org/10.1016/j.bbrc.2015.03.156>.

## Transparency document

Transparency document related to this article can be found online at <http://dx.doi.org/10.1016/j.bbrc.2015.03.156>.

## References

- [1] R.O. Hynes, Integrins: versatility, modulation, and signaling in cell adhesion, *Cell* 69 (1992) 11–25.
- [2] Y. Nojima, D.M. Rothstein, K. Sugita, et al., Ligation of VLA-4 on T cells stimulates tyrosine phosphorylation of a 105-kD protein, *J. Exp. Med.* 175 (1992) 1045–1053.
- [3] M. Minegishi, K. Tachibana, T. Sato, et al., Structure and function of Cas-L, a 105-kD Crk-associated substrate-related protein that is involved in  $\beta$ 1 integrin-mediated signaling in lymphocytes, *J. Exp. Med.* 184 (1996) 1365–1375.
- [4] R. Sakai, A. Iwamatsu, N. Hirano, et al., A novel signaling molecule, p130, forms stable complexes in vivo with v-Crk and v-Src in a tyrosine phosphorylation-dependent manner, *EMBO J.* 13 (1994) 3748–3756.
- [5] S. Kumar, Y. Tomooka, M. Noda, Identification of a set of genes with developmentally down-regulated expression in the mouse brain, *Biochem. Biophys. Res. Commun.* 185 (1992) 1155–1161.
- [6] S.F. Law, J. Estojak, B. Wang, et al., Human enhancer of filamentation 1, a novel p130<sup>cas</sup>-like docking protein, associates with focal adhesion kinase and induces pseudohyphal growth in *Saccharomyces cerevisiae*, *Mol. Cell. Biol.* 16 (1996) 3327–3337.
- [7] G.M. O'Neill, S. Seo, I.G. Serebriiskii, et al., A new central scaffold for metastasis: parsing HGF1/Cas-L/NEDD9, *Cancer Res.* 67 (2007) 8975–8979.
- [8] Y. Ohashi, K. Tachibana, K. Kamiguchi, et al., T cell receptor-mediated tyrosine phosphorylation of Cas-L, a 105-kDa Crk-associated substrate-related protein, and its association of Crk and C3G, *J. Biol. Chem.* 273 (1998) 6446–6451.
- [9] K. Tachibana, T. Urano, H. Fujita, et al., Tyrosine phosphorylation of Crk-associated substrates by focal adhesion kinase. A putative mechanism for the integrin-mediated tyrosine phosphorylation of Crk-associated substrates, *J. Biol. Chem.* 272 (1997) 29083–29090.
- [10] Y. Ohashi, S. Iwata, K. Kamiguchi, C. Morimoto, Tyrosine phosphorylation of Crk-associated substrate lymphocyte-type is a critical element in TCR- and  $\beta$ 1 integrin-induced T lymphocyte migration, *J. Immunol.* 163 (1999) 3727–3734.
- [11] S. Iwata, A. Souta-Kuribara, A. Yamakawa, et al., HTLV-I Tax induces and associates with Crk-associated substrate lymphocyte type (Cas-L), *Oncogene* 24 (2005) 1262–1271.
- [12] R. Miyake-Nishijima, S. Iwata, S. Saijo, et al., Role of Crk-associated substrate lymphocyte type in the pathophysiology of rheumatoid arthritis in tax transgenic mice and in humans, *Arthritis Rheum.* 48 (2003) 1890–1900.
- [13] Y. Iwakura, M. Tosu, E. Yoshida, et al., Induction of inflammatory arthropathy resembling rheumatoid arthritis in mice transgenic for HTLV-I, *Science* 253 (1991) 1026–1028.
- [14] S. Seo, T. Asai, T. Saito, et al., Crk-associated substrate lymphocyte type is required for lymphocyte trafficking and marginal zone B cell maintenance, *J. Immunol.* 175 (2005) 3492–3501.
- [15] E.F. Rosloniec, M. Cremer, A. Kang, L.K. Myers, Collagen-induced arthritis, Chapter 15, *Curr. Protoc. Immunol.* (2001). Unit 15 15.
- [16] D.D. Brand, K.A. Latham, E.F. Rosloniec, Collagen-induced arthritis, *Nat. Protoc.* 2 (2007) 1269–1275.
- [17] S. Iwata, Y. Ohashi, K. Kamiguchi, C. Morimoto,  $\beta$ 1-integrin-mediated cell signaling in T lymphocytes, *J. Dermatol. Sci.* 23 (2000) 75–86.
- [18] K. Kamiguchi, K. Tachibana, S. Iwata, et al., Cas-L is required for  $\beta$ 1 integrin-mediated costimulation in human T cells, *J. Immunol.* 163 (1999) 563–568.
- [19] T. Matsuyama, A. Yamada, J. Kay, et al., Activation of CD4 cells by fibronectin and anti-CD3 antibody. A synergistic effect mediated by the VLA-5 fibronectin receptor complex, *J. Exp. Med.* 170 (1989) 1133–1148.
- [20] S. Inamoto, S. Iwata, T. Inamoto, et al., Crk-associated substrate lymphocyte type regulates transforming growth factor- $\beta$  signaling by inhibiting Smad6 and Smad7, *Oncogene* 26 (2007) 893–904.



ORIGINAL ARTICLE

## Modulation of immunological responses and amelioration of collagen-induced arthritis by the novel roxithromycin derivative 5-I

Noriko Otsuki<sup>1,5</sup>, Satoshi Iwata<sup>1,6</sup>, Taketo Yamada<sup>2</sup>, Osamu Hosono<sup>3</sup>, Nam H. Dang<sup>4</sup>, Ryo Hatano<sup>1,6</sup>, Kei Ohnuma<sup>3,6</sup>, and Chikao Morimoto<sup>1,6</sup>

<sup>1</sup>Division of Clinical Immunology, Advanced Clinical Research Center, The Institute of Medical Science, The University of Tokyo, Minato-ku, Tokyo, Japan,

<sup>2</sup>Department of Pathology, Keio University School of Medicine, Shinjuku-ku, Tokyo, Japan, <sup>3</sup>Department of Rheumatology and Allergy, IMUST Hospital, The Institute of Medical Science, The University of Tokyo, Minato-ku, Tokyo, Japan, <sup>4</sup>Division of Hematology/Oncology, University of Florida, Gainesville, FL, USA, <sup>5</sup>Division of food additives, National Institute of Health Sciences, Setagaya-ku, Tokyo, Japan, and <sup>6</sup>Department of Therapy Development and Innovation for Immune disorders and Cancers, Graduate School of Medicine, Juntendo University, Bunkyo-ku, Tokyo, Japan

### Abstract

**Objective.** Macrolide antibiotics have immunomodulatory properties that are distinct from their antibacterial functions. We synthesized 5-I, which is a new derivative of RXM with less antimicrobial activity, and evaluated its immunomodulatory effects through both *in vitro* and *in vivo* studies.

**Methods.** Proliferative response, cytokine production, and expression of mRNA of T cells stimulated with anti-CD3 and anti-CD28 mAbs in the presence or absence of monocytes, cytokine production of monocytes stimulated with lipopolysaccharide, and transendothelial migration of T cells in various concentrations of 5-I were analyzed. The effect of 5-I treatment was also evaluated in a mouse model of collagen-induced arthritis.

**Results.** 5-I specifically inhibited production of Th1, Th17, and proinflammatory cytokines such as IL-2, IFN- $\gamma$ , TNF- $\alpha$ , IL-6, and IL-17A. 5-I reduced the expression of RORC on CD4<sup>+</sup> T cells, which codes for ROR $\gamma$ t, the master regulator of Th17, and it also inhibited migration of activated T cells. Importantly, administration of 5-I to mice with collagen-induced arthritis reduced the severity of arthritis, and this effect was also observed when treatment was delayed till after the onset of disease.

**Conclusion.** Our findings strongly suggest that 5-I may be useful as a potential therapeutic agent for human rheumatoid arthritis.

### Keywords

5-I, Collagen-induced arthritis, Monocytes, Rheumatoid arthritis, Roxithromycin, T cells

### History

Received 5 August 2014

Accepted 30 October 2014

Published online 20 March 2015

### Introduction

Macrolide antibiotics have many biological activities apart from their antibacterial actions. Low-dose and long-term erythromycin treatment was recently shown to be effective in chronic respiratory tract disease, including diffuse panbronchiolitis [1] and bronchial asthma [2], although the mechanism of action of this drug remains unclear. Moreover, macrolide antibiotics have reported activity in other extra-pulmonary diseases and selected biological conditions including rhinosinusitis [2], bone resorption and remodeling [3], inflammatory bowel diseases [4], and psoriasis [5]. The immunomodulatory effects of these agents are thought to result from processes involved in leukocyte activation such as stimulation of phagocytosis, natural killer cell activity, production of superoxide anion and neutrophil chemotaxis [6, 7]. Roxithromycin (RXM), a macrolide antibiotic, has a 14-member macrocyclin ring

structure resembling that of erythromycin [8]. RXM is characterized by rapid and complete absorption after oral administration, resulting in high serum concentrations [9]. *In vitro* studies revealed that RXM modifies the function of neutrophils [10] and keratinocytes [11]. RXM also affects lymphocyte functions including proliferation induced by mitogens and purified protein derivative [12], as well as proliferation and cytokine secretion induced by mitogens [13].

We showed previously that RXM inhibited *in vitro* production of proinflammatory cytokines by T cells and macrophages, such as tumor necrosis factor- $\alpha$  (TNF- $\alpha$ ) and interleukin 6 (IL-6), as well as suppressing T cell migration [14]. Interestingly, RXM treatment of mice with collagen-induced arthritis reduced the severity of arthritis and serum level of IL-6, along with leukocyte migration into the affected joints and destruction of bones and cartilages [14]. These results indicate that RXM may function both as an immunomodulatory agent and an antibiotic. However, it is of concern that the long-term use of antibiotics such as RXM may potentially induce adverse effects including nausea, QT prolongation, and induction of bacterial resistance. Therefore, components isolated from RXM with immunomodulatory properties may potentially be used for the treatment for autoimmune diseases such as rheumatoid arthritis (RA).

Correspondence to: Dr. Kei Ohnuma, Department of Therapy Development and Innovation for Immune disorders and Cancers, School of Medicine, Juntendo University, 2-1-1, Hongo, Bunkyo-ku, Tokyo 113-8421, Japan. Tel: +81-3-3868-2310. Fax: +81-3-3868-2310. E-mail: kohnuma@juntendo.ac.jp



In the present study, we synthesized a new derivative named 5-I from RXM with less antibiotic property. We then assessed the immunomodulatory activity of 5-I on human peripheral lymphocytes as well as its therapeutic effect on a mouse model of human RA.

## Materials and methods

### Roxithromycin and its derivative, 5-I

RXM was purchased from Sigma (R4393; St. Louis, MO) and 5-I was supplied from Y's Therapeutics Co., Ltd. (Ebisu, Tokyo, Japan). For all *in vitro* experiments, except for transendothelial migration assay, RXM and 5-I were first dissolved in methyl alcohol and further diluted in the culture medium consisting of RPMI-1640 medium supplemented with L-glutamine and 10% fetal calf serum (FCS; Invitrogen, Carlsbad, CA). For assessment of transendothelial migration, RXM and 5-I dissolved in methyl alcohol were further diluted in the assay medium consisting of RPMI-1640 medium with 0.6% bovine serum albumin (Sigma). For oral administration to mice in *in vivo* studies, RXM and 5-I were directly dissolved in 1% carboxymethylcellulose (CMC; Sigma)-containing saline (0.9% NaCl; Otsuka Pharmaceutical Co., Ltd., Tokyo, Japan) using a ground-glass homogenizer.

### Preparation of peripheral blood mononuclear cells (PBMC) and *in vitro* culture

PBMCs were obtained from healthy volunteers. This study was approved by the institutional ethics committee at the Institute of Medical Science, University of Tokyo (No. 20-30-1009) and was conducted according to the principles of the Declaration of Helsinki; each healthy volunteer was provided with a written informed consent. PBMC were isolated by density gradient centrifugation. CD3<sup>+</sup> T cells and CD4<sup>+</sup> T cells were isolated from PBMC by negative selection using human Pan T cell isolation kit II (Miltenyi Biotec GmbH, Bergisch Gladbach, Germany), and human CD4<sup>+</sup> T cell isolation kit (Miltenyi Biotec GmbH), respectively. CD14<sup>+</sup> monocytes were isolated from PBMCs by positive selection using human CD14 MicroBeads (Miltenyi Biotec GmbH). The purities of CD3<sup>+</sup> T cells, CD4<sup>+</sup> T cells, and CD14<sup>+</sup> monocytes were greater than 97%, 97%, and 98% by flow cytometry, respectively. PBMC or CD3<sup>+</sup> T cells were stimulated ( $2 \times 10^5$  cells/well) with immobilized anti-CD3 (1 µg/ml, OKT3, IgG2a) and soluble anti-CD28 (5 µg/ml, 4B10, IgG1) mAb in the presence or absence of RXM or 5-I at the indicated concentration (5, 10, 20 and 40 µg/ml) in 96 well flat-bottom plates. Supernatants from triplicate cultures were collected after 24 h for assessment of IL-2 and IL-4 production. For assessment of IL-5, IL-6, IL-17A, IFN-γ and TNF-α, the supernatants were collected after 48 h. All cytokines except for IL-17A were measured using BD OptEIA ELISA set (BD Biosciences, San Jose, CA). The production of IL-17A was measured using "Ready-set-go!" ELISA Kits (eBioscience, San Diego, CA). For assay of proliferative responses, PBMCs or purified CD3<sup>+</sup> T cells ( $2 \times 10^5$  cells/well) were cultured with or without RXM or 5-I as described above for 72 h. The cells were pulsed with [<sup>3</sup>H]-thymidine (1 mCi/well; Perkin-Elmer, Waltham, MA) for the last 18 h and harvested on a Micro 96 Cell Harvester (Skatron, Sterling, VA). The incorporated radioactivity was measured using a microplate beta counter (Micro Beta Plus; Wallac, Turku, Finland). For monocyte activation, purified CD14<sup>+</sup> monocytes were stimulated with 0.1, 1, 5, or 10 µg/ml of lipopolysaccharide (LPS; Sigma). After 24 h of culture, the supernatants were collected and subjected to ELISA for TNF-α and IL-6.

### Determination of minimal inhibitory concentration (MIC)

For MIC testing, gram-positive bacteria, including *Staphylococcus aureus* (*S. aureus*) (ATCC 29213) or *Streptococcus pneumoniae* (*S. pneumoniae*) (ATCC 49619) was incubated in 96-well flat plates in the presence of RXM or 5-I for 24 h. Mueller-Hinton broth (MH broth; BD Difco, Franklin Lakes, NJ) and MH broth supplemented with 5% horse blood were used for *S. aureus*, or *S. pneumoniae*, respectively. The range of antibiotics concentration was set by two-fold serial dilution, specifically, 100, 50, 25, 12.5, 6.25, 3.13, 1.56, 0.78, 0.39, 0.2, 0.1, and 0.05 µg/ml. After 24 h of culture, growth inhibition was confirmed by visual inspection.

### Transendothelial-migration assay

Transendothelial migration activity was assessed as described previously [15], with some modifications. Human umbilical vein endothelial cells (HUVEC; from KURABO Industries Ltd., Osaka, Japan) were pre-cultured at  $3 \times 10^5$  cells/well to make monolayer sheets on fibronectin-coated Transwell Inserts with 3.0 mm pore size (BD Biosciences, San Jose, CA) for 48 h. Purified CD3<sup>+</sup> T cells ( $1 \times 10^6$  cells/ml) were stimulated 10 µg/ml of PHA in 24-well plates for 3 days. After 3 days of culture, PHA was washed out and IL-2 (100 units/ml; BD Pharmingen, San Diego, CA) was added, and the cells were cultured for an additional 2 days. At day 5, viable cells were isolated by density gradient centrifugation and stained with 5 mM CMFDA (CellTracker® Green, Molecular Probe, Eugene, OR). The assay medium was added to the culture plates in a final volume of 1200 µl in the lower chamber. Pre-activated and stained CD3<sup>+</sup> T cells ( $1 \times 10^6$  cells/ml) were resuspended with the assay medium, and added to each insert in a final volume of 600 µl in the presence or absence of RXM or 5-I for analysis of cell migration. After 24 h of culture, cells that migrated transendothelially into the lower chamber were collected to plastic tubes and stained with 7-amino-actinomycin D (7-AAD, BD Pharmingen) for exclusion of dead cells. FL1<sup>high</sup> 7-AAD<sup>negative</sup> cells were counted at specific time limit (204 sec) and flow rate (high) by flow cytometry using FACSCalibur and CellQuest software (BD Biosciences).

### Induction of collagen-induced arthritis (CIA), macrolides treatment, and clinical assessments of arthritis

CIA was induced as previously described with minor modifications [16]. Briefly, male DBA/1 J mice (7 week old) were injected intradermally at the base of tail with 100 mg of bovine type II collagen (CII) (Collagen Research Center, Tokyo, Japan) in 0.05 M acetic acid, emulsified in complete Freund's adjuvant (CFA) (Difco, Detroit, MI). Twenty-one days after primary immunization, the mice were boosted in the same way. Day of the second immunization (boost) was designated as day 0. Five non-immunized mice were included as the negative control group. The immunized mice were divided into four groups on the basis of body weight, and treated with the following regimens. Each group of mice was treated with either control saline (1% CMC, 200 µl), 5-I (200, 400 µg/body), or RXM (400 µg/body), intraperitoneally from day 0. The treatment was continued until day 20 every other day. In the experiments involving delayed treatment, 400 µg/body of 5-I was administered at alternate days from day 4 to day 20. Each group consisted of 10 mice in all experiments. Mice were examined daily for the onset of CIA. The swelling of four paws was graded from 0 to 4 as follows: grade 0, no swelling; grade 1, swelling of finger joints or focal redness; grade 2, mild swelling of wrist or ankle joints; grade 3, severe swelling of the entire paw; grade 4, deformity or ankylosis. Each paw

was graded, and the four scores were totaled so that the maximal score per mouse was 16. Incidence was expressed as the number of paws that showed swelling in the total number of mice examined, body weight was measured on day 0, 7, 14, and 21, and the time of onset was expressed as the mean time when paw swelling was first observed in individual mouse. Animal experiments were conducted following protocols approved by the Animal Care and Use Committees at the Institute of Medical Science, University of Tokyo.

### Histological analysis

Mice were euthanized by CO<sub>2</sub> asphyxiation and hind paws were then removed from the mice 3 weeks after the second immunization. The paws were fixed in 10% phosphate-buffered formalin (pH7.4), decalcified in 10% EDTA, and embedded in paraffin. Sections (4 µm) were stained with hematoxylin and eosin.

### Quantification of mRNA by real-time RT-PCR

Purified CD4<sup>+</sup> T cells were cultured with immobilized anti-CD3 mAb (1 µg/ml) and soluble anti-CD28 mAbs (10 µg/ml) in the presence or absence of RXM or 5-I for 6 h and 10 h. Total cellular RNA from CD4<sup>+</sup> T cells ( $2 \times 10^6$ ) cultured as above were isolated using High Pure RNA Isolation Kit (Roche Diagnostics GmbH, Mannheim, Germany), according to the manufacturer's instructions. The quality and quantity of total RNA were assessed by NanoDrop spectrophotometer (ND-1000, Thermo Fisher Scientific Inc., MA). Complementary DNA (cDNA) was synthesized from 1 µg of total RNA using Transcriptor First Strand cDNA Synthesis Kit (Roche Diagnostics). The expression levels of *HPRT*, *TNFAIP6*, *WISP1* and *RORC* were evaluated by real-time RT-PCR using LightCycler® TaqMan® Master (Roche Diagnostics) with specific primers (Supplementary Table 1 available online at <http://informahealthcare.com/doi/abs/10.3109/14397595.2014.983262>). Reaction condition was 95°C 10 min, 35 cycles of 95°C 30 sec and 60°C 20 sec. TaqMan® probe (Universal Probe Library, Roche Diagnostics) was used to detect specific PCR products. Amplification and detection of TaqMan® probe were performed with LightCycler® ST300 (Roche Diagnostics). The human *HPRT* gene was used as a housekeeping reference gene to normalize expression levels between the samples.

### Statistical analysis

Data were analyzed by two-tailed Student's *t* test for two group comparison or by ANOVA test for multiple comparison testing followed by the Tukey-Kramer *post-hoc* test. *P* values less than or equal to 0.05 were considered statistically significant.

## Results

### Determination of minimal inhibitory concentration for growth of RXM-susceptible bacteria

The chemical structures of Roxithromycin and its derivative 5-I are outlined in Figure 1A and B, respectively. To ascertain the relative deficiency of antimicrobial activity of 5-I, we determined the MIC for growth of two RXM-susceptible bacterial strains, *S. aureus* and *S. pneumoniae*, for 5-I as compared to RXM. As shown in Figure 1C, the MICs of RXM for *S. aureus* and *S. pneumoniae* were observed at 0.05 µg/ml and 0.78 µg/ml respectively, whereas those of 5-I were observed at 100 µg/ml and 25 µg/ml, respectively. These data hence indicated that 5-I was a defective derivative of RXM in antimicrobial activity, with 5-I antimicrobial activity being approximately 30 to 2,000 fold lower than that of RXM.

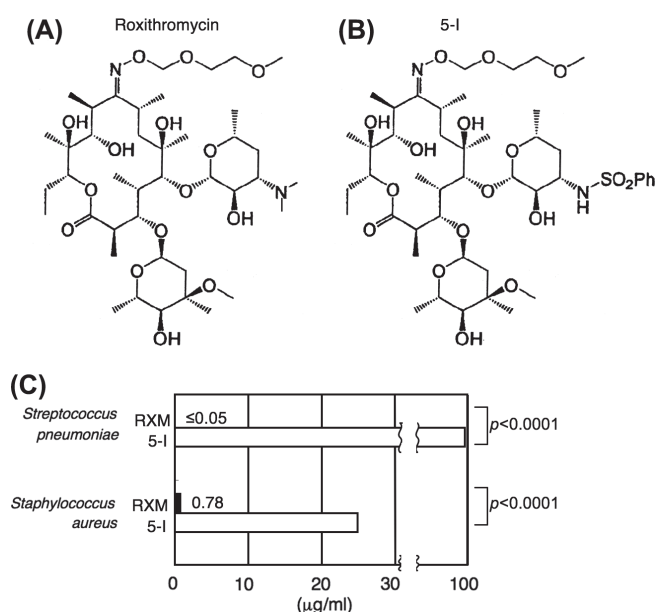


Figure 1. The antibiotic effects of Roxithromycin (RXM) and its new derivative 5-I. (A) The chemical structure of RXM. (B) The chemical structure of 5-I, a new derivative of RXM. (C) *Staphylococcus aureus* or *Streptococcus pneumoniae* were incubated in 96-well flat plates, in the presence of RXM or 5-I for 24 h. After 24 h of incubation, growth inhibition was confirmed by visual inspection. X-axis represents the concentration of RXM or 5-I. One representative set of data from three independent experiments are shown.

### Effect of RXM and 5-I on proliferative response and cytokine production

Since we previously demonstrated the inhibitory effect of RXM on the proliferation and cytokine production of purified T cells [14], we therefore examined the effect of 5-I as well as RXM on CD3<sup>+</sup> T cells purified from PBMC. Both RXM and 5-I had either no inhibitory effect on the proliferative responses of CD3<sup>+</sup> T cells from different donors at concentrations ranging from 5 to 40 µg/ml, with similar results being observed in PBMC which contain monocytes/macrophages as well as T cells (Supplementary Figure 1 available online at <http://informahealthcare.com/doi/abs/10.3109/14397595.2014.983262>). To characterize the immunomodulatory properties of RXM and 5-I, we next assessed their effect on the production of various cytokines by purified CD3<sup>+</sup> T cells alone, and CD3<sup>+</sup> T cells plus CD14<sup>+</sup> monocytes stimulated with anti-CD3 and anti-CD28 mAb, or CD14<sup>+</sup> monocytes stimulated with LPS. Production of IL-2, IL-17A and INF-γ by CD3<sup>+</sup> T cells was reduced by the addition of RXM or 5-I (Figure 2A). TNF-α production by CD3<sup>+</sup> T cells was slightly reduced by the addition of RXM and 5-I (panel a of Figure 2B), while IL-6 production by purified CD3<sup>+</sup> T cells was below the level of detection in our *in vitro* system (data not shown). Since the main sources of TNF-α and IL-6 were monocyte/macrophage cells, we next conducted co-culture experiment using CD3<sup>+</sup> T cells with CD14<sup>+</sup> monocytes at a ratio of 40:1, and assessed the production of TNF-α and IL-6. As shown in Figure 2B, TNF-α (panel b) and IL-6 (panel c) production was clearly suppressed by the addition of RXM or 5-I. When we examined the production of TNF-α and IL-6 by LPS-stimulated CD14<sup>+</sup> monocytes, our data indicated that levels of TNF-α and IL-6 were significantly inhibited (approximately 20%) by the addition of RXM or 5-I (Figure 2C). Since Th2-type CD4<sup>+</sup> T cells may play a role in allergic disorders such as allergic rhinitis and bronchial asthma [17], we also examined the effect of RXM and 5-I on Th2-type cytokine production, and found that RXM and 5-I did not inhibit

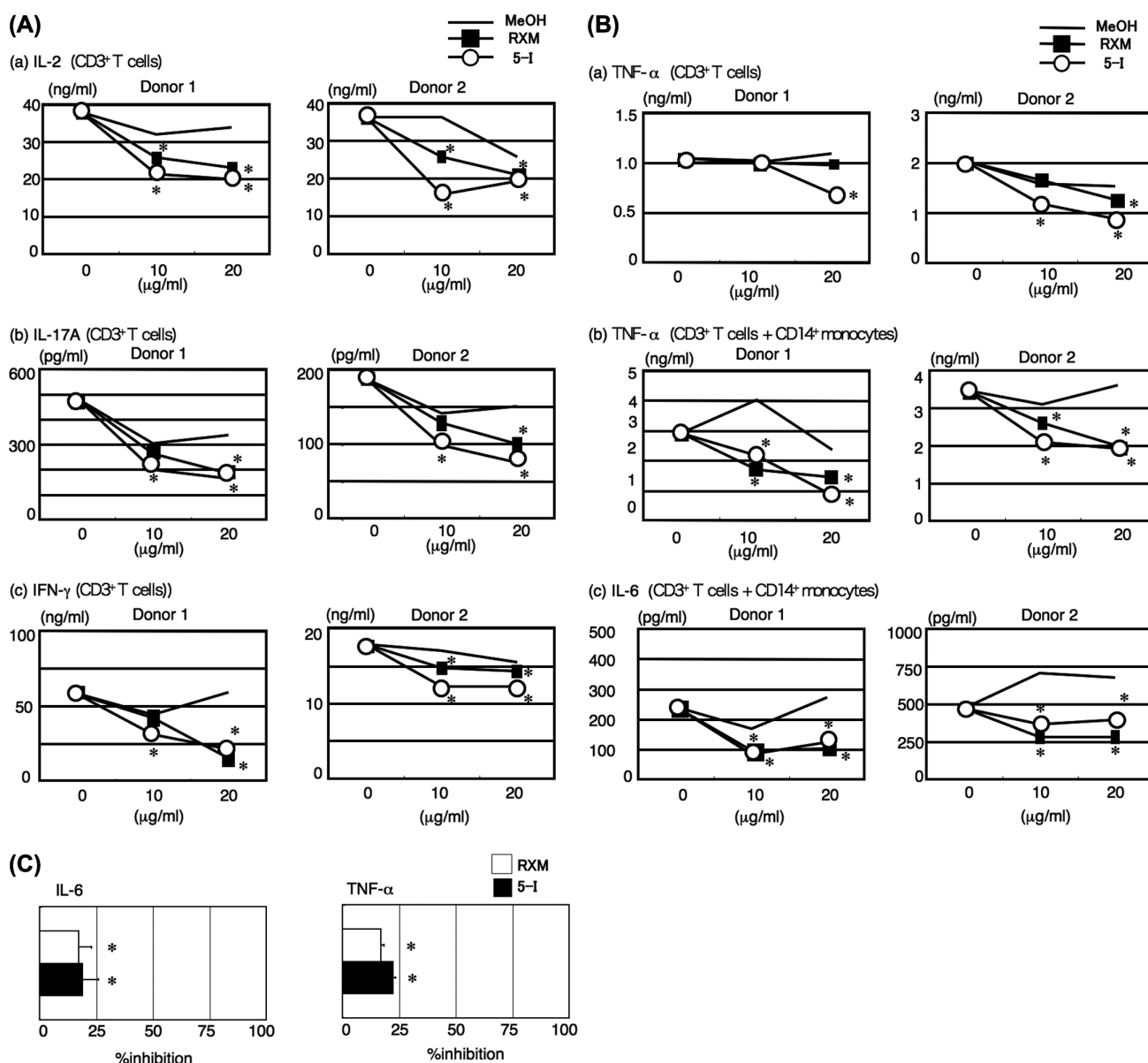


Figure 2. Inhibitory effect of RXM and 5-I on cytokine production by CD3<sup>+</sup> T cells and/or CD14<sup>+</sup> monocytes. (A) Levels of IL-2 (panel a), IL-17A (panel b), and IFN-γ (panel c) in purified CD3<sup>+</sup> T cells ( $2 \times 10^5$  cells) culture supernatants after stimulation with anti-CD3 (1 μg/ml) and anti-CD28 (5 μg/ml) mAbs in the presence or absence of vehicle (MeOH), RXM or 5-I at the indicated concentrations for 24 h (IL-2) and 48 h (IFN-γ and IL-17A) are shown. Results of 2 donors in four independent experiments are shown as representative of 10 different donors, with similar results being obtained. Statistically significant difference compared to the MeOH-treated control is shown (\* $p < 0.01$ ). (B) Level of TNF-α (panel a) in CD3<sup>+</sup> T cells ( $2 \times 10^5$  cells) alone and level of TNF-α (panel b) or IL-6 (panel c) in CD3<sup>+</sup> T cells ( $2 \times 10^5$  cells) plus CD14<sup>+</sup> monocytes ( $5 \times 10^3$  cells) culture supernatants after stimulation by the same method as described in panel (A) for 48 h are shown. Results of 2 donors in four independent experiments are shown as representative of 10 different donors, with similar results being obtained. Statistically significant difference compared to the MeOH-treated control is shown (\* $p < 0.01$ ). (C) Inhibition of TNF-α and IL-6 production in LPS (0.1 μg/ml)-stimulated CD14<sup>+</sup> monocyte culture supernatants in the presence of 20 μg/ml of RXM (open column) or 5-I (closed column) are shown. Data are presented as means  $\pm$  SE of %inhibition to the MeOH-treated control from four experiments using 10 different donors (\* $p < 0.001$ ).

IL-4 or IL-5 production (Supplementary Figures 2A or 2B available online at <http://informahealthcare.com/doi/abs/10.3109/14397595.2014.983262>, respectively). Given the fact that IL-10 regulates anti-inflammatory responses via the activation of T cells, and exerts inhibitory effects on proinflammatory cytokine production, we also assessed the effect of RXM and 5-I on IL-10 production. As shown in Supplementary Figures 2C available online at <http://informahealthcare.com/doi/abs/10.3109/14397595.2014.983262>, RXM and 5-I did not affect IL-10 production at any tested dose. Taken together, our results indicated that RXM and 5-I directly regulated T cell function by inhibiting the production of Th1- and Th17-type cytokines such as IL-2, IFN-γ and IL-17A, and regulated monocyte function by suppressing the production of proinflammatory cytokines such as TNF-α and IL-6, without any effect

on IL-10 mediated anti-inflammatory pathway. Similar to RXM, 5-I therefore modulated activation of both T cells and monocytes by regulating cytokine production without having direct growth inhibitory effect.

#### Effect of 5-I on transendothelial migration of activated T cells as compared to RXM

Having demonstrated previously that RXM inhibited the transendothelial migration of activated T cells, we thus examined the effect of 5-I on this biological activity of PHA-activated T lymphocytes. Pre-activated T cells spontaneously migrate from the upper chamber to the lower chamber through the endothelial monolayer, a process termed chemokinesis. As described in Materi-

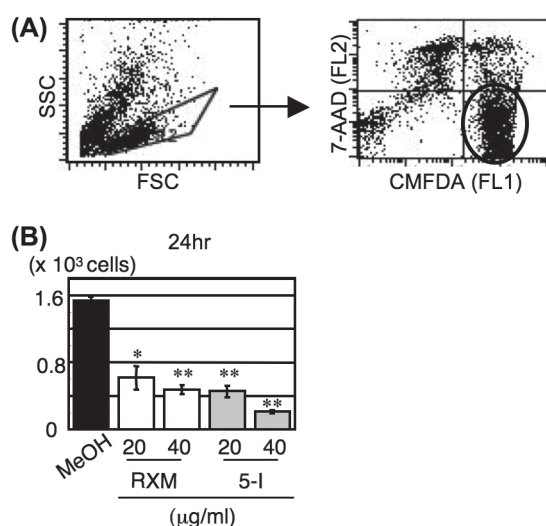


Figure 3. Inhibitory effect of RXM and 5-I on transendothelial migration of PHA-activated T cells. (A) Definition of transendothelially migrated T cells by flow cytometry. T cells pre-stained with CMFDA were acquired by FSC-SSC (gated in the quadrangle area of the left panel) and the migrated live cells were quantified by FL1 positive with 7-AAD negative as viable cells (gated in the circle area of the right panel). (B) The conditions of cell cultures were described as in Materials and Methods. Transendothelially migrated cells were counted by flow cytometry at specific time limit (204 sec) and flow rate (high). Bars show mean of cell numbers  $\pm$  SE of triplicate cultures. Data were obtained from 10 different donors with four independent experiments. Statistically significant difference from the control vehicle-treated group is shown (\* $p < 0.05$ , \*\* $p < 0.01$ ).

als and Methods, migrated viable cells were defined as FL1<sup>high</sup> 7-AAD<sup>negative</sup> cells, which could be analyzed through flow cytometry (Figure 3A). As shown in Figure 3B, T cell migration was significantly inhibited by RXM and 5-I at concentrations of 20 µg/ml and 40 µg/ml when these agents were present during the course of the endothelial migration assay. In contrast, when we pretreated HUVEC with various concentrations of RXM and 5-I for 48 h, and HUVEC were then washed and exposed to PHA-stimulated T cells, neither RXM nor 5-I affected the migration of activated T cells through HUVEC even at highest concentration (80 µg/ml) (data not shown). These findings suggested that inhibition of transendothelial migration of activated T cells was exerted by RXM or 5-I effect on T cells, but not on endothelial cells.

### Regulation of mRNA expression by RXM and 5-I

To elucidate the cellular mechanisms involved in the immunomodulatory effect of RXM or 5-I on human lymphocyte activation, we examined the changes induced by RXM or 5-I in mRNA expression profiles of purified CD4<sup>+</sup> T cells stimulated via CD3 and CD28 pathways (RXM, 5-I or vehicle-treated). Since the addition of RXM or 5-I clearly inhibited production of Th1- and

Th17-type cytokines, such as IL-2 and IL-17, and proinflammatory cytokines, such as TNF- $\alpha$  and IL-6 (Figure 2), we particularly focused on the change of expression of Th-regulated genes. For this purpose, we conducted real-time RT-PCR analysis of the relevant transcription factors in purified CD4<sup>+</sup> T cells. T-bet, GATA-3, and RORC are the master regulators of Th1, Th2, and Th17 subset, respectively. As shown in Figure 4A, the expression of *RORC* was reduced within 10 h of RXM or 5-I treatment whereas we could not detect any enhancing or suppressive effect on *TBX21* (T-bet) and *GATA3* mRNA expression (data not shown). To evaluate the early transcriptional events of cytokine genes involved in the polarization of T helper subsets, the expressions of *IL23R* and *TGFB2* for Th17, *IL13RA1* for Th2, and tumor necrosis factor  $\alpha$ -induced protein 6 (*TNFAIP6*) mRNA were analyzed. Although Th1 and Th17-related cytokine genes were not altered (data not shown), the expression of *TNFAIP6* was diminished within 10 h of RXM or 5-I treatment (Figure 4B). Besides those genes affected by the addition of RXM or 5-I, our data indicated a decrease in the level of WNT1-inducible-signaling pathway protein 1 (*WISP1*) (Figure 4C), a pro-mitogenic, pro-survival factor which mediates TNF- $\alpha$ -induced inflammatory responses. These data suggested that RXM and 5-I inhibited the polarization into Th17 cells by suppressing or delaying *RORC* transcription, and decreased inflammatory responses with subsequent TNF- $\alpha$  secretion in the early phase of CD4<sup>+</sup> T cell activation.

### Preventive and therapeutic effects of 5-I on CIA pathophysiology

Expanding on our findings above, we next investigated the potential effect of 5-I on the development of CIA. For this purpose, DBA/1 J mice were immunized twice with bovine CII in CFA to elicit CIA. Four groups of mice were treated intraperitoneally with either 200, 400 µg of 5-I, 400 µg of RXM, or 200 µl of saline as control solvent. Administration of RXM, 5-I, and saline was started at the time of secondary immunization of CII (day 0), and was continued on a schedule of every-other-day treatment up to day 20. As shown in Figure 5A, mice treated with control saline developed severe arthritis. In contrast, administration of 5-I significantly ameliorated the clinical manifestations of arthritis in a dose-dependent manner (Figure 5A), similar to results observed with 400 µg of RXM. The mean body weight of mice within each group was inversely correlated with their arthritis severity (Figure 5B). As summarized in Table 1, treatment with 400 µg of 5-I significantly decreased the mean arthritis score and the percentage of arthritic paw number. In addition, the mean body weight was markedly different from the saline-treated group, although the day of onset was not affected.

To determine whether 5-I therapy would still be effective even after the onset of disease manifestation, we next conducted a study involving delayed treatment of 5-I. Since disease onset typically occurred on day 4, we initiated a treatment regimen similar to our earlier work from day 4 onward, and then evaluated the clinical scores of the tested animals. As shown in Figure 5C,

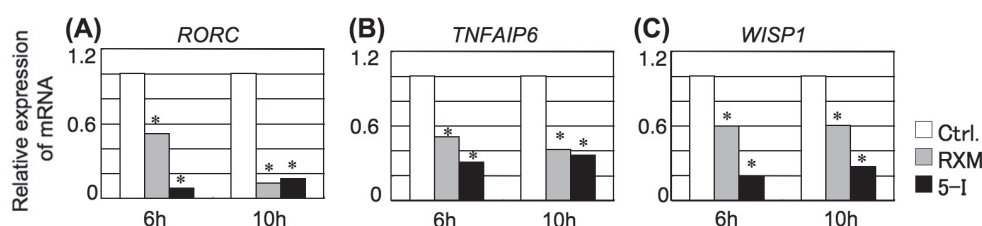


Figure 4. Measurement of gene expression by real-time RT-PCR. Purified CD4<sup>+</sup> T cells were subjected to CD3/CD28-stimulation in the presence or absence of RXM and 5-I. After 24 h of culture, mRNA was extracted and alterations in gene expression in these cells were evaluated. Real-time PCR analysis for (A) *RORC*, (B) *TNFAIP6*, and (C) *WISP1*. Y-axis indicates relative expression level of indicated genes in the cultured CD4<sup>+</sup> T cells (the expression level of control cells was set to 1.0). Data shown were representative of 4 independent experiments from 10 donors. Statistically significant difference from control cells is shown (\* $p < 0.01$ ).

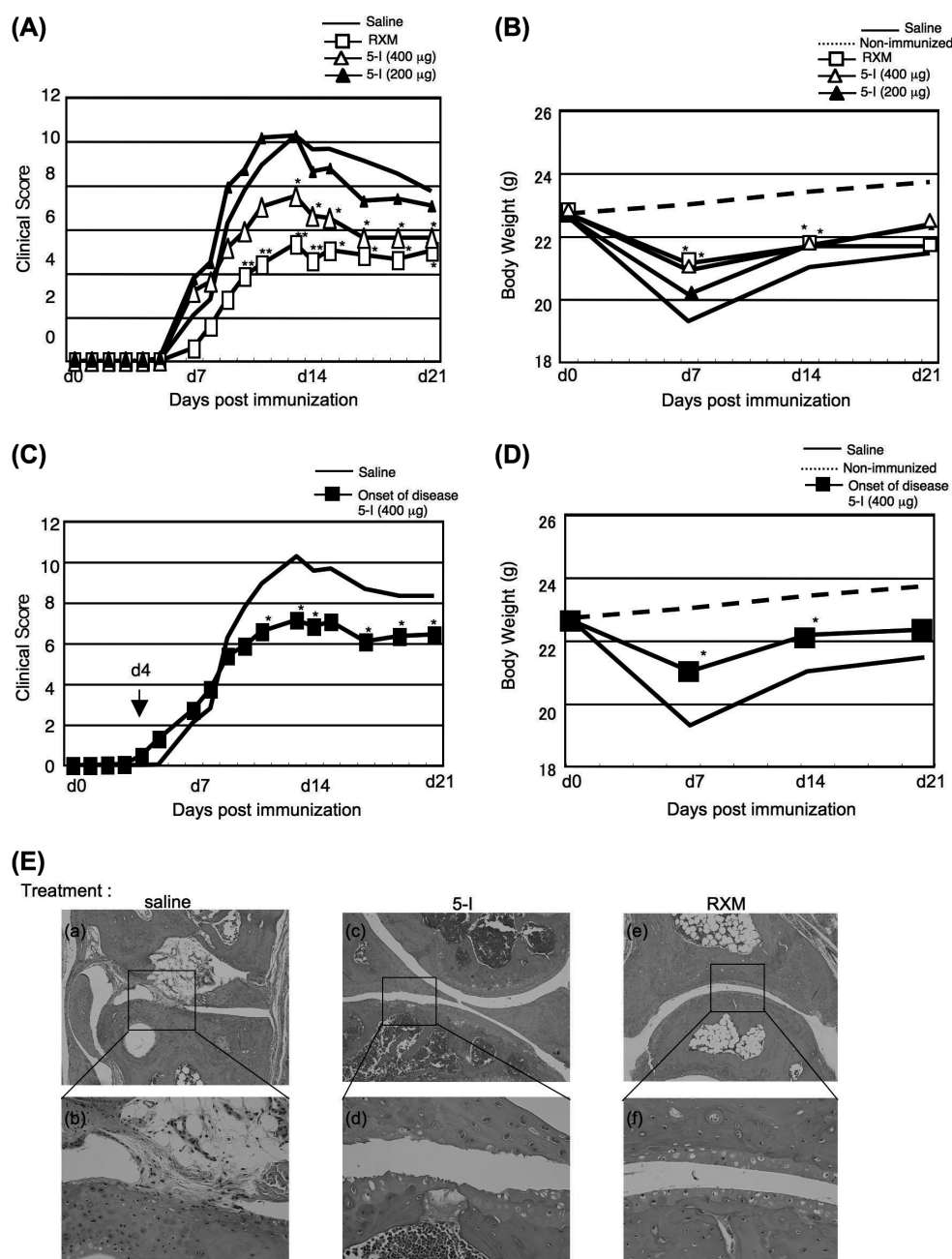


Figure 5. Effect of RXM and 5-I treatment on clinical score, body weight and histopathology of arthritis. Collagen-induced arthritis (CIA) was induced by primary (day - 21) and secondary (day 0) immunization with bovine type II collagen (CII) in complete Freund's adjuvant. (A) Four groups of mice were injected intraperitoneally with either control saline (-), 200 µg of 5-I (▲), 400 µg of 5-I (△), or RXM (□) every other day between day 0 and day 20. Changes of the clinical arthritis score are shown. (B) Body weight change of CIA-mice in A compared with non-immunized mice (-). (C) For studies involving delayed 5-I treatment, two groups of mice were injected intraperitoneally with control saline (-) or 400 µg of 5-I (■) every other day between day 4 and day 20. Changes of the clinical arthritis score are shown. (D) Body weight change of delayed treatment mice, compared with saline-treated mice (-) and non-immunized mice (-). Data were expressed as the mean of ten mice in each group. Data shown were representative of three independent experiments with similar results. Statistically significant difference compared to the control saline-treated group (\* $p < 0.05$ ). (E) Administration of RXM, 5-I, and saline was started on the day of secondary immunization of CII (day 0), and continued on a schedule of every-other-day treatment up to day 20. The mice treated with saline as control solvent developed severe arthritis (panels a and b). In contrast, administration of 5-I or RXM significantly ameliorated destruction of cartilage and bone (panels c and d, or e and f, respectively).

delayed treatment with 5-I was also effective in reducing the clinical arthritis scores. Moreover, as shown in Figure 5D, the mean body weight of the treated group was restored significantly as compared to the saline-treated control group. These results indicated that 5-I therapy started either before or after the onset of disease could reduce the severity of arthritis, suggesting that 5-I-mediated

immunomodulatory effects improved the inflammation associated with CIA.

We also performed histological studies of CIA mice. As shown in Figure 5E, mice treated with control saline developed arthritis with pannus formation (panels a and b). In contrast, RXM administration significantly inhibited destruction of cartilages and bones (panels c and d of Figure 5E). Although the superficial layers of cartilage were degraded slightly in the 5-I treated mice, bone destruction or pannus formation was not observed (panels e and f of Figure 5E). These findings suggest that 5-I, as well as RXM, exert immunomodulatory effects *in vivo*.

Finally, we examined serum levels of anti-CII antibody in CIA mice. As shown in Supplementary Figures 3 available online at <http://informahealthcare.com/doi/abs/10.3109/14397595.2014.983262>, an anti-CII antibody was detected after Day 7 of the second immunization of CII in each cohort, while titers for anti-CII antibody in CIA mice treated with RXAM or 5-I were similar to those of the control group. Taken together with the data of *in vitro* experiments, our observations indicate that 5-I, as well as

Table 1. Effect of 5-I treatment on CIA<sup>a</sup>.

	Saline	RXM	5-I
Day of onset	5.3 ± 2.0	7.4 ± 2.0	6.0 ± 0.5
Clinical Score (day 14)	9.6 ± 2.7	4.6 ± 2.8 <sup>c</sup>	6.6 ± 3.6 <sup>b</sup>
Body weight (grams) (day 7)	19.3 ± 1.8	21.1 g ± 0.7 <sup>b</sup>	21.0 g ± 1.3 <sup>b</sup>
Arthritic paw (day 14)	90.9%	75.0%	77.5%

<sup>a</sup>CIA was induced as described in Figure 5 and treated with either 400 µg of RXM or 5-I, or control saline, for every other day from day 1 to day 21.

<sup>b,c</sup>Statistically different from the control saline-treated group (<sup>b</sup> $p < 0.05$ , <sup>c</sup> $p < 0.01$ ).



RXM, exert immunomodulatory effects resulted from inhibition of proinflammatory cytokines, and strongly suggested that 5-I may be useful as potential therapy for human RA.

## Discussion

In this study, we evaluated the immunomodulatory effects of 5-I, a newly synthesized derivative of RXM. We showed that 5-I exhibited only weak antibacterial activity but clearly reduced production of Th1-, Th17-, and proinflammatory cytokines such as IL-6 and TNF- $\alpha$  by activated T cells and monocytes. In addition, 5-I inhibited transendothelial migration of activated T cells, while suppressing transcription of ROR $\gamma$ t mRNA from CD3- and CD28-stimulated CD4<sup>+</sup> T cells. In addition, and most importantly, 5-I administration ameliorated the clinical manifestations of CIA, with its beneficial effect being similarly seen when given after the onset of CIA-related arthritis symptoms.

Naïve CD4 T cells may differentiate into one of several lineages of Th cells, including Th1, Th2, Th17, and inducible regulatory T cells (iTreg), as defined by their pattern of cytokine production and functions [18], and these T cell subsets play important roles in T cell-dependent immune regulations. The cellular interactions involved in subset differentiation are generally well-defined, with both Th1 and Th2 cells controlling the differentiation of Th17 cells and with Th17 cells inhibiting Th1 and Th2 development [19]. Since RXM and 5-I suppressed *in vitro* production of IL-17, we examined the expression of IL-17A-related mRNAs using real-time RT-PCR assays. *RORC*, a transcription factor coding-gene for the orphan nuclear receptor, retinoic orphan receptor  $\gamma$  t (ROR $\gamma$ t), is uniquely expressed in IL-17A-producing mouse T cells and is required for the *in vitro* and *in vivo* upregulation of this cytokine in T cells [20]. It has been reported recently that ROR $\gamma$ t has a central function in the differentiation of human Th17 cells from naïve CD4<sup>+</sup> T cells [21]. Therefore, data demonstrating suppression of *RORC* expression by RXM or 5-I supported the *in vitro* results of RXM or 5-I-mediated inhibition of IL-17.

Several studies have identified the critical roles of TGF- $\beta$  and IL-6 as proximal factors essential for the induction of Th17 development, and IL-23 has been shown to have a functional role subsequent to Th17 commitment, contingent upon the upregulation of the inducible component of the IL-23 receptor [22]. Based on these reports, it is conceivable that RXM or 5-I may modulate the expression of cytokine receptors or transcription factors required for naïve CD4<sup>+</sup> T cells to differentiate into Th1, Th2, or Th17 subset. We assessed the expression of *IL12RB* and *TBX21* for Th1, *IL13RA* and *GATA3* for Th2, and *IL23R* and *TGFB2* for Th17. However, no detectable modulation in the expression of mRNAs encoding for these molecules, including *IL23R*, was observed following treatment by RXM or 5-I (data not shown). A potential explanation for this observation may be the fact that the optimal time point following RXM or 5-I treatment to detect changes in specific gene expression has yet to be determined. We also performed gene profiling microarray analysis of purified CD4<sup>+</sup> T cells following *in vitro* treatment of RXM or 5-I (data not shown). Although the expression levels of mRNAs encoding numerous genes were altered by the addition of the macrolides, only *TNFAIP6* and *WISP1* mRNAs were consistently down-regulated among all the different donors, as detected by real-time RT-PCR assays. Since *TNFAIP6* (also known as TSG-6) and *WISP1* (also known as CCN4) have been reported to be involved in inflammatory disorders including RA [23–27], it is conceivable that down-regulation of their expression levels by RXM or 5-I may be potentially beneficial in reducing the joint inflammation seen in conditions such as RA. Other investigators have reported that macrolides inhibit TNF or WNT signaling pathways in

inflammation process [25, 28–30]. It is conceivable that 5-I, a derivative of RXM, may have the inhibitory effects on these pathways. Moreover, it will be elucidated in a future study whether 5-I more effectively suppressed *RORC*, *TNFAIP6*, and *WISP1* than RXM.

In both CIA and RA, the inflamed synovium is characterized by elevated level of IL-6, TNF- $\alpha$ , and IL-17 [31–33]. A complex interaction among T cells, monocytes, and fibroblasts in the synovium leads to the development of arthritis. Specifically, activated T cells stimulate monocytes and synoviocytes through direct cell-cell contact and release of cytokines such as IFN- $\gamma$  and IL-17. These cells in turn may amplify the inflammatory cascade through the release of additional cytokines, such as IL-1 and TNF- $\alpha$ , which then stimulate mesenchymal cells to release IL-6 and other factors [31–33]. Local inflammation is triggering and exacerbating cartilage destruction in the joint, and then promotes bone erosion. At the initial step of the perpetuation of this inflammatory process, the *in vivo* effectiveness of 5-I in preventing CIA development likewise RXM, might be intimately linked to the ability of 5-I to inhibit T cell transendothelial migration and cytokine production by T cells and monocytes *in vitro*.

Various costimulatory pathways, which regulate the production of IL-17, TNF- $\alpha$ , or IL-6, have been implicated in the pathogenesis of RA based on studies of human tissues and animal models [34–37]. Advances in understanding disease pathogenesis have led to the identification of molecular targets for immuno-therapeutic intervention. Therapies inhibiting TNF- $\alpha$  activity in patients with active RA result in rapid and sustained improvement in symptoms and signs of disease [38]. It is also conceivable that patients who fail to respond to therapy with specific TNF- $\alpha$  inhibitors could have IL-17-driven disease. Concurrent or sequential inhibition of TNF- $\alpha$  and IL-17 could enable two different cell types with roles in disease pathogenesis to be simultaneously targeted, such as T cells and macrophages.

Other investigators reported that the regulatory mechanism of arthritis involved dysfunction of CII-reactive Th17 cell differentiation by overexpression of T-bet [39]. While titers for anti-CII antibody in CIA mice treated with RXM or 5-I were similar to those of the control group, we could not exclude the possibility that 5-I or RXM exerts an effect on autoreactive lymphocytes, and this possibility will be investigated in a future study involving human cells as well as CIA mice.

Pharmacokinetics data on RXM provided by a pharmaceutical company indicated that the mean peak plasma concentration was 6.6  $\mu$ g/ml and the AUC was 96  $\mu$ g.h/ml following the administration of a single oral dose of RXM 150 mg to healthy young adults [40]. At steady state following doses of 150 mg twice daily, the mean peak plasma concentration was 9.3  $\mu$ g/ml and the AUC was 71  $\mu$ g.h/ml [40]. This information would suggest that the doses of RXM used in this study correspond to the potential physiological ranges. Although pharmacokinetics data on 5-I are not yet available, it is estimated that dosages for 5-I are comparable to those for RXM, based on similar molecular profiles. Therefore, it is conceivable that the concentration ranges of RXM or 5-I used in this study are appropriate physiologically.

In conclusion, 5-I is a potent immunomodulatory macrolide that ameliorates CIA through anti-inflammatory actions and suppression of Th1, Th17, and proinflammatory cytokines such as TNF- $\alpha$  and IL-6. Since 5-I therapy is also effective as delayed treatment following the clinical onset of disease, our results strongly suggest that it may have a role in the clinical setting as an effective therapeutic agent. Since RXM has been used successfully for bronchial asthma, inflammatory bowel disease, and RA, 5-I may also be useful for treating diseases with Th17 having a significant role in disease pathophysiology, such as multiple sclerosis [41], psoriasis [42], and Crohn's disease [43].



## Acknowledgement

This study was supported in part by a grant of the Ministry of Education, Science, Sports and Culture, Japan (K.O. and C.M.), a grant of the Ministry of Health, Labour, and Welfare, Japan (C.M.) and a Grant-in-Aid (E2628 and S1311011) from the Foundation of Strategic Research Projects in Private Universities from the Ministry of Education, Culture, Sports, Science, and Technology, Japan (K.O. and C.M.).

## Authorship contributions

Contributions: N.O., S.I. and R.H. performed the experiments, interpreted the data, O.H. assisted with the paper, K.O. and C.M. designed the research, interpreted the data and wrote the paper, N.H.D. interpreted the data, assisted with the paper, and proofread the manuscript, and T.Y. performed the experiments, analyzed pathological results, interpreted the data and assisted with the paper.

## Conflict of interest

None.

## References

1. Kudoh S, Keicho N. Diffuse panbronchiolitis. *Semin Respir Crit Care Med*. 2003;24(5):607–18.
2. Gotfried MH. Macrolides for the treatment of chronic sinusitis, asthma, and COPD. *Chest*. 2004;125(2 Suppl):52S–60S.
3. Park CS, Park YS, Park YJ, Cho JH, Kang JM, Kim SY. The inhibitory effects of macrolide antibiotics on bone remodeling in chronic rhinosinusitis. *Otolaryngology–head and neck surgery*. 2007;137(2):274–9.
4. Inoue S, Nakase H, Matsuura M, Ueno S, Uza N, Kitamura H, et al. Open label trial of clarithromycin therapy in Japanese patients with Crohn's disease. *J Gastroenterol Hepatol*. 2007;22(7):984–8.
5. Polat M, Lenk N, Yalcin B, Gur G, Tamer E, Artuz F, Alli N. Efficacy of erythromycin for psoriasis vulgaris. *Clin Exp Dermatol*. 2007;32(3):295–7.
6. Frascini F, Scaglione F, Ferrara F, Marelli O, Braga PC, Teodori F. Evaluation of the immunostimulating activity of erythromycin in man. *Chemotherapy*. 1986;32(3):286–90.
7. Anderson R. Erythromycin and roxithromycin potentiate human neutrophil locomotion *in vitro* by inhibition of leukoattractant-activated superoxide generation and autooxidation. *J Infect Dis*. 1989;159(5):966–73.
8. Chantot JF, Bryskier A, Gasc JC. Antibacterial activity of roxithromycin: a laboratory evaluation. *J Antibiot (Tokyo)*. 1986;39(5):660–8.
9. Young RA, Gonzalez JP, Sorkin EM. Roxithromycin. A review of its antibacterial activity, pharmacokinetic properties and clinical efficacy. *Drugs*. 1989;37(1):8–41.
10. Noma T, Hayashi M, Yoshizawa I, Aoki K, Shikishima Y, Kawano Y. A comparative investigation of the restorative effects of roxithromycin on neutrophil activities. *Int J Immunopharmacol*. 1998;20(11):615–24.
11. Wakita H, Tokura Y, Furukawa F, Takigawa M. The macrolide antibiotic, roxithromycin suppresses IFN- $\gamma$ -mediated immunological functions of cultured normal human keratinocytes. *Biol Pharm Bull*. 1996;19(2):224–7.
12. Konno S, Adachi M, Asano K, Okamoto K, Takahashi T. Inhibition of human T-lymphocyte activation by macrolide antibiotic, roxithromycin. *Life Sci*. 1992;51(24):PL231–6.
13. Yoshimura T, Kurita C, Yamazaki F, Shindo J, Morishima I, Machida K, et al. Effects of roxithromycin on proliferation of peripheral blood mononuclear cells and production of lipopolysaccharide-induced cytokines. *Biol Pharm Bull*. 1995;18(6):876–81.
14. Urasaki Y, Nori M, Iwata S, Sasaki T, Hosono O, Kawasaki H, et al. Roxithromycin specifically inhibits development of collagen induced arthritis and production of proinflammatory cytokines by human T cells and macrophages. *J Rheumatol*. 2005;32:1765–74.
15. Iwata S, Yamaguchi N, Munakata Y, Ikushima H, Lee JF, Hosono O, et al. CD26/dipeptidyl peptidase IV differentially regulates the chemotaxis of T cells and monocytes toward RANTES: possible mechanism for the switch from innate to acquired immune response. *Int Immunol*. 1999;11:417–26.

16. Rosloniec EF, Cremer M, Kang A, Myers LK. Collagen-induced arthritis. In: Coligan JE, Kruisbeek AM, Margulies AH, Shevach EM, Strober W, eds. *Current Protocols in Immunology*.
17. Endo Y, Hirahara K, Yagi R, Tumes DJ, Nakayama T. Pathogenic memory type Th2 cells in allergic inflammation. *Trends Immunol*. 2014;35(2):69–78.
18. Christie D, Zhu J. Transcriptional Regulatory Networks for CD4 T Cell Differentiation. *Curr Top Microbiol Immunol*. 2014;381:125–72.
19. Korn T, Bettelli E, Oukka M, Kuchroo VK. IL-17 and Th17 Cells. *Annu Rev Immunol*. 2009;27:485–517.
20. Ivanov II, McKenzie BS, Zhou L, Tadokoro CE, Lepelletier A, Lafaille JJ, et al. The orphan nuclear receptor ROR $\gamma$ t directs the differentiation program of proinflammatory IL-17<sup>+</sup> T helper cells. *Cell*. 2006;126(6):1121–33.
21. Manel N, Unutmaz D, Littman DR. The differentiation of human T<sub>H</sub>-17 cells requires transforming growth factor- $\beta$  and induction of the nuclear receptor ROR $\gamma$ t. *Nat Immunol*. 2008;9(6):641–9.
22. Bettelli E, Oukka M, Kuchroo VK. T<sub>H</sub>-17 cells in the circle of immunity and autoimmunity. *Nat Immunol*. 2007;8(4):345–50.
23. Glant TT, Kamath RV, Bardos T, Gal I, Szanto S, Murad YM, et al. Cartilage-specific constitutive expression of TSG-6 protein (product of tumor necrosis factor alpha-stimulated gene 6) provides a chondroprotective, but not antiinflammatory, effect in antigen-induced arthritis. *Arthritis Rheum*. 2002;46(8):2207–18.
24. Bayliss MT, Howat SL, Dudhia J, Murphy JM, Barry FP, Edwards JC, Day AJ. Up-regulation and differential expression of the hyaluronan-binding protein TSG-6 in cartilage and synovium in rheumatoid arthritis and osteoarthritis. *Osteoarthritis Cartilage*. 2001;9(1):42–8.
25. Milner CM, Day AJ. TSG-6: a multifunctional protein associated with inflammation. *J Cell Sci*. 2003;116(Pt 10):1863–73.
26. Venkatachalam K, Venkatesan B, Valente AJ, Melby PC, Nandish S, Reusch JE, et al. WISP1, a pro-mitogenic, pro-survival factor, mediates tumor necrosis factor-alpha (TNF- $\alpha$ )-stimulated cardiac fibroblast proliferation but inhibits TNF- $\alpha$ -induced cardiomyocyte death. *J Biol Chem*. 2009;284(21):14414–27.
27. Mori H, Nishida K, Ozaki T, Inoue H, Setsu K, Tsujigiwa H, et al. Expression of WISP-1 (ccn4), WISP-2 (ccn5) and WISP-3 (ccn6) in rheumatoid arthritis synovium evaluated by DNA microarrays. *J Hard Tissue Biol*. 2006;15(3):89–95.
28. Takahashi H, Hashimoto Y, Ishida-Yamamoto A, Iizuka H. Roxithromycin suppresses involucrin expression by modulation of activator protein-1 and nuclear factor- $\kappa$ B activities of keratinocytes. *J Dermatol Sci*. 2005;39(3):175–82.
29. Asano K, Tryka E, Cho JS, Keicho N. Macrolide therapy in chronic inflammatory diseases. *Mediators Inflamm*. 2012;2012:692352.
30. Du Q, Geller DA. Cross-Regulation Between Wnt and NF- $\kappa$ B Signaling Pathways. *For Immunopathol Dis Therap*. 2010;1(3):155–81.
31. Aarvak T, Chabaud M, Miossec P, Natvig JB. IL-17 is produced by some proinflammatory Th1/Th0 cells but not by Th2 cells. *J Immunol*. 1999;162(3):1246–51.
32. Chabaud M, Durand JM, Buchs N, Fossiez F, Page G, Frappart L, Miossec P. Human interleukin-17: A T cell-derived proinflammatory cytokine produced by the rheumatoid synovium. *Arthritis Rheum*. 1999;42(5):963–70.
33. Marinova-Mutafchieva L, Williams RO, Mason LJ, Mauri C, Feldmann M, Maini RN. Dynamics of proinflammatory cytokine expression in the joints of mice with collagen-induced arthritis (CIA). *Clin Exp Immunol*. 1997;107(3):507–12.
34. Durie FH, Fava RA, Foy TM, Aruffo A, Ledbetter JA, Noelle RJ. Prevention of collagen-induced arthritis with an antibody to gp39, the ligand for CD40. *Science*. 1993;261(5126):1328–30.
35. Iwai H, Kozono Y, Hirose S, Akiba H, Yagita H, Okumura K, et al. Amelioration of collagen-induced arthritis by blockade of inducible costimulator-B7 homologous protein costimulation. *J Immunol*. 2002;169(8):4332–9.
36. Webb LM, Walmsley MJ, Feldmann M. Prevention and amelioration of collagen-induced arthritis by blockade of the CD28 co-stimulatory pathway: requirement for both B7-1 and B7-2. *Eur J Immunol*. 1996;26(10):2320–8.
37. Yoshioka T, Nakajima A, Akiba H, Ishiwata T, Asano G, Yoshino S, et al. Contribution of OX40/OX40 ligand interaction to the pathogenesis of rheumatoid arthritis. *Eur J Immunol*. 2000;30(10):2815–23.
38. Lipsky PE, van der Heijde DM, St Clair EW, Furst DE, Breedveld FC, Kalden JR, et al. Infliximab and methotrexate in the treatment of rheumatoid arthritis. Anti-Tumor Necrosis Factor Trial in Rheumatoid Arthritis with Concomitant Therapy Study Group. *New Engl J Med*. 2000;343(22):1594–602.

39. Kondo Y, Iizuka M, Wakamatsu E, Yao Z, Tahara M, Tsuboi H, et al. Overexpression of T-bet gene regulates murine autoimmune arthritis. *Arthritis Rheum.* 2012;64(1):162–72.
40. Product Information, RULIDE® & RULIDE® D. [http://www.sanofi.com.au/products/aus\\_pi\\_rulide.pdf](http://www.sanofi.com.au/products/aus_pi_rulide.pdf); 2012.
41. Kebir H, Kreymborg K, Ifergan I, Dodelet-Devillers A, Cayrol R, Bernard M, et al. Human T<sub>H</sub>17 lymphocytes promote blood-brain barrier disruption and central nervous system inflammation. *Nat Med.* 2007;13(10):1173–5.
42. Zaba LC, Cardinale I, Gilleaudeau P, Sullivan-Whalen M, Suarez-Farinas M, Fuentes-Duculan J, et al. Amelioration of epidermal hyperplasia by TNF inhibition is associated with reduced Th17 responses. *J Exp Med.* 2007;204(13):3183–94.
43. Yen D, Cheung J, Scheerens H, Poulet F, McClanahan T, McKenzie B, et al. IL-23 is essential for T cell-mediated colitis and promotes inflammation via IL-17 and IL-6. *J Clin Invest.* 2006; 116(5):1310–6.

### **Supplementary material available online**

Supplementary Table 1 and Figures 1 – 3.



## Comparison of Two Commercial ELISAs against an In-House ELISA for Measuring Soluble CD26 in Human Serum

Kei Ohnuma,<sup>1\*</sup> Tatsuhiko Saito,<sup>2</sup> Ryou Hatano,<sup>1</sup> Osamu Hosono,<sup>3</sup> Satoshi Iwata,<sup>1</sup> Nam H. Dang,<sup>4</sup> Hiroki Ninomiya,<sup>5</sup> and Chikao Morimoto<sup>1</sup>

<sup>1</sup>Department of Therapy Development and Innovation for Immune Disorders and Cancers, Graduate School of Medicine, Juntendo University, Hongo, Bunkyo-ku, Tokyo, Japan

<sup>2</sup>Department of Diabetes and Metabolism Internal Medicine, Kobari General Hospital, Yokouchi, Noda City, Chiba, Japan

<sup>3</sup>Department of Rheumatology and Allergy, Research Hospital, Institute of Medical Science, University of Tokyo, Shrokanedai, Minato-ku, Tokyo, Japan

<sup>4</sup>Division of Hematology/Oncology, University of Florida, Gainesville, Florida,

<sup>5</sup>Kobari General Hospital, Yokouchi, Noda City, Chiba, Japan

**Background:** CD26 is a T-cell costimulatory molecule with dipeptidyl peptidase IV (DPPIV) activity in its extracellular region. The relevance of sCD26 levels and disease activity has been reported in rheumatic or infectious disease. For certain metabolic and endocrine conditions, DPPIV inhibitors were recently developed as a new class of antidiabetic drugs that act by inhibiting DPPIV, the enzyme that inactivates incretin hormone. Higher levels of sCD26 in diabetic patients have been shown to be associated with a poor clinical response to DPPIV inhibitors, with sCD26/DPPIV being an adipokine that may impair insulin sensitivity. With the increasing use of serum sCD26 and DPPIV enzyme activity as biomarkers with potential clinical implications, accurate measurements of serum sCD26 levels and DPPIV enzyme activity are needed. **Methods:** We compare two commercially widely available and an in-house enzyme-linked immunosor-

bent assays (ELISAs) for measurement of serum sCD26 in healthy or diabetic human sera. **Results:** The significant discrepancies among the results obtained from commercially available and the in-house sCD26 assays were found. We also observed that a linear correlation between serum sCD26 level and DPPIV enzyme activity exists with the in-house ELISA, while the commercial ELISAs demonstrate a lack of consistency between serum sCD26 level and DPPIV enzyme activity. **Conclusion:** These data strongly suggest that new commercial assays for sCD26 plasma levels need detailed evaluation and validation with samples from clinically well-characterized patients, and results obtained from these newer assays should be compared to those obtained from well-established in-house assays such as our assay or other validated sCD26 ELISA assays. J. Clin. Lab. Anal. 29:106–111, 2015. © 2014 Wiley Periodicals, Inc.

**Key words:** CD26; dipeptidyl peptidase IV; T cell costimulation

### INTRODUCTION

CD26 is a 110 kDa surface glycoprotein with dipeptidyl peptidase IV (DPPIV, EC 3.4.14.5) activity, being a serine protease that cleaves dipeptides from the N-terminus of peptides at the penultimate position (1). CD26 is also associated with T-cell signal transduction processes as a costimulatory molecule, as well as being a marker of T-cell activation (2). We have previously reported that effector CD26-mediated costimulatory activity is exerted via its DPPIV enzyme activity (2, 3). More recently, we have shown that serum-soluble CD26 (sCD26) and DPPIV

enzyme activity are inversely correlated with disease activity of patients with systemic lupus erythematosus (4).

Grant sponsor: The Ministry of Education, Science, Sports and Culture, Ministry of Health, Labour, and Welfare, Japan.

\*Correspondence to: Kei Ohnuma, Department of Therapy Development and Innovation for Immune Disorders and Cancers, Graduate School of Medicine, Juntendo University, 2-1-1, Hongo, Bunkyo-ku, Tokyo 113-8421, Japan. E-mail: kohnuma@juntendo.ac.jp

Received 7 May 2013; Accepted 12 December 2013

DOI 10.1002/jcla.21736

Published online in Wiley Online Library (wileyonlinelibrary.com).

Other investigators have reported that serum sCD26 level was lower in rheumatoid arthritis (RA) patients than in healthy control or in patients with osteoarthritis (OA) (5, 6). sCD26 lacks transmembrane and cytoplasmic domains (the sequence starting at the 39th amino acid position of the full-length of CD26) (7), although its molecular weight is similar to that of the full-length transmembrane CD26 since it exists as a homodimer in serum/plasma and is heavily glycosylated between the 48 and 324th amino acid positions (8). Meanwhile, DPPIV enzyme activity has been widely studied in metabolic and endocrine disorders, and DPPIV inhibitors have been developed as a new class of antidiabetic drugs that act by inhibiting DPPIV, the enzyme that inactivates incretin hormone (9). For instance, higher serum level of sCD26 was reported to be associated with a worse response to sitagliptin in patients with type 2 diabetes (T2DM) controlled inadequately by metformin and/or sulfonylurea therapy (10). Moreover, other investigators have reported that sCD26/DPPIV is one of the adipokines that may impair insulin sensitivity (11). The potentially important role played by CD26/DPPIV in the clinical setting has led to rising interest in the quantification of serum sCD26 level and DPPIV enzyme activity over the past decade. This is also reflected in the number of publications on this topic and in the recent worldwide availability of commercial CD26 enzyme-linked immunosorbent assays (ELISAs), which can help researchers working in this area avoid the time-consuming process of in-house assay development and maintenance. However, it is our belief that these new commercial assays should be proven to deliver accurate, reliable, and reproducible data prior to usage for analysis of valuable patient-derived samples, even if the assay is certified by the manufacturer. In addition, DPPIV enzymatic activity has been correlated with sCD26 concentration (12), with the enzymatic activity of DPPIV being determined with the use of either chromogenic or fluorogenic substrates. Meanwhile, commercially available DPPIV activity assay kits have been shown to provide comparable results (13). On the other hand, comparative studies of different assay kits for sCD26 quantification have not yet been rigorously performed using human samples. The aim of this study is therefore to compare two commercially worldwide available sCD26 ELISA assays and our own in-house ELISA for detecting both sCD26 level and specific DPPIV enzyme activity.

## MATERIALS AND METHODS

### Serum Collections and Storage

Peripheral blood samples were collected from healthy adult volunteers and T2DM patients (regularly seen and treated at the Kobari General Hospital), using BD Vacu-

tainer blood collection tube SSTII (BD, Franklin Lakes, NJ). Serum was obtained from 5 ml whole blood by centrifugation at  $1,500 \times g$  at  $4^{\circ}\text{C}$  for 10 min, and stored at  $-80^{\circ}\text{C}$  in 500  $\mu\text{l}$  aliquots. Human study protocols were approved by the Ethics Committees at the Kobari General Hospital (Authorization Number 10) and Juntendo University (Authorization Number 2012192). Informed consent was obtained from all patients. Patients' gender and age were matched between normal and T2DM groups. All studies on human subjects were conducted according to the principles set out in the Declaration of Helsinki.

### ELISA Procedure

Serum samples were removed from the  $-80^{\circ}\text{C}$  freezer and quickly thawed in a water bath at  $37^{\circ}\text{C}$ . All samples were centrifuged  $3,000 \times g$  for 5 min to discard debris, and were then assayed in duplicate. Two commercial ELISA kits (Human sCD26 Platinum ELISA Kit, or Human DPPIV/CD26 Quantikine ELISA Kit) were purchased from eBioscience (Vienna, Austria), or R&D Systems, Inc. (Minneapolis, MN), respectively. Measurement of sCD26 level was performed according to the manufacturers' instructions. An in-house sandwich ELISA for sCD26 was established in our laboratory (14). Briefly, Maxisorp ELISA immunoplates (Nunc, Roskilde, Denmark) were coated with 100  $\mu\text{l}$  of 10  $\mu\text{g}/\text{ml}$  anti-CD26 monoclonal antibody (mAb) (clone: 5F8, mouse IgG<sub>1</sub>) in 0.05 M carbonate/bicarbonate buffer, pH 9.6, by incubating overnight at  $4^{\circ}\text{C}$ . Remaining binding sites were blocked with 200  $\mu\text{l}$  of 25% StartingBlock Blocking Buffer (Thermo Scientific, South Logan, UT) for 2 h at room temperature. Plates were then incubated with 100  $\mu\text{l}$  of serum appropriately diluted with 0.01 M phosphate buffered saline (PBS) containing 0.05% Tween 20 at  $4^{\circ}\text{C}$  overnight. Bound sCD26 molecules were detected by incubating with 100  $\mu\text{l}$  of biotin conjugated anti-CD26 mAb (clone: 9C11, mouse IgG<sub>1</sub>) followed by ExtrAvidin-alkaline phosphatase (Sigma-Aldrich, St. Louis, MO). The plates were developed with 1 mg/ml *p*-nitrophenyl phosphate in 10 mM diethanolamine buffer, pH 9.6, containing 0.5 mM  $\text{MgCl}_2$ . Color development was monitored at 405 nm on an iMark Microplate Reader (Bio-Rad Laboratories, Hercules, CA). Absorbance data were analyzed using Microplate Manager 6 Software (Bio-Rad Laboratories). In parallel with sCD26 protein concentration, DPPIV enzyme activity of bound sCD26 to 5F8 was detected by incubation with glycylproline *p*-nitroanilide (Gly-Pro-p-NA, 1 mg/ml in PBS; Sigma-Aldrich). Color development was measured at 405 nm. These results were standardized by a standard curve for *p*-nitroaniline (Sigma-Aldrich). Recombinant CD26/DPPIV (R&D Systems, Inc.) for a standard curve was used as the identical reagent in all three assays. 5F8

TABLE 1. Details of ELISA Assays as Specified by ELISA Manufactures and In-House Protocols

	R&D Quantikine	eBioscience	In-house
Kit format	12 by 8-well strips (flat-bottom)	12 by 8-well strips (flat-bottom)	96-well plate (flat-bottom)
Capture antibody	Rat mAb (no further information)	mAb (no further information)	Mouse mAb (5F8), house-made
Sample dilution and preparation	100-fold dilution	Five-fold dilution	20-fold dilution
Volume/ELISA-well	150 $\mu$ l	100 $\mu$ l	100 $\mu$ l
Dilution buffer	Buffered protein base with blue dye and preservative	No information	0.05% Tween 20-PBS
Sample incubation temperature	Room temperature	Room temperature	4°C
Sample incubation period	2 h	3 h	Overnight
Wash buffer	Buffered surfactant with preservative	1% Tween 20-PBS	0.05% Tween 20-PBS
Detection antibody	HRP conjugated pAb	Biotinylated mAb	Biotinylated mouse mAb (9C11)
Conjugate/substrate	Direct conjugation to detection pAb/TMB	Streptavidin-HRP/TMB	ExtrAvidin-ALP/PNPP
Optical density values (nm)	450	450	405
Standard <sup>a</sup>	Recombinant human DPPIV	Recombinant human DPPIV	Recombinant human DPPIV
Dynamic range (of Standard curve)	0.00031–0.020 ( $\mu$ g/ml)	0.0156–0.5 ( $\mu$ g/ml)	0.005–3.0 ( $\mu$ g/ml)
Data reduction	Log concentration of serial diluted standard against OD values	Log concentration of serial diluted standard against OD values	Log concentration of serial diluted standard against OD values
Precision (intra/interassay)	4–7.3%/8.2–9.1% (precision supplied by manufacturer)	0.8–13.7%/3.3–14.7% (precision supplied by manufacturer)	0.8–14.3%/4.1–15.9%

ALP, alkaline phosphatase; HRP, horseradish peroxidase; PBS, phosphate buffered saline; PNPP, *p*-nitrophenyl phosphate; TMB, tetramethylbenzidine.

<sup>a</sup>Recombinant human DPPIV is composed of the 34–766th amino acids of human CD26/DPPIV, with a C-terminal 6xHis tag, produced with the use of mouse myeloma cells NS0. This human DPPIV is highly glycosylated and shows 115 kDa in reducing sodium dodecyl sulfate-polyacrylamide gel electrophoresis, and presents as a homodimer in nonreducing condition.

was produced by immunizing BALB/cJ mice with a phytohemagglutinin-stimulated T cell line derived from the New World primate species *Aotus trivirgatus* (15). 9C11 was produced by immunizing mice with murine pre-B 300–19 cell line of human CD26 transfectant (16). Selected details for the three sCD26 assays including assay precisions are summarized in Table 1.

### Intra-assay and Interassay Variations

To analyze for intra-assay variation, three replicates of three different samples were run in one assay. To analyze for interassay variation, three different samples were run in three independent assays. The intra-assay or interassay variations were calculated using the following formula:

$$(\text{SD of assay results})/(\text{mean of assay results}) \times 100(\%).$$

### Statistical Analysis

The values measured are shown as mean  $\pm$  standard deviation (SD). The differences between groups were analyzed by one-way repeated measures ANOVA. 95% CIs were calculated and *P* values  $\leq 0.05$  were considered sta-

tistically significant. Correlation was calculated as Pearson product-moment correlation coefficient. Statistical analysis was performed using Microsoft Excel 2011 (Microsoft Corp., Redmond, WA) or GraphPad PRISM version 6 (GraphPad Software Inc., La Jolla, CA).

## RESULTS AND DISCUSSION

As shown in Figure 1A, serum sCD26 concentrations of healthy adults ( $n = 12$ ) measured by the two commercial kits and the in-house assay differed in all samples by approximately fourfold ( $0.34 \pm 0.14 \mu\text{g/ml}$  or  $0.36 \pm 0.15 \mu\text{g/ml}$  vs.  $1.20 \pm 0.31 \mu\text{g/ml}$ ). The values measured by our in-house assay were significantly higher than those by the R&D Quantikine assay ( $P < 0.0001$  [95% CI, 0.65–1.03]), or eBioscience Platinum assay ( $P < 0.0001$  [95% CI, 0.63–1.02]) (Fig. 1A). It has been reported that DPPIV enzymatic activity has been correlated with the concentration of sCD26 using the normal human sera (12). We therefore evaluated for potential correlation between DPPIV enzymatic activity and sCD26 level in the serum samples described above. For this purpose, we performed our in-house capture assay method using anti-human CD26 mAb as a capture antibody for detecting DPPIV specific



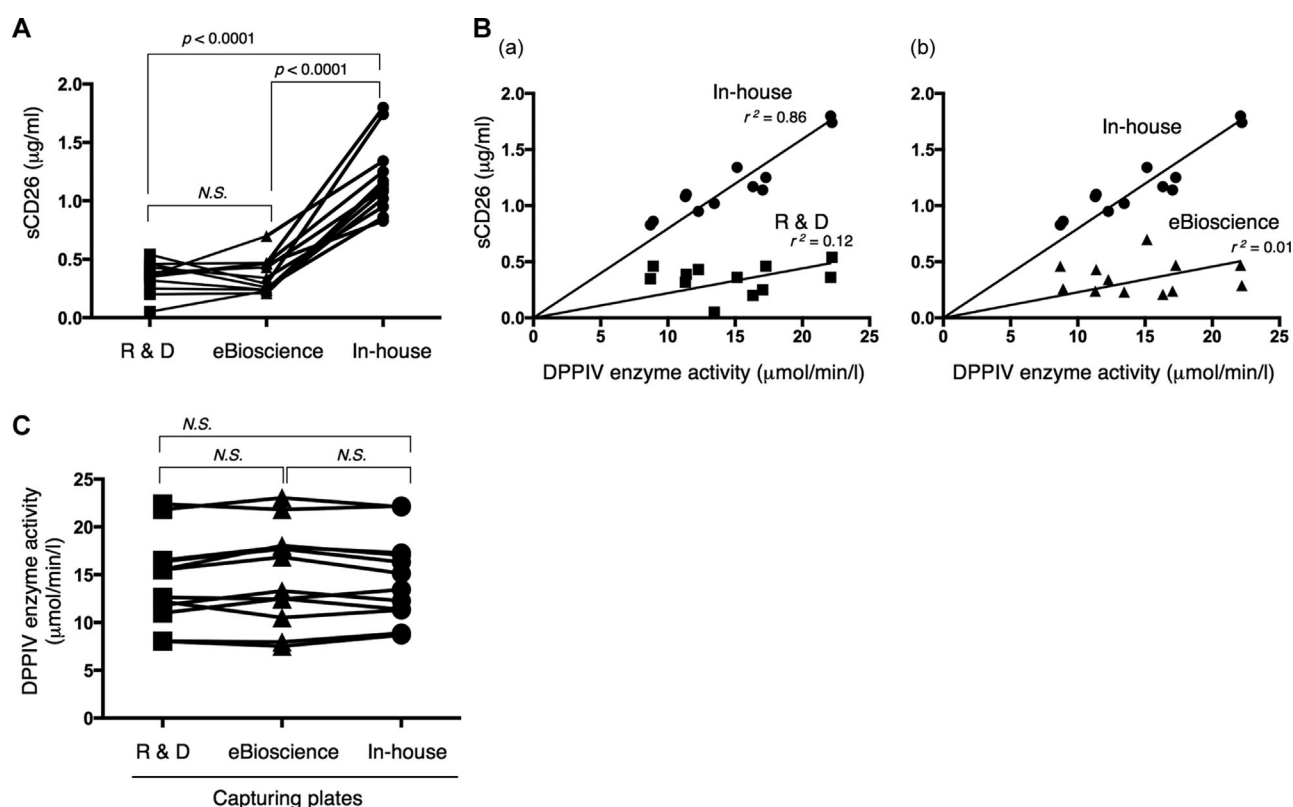


**Fig. 1.** Comparison of 12 normal serum samples, tested with three different ELISA assays for sCD26. (A) sCD26 levels in serum samples of 12 healthy adults were measured using the R&D Quantikine (solid squares), eBioscience Platinum (solid triangles), or in-house ELISA assays (solid circles). Each dot indicates individual value. Data of same samples are connected with horizontal lines. (B) Correlation between levels of sCD26 and DPPIV enzyme activity in serum samples of 12 healthy adults. (a) Comparison between in-house and the R&D Quantikine ELISA assays. (b) Comparison between in-house and the eBioscience Platinum ELISA assays. DPPIV enzyme activity was measured using our in-house capture method as described in Materials and Methods. (C) DPPIV enzyme activity in serum samples of 12 healthy adults was measured using the R&D Quantikine (solid squares), eBioscience Platinum (solid triangles), or in-house ELISA plates (solid circles). The samples were prepared and applied to each plate by the same method as the in-house method. DPPIV enzyme activity was measured using our in-house capture method as described in Materials and Methods. Data of same samples are connected with horizontal lines. N.S. denotes not significant.

to sCD26. It is conceivable that 5F8 is used for capturing sCD26 without affecting DPPIV enzyme activity in the plate since the epitope of human CD26 recognized by 5F8 is in the extracellular region of the truncated human CD26 containing the N-terminal residues 1–449th lacking DPPIV enzyme activity (16). Moreover, 5–10% of DPPIV activity in normal plasma/serum has been reported to be associated with other DPPIV-like peptidases such as DASH (DPPIV activity and/or structure homologues) proteins (17). Therefore, it is also possible to correlate the DPPIV activity with sCD26 level by capturing sCD26 molecules from the samples. As shown in Figure 1B, levels of sCD26 measured by our in-house assay clearly correlated with DPPIV enzyme activity ( $r^2 = 0.86$ ; slope,  $0.08 \pm 0.002$ ) (solid circles in panels a or b), while levels of sCD26 measured by the R&D Quantikine (solid squares in panel a) or eBioscience Platinum assays (solid triangles in panel b) did not correlate with DPPIV enzyme activity ( $r^2 = 0.12$ ; slope,  $0.02 \pm 0.003$ , or  $r^2 = 0.01$ ;

slope,  $0.02 \pm 0.003$ , respectively). To exclude the possibility that the incubation period of samples may influence the results, assays for sCD26 using the R&D Quantikine or eBioscience Platinum kits were conducted in which the sample incubation period in the capture step was extended to overnight at  $4^\circ\text{C}$ , which was the same method as in our in-house sCD26 assay. However, the obtained values were not influenced by extending the incubation period in the capture step (data not shown). Moreover, it was important to determine whether the values for DPPIV enzyme activity measured by the in-house plate were equal to those obtained from the commercial plates. To address this point, we evaluated captured DPPIV enzyme activity on the plates coated with the capture antibody in the R&D Quantikine or eBioscience Platinum kits. As shown in Figure 1C, the values of the captured DPPIV enzyme activity were similar for each assay. These results suggest that the ability to capture sCD26 is similar among the two commercial and our in-house plates, and

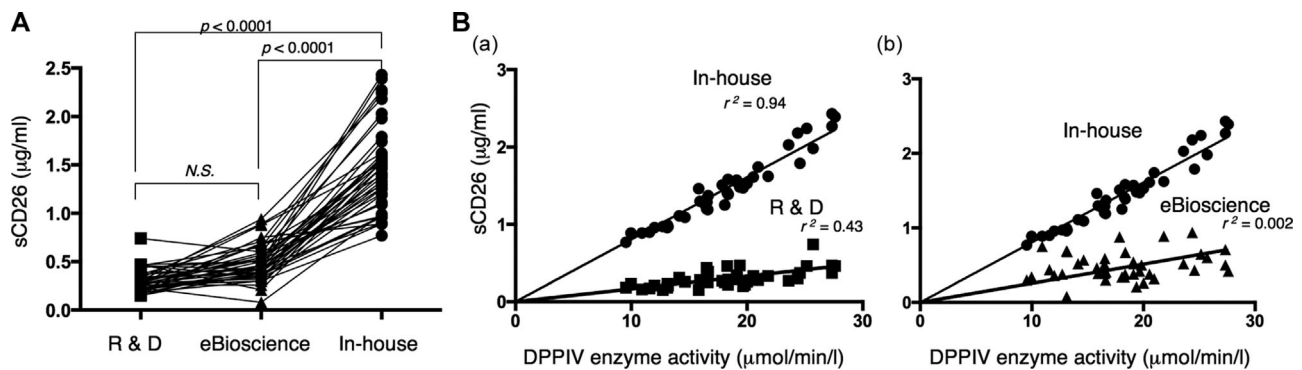


**Fig. 2.** Comparison of 50 serum samples of patients with T2DM, tested with three different ELISA assays for sCD26. (A) sCD26 levels in serum samples of 50 T2DM adults were measured using the R&D Quantikine (solid squares), eBioscience Platinum (solid triangles), or in-house ELISA assays (solid circles). Each dot indicates individual value. Data of same samples are connected with horizontal lines. N.S. denotes not significant. (B) Correlation between levels of sCD26 and DPPIV enzyme activity in serum samples of 50 T2DM patients. (a) Comparison between in-house and the R&D Quantikine ELISA assays. (b) Comparison between in-house and the eBioscience Platinum ELISA assays. DPPIV enzyme activity was measured using our in-house capture method as described in Materials and Methods.

that the observed variability among the assays may be due to differences in the sCD26 detection process.

We next determined serum levels of sCD26 in T2DM patients who were not being treated with DPPIV inhibitor therapy ( $n = 50$ ). As shown in Figure 2A, serum sCD26 concentrations of T2DM patients measured by the two commercial and our in-house assays differed in all samples by approximately four- to fivefold ( $0.30 \pm 0.12$  µg/ml or  $0.40 \pm 0.10$  µg/ml vs.  $1.45 \pm 0.34$  µg/ml). The two commercial assays measured samples of T2DM patients in the range of 0.15–0.74 µg/ml or 0.19–0.74 µg/ml (Fig. 2A), values that were compatible with the previously reported range of serum sCD26 concentrations of T2DM patients, using commercial assays (10, 18). As observed in healthy samples (Fig. 1A), the values measured by our in-house assay were significantly higher than those by the R&D Quantikine assay ( $P < 0.0001$  [95% CI, 1.04–1.27]) or eBioscience Platinum assay ( $P < 0.0001$  [95% CI, 0.91–1.19]) (Fig. 2A). Moreover, levels of sCD26 measured by our in-house assay clearly correlated with DPPIV enzyme activity ( $r^2 = 0.94$ ; slope,  $0.08 \pm 0.001$ ) (solid circles in panels a or b of Fig. 2B), while levels of sCD26 measured by the R&D Quantikine (solid squares in panel a of Fig. 2B) or eBioscience Platinum (solid triangles in panel b of Fig. 2B) assays did not correlate with DPPIV enzyme activity ( $r^2 = 0.43$ ; slope,  $0.02 \pm 0.001$ , or  $r^2 = 0.002$ ; slope,  $0.02 \pm 0.001$ , respectively). These data indicated that serum sCD26 concentration in human samples may be underestimated by the commercially available sCD26 assay, and that poor linearity between DPPIV enzyme activity and sCD26 level may misinterpret the clinical relevance of this molecule.

A critical issue for ELISAs is that the standard curve is stably plotted among different assays. In the present as-

says, we used commercially available recombinant human DPPIV derived from the same lot as the standard compound for all three ELISAs (Table 1), and obtained almost identical standard curves among various assays (data not shown). Therefore, the differences seen in sCD26 levels between the two commercial and our in-house ELISAs were likely not to be due to differences in the quality of the standard. To exclude the possibility that the clones of the capture antibody may influence the results, the in-house DPPIV enzyme activity assay was conducted with 1F7 as a capture antibody, a different epitope from 5F8. However, the obtained values were not influenced by the different epitope capture antibody (data not shown), suggesting higher validity of the in-house DPPIV enzyme activity assay. Moreover, it is theoretically possible that single nucleotide polymorphisms (SNPs) may affect the reactivity of the sandwich antibody sets of the commercial kits. One nonsynonymous coding region SNP Arg492Lys (G→A, exon 18) was reported, although its frequency or functional significance has not yet been determined (19). Since information regarding the clones of the capture and detection antibodies or the concentrations of these antibodies used in the commercial assays is not publicly available, the exact reasons for the observed inconsistencies seen with the commercial assays evaluated in this article are not clear. The epitopes of the anti-human CD26 mAbs used in our in-house assay are distinct from each other (16), that is, 5F8 or 9C11 recognizes 359–449th or 740–766th amino acids of human CD26, respectively. Moreover, these epitopes are also distinct from that of the humanized anti-CD26 mAb, which was developed in our laboratory for clinical uses, such as in the potential treatment of malignant methothelioma, or graft-versus-host disease (20, 21). Therefore, our in-house sCD26 assay can

be used to detect sCD26 or DPP-IV enzyme activity as biomarkers of patients who are subjected to humanized anti-CD26 mAb therapy.

## CONCLUSIONS

Given emerging data indicating the importance of serum levels of sCD26 in certain clinical settings, there is an urgent need for precise measurement and correlation of values obtained from different assays. In light of the discrepancies noted with results obtained from commercially available sCD26 assays in the current study, it seems unlikely that the established associations between sCD26 plasma levels and diseases such as T2DM, RA, OA, chronic infection, or malignant diseases can be reliably reproduced by the commercial assays (1, 10, 17). On the other hand, in view of the linearity observed between sCD26 level and DPP-IV enzyme activity, our in-house assay appears to be superior to the commercial assays as a means to evaluate sCD26/DPP-IV as clinically relevant biomarkers. The current study strongly suggests that new commercial assays for sCD26 plasma levels need detailed evaluation and validation with samples from clinically well-characterized patients, and results obtained from these newer assays should be compared to those obtained from well-established in-house assays such as our assay or other validated sCD26 ELISA assays.

## ACKNOWLEDGEMENTS

The authors thank Ms. Aya Miwa for excellent assistance with measurement of sCD26 and DPP-IV enzyme activity.

## CONFLICT OF INTEREST

The authors declare no competing financial interests associated with this article.

## REFERENCES

- Ohnuma K, Takahashi N, Yamochi T, Hosono O, Dang NH, Morimoto C. Role of CD26/dipeptidyl peptidase IV in human T cell activation and function. *Front Biosci* 2008;13:2299–2310.
- Morimoto C, Schlossman SF. The structure and function of CD26 in the T-cell immune response. *Immunol Rev* 1998;161:55–70.
- Tanaka T, Kameoka J, Yaron A, Schlossman SF, Morimoto C. The costimulatory activity of the CD26 antigen requires dipeptidyl peptidase IV enzymatic activity. *Proc Natl Acad Sci USA* 1993;90:4586–4590.
- Kobayashi H, Hosono O, Mimori T, et al. Reduction of serum soluble CD26/dipeptidyl peptidase IV enzyme activity and its correlation with disease activity in systemic lupus erythematosus. *J Rheumatol* 2002;29:1858–1866.
- Cuchacovich M, Gatica H, Pizzo SV, Gonzalez-Gronow M. Characterization of human serum dipeptidyl peptidase IV (CD26) and analysis of its autoantibodies in patients with rheumatoid arthritis and other autoimmune diseases. *Clin Exp Rheumatol* 2001;19:673–680.
- Sedo A, Duke-Cohan J, Balaziová E, Sedová L. Dipeptidyl peptidase IV activity and/or structure homologs: Contributing factors in the pathogenesis of rheumatoid arthritis? *Arthritis Res Ther* 2005;7:253–269.
- Iwaki-Egawa S, Watanabe Y, Kikuya Y, Fujimoto Y. Dipeptidyl peptidase IV from human serum: Purification, characterization, and N-terminal amino acid sequence. *J Biochem* 1998;124:428–433.
- Durinx C, Lambeir AM, Bosmans E, et al. Molecular characterization of dipeptidyl peptidase activity in serum: Soluble CD26/dipeptidyl peptidase IV is responsible for the release of X-Pro dipeptides. *Eur J Biochem* 2000;267:5608–5613.
- Drucker DJ, Nauck MA. The incretin system: Glucagon-like peptide-1 receptor agonists and dipeptidyl peptidase-4 inhibitors in type 2 diabetes. *Lancet* 2006;368:1696–1705.
- Aso Y, Ozeki N, Terasawa T, et al. Serum level of soluble CD26/dipeptidyl peptidase-4 (DPP-4) predicts the response to sitagliptin, a DPP-4 inhibitor, in patients with type 2 diabetes controlled inadequately by metformin and/or sulfonylurea. *Transl Res* 2011;159:25–31.
- Lamers D, Famulla S, Wronkowitz N, et al. Dipeptidyl peptidase 4 is a novel adipokine potentially linking obesity to the metabolic syndrome. *Diabetes* 2011;60:1917–1925.
- Andrieu T, Thibault V, Malet I, et al. Similar increased serum dipeptidyl peptidase IV activity in chronic hepatitis C and other viral infections. *J Clin Virol* 2003;27:59–68.
- Matheeußen V, Lambeir AM, Jungraithmayr W, et al. Method comparison of dipeptidyl peptidase IV activity assays and their application in biological samples containing reversible inhibitors. *Clin Chim Acta* 2012;413:456–462.
- Hosono O, Homma T, Kobayashi H, et al. Decreased dipeptidyl peptidase IV enzyme activity of plasma soluble CD26 and its inverse correlation with HIV-1 RNA in HIV-1 infected individuals. *Clin Immunol* 1999;91:283–295.
- Torimoto Y, Dang NH, Tanaka T, Prado C, Schlossman SF, Morimoto C. Biochemical characterization of CD26 (dipeptidyl peptidase IV): Functional comparison of distinct epitopes recognized by various anti-CD26 monoclonal antibodies. *Mol Immunol* 1992;29:183–192.
- Dong RP, Tachibana K, Hegen M, et al. Correlation of the epitopes defined by anti-CD26 mAbs and CD26 function. *Mol Immunol* 1998;35:13–21.
- Sedo A, Malik R. Dipeptidyl peptidase IV-like molecules: Homologous proteins or homologous activities? *Biochim Biophys Acta* 2001;1550:107–116.
- Lee SA, Kim YR, Yang EJ, et al. CD26/DPP4 levels in peripheral blood and T cells in patients with type 2 diabetes mellitus. *J Clin Endocrinol Metab* 2013;98:2553–2561.
- Ohnuma K, Morimoto C. DPP4 (dipeptidyl-peptidase 4). *Atlas Genet Cytogenet Oncol Haematol* 2012;17:301–312.
- Inamoto T, Yamada T, Ohnuma K, et al. Humanized anti-CD26 monoclonal antibody as a treatment for malignant mesothelioma tumors. *Clin Cancer Res* 2007;13:4191–4200.
- Hatano R, Ohnuma K, Yamamoto J, Dang NH, Yamada T, Morimoto C. Prevention of acute graft-versus-host disease by humanized anti-CD26 monoclonal antibody. *Br J Haematol* 2013;162:263–277.

# CD26-Mediated Induction of EGR2 and IL-10 as Potential Regulatory Mechanism for CD26 Costimulatory Pathway

Ryo Hatano,<sup>\*,†</sup> Kei Ohnuma,<sup>\*</sup> Haruna Otsuka,<sup>\*</sup> Eriko Komiya,<sup>\*</sup> Izumi Taki,<sup>\*</sup> Satoshi Iwata,<sup>\*</sup> Nam H. Dang,<sup>‡</sup> Ko Okumura,<sup>†</sup> and Chikao Morimoto<sup>\*</sup>

CD26 is associated with T cell signal transduction processes as a costimulatory molecule, and CD26<sup>+</sup> T cells have been suggested to be involved in the pathophysiology of diverse autoimmune diseases. Although the cellular and molecular mechanisms involved in CD26-mediated T cell activation have been extensively evaluated by our group and others, potential negative feedback mechanisms to regulate CD26-mediated activation still remain to be elucidated. In the present study, we examine the expression of inhibitory molecules induced via CD26-mediated costimulation. We show that coengagement of CD3 and CD26 induces preferential production of IL-10 in human CD4<sup>+</sup> T cells, mediated through NFAT and Raf-MEK-ERK pathways. A high level of early growth response 2 (EGR2) is also induced following CD26 costimulation, possibly via NFAT and AP-1-mediated signaling, and knockdown of EGR2 leads to decreased IL-10 production. Furthermore, CD3/CD26-stimulated CD4<sup>+</sup> T cells clearly suppress proliferative activity and effector cytokine production of bystander T cells in an IL-10-dependent manner. Taken together, our data suggest that robust CD26 costimulatory signaling induces preferential expression of EGR2 and IL-10 as a potential mechanism for regulating CD26-mediated activation. *The Journal of Immunology*, 2015, 194: 960–972.

**C**D26 is a 110-kDa type II membrane-bound glycoprotein with dipeptidyl peptidase IV (DPPIV) activity in its extracellular domain (1–3). CD26 is associated with T cell signal transduction processes as a costimulatory molecule, as well as being a marker of T cell activation (4, 5). Whereas CD26 expression is increased following activation of resting T cells, CD4<sup>+</sup> CD26<sup>high</sup> T cells respond maximally to recall Ags such as tetanus toxoid (6). Moreover, crosslinking of CD26 and CD3 with solid-phase immobilized mAbs can induce T cell costimulation and IL-2 production by CD26<sup>+</sup> T cells. Furthermore, high CD26 cell surface expression in CD4<sup>+</sup> T cells is correlated with the production of Th1 and Th17-type cytokines and high migratory activity (4, 7). In fact, patients with autoimmune diseases, such as multiple sclerosis (MS),

Grave's disease, and rheumatoid arthritis, have been found to have increased numbers of CD4<sup>+</sup>CD26<sup>+</sup> T cells in inflamed tissues as well as in their peripheral blood, with enhancement of CD26 expression correlating with the autoimmune disease severity (8–10). We have recently found that cytotoxic activity of CD8<sup>+</sup> T cells is also regulated via CD26-mediated costimulation, and that CD26<sup>+</sup> T cells are deeply involved in the pathophysiology of acute graft-versus-host disease (11, 12). These findings imply that CD26<sup>+</sup> T cells play an important role in the inflammatory process and subsequent tissue damage in such diseases.

Activation of T cells through costimulatory signals is essential for an effective Ag-specific immune response, whereas the suppressive control of excessive immune responses is also critical for maintaining self tolerance and preventing autoimmunity. CD28 is a representative T cell costimulatory molecule, required for optimal production of cytokines and proliferation, and CD28-deficient mice have markedly reduced responses to exogenous Ags (13, 14). Alternatively, CTLA-4 functions as a potent negative regulator of the T cell response, and CTLA-4-deficient mice develop massive lymphadenopathy, autoimmunity, and early death (15, 16). Both CD28 and CTLA-4 are members of the Ig supergene family and are able to bind CD80 and CD86 expressed on APCs. CTLA-4 is not expressed on naive T cells, but it is induced after activation. CTLA-4 interacts with CD80 and CD86 with a 50- to 100-fold higher binding avidity than CD28, leading to interference of CD28 signaling (17). In addition to the ligand competition, the cytoplasmic domain of CTLA-4 associates with phosphatases SHP2 and PP2A to negatively regulate T cell activation, and it also inhibits the formation of lipid rafts (18). We have identified caveolin-1 on APCs as a functional ligand for CD26, and the ligation of CD26 with caveolin-1 recruits a complex consisting of CD26, CARMA1, Bcl10, MALT1, and IκB kinase to lipid rafts, leading to NF-κB activation (19, 20). CD26 possesses DPPIV enzyme activity, able to cleave dipeptides from polypeptides with N-terminal penultimate proline or alanine. Molecules displaying DPPIV-like enzymatic activity and/or structural similarity to the DPPIV/CD26 have been grouped to a family of “dipeptidyl pep-

<sup>\*</sup>Department of Therapy Development and Innovation for Immune Disorders and Cancers, Graduate School of Medicine, Juntendo University, Tokyo 113-8421, Japan; <sup>†</sup>Atopy (Allergy) Research Center, Juntendo University Graduate School of Medicine, Tokyo 113-8421, Japan; and <sup>‡</sup>Division of Hematology/Oncology, University of Florida, Gainesville, FL 32610

Received for publication August 28, 2014. Accepted for publication November 19, 2014.

This work was supported by a grant-in-aid from the Ministry of Education, Culture, Sports, Science and Technology, Japan (to K. Ohnuma and C.M.) and the Ministry of Health, Labor and Welfare, Japan (to C.M.), as well as Foundation of Strategic Research Projects in Private Universities Grant-in-Aid S1311011 from the Ministry of Education, Culture, Sports, Science and Technology, Japan (to C.M.). This work was also supported by Japan Society for the Promotion of Science KAKENHI Grant 26860760 (to R.H.) and Japan Society for the Promotion of Science Research Fellowships for Young Scientists (to R.H.).

Address correspondence and reprint requests to Dr. Chikao Morimoto, Department of Therapy Development and Innovation for Immune Disorders and Cancers, Graduate School of Medicine, Juntendo University, 2-1-1, Hongo, Bunkyo-ku, Tokyo 113-8421, Japan. E-mail address: morimoto@ims.u-tokyo.ac.jp

The online version of this article contains supplemental material.

Abbreviations used in this article: Cav-Ig, fusion protein of the N-terminal domain of human caveolin-1 and human IgG1 Fc; CD26 sup, supernatant of CD3/CD26-stimulated T cells; CD28 sup, supernatant of CD3/CD28-stimulated T cells; CyA, cyclosporin A; DPPIV, dipeptidyl peptidase IV; EGR2, early growth response 2; IRF4, IFN regulatory factor 4; LAG3, lymphocyte-activation gene 3; LAP, latency-associated protein; MFI, mean fluorescence intensity; MS, multiple sclerosis; siRNA, small interfering RNA; Treg, regulatory T cell; Tr1, type 1 regulatory T cell.

Copyright © 2015 by The American Association of Immunologists, Inc. 0022-1767/15/\$25.00

tidase IV activity and/or structure homologs (DASH)," including enzymatically active members such as fibroblast activation protein- $\alpha$ , quiescent cell proline dipeptidase/DPP-II/DPP7, DPP8, DPP9, and enzymatically inactive members such as DPP6 and DPP10 (21). However, a DASH family member that functions as a negative regulator of CD26-caveolin-1-mediated T cell activation has not yet been reported.

Active suppression by regulatory T cells (Tregs) is essential for the control of autoreactive cells. Tregs suppress immune responses through either direct cell-cell interactions or the release of inhibitory cytokines. CD4<sup>+</sup>CD25<sup>high</sup> Tregs expressing FOXP3, a master regulatory gene for the suppressive activity, suppress immune cells mainly through soluble or membrane-bound TGF- $\beta$  (22). Recently, IL-35 has been reported as a new inhibitory cytokine preferentially expressed by mouse Foxp3<sup>+</sup> Tregs, and it is required for their maximal suppressive activity (23). IL-35 is a member of the IL-12 heterodimeric cytokine family, composed of EBV-induced 3 and p35 (also known as IL-12 $\alpha$ ). Type 1 Tregs (Tr1s) are characterized by high-level production of IL-10 with regulatory activity (24). Lymphocyte-activation gene 3 (LAG3) and early growth response 2 (EGR2) have been recently reported as markers of Tr1-like cells (25). LAG3 binds to MHC class II molecules with higher affinity than CD4, leading to transduction of inhibitory signals for both T cells and APCs (26, 27). EGR2 is an essential transcription factor that regulates the T cell anergy program by directly upregulating diacylglycerol kinase  $\alpha$ , and it also plays an important role in the induction of LAG3 and IL-10 expression (28).

Although the signaling events involved in CD26-mediated T cell activation or the cellular functions of CD26-expressing T cells have been studied extensively by our group and others, the potential negative feedback mechanism of CD26-mediated costimulation still remains to be elucidated. The present study focuses on the expression of inhibitory molecules induced in CD4<sup>+</sup> T cells following CD26 costimulation and the signaling pathways involved in this biological process.

## Materials and Methods

### Preparation of human T cells

Human PBMCs were collected from healthy adult volunteers after the documented informed consent and Institutional Review Board approval were obtained. This study has been performed according to the principles set out in the Declaration of Helsinki. For purification, the MACS cell separation system (Miltenyi Biotec, Bergisch Gladbach, Germany) and MACS human CD4<sup>+</sup> T cell isolation kit (Miltenyi Biotec) were used. Purity of CD4<sup>+</sup> T cells was  $\geq 97\%$  as confirmed by FACSCalibur (BD Biosciences, San Jose, CA).

### Abs and reagents

For T cell stimulation, anti-CD3 mAb (OKT3), anti-CD28 mAb (4B10), anti-CD26 mAb (1F7), and the fusion protein of the N-terminal domain of human caveolin-1 and human IgG1 Fc (Cav-Ig) developed in our laboratory were used (20). The following human-specific Abs were used for flow cytometry: FITC-labeled anti-LAG3 mAb (clone 17B4) and FITC-labeled mouse IgG1,  $\kappa$  isotype control (clone MOPC-21) were purchased from Enzo Life Sciences (Farmingdale, NY). PE-labeled anti-CTLA-4 mAb (clone L3D10) and PE-labeled mouse IgG1,  $\kappa$  isotype control (clone MOPC-21) were purchased from BioLegend (San Diego, CA). PE-labeled anti-IL-10 mAb (clone JES3-9D7) and PE-labeled rat IgG1,  $\kappa$  isotype control (clone eBRG1) were purchased from eBioscience (San Diego, CA). PerCP-labeled anti-latency-associated protein (LAP) mAb (clone 27232) and PerCP-labeled mouse IgG1 isotype control (clone 11711) were purchased from R&D Systems (Minneapolis, MN). Alexa Fluor 647-labeled anti-IFN- $\gamma$  mAb (clone B27), Alexa Fluor 647-labeled anti-FOXP3 mAb (clone 259D/C7), and Alexa Fluor 647-labeled mouse IgG1,  $\kappa$  isotype control (clone MOPC-21) were purchased from BD Biosciences. Alexa Fluor 647-labeled anti-CD26 mAb (clone 19) recently developed in our laboratory was used for the detection of CD26 even in the presence of

another anti-CD26 mAb, 1F7 (29). For Western blot analysis, mouse anti-NFAT1 mAb (clone 639402), goat anti-NFAT2 polyclonal Ab, and rabbit anti-p-ERK1 (pT202/pY204)/ERK2 (pT185/pY187) polyclonal Ab were purchased from R&D Systems. Mouse anti-TATA-binding protein mAb (clone mAbcam 51841) and rabbit anti-EGR2 mAb (clone EPR4004) were purchased from Abcam (Cambridge, U.K.). Mouse anti- $\beta$ -actin mAb (clone AC-15) was purchased from Sigma-Aldrich (St. Louis, MO). HRP-conjugated sheep anti-mouse IgG and donkey anti-rabbit IgG were purchased from GE Healthcare (Buckinghamshire, U.K.), and HRP-conjugated donkey anti-goat IgG was purchased from Santa Cruz Biotechnology (Santa Cruz, CA). For neutralizing IL-10, anti-human IL-10 mAb (clone JES3-9D7), anti-human IL-10R mAb (clone 3F9), rat IgG1,  $\kappa$  isotype control (clone RTK2071), and rat IgG2a,  $\kappa$  isotype control (clone RTK2758) were purchased from BioLegend. Recombinant human IL-10 and the NFAT inhibitor cyclosporin A (CyA) were purchased from Sigma-Aldrich. The MEK1/2 inhibitor U0126 and the NF- $\kappa$ B activation inhibitor quinazoline were purchased from Merck Millipore (Billerica, MA).

### Preparation of culture supernatant and measurement of cytokines

Purified CD4<sup>+</sup> T cells ( $1 \times 10^5$ ) were cultured in serum-free AIM-V medium (Invitrogen, Carlsbad, CA) in 96-well flat-bottom plates (Costar; Corning, Corning, NY), with stimulatory mAbs or Cav-Ig being bound in the wells beforehand at the following concentrations: 0.5  $\mu$ g/ml OKT3 and/or 2, 5, 10, 20, or 50  $\mu$ g/ml 4B10 or 1F7 or Cav-Ig. Cells were cultured in 5% CO<sub>2</sub> and 100% humidified incubator at 37°C for 48, 72, 96, or 120 h. After incubation, supernatants were collected and cytokine concentrations were examined using ELISA. BD OptEIA kits for human IL-2, IL-4, IL-5, IL-10, TNF- $\alpha$ , IFN- $\gamma$ , or TGF- $\beta$ 1 were purchased from BD Biosciences, and the Ready-SET-Go! kits for human IL-17A or IL-21 were purchased from eBioscience. The absorbance at 450/570 nm was measured in a microplate reader (Bio-Rad, Hercules, CA), and data were analyzed with Microplate Manager 6 software (Bio-Rad).

### Flow cytometry

Purified CD4<sup>+</sup> T cells ( $1 \times 10^5$ ) were incubated with plate-bound OKT3 (0.5  $\mu$ g/ml) and/or 2, 5, 10, 20, or 50  $\mu$ g/ml of 4B10 or 1F7 in 96-well flat bottom plates for 96 h, and cells were then collected and prepared for the analysis of cell surface expression of CTLA-4, LAG3, and LAP. Acquisition was performed using FACSCalibur, and data were analyzed with FlowJo software (Tree Star, Ashland, OR). For the analysis of intracellular FOXP3 and LAG3, a human FOXP3 buffer set (BD Biosciences) was used. For the staining of intracellular cytokines, cells were treated with Golgi-Stop (monensin) (BD Biosciences) for the last 5 h of culture in the presence or absence of 50 ng/ml PMA (Sigma-Aldrich) plus 1  $\mu$ g/ml ionomycin (Merck Millipore) and then stained using BD Cytofix/Cytoperm Plus fixation/permeabilization kit (BD Biosciences) according to the manufacturer's instructions.

### Preparation of lysates and Western blotting

To analyze nuclear expression of ERK or NFAT, purified CD4<sup>+</sup> T cells ( $1.5 \times 10^6$  cells/well, three wells per sample) were incubated with plate-bound OKT3 (0.5  $\mu$ g/ml) and/or 4B10 (50  $\mu$ g/ml) or 1F7 (50  $\mu$ g/ml) in 24-well flat-bottom plates (Costar) for 0.5, 1, or 2 h. After incubation, cells were collected and nuclear extracts were prepared using EpiQuik nuclear extraction kit (Epigentek, Farmingdale, NY) supplemented with 2% protease inhibitor mixture (Sigma-Aldrich) and 1 $\times$  PhosSTOP (Roche Diagnostics, Tokyo, Japan). For the analysis of EGR2 expression, purified CD4<sup>+</sup> T cells ( $1.5 \times 10^6$  cells/well) were stimulated in the above conditions for 24 or 48 h. After incubation, cells were collected and whole-cell lysates were prepared using RIPA buffer. Each sample was resolved by SDS-PAGE in reducing condition. SDS-PAGE and Western blot analysis were conducted as described previously (30). The images were taken using luminescent image analyzer LAS 4000 (GE Healthcare), and data were analyzed with image reader LAS 4000 and Multi Gauge software (GE Healthcare).

### T cell proliferation assay

Purified CD4<sup>+</sup> T cells ( $1 \times 10^5$ ) were incubated with plate-bound OKT3 (0.5  $\mu$ g/ml) and/or 4B10 or 1F7 in 96-well flat-bottom plates for 96 h in the presence or absence of signal inhibitor or culture supernatant. To evaluate T cell proliferation, a cell proliferation ELISA, BrdU Kit (Roche Diagnostics) was used. BrdU was added to each well for the last 2 h of incubation, and proliferation was assessed by measuring BrdU incorporation by ELISA. The absorbance at 450/655 nm was measured in a microplate reader, and data were analyzed with Microplate Manager 6 software. T cell proliferation was also assessed by using Cell Counting



Kit-8 (Dojindo, Kumamoto, Japan). 2-(2-Methoxy-4-nitrophenyl)-3-(4-nitrophenyl)-5-(2,4-disulphophenyl)-2H tetrazolium monosodium salt (WST-8) was added to each well at a concentration of 1/10 volume for the last 3 h, and the absorbance at 450/595 nm was measured. For the analysis of the number of cell divisions, a Vybrant CFDA SE cell tracer kit (Molecular Probes, Carlsbad, CA) was used. Purified CD4<sup>+</sup> T cells labeled with 2  $\mu$ Mol/l CFSE were incubated for 96 h with plate-bound stimulatory mAbs as described above, and cells were then harvested and analyzed by FACSCalibur.

#### Small interfering RNA against human EGR2

We selected two target sequences from nucleotides +1802 to 1820 (sense1) and +1890 to 1908 (sense2) downstream of the start codon of human EGR2 mRNA: sense1 small interfering RNA (siRNA), 5'-GAGUUGAUCUAA-GACGUUUdTdT-3', and sense2 siRNA, 5'-CACUUUAUGGCUUGGG-ACUdTdT-3'. siRNAs against EGR2 were purchased from Sigma-Aldrich, and negative control siRNA (oligonucleotide sequences are not disclosed) was purchased from Qiagen (Valencia, CA). Fifty picomoles siRNA duplexes were transfected into  $5 \times 10^5$  purified CD4<sup>+</sup> T cells by using HVJ-E vector (GenomONE-Si; Ishihara Sangyo Kaisha, Osaka, Japan) according to the manufacturer's instructions (19, 20).

#### Quantitative real-time RT-PCR assay

Purified CD4<sup>+</sup> T cells or siRNA transfected CD4<sup>+</sup> T cells ( $5 \times 10^5$ ) were incubated with plate-bound OKT3 (0.5  $\mu$ g/ml) and/or 4B10 or 1F7 or Cav-Ig in 24-well flat-bottom plates for 6, 12, 24, 48, or 72 h in the presence or absence of signal inhibitor or culture supernatant. After incubation, cells were collected and total RNA was extracted by the use of an RNeasy Micro kit according to the manufacturer's instructions (Qiagen). cDNA was produced by using a PrimeScript II first strand cDNA synthesis kit (TaKaRa Bio, Shiga, Japan) with oligo(dT) primers. Quantification of mRNA was performed using the 7500 real-time PCR System and SYBR Select Master Mix (Applied Biosystems, Foster City, CA). The obtained data were analyzed with 7500 System SDS software (Applied Biosystems), being normalized to hypoxanthine phosphoribosyltransferase expression. Sequences of primers used in quantitative real-time RT-PCR analysis are shown in Supplemental Table I.

#### Statistical analysis

Data were analyzed by the paired Student *t* test (two-tailed) for two group comparison, or by the ANOVA test for multiple comparison testing. The assay was performed in triplicate wells, and data are presented as mean  $\pm$  SD of triplicate samples of the representative experiment, or mean  $\pm$  SE of triplicate samples of independent experiments. Significance was analyzed using MS Excel (Microsoft) and *p* values < 0.01 were considered significant and are indicated in the corresponding figures and figure legends.

## Results

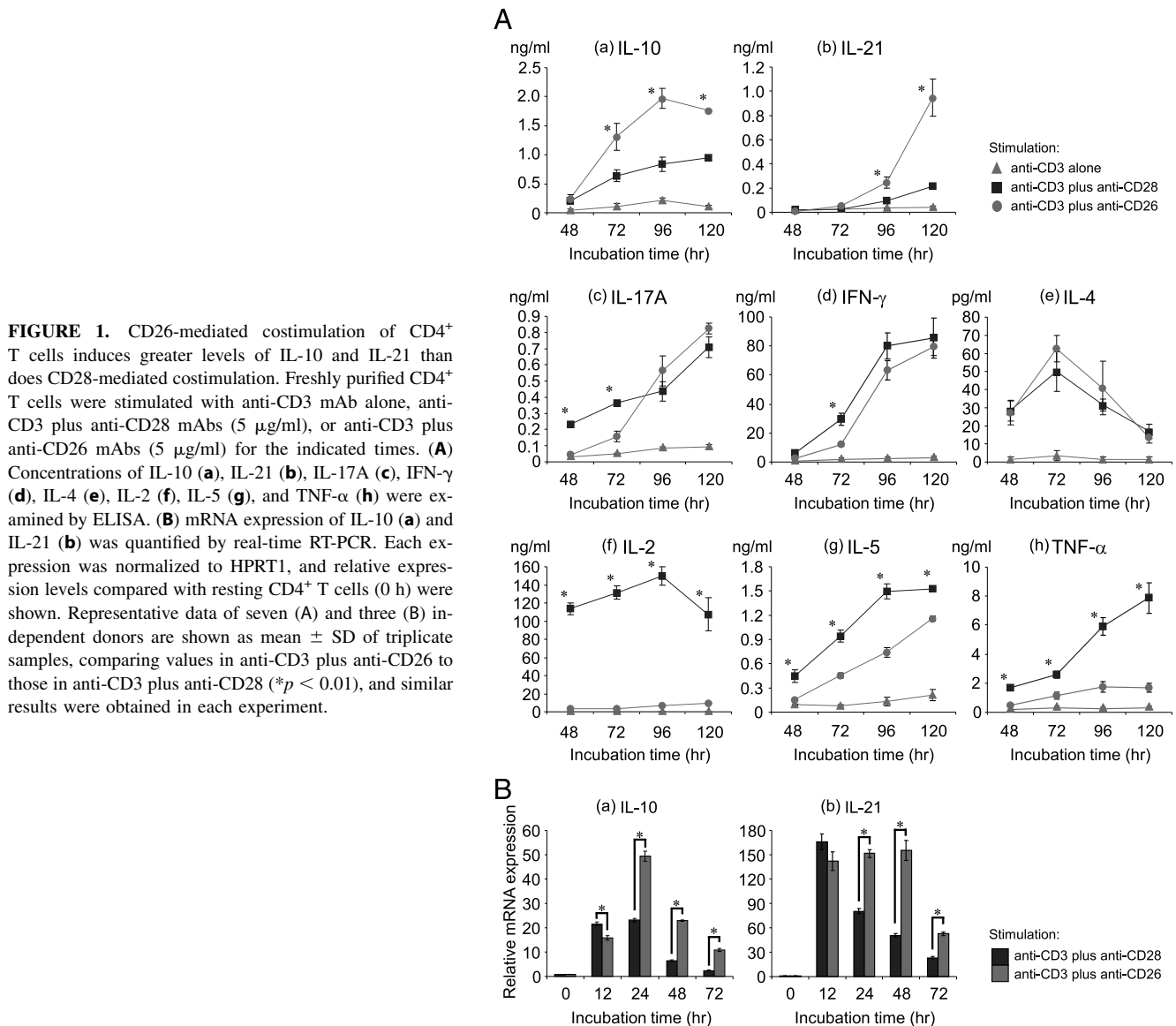
#### CD26-mediated costimulation induces the development of CD4<sup>+</sup> T cells to a Tr1-like phenotype with high IL-10 production

To explore the negative feedback mechanism associated with CD26-mediated costimulation, we first examined the cytokine production profile of CD4<sup>+</sup> T cells, focusing particularly on the production of immunosuppressive cytokines such as TGF- $\beta$  and IL-10. To characterize the specific phenotype associated with CD26 costimulation, we compared the level of cytokine production following costimulation with either CD26 or CD28, a representative T cell costimulatory pathway. As shown in Fig. 1A, only a small amount of cytokines was produced following stimulation with anti-CD3 mAb alone (gray lines), whereas both anti-CD3 plus anti-CD26 and anti-CD3 plus anti-CD28 costimulation greatly enhanced cytokine production (red or blue lines). Production of IL-10 by CD4<sup>+</sup> T cells was preferentially increased following CD26-mediated costimulation compared with CD28-mediated costimulation over the tested time intervals (Fig. 1Aa). IL-21 production was also greatly enhanced in the late phase of CD26 costimulation (Fig. 1Ab). Alternatively, production of IL-2, IL-5, or TNF- $\alpha$  was much lower following CD26 costimulation than CD28 costimulation (Fig. 1Af–h). In contrast, no difference in the production of IL-17A, IFN- $\gamma$ , or IL-4 was observed following

CD26- or CD28-mediated costimulation (Fig. 1Ac–e). Real-time RT-PCR analysis was then conducted to confirm the above results. As shown in Fig. 1B, IL-10 and IL-21 mRNA expression levels were higher after 24 h of CD26 costimulation than CD28 costimulation. Meanwhile, the amount of TGF- $\beta$ 1 was below the detection limit (0.125 ng/ml), and mRNA expression level of IL-35 subunits (EBV-induced 3 and p35) was not elevated following CD26- or CD28-mediated costimulation (data not shown). These data indicate that CD26 and CD28 costimulation of CD4<sup>+</sup> T cells results in different profiles of cytokine production, with IL-10 production being preferentially enhanced following CD26 costimulation.

To further characterize the biological process involved in IL-10 production following CD26 costimulation, we evaluated the effect of a wide range of concentrations of anti-CD26 and anti-CD28 mAbs. Additionally, to assess whether caveolin-1, a physiological ligand of CD26, can induce IL-10, we activated CD4<sup>+</sup> T cells with anti-CD3 mAb and Cav-Ig as described in *Materials and Methods*. As shown in Fig. 2Aa, CD26-mediated costimulation by both anti-CD3 plus anti-CD26 and anti-CD3 plus Cav-Ig greatly enhanced IL-10 production compared with CD28-mediated costimulation. It is noteworthy that the enhancement in CD26-mediated IL-10 production via either anti-CD26 mAb or Cav-Ig was dose-dependent, whereas IL-10 production decreased with increasing doses of anti-CD28 mAb (Fig. 2Aa). IL-17A production following CD26-mediated costimulation was similar to that observed following CD28-mediated costimulation (Fig. 2Ab). Although the amount of IL-2 produced by CD4<sup>+</sup> T cells following CD26 costimulation was 1–10 ng/ml and significantly higher than anti-CD3 mAb alone, it was consistently lower than that induced by CD28 costimulation (Fig. 2Ac, Supplemental Fig. 1A). T cell proliferation in response to CD26 costimulation was significantly decreased in the presence of neutralizing anti-IL-2 mAb, indicating that a relatively small amount of IL-2 induced by CD26 costimulation was sufficiently functional for enhancing T cell proliferation (Supplemental Fig. 1B). For further confirmation, we analyzed the intracellular expression of IL-10 in CD4<sup>+</sup> T cells through flow cytometry. Because inhibition of protein transport by monensin or brefeldin A is essential for intracellular cytokine staining, we analyzed IL-10 expression in T cells stimulated by anti-CD3 plus a high dose (50  $\mu$ g/ml) of anti-CD26 or anti-CD28 with monensin for the last 5 h of culture. As shown in Fig. 2B, IL-10 and IFN- $\gamma$  were equally induced in CD4<sup>+</sup> T cells following CD26 costimulation (Fig. 2Bb), whereas CD28 costimulation induced only IFN- $\gamma$  but hardly induced IL-10 (Fig. 2Ba). Note that only ~2% of CD4<sup>+</sup> T cells expressed IL-10 following CD26 costimulation, but this induction was significant and was consistently seen in all the repeated experiments. In contrast with IFN- $\gamma$  level, which was clearly detected by restimulation with PMA plus ionomycin, detection of the IL-10 level was relatively difficult because restimulation with PMA plus ionomycin hardly affected the percentage of IL-10-expressing cells following either CD26- or CD28-mediated costimulation (the results with similar stimulatory condition are shown in Fig. 6B). Previous work by Jonuleit et al. (31) investigating IL-10 expression also demonstrated a relatively low level of IL-10 expression when human peripheral blood CD4<sup>+</sup> T cells from healthy volunteers were primed and restimulated with allogeneic dendritic cells. We also noted that another anti-human IL-10 mAb from BD Biosciences gave similar results (data not shown). To define whether IL-10-expressing CD4<sup>+</sup> T cells following CD26-mediated costimulation expressed CD26, we stained cell surface CD26 and intracellular IL-10. For this purpose, as described in *Materials and Methods*, we used an anti-human CD26 mAb recognizing a different epitope from the one recognized by





the immobilized anti-CD26 mAb, 1F7, used for CD26 costimulation. As shown in Fig. 2Bc, all of the IL-10-expressing CD4<sup>+</sup> T cells were shown to express CD26. Taken together, these results indicate that CD26-mediated costimulation in CD4<sup>+</sup>CD26<sup>+</sup> T cells preferentially induces IL-10, and this effect increases with enhancing intensity of CD26-mediated signaling.

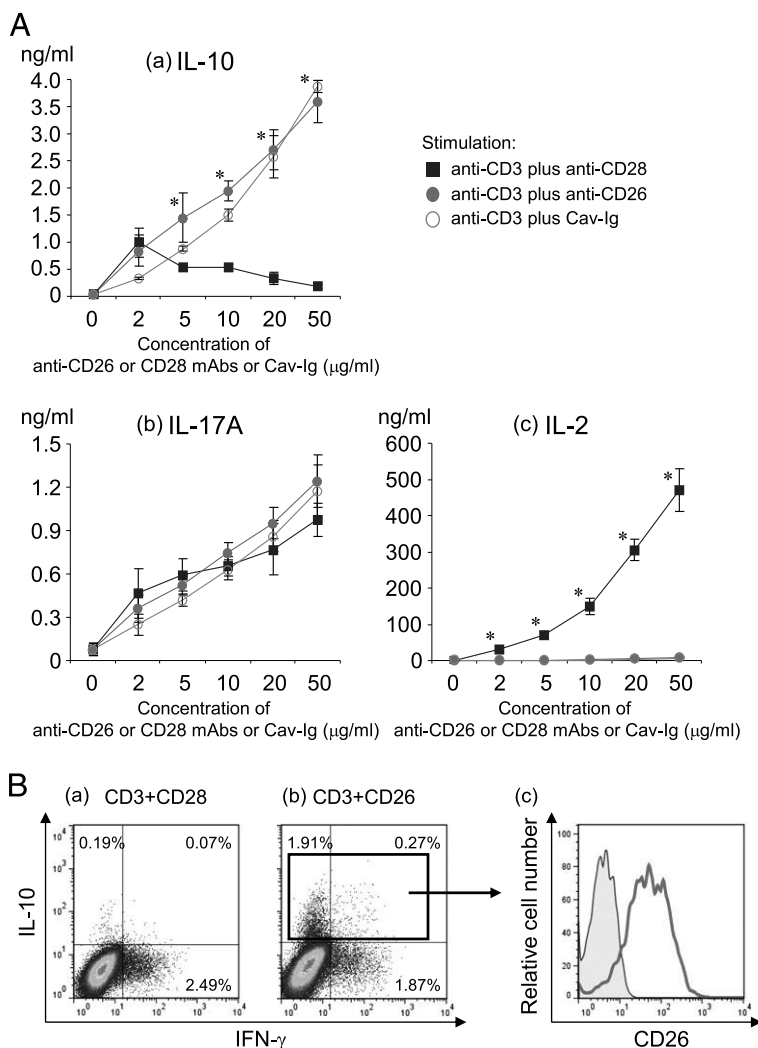
We next examined the expression of selected molecules with well-characterized immunosuppressive functions by flow cytometry, including the cell surface expression of CTLA-4 and LAP complexed with TGF-β1, and the intracellular expression of transcription factor FOXP3. Because LAG3 has been reported to be continuously recycled and rapidly translocated to the plasma membrane in response to antigenic stimulation (32), we analyzed both the cell surface and intracellular expression of LAG3. As shown in Fig. 3, both the cell surface and intracellular expression of LAG3 was clearly enhanced with increasing doses of anti-CD26 mAb, and CD26-induced enhancement of LAG3 was more pronounced than the effect of CD28-mediated costimulation (Fig. 3Aa). Alternatively, both CD26- and CD28-mediated costimulation enhanced the expression of CTLA-4 and FOXP3, with no significant difference being detected between these two costimulatory pathways (Fig. 3Ac, d). In contrast with CD28 costimulation, LAP was hardly induced following CD26 costimulation (Fig. 3Ab). Although the

mean fluorescence intensity (MFI) results of LAP, CTLA-4, or FOXP3 correlated with those of percentage of cells expressing LAP, CTLA-4, or FOXP3 shown in Fig. 3A, the values of MFI, especially for LAP and FOXP3, were low and the difference between CD26- and CD28-mediated costimulation was minimal (data not shown). Alternatively, as shown in Fig. 3B, all of the CD4<sup>+</sup> T cells expressed LAG3 following CD26 or CD28 costimulation, and no difference was observed in the percentage of LAG3-expressing cells, whereas the expression intensity of LAG3 after CD26-mediated costimulation was higher than after CD28-mediated costimulation. LAG3 also serves as a marker of IL-10-producing Tregs (25), suggesting that signaling events via CD26 may induce the development of CD4<sup>+</sup> T cells to a Tr1-like phenotype.

#### *NFAT and Raf-MEK-ERK signalings are indispensable for CD26-mediated T cell activation*

We next examined the signaling events associated with CD26-mediated enhancement in IL-10 production in CD4<sup>+</sup> T cells. Although cytokine receptor signaling through JAK-STAT plays a crucial role in T cell differentiation into specific effector subsets or Tregs, the initial signaling events for inducing cytokine production in T cells are associated with the TCR signaling pathway. Therefore, we first examined the effect of signal inhibitors against

**FIGURE 2.** CD26-mediated costimulation of CD4<sup>+</sup> T cells greatly enhances IL-10 in a stimulation intensity-dependent manner. **(A)** Freshly purified CD4<sup>+</sup> T cells were stimulated with anti-CD3 mAb alone, anti-CD3 plus anti-CD28 mAbs, anti-CD3 plus anti-CD26 mAbs, or anti-CD3 mAb plus Cav-Ig at the indicated concentrations for 96 h. Concentrations of IL-10 (**Aa**), IL-17A (**Ab**), and IL-2 (**Ac**) were examined by ELISA. Representative data of five independent donors are shown as mean  $\pm$  SD of triplicate samples, comparing values in anti-CD3 plus anti-CD26 or anti-CD3 plus Cav-Ig to those in anti-CD3 plus anti-CD28 (\* $p < 0.01$ ), and similar results were obtained in each experiment. **(B)** Freshly purified CD4<sup>+</sup> T cells were stimulated with anti-CD3 plus anti-CD28 mAbs (50  $\mu$ g/ml) (**a**) or anti-CD3 plus anti-CD26 mAbs (50  $\mu$ g/ml) (**b** and **c**) for 72 h. Cells were treated with monensin in the absence of PMA plus ionomycin restimulation for the last 5 h of culture, and cell surface CD26, intracellular IFN- $\gamma$ , and IL-10 were detected by flow cytometry. **(Ba and b)** Two-dimensional dot plot of IFN- $\gamma$  or IL-10 staining gated for CD4<sup>+</sup> T cells is shown. **(Bc)** Following gating for CD4<sup>+</sup>IL-10<sup>+</sup> population as indicated in **(Bb)**, the expression of CD26 was analyzed. The data are shown as histogram of CD26 intensity, and the gray area in the histogram show the data on the isotype control. A representative plot or histogram of four independent donors is shown, and similar results were obtained in each experiment.

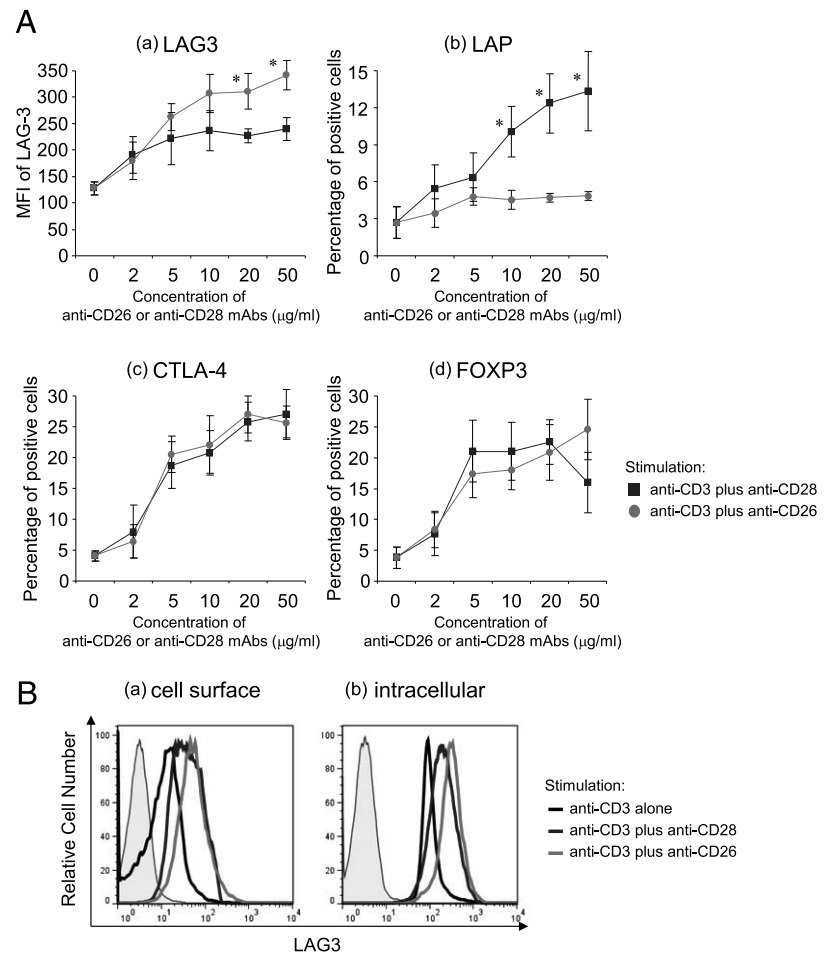


NFAT, AP-1, or NF- $\kappa$ B, essential transcription factors for T cell activation located at the terminal end of TCR signaling. We first assessed T cell proliferation by measuring BrdU incorporation by ELISA, which is generally accepted to be equivalent to the [<sup>3</sup>H]thymidine incorporation assay. As shown in Fig. 4A, the NFAT inhibitor CyA and the MEK1/2 inhibitor U0126 markedly inhibited the proliferative activity of CD4<sup>+</sup> T cells following CD26 or CD28 costimulation. Of note, T cells activated with anti-CD3 and anti-CD26 were much more sensitive to these inhibitors as compared with CD28 costimulation, and a high dose of CyA and U0126 suppressed the proliferation of T cells to the same level of proliferative activity as anti-CD3 alone (Fig. 4A). Additionally, we conducted a T cell proliferation assay by using tetrazolium salt, and results similar to those obtained with the BrdU incorporation assay were observed (Fig. 4B). As shown in Fig. 4C, the effects of NFAT and MEK1/2 inhibitors on IL-10 production were very similar to those on T cell proliferation. Whereas the NF- $\kappa$ B inhibitor quinazoline also suppressed T cell proliferation and IL-10 production in a dose-dependent manner, its effect on CD4<sup>+</sup> T cells following CD26 costimulation was less apparent as compared with NFAT and MEK1/2 inhibitors (Fig. 4A–C). These three inhibitors had similar effects on IL-17A and IFN- $\gamma$  production as they did with IL-10 production (data not shown). These results indicate that both NFAT- and Raf-MEK-ERK-related signals are indispensable for CD26-mediated T cell activation, and they suggest that the intensity or persistence of these two signal

pathways in CD4<sup>+</sup> T cells are different between CD26 and CD28 costimulation.

To further define the difference between CD26- and CD28-mediated costimulatory signaling pathways, we next examined the amount of NFAT and p-ERK1/2 translocated to the nucleus of CD4<sup>+</sup> T cells following CD26 or CD28 costimulation. The NFAT family consists of five members (NFAT1–5), and only NFAT5 is regulated by osmotic stress, not by calcium–calcein signaling (33). Because NFAT3 is reported to be absent in T cells, we analyzed the expression of NFAT1, NFAT2, and NFAT4. As shown in Fig. 4D, stimulation with both anti-CD3 plus anti-CD28 and anti-CD3 plus anti-CD26 resulted in increased nuclear levels of p-ERK1/2 and NFAT2 compared with anti-CD3 alone. Nuclear levels of p-ERK1/2 peaked at 30 min and then gradually decreased following CD28-mediated costimulation, whereas accumulation of NFAT2 in the nucleus reached a maximum after 2 h of CD28 costimulation. Alternatively, CD26-mediated costimulation resulted in greater enhancement of nuclear level of NFAT2 compared with CD28 costimulation, whereas the maximum level of p-ERK1/2 following CD26-mediated costimulation was lower than that seen with CD28 costimulation, but the effect of CD26 costimulation on p-ERK1/2 persisted until 2 h after stimulation. In contrast, no difference in nuclear level of NFAT1 was observed following CD26 or CD28 costimulation. As shown in Fig. 4D, when each sample was immunoblotted with anti-NFAT2, two bands were detected in molecular mass regions at ~110,000 and

**FIGURE 3.** CD26-mediated costimulation of CD4<sup>+</sup> T cells induces greater LAG3 expression than does CD28-mediated costimulation. **(A)** Freshly purified CD4<sup>+</sup> T cells were stimulated with anti-CD3 mAb alone, anti-CD3 plus anti-CD28 mAbs, or anti-CD3 plus anti-CD26 mAbs at the indicated concentrations for 96 h. Cell surface LAP (**Ab**), CTLA-4 (**Ac**), intracellular LAG3 (**Aa**), and FOXP3 (**Ad**) gated for CD4<sup>+</sup> T cells were detected by flow cytometry. Data are shown as mean  $\pm$  SE of MFI (**Aa**) or percentage positive cells (**Ab–d**) from five independent donors, comparing values in anti-CD3 plus anti-CD26 to those in anti-CD3 plus anti-CD28 (\* $p < 0.01$ ), and similar results were obtained in each experiment. **(B)** Freshly purified CD4<sup>+</sup> T cells were stimulated with anti-CD3 mAb alone, anti-CD3 plus anti-CD28 mAbs (50  $\mu$ g/ml), or anti-CD3 plus anti-CD26 mAbs (50  $\mu$ g/ml) for 96 h. After stimulation, cell surface (a) or intracellular (b) expression of LAG3 gated for CD4<sup>+</sup> T cells was analyzed by flow cytometry. Data are shown as histogram of LAG3 and are representative of five independent donors. The gray areas in each histogram show the data of isotype control.



130,000 Da. The band with the higher molecular mass is thought to represent the constitutively expressed NFAT2 isoform, and the one with the lower molecular mass probably represents the inducible NFAT2 isoform (33). In contrast with NFAT4, which was only slightly expressed both in the cytoplasm and the nucleus of peripheral blood CD4<sup>+</sup> T cells (data not shown), the protein level of NFAT2 was abundant and clearly increased in response to CD26 or CD28 costimulation compared with NFAT1, suggesting that among the NFAT family, NFAT2 plays a crucial role in regulating human CD4<sup>+</sup> T cell activation. NFAT protein is known to synergistically interact with many transcription factors, including AP-1, which is the main transcriptional partner of NFAT during T cell activation. Alternatively, in the absence of AP-1, NFAT directs transcription of a specific program of gene expression that may be responsible for blocking TCR signaling (33). Taken together, these results strongly suggest that persistent NFAT–AP-1 cooperation is responsible for CD26-mediated T cell activation, leading to a specific pattern of gene expression different from CD28-mediated costimulation.

#### *Increased EGR2 expression following CD26-mediated costimulation is associated with preferential IL-10 production*

The findings above suggest that persistent NFAT–AP-1 activation following CD26-mediated costimulation is associated with enhanced IL-10 production. The molecular mechanisms involved in the process of IL-10 transcription in T cells have been well characterized, with the involvement of many transcription factors having been reported previously. c-Maf and IRF4 directly transactivate IL-10 gene expression through binding to the IL-10 promoter (34, 35), whereas Blimp-1 posi-

tioned downstream of EGR2, GATA-3, and E4BP4 (also known as NFIL3) enhances IL-10 expression epigenetically by acetylating or methylating histones to change the chromatin structure at the IL-10 locus (36–38). We hypothesized that preferential IL-10 production of CD4<sup>+</sup> T cells following CD26-mediated costimulation was associated with the induction of such transcription factors. To validate the above assumption, we conducted a real-time RT-PCR assay to analyze the expression levels of the transcription factors discussed above following CD26 or CD28 costimulation. As shown in Fig. 5Aa, CD26 costimulation resulted in greater enhancement of EGR2 expression in CD4<sup>+</sup> T cells during the tested time intervals as compared with CD28 costimulation. Alternatively, both CD26 and CD28 costimulation markedly increased the expression of IRF4 compared with unstimulated T cells, but no difference was observed between these two costimulatory pathways (Fig. 5Ab). In contrast, both CD26 and CD28 costimulation of T cells led to a decrease in c-Maf or Blimp-1 expression (Fig. 5Ac, d), as well as a decline in expression levels of GATA-3 and E4BP4 (data not shown), indicating that EGR2 expression was preferentially induced following CD26-mediated costimulation. Western blot analysis was then conducted to confirm the above results. As shown in Fig. 5B, the protein level of EGR2 was higher after 24 or 48 h of CD26 costimulation than CD28 costimulation. Because it has been reported that EGR2 transcription is regulated by NFAT (39), we next examined the potential involvement of NFAT in the induction of EGR2 expression following CD26 costimulation. As shown in Fig. 5C, stimulation with both anti-CD3 plus anti-CD26 and anti-CD3 plus Cav-Ig clearly enhanced EGR2 expression compared with CD28 costimulation, a process that was partially inhibited by the NFAT

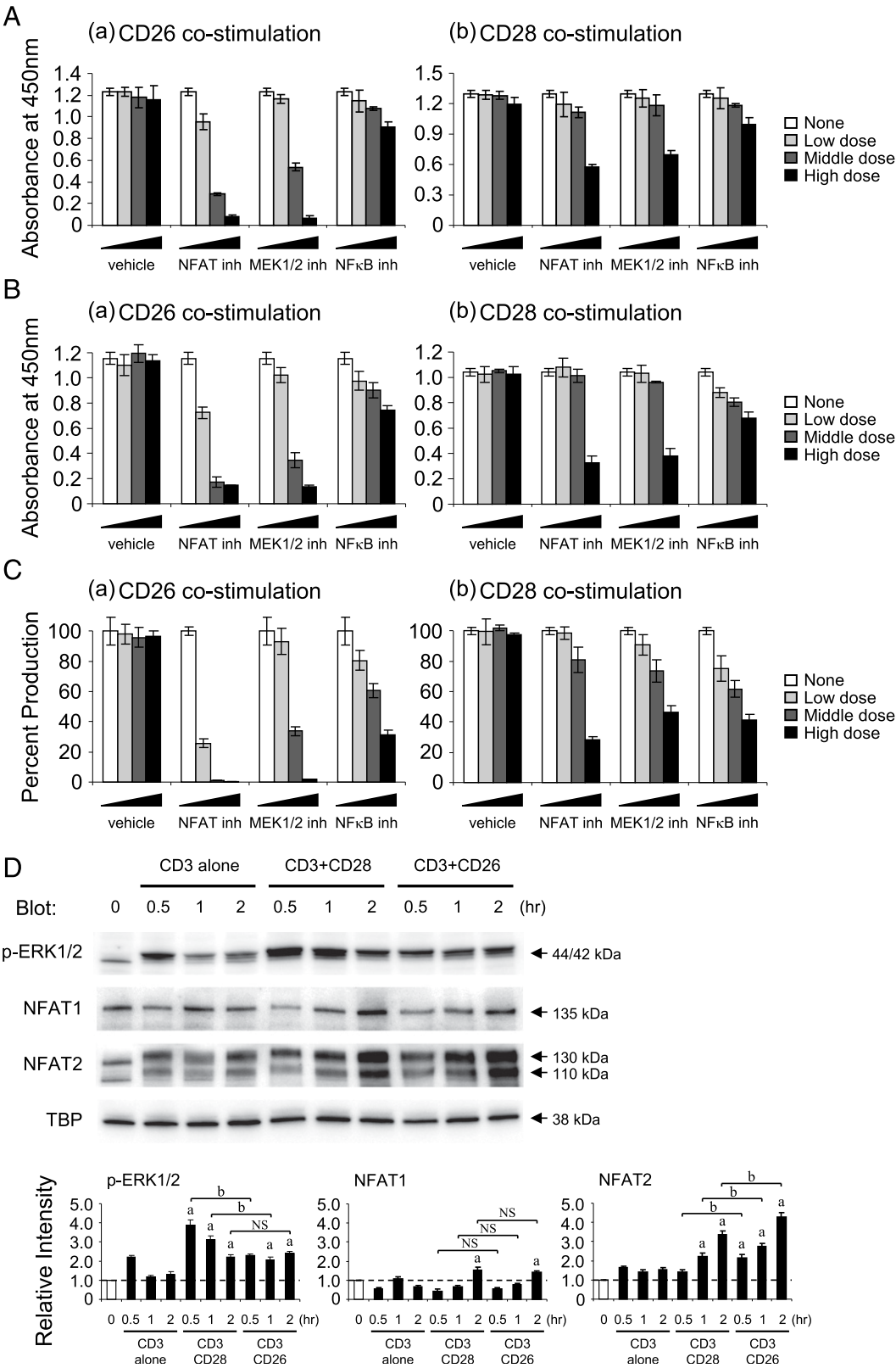


**FIGURE 4.** NFAT and Raf-MEK-ERK signaling events are indispensable for CD26-mediated CD4<sup>+</sup> T cell activation. (**A–C**) Freshly purified CD4<sup>+</sup> T cells were stimulated with anti-CD3 plus anti-CD26 mAbs (25  $\mu$ g/ml) (**a**) or anti-CD3 plus anti-CD28 mAbs (25  $\mu$ g/ml) (**b**) for 96 h in the presence of increasing doses of vehicle (DMSO, 0.0025, 0.0075, 0.025%), NFAT inhibitor (CyA, 0.01, 0.1, 1  $\mu$ M), MEK1/2 inhibitor (U0126, 0.5, 1.5, 5  $\mu$ M), or NF- $\kappa$ B inhibitor (quinazoline, 0.1, 0.5, 2.5  $\mu$ M). (**A**) BrdU was added for the last 2 h of culture, and proliferation was assessed by measuring BrdU incorporation by ELISA. (**B**) Tetrazolium was added for the last 3 h of culture, and the absorbance at 450 nm was measured. (**C**) Concentration of IL-10 was examined by ELISA. Representative data of two (**A**) and four (**B** and **C**) independent donors are shown as mean  $\pm$  SD of triplicate samples, and similar results were obtained in each experiment. (**D**) Freshly purified CD4<sup>+</sup> T cells were stimulated with anti-CD3 mAb alone, anti-CD3 plus anti-CD28 mAbs (50  $\mu$ g/ml), or anti-CD3 plus anti-CD26 mAbs (50  $\mu$ g/ml) for the indicated times. Nuclear extracts were separated by SDS-PAGE (each at 5  $\mu$ g), and p-ERK1/2, NFAT1, or NFAT2 were detected by immunoblotting. The same blots were stripped and reprobed with Abs specific (Figure legend continues)

inhibitor alone and completely abrogated by the combination of the NFAT and MEK1/2 inhibitors. Furthermore, to determine whether EGR2 expression was associated with IL-10 production, we conducted knockdown experiments using siRNA against EGR2 in primary CD4<sup>+</sup> T cells. Expression level of EGR2 in T cells following CD26 costimulation was determined by real-time RT-PCR in the presence of control siRNA or two different sequences of EGR2-siRNA. As shown in Fig. 5Da, b, EGR2-siRNA treatment reduced EGR2 expression by ~50% as compared with control siRNA, which was associated with a significant decrease in IL-10 production by CD4<sup>+</sup> T cells. Because similar results were also obtained with a different siRNA sense2 designed to target a separate EGR2 site, data obtained with EGR2-siRNA sense1 as described in *Materials and Methods* are shown. Because it has been shown that EGR2-deficient CD4<sup>+</sup> T cells in mice produced high levels of IFN- $\gamma$  and IL-17 following TCR stimulation (40), we therefore examined the effect of EGR2 knockdown on IL-17A and IFN- $\gamma$  production by human CD4<sup>+</sup> T cells. As shown in Fig. 5Dc, d, production of both cytokines was vigorously enhanced by EGR2-siRNA compared with control siRNA. These results rule out the possibility that the decrease in IL-10 production seen with EGR2-siRNA treatment was due to the nonspecific off-target effects of siRNA. Taken together, these observations strongly suggest that CD26-mediated costimulation of CD4<sup>+</sup> T cells results in enhanced NFAT/AP-1-dependent EGR2 expression, which is associated with the preferential production of IL-10.

*Supernatants of CD3/CD26-stimulated CD4<sup>+</sup> T cells suppress activation of bystander T cells in an IL-10-dependent manner*

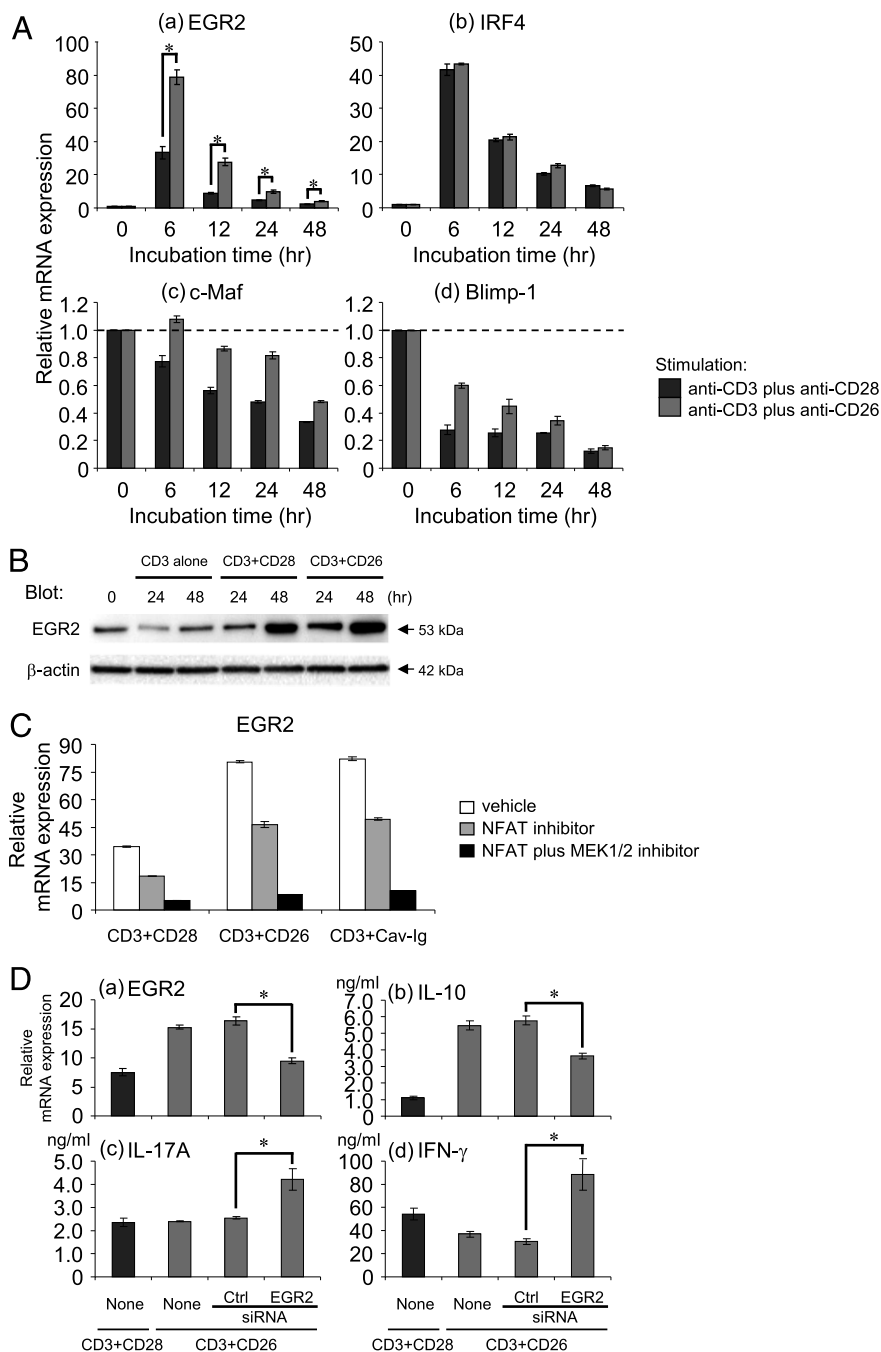
To address the functional significance of enhanced IL-10 production by CD4<sup>+</sup> T cells following CD26-mediated costimulation, we prepared culture supernatant of CD4<sup>+</sup> T cells stimulated with anti-CD3 plus a high dose (50  $\mu$ g/ml) of anti-CD26 or anti-CD28 as a control and then examined whether the supernatant of CD3/CD26-stimulated T cells (CD26 sup) suppressed activation of bystander T cells. We confirmed that higher levels of IL-10 and lower levels of IL-2 were contained in CD26 sup as compared with the supernatant of CD3/CD28-stimulated T cells (CD28 sup), as shown in Fig. 2A. As shown in Fig. 6Aa, b, addition of CD26 sup to freshly purified CD4<sup>+</sup> T cells incubated under stimulatory condition with anti-CD3 plus anti-CD26 for 24 h resulted in a significant reduction in expression levels of both IL-2 and IFN- $\gamma$  as compared with AIM-V medium, and this inhibitory effect was abrogated by the addition of anti-IL-10 plus anti-IL-10R. In contrast, IL-10 expression in CD4<sup>+</sup> T cells was significantly enhanced by CD26 sup, and this enhancing effect was almost completely reversed by anti-IL-10 plus anti-IL-10R (Fig. 6Ac). These results indicate that IL-10 contained in the CD26 sup suppresses the expression of effector cytokines such as IL-2 and IFN- $\gamma$  but upregulated the expression of IL-10. Alternatively, treatment with CD28 sup markedly upregulated IL-2 expression, suggesting the presence in CD28 sup of soluble factors such as IL-2 that enhance the process of T cell activation (Fig. 6Aa). In contrast, addition of anti-IL-10 plus anti-IL-10R in the presence of CD28 sup increased the expression of IFN- $\gamma$  but decreased IL-10 expression, suggesting that the relatively small amount of IL-10 in the CD28 sup was sufficient to regulate CD4<sup>+</sup> T cell cytokine production (Fig. 6Ab, c). To analyze the effect of CD26 sup on the

proportion of IL-10 or effector cytokine-expressing cells, we next performed intracellular staining of IL-10 and IFN- $\gamma$  in CD4<sup>+</sup> T cells. As shown in Fig. 6Ba, d, stimulation of freshly purified CD4<sup>+</sup> T cells with anti-CD3 plus anti-CD26 in the presence of CD26 sup for 3 d resulted in a decrease in the relative percentage of IFN- $\gamma$ -expressing cells (from 18.5 to 11.1%) as compared with AIM-V medium, whereas the proportion of IL-10-expressing cells was hardly affected by CD26 sup. The effect of CD26 sup on the proportion of IFN- $\gamma$ -expressing cells was reversed by anti-IL-10 plus anti-IL-10R (Fig. 6Be). Alternatively, addition of CD28 sup to CD4<sup>+</sup> T cells did not change the proportion of IFN- $\gamma$ -expressing cells, but CD28 sup treatment in the presence of anti-IL-10 and anti-IL-10R led to an increase in the level of IFN- $\gamma$  cells (Fig. 6Bb, c), suggesting that the CD28 sup contained both activating and inhibitory factors such as IL-10. These findings strongly suggest that CD26 sup preferentially suppresses the proliferation of effector cytokine-expressing cells in an IL-10-dependent manner.

We next analyzed the effect of CD26 sup on T cell proliferation. As shown in Fig. 7A, CD26 sup clearly inhibited the proliferative activity of freshly purified CD4<sup>+</sup> T cells following CD26 costimulation. Although CD28 sup also slightly suppressed the proliferation of T cells following CD26 costimulation, the suppressive effect of CD26 sup was much more pronounced compared with CD28 sup. Interestingly, the suppressive effect on T cells following CD26 costimulation was more evident compared with T cells following CD28 costimulation (Fig. 7A). To further evaluate this observed difference, we conducted the same T cell proliferation assay in the presence of rIL-10. As shown in Supplemental Fig. 2A and 2B, T cells stimulated with anti-CD3 plus anti-CD26 were much more sensitive to the inhibitory effect of IL-10 as compared with CD28 costimulation, and the difference between CD26 and CD28 costimulation was markedly evident in cytokine production compared with proliferative activity. We further analyzed the expression of IL-10R on CD4<sup>+</sup> T cells following CD26- or CD28-mediated costimulation but observed no difference in the expression intensity of IL-10R between these two costimulatory approaches (Supplemental Fig. 2C). To characterize in more detail the effect of CD26 sup on T cell proliferation, we analyzed the cell division process of CFSE-labeled CD4<sup>+</sup> T cells by flow cytometry. As shown in Fig. 7Ba, b, d, e, CD26 sup exhibited a very potent suppressive effect on the proliferation of T cells stimulated with anti-CD3 plus anti-CD26 compared with CD28 sup, and this effect was partially reversed by addition of anti-IL-10 plus anti-IL-10R. It is noteworthy that 10 ng/ml rIL-10, a higher concentration than that found in CD26 sup, clearly suppressed T cell proliferation, but this effect was not more potent than CD26 sup (Fig. 7Bd, f). Alternatively, CD26 sup only slightly inhibited the proliferation of T cells stimulated with anti-CD3 plus anti-CD28, and these CD3/CD28-stimulated CD4<sup>+</sup> T cells were much less sensitive to the inhibitory effect of IL-10 as compared with CD3/CD26-stimulated T cells (Fig. 7Cc, d). These results correlated strongly with the proliferative activity shown in Fig. 7A. Taken together, these data strongly suggest that soluble factors secreted from CD4<sup>+</sup> T cells following CD26-mediated costimulation profoundly suppress bystander T cell proliferation, with IL-10 having a synergistic effect on the suppressive activity of these soluble factors.

for TATA-binding protein (TBP) as a loading control. Band intensity of p-ERK1/2, NFAT1, or NFAT2 was normalized to TBP, and relative intensity compared with resting CD4<sup>+</sup> T cells (0 h) is indicated in the *bottom panel*. Data are shown as mean  $\pm$  SE of relative intensity from three independent donors, comparing values in anti-CD3 plus anti-CD28 or anti-CD3 plus anti-CD26 to those in anti-CD3 alone at the same stimulation period (<sup>a</sup> $p < 0.01$ ), and anti-CD3 plus anti-CD26 to those in anti-CD3 plus anti-CD28 at the same stimulation period (<sup>b</sup> $p < 0.01$ ).

**FIGURE 5.** EGR2 expression strongly induced via CD26-mediated costimulation is associated with IL-10 production. **(A and B)** Freshly purified CD4<sup>+</sup> T cells were stimulated with anti-CD3 alone, anti-CD3 plus anti-CD28 mAbs (25  $\mu$ g/ml), or anti-CD3 plus anti-CD26 mAbs (25  $\mu$ g/ml) for the indicated times. **(A)** mRNA expression of EGR2 **(a)**, IRF4 **(b)**, c-Maf **(c)**, and Blimp-1 **(d)** was quantified by real-time RT-PCR. Each expression was normalized to HPRT1, and relative expression levels compared with resting CD4<sup>+</sup> T cells (0 h) are shown. Representative data of four independent donors are shown as mean  $\pm$  SD of triplicate samples, comparing values in anti-CD3 plus anti-CD26 to those in anti-CD3 plus anti-CD28 (\* $p$  < 0.01). **(B)** Whole-cell lysates were separated by SDS-PAGE (each 10  $\mu$ g), and EGR2 was detected by immunoblotting. The same blots were stripped and reprobed with Abs specific for  $\beta$ -actin as a loading control. Data shown are representative of two independent experiments with similar results. **(C)** Freshly purified CD4<sup>+</sup> T cells were stimulated with anti-CD3 plus anti-CD28 mAbs (25  $\mu$ g/ml), anti-CD3 plus anti-CD26 mAbs (25  $\mu$ g/ml), or anti-CD3 mAb plus Cav-Ig (25  $\mu$ g/ml) for 6 h in the presence of vehicle (DMSO, 0.025%), NFAT inhibitor (CyA, 1  $\mu$ M), or NFAT inhibitor plus MEK1/2 inhibitor (U0126, 5  $\mu$ M). mRNA expression of EGR2 was quantified by real-time RT-PCR, and the relative expression level is shown as in **(A)**. Representative data of three independent donors are shown as mean  $\pm$  SD of triplicate samples. **(D)** Freshly purified CD4<sup>+</sup> T cells were transfected with siRNA against EGR2 or control siRNA (Ctrl) and stimulated with anti-CD3 plus anti-CD28 mAbs (25  $\mu$ g/ml) or anti-CD3 plus anti-CD26 mAbs (25  $\mu$ g/ml) for 24 h **(a)** or 96 h **(b–d)**. **(Da)** mRNA level of EGR2 is shown as in **(A)**. **(Db–d)** Concentrations of IL-10 **(b)**, IL-17A **(c)**, and IFN- $\gamma$  **(d)** were examined by ELISA. Representative data of four independent donors are shown as mean  $\pm$  SD of triplicate samples, comparing values with EGR2 siRNA to those with control siRNA (\* $p$  < 0.01), and similar results were obtained in each experiment.



## Discussion

In the present study, we show that coengagement of CD3 and CD26 induces the development of CD4<sup>+</sup> T cells to a Tr1-like phenotype with a high level of IL-10 production and LAG3 expression. CD26 costimulation also induces a high level of EGR2 associated with preferential IL-10 production, possibly via NFAT- and AP-1-mediated signaling. Furthermore, supernatants of these CD3/CD26-stimulated CD4<sup>+</sup> T cells clearly suppress the proliferative activity and effector cytokine production of bystander T cells in an IL-10-dependent manner.

Because the maintenance of peripheral tolerance by Tregs is critical to the potential development of autoimmunity, there is considerable interest in elucidating the molecular mechanisms for inducing the differentiation of CD4<sup>+</sup> T cells into specific Treg subsets. Although the mechanisms of Treg induction through exogenous cytokine stimulation have been extensively studied, such

as TGF- $\beta$  for Foxp3<sup>+</sup> Tregs or IL-27 for Tr1 cells (41), costimulatory signals for the induction of Tregs have not been fully understood. ICOS and CD46 have been reported as costimulatory signals inducing Tr1-type cells (42, 43). ICOS costimulation regulates c-Maf expression possibly through the enhancement of NFAT2 signal (44). CD46 costimulation induces interaction of the cytoplasmic tail of CD46 (CYT-1-BC1) with SPAK, leading to sustained phosphorylation of ERK1/2 (45). The importance of sustained phosphorylation of ERK1/2 has also been reported for the development of IL-10-producing Th1 cells (46). However, sustained phosphorylation of ERK1/2 alone is not sufficient to explain the preferential IL-10 production, and transcription factors such as c-Maf, IRF4, Blimp-1, GATA-3, and E4BP4 (NFIL3) may be associated with the transcription of IL-10 (34–38). Our present study indicates that EGR2 expression is enhanced in CD4<sup>+</sup> T cells following CD26-mediated costimulation (Fig. 5A, B), and EGR2



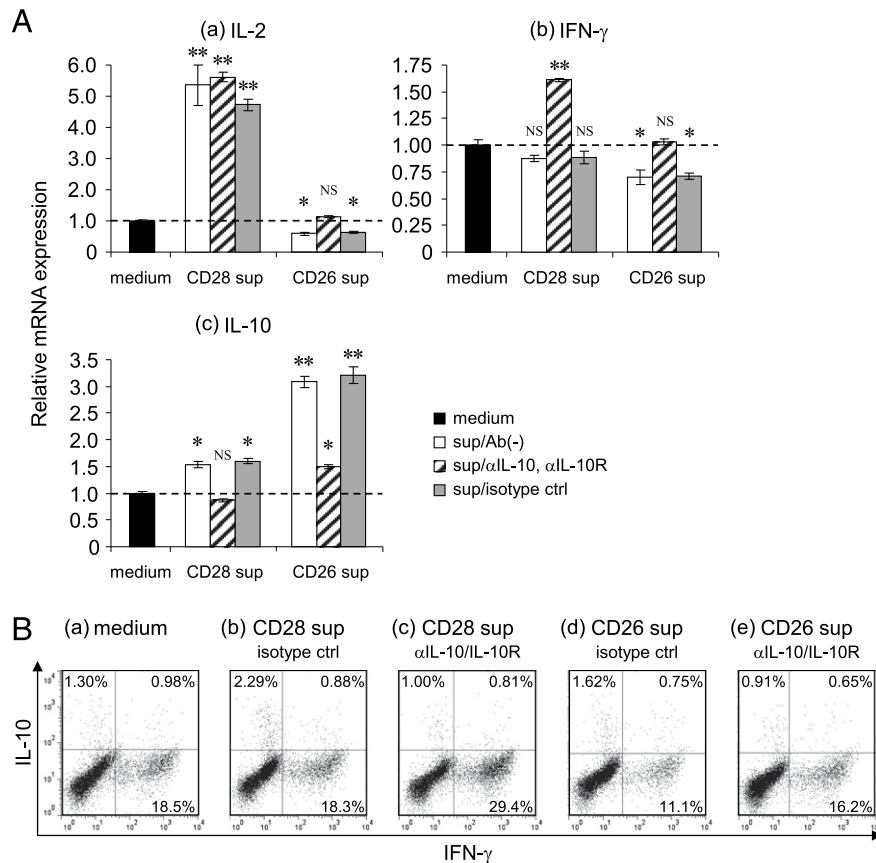


**FIGURE 6.** Supernatants of CD3/CD26-activated CD4<sup>+</sup> T cells suppress effector function of bystander T cells while augmenting IL-10 expression in an IL-10-dependent manner. Culture supernatants of CD4<sup>+</sup> T cells stimulated with anti-CD3 plus anti-CD28 mAbs (50  $\mu$ g/ml) or anti-CD3 plus anti-CD26 mAbs (50  $\mu$ g/ml) for 72 h were collected, and freshly purified CD4<sup>+</sup> T cells were stimulated with anti-CD3 plus anti-CD26 mAbs (5  $\mu$ g/ml) in the presence of the supernatant (CD28 sup or CD26 sup) or AIM-V medium as a control. Prior to the onset of culture, the combination of anti-human IL-10 mAb and anti-human IL-10 receptor mAb ( $\alpha$ IL10/IL10R) or isotype control mAbs (isotype ctrl) were added to the culture wells to give a final concentration of 20  $\mu$ g/ml each. **(A)** After 24 h of incubation, cells were harvested and mRNA expression of IL-2 (**a**), IFN- $\gamma$  (**b**), or IL-10 (**c**) was quantified by real-time RT-PCR. Each expression was normalized to HPRT1, and relative expression levels compared with the sample of control medium are shown. Representative data of three independent donors are shown as mean  $\pm$  SD of triplicate samples, comparing values in each sample to that in control medium. \* $p$  < 0.01, \*\* $p$  < 0.0001. **(B)** On day 3, cells were restimulated with PMA plus ionomycin in the presence of monensin for the last 5 h of culture, and the intracellular expression of IFN- $\gamma$  and IL-10 was detected by flow cytometry. Two-dimensional dot plot of IFN- $\gamma$  or IL-10 staining gated for CD4<sup>+</sup> T cells is shown as a representative plot of three independent donors, and similar results were obtained in each experiment.

knockdown in CD4<sup>+</sup> T cells decreases IL-10 while markedly enhancing IL-17A and IFN- $\gamma$  production (Fig. 5D). These observations strongly suggest that the induction of EGR2 expression is associated with the preferential production of IL-10 after CD26 costimulation. In mice, it has been recently reported that a high level of EGR2 expression is induced by IL-27/IL-27R–STAT3 signaling, and Blimp-1 induced by EGR2 is important for IL-10 production in CD4<sup>+</sup> T cells (47). In contrast with the marked upregulation of EGR2 following CD26-mediated costimulation, the expression level of Blimp-1 is not enhanced as compared with unstimulated T cells, although the decrease is more apparent in T cells following CD28 costimulation (Fig. 5A). To characterize more precisely the molecular mechanisms involved in IL-10 induction following CD26-mediated costimulation, the role of Blimp-1 or c-Maf needs to be better defined. NFAT is considered to be a regulator of EGR2 expression in T cells (39). Our present work shows that EGR2 is highly induced via CD26 costimulatory signal, and its expression is partially decreased by the NFAT inhibitor CyA and completely abrogated by the combination of CyA and the MEK1/2 inhibitor U0126 (Fig. 5C). These results strongly suggest that not only NFAT but also Raf-MEK-ERK signaling is involved in the induction of EGR2 expression. The association of

ERK1/2 signaling in the induction of EGR2 expression has been recently reported in osteoprogenitors or breast adipose fibroblasts (48, 49), suggesting that the ERK signaling pathway is also associated with the transcription of EGR2 in T cells.

The importance of the anti-inflammatory effects of IL-10 has been confirmed in IL-10-deficient mice. IL-10-deficient mice develop spontaneous colitis at an early age, indicating that IL-10 is essential for intestinal homeostasis (50). IL-10-deficient mice also exhibit severe neuroinflammation with loss of recovery in experimental autoimmune encephalomyelitis (51). Furthermore, the generation of Tr1 cells from peripheral CD4<sup>+</sup> T cells has been shown to be greatly impaired in MS patients in comparison with healthy controls (52). Therefore, Tr1-mediated immunotherapy may be a potentially effective approach for the treatment of many autoimmune disorders, including inflammatory bowel disease or MS. Several groups have attempted to generate large numbers of Tr1 in vitro for clinical applications, and IL-27 is being considered currently to be an essential factor for the generation of Tr1 cells (53). In addition to IL-27, costimulatory signals through ICOS or CD46 play an important role in the generation or expansion of Tr1 cells. Our present study raises the possibility that CD26 is a novel costimulatory molecule inducing preferential IL-10 production in

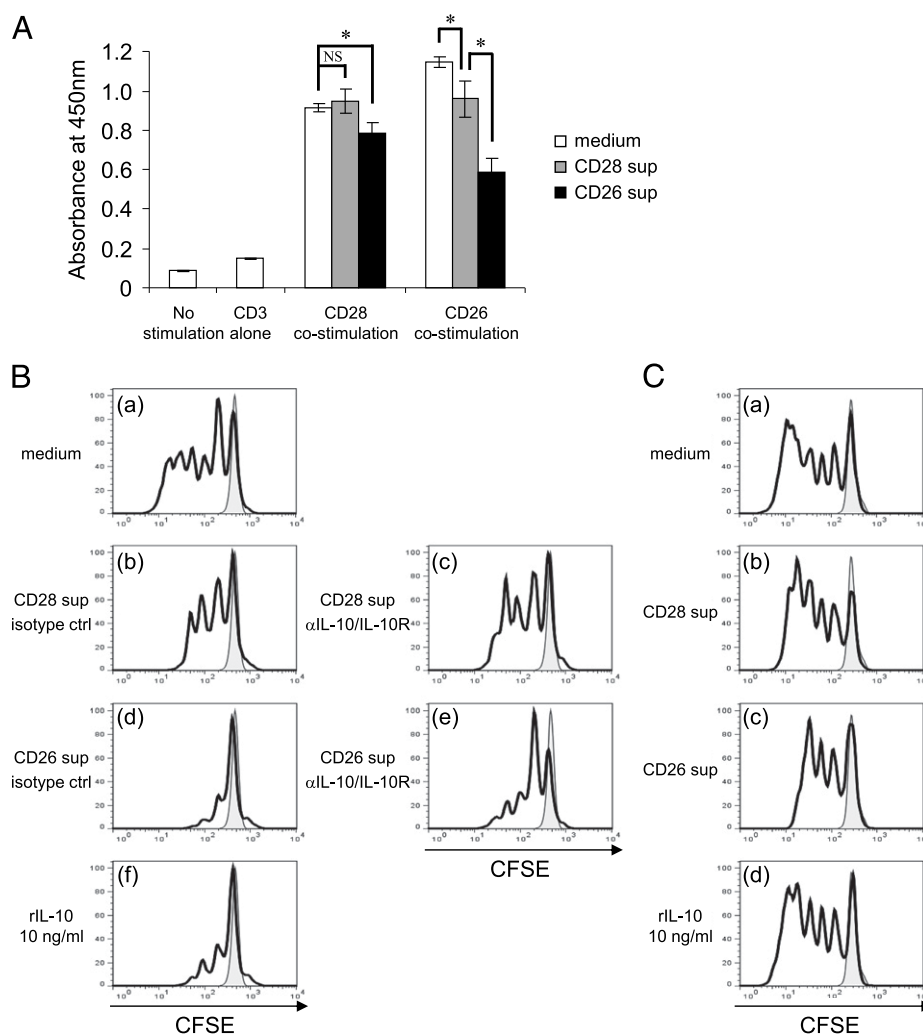


**FIGURE 7.** Supernatants of CD3/CD26-activated CD4<sup>+</sup> T cells significantly suppress the proliferation of bystander T cells through partial dependence on IL-10. Culture supernatants were prepared by the same method as shown in Fig. 6. **(A)** Freshly purified CD4<sup>+</sup> T cells were stimulated with anti-CD3 mAb alone, anti-CD3 plus anti-CD28 mAbs (5  $\mu$ g/ml), or anti-CD3 plus anti-CD26 mAbs (5  $\mu$ g/ml) for 96 h in the presence of the supernatant (CD28 sup or CD26 sup) or AIM-V medium as a control. Tetrazolium was added for the last 3 h of culture, and the absorbance at 450 nm was measured. Representative data of five independent donors are shown as mean  $\pm$  SD of triplicate samples, comparing values with culture supernatants to those with control medium (\* $p$  < 0.01). **(B)** CFSE-labeled freshly purified CD4<sup>+</sup> T cells were stimulated with anti-CD3 plus anti-CD26 mAbs (5  $\mu$ g/ml) in the presence of the supernatant [CD28 sup (**b** and **c**) or CD26 sup (**d** and **e**)] or recombinant human IL-10 (rIL-10, 10 ng/ml) (**f**) or AIM-V medium (**a**) as a control. Prior to the onset of culture, the combination of anti-human IL-10 mAb and anti-human IL-10 receptor mAb ( $\alpha$ IL-10/IL-10R) (**b** and **e**) or isotype control mAbs (isotype ctrl) (**b** and **d**) were added to the culture wells to give a final concentration of 20  $\mu$ g/ml each. **(C)** CFSE-labeled freshly purified CD4<sup>+</sup> T cells were stimulated with anti-CD3 plus anti-CD28 mAbs (5  $\mu$ g/ml) in the presence of the supernatant [CD28 sup (**b**) or CD26 sup (**c**)] or recombinant human IL-10 (rIL-10, 10 ng/ml) (**d**) or AIM-V medium (**a**) as a control. After 96 h of incubation, cells were harvested and analyzed by flow cytometry. The data are shown as histograms of CFSE intensity gated for CD4<sup>+</sup> T cells and are representative of three independent donors, and similar results were obtained in each experiment. The gray areas in each histogram show the data of T cells cultured for 96 h without any stimulation.

CD4<sup>+</sup> T cells. Because CD26, ICOS, and CD46 belong to different families and their downstream signaling events are considered to be different, the combination of these costimulatory pathways may have additive effects on the induction of Tr1 cells. For this purpose, identification of the T cell subsets producing a high level of IL-10 following CD26 costimulation is needed. Because the CD4<sup>+</sup> T cells used in this study contained all the T cell subsets such as naive, Th1, Th2, Th17, follicular helper T, or Treg, we conducted costimulation assays following purification of CD4<sup>+</sup> naive, memory, or Treg subsets. Although the absolute amount of IL-10 produced by CD45RO<sup>+</sup> memory T cells was higher than CD45RA<sup>+</sup> naive T cells, both naive and memory CD4<sup>+</sup> T cells costimulated through CD26 produced greater levels of IL-10 compared with CD28 costimulation (Supplemental Fig. 3). In contrast, purified CD4<sup>+</sup>CD25<sup>high</sup>CD127<sup>low</sup>FOXP3<sup>+</sup> cells appar-

ently produced a low level of IL-10 following CD26 costimulation compared with other populations of CD4<sup>+</sup> T cells (Supplemental Fig. 3). These observations indicate that naturally occurring CD4<sup>+</sup>CD25<sup>high</sup>CD127<sup>low</sup>FOXP3<sup>+</sup> cells are not the source of IL-10 production, and they suggest that the subpopulation included in memory CD4<sup>+</sup> T cells is the main source of IL-10, whereas naive CD4<sup>+</sup> T cells also produce IL-10 in response to CD26 costimulation. Additionally, in vivo studies focusing on the suppressive activity of this population of in vitro-differentiated CD4<sup>+</sup> T cells, or the stability or plasticity of this IL-10-producing phenotype, need to be considered in future work.

CD28 is a representative T cell costimulatory pathway, and the negative feedback mechanism through CTLA-4 is associated with this pathway as a means of controlling excessive T cell activation. CD26 also functions as a costimulatory molecule in human T cells,

and CD26<sup>+</sup> T cells have been suggested to be involved in the pathophysiology of various immune disorders such as MS, rheumatoid arthritis, and graft-versus-host disease (8, 10, 12). Our present study shows that stimulation through TCR and high-intensity interaction of caveolin-1–CD26-mediated signaling induces the development of CD4<sup>+</sup> T cells to a Tr1-like phenotype. Caveolin-1 is a ubiquitously expressed ligand of CD26 in many cell types such as epithelial cells, endothelial cells, fibroblasts, macrophages, and neutrophils. We have previously shown that caveolin-1 was detected on the cell surface of monocytes 12–24 h after Ag uptake, and that CD26 and caveolin-1 colocalized at the T cell/monocyte contact site (19). Moreover, caveolin-1 expression is regulated by NF- $\kappa$ B, and stimulation with LPS or TNF- $\alpha$  increases the expression of caveolin-1 mRNA and protein (54), suggesting that expression of caveolin-1 may be increased on cells accumulated at sites of inflammation, leading to the transduction of intensive CD26-mediated signaling in CD26<sup>+</sup> T cells. Taken together, our data strongly suggest that CD4<sup>+</sup> T cells receiving robust caveolin-1–CD26-mediated signaling at the inflammatory site produce a high level of IL-10 and potentially other inhibitory factors to curtail the inflammatory process. Because striking defects in the induction of Tr1 cells through CD46 costimulation have been reported in patients with MS (52), it is conceivable that negative feedback mechanisms for regulating excessive CD26-mediated activation may be impaired in patients with autoimmune diseases, and further research is required to evaluate this hypothesis.

The cytoplasmic domain of CD28 has several common motifs that bind to signaling molecules such as PI3K, growth factor receptor-bound protein 2, or IL-2-inducible T cell kinase, whereas the cytoplasmic tail of CD26 consists of only 6 aa without any conserved kinase or protein-binding motifs (18). We have previously shown that CD26 localizes into lipid rafts, and stimulation with anti-CD3 plus anti-CD26 promotes aggregation of lipid rafts, leading to colocalization of CD45 to TCR signaling molecules such as p56<sup>Lck</sup>, ZAP-70, or TCR $\zeta$  (30). Our present data strongly suggest that persistent NFAT–AP-1 cooperation is responsible for CD26-mediated T cell activation, and sustained activation of NFAT and ERK1/2 is possibly due to the aggregation of signaling molecules in lipid rafts following CD26-mediated costimulation. Furthermore, we have previously shown that DPPIV enzyme activity is partially involved in the costimulatory activity of CD26 through studies using wild-type CD26 (DPPIV<sup>+</sup>) or mutant CD26 (DPPIV<sup>−</sup>)–transfected Jurkat T cell lines (55). Other groups reported that the synthetic competitive DPPIV inhibitor Lys[Z(NO<sub>2</sub>)] significantly suppressed the proliferation and production of IL-2, IL-10, and IFN- $\gamma$  in PWM-stimulated human T cells (56). They showed that these DPPIV inhibitors markedly increased the secretion of latent TGF- $\beta$ 1 by PWM-stimulated T cells, resulting in suppression of T cell activation. To further characterize the role of DPPIV enzyme activity in T cell activation, we are now examining the effect of the clinically used DPPIV specific inhibitor sitagliptin. Our preliminary data indicate that sitagliptin strongly suppresses the proliferative activity and production of cytokines including IL-10 of human CD4<sup>+</sup> T cells following CD26-mediated costimulation compared with CD28-mediated costimulation (data not shown), with the precise molecular mechanisms involved in this process being currently investigated.

In conclusion, intensive CD26 costimulatory signaling induces the development of CD4<sup>+</sup> T cells to a Tr1-like phenotype with a high level of IL-10 production, possibly for regulating potentially excessive CD26-mediated activation. Whether this possible negative feedback mechanism of CD26 costimulation is normally maintained or impaired in patients with autoimmune diseases is the subject of future investigations.

## Disclosures

The authors have no financial conflicts of interest.

## References

1. Fox, D. A., R. E. Hussey, K. A. Fitzgerald, O. Acuto, C. Poole, L. Palley, J. F. Daley, S. F. Schlossman, and E. L. Reinherz. 1984. Ta1, a novel 105 KD human T cell activation antigen defined by a monoclonal antibody. *J. Immunol.* 133: 1250–1256.
2. Nanus, D. M., D. Engelstein, G. A. Gastl, L. Gluck, M. J. Vidal, M. Morrison, C. L. Finstad, N. H. Bander, and A. P. Albino. 1993. Molecular cloning of the human kidney differentiation antigen gp160: human aminopeptidase A. *Proc. Natl. Acad. Sci. USA* 90: 7069–7073.
3. Tanaka, T., D. Camerini, B. Seed, Y. Torimoto, N. H. Dang, J. Kameoka, H. N. Dahlberg, S. F. Schlossman, and C. Morimoto. 1992. Cloning and functional expression of the T cell activation antigen CD26. *J. Immunol.* 149: 481–486.
4. Morimoto, C., and S. F. Schlossman. 1998. The structure and function of CD26 in the T-cell immune response. *Immunol. Rev.* 161: 55–70.
5. Ohnuma, K., N. H. Dang, and C. Morimoto. 2008. Revisiting an old acquaintance: CD26 and its molecular mechanisms in T cell function. *Trends Immunol.* 29: 295–301.
6. Morimoto, C., Y. Torimoto, G. Levinson, C. E. Rudd, M. Schrieber, N. H. Dang, N. L. Letvin, and S. F. Schlossman. 1989. IF7, a novel cell surface molecule, involved in helper function of CD4 cells. *J. Immunol.* 143: 3430–3439.
7. Bengsch, B., B. Seigel, T. Flecken, J. Wolanski, H. E. Blum, and R. Thimme. 2012. Human Th17 cells express high levels of enzymatically active dipeptidylpeptidase IV (CD26). *J. Immunol.* 188: 5438–5447.
8. Krakauer, M., P. S. Sorensen, and F. Sellebjerg. 2006. CD4<sup>+</sup> memory T cells with high CD26 surface expression are enriched for Th1 markers and correlate with clinical severity of multiple sclerosis. *J. Neuroimmunol.* 181: 157–164.
9. Eguchi, K., Y. Ueki, C. Shimomura, T. Otsubo, H. Nakao, K. Migita, A. Kawakami, M. Matsunaga, H. Tezuka, N. Ishikawa, et al. 1989. Increment in the Ta1<sup>+</sup> cells in the peripheral blood and thyroid tissue of patients with Graves' disease. *J. Immunol.* 142: 4233–4240.
10. Ohnuma, K., H. Inoue, M. Uchiyama, T. Yamochi, O. Hosono, N. H. Dang, and C. Morimoto. 2006. T-cell activation via CD26 and caveolin-1 in rheumatoid synovium. *Mod. Rheumatol.* 16: 3–13.
11. Hatano, R., K. Ohnuma, J. Yamamoto, N. H. Dang, and C. Morimoto. 2013. CD26-mediated co-stimulation in human CD8<sup>+</sup> T cells provokes effector function via pro-inflammatory cytokine production. *Immunology* 138: 165–172.
12. Hatano, R., K. Ohnuma, J. Yamamoto, N. H. Dang, T. Yamada, and C. Morimoto. 2013. Prevention of acute graft-versus-host disease by humanized anti-CD26 monoclonal antibody. *Br. J. Haematol.* 162: 263–277.
13. Bluestone, J. A. 1995. New perspectives of CD28-B7-mediated T cell costimulation. *Immunity* 2: 555–559.
14. Shahinian, A., K. Pfeffer, K. P. Lee, T. M. Kündig, K. Kishihara, A. Wakeham, K. Kawai, P. S. Ohashi, C. B. Thompson, and T. W. Mak. 1993. Differential T cell costimulatory requirements in CD28-deficient mice. *Science* 261: 609–612.
15. Tivol, E. A., F. Borriello, A. N. Schweitzer, W. P. Lynch, J. A. Bluestone, and A. H. Sharpe. 1995. Loss of CTLA-4 leads to massive lymphoproliferation and fatal multiorgan tissue destruction, revealing a critical negative regulatory role of CTLA-4. *Immunity* 3: 541–547.
16. Waterhouse, P., J. M. Penninger, E. Timms, A. Wakeham, A. Shahinian, K. P. Lee, C. B. Thompson, H. Griesser, and T. W. Mak. 1995. Lymphoproliferative disorders with early lethality in mice deficient in Ctla-4. *Science* 270: 985–988.
17. Stamper, C. C., Y. Zhang, J. F. Tobin, D. V. Erbe, S. Ikemizu, S. J. Davis, M. L. Stahl, J. Seehra, W. S. Somers, and L. Mosyak. 2001. Crystal structure of the B7-1/CTLA-4 complex that inhibits human immune responses. *Nature* 410: 608–611.
18. Rudd, C. E., and H. Schneider. 2003. Unifying concepts in CD28, ICOS and CTLA4 co-receptor signalling. *Nat. Rev. Immunol.* 3: 544–556.
19. Ohnuma, K., T. Yamochi, M. Uchiyama, K. Nishibashi, N. Yoshikawa, N. Shimizu, S. Iwata, H. Tanaka, N. H. Dang, and C. Morimoto. 2004. CD26 up-regulates expression of CD86 on antigen-presenting cells by means of caveolin-1. *Proc. Natl. Acad. Sci. USA* 101: 14186–14191.
20. Ohnuma, K., M. Uchiyama, T. Yamochi, K. Nishibashi, O. Hosono, N. Takahashi, S. Kina, H. Tanaka, X. Lin, N. H. Dang, and C. Morimoto. 2007. Caveolin-1 triggers T-cell activation via CD26 in association with CARMA1. *J. Biol. Chem.* 282: 10117–10131.
21. Stremenová, J., V. Mares, V. Lisá, M. Hilser, E. Krepela, Z. Vanicková, M. Syrucek, O. Soula, and A. Sedo. 2010. Expression of dipeptidyl peptidase-IV activity and/or structure homologs in human meningiomas. *Int. J. Oncol.* 36: 351–358.
22. Nakamura, K., A. Kitani, and W. Strober. 2001. Cell contact-dependent immunosuppression by CD4<sup>+</sup>CD25<sup>+</sup> regulatory T cells is mediated by cell surface-bound transforming growth factor  $\beta$ . *J. Exp. Med.* 194: 629–644.
23. Collison, L. W., C. J. Workman, T. T. Kuo, K. Boyd, Y. Wang, K. M. Vignali, R. Cross, D. Sehy, R. S. Blumberg, and D. A. Vignali. 2007. The inhibitory cytokine IL-35 contributes to regulatory T-cell function. *Nature* 450: 566–569.
24. Groux, H., A. O'Garra, M. Bigler, M. Rouleau, S. Antonenko, J. E. de Vries, and M. G. Roncarolo. 1997. A CD4<sup>+</sup> T-cell subset inhibits antigen-specific T-cell responses and prevents colitis. *Nature* 389: 737–742.
25. Okamura, T., K. Fujio, M. Shibuya, S. Sumitomo, H. Shoda, S. Sakaguchi, and K. Yamamoto. 2009. CD4<sup>+</sup>CD25<sup>+</sup>LAG3<sup>+</sup> regulatory T cells controlled by the transcription factor Egr-2. *Proc. Natl. Acad. Sci. USA* 106: 13974–13979.

26. Huard, B., P. Prigent, F. Pagès, D. Bruniquel, and F. Triebel. 1996. T cell major histocompatibility complex class II molecules down-regulate CD4<sup>+</sup> T cell clone responses following LAG-3 binding. *Eur. J. Immunol.* 26: 1180–1186.
27. Maçon-Lemaître, L., and F. Triebel. 2005. The negative regulatory function of the lymphocyte-activation gene-3 co-receptor (CD223) on human T cells. *Immunology* 115: 170–178.
28. Zheng, Y., Y. Zha, G. Driessens, F. Locke, and T. F. Gajewski. 2012. Transcriptional regulator early growth response gene 2 (Egr2) is required for T cell anergy in vitro and in vivo. *J. Exp. Med.* 209: 2157–2163.
29. Hatano, R., T. Yamada, S. Matsuoka, S. Iwata, H. Yamazaki, E. Komiya, T. Okamoto, N. H. Dang, K. Ohnuma, and C. Morimoto. 2014. Establishment of monoclonal anti-human CD26 antibodies suitable for immunostaining of formalin-fixed tissue. *Diagn. Pathol.* 9: 30.
30. Ishii, T., K. Ohnuma, A. Murakami, N. Takasawa, S. Kobayashi, N. H. Dang, S. F. Schlossman, and C. Morimoto. 2001. CD26-mediated signaling for T cell activation occurs in lipid rafts through its association with CD45RO. *Proc. Natl. Acad. Sci. USA* 98: 12138–12143.
31. Jonuleit, H., E. Schmitt, M. Stassen, A. Tuettenberg, J. Knop, and A. H. Enk. 2001. Identification and functional characterization of human CD4<sup>+</sup>CD25<sup>+</sup> T cells with regulatory properties isolated from peripheral blood. *J. Exp. Med.* 193: 1285–1294.
32. Okamura, T., K. Fujio, S. Sumitomo, and K. Yamamoto. 2012. Roles of LAG3 and EGR2 in regulatory T cells. *Ann. Rheum. Dis.* 71(Suppl. 2): i96–i100.
33. Macian, F. 2005. NFAT proteins: key regulators of T-cell development and function. *Nat. Rev. Immunol.* 5: 472–484.
34. Xu, J., Y. Yang, G. Qiu, G. Lal, Z. Wu, D. E. Levy, J. C. Ochando, J. S. Bromberg, and Y. Ding. 2009. c-Maf regulates IL-10 expression during Th17 polarization. *J. Immunol.* 182: 6226–6236.
35. Ahyi, A. N., H. C. Chang, A. L. Dent, S. L. Nutt, and M. H. Kaplan. 2009. IFN regulatory factor 4 regulates the expression of a subset of Th2 cytokines. *J. Immunol.* 183: 1598–1606.
36. Cretney, E., A. Xin, W. Shi, M. Minnich, F. Masson, M. Miasari, G. T. Belz, G. K. Smyth, M. Busslinger, S. L. Nutt, and A. Kallies. 2011. The transcription factors Blimp-1 and IRF4 jointly control the differentiation and function of effector regulatory T cells. *Nat. Immunol.* 12: 304–311.
37. Shoemaker, J., M. Saraiva, and A. O'Garra. 2006. GATA-3 directly remodels the IL-10 locus independently of IL-4 in CD4<sup>+</sup> T cells. *J. Immunol.* 176: 3470–3479.
38. Motomura, Y., H. Kitamura, A. Hijikata, Y. Matsunaga, K. Matsumoto, H. Inoue, K. Atarashi, S. Hori, H. Watarai, J. Zhu, et al. 2011. The transcription factor E4BP4 regulates the production of IL-10 and IL-13 in CD4<sup>+</sup> T cells. *Nat. Immunol.* 12: 450–459.
39. Safford, M., S. Collins, M. A. Lutz, A. Allen, C. T. Huang, J. Kowalski, A. Blackford, M. R. Horton, C. Drake, R. H. Schwartz, and J. D. Powell. 2005. Egr-2 and Egr-3 are negative regulators of T cell activation. *Nat. Immunol.* 6: 472–480.
40. Zhu, B., A. L. Symonds, J. E. Martin, D. Kioussis, D. C. Wraith, S. Li, and P. Wang. 2008. Early growth response gene 2 (Egr-2) controls the self-tolerance of T cells and prevents the development of lupuslike autoimmune disease. *J. Exp. Med.* 205: 2295–2307.
41. Sabat, R., G. Grütz, K. Warszawska, S. Kirsch, E. Witte, K. Wolk, and J. Geginat. 2010. Biology of interleukin-10. *Cytokine Growth Factor Rev.* 21: 331–344.
42. Hutloff, A., A. M. Dittrich, K. C. Beier, B. Eljaschewitsch, R. Kraft, I. Anagnostopoulos, and R. A. Kroczeck. 1999. ICOS is an inducible T-cell co-stimulator structurally and functionally related to CD28. *Nature* 397: 263–266.
43. Kemper, C., A. C. Chan, J. M. Green, K. A. Brett, K. M. Murphy, and J. P. Atkinson. 2003. Activation of human CD4<sup>+</sup> cells with CD3 and CD46 induces a T-regulatory cell 1 phenotype. *Nature* 421: 388–392.
44. Nurieva, R. I., J. Duong, H. Kishikawa, U. Dianzani, J. M. Rojo, I. C. Ho, R. A. Flavell, and C. Dong. 2003. Transcriptional regulation of th2 differentiation by inducible costimulator. *Immunity* 18: 801–811.
45. Cardone, J., G. Le Friec, P. Vantourout, A. Roberts, A. Fuchs, I. Jackson, T. Suddason, G. Lord, J. P. Atkinson, A. Cope, et al. 2010. Complement regulator CD46 temporally regulates cytokine production by conventional and unconventional T cells. *Nat. Immunol.* 11: 862–871.
46. Saraiva, M., J. R. Christensen, M. Veldhoen, T. L. Murphy, K. M. Murphy, and A. O'Garra. 2009. Interleukin-10 production by Th1 cells requires interleukin-12-induced STAT4 transcription factor and ERK MAP kinase activation by high antigen dose. *Immunity* 31: 209–219.
47. Iwasaki, Y., K. Fujio, T. Okamura, A. Yanai, S. Sumitomo, H. Shoda, T. Tamura, H. Yoshida, P. Charnay, and K. Yamamoto. 2013. Egr-2 transcription factor is required for Blimp-1-mediated IL-10 production in IL-27-stimulated CD4<sup>+</sup> T cells. *Eur. J. Immunol.* 43: 1063–1073.
48. Chandra, A., S. Lan, J. Zhu, V. A. Siclari, and L. Qin. 2013. Epidermal growth factor receptor (EGFR) signaling promotes proliferation and survival in osteoprogenitors by increasing early growth response 2 (EGR2) expression. *J. Biol. Chem.* 288: 20488–20498.
49. To, S. Q., K. C. Knowler, and C. D. Clyne. 2013. NFκB and MAPK signalling pathways mediate TNFα-induced early growth response gene transcription leading to aromatase expression. *Biochem. Biophys. Res. Commun.* 433: 96–101.
50. Kühn, R., J. Löhler, D. Rennick, K. Rajewsky, and W. Müller. 1993. Interleukin-10-deficient mice develop chronic enterocolitis. *Cell* 75: 263–274.
51. Bettelli, E., M. P. Das, E. D. Howard, H. L. Weiner, R. A. Sobel, and V. K. Kuchroo. 1998. IL-10 is critical in the regulation of autoimmune encephalomyelitis as demonstrated by studies of IL-10- and IL-4-deficient and transgenic mice. *J. Immunol.* 161: 3299–3306.
52. Astier, A. L., G. Meiffren, S. Freeman, and D. A. Hafler. 2006. Alterations in CD46-mediated Tr1 regulatory T cells in patients with multiple sclerosis. *J. Clin. Invest.* 116: 3252–3257.
53. Vasanthakumar, A., and A. Kallies. 2013. IL-27 paves different roads to Tr1. *Eur. J. Immunol.* 43: 882–885.
54. Tirupathi, C., J. Shimizu, K. Miyawaki-Shimizu, S. M. Vogel, A. M. Bair, R. D. Minshall, D. Predescu, and A. B. Malik. 2008. Role of NF-κB-dependent caveolin-1 expression in the mechanism of increased endothelial permeability induced by lipopolysaccharide. *J. Biol. Chem.* 283: 4210–4218.
55. Tanaka, T., J. Kameoka, A. Yaron, S. F. Schlossman, and C. Morimoto. 1993. The costimulatory activity of the CD26 antigen requires dipeptidyl peptidase IV enzymatic activity. *Proc. Natl. Acad. Sci. USA* 90: 4586–4590.
56. Reinhold, D., U. Bank, F. Bühlung, U. Lendeckel, J. Faust, K. Neubert, and S. Ansorge. 1997. Inhibitors of dipeptidyl peptidase IV induce secretion of transforming growth factor-β<sub>1</sub> in PWM-stimulated PBMC and T cells. *Immunology* 91: 354–360.



# Hair follicle–derived IL-7 and IL-15 mediate skin-resident memory T cell homeostasis and lymphoma

Takeya Adachi<sup>1</sup>, Tetsuro Kobayashi<sup>1,2</sup>, Eiji Sugihara<sup>3</sup>, Taketo Yamada<sup>4,7</sup>, Koichi Ikuta<sup>5</sup>, Stefania Pittaluga<sup>6</sup>, Hideyuki Saya<sup>3</sup>, Masayuki Amagai<sup>1</sup> & Keisuke Nagao<sup>1,2</sup>

The skin harbors a variety of resident leukocyte subsets that must be tightly regulated to maintain immune homeostasis. Hair follicles are unique structures in the skin that contribute to skin dendritic cell homeostasis through chemokine production. We demonstrate that CD4<sup>+</sup> and CD8<sup>+</sup> skin-resident memory T cells (T<sub>RM</sub> cells), which are responsible for long-term skin immunity, reside predominantly within the hair follicle epithelium of the unperturbed epidermis. T<sub>RM</sub> cell tropism for the epidermis and follicles is herein termed epidermotropism. Hair follicle expression of IL-15 was required for CD8<sup>+</sup> T<sub>RM</sub> cells, and IL-7 for CD8<sup>+</sup> and CD4<sup>+</sup> T<sub>RM</sub> cells, to exert epidermotropism. A lack of either cytokine in the skin led to impaired hapten-induced contact hypersensitivity responses. In a model of cutaneous T cell lymphoma, epidermotropic CD4<sup>+</sup> T<sub>RM</sub> lymphoma cell localization depended on the presence of hair follicle–derived IL-7. These findings implicate hair follicle–derived cytokines as regulators of malignant and non-malignant T<sub>RM</sub> cell tissue residence, and they suggest that the cytokines may be targeted therapeutically in inflammatory skin diseases and lymphoma.

Hair follicles are unique structures in the mammalian skin that provide a niche for keratinocyte and melanocyte stem cells<sup>1,2</sup>. Various leukocyte subsets localize to hair follicles<sup>3</sup>. We recently demonstrated that hair follicles recruit skin dendritic cells to sites of minor trauma<sup>4</sup>. Keratinocytes in the hair follicle infundibulum and isthmus produce the chemokines CCL2 and CCL20, recruiting myeloid cells after experiencing physical perturbation. A subset of keratinocytes in the suprabasal layer of the follicular bulge region express another chemokine, CCL8, which prevents local Langerhans cell (LC) accumulation, a mechanism that may protect bulge stem cells from excessive leukocyte infiltration<sup>4</sup>. These data establish that hair follicles actively promote immune homeostasis.

T cells that reside in peripheral tissues have been described in recent years, and their importance is now well established<sup>5–9</sup>. Skin-resident T<sub>RM</sub> cells display an effector memory phenotype, and are generated after immunological insults such as viral infection<sup>6,8</sup>. In the context of infection, CD4<sup>+</sup> memory T cells accumulate primarily in the dermis, whereas CD8<sup>+</sup> T<sub>RM</sub> cells accumulate within the epidermis<sup>7</sup>. Both T cell subsets exhibited tropism to the hair follicles<sup>7</sup>. Skin T<sub>RM</sub> cells express CD69 and CD103 (ref. 10). CD69 suppresses sphingosine-1-phosphate receptor 1 expression, which prevents T cells from emigrating from lymphoid organs or other tissues into circulation<sup>11,12</sup>. CD103-mediated retention of T cells in the skin probably occurs by adhesion to E-cadherin<sup>13</sup>. The non-migratory nature of CD8<sup>+</sup> T<sub>RM</sub> cells has been established in parabiotic mice<sup>8</sup>, and CD4<sup>+</sup> T<sub>RM</sub> cells in human skin have been engrafted onto immunodeficient mice<sup>14</sup>.

Infiltration of T cells into the epidermis is a prominent feature in both inflammatory and neoplastic human diseases, including graft-versus-host disease, drug eruptions and cutaneous T cell lymphoma (CTCL). In fixed drug eruption, CD8<sup>+</sup> T cells attack the epidermis to cause keratinocyte cell death in the presence of the drug(s)<sup>15</sup>. After clinical resolution, CD8<sup>+</sup> T cells with a memory phenotype persist within the epidermis<sup>15,16</sup>. The majority of CTCL is caused by CD4<sup>+</sup> lymphoma cells<sup>17</sup>. In the classic form—mycosis fungoides—lymphoma cells with a T<sub>RM</sub> cell phenotype infiltrate the epidermis, including the follicular epithelium<sup>18,19</sup>, and they slowly accumulate and proliferate to form tumors. Such epidermis- and follicle-infiltrating T cells are termed epidermotropic T cells<sup>20</sup>.

Given the importance of T<sub>RM</sub> cells in conferring long-term immunological memory<sup>6,8</sup> and regulatory functions that maintain immunological homeostasis<sup>13,21,22</sup>, elucidation of mechanisms that support long-term persistence in the skin may provide insight into T cell homeostasis in health and disease. Here we demonstrate that the epidermotropism of T<sub>RM</sub> cells is supported by the hair follicle–derived cytokines IL-7 and IL-15.

## RESULTS

### CD4<sup>+</sup> and CD8<sup>+</sup> T cells in steady-state epidermis

To characterize T<sub>RM</sub> cells in the epidermis, we prepared vertical sections of frozen skin samples taken from unmanipulated adult C57BL/6J mice, and then visualized CD4<sup>+</sup> and CD8<sup>+</sup> T cells

<sup>1</sup>Department of Dermatology, Keio University School of Medicine, Tokyo, Japan. <sup>2</sup>Dermatology Branch, Center for Cancer Research, National Cancer Institute, National Institutes of Health, Bethesda, Maryland, USA. <sup>3</sup>Division of Gene Regulation, Institute for Advanced Medical Research, Keio University School of Medicine, Tokyo, Japan. <sup>4</sup>Department of Pathology, Keio University School of Medicine, Tokyo, Japan. <sup>5</sup>Laboratory of Biological Protection, Department of Biological Responses, Institute for Virus Research, Kyoto University, Kyoto, Japan. <sup>6</sup>Laboratory of Pathology, Center for Cancer Research, National Cancer Institute, National Institutes of Health, Bethesda, Maryland, USA. <sup>7</sup>Present address: Department of Pathology, Saitama Medical University School of Medicine, Saitama, Japan. Correspondence should be addressed to K.N. (keisuke.nagao@nih.gov).

Received 2 July; accepted 2 September; published online 19 October 2015; doi:10.1038/nm.3962



using immunofluorescence microscopy. We routinely observed small numbers of both CD4<sup>+</sup> and CD8<sup>+</sup> T cells in the follicular epithelium (**Fig. 1a**). Visualization of the basement membrane using integrin  $\alpha_6$  staining confirmed that both CD4<sup>+</sup> and CD8<sup>+</sup> T cells resided within the follicular epithelium (**Supplementary Fig. 1a**). Staining epidermal sheets revealed that CD8<sup>+</sup> T cells were present both in hair follicles and in the interfollicular epidermis, whereas CD4<sup>+</sup> T cells were localized exclusively around hair follicles (**Supplementary Fig. 1b**). In flow cytometry analysis of epidermal cell suspensions, exclusion of LCs and dendritic epidermal T cells enabled the identification of small numbers of CD4<sup>+</sup> and CD8<sup>+</sup> T cells, consistent with the immunofluorescence microscopy results (**Fig. 1b**). The number of CD4<sup>+</sup> T cells in the epidermis was comparable to that in the dermis (**Fig. 1c**). CD8<sup>+</sup> T cells were found exclusively in epidermal cell suspensions (**Fig. 1c**)<sup>7</sup>. Contamination of the

epidermal preparation with dermal leukocytes and vice versa seemed unlikely (**Supplementary Fig. 1c,d**).

Phenotypic analysis suggests that most of these CD4<sup>+</sup> and CD8<sup>+</sup> T cells are effector memory T cells, as assessed by their cell surface expression of CD44 and CD62L, and they are resident cells, as suggested by CD103 and CD69 co-expression (**Fig. 1d**). CD4<sup>+</sup> T cells in the epidermis expressed slightly lower levels of CD103 than did those in the dermis (**Fig. 1e**). Furthermore, the epidermis contained fewer CD4<sup>+</sup> FoxP3<sup>+</sup> regulatory T<sub>RM</sub> cells than did the dermis (**Fig. 1f**), suggesting that the organization of CD4<sup>+</sup> T<sub>RM</sub> cells in the two skin compartments may be differentially regulated. Hereafter, memory T cells that reside in the epidermis and the follicles will be referred to as epidermotropic T<sub>RM</sub> cells, not to indicate their entity as a distinct T cell subset, but solely to describe their localization in the skin.

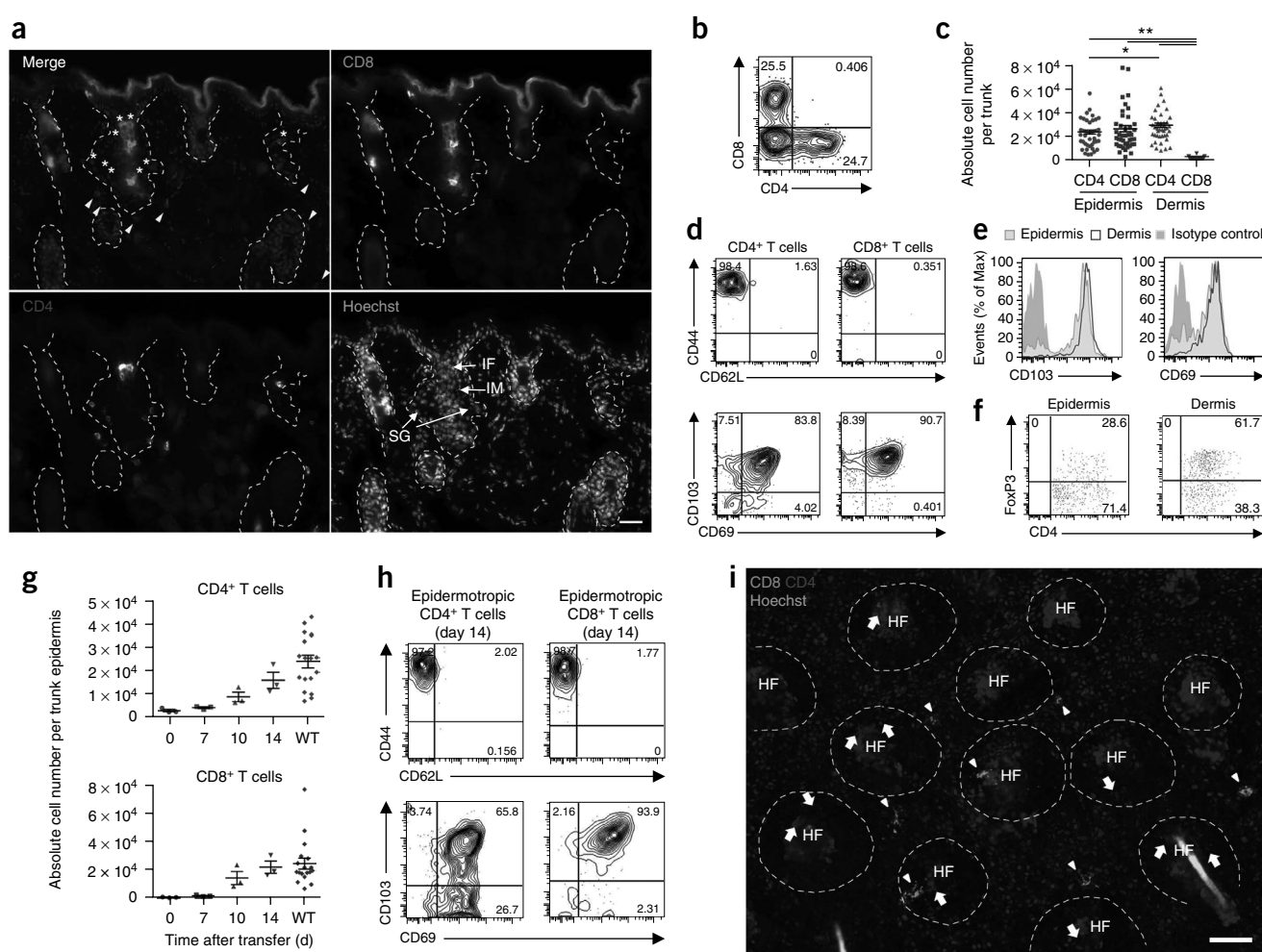
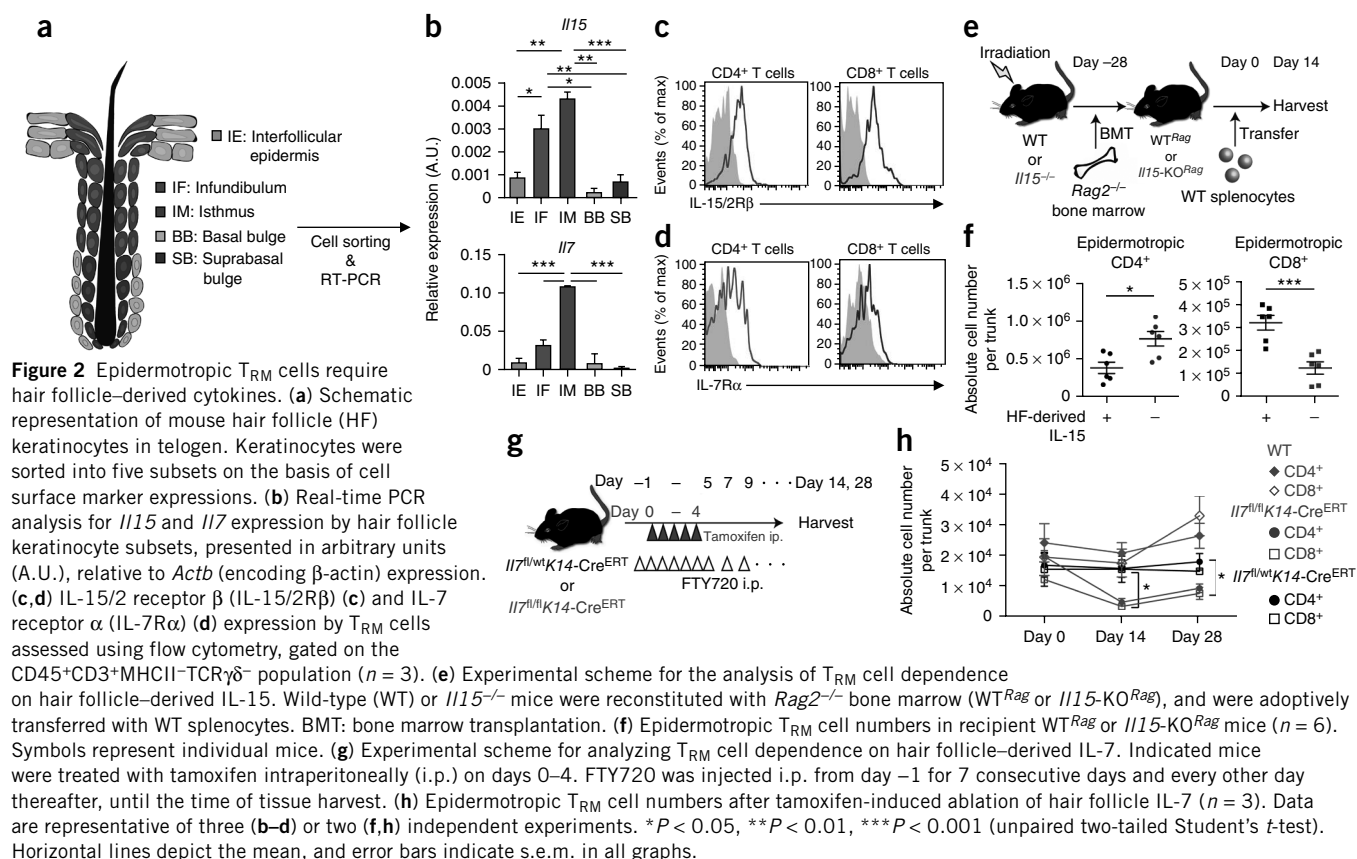


**Figure 1** Epidermotropic CD4<sup>+</sup> and CD8<sup>+</sup> T<sub>RM</sub> cells associate with hair follicles. **(a)** Skin sections from wild-type (WT) mice, stained as indicated. Dotted lines delineate hair follicles. Asterisks and arrowheads depict CD4<sup>+</sup> T cells in epidermis and dermis, respectively. Scale bar, 50  $\mu$ m. IF: infundibulum, IM: isthmus, SG: sebaceous glands. **(b)** Flow cytometry analysis of CD45<sup>+</sup>CD3<sup>+</sup>MHCII (class II MHC)-TCR (T cell receptor)  $\gamma\delta$ -epidermal cells from WT mice. Numbers represent frequencies (%) of gated subsets among the analyzed population. **(c)** T cell numbers in the epidermis and dermis. \**P* < 0.05, \*\**P* < 0.01 (unpaired two-tailed Student's *t*-test). **(d)** CD44 and CD62L, and CD103 and CD69 expression on T cells in the epidermis. **(e)** CD103 and CD69 expression levels on CD4<sup>+</sup> T cells in the epidermis (blue) and dermis (red) with isotype controls (gray). **(f)** Frequency of CD4<sup>+</sup>FoxP3<sup>+</sup> T<sub>reg</sub> cells in the epidermis and dermis. **(g)** Number of donor T cells in *Rag2*<sup>-/-</sup> recipient epidermis monitored by flow cytometry at the indicated dates after adoptive transfer of WT splenocytes. **(h)** Epidermotropic T cells from **g** were analyzed using flow cytometry as in **d**, 14 d after transfer. **(i)** Epidermal sheets of a mouse from **g**, day 14 after transfer, were stained as indicated. Dashed lines delineate hair follicles (HF), arrows and arrowheads indicate CD4<sup>+</sup> and CD8<sup>+</sup> T cells, respectively. Scale bar, 100  $\mu$ m. Data are from one experiment representative of three independent experiments with three mice per group (**a,b,d-i**), or from ten independent experiments with a total of 42 mice (**c**). Each symbol represents an individual mouse; horizontal lines depict the mean; error bars indicate s.e.m. (**c,g**).



### $T_{RM}$ cells associate with hair follicles during epidermal entry

$T_{RM}$  cells are generated during skin infection and accumulate not only at sites of primary inoculation, but also at distant sites<sup>8,23</sup>. To model this distribution of  $T_{RM}$  cells, we adoptively transferred wild-type (WT) splenocytes into *Rag2*<sup>-/-</sup> mice, which lack lymphocytes. After being transferred into a lymphopenic environment, donor T cells undergo homeostatic proliferation, and we hypothesized that such T cells might distribute to peripheral tissues such as the epidermis and skin. Indeed, CD4<sup>+</sup> and CD8<sup>+</sup> T cells appeared in the epidermis of *Rag2*<sup>-/-</sup> recipients 10 d after transfer, and by day 14, their numbers had reached levels detectable in WT mice (Fig. 1g). Donor T cells displayed effector memory and resident cell phenotypes (Fig. 1h), and thus represent epidermotropic  $T_{RM}$  cells.

Visualization of CD4<sup>+</sup> and CD8<sup>+</sup>  $T_{RM}$  cells during active epidermal repopulation revealed close association with hair follicles (Fig. 1i). CD4<sup>+</sup>  $T_{RM}$  cells initially appeared within the dermis, accumulated around hair follicles in frozen sections on day 7 after transfer, and then distributed within the epidermis and dermis thereafter (Supplementary Fig. 1e). In contrast to CD4<sup>+</sup>  $T_{RM}$  cells, CD8<sup>+</sup>  $T_{RM}$  cells appeared directly within the interfollicular epidermis, and then accumulated around the hair follicles (Supplementary Fig. 1e, f). Thus, the anatomical modes of entry for CD4<sup>+</sup> and CD8<sup>+</sup>  $T_{RM}$  cells seem to be distinct.

### Hair follicle keratinocytes express *Il15* and *Il7*

IL-15 and IL-7 are important cytokines that enable the generation and maintenance of memory T cells<sup>24,25</sup>. Our previous study<sup>4</sup> revealed that hair follicle keratinocyte subsets exhibit distinct chemokine expression profiles. To determine whether hair follicle keratinocytes expressed mRNA encoding IL-15 and IL-7, we sorted epidermal keratinocytes

into those from the interfollicular epidermis, infundibulum, isthmus, basal layer bulge or suprabasal layer bulge<sup>4</sup> (Fig. 2a). Similarly to previously described patterns of chemokine expression<sup>4</sup>, real-time PCR analysis revealed that both *Il15* and *Il7* mRNA were predominantly expressed by keratinocytes in the infundibulum and isthmus (Fig. 2b). Because most of the mouse pelage hair follicles are in telogen, we studied the vibrissae to determine whether cytokines were expressed during anagen. The transient portions of anagen hair follicles did not express *Il7*, but the bulb expressed low levels of *Il15* (Supplementary Fig. 2a). We also analyzed cytokine mRNA expression in major leukocyte subsets in the epidermis and found that LCs, but not dendritic epidermal T cells, expressed *Il15* (Supplementary Fig. 2b). Both leukocyte subsets lacked *Il7* expression (data not shown).

### Epidermotropic $T_{RM}$ cells require hair follicle-derived cytokines

Analysis of CD4<sup>+</sup> and CD8<sup>+</sup>  $T_{RM}$  cells using flow cytometry revealed that both T cell subsets expressed IL-15/2R $\beta$  and IL-7R $\alpha$  (Fig. 2c, d). Given the unavailability of an animal model enabling conditional ablation of IL-15, we generated bone marrow (BM) chimeric mice to determine whether epidermotropic  $T_{RM}$  cells were influenced by hair follicle-derived cytokines. Reconstitution of WT or *Il15*<sup>-/-</sup> mice with BM from *Rag2*<sup>-/-</sup> mice led to the generation of lymphopenic mice that either expressed (WT<sup>Rag</sup>) or lacked (*Il15*-knockout (KO)<sup>Rag</sup>) IL-15 in peripheral tissues, including the skin (Fig. 2e). We then transferred WT splenocytes into these BM chimeric mice and analyzed the numbers of epidermotropic  $T_{RM}$  cells at day 14 after the transfer (Fig. 2e). The numbers of epidermotropic CD4<sup>+</sup>  $T_{RM}$  cells had slightly increased in recipient *Il15*-KO<sup>Rag</sup> mice, whereas epidermotropic CD8<sup>+</sup>  $T_{RM}$  numbers had been reduced (Fig. 2f). The numbers of CD4<sup>+</sup> and

CD8<sup>+</sup> T cells in the spleen were comparable in recipient *Il15*-KO<sup>Rag</sup> and WT<sup>Rag</sup> mice (Supplementary Fig. 2c), indicating that the difference in the numbers of epidermotropic CD8<sup>+</sup> T<sub>RM</sub> cells was due to the loss of IL-15 in the skin. The numbers of epidermotropic CD8<sup>+</sup> T<sub>RM</sub> cells were tenfold higher than those of unmanipulated WT mice. Upregulation of IL-15 mRNA expression in keratinocytes in lethally irradiated mice may have contributed to the enhanced population of CD8<sup>+</sup> T<sub>RM</sub> cells in the epidermis (Supplementary Fig. 2d).

Because LCs also expressed *Il15* mRNA, we studied the effect of LC depletion on epidermotropic T<sub>RM</sub> cells using two different models. Neither constitutive loss nor depletion of LCs affected the numbers of epidermotropic T<sub>RM</sub> cells (Supplementary Fig. 3a–c). Thus, hair follicle-derived IL-15 is crucial for the maintenance of epidermotropic CD8<sup>+</sup> T<sub>RM</sub> cells.

A different approach was taken to evaluate the contribution of hair follicle-derived IL-7, because T cells failed to undergo homeostatic proliferation when transferred into *Il7*-KO<sup>Rag</sup> mice (data not shown). We crossed *K14*-Cre<sup>ERT</sup> mice<sup>26</sup> with *Il7*-floxed mice to generate mice in which ablation of IL-7 in the epidermis could be specifically induced in the skin of adult mice by administering tamoxifen injections (Supplementary Fig. 2e). Because of the potential for a continuous influx of newly generated T<sub>RM</sub> cells, which could alter total cell numbers during and after IL-7 ablation, we treated mice with FTY720, a sphingosine-1-phosphate receptor 1 inhibitor that inhibits lymphocyte egress from lymph nodes, thereby preventing the influx of endogenous T<sub>RM</sub> cells into the epidermis (Fig. 2g). Epidermal ablation of IL-7 reduced the numbers of both CD4<sup>+</sup> and CD8<sup>+</sup> T<sub>RM</sub> cells 14 d after the loss of IL-7, an effect that persisted for at least 28 d (Fig. 2h). The numbers of splenic T cells remained unaffected by the loss of IL-7 in the skin (Supplementary Fig. 2f). Therefore, hair

follicle-derived IL-7 is required for both CD4<sup>+</sup> and CD8<sup>+</sup> T<sub>RM</sub> cells to persist in the epidermis.

### Impaired contact hypersensitivity responses in the absence of IL-7 and IL-15

Impaired anatomical localization of T<sub>RM</sub> cells during the steady state in the absence of hair follicle-derived IL-15 and IL-7 might affect subsequent immune responses in the skin. To address this, we induced contact hypersensitivity (CHS) with a hapten in mice that lacked hair follicle-derived cytokines. To analyze the effect of IL-15 deficiency in the context of CD8<sup>+</sup> T<sub>RM</sub> cells, we generated WT<sup>Rag</sup> and *Il15*-KO<sup>Rag</sup> mice using BM transplantation (Fig. 2e). These BM chimeric mice were injected with CD8<sup>+</sup> T cells obtained from skin-draining lymph nodes of 1-fluoro-2,4-dinitrobenzene (DNFB)-sensitized mice (Fig. 3a). Transferred CD8<sup>+</sup> T cells are expected to undergo homeostatic proliferation and distribute to peripheral tissues, including the skin, in WT<sup>Rag</sup>, but not in *Il15*-KO<sup>Rag</sup> mice (Figs. 1g and 2f). Recipient mice were then challenged with DNFB, and ear-swelling responses were monitored. Both ear swelling and lymphocytic infiltration were reduced in the absence of tissue-derived IL-15 (Fig. 3b,c).

The roles of hair follicle-derived IL-7 and T<sub>RM</sub> cells were assessed in the context of CD4<sup>+</sup> T cell-mediated CHS. To generate lymphopenic mice that constitutively lack IL-7 in the epidermis, *K5*-Cre mice and *Il7*-floxed mice<sup>27</sup> were each crossed to the *Rag2*<sup>-/-</sup> background (*Il7*<sup>fl/fl</sup>*K5*-Cre × *Rag2*<sup>-/-</sup> mice). CD4<sup>+</sup> T cells isolated from skin-draining lymph nodes of DNFB-sensitized WT mice were transferred into *Il7*<sup>fl/fl</sup>*K5*-Cre × *Rag2*<sup>-/-</sup> mice or control *Rag2*<sup>-/-</sup> mice. Recipient mice were challenged with DNFB 14 d after transfer, and ear-swelling responses were assessed (Fig. 3d). Ear swelling and

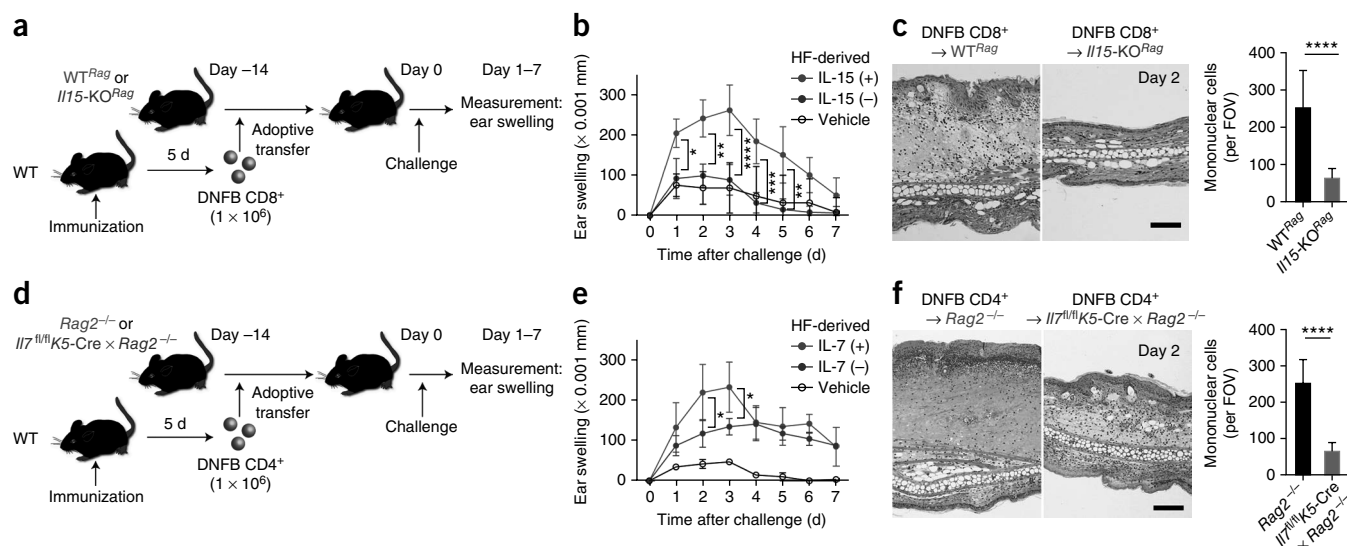


**Figure 3** Impaired CHS responses in the absence of hair follicle-derived cytokines. (a) Experimental scheme for the analysis of CD8<sup>+</sup> T<sub>RM</sub> cell-mediated CHS in the absence of peripheral tissue (hair follicle)-derived IL-15. CD8<sup>+</sup> T cells from DNFB (DNFB CD8<sup>+</sup>) or vehicle-immunized (vehicle CD8<sup>+</sup>) WT mice were transferred into indicated lymphopenic mice. 14 d later, recipients were challenged with DNFB on their ears, and ear-swelling responses were measured. (b) Ear thickness (Δmm) of DNFB CD8<sup>+</sup>-transferred WT<sup>Rag</sup> (red), *Il15*-KO<sup>Rag</sup> (blue) and vehicle CD8<sup>+</sup>-transferred WT<sup>Rag</sup> (black) (*n* = 3). (c) H&E staining of ear sections from indicated mice, day 2 after challenge and quantification of skin-infiltrating mononuclear cells. (d) Experimental scheme for analyzing CD4<sup>+</sup> T<sub>RM</sub> cell-mediated CHS in the absence of hair follicle-derived IL-7. DNFB CD4<sup>+</sup> or vehicle CD4<sup>+</sup> were adoptively transferred into indicated lymphopenic mice. (e) Ear thickness (Δmm) of DNFB CD4<sup>+</sup>-transferred *Rag2*<sup>-/-</sup> (red), *Il7*<sup>fl/fl</sup>*K5*-Cre × *Rag2*<sup>-/-</sup> (blue) or vehicle CD4<sup>+</sup>-transferred *Rag2*<sup>-/-</sup> (black) (*n* = 3). (f) H&E staining of ear sections from indicated mice, day 2 after challenge and quantification of skin-infiltrating mononuclear cells. Data are from one experiment, representative of two independent experiments with three mice per group in each (b,c,e,f). Cell counts represent pools of three fields of view per section (original magnification: 100×) from three mice per group (c,f). Scale bars, 100 μm (c,f).

\**P* < 0.05, \*\**P* < 0.01, \*\*\**P* < 0.001, \*\*\*\**P* < 0.0001 (two-way ANOVA). Error bars are s.e.m.

lymphocytic infiltration were both reduced in  $Il7^{fl/fl}K5-Cre \times Rag2^{-/-}$  mice on days 2 and 3 after the challenge (Fig. 3e,f). This transient effect might reflect the generation and influx of newly generated recipient  $T_{RM}$  cells after DNFB challenge.

### A CD4<sup>+</sup> T cell lymphoma model with skin involvement

Epidermotropism of T cells is a histological hallmark in human CTCL. In particular, lymphoma cells in mycosis fungoides exhibit a  $T_{RM}$  cell phenotype<sup>18,19,28</sup>. *IL7* expression is increased in CTCL skin<sup>29</sup>. Whether lymphoma cells also require hair follicle-derived cytokines remains unclear. Thus, we extended our  $T_{RM}$  cell repopulation model in  $Rag2^{-/-}$  mice by generating a novel lymphoma model.

Mutations in, or upregulation of, the oncogene *MYC*<sup>30,31</sup>, as well as mutations in the tumor-suppressor gene *INK4A/ARF* (officially known as *CDKN2A*), have been implicated<sup>17,30</sup> in human lymphoma and CTCL. *Cdkn2a*<sup>-/-</sup> mice are prone to tumor development, including T cell lymphoma<sup>32,33</sup>. *Cdkn2a*<sup>-/-</sup> progenitor B cells transduced with *Myc* generate B cell lymphoma<sup>34</sup>. Taking advantage of these previous findings, we isolated CD4<sup>+</sup> T cells from *Cdkn2a*<sup>-/-</sup> mice and retrovirally transduced them with *Myc* (Fig. 4a). Approximately 50% of T cells were transduced, as determined by GFP expression (*Myc*<sup>+</sup>*Cdkn2a*<sup>-/-</sup> CD4<sup>+</sup> T cells) (Fig. 4b). Recipient  $Rag2^{-/-}$  mice developed erythroderma (redness and fine scaling of the entire skin surface) approximately 3 weeks after the transfer of *Myc*<sup>+</sup>*Cdkn2a*<sup>-/-</sup> CD4<sup>+</sup> T cells (Fig. 4c). Flow cytometry analysis revealed increased numbers of epidermotropic CD4<sup>+</sup> T cells in  $Rag2^{-/-}$  mice that had been transferred with *Myc*<sup>+</sup>*Cdkn2a*<sup>-/-</sup> CD4<sup>+</sup> T cells as compared to those transferred with WT CD4<sup>+</sup> T cells (Fig. 4d). The majority of

epidermotropic CD4<sup>+</sup> T cells in *Myc*<sup>+</sup>*Cdkn2a*<sup>-/-</sup> CD4<sup>+</sup> T cell-transferred mice expressed *Myc*-GFP (Fig. 4e) with increased IL-7R $\alpha$  expression (Fig. 4e).

Histology revealed epidermotropism of lymphocytes with large, atypical nuclei, recapitulating that of human CTCL (Fig. 4f)<sup>17</sup>. Consistently, flow cytometry analysis revealed that *Myc*<sup>+</sup>*Cdkn2a*<sup>-/-</sup> CD4<sup>+</sup> T cells were enlarged in size (Fig. 4g). Infiltrating lymphocytes expressed *Ki-67*, demonstrating that they were proliferative (Fig. 4h). Epidermotropic CD4<sup>+</sup> T cells were of the  $T_{RM}$  cell phenotype (Fig. 4i), and they accumulated around the hair follicles (Fig. 4f,j). Collectively, *Myc*<sup>+</sup>*Cdkn2a*<sup>-/-</sup> CD4<sup>+</sup> T cells that had been transferred into  $Rag2^{-/-}$  mice infiltrated the skin and epidermis, exhibiting histologic features of human CTCL. These mice also exhibited lymphoma in the lymph nodes and spleen, and they died within 10 weeks after transfer (Supplementary Fig. 4), thereby also recapitulating an aspect of Sezary's syndrome, a leukemic subtype of CTCL<sup>30</sup>.

### Epidermotropism in CTCL depends on IL-7

To determine whether CD4<sup>+</sup> lymphoma cells also relied on hair follicle-derived IL-7, we transferred *Myc*<sup>+</sup>*Cdkn2a*<sup>-/-</sup> CD4<sup>+</sup> T cells into  $Rag2^{-/-}$  or  $Il7^{fl/fl}K5-Cre \times Rag2^{-/-}$  mice (Fig. 5a). In contrast to  $Rag2^{-/-}$  mice,  $Il7^{fl/fl}K5-Cre \times Rag2^{-/-}$  mice did not develop erythroderma (Fig. 5b). Furthermore, the absolute numbers of epidermotropic lymphoma cells were reduced in the absence of hair follicle-derived IL-7 (Fig. 5c), whereas significant differences were not observed in the lymph nodes and spleen (Fig. 5d). Histologic analysis of control  $Rag2^{-/-}$  mice revealed abundant epidermotropic

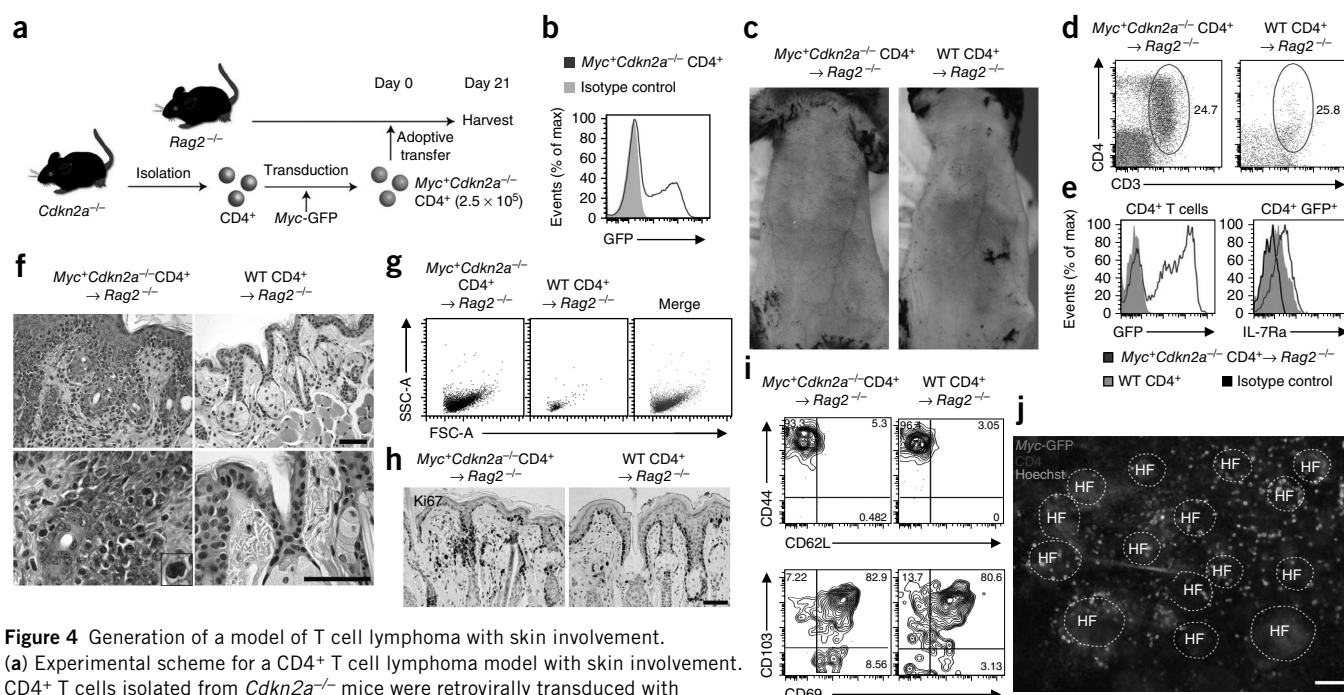
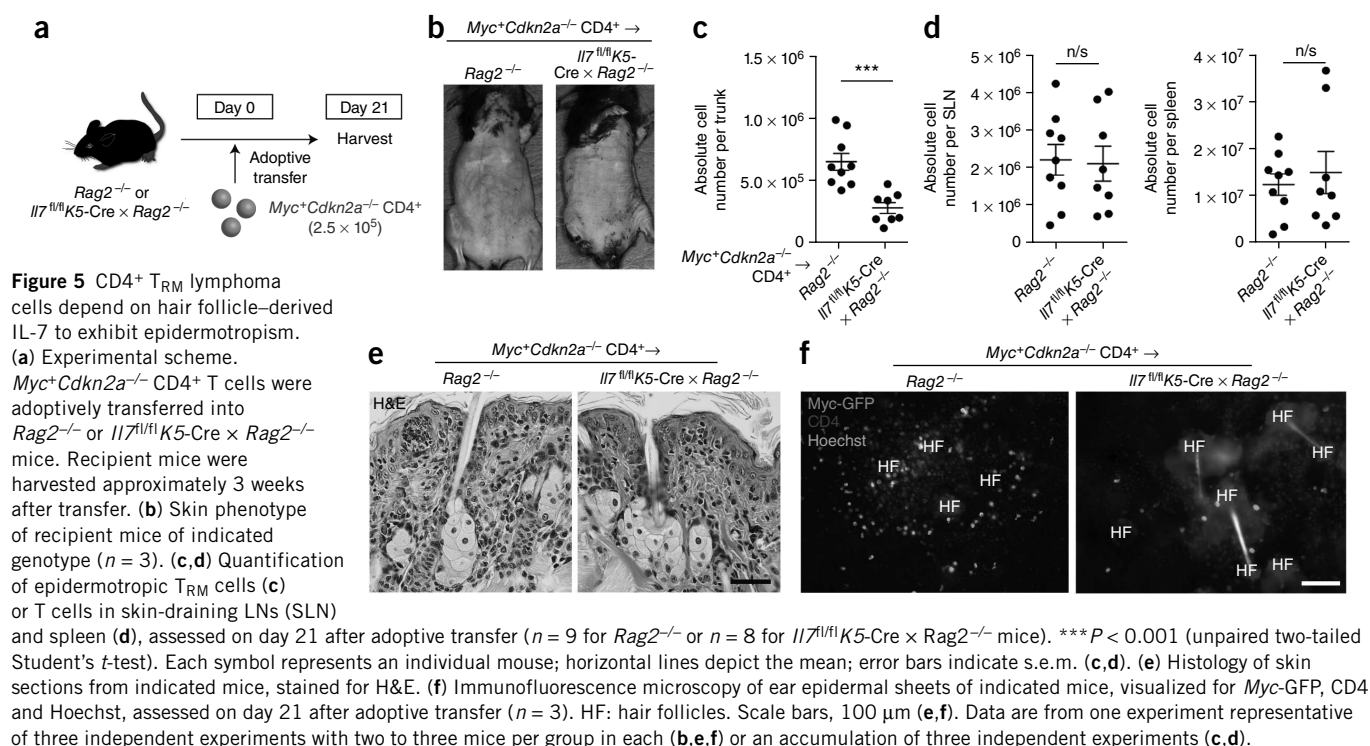


**Figure 4** Generation of a model of T cell lymphoma with skin involvement.

(a) Experimental scheme for a CD4<sup>+</sup> T cell lymphoma model with skin involvement. CD4<sup>+</sup> T cells isolated from *Cdkn2a*<sup>-/-</sup> mice were retrovirally transduced with *Myc*-GFP (*Myc*<sup>+</sup>*Cdkn2a*<sup>-/-</sup> CD4<sup>+</sup>) and were adoptively transferred into  $Rag2^{-/-}$  mice. (b) Flow cytometry analysis of *Myc*-GFP expression on *Myc*<sup>+</sup>*Cdkn2a*<sup>-/-</sup> CD4<sup>+</sup> T cells before transfer. (c) Skin phenotype of *Myc*<sup>+</sup>*Cdkn2a*<sup>-/-</sup> CD4<sup>+</sup>-transferred (left) or wild-type (WT) CD4<sup>+</sup>-transferred  $Rag2^{-/-}$  mice (right). (d) Flow cytometry analysis of CD3<sup>+</sup>CD4<sup>+</sup> epidermotropic cells in recipient mice, as indicated by the purple gate. CD45<sup>+</sup>MHCII<sup>+</sup>TCR $\gamma\delta$ <sup>-</sup> cells are shown. (e) Expression of GFP and IL-7R $\alpha$  on cells within the purple gate in d. (f) H&E staining of skin sections from indicated mice. (g) Forward scatter (FSC) and side scatter (SSC) profiles of cells within the purple gate in d. (h) Immunohistochemical staining for *Ki-67*. (i) CD44 versus CD62L, and CD103 versus CD69 expression on CD45<sup>+</sup>MHCII<sup>+</sup>TCR $\gamma\delta$ <sup>-</sup> CD3<sup>+</sup>CD4<sup>+</sup>GFP<sup>+</sup> cells (left panels) or CD45<sup>+</sup>MHCII<sup>+</sup>TCR $\gamma\delta$ <sup>-</sup> CD3<sup>+</sup>CD4<sup>+</sup> cells (right panels). (j) Immunofluorescence microscopy of epidermal sheets, visualized for *Myc*-GFP, CD4 and Hoechst. Dashed lines delineate the hair follicles (HF). Scale bar, 100  $\mu$ m (f,h,j). All data are from one experiment representative of three independent experiments with three mice per group in each.



lymphocytes with epidermal thickening, but histological changes were minimal in *Il7<sup>fl/fl</sup>K5-Cre × Rag2<sup>-/-</sup>* mice (Fig. 5e). Visualization of CD4<sup>+</sup> T cells in epidermal sheets confirmed these findings (Fig. 5f). Thus, epidermotropic CD4<sup>+</sup> T<sub>RM</sub> cells continued to require hair follicle-derived IL-7 after neoplastic transformation.

#### In CTCL, IL-7 is upregulated in human hair follicles

To examine whether our findings could be extended to humans, we studied human hair follicles. Whereas hair follicles in the trunk skin

of mice and humans are mostly found in telogen, the majority of those in human scalp are in anagen. The terminus end is called the bulb, and the portion between the bulb and the stem cell-containing bulge is referred to as the suprabulb (Fig. 6a and Supplementary Fig. 5). We dissected hair follicles from normal human scalp to isolate the interfollicular epidermis, infundibulum, bulge, suprabulb and bulb, and we obtained RNA from each of these sites (Fig. 6a)<sup>4</sup>. We then performed real-time PCR for *IL15* and *IL7*. *IL15* was predominantly expressed by hair follicle keratinocytes in the

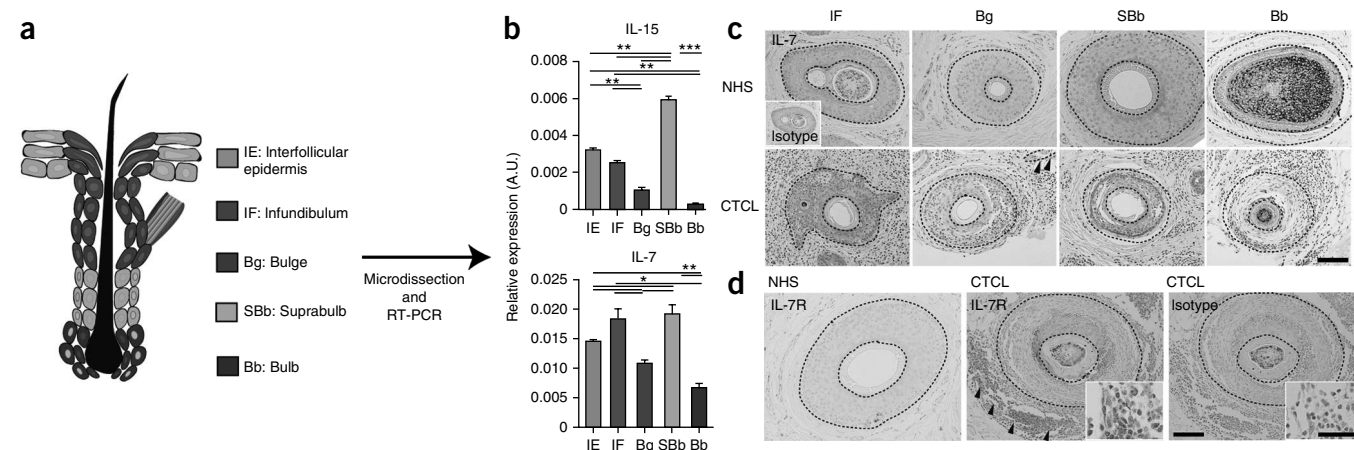


**Figure 6** IL-7 and IL-15 expression in human hair follicles from normal scalp and cutaneous T cell lymphoma. (a) Schematic representation of human hair follicle keratinocytes. (b) Real-time PCR analysis for *IL15* and *IL7* expression at distinct sites in the hair follicle. \**P* < 0.05, \*\*\**P* < 0.001 (unpaired two-tailed Student's *t*-test). Horizontal lines depict the mean, and error bars indicate s.e.m. (c) Immunohistochemistry of normal scalp sections from humans (NHS) (*n* = 3 samples from three subjects) and from subjects with CTCL (*n* = 6 samples from three subjects), stained with an IL-7-specific antibody or with an isotype control. Scale bar, 100 μm. Arrowheads indicate arrector pili muscle (reflecting the bulge region). (d) Immunohistochemistry of scalp sections from patients with CTCL, stained with an IL-7R-specific antibody or with an isotype control (*n* = 6 samples from three subjects). Scale bar, 100 μm in low-power field, 50 μm in high-power field. Dashed lines delineate hair follicles. Arrowheads indicate IL-7R-positive lymphoma cells. Data are from one experiment representative of three (b,c) or two (d) independent experiments.

suprabulb, and *IL7* expression was highest in the infundibulum and suprabulb (Fig. 6b).

We additionally evaluated *IL-7* expression in hair follicles from both normal human scalp and lesional scalp skin of patients with CTCL. Faint immunohistochemical staining for *IL-7* was detected in normal human hair follicles. *IL-7* expression was apparent in a CTCL-affected subject, in which the staining was detected in the infundibulum and the suprabulbar area (Fig. 6c), consistent with the real-time PCR data from normal human scalp. In other patients, *IL-7* staining was increased not only in hair follicle keratinocytes, but also in keratinocytes in the interfollicular epidermis (Supplementary Fig. 6).

Consistent with our observations in mice, *IL-7R* expression by T cells was increased in lesional CTCL epidermis in comparison to that on T cells in normal human scalp skin (Fig. 6d and Supplementary Fig. 5). *IL-7R* expression in lesional keratinocytes in CTCL seems to be increased relative to keratinocytes in normal scalp skin, although the significance of this has yet to be determined.

## DISCUSSION

Epidermotropism of  $T_{RM}$  cells, both non-malignant and malignant, is regulated by the hair follicle-derived cytokines *IL-7* and *IL-15*. Previous studies<sup>6–8</sup> have focused on  $T_{RM}$  cell biology in the context of viral infections. We studied the requirement of epidermotropic  $T_{RM}$  cells during the steady state by using non-malignant and malignant models. The lack of hair follicle-derived cytokines led to the failure of both  $CD4^+$  and  $CD8^+$   $T_{RM}$  cells to persist in skin. Impaired CHS responses in the absence of hair follicle-derived cytokines highlight the importance of homeostatic organization of  $T_{RM}$  cells before inflammation.

The requirement of *IL-7* and *IL-15* for the generation and maintenance of memory T cells is well established<sup>24,25</sup>, but the fate of  $T_{RM}$  cells in peripheral tissues that are deprived of these cytokines remains unclear. In particular, whether the cells undergo cell death or migration deserves further attention in the context of lymphoma.

The tropism that  $CD4^+$   $T_{RM}$  cells exhibit to the hair follicles demonstrated in this study is compatible with and complementary to a previous report<sup>7</sup> in which approximately 30% of virus-specific  $CD4^+$  memory T cells were found to associate with the hair follicles after herpes simplex virus skin infection. To date,  $T_{RM}$  cells in the skin have mainly been characterized in the context of  $CD8^+$  T cells. Although  $CD4^+$  memory T cells may well be comparable to  $CD8^+$   $T_{RM}$  cells as skin residents on the basis of surface marker expression and past reports<sup>13,22</sup>, thorough studies on  $CD4^+$  memory T cells as bona fide  $T_{RM}$  cells have yet to be performed. Our observation that epidermal and dermal  $T_{RM}$  cells have subtle differences in *CD103* expression, in conjunction with the higher observed ratio of  $CD4^+$   $FoxP3^+$   $T_{RM}$  cells in the dermis, suggests that  $CD4^+$   $T_{RM}$  cells in these skin compartments might be regulated through distinct mechanisms.

In conclusion, we have demonstrated the importance of hair follicle-derived *IL-7* and *IL-15* in  $T_{RM}$  cell homeostasis in the epidermis, which represents an attractive therapeutic target in inflammatory skin diseases and malignant lymphoma, and which may also be relevant in other peripheral tissues.

## METHODS

Methods and any associated references are available in the online version of the paper.

Note: Any Supplementary Information and Source Data files are available in the online version of the paper.

## ACKNOWLEDGMENTS

We thank M. Ohyama for helpful discussion on human hair follicles; N. Sakai, K. Eguchi and S. Sato (Keio University School of Medicine) for their technical assistance; H. Kong (National Institutes of Health) for their discussions on human CTCL; Y. Madokoro (Keio University School of Medicine) for human CTCL immunohistochemical staining; T. Kitamura (University of Tokyo) for providing the retroviral vector pMXs-IG and Plat-E cells; J. Takeda (Osaka University) for providing *K5-Cre* mice; D.H. Kaplan (University of Minnesota) for providing Langerin-DTA mice; and B.E. Clausen (Johannes Gutenberg University of Mainz) for providing Langerin-DTR mice. This work was supported by the Japan Society for the Promotion of Science, The Kanae Foundation for the Promotion of Medical Science, the Japanese Society for Investigative Dermatology's (JSID's) Fellowship Shiseido Award and the NIH NCI Intramural Research Programs.

## AUTHOR CONTRIBUTIONS

T.A. and K.N. conceived of and designed all experiments. Experiments were performed by T.A. with the assistance of T.K.; E.S. and H.S. provided *Cdkn2a*<sup>-/-</sup> mice and assisted with retroviral transduction; T.Y. assisted with immunohistochemical staining; K.I. provided *IL7*-floxed mice; S.P. provided human CTCL samples; M.A. discussed the data and provided administrative support; K.N. guided the project; and T.A. and K.N. wrote the manuscript.

## COMPETING FINANCIAL INTERESTS

The authors declare no competing financial interests.

Reprints and permissions information is available online at <http://www.nature.com/reprints/index.html>.

- Cotsarelis, G., Sun, T.T. & Lavker, R.M. Label-retaining cells reside in the bulge area of pilosebaceous unit: implications for follicular stem cells, hair cycle, and skin carcinogenesis. *Cell* **61**, 1329–1337 (1990).
- Nishimura, E.K. *et al.* Dominant role of the niche in melanocyte stem-cell fate determination. *Nature* **416**, 854–860 (2002).
- Christoph, T. *et al.* The human hair follicle immune system: cellular composition and immune privilege. *Br. J. Dermatol.* **142**, 862–873 (2000).
- Nagao, K. *et al.* Stress-induced production of chemokines by hair follicles regulates the trafficking of dendritic cells in skin. *Nat. Immunol.* **13**, 744–752 (2012).
- Clark, R.A. *et al.* The vast majority of CLA<sup>+</sup> T cells are resident in normal skin. *J. Immunol.* **176**, 4431–4439 (2006).
- Gebhardt, T. *et al.* Memory T cells in nonlymphoid tissue that provide enhanced local immunity during infection with herpes simplex virus. *Nat. Immunol.* **10**, 524–530 (2009).
- Gebhardt, T. *et al.* Different patterns of peripheral migration by memory  $CD4^+$  and  $CD8^+$  T cells. *Nature* **477**, 216–219 (2011).
- Jiang, X. *et al.* Skin infection generates non-migratory memory  $CD8^+$   $T_{RM}$  cells providing global skin immunity. *Nature* **483**, 227–231 (2012).
- Wakim, L.M., Waithman, J., van Rooijen, N., Heath, W.R. & Carbone, F.R. Dendritic cell-induced memory T cell activation in nonlymphoid tissues. *Science* **319**, 198–202 (2008).
- Mackay, L.K. *et al.* The developmental pathway for  $CD103^+CD8^+$  tissue-resident memory T cells of skin. *Nat. Immunol.* **14**, 1294–1301 (2013).
- Shiow, L.R. *et al.* *CD69* acts downstream of interferon- $\alpha/\beta$  to inhibit *S1P1* and lymphocyte egress from lymphoid organs. *Nature* **440**, 540–544 (2006).
- Bromley, S.K., Yan, S., Tomura, M., Kanagawa, O. & Luster, A.D. Recirculating memory T cells are a unique subset of  $CD4^+$  T cells with a distinct phenotype and migratory pattern. *J. Immunol.* **190**, 970–976 (2013).
- Suffia, I., Reckling, S.K., Salay, G. & Belkaid, Y. A role for *CD103* in the retention of  $CD4^+CD25^+$   $T_{reg}$  and control of *Leishmania major* infection. *J. Immunol.* **174**, 5444–5455 (2005).
- Sanchez Rodriguez, R. *et al.* Memory regulatory T cells reside in human skin. *J. Clin. Invest.* **124**, 1027–1036 (2014).
- Shiohara, T. & Moriya, N. Epidermal T cells: their functional role and disease relevance for dermatologists. *J. Invest. Dermatol.* **109**, 271–275 (1997).
- Mizukawa, Y. *et al.* Direct evidence for interferon- $\gamma$  production by effector-memory-type intraepidermal T cells residing at an effector site of immunopathology in fixed drug eruption. *Am. J. Pathol.* **161**, 1337–1347 (2002).
- Hwang, S.T., Janik, J.E., Jaffe, E.S. & Wilson, W.H. Mycosis fungoides and Sezary syndrome. *Lancet* **371**, 945–957 (2008).
- Campbell, J.J., Clark, R.A., Watanabe, R. & Kupper, T.S. Sezary syndrome and mycosis fungoides arise from distinct T-cell subsets: a biologic rationale for their distinct clinical behaviors. *Blood* **116**, 767–771 (2010).
- Clark, R.A. *et al.* Skin effector memory T cells do not recirculate and provide immune protection in alemtuzumab-treated CTCL patients. *Sci. Transl. Med.* **4**, 117ra7 (2012).
- Edelson, R.L. Cutaneous T cell lymphoma: mycosis fungoides, Sezary syndrome, and other variants. *J. Am. Acad. Dermatol.* **2**, 89–106 (1980).
- Seneschal, J., Clark, R.A., Gehad, A., Baecher-Allan, C.M. & Kupper, T.S. Human epidermal Langerhans cells maintain immune homeostasis in skin by activating skin resident regulatory T cells. *Immunity* **36**, 873–884 (2012).
- Sanchez Rodriguez, R. *et al.* Memory regulatory T cells reside in human skin. *J. Clin. Invest.* **124**, 1027–1036 (2014).



23. Ariotti, S. *et al.* T cell memory. Skin-resident memory CD8<sup>+</sup> T cells trigger a state of tissue-wide pathogen alert. *Science* **346**, 101–105 (2014).
24. Lanzavecchia, A. & Sallusto, F. Understanding the generation and function of memory T cell subsets. *Curr. Opin. Immunol.* **17**, 326–332 (2005).
25. van Leeuwen, E.M., Sprent, J. & Surh, C.D. Generation and maintenance of memory CD4<sup>+</sup> T cells. *Curr. Opin. Immunol.* **21**, 167–172 (2009).
26. Vasioukhin, V., Degenstein, L., Wise, B. & Fuchs, E. The magical touch: genome targeting in epidermal stem cells induced by tamoxifen application to mouse skin. *Proc. Natl. Acad. Sci. USA* **96**, 8551–8556 (1999).
27. Liang, B. *et al.* Role of hepatocyte-derived IL-7 in maintenance of intrahepatic NKT cells and T cells and development of B cells in fetal liver. *J. Immunol.* **189**, 4444–4450 (2012).
28. Dorfman, D.M. & Shahsafaie, A. CD69 expression correlates with expression of other markers of Th1 T cell differentiation in peripheral T cell lymphomas. *Hum. Pathol.* **33**, 330–334 (2002).
29. Yamanaka, K. *et al.* Skin-derived interleukin-7 contributes to the proliferation of lymphocytes in cutaneous T-cell lymphoma. *Blood* **107**, 2440–2445 (2006).
30. Espinet, B. & Salgado, R. Mycosis fungoides and Sezary syndrome. *Methods Mol. Biol.* **973**, 175–188 (2013).
31. Kanavaros, P. *et al.* Mycosis fungoides: expression of C-myc p62 p53, bcl-2 and PCNA proteins and absence of association with Epstein-Barr virus. *Pathol. Res. Pract.* **190**, 767–774 (1994).
32. Kamijo, T., Bodner, S., van de Kamp, E., Randle, D.H. & Sherr, C.J. Tumor spectrum in *ARF*-deficient mice. *Cancer Res.* **59**, 2217–2222 (1999).
33. Serrano, M. *et al.* Role of the *INK4a* locus in tumor suppression and cell mortality. *Cell* **85**, 27–37 (1996).
34. Sugihara, E. *et al.* Ink4a and Arf are crucial factors in the determination of the cell of origin and the therapeutic sensitivity of Myc-induced mouse lymphoid tumor. *Oncogene* **31**, 2849–2861 (2012).

## CONCISE COMMUNICATION

# Recurrent gastrointestinal perforation in a patient with Ehlers–Danlos syndrome due to tenascin-X deficiency

Tomo SAKIYAMA,<sup>1,2</sup> Akiharu KUBO,<sup>2</sup> Takashi SASAKI,<sup>2,3</sup> Taketo YAMADA,<sup>4,5</sup> Nobushige YABE,<sup>6</sup> Ken-ichi MATSUMOTO,<sup>7</sup> Yuko FUTEI<sup>1</sup>

<sup>1</sup>Division of Dermatology, Ogikubo Hospital, <sup>2</sup>Department of Dermatology, Keio University School of Medicine, <sup>3</sup>KOSÉ Endowed Program for Skin Care and Allergy Prevention, Keio University School of Medicine, <sup>4</sup>Department of Pathology, Keio University School of Medicine, Tokyo, <sup>5</sup>Department of Pathology, Saitama Medical University, Saitama, <sup>6</sup>Division of Surgery, Ogikubo Hospital, Tokyo, <sup>7</sup>Department of Biosignaling and Radioisotope Experiment, Interdisciplinary Center for Science Research, Organization for Research, Shimane University, Shimane, Japan

## ABSTRACT

**Ehlers–Danlos syndrome (EDS) is a clinically and genetically heterogeneous disorder. Using a customized targeted exome-sequencing system we identified nonsense mutations in *TNXB* in a patient who had recurrent gastrointestinal perforation due to tissue fragility. This case highlights the utility of targeted exome sequencing for the diagnosis of congenital diseases showing genetic heterogeneity, and the importance of attention to gastrointestinal perforation in patients with tenascin-X deficient type EDS.**

**Key words:** customized targeted exome sequencing, Ehlers–Danlos syndrome, gastrointestinal perforation, next-generation sequencer, tenascin-X.

## INTRODUCTION

Ehlers–Danlos syndrome (EDS) is a heritable connective-tissue disorder characterized by skin hyperextensibility, joint hypermobility and tissue fragility. EDS is classified into six major types and other minor forms according to clinical features and causative gene mutations. A total of 22 types and 15 causative genes have been reported.<sup>1</sup> EDS due to tenascin-X (TNX) deficiency is a rare variant of EDS. TNX-deficient EDS was first reported by Burch *et al.* in 1997,<sup>2</sup> and only 18 cases have been reported to date. TNX, encoded by *TNXB* located on chromosome 6p, is a glycoprotein that is widely distributed in the extracellular matrix of tissues throughout the body, especially in muscle.<sup>3</sup> TNX plays a role in collagen fibrillogenesis and regulation of type VI collagen synthesis.<sup>4</sup> Herein, we report the first Asian patient diagnosed with TNX-deficient EDS. She had a history of recurrent gastrointestinal perforation, and two novel nonsense mutations in *TNXB* were detected by customized targeted exome sequencing for genodermatoses.

## CASE REPORT

A 45-year-old woman was initially referred to the dermatology department of our hospital with a history suggestive of EDS. She had had skin hyperextensibility, easy bruising, scoliosis and recurrent subluxations since childhood. She underwent

multiple surgical procedures for subluxations of her hip joints. In her 20s, recurrent periodontitis and abdominal pain were recognized. Episodes of both spontaneous and secondary gastrointestinal ileus and perforations were repeatedly observed commencing in her 40s with diverticular perforation of the sigmoid colon, followed by incarcerated hernia at the drain tube insertion site and ileus after stoma closure. At 45 years of age, the patient experienced a spontaneous ileus followed by duodenal perforation (likely due to ileus tube insertion). An ovarian cyst was observed at 41 years of age. There was no apparent delay in wound healing of her skin or intestine, although both were very fragile. In her 40s, she had felt numbness in her fingers, neck pain and reduced grip strength. The family history was uncertain because her parents had already died, but no symptoms of joint hypermobility or skin hyperextensibility had been recognized. Her elder sister (II-3 in Fig. 1a) had mild skin hyperelasticity, mild joint hypermobility and pes planus. Her niece (III-2 in Fig. 1a) had mild skin hyperelasticity and her nephew (III-1 in Fig. 1a) had pes planus.

On examination, her face was slack-skinned with prominent eyes and a thin nose (Fig. 1b). Periodontitis was observed (Fig. 1b). Her hyperextensive skin was thin, translucent, soft and velvety. Although she had mild joint hypermobility, her Beighton score was 3 of 9 (a 9-point scale to define joint hypermobility, with cut-off points for generalized joint hypermobility of  $\geq 4/9$  for men and  $\geq 5/9$  for women). She had pes planus, piezogenic papules on her feet and deformity due to

Correspondence: Akiharu Kubo, M.D., Ph.D., Department of Dermatology, Keio University School of Medicine, 35 Shinanomachi, Shinjuku-ku, Tokyo 160-8582, Japan. Email: akiharu@a5.keio.jp

Received 3 December 2014; accepted 26 January 2015.

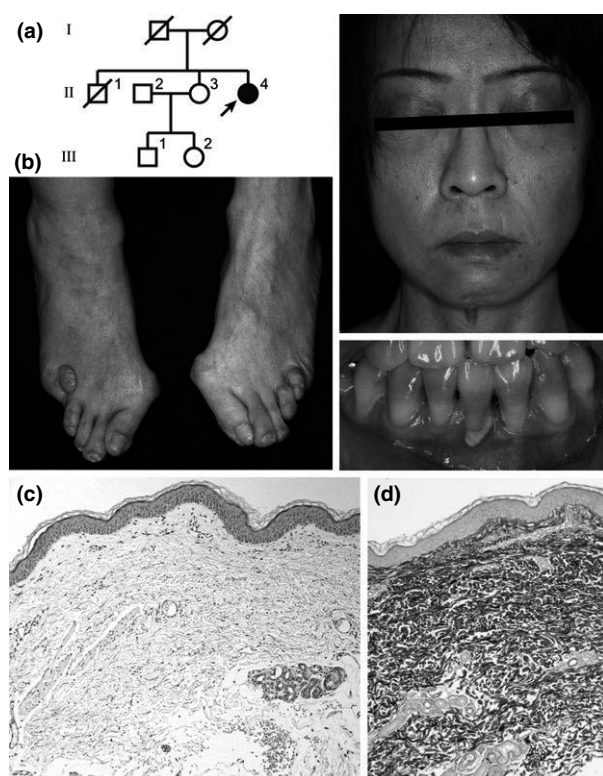


**Figure 1.** (a) Patient pedigree. (b) The patient's face was slack-skinned with prominent eyes and a thin nose. She had periodontitis, pes planus and deformity due to subluxation of the right little toe. (c) Hematoxylin–eosin stain of the patient's skin (original magnification  $\times 100$ ). (d) Elastica van Gieson stain of skin ( $\times 100$ ).

subluxation of the right little toe (Fig. 1b). There was non-atrophic broad scar formation on her knees and elbows. Ophthalmologic examination showed conjunctivochalasis in both eyes. Computed tomography (CT) scan and echocardiography revealed no cardiovascular abnormality. She was incapable of opening a bottle cap due to numbness in her thumbs and reduced grip strength (right, 10.0 kg; left, 6.8 kg). Electromyogram and nerve conduction studies from her upper extremities showed bilateral median, left musculocutaneous and mild left radial sensory neuropathy. Skin biopsy from her left upper arm showed thin and loosely assembled collagen bundles, especially apparent around the sweat glands (Fig. 1c). There was marked hemorrhage around blood vessels in the dermis (Fig. 1c). Fragmented and curly elastin fibers were confirmed by elastica van Gieson staining as previously described (Fig. 1d).<sup>5</sup>

We developed a custom panel for mutation screening of approximately 450 genes of genodermatoses using the Sure-Design program and Haloplex target enrichment system (Agilent Technologies, Santa Clara, CA, USA). The custom panel included 13 EDS-associated genes (Fig. 2a) with the exclusion of two of these (*B3GALT6* and *DSE*)<sup>1</sup> that were identified after

the panel was established. Next-generation sequencing analysis was performed using the panel according to the supplier's protocol, and two novel nonsense mutations in *TNXB*, c.2539C>T (p.R847\*) and c.3574C>T (p.Q1192\*) were identified. No disease-associated mutations were identified in the other 12 genes tested (Fig. 2a). The nonsense mutations in *TNXB* were confirmed by Sanger DNA sequencing (Fig. 2b). We further confirmed complete absence of TNX protein in the patient's serum and skin. Immunoblot analysis of the patient's serum using rabbit polyclonal anti-tenascin-X antibody ( $\alpha$ -hu30),<sup>6</sup> detected with IRDye 680-conjugated donkey anti-rabbit immunoglobulin (IgG) (LI-COR Biosciences, Lincoln, NE, USA) using an Odyssey infrared imaging system (LI-COR) demonstrated the complete absence of soluble 75- and 140-kDa forms of TNX protein (Fig. 3a).<sup>7</sup> Immunostaining with an anti-TNX antibody (AF6999 polyclonal sheep IgG; R&D Systems, Minneapolis, MN, USA) detected by means of rabbit anti-sheep Ig conjugated with horseradish peroxidase (DAKO, Glostrup, Denmark), VECTOR SG Kit (Vector Laboratories, Burlingame, CA, USA) and 3,3'-diaminobenzidine-tetrachloride (DAB; Dojindo Laboratories, Kumamoto, Japan) revealed that skin sections were negative for TNX expression (Fig. 3b). Together with the results of genetic testing, the patient was diagnosed with TNX-deficient type EDS due to probable compound heterozygosity of the two novel nonsense mutations in *TNXB*.

## DISCUSSION

Tenascin-X-deficient type EDS is clinically characterized by hyperextensibility, joint hypermobility, easy bruising, normal wound healing and lack of atrophic scar formation. Neuromuscular complaints are seen in several types of EDS, and axonal sensorimotor polyneuropathy is predominant in the TNX-deficient type.<sup>8</sup> Patients can also suffer from luxation, valvular heart disease, pes planus and piezogenic papules on the feet. Based on clinical features alone, it is difficult to distinguish TNX-deficient type EDS from other types of EDS, and especially from classical EDS exhibiting a mild clinical phenotype. Therefore, genetic testing is important for diagnosis of the EDS type.

The genetic heterozygosity of EDS and the large size of several of the causative genes (including *TNXB*) make it difficult to routinely diagnose EDS genetically. Targeted exome sequencing has enabled comprehensive screening of causative mutations in a set of selected genes associated with disease. We developed a custom panel for next-generation sequencing to screen mutations in approximately 450 causative genes for genodermatoses. With this system, 13 causative genes for EDS and EDS-related diseases (including *TNXB*) were sequenced comprehensively (Fig. 2a), enabling identification of the two novel nonsense mutations of *TNXB* rapidly and at low cost. Targeted exome sequencing is considered very useful for the diagnosis of genodermatoses that show genetic and clinical heterogeneity, such as EDS, epidermolysis bullosa, ichthyosiform erythroderma and palmoplantar keratoderma.

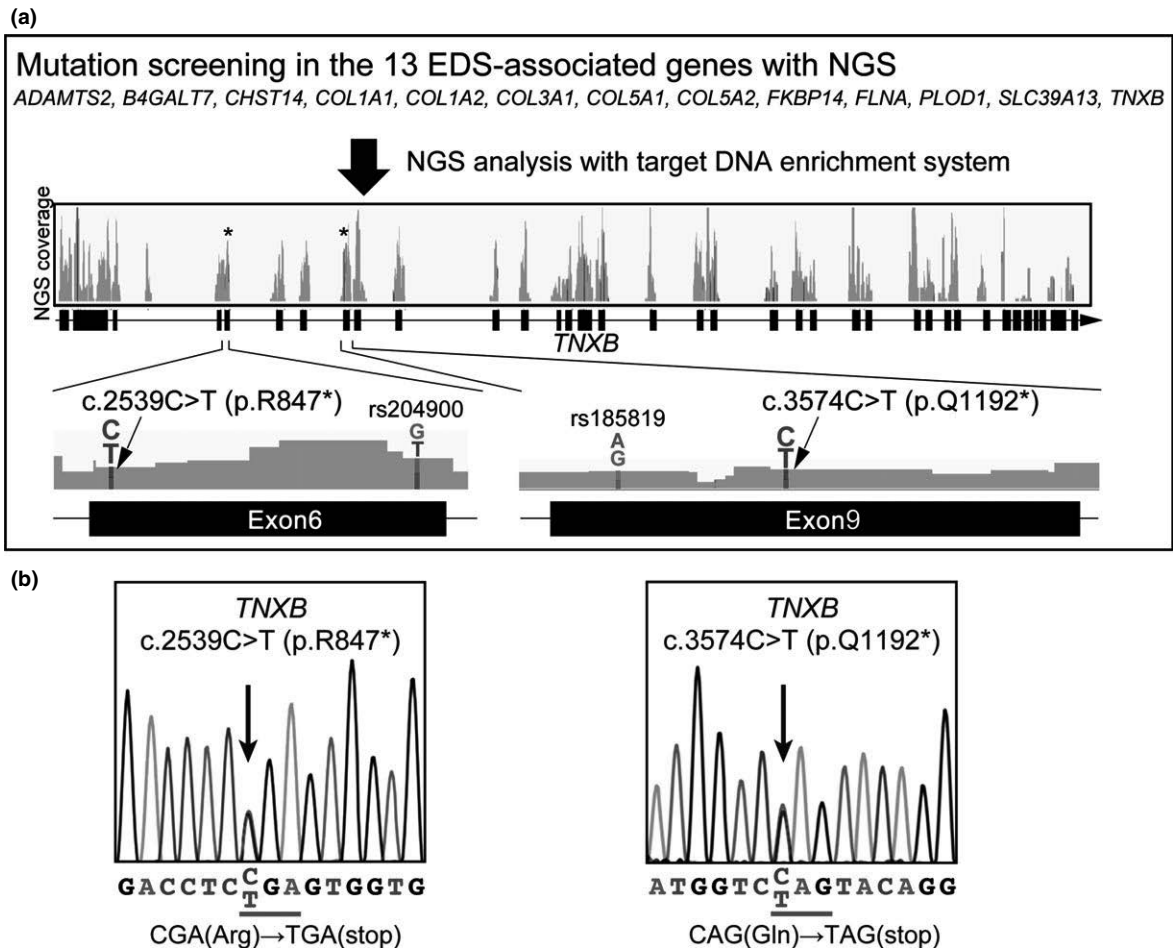


**Figure 2.** (a) Targeted exome sequencing analysis with next-generation sequencing (NGS) of 13 Ehlers–Danlos syndrome (EDS)-associated genes, including *TNXB*. Single nucleotide polymorphisms including two nonsense mutations were identified. (b) Sanger DNA sequencing analysis of *TNXB* revealed p.R847\* and p.Q1192\* nonsense mutations.

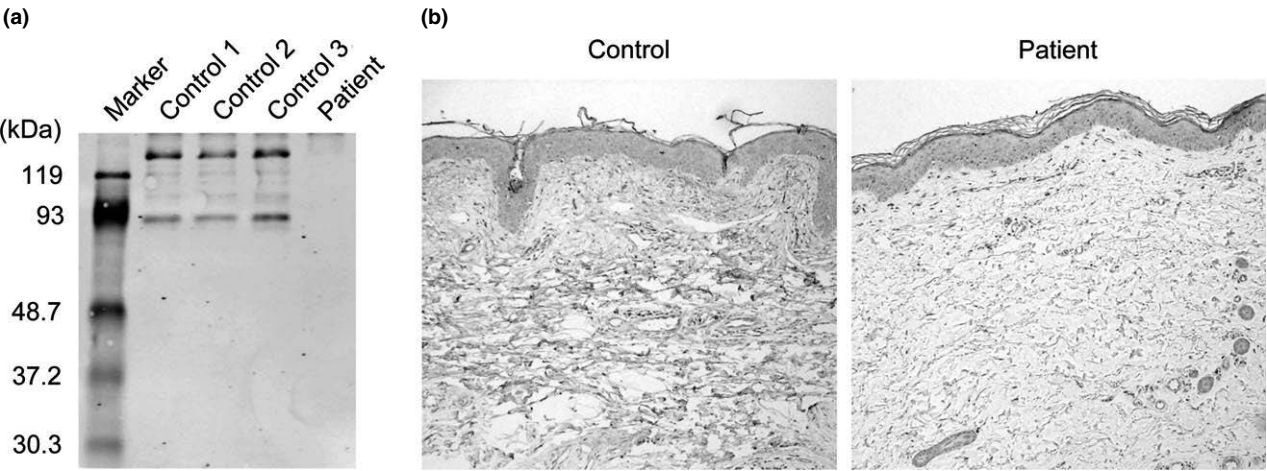


**Figure 3.** (a) Western blot of the patient's serum revealed complete deficiency of both the 140- and 75-kDa species of serum tenascin-X (TNX). (b) TNX immunostaining of the patient's skin and that of a control individual (original magnification  $\times 100$ ).

Recurrent gastrointestinal perforation and fragility of the intestinal tract were distinctive features in this patient. The intestinal specimen obtained during the surgery for duodenum perforation showed very loose interstitium. Of the six major types of EDS, vascular type EDS patients are known to have the highest risk of gastrointestinal complications, namely, spontaneous and/or iatrogenic rupture of the sigmoid colon.<sup>9</sup> Upon review of the published work, we found that five of 19 patients of TNX-deficient type EDS (including this case) had gastrointestinal involvement (three hernias,<sup>10,11</sup> three diverticuloses,<sup>10</sup> two bowel perforations,<sup>10</sup> one recurrent rectal prolapse<sup>10</sup> and one gastrointestinal bleeding<sup>12</sup>). Mutations in *TNXB* were identified in three of the five patients, and no apparent genotype–phenotype correlation was observed compared with other patients.<sup>11,12</sup> The high incidence of gastrointestinal involvement in TNX-deficient type EDS patients indicates the importance of attention to invasive procedures and treatment of gastrointestinal disorders, not only in vascular type EDS but also in TNX-deficient type EDS.

*TNXB* haploinsufficiency is observed prevalently in heterozygous females with *TNXB* deficiency showing generalized joint hypermobility.<sup>13</sup> Examination of 20 heterozygous family members revealed that nine of 14 females and zero of six males exhibited generalized joint hypermobility similar to hypermobility type EDS.<sup>13</sup> *TNXB* haploinsufficiency is dominantly inherited and appears to produce clinical findings primarily in females, consistent with clinical descriptions of hypermobility type EDS. In our case, the proband's sister and her daughter revealed mild skin hyperelasticity. However, as no genetic tests were performed whether they were heterozygous for TNX deficiency remains unknown.

In conclusion, we report the first Asian case of TNX deficiency, diagnosed by customized targeted exome sequencing. This case indicates the importance of attention to gastrointestinal perforation due to tissue fragility in TNX-deficient type EDS patients.

**ACKNOWLEDGMENT:** This work was supported in parts by grants from the Ministry of Health, Labour and Welfare of Japan.

**CONFLICT OF INTEREST:** None declared.

## REFERENCES

- 1 Online Mendelian Inheritance in Man (130000, 130010, 130020, 130050, 130060, 130070, 130080, 130090, 225310, 225320, 225400, 225410, 300537, 305200, 601776, 615539, 606408, 608763, 612350, 614557, 615349). [cited 4 Sept 2014.] Available from URL: <http://www.ncbi.nlm.nih.gov/omim>
- 2 Burch GH, Gong Y, Liu W *et al.* Tenascin-X deficiency is associated with Ehlers-Danlos syndrome. *Nat Genet* 1997; **17**: 104–108.
- 3 Matsumoto K, Saga Y, Ikemura T *et al.* The distribution of tenascin-X is distinct and often reciprocal to that of tenascin-C. *J Cell Biol* 1994; **125**: 483–493.
- 4 Minamitani T, Ariga H, Matsumoto K. Deficiency of tenascin-X causes a decrease in the level of expression of type VI collagen. *Exp Cell Res* 2004; **297**: 49–60.
- 5 Zweers MC, van Vlijmen-Willems IM, van Kuppevelt TH *et al.* Deficiency of tenascin-X causes abnormalities in dermal elastic fiber morphology. *J Invest Dermatol* 2004; **122**: 885–891.
- 6 Satoh K, Tsukamoto M, Shindoh M *et al.* Increased expression of tenascin-X in thoracic and abdominal aortic aneurysm tissues. *Biol Pharm Bull* 2010; **33**: 1898–1902.
- 7 Egging DF, Peeters ACTM, Grebenchtchikov N *et al.* Identification and characterization of multiple species of tenascin-X in human serum. *FEBS J* 2007; **274**: 1280–1289.
- 8 Voermans NC, Van Alfen N, Pillen S *et al.* Neuromuscular involvement in various types of Ehlers-Danlos syndrome. *Ann Neurol* 2009; **65**: 687–697.
- 9 Burcharth J, Rosenberg J. Gastrointestinal surgery and related complications in patients with Ehlers-Danlos syndrome: a systematic review. *Dig Surg* 2012; **29**: 349–357.
- 10 Lindor NM, Bristow J. Tenascin-X deficiency in autosomal recessive Ehlers-Danlos syndrome. *Am J Med Genet A* 2005; **135**: 75–80.
- 11 Penisson-Besnier I, Allamand V, Beurrier P *et al.* Compound heterozygous mutations of the *TNXB* gene cause primary myopathy. *Neuromuscul Disord* 2013; **23**: 664–669.
- 12 Schalkwijk J, Zweers MC, Steijlen PM *et al.* A recessive form of the Ehlers-Danlos syndrome caused by tenascin-X deficiency. *N Engl J Med* 2001; **345**: 1167–1175.
- 13 Zweers MC, Bristow J, Steijlen PM *et al.* Haploinsufficiency of *TNXB* is associated with hypermobility type of Ehlers-Danlos syndrome. *Am J Hum Genet* 2003; **73**: 214–217.

RESEARCH ARTICLE

# A Novel Phthalimide Derivative, TC11, Has Preclinical Effects on High-Risk Myeloma Cells and Osteoclasts

Maiko Matsushita<sup>1</sup>, Yoshie Ozaki<sup>1</sup>, Yuka Hasegawa<sup>1</sup>, Fukiko Terada<sup>1</sup>, Noriko Tabata<sup>2</sup>, Hirokazu Shiheido<sup>2</sup>, Hiroshi Yanagawa<sup>2</sup>, Tsukasa Oikawa<sup>3</sup>, Koichi Matsuo<sup>3</sup>, Wenlin Du<sup>4</sup>, Taketo Yamada<sup>4</sup>, Masashi Hozumi<sup>1</sup>, Daiju Ichikawa<sup>1</sup>, Yutaka Hattori<sup>1\*</sup>

**1** Clinical Physiology and Therapeutics, Faculty of Pharmacy, Keio University, Tokyo, Japan, **2** Department of Biosciences and Informatics, Faculty of Science and Technology, Keio University, Yokohama, Japan, **3** Cell and Tissue Biology, School of Medicine, Keio University, Tokyo, Japan, **4** Department of Pathology, School of Medicine, Keio University, Tokyo, Japan

\* [hattori-yt@pha.keio.ac.jp](mailto:hattori-yt@pha.keio.ac.jp)



## OPEN ACCESS

**Citation:** Matsushita M, Ozaki Y, Hasegawa Y, Terada F, Tabata N, Shiheido H, et al. (2015) A Novel Phthalimide Derivative, TC11, Has Preclinical Effects on High-Risk Myeloma Cells and Osteoclasts. PLoS ONE 10(1): e0116135. doi:10.1371/journal.pone.0116135

**Academic Editor:** Dominique Heymann, Faculté de médecine de Nantes, FRANCE

**Received:** April 18, 2014

**Accepted:** November 24, 2014

**Published:** January 24, 2015

**Copyright:** © 2015 Matsushita et al. This is an open access article distributed under the terms of the [Creative Commons Attribution License](https://creativecommons.org/licenses/by/4.0/), which permits unrestricted use, distribution, and reproduction in any medium, provided the original author and source are credited.

**Data Availability Statement:** All relevant data are within the paper.

**Funding:** This work was supported in part by a Grant-in-Aid for Scientific Research (Y. Hattori, MM) and a grant from the Private University Strategic Research Base Development Program (Y. Hattori) of MEXT (the Ministry of Education, Culture, Sports, Science and Technology) of Japan, Keio Gijuku Academic development Funds (Y. Hattori) and Japan Leukemia Research Fund (Y. Hattori, MM). The funders had no role in study design, data collection and

## Abstract

Despite the recent advances in the treatment of multiple myeloma (MM), MM patients with high-risk cytogenetic changes such as t(4;14) translocation or deletion of chromosome 17 still have extremely poor prognoses. With the goal of helping these high-risk MM patients, we previously developed a novel phthalimide derivative, TC11. Here we report the further characterization of TC11 including anti-myeloma effects *in vitro* and *in vivo*, a pharmacokinetic study in mice, and anti-osteoclastogenic activity. Intraperitoneal injections of TC11 significantly delayed the growth of subcutaneous tumors in human myeloma-bearing SCID mice. Immunohistochemical analyses showed that TC11 induced apoptosis of MM cells *in vivo*. In the pharmacokinetic analyses, the  $C_{max}$  was 2.1  $\mu$ M at 1 h after the injection of TC11, with 1.2 h as the half-life. TC11 significantly inhibited the differentiation and function of tartrate-resistant acid phosphatase (TRAP)-positive multinucleated osteoclasts in mouse osteoclast cultures using M-CSF and RANKL. We also revealed that TC11 induced the apoptosis of myeloma cells accompanied by  $\alpha$ -tubulin fragmentation. In addition, TC11 and lenalidomide, another phthalimide derivative, directly bound to nucleophosmin 1 (NPM1), whose role in MM is unknown. Thus, through multiple molecular interactions, TC11 is a potentially effective drug for high-risk MM patients with bone lesions. The present results suggest the possibility of the further development of novel thalidomide derivatives by drug designing.

## Introduction

Multiple myeloma (MM) is a neoplasm of plasma cells that is accompanied by various clinical manifestations including lytic bone lesions, hypercalcemia, renal dysfunction, immunodeficiency, and anemia [1, 2]. Despite recent advances in the use of newly developed drugs



analysis, decision to publish, or preparation of the manuscript.

**Competing Interests:** The authors have declared that no competing interests exist.

including immune-modulatory drugs (IMiDs) such as thalidomide, lenalidomide, and pomalidomide and proteasome inhibitors such as bortezomib, carfilzomib, and MLN9708, MM is still an incurable disease [3–7]. In particular, MM patients harboring 17p deletion, t(14;16), t(14;20), or t(4;14) are classified as a high-risk group and have shown significantly shorter survival [8–10]. For example, it is reported that even lenalidomide plus dexamethasone or bortezomib could not substantially improve the survival of refractory patients with del 17p [11, 12]. With the goal of helping prolong the survival of these high-risk MM patients, we screened 29 synthetic phthalimide derivatives and found a novel compound, 2-(2,6-diisopropylphenyl)-5-amino-1*H*-isoindole-1,3-dione (TC11), which induced the apoptosis of KMS34 cells with t(4;14) and del17p13 [13].

Bone lytic lesions, which are seen in 80%–90% of MM patients, have clinical manifestations that include pain, pathologic fractures, spinal cord compression, and hypercalcemia, thus providing a negative impact on the quality of life of MM patients [1]. In the clinical setting, bisphosphonate, radiotherapy, and surgery are used to treat bone disease. Bisphosphonate can significantly reduce skeletal-related events in MM patients [14], but side effects such as renal impairment and osteonecrosis of the jaw are seen in some patients [15, 16]. The development of novel agents to effectively treat bone lesions without severe side effects is thus necessary.

In the present study, we evaluate the anti-myeloma effects of TC11 *in vitro* and *in vivo*, and we investigated the effects of TC11 on the differentiation of osteoclasts to determine whether this new drug could be effective for treating high-risk MM patients with bone lesions. We also examined nucleophosmin-1 (NPM1) as a molecule that binds directly to phthalimide, and the results raised the possibility that  $\alpha$ -tubulin is involved in the anti-myeloma effect of TC11.

## Materials and Methods

### Cell lines

Human myeloma cell lines KMS11, KMS 26, KMS28, and KMS34 were established by Dr. T. Otsuki (Kawasaki Medical School, Kurashiki, Japan) from Japanese patients [17, 18] and these cell lines were kindly provided by him. MUM24 was established from a patient with thalidomide-resistant MM [19]. These cell lines were maintained in RPMI1640 medium (Sigma-Aldrich, St. Louis, MO) containing 10% fetal bovine serum (FBS). The human macrophage cell line RAW264.7 was purchased from American Type Culture Collection (Rockville, MD) and cultured in DMEM medium (Sigma-Aldrich) containing 10% FBS (Hyclone Laboratories, Logan, UT).

### Reagents

We synthesized TC11 [2-(2,6-diisopropylphenyl)-5-amino-1*H*-isoindole-1,3-dione] from phthalic acid anhydride with a nitro group and amines, followed by catalytic hydrogenation under a nitrogen atmosphere. The benzene ring moiety of TC11 is different from those of thalidomide and lenalidomide (Fig. 1A). Dexamethasone sodium phosphate (MSD K.K., Tokyo) was used for *in vitro* proliferation assay.

### Patients' samples

Bone marrow samples were obtained from patients with MM treated in Keio University Hospital. Mononuclear cells were isolated by Ficoll density gradient centrifugation and cryopreserved in a liquid nitrogen tank until further use. All samples contained more than 30% myeloma cells. This study was approved by the ethics committee of the Keio University School of

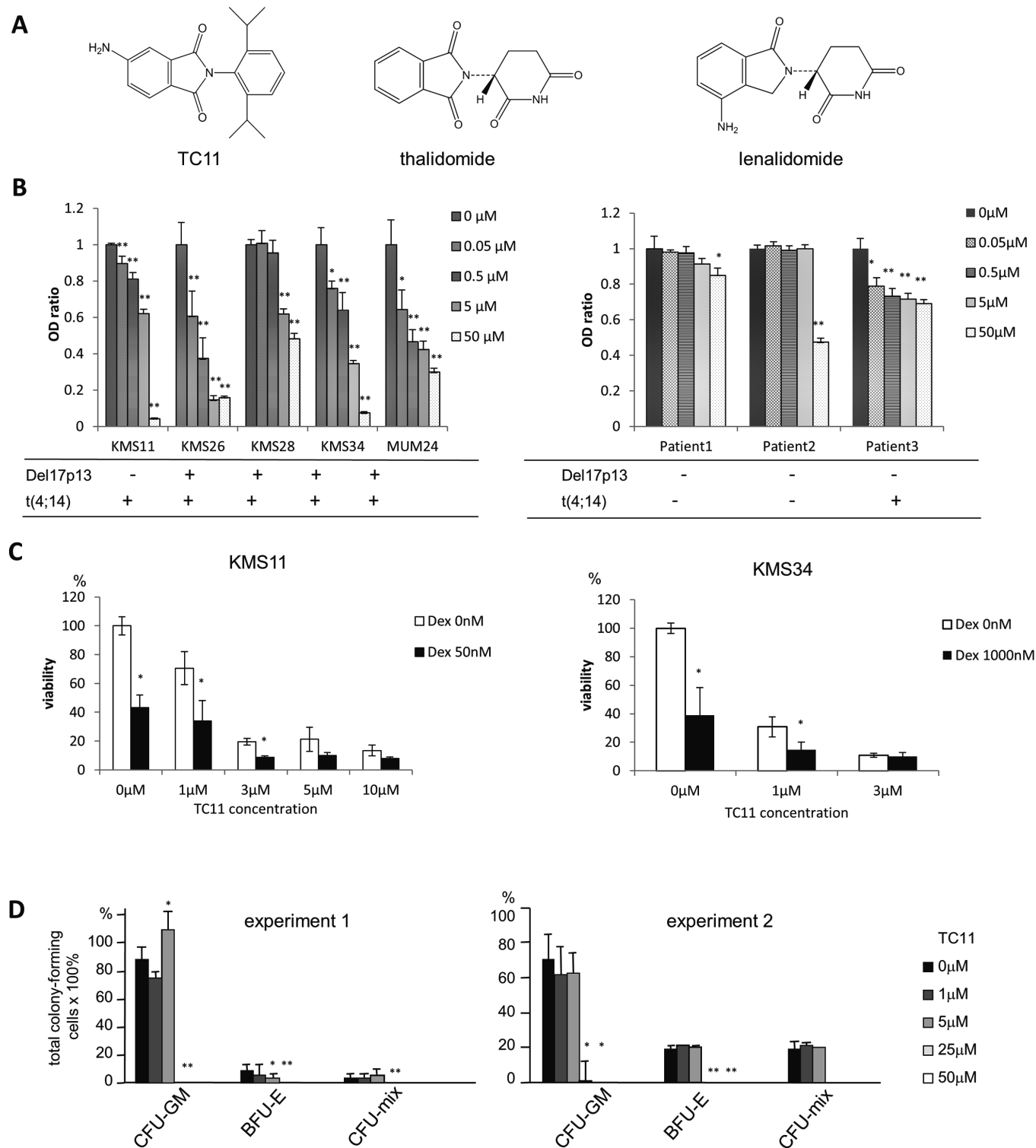


**Figure 1. TC11 inhibited the growth of MM cell lines.** (A) The chemical structures of TC11, thalidomide, and lenalidomide. (B) The dose-dependent inhibition of MM cells by TC11. Cell lines KMS11, KMS26, KMS28, KMS34, MUM24 with del 17p13 and/or t(4;14) were cultured for 48 h with the indicated dose of TC11, followed by an assessment of cell viability using MTT assays. Mononuclear cells separated from bone marrow samples of three MM patients were also treated with TC11 and examined by MTT assay. (C) Synergistic effects of TC11 with dexamethasone were examined by MTT assay. Bars indicate means±SD. \* $p < 0.05$  (Student's *t*-test). (D) The effect of TC11 on the number of hematopoietic progenitor cells was examined by colony assay. Mice bone

marrow cells were plated in 1.2% methylcellulose medium containing 20 ng/mL mL-3, 10 ng/mL mL-6, 20 ng/mL mSCF and 1 U/mL hEPO in the presence or absence of TC11. The numbers of colony-forming cells were counted after 14 days. Bars indicate means $\pm$ SD. \* $p$ <0.05, \*\* $p$ <0.01 (Student's *t*-test).

doi:10.1371/journal.pone.0116135.g001

Medicine (99–7 and 15–21) and Faculty of Pharmacy (G110107–1). Written informed consent was obtained from all patients.

### Cell viability assay

MM cells ( $2 \times 10^4$  cells per well) were seeded in 96-well plates and incubated with various concentrations of TC11 (0–50  $\mu$ M) at 37°C for 48 h. The number of viable cells was assessed by MTT dye absorbance (Roche Diagnostics, Indianapolis, IN) according to the manufacturer's instructions.

### Colony-forming cell assay

To evaluate the hematological toxicity of TC11,  $4 \times 10^4$  cells/mL of bone marrow cells from 13-wk-old male ICR mice were cultured in methylcellulose medium (Stem Cell Technologies, Vancouver, BC) containing FBS, 2-mercaptoethanol, 20 ng/mL mouse stem cell factor (mSCF), 20 ng/mL mouse interleukin 3 (mIL-3), 10 ng/mL mouse interleukin-6 (mIL-6), and 1 U/mL human erythropoietin (hEPO) (kindly provided by Kyowa Hakko Kirin Co., Tokyo) in the presence or absence of TC11. On day 14, various types of colony-forming cells were counted.

### *In vivo* tumor growth assay

All of the animal experiments were approved by the Ethics Committee for Animal Experiments at Keio University Faculty of Pharmacy (Approval no.09118-(0), 09118-(1)). The *in vivo* tumor-inhibitory activity assay was performed as described with several modifications [18]. Briefly,  $3 \times 10^7$  KMS34 or KMS11 cells were subcutaneously inoculated into 5-wk-old male ICR/SCID mice (Clea Japan, Tokyo) and plasmacytoma developed in 4–7 wks. In addition, twenty mg/kg of TC11 dissolved in 10% DMSO (Sigma-Aldrich)-1% Tween80 at the concentration of 2.5 mg/mL or only 10% DMSO-1% Tween80 as a control was injected intraperitoneally twice every 3 days for 15 days ( $n = 7$ ). The tumor volume was calculated according to the following formula as described [18]: width  $\times$  length<sup>2</sup>  $\times$  0.52.

### Histopathologic examination

The histopathologic analysis was performed as described with several modifications [18]. When the subcutaneous tumors reached 50 mm<sup>3</sup>, the intraperitoneal injections of TC11 was started. After 14 days of observation, the mice were sacrificed and the isolated tumors were fixed with 10% formalin and embedded in paraffin. Sliced sections were stained with hematoxylin and eosin (H. E.). Anti-human cleaved PARP (Asp214) polyclonal antibody (Cell Signaling Technology Japan, Tokyo), anti-cleaved caspase-3 (Asp175) polyclonal antibody (Cell Signaling Technology Japan) and anti-human Ki-67 monoclonal antibody (clone MIB-1) (Dako Japan, Tokyo) were used for immunohistochemistry.

### Pharmacokinetics study

To evaluate the pharmacokinetics of TC11, we obtained peripheral blood with a heparinized needle from the tail veins of 5-wk-old male ICR mice at 0.5, 1, 1.5, 4, 8, 12, and 24 h after an injection of a low dose (20 mg/kg) or a high dose (100 mg/kg) of TC11. Blood samples were

centrifuged immediately at 3400g for 15 min at 4°C. The plasma fraction was transferred to a polypropylene tube and stored at -80°C until the assay. The plasma samples were thawed and diluted with 10% ethanol in phosphate-buffered saline (PBS). A stock solution of TC11 was prepared in ethanol at 1 mg/mL. A series of standard solutions at designated concentrations were prepared by diluting the stock solution with ethanol. All of the samples were analyzed by high-pressure liquid chromatography (HPLC; a Jasco HPLC system, Jasco, Tokyo). The C18 column (Sep-Pak; Waters Associates, Milford, MA) was used. The mobile phases were acetonitrile and 25 mM ammonium acetate (60:40).

### Osteoclast differentiation assay

We prepared murine osteoclasts from bone marrow cells as described [20]. In brief, cells obtained from the bone marrow of 5-wk-old male ICR mice were cultured in  $\alpha$ -MEM containing 10% FBS with macrophage-colony stimulating factor (M-CSF; R&D Systems, Minneapolis, MN) (10 ng/mL). After 3 days of culture, we removed the floating cells and used the attached cells including bone marrow-derived macrophages (BMMs) as osteoclast precursors. To generate osteoclasts, BMMs were further cultured with M-CSF (10 ng/mL) and receptor activator of nuclear factor  $\kappa$ B ligand (RANKL; R&D Systems) (10 ng/mL). After an additional 3–6 days of culture, the cells were fixed and stained for tartrate-resistant acid phosphatase (TRAP) as described [20]. TRAP-positive multinucleated cells containing more than three nuclei were considered TRAP<sup>+</sup> multinuclear osteoclasts (TRAP<sup>+</sup> MNCs).

### Pit formation assay

RAW 264.7 cells were incubated for 5–8 days with RANKL (10 ng/mL). After maturation into osteoclasts, the cells were seeded on BioCoat Osteologic multi-test slides (BD Falcon, BD Biosciences, San Jose, CA). Various concentrations of TC11, thalidomide (Wako, Osaka, Japan), bortezomib (Toronto Research Chemicals Inc., ON, Canada), and osteoprotegerin (OPG; R&D Systems) were added every 2 days for 7 days. Finally Von Kossa stain was conducted to visualize resorption pits. The resorption pits were observed by fluorescence microscopy (BZ-9000, Keyence, Tokyo). The pit area was quantified using Image J software (NIH).

### Immunocytochemistry

KMS34 cells were treated with 5  $\mu$ M TC11 for 4 h and attached to a slide using CYTOSPIN4 (Thermo Fisher Scientific, Rockford, IL), then fixed with 2% paraformaldehyde and permeabilized with 0.5% Triton X followed by blocking with 1% bovine serum albumin (BSA) in PBS. The sample was stained with antibody against  $\alpha$ -tubulin (Sigma-Aldrich) followed by FITC-conjugated anti-mouse IgG (Takara Bio, Shiga, Japan), and then observed by fluorescence microscopy (BZ-9000).

### Surface plasmon resonance (SPR) analysis

We determined the binding kinetics by a surface plasmon resonance (SPR) analysis with the Biacore 3000 system (GE Healthcare, Buckinghamshire, UK). All experiments were performed at 25°C using TBS buffer (25 mM Tris-HCl, pH 7.4, 137 mM NaCl, 3 mM KCl). Recombinant NPM1 was expressed in *E. coli* and purified. The NPM1 obtained (1.84  $\mu$ M, 100  $\mu$ L) was immobilized onto the sensor chip NTA (GE Healthcare). The measurements were performed under conditions of 662 resonance units of the ligand and at a flow rate of 30  $\mu$ L/min. To determine the dissociation constants, we injected three different concentrations of TC11 and lenalidomide (Santa Cruz Biotechnology, Santa Cruz, CA). The injection periods for association and

dissociation were 60 and 300 s, respectively. The binding data were analyzed with 1:1 binding with the mass transfer model in the BIA evaluation software ver. 4.1 (Biacore).

### Statistical analysis

The significance of differences was determined using Student's *t*-test. The level of significance was specified as  $p < 0.05$ .

## Results

### TC11 inhibited the growth of MM cells with chromosomal abnormalities *in vitro*

We examined whether TC11 could inhibit the growth of four different MM cell lines harboring del 17p and/or t(4;14) in addition to previously reported KMS34 cells [13]. We also analyzed TC11's effect on the bone marrow cells obtained from three MM patients. In an MTT assay, TC11 inhibited the proliferation of the KMS11, KMS26, KMS28, and MUM24 cells as well as the proliferation of all of the bone marrow cells from the MM patients, in a dose-dependent manner (Fig. 1B). TC11 was effective both for high risk and standard risk myeloma cells. As shown in Fig. 1C, dexamethasone (Dex) potentiated TC11 anti-myeloma effect of TC11 in KMS 11 as well as KMS34 cells.

### Suppression of the growth of normal hematopoietic cells by TC11

To evaluate the effect of TC11 on normal hematopoiesis, we conducted a colony formation assay using bone marrow cells from ICR mice (Fig. 1D). 1–5  $\mu$ M of TC11 (IC<sub>50</sub> values of most MM cell lines were 3–5  $\mu$ M) did not suppress the production of the total colonies of normal hematopoietic cells. 25  $\mu$ M or higher concentrations of TC11 almost completely inhibited the colony formation. TC11 did not inhibit the production of colony-forming unit-granulocyte macrophage (CFU-GM), even though the number of burst-forming unit-erythroid (BFU-E) was decreased by the addition of a 5  $\mu$ M of TC11 ( $p < 0.05$ ) (Fig. 1D).

### TC11 inhibited the growth of MM cells in the xenograft mouse model through the induction of apoptosis *in vivo*

We evaluated the anti-myeloma effect of TC11 *in vivo* in the KMS34-bearing xenograft model. KMS34 tumor xenografts ( $\sim 50$  mm<sup>3</sup>) were treated with intraperitoneal injections of 20 mg/kg TC11 twice every 3 days for 2 wks, followed by a time-course analysis of the tumor volumes for 15 days. Fig. 2A shows that the tumor growth was significantly suppressed by the TC11 injections compared to the control ( $p < 0.01$ ). The average weight of the tumors of the TC11-treated mice on day 14 was 153.94 mg, whereas that of the control mice was 314.14 mg ( $p < 0.01$ ) (Fig. 2C). In addition, neither weight loss nor organ damage in lung, kidney or liver was observed macroscopically after the administration of TC11 (data not shown). Higher dose of TC11 (100 mg/kg) was injected to the xenograft model derived from another myeloma cell line, KMS11. As shown in Fig. 2D, TC11 significantly delayed the tumor growth. In one xenograft model, the tumor had almost disappeared after injection of TC11. During treatment of higher dose of TC11, significant body weight loss was not observed in TC11-treated mice.

The hematoxylin-eosin (H.E.) staining of KMS34 and KMS11-derived tumor tissues revealed elevated numbers of cells with aggregated chromatin in the TC11-treated mice compared to the untreated mice (Fig. 2B and 2E). Immunohistochemical analyses showed that cleaved PARP and cleaved caspase 3 were intensely stained in TC11-treated KMS11 tumors, especially in the cell death area (Fig. 2E). Ki-67 antigen, which is preferentially expressed during

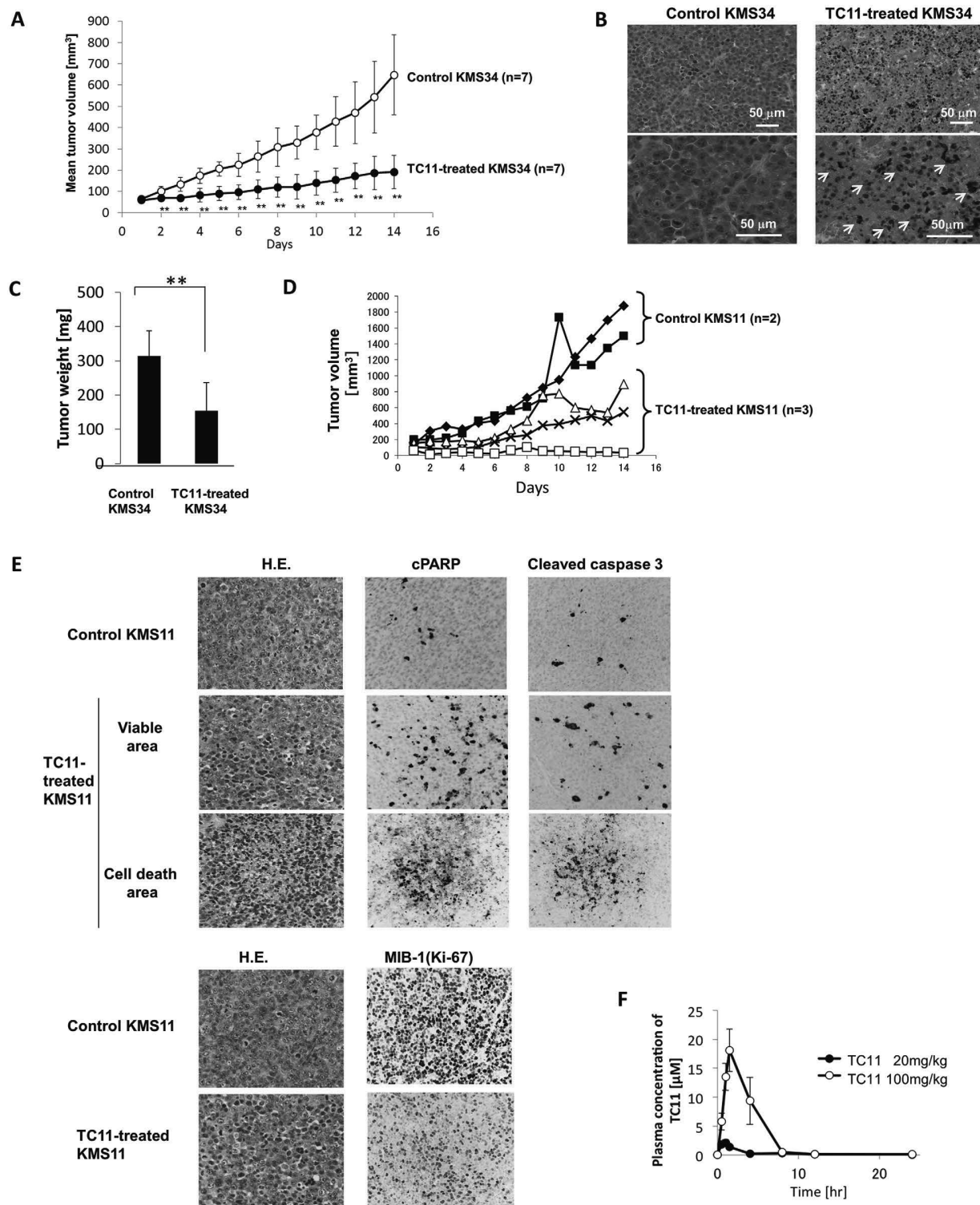


**Figure 2. *In vivo* growth inhibition of myeloma cells by intraperitoneal injections of TC11.** A total of  $3 \times 10^7$  KMS34 or KMS11 cells were inoculated subcutaneously into ICR/SCID mice. When the tumors reached  $50 \text{ mm}^3$  (day 0), TC11 (20 mg/kg or 100 mg/kg) or vehicle was administered intraperitoneally twice every 3 days for 2 wks. (A) Growth of KMS34-derived subcutaneous plasmacytomas was examined (n = 7). (B) Sections of dissected KMS34-derived tumors were stained with hematoxylin and eosin. The arrows indicate nuclear fragmentation of TC11-treated cells. (C) The weights of KMS34-derived tumors dissected from the KMS34-inoculated mice were measured on day 14. Bars: means  $\pm$ SD.  $^{**}p < 0.01$  (Students *t*-test). (D) Growth of KMS11-derived



subcutaneous plasmacytomas was examined. (E) Pathological examination of KMS11-derived tumors was shown. Immunohistochemical staining of the KMS11-derived tumors were also shown. (F) Pharmacokinetics of TC11. Plasma concentrations of TC11 in mice after a single injection of 20 mg/kg or 100 mg/kg of TC11 determined by HPLC.

doi:10.1371/journal.pone.0116135.g002

all active phases of the cell cycle but is absent in resting cells, was less weakly stained in TC11-treated tumors (Fig. 2E). These results suggested that TC11 exhibited anti-tumor activity *in vivo* through the inhibition of cell proliferation and the induction of apoptosis of myeloma cells.

### Pharmacokinetics of TC11 in the mouse model

For the pharmacokinetic study, we examined the plasma concentrations of TC11 in mice after a single injection of 20 mg/kg or 100 mg/kg of TC11 using HPLC (Fig. 2F). The maximum concentration ( $C_{max}$ ) was 2.1  $\mu$ M, which was observed at 1 hr after the injection ( $T_{max}$ ). The plasma concentration of TC11 gradually decreased to 0.25  $\mu$ M at 4 h and to 0.04  $\mu$ M at 24 h. The elimination half-life ( $T_{1/2}$ ) was estimated to be 1.2 h. When a higher dose of TC11 (100 mg/kg) was injected, the  $C_{max}$  was 18.1  $\mu$ M and the  $T_{max}$  was 1.5 h; the plasma concentration was 0.45  $\mu$ M at 8 h and 0.16  $\mu$ M at 24 h. The  $T_{1/2}$  was estimated to be 2.6 h.

### TC11 inhibited the differentiation of osteoclasts and bone resorption

The hyperactivity of osteoclasts is considered one of the causes of lytic bone lesions, suggesting that the control of osteoclast activity could be a key to treating bone lesions in MM patients. We therefore examined the effects of TC11 on the differentiation and function of osteoclasts using mouse bone marrow primary cell culture. We analyzed M-CSF and RANKL-treated osteoclasts by TRAP staining after treatment with various concentrations of TC11 (0.01  $\mu$ M–5  $\mu$ M) (Fig. 3A). The number of TRAP-positive multinuclear cells was significantly lower in the cells treated with more than 0.5  $\mu$ M of TC11 (Fig. 3B). In contrast, 10  $\mu$ M of thalidomide or 1 nM of bortezomib did not affect the number of TRAP-positive cells.

We next examined TC11's effect on the bone resorption activity of TC11 in a pit formation assay (Fig. 3C). After the treatment of RAW264.7 cells with TC11 (3  $\mu$ M, 5  $\mu$ M), the bone resorption area was reduced in a dose-dependent manner (Fig. 3D). Treatment with thalidomide (10  $\mu$ M) or bortezomib (1 nM) did not change the resorption area compared to the control.

### TC11 induced the fragmentation of $\alpha$ -tubulin

Because we previously found that TC11 binds to  $\alpha$ -tubulin, we examined the tubulin formation in KMS34 cells after TC11 treatment. The immunohistochemical analysis showed that TC11-treated cells exhibited elevated levels of  $\alpha$ -tubulin fragmentation (Fig. 4A). The percentage of cells with tubulin fragmentation was 6.5% in the cells treated with TC11, which is significantly higher compared to the 0.8% in the untreated cells (Fig. 4B).

### Binding between NPM and TC11 or lenalidomide

We previously identified NPM1 as one of the TC11-binding proteins, by mRNA display. In our previous observation, TC11 bound to the NH<sub>2</sub>-terminal 183-amino-acid (aa) region of monomeric NPM1. In the present study, we assessed the binding capacity of both TC11 and lenalidomide to the full length of NPM1. The SPR analysis showed that not only TC11 but also lenalidomide could bind to NPM1 (Fig. 5A,B). The  $K_D$  values of TC11 and lenalidomide were  $6.23 \times 10^{-8}$  M and  $7.66 \times 10^{-7}$  M, respectively.

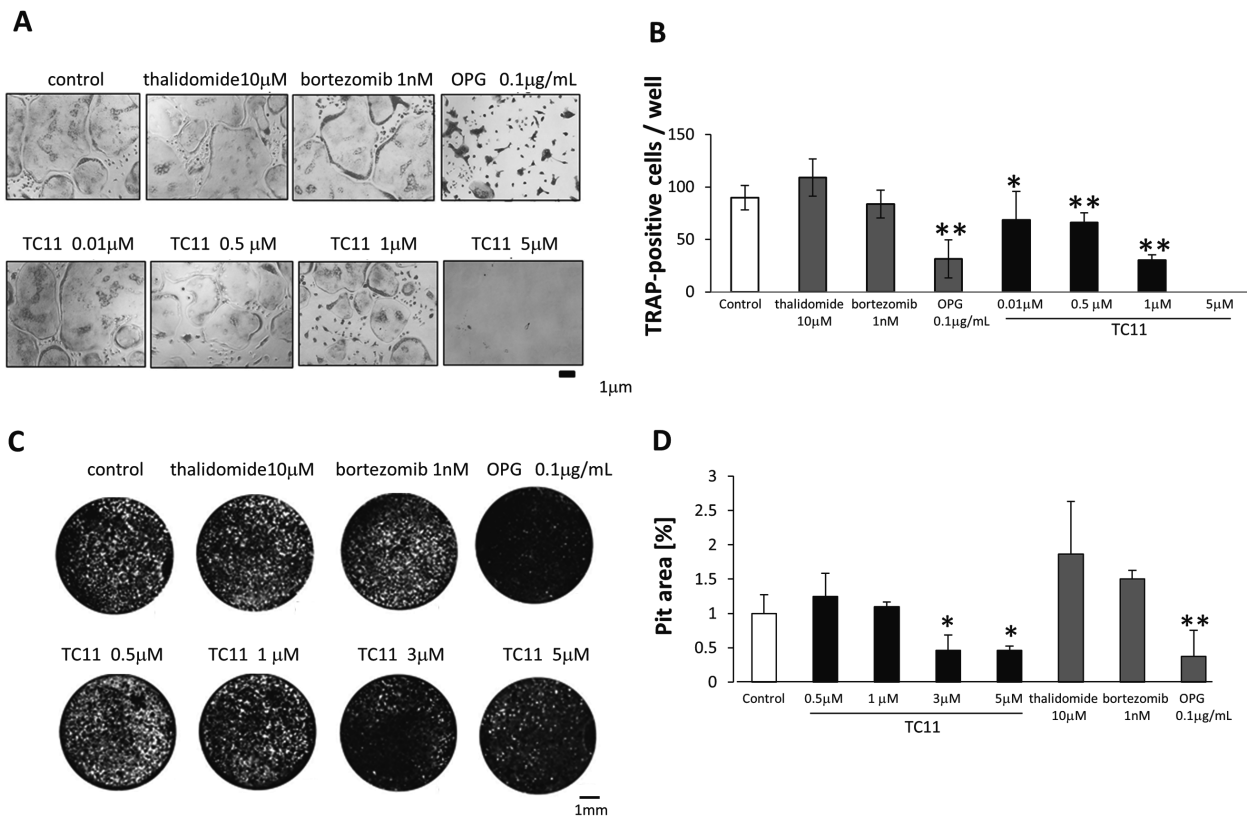


**Figure 3. TC11 inhibited both the maturation and function of bone marrow-derived osteoclasts.** Mice bone marrow cells were cultured with M-CSF (10 ng/mL) for 3 days, then further cultured with M-CSF (10 ng/mL) and RANKL (10 ng/mL). After an additional 3–6 days of culture with the indicated concentration of TC11, thalidomide, bortezomib, or DMSO, the cells were fixed and stained for TRAP as described in the [Materials and Methods](#) section. TRAP-positive multinucleated cells containing more than three nuclei were considered TRAP<sup>+</sup> multinuclear osteoclasts. (A) The number and size of TRAP<sup>+</sup> multinuclear osteoclasts were decreased by treatment with 0.5–1  $\mu$ M of TC11. (B) The number of TRAP<sup>+</sup> multinuclear osteoclasts in each well of a 96-well plate was counted. Bars: means  $\pm$  SD. \* $p$  < 0.05, \*\* $p$  < 0.01 (Student's *t*-test). (C) RAW 264.7 cells were incubated for 5–8 days with RANKL (10 ng/mL) and seeded on multi-test slides. The indicated concentrations of TC11, thalidomide, bortezomib, or OPG were added every 2 days for 7 days, followed by Von Kossa staining. The resorption pits were observed by fluorescence microscopy and the number of the pits was quantified using Image J software. (D) Bone resorption is indicated by white spots (pit). Bone resorption was suppressed by treatment with 3–5  $\mu$ M of TC11. (D) The pit area was measured by ImageJ software. The pit area of the DMSO-treated wells was used as the control (= 1). Data shown are representative of three independent experiments. Bars: means  $\pm$  SD. \* $p$  < 0.05, \*\* $p$  < 0.01 (Student's *t*-test)

doi:10.1371/journal.pone.0116135.g003

## Discussion

MM remains difficult to treat and cure, and MM patients with high-risk cytogenetic changes in particular have shown very poor prognosis when treated with existing drugs. To overcome this unmet clinical need, in previous work we screened phthalimide derivatives and identified TC11 as a novel candidate drug for MM. TC11 is different from other IMiDs in chemical structure, lacking glutarimide moiety. That is, TC11 is a phthalimide derivative containing a benzene ring instead of a glutarimide structure (Fig. 1A). In the present study, we observed that TC11 inhibited the growth of MM cell lines, even though some of the myeloma cells harbored high-risk chromosomal abnormalities such as del17, or t(4;14). In addition, growth inhibition of bone marrow cells obtained from the relapsed MM patients was also examined. TC11 more or less inhibited proliferation of myeloma cells obtained from all the patients. Patient #3 showed t(4;14), and patient #2 had extramedullary disease in the liver. Even though these two patients were high-risk cases, TC11 regulated proliferation of the tumor cells (Fig. 1B). Moreover, the growth of total colony-forming cells was not suppressed by the treatment with 1–5

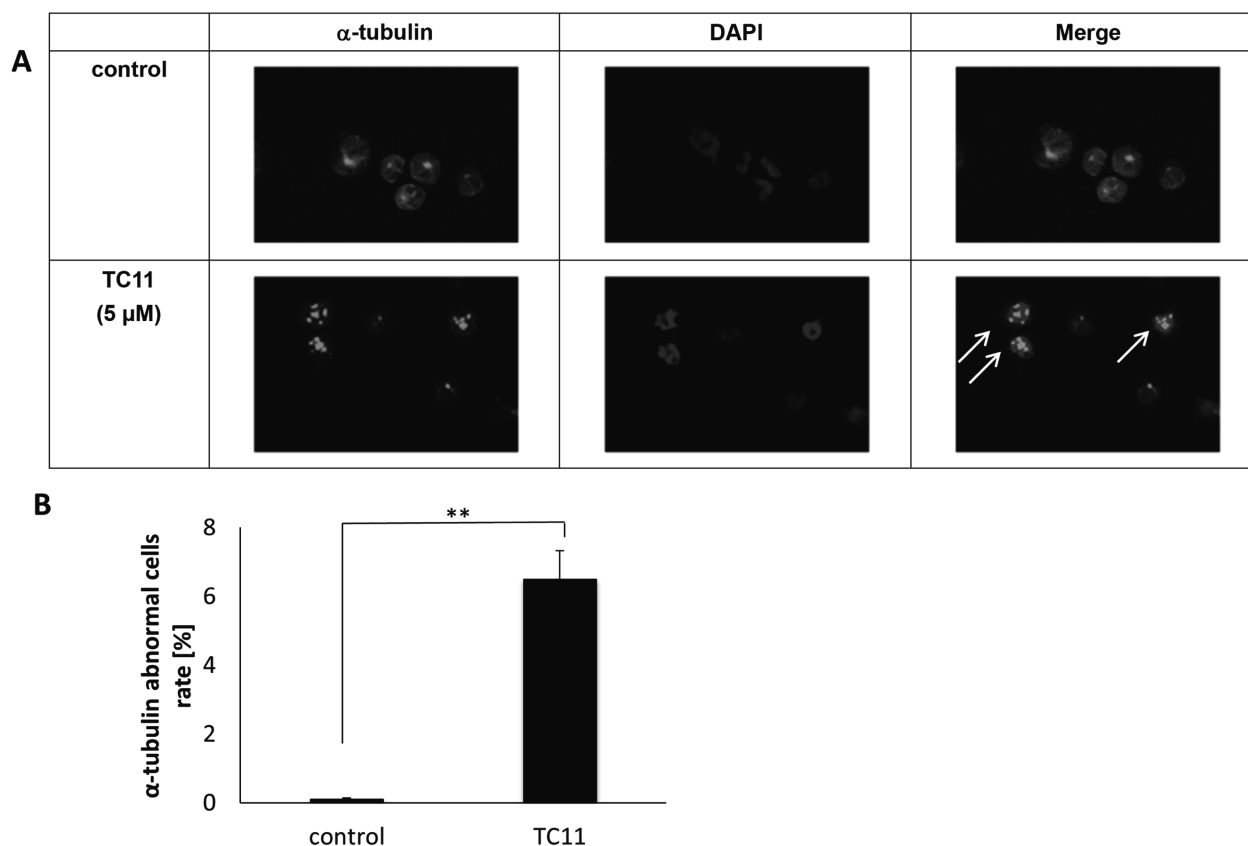


**Figure 4. TC11 altered the  $\alpha$ -tubulin formation of myeloma cells.** KMS34 was treated with 5 $\mu$ M TC11 for 4 hours and attached to a slide by cytospin. The sample was fixed and stained with antibody against  $\alpha$ -tubulin followed by FITC-conjugated anti-mouse IgG (green). Nucleus was stained with DAPI (blue). A, Representative mitotic cells with or without TC11 treatment. B, The percentage of cells with fragmented  $\alpha$ -tubulin in 2500 cells was calculated independently in 9 areas. \*\* $P < 0.01$  (Student *t*-test). A and B indicate representative data from 3 experiments.

doi:10.1371/journal.pone.0116135.g004

$\mu$ M of TC11 even though TC11 significantly inhibited the growth of all MM cell lines in such concentrations, suggesting low hematological toxicity. It is speculated that myeloma cells may proliferate more dependently on TC11-associated molecules such as NPM1. Further study is needed to discriminate the molecular function of TC11 on myeloma cells from that on normal hematopoietic cells.

We also confirmed an *in vivo* anti-myeloma effect of TC11 by using intraperitoneal injections of TC11 to KMS34 and KMS11-bearing ICR/SCID mice. The tumor growth in these mice was significantly delayed by the administration of 20 mg/kg or higher dose of TC11. The histopathological examination revealed apoptosis of MM cells, which is consistent with our previous study showing that TC11 induces apoptosis through the activation of caspase 3, 8 and 9 *in vitro* [13]. In addition, no systemic side effects including weight loss occurred.

Our pharmacokinetics study indicated that TC11 was completely eliminated from the plasma at 4 h after the injection of a low dose (20 mg/kg) of TC11 and at 8 h after the injection of a high dose (100 mg/kg) of TC11. These data suggest that TC11 would not accumulate in patients by the administration of TC11 twice at a 3-day interval. To obtain stronger anti-tumor effects, it might be necessary to develop a new drug-delivery system or change the schedule of drug administration.

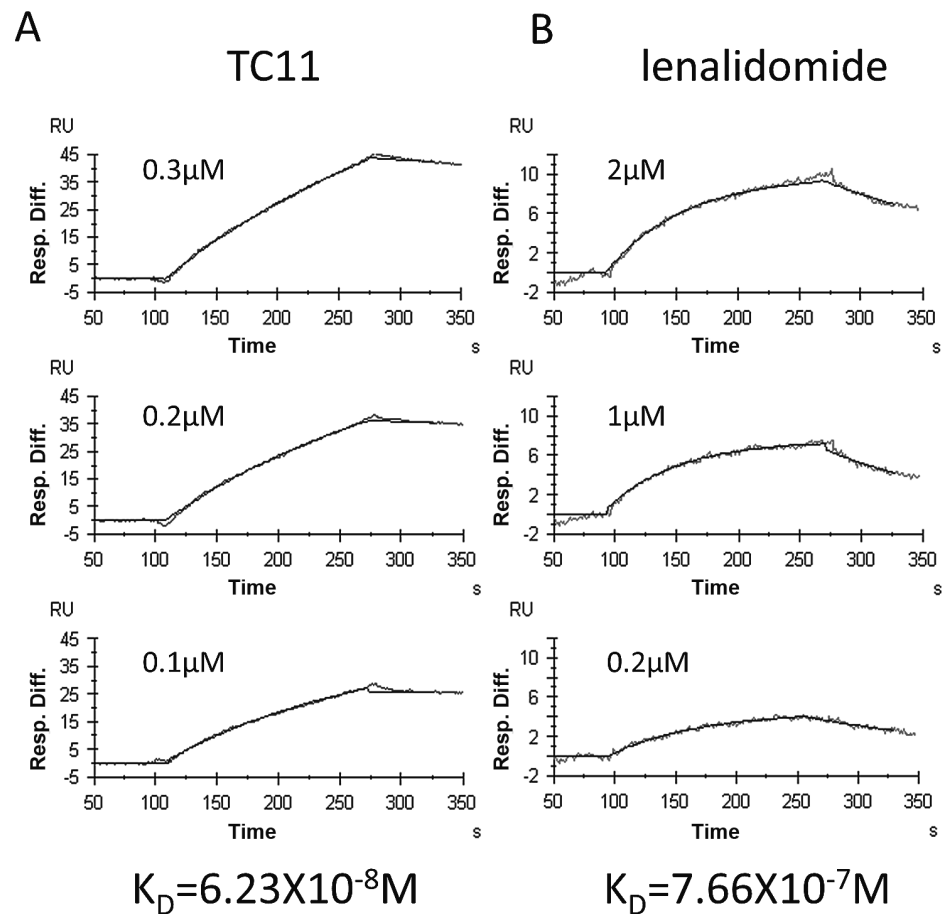


**Figure 5. NPM1 interacts with TC11 and lenalidomide.** Recombinant NPM1 was expressed in *E. coli* and purified. The NPM1 obtained was immobilized onto the sensor chip NTA followed by an SPR analysis. Panels A and B show representative biosensorgrams of TC11 and lenalidomide, respectively.

doi:10.1371/journal.pone.0116135.g005

Lytic bone disease in MM is thought to be associated with both enhanced activity of osteoclasts and impaired function of osteoblasts. It was reported that bortezomib could cause an increase in bone formation by activating osteoblastic function, which leads to the improvement of osteolytic lesions [21]. Here, we found that TC11 inhibited both the maturation and function of osteoclasts. Osteoclasts are differentiated from hematopoietic stem cells through stimulation with M-CSF and RANKL. Under normal conditions, the balance between bone formation and bone resorption is well-controlled.

However, MM cells produce macrophage inflammatory protein-1 (MIP-1), which stimulates osteoclasts to express receptor activator of nuclear factor- $\kappa$ B (RANK). RANK interacts with RANKL on stromal cells or osteoblasts. This interaction leads to the activation of nuclear factor-kappa B (NF- $\kappa$ B) and nuclear factor of activated T cell c1 (NFATc1) via an activation of AP-1 [22]. In our M-CSF and RANKL-stimulated mouse bone marrow model, we observed that the differentiation of osteoclasts was significantly suppressed by at least 0.5  $\mu$ M TC11. We also found that the function of osteoclasts was reduced by 3  $\mu$ M TC11. These anti-osteoclastic effects might be characteristic of TC11, because these effects were not seen in the cells treated with thalidomide nor bortezomib. We also found that this effect was not due simply to the induction of apoptosis of the bone marrow cells, but rather occurred by a direct inhibition of

osteoclast maturation, since apoptosis of osteoclasts was not observed after treatment with 3  $\mu$ M TC11 (data not shown). It would be worthwhile to investigate the effects of TC11 on the expression of osteoclast-related genes such as AP-1.

To clarify the mechanism of TC11's anti-myeloma effect, we investigated the effects of TC11 on NPM1, since we have found that NPM1 is one of the binding targets of TC11 by an mRNA display (i.e., the IVV method) [13]. In the present study, the results obtained by the SPR analysis indicated that TC11 binds to the full length of NPM1, with the  $K_D$  value of  $6.23 \times 10^{-8}$  M. However, the pharmacological significance of the binding of TC11 to NPM1 has not been elucidated.

NPM1 is a nuclear phosphoprotein which plays a variety of roles in cancer cells by affecting DNA repair, centrosome duplication, and molecular chaperoning [23–25]. NPM1 is also important in hematopoiesis by controlling the cell cycle of hematopoietic progenitor cells [26]. In addition, mutation of NPM1 is found in one-third of acute myelogenous leukemia (AML) patients, which changes the localization of NPM1 from the nucleus to the cytoplasm [27–29].

Little is known about the role of NPM1 in MM patients. To our knowledge, there is only one report on NPM and MM, showing an overexpression of NPM1 in hyperdiploid MM cells [30]. All of the MM cell lines we used in the present study expressed NPM1 proteins, but NPM1 gene mutation was not observed in these MM cell lines, and TC11 did not cause an accumulation of NPM1 in the cytoplasm of KMS34 as seen in leukemic cells (data not shown).

Another possibility explaining the role of NPM1 in TC11's effects is that TC11 blocks the oligomerization of NPM1, since the binding site of TC11 contains the oligomerization domain of NPM1. NPM1 normally exists in oligomer form [31]. Therefore, TC11 might affect myeloma cells by blocking the oligomerization of NPM1 and inhibiting its various functions. Qi et al. showed that the inhibition of the oligomerization of NPM1 by a small-molecule inhibitor, NSC348884, induces the apoptosis of cancer cells through the activation of p53 [32]. Balusu et al. reported that NSC348884 could induce the apoptosis of AML cell lines [33].

It is also possible that TC11 impairs centrosomal disruption by binding to NPM1, because NPM1 has been reported to be indispensable to normal centrosomal duplication [34]. The NPM1 gene is located on chromosome 5q35, which is occasionally deleted in myelodysplastic syndrome (5q<sup>−</sup>MDS) [35]. Considering our observation that lenalidomide could also bind to NPM1, the contribution of these interactions to the anti-tumor effects should be further investigated.

We then analyzed the effects of TC11 on  $\alpha$ -tubulin's structure, since we identified  $\alpha$ -tubulin as another TC11-binding protein using the IVV method in our previous work [13]. Alpha-tubulin is a component of microtubules that is important for cell division and cellular transport. Drugs that alter the formation of microtubules, such as vinca alkaloids, have been used in cancer therapy. However, the target sites and effects of these drugs on microtubules are different [36, 37]. In the case of TC11, we observed abnormal  $\alpha$ -tubulin fragmentation in TC11-treated KMS34 cells (Fig. 4), which suggests that the apoptosis induced by TC11 might be triggered by an abnormal formation of microtubules. In the previous report, knockdown of NPM1 gene induced centrosomal disruption followed by activation of caspase-9 and significant reduction in cell viability [12]. Therefore, it is speculated that the principal actions of TC11 on myeloma cells are centrosomal disruption and abnormal microtubule assembly by binding to NPM1 and  $\alpha$ -tubulin, respectively. Consequently, TC11-treated myeloma cells fall into mitotic catastrophe because NPM1 and tubulin families are key molecules for cell division. After these series of actions initiated by TC11-treatment, those cells caused apoptosis. As a next step to clarify exact signaling pathway after binding of TC11 to NPM1, we are trying to knock-down of NPM1 gene in myeloma cells and examine the effects of TC11 on oligomerization and phosphorylation of NPM1 in myeloma cells.

Cereblon (CRBN: cerebral protein with ion protease), a component of the E3 ubiquitin ligase complex, has been identified as a target of thalidomide-mediated teratogenicity [38, 39]. It was shown that not only thalidomide but also lenalidomide and pomalidomide bind to CRBN, attenuating the proliferation of myeloma cells through several pathways such as the down-regulation of autoubiquitination of CRBN [40–41]. However, our experiments using the IVV method failed to screen CRBN as a TC11-binding protein. The difference might be explained by the structure of TC11, because CRBN was reported to bind to a glutarimide moiety of lenalidomide or pomalidomide, which was not included in TC11. On the other hand, NPM1 may bind to the phthalimide moiety which is a common component of TC11 and other IMiDs, since our data showed both TC11 and lenalidomide could bind to NPM1.

Thus, TC11 exerts its anti-myeloma effect via molecular interactions which do not involve CRBN. In addition, TC11 does not form racemate and is expected to lack teratogenicity. The results of our present study suggest that new phthalimide derivatives other than thalidomide, lenalidomide and pomalidomide could be developed by drug designing for the treatment of MM.

In conclusion, we have demonstrated that TC11, a novel phthalimide derivative, has anti-tumor activity against MM cells with high-risk genetic abnormality including del 17p and t (4;14), *in vitro* and *in vivo*. This novel compound also down-regulates the differentiation and function of osteoclasts. Our data provide a strong preclinical rationale for TC11 as a safe and effective drug for the treatment of high-risk MM patients with bone disease. The actions of this drug relating to  $\alpha$ -tubulin and NPM1 remain to be further investigated.

## Acknowledgments

We thank Dr. Takemi Otsuki for gift of multiple myeloma cell lines.

## Author Contributions

Conceived and designed the experiments: HY TO KM TY Y. Hattori. Performed the experiments: YO Y. Hasegawa FT NT HY TO WD TY MH Y. Hattori. Analyzed the data: MM YO Y. Hasegawa FT NT HS HY TO KM WD TY DI Y. Hattori. Wrote the paper: MM HY TO KM DI Y. Hattori.

## References

1. Rajkumar SV (2013) Multiple myeloma: 2013 update on diagnosis, risk-stratification, and management. *Am J Hematol.* 88(3): 226–235. doi: [10.1002/ajh.23390](https://doi.org/10.1002/ajh.23390)
2. Bird JM, Owen RG, D'Sa S, Snowden JA, Pratt G, et al. (2011) Guidelines for the diagnosis and management of multiple myeloma 2011. *Br J Haematol.* 154(1): 32–75. doi: [10.1111/j.1365-2141.2011.08573.x](https://doi.org/10.1111/j.1365-2141.2011.08573.x) PMID: [21569004](https://pubmed.ncbi.nlm.nih.gov/21569004/)
3. Terpos E, Kanellias N, Christoulas D, Kastritis E, Dimopoulos MA (2013) Pomalidomide: a novel drug to treat relapsed and refractory multiple myeloma. *Onco Targets Ther.* 6: 531–538. doi: [10.2147/OTT.S34498](https://doi.org/10.2147/OTT.S34498) PMID: [23690693](https://pubmed.ncbi.nlm.nih.gov/23690693/)
4. McCurdy AR, Lacy MQ (2013) Pomalidomide and its clinical potential for relapsed or refractory multiple myeloma: an update for the hematologist. *Ther Adv Hematol.* 4(3): 211–216. doi: [10.1177/2040620713480155](https://doi.org/10.1177/2040620713480155) PMID: [23730498](https://pubmed.ncbi.nlm.nih.gov/23730498/)
5. Siegel DS (2012) Relapsed/Refractory multiple myeloma: defining refractory disease and identifying strategies to overcome resistance. *Semin Hematol.* 49 Suppl 1: S3–15. doi: [10.1053/j.seminhematol.2012.05.005](https://doi.org/10.1053/j.seminhematol.2012.05.005) PMID: [22727390](https://pubmed.ncbi.nlm.nih.gov/22727390/)
6. Lacy MQ (2011) New immunomodulatory drugs in myeloma. *Curr Hematol Malig Rep.* 6(2): 120–125. doi: [10.1007/s11899-011-0077-y](https://doi.org/10.1007/s11899-011-0077-y) PMID: [21327565](https://pubmed.ncbi.nlm.nih.gov/21327565/)
7. Pan B, Lentzsch S (2012) The application and biology of immunomodulatory drugs (IMiDs) in cancer. *Pharmacol Ther.* 136(1): 56–68. doi: [10.1016/j.pharmthera.2012.07.004](https://doi.org/10.1016/j.pharmthera.2012.07.004) PMID: [22796518](https://pubmed.ncbi.nlm.nih.gov/22796518/)

8. Bergsagel PL, Mateos MV, Gutierrez NC, Rajkumar SV, San Miguel JF (2013) Improving overall survival and overcoming adverse prognosis in the treatment of cytogenetically high-risk multiple myeloma. *Blood*. 121(6): 884–892. doi: [10.1182/blood-2012-05-432203](https://doi.org/10.1182/blood-2012-05-432203) PMID: [23165477](https://pubmed.ncbi.nlm.nih.gov/23165477/)
9. Avet-Loiseau H, Attal M, Campion L, Caillot D, Hulin C, et al. (2012) Long-term analysis of the IFM 99 trials for myeloma: cytogenetic abnormalities [t(4;14), del(17p), 1q gains] play a major role in defining long-term survival. *J Clin Oncol*. 30(16): 1949–1952. doi: [10.1200/JCO.2011.36.5726](https://doi.org/10.1200/JCO.2011.36.5726) PMID: [22547600](https://pubmed.ncbi.nlm.nih.gov/22547600/)
10. Sawyer JR (2011) The prognostic significance of cytogenetics and molecular profiling in multiple myeloma. *Cancer Genet*. 204(1): 3–12. doi: [10.1016/j.cancergencyto.2010.11.002](https://doi.org/10.1016/j.cancergencyto.2010.11.002) PMID: [21356186](https://pubmed.ncbi.nlm.nih.gov/21356186/)
11. Mateos MV, Gutierrez NC, Martin-Ramos ML, Paiva B, Montalban MA, et al. (2011) Outcome according to cytogenetic abnormalities and DNA ploidy in myeloma patients receiving short induction with weekly bortezomib followed by maintenance. *Blood*. 118(17): 4547–4553. doi: [10.1182/blood-2011-04-345801](https://doi.org/10.1182/blood-2011-04-345801) PMID: [21900193](https://pubmed.ncbi.nlm.nih.gov/21900193/)
12. Chang H, Jiang A, Qi C, Trieu Y, Chen C, et al. (2010) Impact of genomic aberrations including chromosome 1 abnormalities on the outcome of patients with relapsed or refractory multiple myeloma treated with lenalidomide and dexamethasone. *Leuk Lymphoma*. 51(11):2084–2091. doi: [10.3109/10428194.2010.524325](https://doi.org/10.3109/10428194.2010.524325) PMID: [20929319](https://pubmed.ncbi.nlm.nih.gov/20929319/)
13. Shiheido H, Terada F, Tabata N, Hayakawa I, Matsumura N, et al. (2012) A phthalimide derivative that inhibits centrosomal clustering is effective on multiple myeloma. *PLoS One*. 7(6):e38878. doi: [10.1371/journal.pone.0038878](https://doi.org/10.1371/journal.pone.0038878) PMID: [22761710](https://pubmed.ncbi.nlm.nih.gov/22761710/)
14. Chesi M, Bergsagel PL (2013) Molecular pathogenesis of multiple myeloma: basic and clinical updates. *Int J Hematol*. 97(3): 313–323. doi: [10.1007/s12185-013-1291-2](https://doi.org/10.1007/s12185-013-1291-2) PMID: [23456262](https://pubmed.ncbi.nlm.nih.gov/23456262/)
15. Modi ND, Lentzsch S (2012) Bisphosphonates as antimyeloma drugs. *Leukemia*. 26(4): 589–594. doi: [10.1038/leu.2011.282](https://doi.org/10.1038/leu.2011.282) PMID: [22005788](https://pubmed.ncbi.nlm.nih.gov/22005788/)
16. Raje N, Roodman GD (2011) Advances in the biology and treatment of bone disease in multiple myeloma. *Clin Cancer Res*. 17(6):1278–1286. doi: [10.1158/1078-0432.CCR-10-1804](https://doi.org/10.1158/1078-0432.CCR-10-1804) PMID: [21411443](https://pubmed.ncbi.nlm.nih.gov/21411443/)
17. Namba M, Ohtsuki T, Mori M, Togawa A, Wada H, et al. (1989) Establishment of five human myeloma cell lines. *In Vitro Cell Dev Biol*. 25(8): 723–729. doi: [10.1007/BF02623725](https://doi.org/10.1007/BF02623725) PMID: [2768132](https://pubmed.ncbi.nlm.nih.gov/2768132/)
18. Du W, Hattori Y, Yamada T, Matsumoto K, Nakamura T, et al. (2007) NK4, an antagonist of hepatocyte growth factor (HGF), inhibits growth of multiple myeloma cells: molecular targeting of angiogenic growth factor. *Blood*. 109(7): 3042–3049. PMID: [17179234](https://pubmed.ncbi.nlm.nih.gov/17179234/)
19. Hattori Y, Du W, Yamada T, Ichikawa D, Matsunami S, et al. (2013) A myeloma cell line established from a patient refractory to thalidomide therapy revealed high-risk cytogenetic abnormalities and produced vascular endothelial growth factor. *Blood Cancer J*. 3:e115. doi: [10.1038/bcj.2013.13](https://doi.org/10.1038/bcj.2013.13) PMID: [23686003](https://pubmed.ncbi.nlm.nih.gov/23686003/)
20. Oikawa T, Oyama M, Kozuka-Hata H, Uehara S, Udagawa N, et al. (2012) Tks5-dependent formation of circumferential podosomes/invadopodia mediates cell-cell fusion. *J Cell Biol*. 197(4): 553–568. doi: [10.1083/jcb.201111116](https://doi.org/10.1083/jcb.201111116) PMID: [22584907](https://pubmed.ncbi.nlm.nih.gov/22584907/)
21. Zangari M, Terpos E, Zhan F, Tricot G (2012) Impact of bortezomib on bone health in myeloma: a review of current evidence. *Cancer Treat Rev*. 38(8):968–980. doi: [10.1016/j.ctrv.2011.12.007](https://doi.org/10.1016/j.ctrv.2011.12.007) PMID: [22226939](https://pubmed.ncbi.nlm.nih.gov/22226939/)
22. Matsuo K, Galson DL, Zhao C, Peng L, Laplace C, et al. (2004) Nuclear factor of activated T-cells (NFAT) rescues osteoclastogenesis in precursors lacking c-Fos. *J Biol Chem*. 279(25): 26475–26480. doi: [10.1074/jbc.M313973200](https://doi.org/10.1074/jbc.M313973200) PMID: [15073183](https://pubmed.ncbi.nlm.nih.gov/15073183/)
23. Lindstrom MS (2011) NPM1/B23: A Multifunctional Chaperone in Ribosome Biogenesis and Chromatin Remodeling. *Biochem Res Int*:195–209.
24. Colombo E, Alcalay M, Pelicci PG (2011) Nucleophosmin and its complex network: a possible therapeutic target in hematological diseases. *Oncogene*. 30(23): 2595–2609. doi: [10.1038/onc.2010.646](https://doi.org/10.1038/onc.2010.646) PMID: [21278791](https://pubmed.ncbi.nlm.nih.gov/21278791/)
25. Grisendi S, Mecucci C, Falini B, Pandolfi PP (2006) Nucleophosmin and cancer. *Nat Rev Cancer*. 6(7): 493–505. doi: [10.1038/nrc1885](https://doi.org/10.1038/nrc1885) PMID: [16794633](https://pubmed.ncbi.nlm.nih.gov/16794633/)
26. Li J, Sejas DP, Rani R, Koretsky T, Bagby GC, et al. (2006) Nucleophosmin regulates cell cycle progression and stress response in hematopoietic stem/progenitor cells. *J Biol Chem*. 281(24):16536–16545. doi: [10.1074/jbc.M601386200](https://doi.org/10.1074/jbc.M601386200) PMID: [16608843](https://pubmed.ncbi.nlm.nih.gov/16608843/)
27. Estey EH (2013) Acute myeloid leukemia: 2013 update on risk-stratification and management. *Am J Hematol*. 88(4): 318–327. doi: [10.1002/ajh.23404](https://doi.org/10.1002/ajh.23404) PMID: [23526416](https://pubmed.ncbi.nlm.nih.gov/23526416/)
28. Falini B, Gionfriddo I, Cecchetti F, Ballanti S, Pettrossi V, et al. (2011) Acute myeloid leukemia with mutated nucleophosmin (NPM1): any hope for a targeted therapy? *Blood Rev*. 25(6):247–254. doi: [10.1016/j.blre.2011.06.001](https://doi.org/10.1016/j.blre.2011.06.001) PMID: [21724308](https://pubmed.ncbi.nlm.nih.gov/21724308/)



29. Falini B, Bolli N, Liso A, Martelli MP, Mannucci R, et al. (2009) Altered nucleophosmin transport in acute myeloid leukaemia with mutated NPM1: molecular basis and clinical implications. *Leukemia*. 23(10): 1731–1743. doi: [10.1038/leu.2009.124](https://doi.org/10.1038/leu.2009.124) PMID: [19516275](https://pubmed.ncbi.nlm.nih.gov/19516275/)
30. Weinhold N, Moreaux J, Raab MS, Hose D, Hielscher T, et al. (2010) NPM1 is overexpressed in hyperdiploid multiple myeloma due to a gain of chromosome 5 but is not delocalized to the cytoplasm. *Genes Chromosomes Cancer*. 49(4): 333–341. PMID: [20073075](https://pubmed.ncbi.nlm.nih.gov/20073075/)
31. Lee HH, Kim HS, Kang JY, Lee BI, Ha JY, et al. (2007) Crystal structure of human nucleophosmin-core reveals plasticity of the pentamer-pentamer interface. *Proteins*. 69(3): 672–678. doi: [10.1002/prot.21504](https://doi.org/10.1002/prot.21504) PMID: [17879352](https://pubmed.ncbi.nlm.nih.gov/17879352/)
32. Qi W, Shakalya K, Stejskal A, Goldman A, Beeck S, et al. (2008) NSC348884, a nucleophosmin inhibitor disrupts oligomer formation and induces apoptosis in human cancer cells. *Oncogene*. 27(30): 4210–4220. doi: [10.1038/onc.2008.54](https://doi.org/10.1038/onc.2008.54) PMID: [18345031](https://pubmed.ncbi.nlm.nih.gov/18345031/)
33. Balusu R, Fiskus W, Rao R, Chong DG, Nalluri S, et al. (2011) Targeting levels or oligomerization of nucleophosmin 1 induces differentiation and loss of survival of human AML cells with mutant NPM1. *Blood*. 118(11): 3096–3106. doi: [10.1182/blood-2010-09-309674](https://doi.org/10.1182/blood-2010-09-309674) PMID: [21719597](https://pubmed.ncbi.nlm.nih.gov/21719597/)
34. Okuda M, Horn HF, Tarapore P, Tokuyama Y, Smulian AG, et al. (2000) Nucleophosmin/B23 is a target of CDK2/cyclin E in centrosome duplication. *Cell*. 103(1): 127–140. doi: [10.1016/S0092-8674\(00\)00093-3](https://doi.org/10.1016/S0092-8674(00)00093-3) PMID: [11051553](https://pubmed.ncbi.nlm.nih.gov/11051553/)
35. Ebert BL (2011) Molecular dissection of the 5q deletion in myelodysplastic syndrome. *Semin Oncol*. 38(5): 621–626. doi: [10.1053/j.seminoncol.2011.04.010](https://doi.org/10.1053/j.seminoncol.2011.04.010) PMID: [21943668](https://pubmed.ncbi.nlm.nih.gov/21943668/)
36. Spagnuolo PA, Hu J, Hurren R, Wang X, Gronda M, et al. (2010) The antihelminthic flubendazole inhibits microtubule function through a mechanism distinct from Vinca alkaloids and displays preclinical activity in leukemia and myeloma. *Blood*. 115(23):4824–4833. doi: [10.1182/blood-2009-09-243055](https://doi.org/10.1182/blood-2009-09-243055) PMID: [20348394](https://pubmed.ncbi.nlm.nih.gov/20348394/)
37. Perez EA (2009) Microtubule inhibitors: Differentiating tubulin-inhibiting agents based on mechanisms of action, clinical activity, and resistance. *Mol Cancer Ther*. 8(8): 2086–2095. doi: [10.1158/1535-7163.MCT-09-0366](https://doi.org/10.1158/1535-7163.MCT-09-0366) PMID: [19671735](https://pubmed.ncbi.nlm.nih.gov/19671735/)
38. Ito T, Ando H, Handa H (2011) Teratogenic effects of thalidomide: molecular mechanisms. *Cell Mol Life Sci*. 68(9):1569–1579. doi: [10.1007/s00018-010-0619-9](https://doi.org/10.1007/s00018-010-0619-9) PMID: [21207098](https://pubmed.ncbi.nlm.nih.gov/21207098/)
39. Ito T, Ando H, Suzuki T, Ogura T, Hotta K, et al. (2010) Identification of a primary target of thalidomide teratogenicity. *Science*. 327(5971):1345–1350. doi: [10.1126/science.1177319](https://doi.org/10.1126/science.1177319) PMID: [20223979](https://pubmed.ncbi.nlm.nih.gov/20223979/)
40. Lopez-Girona A, Mendy D, Ito T, Miller K, Gandhi AK, et al. (2012) Cereblon is a direct protein target for immunomodulatory and antiproliferative activities of lenalidomide and pomalidomide. *Leukemia*. 26(11):2326–2335. doi: [10.1038/leu.2012.119](https://doi.org/10.1038/leu.2012.119) PMID: [22552008](https://pubmed.ncbi.nlm.nih.gov/22552008/)
41. Zhu YX, Braggio E, Shi CX, Bruins LA, Schmidt JE, et al. (2011) Cereblon expression is required for the antimyeloma activity of lenalidomide and pomalidomide. *Blood*. 118(18):4771–4779. doi: [10.1182/blood-2011-05-356063](https://doi.org/10.1182/blood-2011-05-356063) PMID: [21860026](https://pubmed.ncbi.nlm.nih.gov/21860026/)



Original Article

## Pilot Analysis of Asbestos-induced Diffuse Pleural Thickening with Respiratory Compromise

Daisuke Nojima<sup>a,f</sup>, Nobukazu Fujimoto<sup>b\*</sup>, Katsuya Kato<sup>c</sup>, Yasuko Fuchimoto<sup>d</sup>,  
Katsuyuki Kiura<sup>e</sup>, Takumi Kishimoto<sup>f</sup>, and Mitsune Tanimoto<sup>a</sup>

<sup>a</sup>Department of Hematology, Oncology and Respiratory Medicine, Okayama University Graduate School of Medicine, Dentistry and Pharmaceutical Sciences, Departments of <sup>c</sup>Radiology and <sup>e</sup>Allergy and Respiratory Medicine (Thoracic Oncology), Okayama University Hospital, Okayama 700-8558, Japan, Department of <sup>b</sup>Medical Oncology, <sup>d</sup>Respiratory Medicine, and <sup>f</sup>Internal Medicine, Okayama Rosai Hospital, Okayama 702-8055, Japan

We investigated the clinical features of asbestos-induced diffuse pleural thickening (DPT) with severe respiratory compromise. We conducted a retrospective study of consecutive subjects with asbestos-induced DPT. Medical data such as initial symptoms, radiological findings, respiratory function test results, and clinical course were collected and analyzed. There were 24 patients between 2003 and 2012. All were men, and the median age at the development of DPT was 74 years. The top occupational category associated with asbestos exposure was dockyard workers. The median duration of asbestos exposure was 35.0 years, and the median latency from first exposure to the onset of DPT was 49.0 years. There were no significant differences in respiratory function test results between the higher and lower Brinkman index groups or between unilateral and bilateral DPT. Thirteen patients had a history of benign asbestos pleural effusion (BAPE), and the median duration from pleural fluid accumulation to DPT with severe respiratory compromise was 28.4 months. DPT with severe respiratory compromise can develop after a long latency following occupational asbestos exposure and a history of BAPE.

**Key words:** asbestos, pleural thickening, MRC dyspnea scale, respiratory function test, costophrenic angle

Asbestos-related health problems remain a major public health concern. Asbestos-related pleural diseases include malignant pleural mesothelioma (MPM), benign asbestos pleural effusion (BAPE), and diffuse pleural thickening (DPT) [1]; cases of these diseases will continue to be seen in the next several decades due to past industrial asbestos use. Asbestos-induced DPT is considered to be a consequence of asbestos-induced inflammation of the visceral pleura, which leads to adhesion to the parietal pleura.

However, the actual pathogenesis is still unknown and the radiological definition of DPT is ambiguous. McLoud *et al.* described DPT on chest X-rays as a smooth, uninterrupted pleural density extending over at least one-quarter of the chest wall, with or without involvement of the costophrenic angle (CPA) [2]. Yates *et al.* also proposed a definition of DPT based on dimensional criteria, in which DPT is characterized by pleural thickening of  $\geq 5$  mm that extends over more than one-quarter of the chest wall, with or without obliteration of the CPA [3].

Received January 29, 2015; accepted April 20, 2015.

\*Corresponding author. Phone: +81-86-262-0131; Fax: +81-86-262-3391  
E-mail: nobufujimot@gmail.com (N. Fujimoto)

Conflict of Interest Disclosures: No potential conflict of interest relevant to this article was reported.

Several studies have examined the characteristics of DPT [2, 4–7]. A major limitation of these earlier studies is that their definitions of DPT varied; as such, some studies may have included patients with pleural plaques, BAPE, and MPM, mainly due to the difficulty of confirming a diagnosis of DPT based on chest X-ray without computed tomography (CT) images.

DPT often induces significant impairment of lung function [8]. In Japan, patients with DPT are provided worker's compensation or given financial relief by the Act on Asbestos Health Damage Relief if they present severe respiratory compromise. We recently retrospectively analyzed the clinical features and radiological findings of DPT, and we reported that some of the radiological findings, such as the involvement of CPA and pleural thickness and the craniocaudal and horizontal extension of pleural thickening (as determined by chest CT) were correlated with impaired respiratory function in patients with DPT [9]. There are few reports concerning the features of DPT in patients with severe respiratory compromise, however.

The objectives of the present retrospective analysis, which was conducted in a single region of Japan, were to clarify the clinical features of DPT patients with severe respiratory compromise, including the clinical course. We focused on the association between BAPE and DPT. We also investigated clinical issues associated with the diagnosis, evaluation, and handling of compensation for DPT.

## Materials and Methods

**Subjects.** The consecutive subjects diagnosed as having asbestos-induced DPT in Okayama Rosai Hospital (Okayama, Japan) between 2003 and 2012 were identified. The inclusion criteria were a history of occupational asbestos exposure, pleural thickening > 5mm on chest X-ray extending for more than one-half of the lateral thoracic wall (LTW) in patients with unilateral DPT or more than one-quarter of the LTW in patients with bilateral DPT, and impaired respiratory function (defined below). The subjects had to have been followed up for at least 6 months after the diagnosis of DPT. Medical data from these patients were collected and analyzed retrospectively. The medical information included age, gender, initial symptoms, modified Medical Research Council (mMRC)

dyspnea grade, smoking history, radiological findings, respiratory function test results, and the clinical course. Former smoker was defined as those quit smoking for more than 6 months. Information about the history of asbestos exposure was also collected. In some patients who changed to local hospitals or clinics, we made inquiries about their information at outcome at the relevant medical institutions.

This study was done according to Ethical Guidelines for Epidemiological Research issued by the Japanese Ministry of Education, Culture, Sports, Science and Technology and the Japanese Ministry of Health, Labour and Welfare. This study was approved by the ethics committee of the Japan Labour Health and Welfare Organization and the institutional review board of Okayama Rosai Hospital.

**Respiratory function test.** Respiratory function tests were performed in clinical settings based on the guidelines set forth in the Official Statement of the American Thoracic Society [10]. The data obtained included the percentage of vital capacity (%VC) and the forced expiratory volume percentage in 1 sec (FEV1). Blood gas data such as PaO<sub>2</sub> (the partial pressure of O<sub>2</sub> in arterial blood) and PaCO<sub>2</sub> (the partial pressure of carbon dioxide in arterial blood) were also extracted. The data obtained closest in time to when the chest CT was performed were used for the analyses. Impaired respiratory function was defined as (1) %VC < 60% or (2) %VC 60–80%, FEV1 ≤ 70%, and FEV1/forced vital capacity (FVC) < 50% or PaO<sub>2</sub> on arterial blood gas test ≤ 60 Torr.

**Statistical analysis.** Comparisons between groups were performed using a nonparametric analysis with the Wilcoxon rank-sum test. The latency period of DPT was calculated as the time between the first exposure to asbestos and the onset of DPT. In the patients with a history of BAPE, the period from the detection of pleural effusion to the onset of DPT and the development of severe respiratory impairment were calculated. Correlations were examined in a regression analysis. The software package used for the statistical analyses was JMP 10.0.2 (SAS Institute, Cary, NC, USA).

## Results

**Patient characteristics.** A total of 24 patients were analyzed retrospectively. The patients' demo-

graphic details are listed in Table 1. All of the patients were men, and the median age at the diagnosis of DPT was 74 years. More than 90% of the patients smoked, and the Brinkman index was  $\geq 600$  in 14 (58.3%) of the patients. Fifteen patients had visited a clinic or a hospital with symptoms, 5 had an abnormal shadow on a chest X-ray at a medical checkup, and 4 were diagnosed with DPT while receiving medical treatment for other diseases. The mMRC dyspnea grade at the diagnosis of DPT was 1 in 3 patients, 2 in 15 patients, 3 in 3 patients, and 4 in 3 patients.

#### **Occupational asbestos exposure history.**

Occupational categories associated with asbestos exposure are listed in Table 2 and included dockyard, construction, and heating trade work and more. The median (range) duration of asbestos exposure was 35.0 (3.0–50.0) years. The median (range) latency period since the first exposure to the onset of DPT was 49.0 (37.0–64.0) years.

**Radiological findings.** Unilateral DPT was found in the thorax in 6 cases and bilateral DPT was found in 18 cases at the time of diagnosis. In the 6 cases with unilateral DPT, DPT was found in the right thorax in 4 cases and in the left thorax in 2 cases. Radiographic findings associated with DPT are listed in Table 3. All of the cases showed CPA involvement on chest X-ray. Pleural plaques were detected in most of the patients. Pulmonary asbestosis was diagnosed in 3 (12.5%) cases, and the profusion rate according to the International Labour Organization criteria [11] was 1 in 2 cases and 3 in one case. Rounded atelectasis was detected in 18 (75.0%) cases on chest CT. Crow's feet signs, defined as fibrous strands with accompanying circumscribed pleural thickening, was detected in all cases on chest CT.

**Respiratory function test.** The median (range) value of %VC was 51.4% (31.2–70.7%); the %VC was  $< 60\%$  in 22 (91.7%) patients. The median (range) value for FEV1 was 82.9% (47.7–100%). Eighteen (75.0%) patients showed restrictive ventilatory impairment, and 6 (25.0%) showed combined restrictive and obstructive ventilatory impairment. Blood gas data were available in 23 cases, and the median (range) values for PaO<sub>2</sub> and PaCO<sub>2</sub> were 78.9 (53–86) Torr and 43.3 (35.8–56.5) Torr, respectively.

We then examined the association between respira-

**Table 1** Demographics of the study population ( $n = 24$ )

Characteristics	No. of patients (%)
Median age (range)	74 (63–92) years
Gender	Male 24 (100.0%)
Smoking	Never 6 (25.0%)
	Former 16 (66.7%)
	Present 2 (8.3%)
Initial symptom	Cough 14 (56.0%)
	Chest pain 3 (12.0%)
	Sputum 1 (4.0%)
mMRC* grade	0/1/2/3/4 0/3/15/3/3

\*modified Medical Research Council.

**Table 2** Occupational category of asbestos exposure ( $n = 24$ )

Occupation	No. of patients
Dockyards	7
Construction	4
Heating trade	3
Demolition work	2
Asbestos product industry	2
Furnace installation	1
Electric work	1
Painting	1
Plumbing	1
Welding	1
Shipman	1

**Table 3** Radiographic findings associated with DPT

Findings	No. of patients (%)
Asbestosis	3 (12.5%)
Pleural plaques (X-ray)	14 (58.3%)
Pleural plaque (CT*)	22 (91.7%)
Rounded atelectasis	18 (75.0%)
Crow's feet sign	24 (100.0%)
Costophrenic angle involvement	24 (100.0%)

\*Computed tomography. DPT: diffuse pleural thickening.

tory function and smoking history. First, we compared %VC and FEV1 between lower ( $< 600$ ) and higher ( $\geq 600$ ) Brinkman index groups ( $n = 10$  and 14, respectively). Never-smokers were included in lower Brinkman index group. The median values for %VC in the lower ( $< 600$ ) and higher ( $\geq 600$ ) Brinkman index groups were 50.9% and 51.4%, respectively. The median values for FEV1 in the lower ( $< 600$ ) and higher ( $\geq 600$ ) Brinkman index groups were 71.7% and 85.4%, respectively. There

were no significant differences in %VC ( $p = 0.5780$ ) and FEV1 ( $p = 0.5387$ ) between the 2 Brinkman index groups (Fig. 1). We also compared the %VC and FEV1 values between lower ( $< 400$ ) and higher ( $\geq 400$ ) Brinkman index groups ( $n = 6$  and 18, respectively). The median values for %VC in the lower ( $< 400$ ) and higher ( $\geq 400$ ) Brinkman index groups were 56.3% and 50.1%, respectively. The median values for FEV1 in the lower ( $< 400$ ) and higher ( $\geq 400$ ) Brinkman index groups were 68.1% and 86.4%, respectively. There were no significant differences in %VC ( $p = 0.5709$ ) and FEV1 ( $p = 0.0773$ ) between these 2 Brinkman index groups.

We next examined the association between respiratory function and unilateral or bilateral DPT. The median values for %VC in the unilateral ( $n = 6$ ) and bilateral ( $n = 18$ ) DPT cases were 53.3% and 51.4%, respectively. The median values for FEV1 in the unilateral and bilateral DPT cases were 67.7% and 84.4%, respectively. There were no significant differences in %VC ( $p = 0.7642$ ) or FEV1 ( $p = 0.3014$ ) between the cases of unilateral and bilateral DPT.

We compared respiratory function between 2 groups: those with longer asbestos exposure ( $\geq 30$  years:  $n = 16$ ) and those with shorter asbestos exposure ( $< 30$  years:  $n = 8$ ). The median VC values in the longer- and shorter-exposure groups were 48.4% and 54.2%, respectively. The median FEV1 values in the longer- and shorter-exposure groups were 76.4% (41.3–70.7%) and 85.4%, respectively. The longer-exposure group showed more impaired respiratory function, although the difference was not significant ( $p = 0.3123$  for

%VC and  $p = 0.4813$  for FEV1).

**Clinical course of DPT.** Thirteen patients had a medical history of BAPE that preceded the diagnosis of DPT. The date of the accumulation of pleural effusion was identified based on their medical records, except in one case. The median (range) duration from the accumulation of pleural effusion to the development of DPT was 28.4 (8.9–255.3) months. The median duration from the accumulation of pleural effusion to the development of impaired respiratory function was 35.1 (2.8–255.3) months. We examined the correlation between the duration from the fluid accumulation to the onset of DPT and the duration of asbestos exposure using a regression analysis, but there was no significant correlation ( $r = 0.09$ ). In 2 of the 6 cases with unilateral DPT, the DPT had progressed to the other side of the thorax in 3.2 and 18.7 months, respectively. At the time of the analysis, 15 patients were alive and 9 patients had died. Of the 9 patients who had died, 4 died of respiratory failure, and 1 died of lung cancer. The other 4 patients died of unknown causes. There was no patient who developed MPM.

## Discussion

We retrospectively analyzed the characteristic features of asbestos-induced DPT. We focused in particular on DPT cases with severe respiratory compromise. The criteria that we applied are those used for worker's compensation and the Act on Asbestos Health Damage Relief in Japan. The top

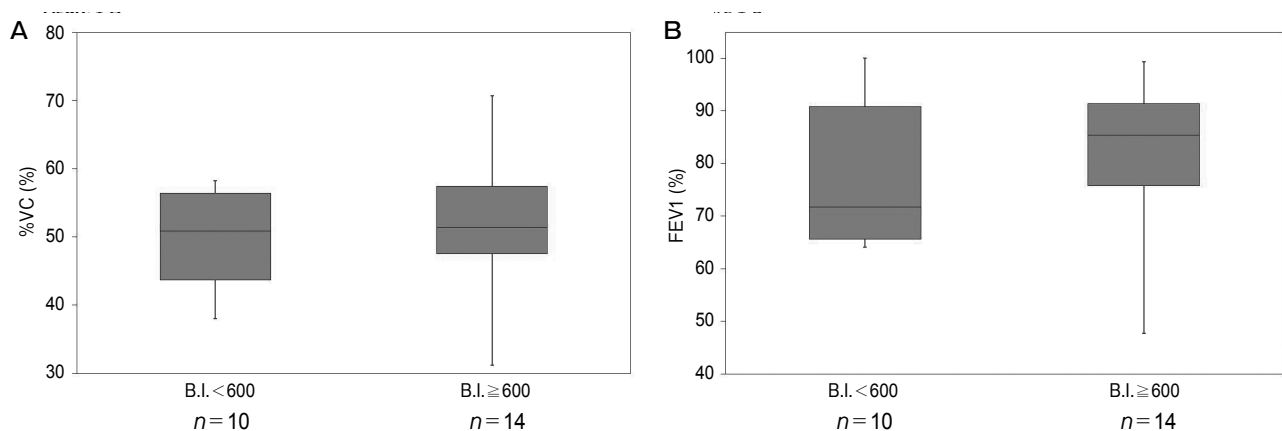


Fig. 1 Comparison of the percentage of vital capacity (%VC) (A) and the forced expiratory volume percentage in 1 sec (FEV1) (B), between the groups with lower and higher Brinkman index values.

occupational category in which the patients had been exposed to asbestos was dockyard workers, as there is a dockyard facility in the suburbs of the Okayama area. The median duration of asbestos exposure was 35 years, and the median latency period for the development of DPT from the first asbestos exposure was 49.0 years. These results are similar to those of our previous study [9] and those from other groups [7, 12]. The results of the present study confirm that DPT can develop after long latency periods following occupational asbestos exposure.

Making a diagnosis of DPT is challenging. In the present study, we defined DPT as pleural thickening of  $> 5$  mm on a posteroanterior chest X-ray, extending for more than one-half of the LTW in the patients with unilateral DPT, or over more than one-quarter of the LTW in the patients with bilateral DPT. These definitions were made based on dimensional criteria [3], because these are the criteria that are applied when making a diagnosis for the certification of worker's compensation or the Act on Asbestos Health Damage Relief in Japan. However, these criteria are based on chest X-rays and are ambiguous and subjective.

Ameille *et al.* reported that obliteration of the CPA was a far more reliable sign than dimensional criteria in the characterization of DPT [13]. Accordingly, the revised International Labor Office (ILO) Classification of Radiographs of Pneumoconiosis provided clearer criteria, in which involvement of the CPA had to be demonstrated for DPT [11]. We recently reported that the involvement of the CPA was negatively correlated with %VC [9]. This finding supports the use of CPA involvement not only for making a diagnosis of DPT, but also for assessing the severity of DPT. There is still room for discussion regarding the most relevant radiological diagnostic criteria for DPT.

Our present findings demonstrated that breathlessness, cough, and chest pain were the most frequent symptoms of DPT; this finding was similar to that of Yates *et al.* [3]. Moreover, 75.0% of the patients showed restrictive ventilatory impairment, and 25.0% of the patients showed combined ventilatory impairment. The characteristic features of DPT with respect to respiratory function testing are a restrictive ventilator defect, decreased compliance, a reduction in total lung capacity, and impairment of gas transfer

[8]. We suggest that the obstructive ventilatory impairment demonstrated in some of the patients in our study may be due to a history of smoking, although we could find no clear association between respiratory function and smoking history.

Unilateral DPT has been reported to cause less severe ventilatory impairment than bilateral DPT [8]. However, there were no differences in ventilatory impairment between the patients with unilateral or bilateral DPT in the present study and in our previous study [9]. However, caution should be used when drawing conclusions from these results, since the sample size was small. In the present study, FEV1 in unilateral DPT was lower than that in bilateral DPT. In fact, among 6 cases with unilateral DPT, there were 3 cases with mild pulmonary emphysema, 1 case with asbestosis, and 1 case with pulmonary emphysema and bronchial asthma. We consider that these concomitant diseases contributed to lower FEV1 in unilateral DPT.

Severe respiratory compromise is the key factor for approval for worker's compensation, and thus the most appropriate method for assessing respiratory impairment associated with DPT should be investigated further.

In the present study, we focused on the sequence of DPT and BAPE (also known as asbestos pleuritis). Epler *et al.* advocated the following diagnostic criteria for BAPE: (1) previous asbestos exposure, (2) determination of pleural effusion by chest X-ray or thoracentesis, and (3) absence of other causes of effusion [4]. We examined the patients' history of pleural fluid accumulation based on the medical information available and their subsequent clinical courses. We found that 54.2% of the 24 DPT cases had a history of pleural fluid accumulation, and they subsequently developed DPT at a median of 28.4 months. In addition, these patients developed severe respiratory compromise at a median of 35.1 months following the episode of pleural fluid accumulation. In a previous report, 40% of DPT cases were preceded by the development of pleural effusion [7]. However, in the present study, there were some cases in which it was difficult to determine the radiological change from BAPE to DPT, especially in patients with BAPE in the organizing stage. Diagnostic criteria for differentiating between BAPE in the organizing stage and DPT would be of critical importance with respect to



worker's compensation in Japan.

Our present findings demonstrated that the main cause of death was respiratory failure. Karjalainen *et al.* reported that asbestos-induced benign pleural disease raised the risk of MPM, but the risk of lung cancer was only slightly elevated [14]. In our study, only one of the 24 patients died of lung cancer and there were no patients with MPM. Associations between DPT and MPM or lung cancer should be clarified in a large-scale, long-term study.

In conclusion, our results indicate that DPT can develop after a long latency period following occupational asbestos exposure and a history of BAPE. Radiological diagnostic criteria that are suitable for practical use and appropriate methods for assessing respiratory impairment due to DPT should be established. Clinical, pathological, and temporal alterations that occur in the transition from BAPE to DPT should be clarified, and the association between DPT and MPM or lung cancer should be examined in large-scale, long-term prospective studies.

**Acknowledgments.** This study was supported by the Japanese Ministry of the Environment. This study is a part of the research and development and dissemination projects related to 9 fields of occupational injuries and illnesses of the Japan Labour Health and Welfare Organization.

## References

1. American Thoracic Society: Diagnosis and initial management of nonmalignant diseases related to asbestos. *Am J Respir Crit Care Med* (2004) 170: 691–715.
2. McLoud TC, Woods BO, Carrington CB, Epler GR and Gaensler EA: Diffuse pleural thickening in an asbestos-exposed population: prevalence and causes. *AJR Am J Roentgenol* (1985) 144: 9–18.
3. Yates DH, Browne K, Stidolph PN and Neville E: Asbestos-related bilateral diffuse pleural thickening: natural history of radiographic and lung function abnormalities. *Am J Respir Crit Care Med* (1996) 153: 301–306.
4. Epler GR, McLoud TC and Gaensler EA: Prevalence and incidence of benign asbestos pleural effusion in a working population. *JAMA* (1982) 247: 617–622.
5. Hillerdal G and Ozesmi M: Benign asbestos pleural effusion: 73 exudates in 60 patients. *Eur J Respir Dis* (1987) 71: 113–121.
6. de Klerk NH, Cookson WO, Musk AW, Armstrong BK and Glancy JJ: Natural history of pleural thickening after exposure to crocidolite. *Br J Ind Med* (1989) 46: 461–467.
7. Jeebun V and Stenton SC: The presentation and natural history of asbestos-induced diffuse pleural thickening. *Occup Med (Lond)* (2012) 62: 266–268.
8. Rudd RM: New developments in asbestos-related pleural disease. *Thorax* (1996) 51: 210–216.
9. Fujimoto N, Kato K, Usami I, Sakai F, Tokuyama T, Hayashi S, Miyamoto K and Kishimoto T: Asbestos-related diffuse pleural thickening. *Respiration* (2014) 88: 277–284.
10. American Thoracic Society: Standardization of Spirometry, 1994 Update. *Am J Respir Crit Care Med* (1995) 152: 1107–1136.
11. International Labour Office: Guidelines for the use of the ILO International Classification of Radiographs of Pneumoconioses. Revised edition 2011. (2011) Geneva, International Labour Office.
12. Kee ST, Gamsu G and Blanc P: Causes of pulmonary impairment in asbestos-exposed individuals with diffuse pleural thickening. *Am J Respir Crit Care Med* (1996) 154: 789–793.
13. Ameille J, Matrat M, Paris C, Joly N, Raffaelli C, Brochard P, Iwatsubo Y, Paire JC and Letourneux M: Asbestos-related pleural diseases: dimensional criteria are not appropriate to differentiate diffuse pleural thickening from pleural plaques. *Am J Ind Med* (2004) 45: 289–296.
14. Karjalainen A, Pukkala E, Kauppinen T and Partanen T: Incidence of cancer among Finnish patients with asbestos-related pulmonary or pleural fibrosis. *Cancer Causes Control* (1999) 10: 51–57.



# Prognostic significance of the lymphocyte-to-monocyte ratio in patients with malignant pleural mesothelioma<sup>☆</sup>



Tomoko Yamagishi<sup>a</sup>, Nobukazu Fujimoto<sup>b,\*</sup>, Hideyuki Nishi<sup>c</sup>, Yosuke Miyamoto<sup>a</sup>, Naofumi Hara<sup>a</sup>, Michiko Asano<sup>a</sup>, Yasuko Fuchimoto<sup>a</sup>, Sae Wada<sup>a</sup>, Kenichi Kitamura<sup>a</sup>, Shinji Ozaki<sup>a</sup>, Takumi Kishimoto<sup>d</sup>

<sup>a</sup> Department of Respiratory Medicine, Okayama Rosai Hospital, Okayama, Japan

<sup>b</sup> Department of Medical Oncology, Okayama Rosai Hospital, Okayama, Japan

<sup>c</sup> Department of Surgery, Okayama Rosai Hospital, Okayama, Japan

<sup>d</sup> Department of Internal Medicine, Okayama Rosai Hospital, Okayama, Japan

## ARTICLE INFO

### Article history:

Received 4 April 2015

Received in revised form 2 July 2015

Accepted 27 July 2015

### Keywords:

Asbestos

Lymphocyte-to-monocyte ratio

Malignant pleural mesothelioma

Prognostic score

## ABSTRACT

**Objectives:** Chronic inflammation plays a key role in the pathogenesis of malignant pleural mesothelioma (MPM) as a result of asbestos exposure. Several inflammation-based prognostic scores including the lymphocyte-to-monocyte ratio (LMR), Glasgow Prognostic Score (GPS), neutrophil-to-lymphocyte ratio (NLR), and platelet-to-lymphocyte ratio (PLR) reportedly predict survival in many malignancies, while the role of LMR in MPM remains unclear. The aim of this study was to evaluate the clinical value of LMR and to compare the prognostic value of these inflammation-based scores in predicting overall survival (OS) in MPM.

**Materials and methods:** One hundred and fifty patients with histologically proven MPM were included in this retrospective study. Kaplan–Meier curves and multivariate Cox-regression analyses were calculated for OS. The area under the receiver operating characteristics curve (AUC) was calculated to compare the discriminatory ability of each scoring system.

**Results:** An elevated LMR was significantly associated with prolonged OS. Patients with LMR <2.74 had significantly poor survival compared with LMR ≥2.74 (median, 5.0 versus 14.0 months;  $p=0.000$ ). The LMR consistently had a higher AUC value at 6 months (0.722), 12 months (0.712), and 24 months (0.670), compared with other scores. Multivariate analysis showed that the LMR was independently associated with OS.

**Conclusions:** The LMR is an independent prognostic marker for OS in patients with MPM and is superior to other inflammation-based prognostic scores with respect to prognostic ability.

© 2015 Elsevier Ireland Ltd. All rights reserved.

## 1. Introduction

Malignant pleural mesothelioma (MPM) is a rare but aggressive primary pleural malignancy that is associated with asbestos exposure [1]. Its prognosis remains poor, as most patients present with unresectable disease at diagnosis or are deemed inoperable owing to age or medical comorbidities. Although several treatment options have been delivered to patients with MPM, the median

survival time is approximately 12 months [2]. Despite a very poor prognosis, some selected patients live with the disease for a considerable period of time; median survival is 12.8–46.9 months when treated using a multimodality therapy that contains either (1) neoadjuvant chemotherapy and surgery with or without radiation therapy, or (2) adjuvant chemotherapy [3].

The best-known clinical prognostic scoring systems for MPM have originated from the European Organization for Research and Treatment of Cancer (EORTC) [4] and the Cancer and Leukemia Group B (CALGB) [5], and take into account a combination of biological and clinical factors. However, these scoring systems are not routinely used in MPM prognosis because they are time-consuming to perform.

It is well known that systemic inflammatory response plays an important role in cancer progression [6]. Although the mechanisms

<sup>☆</sup> This study is supported by "the research and development and the dissemination projects related to the 9 fields of occupational injuries and illnesses" of the Japan Labour Health and Welfare Organization.

\* Corresponding author at: Department of Medical Oncology, Okayama Rosai Hospital, 1-10-25 Chikkomidorimachi, Okayama 7028055, Japan. Fax: +81 86 2623391.

E-mail address: [nobufujimoto@gmail.com](mailto:nobufujimoto@gmail.com) (N. Fujimoto).

of carcinogenesis in MPM are incompletely understood, chronic inflammation is critically involved in the pathogenesis of MPM as a result of asbestos exposure. In addition to its involvement in the pathogenesis of cancer-related cachexia, systemic inflammation can predict clinically meaningful outcomes, such as overall survival (OS) and response to systemic treatment [7]. Several studies have shown that inflammation-based prognostic scores that include a combination of serum C-reactive protein (CRP) and albumin (ALB) (e.g., the Glasgow Prognostic Score [GPS] and modified GPS [mGPS]), a combination of neutrophil and lymphocyte counts (e.g., the neutrophil-to-lymphocyte ratio, NLR), and a combination of platelet (PLT) and lymphocyte counts (e.g., the platelet-to-lymphocyte ratio, PLR) are associated with survival in patients with various cancers, including MPM [8,9]. Lymphocytes act as tumor suppressors by inducing cytotoxic cell death and inhibiting tumor cell proliferation and migration [10]. The important role of monocytes and macrophages in cancer, including thoracic malignancies, has recently been uncovered [11]. More recently, some studies demonstrated that lymphocyte-to-monocyte ratio (LMR) is associated with prognosis in several cancers, including hematological malignancy [12] and some solid tumors. However, to the best of our knowledge, there is no evidence determining the association between LMR and the survival of MPM patients.

The aim of this study was to assess the prognostic role of inflammation-based prognostic scores such as the GPS, mGPS, NLR, PLR, and LMR in patients with MPM.

## 2. Materials and methods

### 2.1. Patient population

The study included 150 consecutive patients with histologically proven MPM between July 1993 and October 2014, at Okayama Rosai Hospital. No patients showed obvious clinical evidence of infection or other inflammatory conditions such as rheumatoid arthritis at the diagnosis of MPM. Baseline prognostic clinical and laboratory variables were collected retrospectively from patients' medical records. These included age, gender, histological subtype, stage, and Eastern Cooperative Oncology Group (ECOG) performance status (PS). Staging was determined according to the International Mesothelioma Interest Group (IMIG) staging system [13], based on enhanced CT of whole body, magnetic resonance imaging of the brain, and bone scintigraphy. Positron-emission tomography was available since 2012 and substituted to bone scintigraphy in 20 cases.

This study followed REMARK guidelines [14] and was conducted according to The Ethical Guidelines for Epidemiological Research by Japanese Ministry of Education, Culture, Sports, Science and Technology, and the Ministry of Health, Labour and Welfare. This study was approved by the Japan Labour, Health and Welfare Organization and the institutional review boards of Okayama Rosai Hospital. Patient confidentiality was strictly maintained.

### 2.2. Inflammation-based prognostic scores and other variables

Blood samples were obtained at the time of diagnosis of MPM for measurement of white blood cell count (WBC), absolute neutrophil count (ANC), absolute lymphocyte count (ALC), absolute monocyte count (AMC), PLT, CRP, and ALB. The LMR was defined as the ALC divided by the AMC. The NLR was calculated by dividing the ANC by the ALC; we applied a cutoff value of  $\leq 5$  versus  $> 5$  in accordance with the first report of NLR in MPM [15]. The same calculation was applied to derive the PLR; the cutoff for positivity was 150 [16].

The GPS was calculated as described in previous studies [17]. Briefly, patients with both elevated CRP ( $> 1.0$  mg/dL) and low ALB

( $< 3.5$  g/dL) were allocated a score of 2. Patients in whom only one of these biochemical abnormalities was present were allocated a score of 1. Patients in whom neither abnormality was present were allocated a score of 0. Regarding mGPS, patients with both elevated CRP ( $> 1.0$  mg/dL) and low ALB ( $< 3.5$  g/dL) were allocated a score of 2, patients in whom only CRP was elevated ( $> 1.0$  mg/dL) were allocated a score of 1, and those with normal CRP were allocated a score of 0 [18]. The EORTC Prognostic Score (EPS) was devised to subcategorize patients into low-risk or high-risk groups based on age, gender, histology, probability of diagnosis, and leukocyte count [4]. The CALGB score incorporates the presence of non-epithelial histology, weight loss, or chest pain; high platelet (PLT) and WBC; low hemoglobin; high serum lactate dehydrogenase; advanced age; and PS [5]. The CALGB groups were combined into three prognostic groups (e.g., groups 1/2, 3/4, or 5/6), because of the small numbers in the even numbered groups [19].

### 2.3. Statistical analysis

Receiver operating characteristic (ROC) curve analysis was performed to select the most appropriate cut-off point for LMR, AMC, and ALC to predict poor prognosis in patients with MPM. The score with the maximum sensitivity and specificity was selected as the best cut-off value. Survival outcomes were dichotomized by survival (alive versus death) in the ROC analysis. The relationships between the LMR and clinico-pathological features were evaluated using the chi-squared test. The primary objective of this study was to assess the association of inflammation-based scores and OS, which was defined as the time from diagnosis until death from any cause. OS was obtained by using Kaplan–Meier methods, and between-group differences were compared using the log-rank test. Univariate and multivariate analyses were performed regarding the potential prognostic factors using the Cox proportional hazard model. A stepwise backward procedure was used to derive a final model of the variables. Age ( $< 70$  versus  $\geq 70$  years), gender (male versus female), ECOG PS ( $\leq 1$  versus  $> 1$ ), histological subtype (epithelioid versus non-epithelioid), IMIG stage (I/II versus III/IV), EPS (high-risk versus low-risk), CALGB scoring system (group 1/2 versus group 3/4 versus group 5/6), surgical intervention (yes versus no), baseline WBC ( $\leq 8.3 \times 10^9/L$  versus  $> 8.3 \times 10^9/L$ ) and PLT ( $\leq 400 \times 10^9/L$  versus  $> 400 \times 10^9/L$ ), ALB ( $\geq 3.5$  g/dL versus  $< 3.5$  g/dL), and difference in hemoglobin ( $< 10$  g/L versus  $\geq 10$  g/L) entered the calculations. An ROC curve was also generated and the area under the curve (AUC) was calculated to evaluate the discriminatory ability of each scoring system. A two-tailed  $p$ -value  $< 0.05$  was considered statistically significant. All statistical analysis was performed using STATA software (version 12.1; StataCorp, College Station, Texas).

## 3. Results

### 3.1. Patient characteristics

The patient and tumor characteristics at baseline are shown in Table 1. Median age at the time of diagnosis was 70 (range: 38–92) years. The majority of study participants were male (93.3%) and had a diagnosis of stage III/IV (64.0%). Surgery was performed in 44 (29.3%) patients including 38 extrapleural pneumonectomy, 3 pleural decortication, and 3 tumor excision. Systemic chemotherapy and radiotherapy were delivered as initial treatment to 86 (57.3%) and 3 (2.0%) patients, respectively. The remaining 17 (11.3%) patients received best supportive care. The median follow-up duration was 11 (range: 1.0–150.0) months. At the time of analysis, 116 (77.3%) patients had died, and the median OS was 13.0 [95% confidence interval (CI), 10.0–16.0] months.

**Table 1**  
Patient characteristics (n = 150).

	No. of patients	%
Median age at diagnosis (range)	70 (38–92)	
Gender		
Male	140	93.3
Female	10	6.7
ECOG PS		
≤1	129	86.0
>1	21	14.0
Histological subtype		
Epithelioid	97	64.7
Non-epithelioid	53	36.3
IMIG stage at diagnosis		
I/II	54	36.0
III/IV	96	64.0
Treatment modalities		
Surgery (including multimodal treatment)	44	29.3
Systemic chemotherapy only	86	57.3
Radiotherapy only	3	2.0
Best supportive care only	17	11.3
CALGB group		
1–2	49	32.7
3–4	68	45.3
5–6	33	22.0
EORTC prognostic score		
Low risk	91	60.7
High risk	59	39.3
Platelet counts, mean ± SD (×10 <sup>9</sup> /L)	299.5 ± 102.1	
≤400	130	86.7
>400	20	13.3
Hemoglobin difference (g/L)		
<10	18	12.0
≥10	132	88.0
Albumin (g/dL)		
≥3.5	76	50.7
<3.5	74	49.3
White cell count, mean ± SD (×10 <sup>9</sup> /L)	8.32 ± 5.25	
≤8.3	102	68.0
>8.3	48	32.0
Neutrophil count, mean ± SD (×10 <sup>9</sup> /L)	6.01 ± 5.00	
Lymphocyte count, mean ± SD (×10 <sup>9</sup> /L)	1.50 ± 0.57	
Monocyte count, mean ± SD (×10 <sup>9</sup> /L)	0.57 ± 0.42	
Neutrophil-to-lymphocyte ratio, mean ± SD	5.63 ± 10.99	
≤5	112	74.7
>5	38	25.3
Platelet-to-lymphocyte ratio, mean ± SD	228.40 ± 114.18	
<150	44	29.3
≥150	106	70.7
Lymphocyte-to-monocyte ratio, mean ± SD	3.36 ± 2.26	
≥2.74	109	72.7
<2.74	41	27.3
The Glasgow Prognostic Score		
0	45	30.0
1	37	24.7
2	68	45.3
The modified Glasgow Prognostic Score		
0	51	34.0
1	31	20.7
2	68	45.3

ECOG: Eastern Cooperative Oncology Group; PS: performance status; IMIG: International Mesothelioma Interest Group; CALGB: Cancer and Leukemia Group B; EORTC: European Organisation for Research and Treatment of Cancer.

### 3.2. The cutoff value for ALC, AMC, and LMR at diagnosis for survival analysis

The mean (±SD) lymphocyte count was 1.50 (±0.57) × 10<sup>9</sup>/L, and the mean monocyte count was 0.57 (±0.42) × 10<sup>9</sup>/L. The mean (±SD) LMR level was 3.36 (±2.26). Applying ROC analysis, the optimal LMR cut-off was 2.74 (AUC, 0.736; 95% CI, 0.647–0.824)

for OS. All patients were categorized as either high-LMR (≥2.74) or low-LMR (<2.74). Overall, there were 41 (27.3%) patients with LMR <2.74 and 109 (72.7%) patients with LMR ≥2.74. Similarly, AMC of 0.28 × 10<sup>9</sup>/L (AUC, 0.741; 95% CI, 0.648–0.834) and ALC of 1.73 × 10<sup>9</sup>/L (AUC, 0.532; 95% CI, 0.408–0.656) were selected as the optimal cut-off values.

### 3.3. Prognostic factor analysis for OS

Univariate analysis variables that predicted poor OS included male gender ( $p=0.022$ ), PS >1 ( $p=0.001$ ), non-epithelioid histologic subtype ( $p=0.000$ ), stages III–IV ( $p=0.000$ ), no surgical intervention ( $p=0.000$ ), baseline WBC >8.30 × 10<sup>9</sup>/L ( $p=0.038$ ), baseline ALB <3.5 g/L ( $p=0.031$ ), high CALGB ( $p=0.010$ ), high-risk EPS ( $p=0.014$ , Fig. 1A), NLR >5 ( $p=0.002$ , Fig. 1B), PLR >150 ( $p=0.014$ , Fig. 1C), LMR <2.74 ( $p=0.000$ , Fig. 1D), high GPS ( $p=0.006$ ), high mGPS ( $p=0.014$ ), AMC ≥0.28 × 10<sup>9</sup>/L ( $p=0.011$ , Fig. 1E), and ALC <1.73 × 10<sup>9</sup>/L ( $p=0.009$ , Fig. 1F). Multivariate analysis revealed PS >1 (hazard ratio [HR], 1.84; 95% CI, 1.07–3.16;  $p=0.027$ ), non-epithelioid histologic subtype (HR, 2.24; 95% CI, 1.51–3.33;  $p=0.000$ ), stage III/IV (HR, 1.70; 95% CI, 1.08–2.69;  $p=0.022$ ), no surgical intervention (HR, 2.41; 95% CI, 1.43–4.04;  $p=0.001$ ), LMR <2.74 (HR, 2.34; 95% CI, 1.58–3.47;  $p=0.000$ ) as independent prognostic factors of OS (Table 3).

ROC curves were constructed for survival status at 6, 12, and 24 months of follow-up, and the areas under the ROC curves were compared to assess the discrimination ability of each inflammation scoring system. The LMR consistently had higher AUC value at 6 months (0.772), 12 months (0.712), and 24 months (0.670) in comparison with other inflammation-based prognostic scores (Fig. 2).

An elevated LMR was significantly associated with prolonged OS. Patients with an LMR of <2.74 exhibited a median OS of 5.0 (95% CI, 4.0–10.0) months, while patients with an LMR ≥2.74 had a median OS of 14.0 (95% CI, 13.0–23.0) months ( $p=0.000$ ). Sub-group analyses were performed regarding histological subtype (epithelioid versus non-epithelioid), stage (I/II versus III/IV), and surgical intervention (yes versus no). In univariate analysis, the prognostic value of LMR was significant in patients with epithelioid subtype (HR, 2.76; 95% CI, 1.61–4.71;  $p=0.000$ ), patients with non-epithelioid subtype (HR, 3.38; 95% CI, 1.67–6.87;  $p=0.001$ ), and patients designated stage I/II (HR, 2.85; 95% CI, 1.21–6.71;  $p=0.016$ ) or stage III/IV (HR, 2.71; 95% CI, 1.69–4.35;  $p=0.000$ ). In addition, the predictive value of LMR was significantly stratified by surgical intervention (HR, 2.90; 95% CI, 1.20–6.98;  $p=0.017$ ) and by no surgical intervention (HR, 3.15; 95% CI, 1.98–5.05;  $p=0.000$ ). Kaplan–Meier curves revealed that decreased LMR (<2.74) about these factors was significantly associated with decreased OS (Fig. 3).

This study demonstrated that the LMR was associated with ECOG PS ( $p=0.001$ ), histological subtype ( $p=0.035$ ), stage ( $p=0.010$ ), surgical intervention ( $p=0.043$ ), CALGB ( $p=0.022$ ), EPS ( $p=0.001$ ), and baseline ALC ( $p=0.000$ ) and AMC ( $p=0.000$ ) (Table 2).

## 4. Discussion

In the present study, we demonstrated that elevated LMR, an inflammation-based prognostic score, was a favorable prognosis factor for OS in MPM. To the best of our knowledge, this study is the first to demonstrate that the LMR is an independent marker of prognosis in patients with MPM and features prognostic ability superior to that of the NLR, PLR, GPS, and mGPS.

Accumulating studies have demonstrated a strong link between systemic inflammatory responses (including neutrophils, lymphocytes, and monocytes) and cancer, and those responses have been

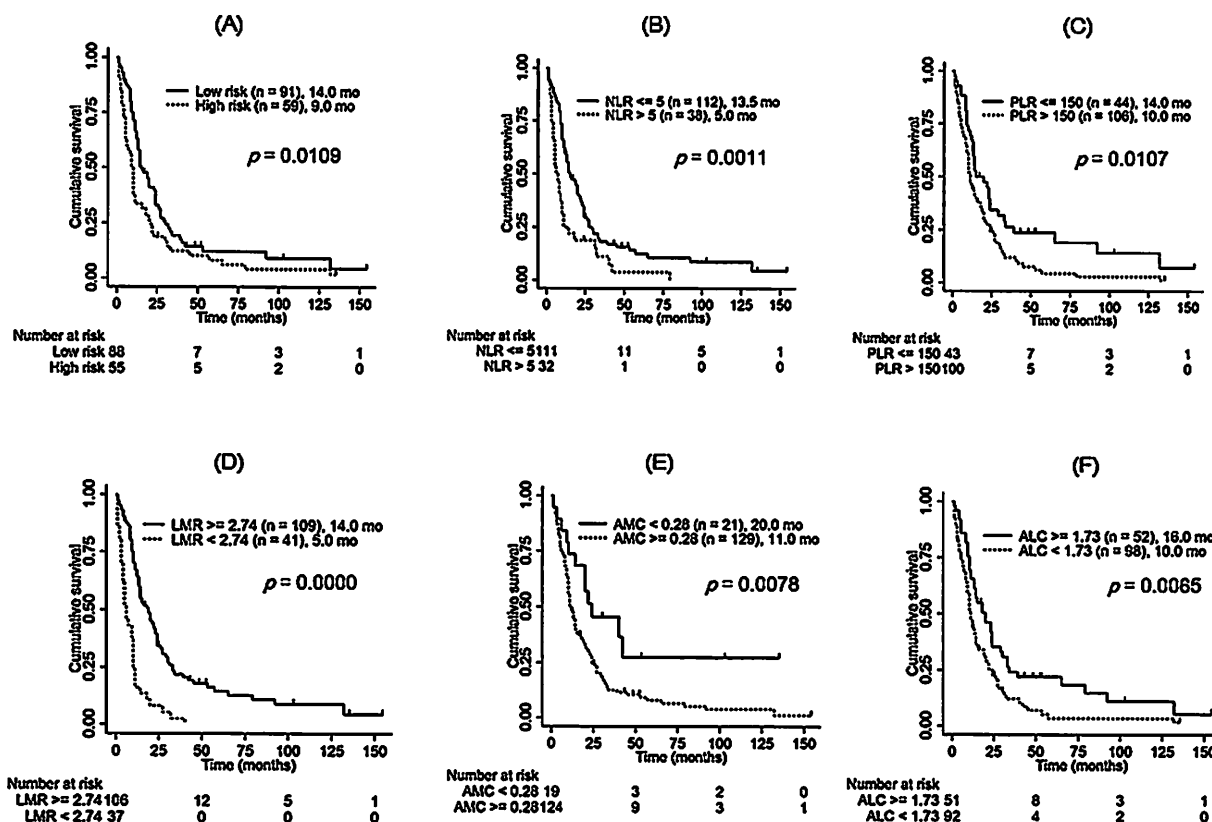


Fig. 1. Kaplan-Meier survival curves for patients affected by malignant pleural mesothelioma, stratified by European Organisation for Research and Treatment of Cancer prognostic score (A), neutrophil-to-lymphocyte ratio (NLR) (B), platelet-to-lymphocyte ratio (PLR) (C), lymphocyte-to-monocyte ratio (LMR) (D), absolute monocyte count (AMC) (E), and absolute lymphocyte count (ALC) (F).

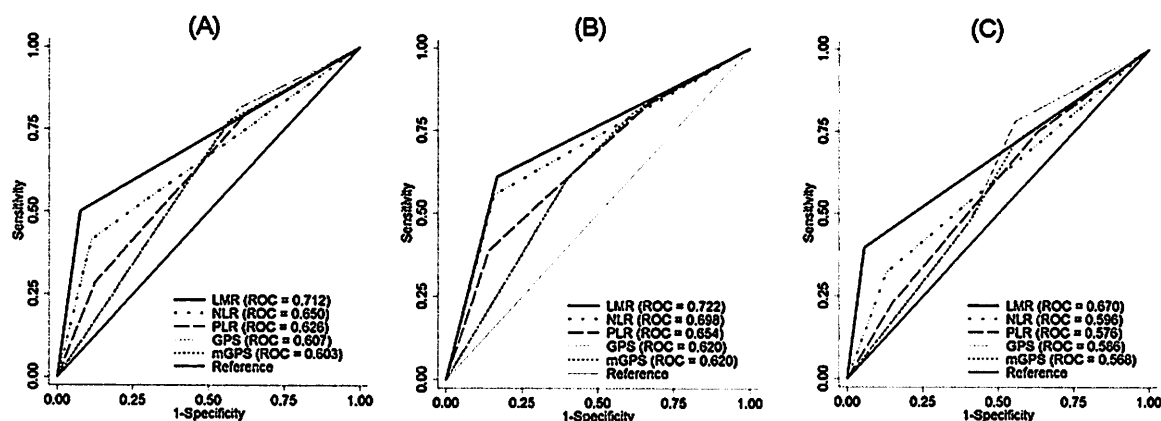


Fig. 2. Comparison of the areas under the receiver operating characteristic curves, for outcome prediction between the inflammation-based prognostic scores at (A) 6 months, (B) 12 months, and (C) 24 months in patients with malignant pleural mesothelioma. LMR, lymphocyte-to-monocyte ratio; NLR, neutrophil-to-lymphocyte ratio; PLR, platelet-to-lymphocyte ratio; GPS, Glasgow Prognostic Score; mGPS, modified Glasgow Prognostic Score.

significantly associated with clinical outcomes in cancer patients [20,21]. Among some inflammation-based scores, GPS is the most extensively validated [22]. However, recent years have seen a wealth of information about the prognostic value of ALC and AMC, together with their ratio, LMR.

Lymphocytes are components of the host immunity; they are important in the destruction of residual tumor cells and related micrometastases [23], and infiltrating lymphocytes can activate an effective antitumor cellular immune response [24]. Over the last few decades, a vast amount of evidence has highlighted the importance of monocytes and macrophages in cancer. Macrophages are derived from circulating monocytes and myeloid progenitor cells

when entering tissues. Macrophages in tumors, which are usually referred to as tumor-associated macrophages (TAM), promote tumor cell invasion, migration, tumor-associated angiogenesis [25], and the suppression of antitumor immune reactions [26]. The role of TAMs in tumor biology and their prognostic value in various cancers, including thoracic malignancies, has become a major topic of interest [11]. The peripheral monocytes may reflect an increased production of tissue macrophage as a surrogate marker of high tumor burden. Burt et al. reported that higher numbers of circulating monocytes are associated with poor survival in all patients with MPM and higher densities of tumor-infiltrating macrophages are associated with poor survival in patients with the non-epithelioid

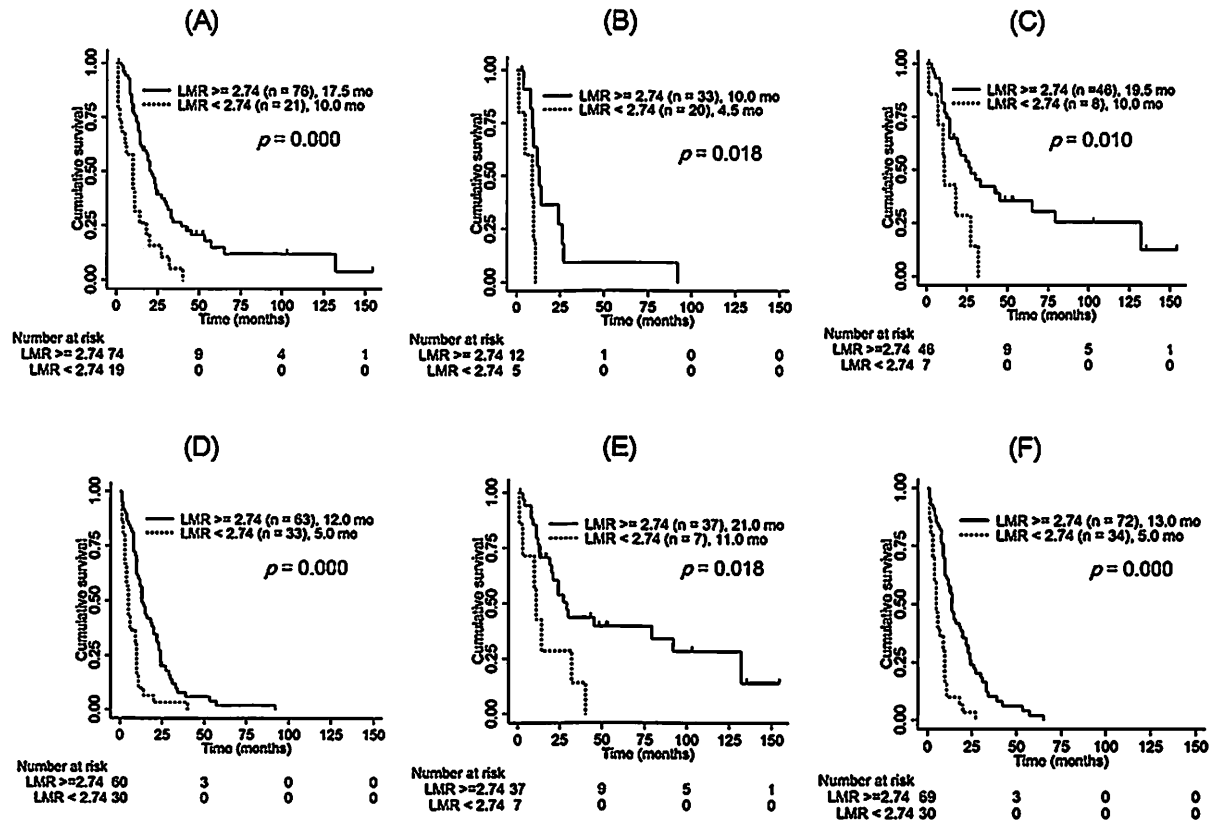


Fig. 3. Kaplan-Meier survival curves, stratified by lymphocyte-to-monocyte ratio (LMR) in patients with epithelioid subtype (A), with non-epithelioid subtype (B), with stage I/II disease (C), with stage III/IV disease (D), with surgical intervention (E), and without surgical intervention (F).

Table 2  
Association of LMR with baseline clinical characteristics.

Variable	LMR $\geq 2.74$ N = 109 (%)	LMR < 2.74 N = 41 (%)	p
Age, years			0.828
<70	51 (47)	20 (49)	
$\geq 70$	58 (53)	21 (51)	
Gender			0.352
Male	103 (95)	37 (90)	
Female	6 (5)	4 (10)	
ECOG PS			0.001
$\leq 1$	100 (92)	29 (70)	
>1	9 (8)	12 (30)	
Histological subtype			0.035
Epithelioid	76 (70)	21 (51)	
Non-epithelioid	33 (30)	20 (49)	
IMIG stage			0.010
I/II	46 (42)	8 (20)	
III/IV	63 (58)	33 (80)	
Surgery			0.043
Yes	72 (66)	34 (83)	
No	37 (34)	7 (17)	
CALGB group			0.022
1–2	40 (37)	9 (22)	
3–4	51 (47)	17 (41)	
5–6	18 (16)	15 (37)	
EORTC prognostic score			0.001
Low risk	75 (69)	16 (39)	
High risk	34 (31)	25 (61)	
Lymphocyte count, mean $\pm$ SD ( $\times 10^9/L$ )	1.63 $\pm$ 0.54	1.13 $\pm$ 0.48	0.000
Monocyte count, mean $\pm$ SD ( $\times 10^9/L$ )	0.44 $\pm$ 0.17	0.93 $\pm$ 0.62	0.000

LMR: lymphocyte-to-monocyte ratio; ECOG: Eastern Cooperative Oncology Group; PS: performance status; IMIG: International Mesothelioma Interest Group; CALGB: Cancer and Leukemia Group B; EORTC: European Organisation for Research and Treatment of Cancer.

subtype [27]. These findings might explain how decreasing LMR confers a negative prognosis in cancer patients.

Historically, the prognostic value of LMR was investigated mainly in hematological malignancies [12,28], and data were sparse in the context of solid tumors. In recent years, LMR has also been documented as an independent predictor of survival in a variety of patients with solid tumors, including colorectal tumor [29], breast cancer [30], lung cancer [31,32], pancreatic cancer [33], bladder cancer [34], and nasopharyngeal carcinoma [35]. However, until now, LMR data has not been reported in patients with MPM.

MPM is strongly associated with exposure to airborne asbestos fibers. Inhaled asbestos fibers present in the lung cause circulating macrophages to infiltrate the pleural space, where they attempt to phagocytose the inhaled foreign bodies [36]. As the macrophages are unable to eliminate the asbestos fibers, a state of chronic inflammation occurs, during which the secretion of free radicals causes genotoxic damage, which in turn facilitates the transformation of normal mesothelial cells to malignant mesothelioma [37].

In the present study, we initially evaluated the usefulness of LMR for predicting OS in patients with MPM. This study demonstrated that the ALC ( $\geq 1.73 \times 10^9/L$ ) was a favorable prognosis factor and the AMC ( $\geq 0.28 \times 10^9/L$ ) was an inferior prognostic factor for MPM patients. Multivariate analysis showed that LMR, ECOG PS, histological subtype, stage, and surgical intervention were significantly associated with OS. Moreover, AUC analysis has shown that the LMR was superior to other inflammation-based prognostic scores regarding predictive accuracy. In our study cohort, an elevated LMR ( $\geq 2.74$ ) was significantly associated with increased OS. Similar results were observed in Hodgkin's lymphoma [38], diffuse large B-cell lymphoma [28], and nasopharyngeal carcinoma [35]. We also focused on the relationship between LMR and prognosis according to subtype. Our results showed that decreased

**Table 3**  
Analysis of prognostic factors regarding overall survival.

Variable	OS (univariate analysis)		OS (multivariate analysis)	
	Hazard ratio (95% CI)	p	Hazard ratio (95% CI)	p
Age (<70/≥70 years)	1.00 (0.69–1.43)	0.993	NI	
Gender (male/female)	2.36 (1.13–4.93)	0.022	NI	
ECOG PS (≤1/>1)	2.39 (1.44–3.98)	0.001	1.84 (1.07–3.16)	0.027
Histological subtype (epithelioid/non-epithelioid)	1.95 (1.34–2.84)	0	2.24 (1.51–3.33)	0
IMIG stage (I/II vs. III/IV)	2.73 (1.81–4.12)	0	1.70 (1.08–2.69)	0.022
Surgery (yes/no)	0.35 (0.22–0.55)	0	2.41 (1.43–4.04)	0.001
Hemoglobin difference (g/L) (<10/≥10)	1.33 (0.76–2.33)	0.31	NI	
White cell count ( $\times 10^9/L$ ) ( $\leq 8.30$ / $> 8.30$ )	1.49 (1.02–2.17)	0.038	NI	
Platelet count ( $\times 10^9/L$ ) ( $\leq 400$ / $> 400$ )	1.17 (0.72–1.90)	0.517	NI	
Albumin (g/dL) ( $\geq 3.5$ / $< 3.5$ )	1.48 (1.03–2.12)	0.031	NI	
CALGB group (1–2/3–4/5–6)	1.43 (1.09–1.89)	0.01	NI	
EPS (low risk/high risk)	1.57 (1.09–2.26)	0.014	NI	
NLR ( $\leq 5$ / $> 5$ )	1.93 (1.28–2.92)	0.002	NI	
PLR ( $\leq 150$ / $> 150$ )	1.65 (1.10–2.47)	0.014	NI	
LMR ( $\geq 2.74$ / $< 2.74$ )	3.10 (2.07–4.66)	0	2.34 (1.58–3.47)	0
GPS (0/1/2)	1.32 (1.08–1.63)	0.006	NI	
mGPS (0/1/2)	1.28 (1.05–1.56)	0.014	NI	
AMC ( $\times 10^9/L$ ) ( $< 0.28$ / $\geq 0.28$ )	2.16 (1.19–3.93)	0.011	NI	
ALC ( $\times 10^9/L$ ) ( $\geq 1.73$ / $< 1.73$ )	1.66 (1.13–2.44)	0.009	NI	

ECOG: Eastern Cooperative Oncology Group; PS: performance status; IMIG: International Mesothelioma Interest Group; CALGB: Cancer and Leukemia Group B; EPS: European Organisation for Research and Treatment of Cancer prognostic score; NLR: neutrophil-to-lymphocyte ratio; PLR: platelet-to-lymphocyte ratio; LMR: lymphocyte-to-monocyte ratio; GPS: Glasgow Prognostic Score; mGPS: modified Glasgow Prognostic Score; AMC: absolute monocyte count; ALC: absolute lymphocyte count; NI: Not included.

LMR was significantly associated with poor prognosis for patients with the epithelioid subtype, as well as for those with the non-epithelioid subtype. In addition, the predictive value of LMR was also significant in patients with stage I/II and stage III/IV disease, and in patients with or without surgical intervention. Some studies reported that the inflammation-based prognostic scores are associated with responses to treatment (e.g., chemotherapy and radiotherapy) and perioperative outcomes (e.g., post-operative mortality and complications) [17,21]. Additional work is required to define the clinical utility of LMR within the individual therapeutic process.

Although the roles of monocytes and macrophage in tumor biology and their prognostic value in cancer have become major topics of interest, and much recent research has been dedicated to targeting these cells, there is currently no available clinical therapy to target these cells in patients with MPM. Conventional treatment strategies have met with limited success for patients with MPM. The combination strategy, which targets cancer cells directly, as well as macrophages and monocytes, may present a potentially new therapeutic approach [39]. Additional research is warranted regarding the use of immune-modulatory therapies to treat this malignancy.

One potential limitation of this study is that this is a retrospective and single-centre study. In addition, the study did not assess potential confounding factors (e.g., local or systemic infection, ischemia, acute coronary syndrome, metabolic syndrome, diabetes mellitus, and renal or hepatic dysfunction) that might affect the lymphocyte and monocyte counts. A large-scale prospective validation study is needed to confirm the results.

## 5. Conclusion

Our study is the first to demonstrate that the LMR is an independent marker of prognosis in patients with MPM and is superior to the other inflammation-based scores regarding prognostic ability. LMR is easily assessed using a simple complete blood count test, and is both technically and financially feasible to predict patients' clinical outcomes in routine practice. The identification of simple and valuable prognostic markers for MPM will enable clinicians to select patients who are most likely to benefit from intensive therapy, and avoid subjecting unsuitable candidates to futile treatment.

## Conflict of interest

The authors declare that they have no competing interests.

## Acknowledgements

The authors thank Dr. Nobuaki Ochi, Kawasaki Medical School, Okayama, Japan, for expert advice regarding statistical analyses.

This study is a part of "the research and development and the dissemination projects related to the 9 fields of occupational injuries and illnesses" of the Japan Labour Health and Welfare Organization. This sponsor had no involvement in the study design, collection, analysis and interpretation of the data, writing of the manuscript, or decision to submit the manuscript for publication.

## References

- [1] K. Gemba, N. Fujimoto, K. Kato, K. Aoe, Y. Takeshima, K. Inai, et al., National survey of malignant mesothelioma and asbestos exposure in Japan, *Cancer Sci.* 103 (2012) 483–490.
- [2] C. Cao, D. Tian, J. Park, J. Allan, K.A. Pataky, T.D. Yan, A systematic review and meta-analysis of surgical treatments for malignant pleural mesothelioma, *Lung Cancer* 83 (2014) 240–245.
- [3] C. Cao, D. Tian, C. Manganas, P. Matthews, T.D. Yan, Systematic review of trimodality therapy for patients with malignant pleural mesothelioma, *Ann. Cardiothorac. Surg.* 1 (2012) 428–437.
- [4] D.A. Fennell, A. Parmar, J. Shamash, M.T. Evans, M.T. Sheaff, R. Sylvester, et al., Statistical validation of the EORTC prognostic model for malignant pleural mesothelioma based on three consecutive phase II trials, *J. Clin. Oncol.* 23 (2005) 184–189.
- [5] J.E. Herndon, M.R. Green, A.P. Chahinian, J.M. Corson, Y. Suzuki, N.J. Vogelzang, Factors predictive of survival among 337 patients with mesothelioma treated between 1984 and 1994 by the Cancer and Leukemia Group B, *Chest* 113 (1998) 723–731.
- [6] A. Mantovani, P. Allavena, A. Sica, F. Balkwill, Cancer-related inflammation, *Nature* 454 (2008) 436–444.
- [7] A. Linton, N. van Zandwijk, G. Reid, S. Clarke, C. Cao, S. Kao, Inflammation in malignant mesothelioma—friend or foe? *Ann. Cardiothorac. Surg.* 1 (2012) 516–522.
- [8] D. Bugada, M. Allegri, P. Lavand'homme, M. De Kock, G. Fanelli, Inflammation-based scores: a new method for patient-targeted strategies and improved perioperative outcome in cancer patients, *Biomed. Res. Int.* 2014 (2014) 142425.
- [9] D.J. Pinato, F.A. Mauri, R. Ramakrishnan, L. Wahab, T. Lloyd, R. Sharma, Inflammation-based prognostic indices in malignant pleural mesothelioma, *J. Thorac. Oncol.* 7 (2012) 587–594.
- [10] L.M. Coussens, Z. Werb, Inflammation and cancer, *Nature* 420 (2002) 806–867.



- [11] L.A. Lievense, K. Bezemer, J.G. Aerts, J.P. Hegmans, Tumor-associated macrophages in thoracic malignancies, *Lung Cancer* 80 (2013) 256–262.
- [12] L.F. Porrata, D.J. Inwards, S.M. Ansell, I.N. Micallef, P.B. Johnston, W.J. Hogan, et al., Day 100 peripheral blood absolute lymphocyte/monocyte ratio and survival in classical Hodgkin's lymphoma postautologous peripheral blood hematopoietic stem cell transplantation, *Bone Marrow Res.* (2013) 658371, <http://dx.doi.org/10.1155/2013/658371>
- [13] V.W. Rusch, A proposed new international TNM staging system for malignant pleural mesothelioma. From the International Mesothelioma Interest Group, *Chest* 108 (1995) 1122–1128.
- [14] L.M. McShane, D.G. Altman, W. Sauerbrei, S.E. Taube, M. Gion, G.M. Clark, Reporting recommendations for tumor marker prognostic studies, *J. Clin. Oncol.* 23 (2005) 9067–9072.
- [15] S.C. Kao, N. Pavlakakis, R. Harvie, J.L. Vardy, M.J. Boyer, Z. van, N. andwijk, et al., High blood neutrophil-to-lymphocyte ratio is an indicator of poor prognosis in malignant mesothelioma patients undergoing systemic therapy, *Clin. Cancer Res.* 16 (2010) 5805–5813.
- [16] Ji-Feng Feng, Ying Huang, Qi-Xun Chen, Preoperative platelet lymphocyte ratio (PLR) is superior to neutrophil lymphocyte ratio (NLR) as a predictive factor in patients with esophageal squamous cell carcinoma, *World J. Surg. Oncol.* 12 (2014) 58.
- [17] D.C. McMillan, The systemic inflammation-based Glasgow Prognostic Score: a decade of experience in patients with cancer, *Cancer Treat. Rev.* 39 (2013) 534–540.
- [18] M.J. Proctor, D.S. Morrison, D. Talwar, S.M. Balmer, D.S. O'Reilly, A.K. Foulis, et al., An inflammation-based prognostic score (mGPS) predicts cancer survival independent of tumour site: a Glasgow Inflammation Outcome Study, *Br. J. Cancer* 104 (2011) 726–734.
- [19] J. Edwards, K. Abrams, J. Leverment, T. Spyt, D. Waller, K. O'Byrne, Prognostic factors for malignant mesothelioma in 142 patients: validation of CALGB and EORTC prognostic scoring systems, *Thorax* 55 (2000) 731–735.
- [20] A. Kinoshita, H. Onoda, N. Imai, A. Iwaku, M. Oishi, N. Fushiya, et al., Comparison of the prognostic value of inflammation-based prognostic scores in patients with hepatocellular carcinoma, *Br. J. Cancer* 107 (2012) 988–993.
- [21] D. Bugada, M. Allegri, P. Lavand'homme, M. De Kock, G. Fanelli, Inflammation-based scores: a new method for patient-targeted strategies and improved perioperative outcome in cancer patients, *Biomed. Res. Int.* (2014) 142425, <http://dx.doi.org/10.1155/2014/142425>
- [22] M.J. Proctor, D.S. Morrison, D. Talwar, S.M. Balmer, D.S. O'Reilly, A.K. Foulis, et al., An inflammation-based prognostic score (mGPS) predicts cancer survival independent of tumour site: a Glasgow Inflammation Outcome Study, *Br. J. Cancer* 104 (2011) 726–734.
- [23] P. Fogar, C. Sperti, D. Basso, M.C. Sanzari, E. Greco, C. Davoli, et al., Decreased total lymphocyte counts in pancreatic cancer: an index of adverse outcome, *Pancreas* 32 (2006) 22–28.
- [24] H. Rabinowich, R. Cohen, I. Bruderman, Z. Steiner, A. Klajman, Functional analysis of mononuclear cells infiltrating into tumors: lysis of autologous human tumor cells by cultured infiltrating lymphocytes, *Cancer Res.* 47 (1987) 173–177.
- [25] J.W. Pollard, Tumour-educated macrophages promote tumour progression and metastasis, *Nat. Rev. Cancer* 4 (2004) 71–78.
- [26] D.I. Gabrilovich, S. Nagaraj, Myeloid-derived suppressor cells as regulators of the immune system, *Nat. Rev. Immunol.* 9 (2009) 162–174.
- [27] B.M. Burt, S.J. Rodig, T.R. Tillemann, A.W. Elbardissi, R. Bueno, D.J. Sugarbaker, Circulating and tumor-infiltrating myeloid cells predict survival in human pleural mesothelioma, *Cancer* 117 (2011) 5234–5244.
- [28] Z.M. Li, J.J. Huang, Y. Xia, J. Sun, Y. Huang, Y. Wang, et al., Blood lymphocyte-to-monocyte ratio identifies high-risk patients in diffuse large B-cell lymphoma treated with R-CHOP, *PLoS One* 7 (2012) e41658, <http://dx.doi.org/10.1371/journal.pone.0041658>
- [29] M. Stotz, M. Pichler, G. Absenger, J. Szkandera, F. Arminger, R. Schabert-Moser, et al., The preoperative lymphocyte to monocyte ratio predicts clinical outcome in patients with stage III colon cancer, *Br. J. Cancer* 110 (2014) 435–440.
- [30] X.J. Ni, X.L. Zhang, Q.W. Ou-Yang, G.W. Qian, L. Wang, S. Chen, et al., An elevated peripheral blood lymphocyte-to-monocyte ratio predicts favorable response and prognosis in locally advanced breast cancer following neoadjuvant chemotherapy, *PLoS One* 9 (2014) e111886, <http://dx.doi.org/10.1371/journal.pone.0111886>
- [31] P. Hu, H. Shen, G. Wang, P. Zhang, Q. Liu, J. Du, Prognostic significance of systemic inflammation-based lymphocyte-monocyte ratio in patients with lung cancer: based on a large cohort study, *PLoS One* 9 (2014) e108062, <http://dx.doi.org/10.1371/journal.pone.0108062>
- [32] G.N. Lin, J.W. Peng, J.J. Xiao, D.Y. Liu, Z.J. Xia, Prognostic impact of circulating monocytes and lymphocyte-to-monocyte ratio on previously untreated metastatic non-small cell lung cancer patients receiving platinum-based doublet, *Med. Oncol.* 31 (2014) 70.
- [33] Y. Fujiwara, T. Misawa, H. Shiba, Y. Shirai, R. Iwase, K. Haruki, et al., Postoperative peripheral absolute blood lymphocyte-to-monocyte ratio predicts therapeutic outcome after pancreatic resection in patients with pancreatic adenocarcinoma, *Anticancer Res.* 34 (2014) 5133–5138.
- [34] S. Temraz, D. Mukherji, Z.A. Farhat, R. Nasr, M. Charafeddine, M. Shahait, et al., Preoperative lymphocyte-to-monocyte ratio predicts clinical outcome in patients undergoing radical cystectomy for transitional cell carcinoma of the bladder: a retrospective analysis, *BMC Urol.* 14 (2014) 76.
- [35] J. Li, R. Jiang, W.S. Liu, Q. Liu, M. Xu, Q.S. Feng, et al., A large cohort study reveals the association of elevated peripheral blood lymphocyte-to-monocyte ratio with favorable prognosis in nasopharyngeal carcinoma, *PLoS One* 8 (2013) e83069, <http://dx.doi.org/10.1371/journal.pone.0083069>
- [36] B.T. Mossman, A. Churg, Mechanisms in the pathogenesis of asbestosis and silicosis, *Am. J. Respir. Crit. Care Med.* 157 (1998) 1666–1680.
- [37] A.J. Bograd, K. Suzuki, E. Vertes, C. Colovos, E.A. Morales, M. Sadelain, et al., Immune responses and immunotherapeutic interventions in malignant pleural mesothelioma, *Cancer Immunol. Immunother.* 60 (2011) 1509–1527.
- [38] L.F. Porrata, K. Ristow, J.P. Colgan, T.M. Habermann, T.E. Witzig, D.J. Inwards, et al., Peripheral blood lymphocyte/monocyte ratio at diagnosis and survival in classical Hodgkin's lymphoma, *Haematologica* 97 (2012) 262–269.
- [39] M.A. Lameijer, J. Tang, M. Nahrendorf, R.H. Beelen, W.J. Mulder, Monocytes and macrophages as nanomedicinal targets for improved diagnosis and treatment of disease, *Expert Rev. Mol. Diagn.* 13 (2013) 567–580.



# DNA copy number gains in malignant pleural mesothelioma

MASASHI FURUKAWA<sup>1</sup>, SHINICHI TOYOOKA<sup>1,2</sup>, TATSURO HAYASHI<sup>1,3</sup>, HIROMASA YAMAMOTO<sup>1,3</sup>, NOBUKAZU FUJIMOTO<sup>4</sup>, JUNICHI SOH<sup>1</sup>, SHINSUKE HASHIDA<sup>1,2</sup>, KAZUHIKO SHIEN<sup>1,2</sup>, HIROAKI ASANO<sup>1</sup>, KEISUKE AOE<sup>5</sup>, KAZUNORI OKABE<sup>3</sup>, HARVEY I. PASS<sup>6</sup>, KAZUNORI TSUKUDA<sup>1</sup>, TAKUMI KISHIMOTO<sup>4</sup> and SHINICHIRO MIYOSHI<sup>1</sup>

Departments of <sup>1</sup>Thoracic, Breast and Endocrinological Surgery, and <sup>2</sup>Clinical Genomic Medicine, Okayama University Graduate School of Medicine, Dentistry and Pharmaceutical Sciences, Okayama, Okayama 700-8558; <sup>3</sup>Department of Thoracic Surgery, National Hospital Organization Yamaguchi-Ube Medical Center, Ube, Yamaguchi 755-0241; <sup>4</sup>Department of Internal Medicine, Okayama Rosai Hospital, Okayama, Okayama 702-8055; <sup>5</sup>Department of Medical Oncology, National Hospital Organization Yamaguchi-Ube Medical Center, Ube, Yamaguchi 755-0241, Japan; <sup>6</sup>Division of Thoracic Surgery, Department of Cardiothoracic Surgery, New York University Langone Medical Center, NY 10016, USA

Received October 15, 2014; Accepted July 30, 2015

DOI: 10.3892/ol.2015.3652

**Abstract.** Malignant pleural mesothelioma (MPM) is a highly aggressive tumor with an extremely poor prognosis. The incidence of MPM is increasing as a result of widespread exposure to asbestos. The molecular pathogenesis of MPM remains unclear. The present study analyzed the frequency of various genomic copy number gains (CNGs) in MPM using reverse transcription-quantitative polymerase chain reaction. A total of 83 primary MPMs and 53 primary lung adenocarcinomas were analyzed to compare the CNGs of *EGFR*, *KRAS*, *MET*, *FGFR1* and *SOX2*. In MPM, the CNGs of *EGFR*, *KRAS*, *MET*, *FGFR1* and *SOX2* were detected in 12 (14.5%), 8 (9.6%), 5 (6.0%), 4 (4.8%) and 1 (1.2%) of the samples, respectively. In lung adenocarcinomas, the CNGs of *EGFR*, *KRAS*, *MET*, *FGFR1* and *SOX2* were detected in 21 (39.6%), 12 (22.6%), 5 (9.4%), 10 (18.9%) and 0 (0.0%) of the samples, respectively. The CNGs of *EGFR*, *KRAS* and *FGFR1* were significantly less frequent in the MPMs compared with the lung adenocarcinomas ( $P=0.0018$ , 0.048 and 0.018, respectively). Overall, the MPMs exhibited these CNGs less frequently compared with the lung adenocarcinomas ( $P=0.0002$ ). The differences in CNGs between the two tumor types suggested that they are genetically different.

## Introduction

Malignant pleural mesothelioma (MPM) is a tumor derived from the mesothelial cells lining the pleural spaces. MPM has highly invasive and aggressive clinical characteristics. Approximately 80% of MPM patients have a history of occupational asbestos exposure, which is considered to be a risk factor for the development of the disease (1). The molecular pathogenesis of MPM is not well understood. The most common mutations in MPMs are losses in 9p21, 1p36, 14q32 and 22q12, and gains in 5p, 7p and 8q24, which have been detected by comparative genomic hybridization analysis (2,3). Homozygous deletion of the 9p21 locus encoding two critical cyclin-dependent kinase inhibitors, p16<sup>INK4a</sup> and p15<sup>INK4b</sup>, have been reported in up to 80% of MPMs, and this mutation may be of diagnostic utility (4,5). The tumor suppressor neurofibromin 2 is encoded by the *NF2* gene, located on chromosome 22q12. Mutations in *NF2* are found in ~40% of MPMs, and heterozygous loss of *NF2* is identified in ~74% of MPMs (6,7). Mutations are rare in the *TP53* and *RAS* genes, which are frequently present in epithelial solid tumors (8,9). Epigenetic alterations, such as DNA methylation, have been found in MPMs, which have a different profile compared with lung cancer (10-12). MPMs, particularly of the epithelioid subtype, may be hard to differentiate from adenocarcinoma arising in the lung periphery, and epidemiological evidence indicates that asbestos and smoking are shared risk factors for these diseases (2,13,14). Currently, the differential diagnosis of MM is based on a range of morphological analyses, including a combination of histological and immunohistochemical staining, and electron microscopy (13,15,16).

Cytogenetic studies have been performed on MPMs and adenocarcinomas arising in the lung periphery, however, no chromosomal aberrations specific to either of the tumor types have been identified (2,14).

Reverse transcription-quantitative polymerase chain reaction (RT-qPCR) is a method for evaluating DNA copy number

---

**Correspondence to:** Professor Shinichi Toyooka, Department of Clinical Genomic Medicine, Okayama University Graduate School of Medicine, Dentistry and Pharmaceutical Sciences, 2-5-1 Shikata, Kita, Okayama, Okayama 700-8558, Japan  
E-mail: toyooka@md.okayama-u.ac.jp

**Key words:** malignant pleural mesothelioma, lung adenocarcinoma, copy number, reverse transcription-quantitative polymerase chain reaction

changes, including losses, gains and amplifications of DNA sequences (17-19). Copy number gains (CNGs) of *EGFR* and *KRAS* have been observed in lung cancer, particularly in adenocarcinoma (18,20). Furthermore, CNGs of *FGFR1* and *SOX2* have been observed in lung cancer, particularly in squamous cell carcinoma (21-25). c-Met was recently reported to be activated in MPM by overexpression or mutations in *MET* (26), and *MET* amplification is a known cause of resistance to *EGFR*-tyrosine kinase inhibitor (TKI) treatment in lung cancer (27). RT-qPCR was used in the present study on 83 primary MPM and 53 primary lung adenocarcinomas to compare the CNGs of *EGFR*, *KRAS*, *MET*, *FGFR1* and *SOX2*.

## Materials and methods

**Tumor samples.** Surgically resected specimens of 53 lung adenocarcinomas and 83 MPMs (57 epithelioid, 8 sarcomatoid, 15 biphasic, 2 desmoplastic and 1 lymphohistiocytic) were obtained. All the lung adenocarcinomas and 11 of the MPM samples were obtained from Okayama University Hospital (Okayama, Japan). Another 18 MPMs were obtained from Yamaguchi-Ube Medical Center (Ube, Japan), 2 were obtained from Okayama Rosai Hospital (Okayama, Japan) and the remaining 52 were obtained from Karmanos Cancer Center (Detroit, MI, USA). All Japanese samples were collected between March 2002 and September 2011, and all samples from the USA were collected >10 years ago. Resected tumors were stored at -80°C until DNA extraction. Permission from the Institutional Review Board and informed consent were obtained at each collection site.

**DNA extraction.** Genomic DNA was obtained from primary tumors by standard phenol:chloroform (1:1) extraction, followed by ethanol precipitation, or using a DNeasy Tissue kit (Qiagen, Inc., Valencia, CA, USA).

**RT-qPCR for copy number evaluation.** CNGs of *EGFR*, *KRAS*, *MET*, *FGFR1* and *SOX2* genes were determined by RT-qPCR assays using Power SYBR® Green PCR Master Mix (Thermo Fisher Scientific, Waltham, MA, USA), as previously described (18,19). Briefly, samples of 1 µl were analyzed per assay using with StepOne Plus Real-Time PCR System (Thermo Fisher Scientific). PCR conditions were initial denaturation at 95°C for 10 min followed by 40 cycles of amplification at 95°C for 15 sec and 60°C for 60 sec. The samples were analyzed in triplicate using StepOne Plus RT PCR software (version 2.0; Thermo Fisher Scientific) and the *LINE1* gene was used as a reference gene for all copy number analyses, as this is the most abundant autonomous retrotransposon in the human genome, constituting 17%. Each amplification reaction was checked for the absence of non-specific PCR products by performing a melting curve analysis. The copy number calculation was conducted using the comparative cycle threshold (Ct) method following validation of the PCR reaction efficiency of *EGFR*, *KRAS*, *MET*, *FGFR1*, *SOX2* and *LINE1*. The PCR primer sequences for *EGFR*, *KRAS*, *MET* and *LINE1* primers have previously been described (17-19). The PCR primer sequences for *FGFR1* and *SOX2* were designed by Primer 3 plus software and by modification of the sequences. The PCR primer sequences were as follows: *FGFR1* forward, 5'-AGC CAC CAC ATG GCA TAC

TT-3' and reverse, 5'-GGT GAC AAG GCT CCA CAT CT-3'; and *SOX2* forward, 5'-CGT CAC ATG GAT GGT TGT CT-3' and reverse, 5'-GCC GCC GAT GAT TGT TAT TA-3'. The relative copy number of each sample was determined by comparing the ratio of the target gene to *LINE1* in each sample with the ratio of these genes in normal human genomic DNA (EMD Biosciences, Darmstadt, Germany) prepared from a mixture of human blood cells from 6-8 donors, as a diploid control. Our previous study defined a copy number of ≥4 as a gene gain in cell lines (17,18). However, considering the contamination by non-malignant cells in primary samples (estimated mean per tumor, 50% tumor cells and 50% non-malignant cells), the cut-off value of 3 copy numbers rather than 4 was used for primary tumors in this study (17).

**Detection of *EGFR* mutations.** The *EGFR* mutational status was determined using a PCR-based length polymorphism and restriction fragment length polymorphism assay, as previously described (28). Briefly, the common deletions of exon 19 were distinguished from the wild-type based on PCR product length polymorphisms using 12% polyacrylamide gel electrophoresis (PAGE) and ethidium bromide staining. For the exon 21 L858R mutation, *Sau96I* digestion, which specifically digests the mutant type, was performed prior to 12% PAGE.

**Statistical analyses.** Differences between the two groups were assessed using the  $\chi^2$  test or Fisher's exact test as required. All data were analyzed using JMP software version 9.0.0 (SAS Institute Inc., Cary, NC, USA). For all analyses, P<0.05 was considered to indicate a statistically significant difference.

## Results

**CNGs in MPMs and lung adenocarcinomas.** In the 83 MPM samples, the CNGs of *EGFR*, *KRAS*, *MET*, *FGFR1* and *SOX2* were detected in 12 (14.5%), 8 (9.6%), 5 (6.0%), 4 (4.8%), and 1 (1.2%) of the samples, respectively. In the epithelioid subtype of MPM (n=57), the CNGs of *EGFR*, *KRAS*, *MET*, *FGFR1* and *SOX2* were detected in 7 (12.3%), 5 (8.8%), 3 (5.3%), 4 (7.0%) and 0 (0.0%) of the samples, respectively. In the other subtypes of MPMs (n=26), the CNGs of *EGFR*, *KRAS*, *MET*, *FGFR1* and *SOX2* were detected in 5 (19.2%), 3 (11.5%), 2 (7.7%), 0 (0%) and 1 (3.8%) of the samples, respectively. In the 53 lung adenocarcinomas, the CNGs of *EGFR*, *KRAS*, *MET*, *FGFR1* and *SOX2* were detected in 21 (39.6%), 12 (22.6%), 5 (9.4%), 10 (18.9%) and 0 (0.0%) of the samples, respectively (Table I; Fig. 1). Three cases of MPMs were demonstrated to have numerous CNGs of *EGFR* (269, 62 and 14, respectively). The CNGs of *EGFR*, *KRAS* and *FGFR1* were significantly less frequent in the MPMs compared with the lung adenocarcinomas (P=0.0018, 0.048 and 0.018, respectively). In the epithelioid subtype of MPMs, the CNGs of *EGFR* were significantly less frequent than those in the lung adenocarcinomas (P=0.0018), and in other subtypes of MPMs, the CNGs of *FGFR1* were significantly less frequent compared with those of the lung adenocarcinomas (P=0.026). In the MPMs, an absence and presence of CNGs were observed in 64 (77.1%) and 19 (22.9%) of the 83 cases, respectively. In the epithelioid MPMs, absent/present CNGs were observed in 47 (82.5%) and 10 (17.5%) of the 57 cases, respectively. In the other subtypes of

Table I. CNGs of *EGFR*, *KRAS*, *MET*, *FGFR1* and *SOX2* in MPMs and lung adenocarcinomas.

Genes	MPMs (n=83)						Lung adenocarcinoma (n=53)	
	All (n=83)		Epithelioid subtype (n=57)		Other subtypes (n=26)			
	No.	%	No.	%	No.	%	No.	%
<i>EGFR</i>	12 <sup>a</sup>	14.5	7 <sup>a</sup>	12.3	5	19.2	21	39.6
<i>KRAS</i>	8 <sup>b</sup>	9.6	5	8.8	3	11.5	12	22.6
<i>MET</i>	5	6.0	3	5.3	2	7.7	5	9.4
<i>FGFR1</i>	4 <sup>b</sup>	4.8	4	7.0	0 <sup>b</sup>	0.0	10	18.9
<i>SOX2</i>	1	1.2	0	0.0	1	3.8	0	0.0

CNGs of *FGFR1* and *KRAS* were significantly less frequent in MPMs compared with lung adenocarcinomas. In epithelioid MPMs, CNGs of *EGFR* were found to be significantly less frequent compared with lung adenocarcinomas. In other types of MPMs, CNGs of *FGFR1* were found to be significantly less frequent compared with lung adenocarcinomas (<sup>a</sup>P<0.05; <sup>b</sup>P<0.01). CNGs, copy number gains; MPMs, malignant pleural mesotheliomas.

Table II. Frequency of the absence or presence of CNGs in MPMs and lung adenocarcinomas.

Cancer type	Absence of CNGs		Presence of CNGs	
	No.	%	No.	%
Malignant pleural mesothelioma (n=83) <sup>a</sup>	64 <sup>a</sup>	77.1	19	22.9
Epithelioid subtype (n=57) <sup>a</sup>	47 <sup>a</sup>	82.5	10	17.5
Other subtypes (n=26)	17	65.4	9	34.6
Lung adenocarcinoma (n=53)	24	45.3	29	54.7

Frequency of none of CNGs in MPMs and epithelioid MPMs was significantly higher compared with lung adenocarcinomas (<sup>a</sup>P<0.01). CNGs, copy number gains; MPM, malignant pleural mesothelioma.

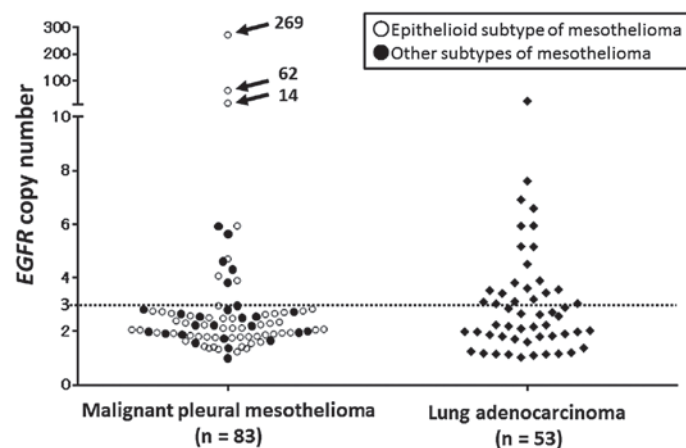


Figure 1. *EGFR* gene copy number, determined by reverse transcription-quantitative polymerase chain reaction in malignant pleural mesotheliomas (MPMs) and lung adenocarcinomas. Copy numbers >3 were considered as copy number gain (CNG). Three cases of MPMs were shown to have high CNGs of *EGFR* (269, 62 and 14, respectively).

the MPMs, the absence and presence of CNGs were observed in 17 (65.4%) and 9 (34.6%) of the 26 cases, respectively. In the lung adenocarcinomas, the absence and presence of CNGs were observed in 24 (45.3%) and 29 (54.7%) of the 53 cases, respectively (Table II). The MPMs and the epithelioid subtypes

of the MPMs had less frequent CNGs than the lung adenocarcinomas (P=0.0002 and P=0.0001, respectively).

***EGFR* mutations.** No *EGFR* mutation was detected in the 83 MPMs. In the lung adenocarcinomas, *EGFR* mutations

were detected in 21 (39.6%) cases; 14 cases exhibited an exon 19 deletion and 7 cases exhibited an exon 21 mutation (L858R).

## Discussion

The main finding of the present study is that the pattern of DNA CNGs of MPM is different from that in lung adenocarcinoma. MPMs exhibited less CNGs of the genes examined in compared with the lung adenocarcinomas. The epithelioid subtype of MPM, which is often difficult to distinguish from lung adenocarcinoma, similarly exhibited these CNGs less frequently compared with the lung adenocarcinomas. To the best of our knowledge, only a limited number of studies have previously analyzed the presence and frequency of *EGFR* CNGs in MPMs (2,29-32), and no studies have focused on CNGs of *KRAS*, *MET*, *FGFR1* or *SOX2* in MPM. A large number of samples (n=83) were screened in the present study, whereas the previous studies were based on smaller sample sizes and may have underestimated the true frequency of such CNGs.

Although CNGs of *SOX2* were seldom observed in the MPMs and lung adenocarcinomas, the CNGs of the remaining four genes were detected in the MPM samples to a certain extent. The fact that the CNGs of four genes in the MPMs were less frequent in comparison to the lung adenocarcinomas suggested that CNG may not be a pivotal mechanism for the activation of oncogenes in MPMs, and that different mechanisms may be of greater importance. It has been previously reported that *EGFR* is overexpressed in 60-70% of MPM tissue specimens; however, it is not overexpressed in the normal mesothelium (29,33). Furthermore, exposure to asbestos fibers is known to cause *EGFR* aggregation (34). In the present study, *EGFR*, located at 7p12-p13, was the most frequent gene to exhibit CNGs (12 out of 83 MPMs and 20 out of 53 lung adenocarcinomas). Björkqvist *et al* (2) reported similar results, such as gains of genetic material in 5p, 6p and 7p between MPMs and lung adenocarcinomas. The study detected a gain in 7p in 7 out of 34 MPMs and 11 out of 30 lung adenocarcinomas (2). MPMs rarely harbor *EGFR* mutations (31,35-37). There were no *EGFR* mutations detected in MPMs in the present study, as expected. Upon analysis, three cases of MPMs exhibited high *EGFR* gene amplification (CNG>10), and these cases were all epithelioid MPMs, which was consistent with the previous studies by Okuda *et al* (29) and Enomoto *et al* (31). It remains unclear whether high-level amplification of *EGFR* is more prominent in MPMs compared with lung adenocarcinomas, although the frequency of CNGs for *EGFR* is lower in MPMs compared with lung adenocarcinomas. In MPMs with *EGFR* amplification, the inhibition of *EGFR* pathways should exert an antitumor effect. In lung cancer, the results of two randomized phase III trials that compared a placebo to erlotinib or gefitinib treatment indicated that *EGFR* copy number detected by fluorescence *in situ* hybridization was the best predictor of survival (38). Patients with colorectal cancer who responded to anti-*EGFR* treatment with cetuximab or panitumumab exhibited an increased *EGFR* copy number (39). Although two phase II studies of single-agent *EGFR*-TKI therapy to treat MPMs failed to demonstrate their clinical efficacy, in the gefitinib trial, 2 of 43 MPM patients responded to gefitinib (40,41). These data suggest that a small proportion of patients (with

*EGFR* gene amplification) may be candidates for anti-*EGFR* treatment (29).

In conclusion, the present study detected novel CNGs in genes other than *EGFR*. MPM samples exhibited these CNGs less frequently compared with lung adenocarcinomas. The differences in DNA CNG between the two tumor types suggested that they are genetically different.

## Acknowledgements

The authors would like to thank Ms. Fumiko Isobe for providing excellent technical support. The study received Grant-in-Aids for the 13 fields of occupational injuries and illnesses of the Japan Labor Health and Welfare Organization.

## References

1. Spirtas R, Heineman EF, Bernstein L, Beebe GW, Keehn RJ, Stark A, Harlow BL and Benichou J: Malignant mesothelioma: Attributable risk of asbestos exposure. *Occup Environ Med* 51: 804-811, 1994.
2. Björkqvist AM, Tammilehto L, Nordling S, Nurminen M, Anttila S, Mattson K and Knuutila S: Comparison of DNA copy number changes in malignant mesothelioma, adenocarcinoma and large-cell anaplastic carcinoma of the lung. *Br J Cancer* 77: 260-269, 1998.
3. Taniguchi T, Karnan S, Fukui T, Yokoyama T, Tagawa H, Yokoi K, Ueda Y, Mitsudomi T, Horio Y, Hida T, *et al*: Genomic profiling of malignant pleural mesothelioma with array-based comparative genomic hybridization shows frequent non-random chromosomal alteration regions including JUN amplification on 1p32. *Cancer Sci* 98: 438-446, 2007.
4. Chiosea S, Krasinskas A, Cagle PT, Mitchell KA, Zander DS and Dacic S: Diagnostic importance of 9p21 homozygous deletion in malignant mesotheliomas. *Mod Pathol* 21: 742-747, 2008.
5. Toyooka S, Kishimoto T and Date H: Advances in the molecular biology of malignant mesothelioma. *Acta Med Okayama* 62: 1-7, 2008.
6. Fleury-Feith J, Lecomte C, Renier A, Matrat M, Kheuang L, Abramowski V, Levy F, Janin A, Giovannini M and Jaurand MC: Hemizygosity of Nf2 is associated with increased susceptibility to asbestos-induced peritoneal tumours. *Oncogene* 22: 3799-3805, 2003.
7. Nemoto H, Tate G, Kishimoto K, Saito M, Shirahata A, Umemoto T, Matsubara T, Goto T, Mizukami H, Kigawa G, *et al*: Heterozygous loss of NF2 is an early molecular alteration in well-differentiated papillary mesothelioma of the peritoneum. *Cancer Genet* 205: 594-598, 2012.
8. Metcalf RA, Welsh JA, Bennett WP, *et al*: p53 and Kirsten-ras mutations in human mesothelioma cell lines. *Cancer Res* 52: 2610-2615, 1992.
9. Papp T, Schipper H, Pemsel H, *et al*: Mutational analysis of N-ras, p53, p16INK4a, p14ARF and CDK4 genes in primary human malignant mesotheliomas. *Int J Oncol* 18: 425-433, 2001.
10. Toyooka S, Pass HI, Shivapurkar N, Fukuyama Y, *et al*: Aberrant methylation and simian virus 40 tag sequences in malignant mesothelioma. *Cancer Res* 61: 5727-5730, 2001.
11. Kobayashi N, Toyooka S, Yanai H, *et al*: Frequent p16 inactivation by homozygous deletion or methylation is associated with a poor prognosis in Japanese patients with pleural mesothelioma. *Lung Cancer* 62: 120-125, 2008.
12. Goto Y, Shinjo K, Kondo Y, *et al*: Epigenetic profiles distinguish malignant pleural mesothelioma from lung adenocarcinoma. *Cancer Res* 69: 9073-9082, 2009.
13. Addis B and Roche H: Problems in mesothelioma diagnosis. *Histopathology* 54: 55-68, 2009.
14. Gee GV, Koestler DC, Christensen BC, *et al*: Downregulated microRNAs in the differential diagnosis of malignant pleural mesothelioma. *Int J Cancer* 127: 2859-2869, 2010.
15. Betta PG, Magnani C, Bensi T, Trinchieri NF and Orecchia S: Immunohistochemistry and molecular diagnostics of pleural malignant mesothelioma. *Arch Pathol Lab Med* 136: 253-261, 2012.

16. Husain AN, Colby T, Ordóñez N, Krausz T, Attanoos R, Beasley MB, Borczuk AC, Butnor K, Cagle PT, Chirieac LR, *et al*; International Mesothelioma Interest Group: Guidelines for pathologic diagnosis of malignant mesothelioma: 2012 update of the consensus statement from the International Mesothelioma Interest Group. *Arch Pathol Lab Med* 137: 647-667, 2013.
17. Yamamoto H, Shigematsu H, Nomura M, Lockwood WW, Sato M, Okumura N, Soh J, Suzuki M, Wistuba II, Fong KM, *et al*: PIK3CA mutations and copy number gains in human lung cancers. *Cancer Res* 68: 6913-6921, 2008.
18. Soh J, Okumura N, Lockwood WW, Yamamoto H, Shigematsu H, Zhang W, Chari R, Shames DS, Tang X, MacAulay C, *et al*: Oncogene mutations, copy number gains and mutant allele specific imbalance (MASI) frequently occur together in tumor cells. *PLoS One* 4: e7464, 2009.
19. Kubo T, Yamamoto H, Lockwood WW, Valencia I, Soh J, Peyton M, Jida M, Otani H, Fujii T, Ouchida M, *et al*: *MET* gene amplification or *EGFR* mutation activate *MET* in lung cancers untreated with *EGFR* tyrosine kinase inhibitors. *Int J Cancer* 124: 1778-1784, 2009.
20. Sasaki H, Hikosaka Y, Kawano O, Moriyama S, Yano M and Fujii Y: Evaluation of Kras gene mutation and copy number gain in non-small cell lung cancer. *J Thorac Oncol* 6: 15-20, 2011.
21. Zhao X, Weir BA, LaFramboise T, Lin M, Beroukhi R, Garraway L, Beheshti J, Lee JC, Naoki K, Richards WG, *et al*: Homozygous deletions and chromosome amplifications in human lung carcinomas revealed by single-nucleotide polymorphism array analysis. *Cancer Res* 65: 5561-5570, 2005.
22. Yuan P, Kadara H, Behrens C, Tang X, Woods D, Solis LM, Huang J, Spinola M, Dong W, Yin G, *et al*: Sex-determining region Y-Box 2 (*SOX2*) is a potential cell-lineage gene highly expressed in the pathogenesis of squamous cell carcinomas of the lung. *PLoS One* 5: e9112, 2010.
23. Kohler LH, Mireskandari M, Knösel T, Altendorf-Hofmann A, Kunze A, Schmidt A, Presselt N, Chen Y and Petersen I: *FGFR1* expression and gene copy numbers in human lung cancer. *Virchows Arch* 461: 49-57, 2012.
24. Heist RS, Mino-Kenudson M, Sequist LV, Tammireddy S, Morrissey L, Christiani DC, Engelman JA and Iafrate AJ: *FGFR1* amplification in squamous cell carcinoma of the lung. *J Thorac Oncol* 7: 1775-1780, 2012.
25. Sasaki H, Yokota K, Hikosaka Y, Moriyama S, Yano M and Fujii Y: Increased *SOX2* copy number in lung squamous cell carcinomas. *Exp Ther Med* 3: 44-48, 2012.
26. Jagadeeswaran R, Ma PC, Seiwert TY, Jagadeeswaran S, Zumba O, Nallasura V, Ahmed S, Filiberti R, Paganuzzi M, Puntoni R, *et al*: Functional analysis of c-met hepatocyte growth factor pathway in malignant pleural mesothelioma. *Cancer Res* 66: 352-361, 2006.
27. Engelman JA, Zejnullahu K, Mitsudomi T, Song Y, Hyland C, Park JO, Lindeman N, Gale CM, Zhao X, Christensen J, *et al*: *MET* amplification leads to gefitinib resistance in lung cancer by activating ERBB3 signaling. *Science* 316: 1039-1043, 2007.
28. Asano H, Toyooka S, Tokumo M, Ichimura K, Aoe K, Ito S, Tsukuda K, Ouchida M, Aoe M, Katayama H, *et al*: Detection of *EGFR* gene mutation in lung cancer by mutant-enriched polymerase chain reaction assay. *Clin Cancer Res* 12: 43-48, 2006.
29. Okuda K, Sasaki H, Kawano O, Yukiue H, Yokoyama T, Yano M and Fujii Y: Epidermal growth factor receptor gene mutation, amplification and protein expression in malignant pleural mesothelioma. *J Cancer Res Clin Oncol* 134: 1105-1111, 2008.
30. Rena O, Boldorini LR, Gaudino E and Casadio C: Epidermal growth factor receptor overexpression in malignant pleural mesothelioma: Prognostic correlations. *J Surg Oncol* 104: 701-705, 2011.
31. Enomoto Y, Kasai T, Takeda M, Takano M, Morita K, Kadota E, Iizuka N, Maruyama H, Haratake J, Kojima Y, *et al*: A comparison of epidermal growth factor receptor expression in malignant peritoneal and pleural mesothelioma. *Pathol Int* 62: 226-231, 2012.
32. Takeda M, Kasai T, Enomoto Y, Takano M, Morita K, Kadota E, Iizuka N, Maruyama H and Nonomura A: Genomic gains and losses in malignant mesothelioma demonstrated by FISH analysis of paraffin-embedded tissues. *J Clin Pathol* 65: 77-82, 2012.
33. Destro A, Ceresoli GL, Falleni M, Zucali PA, Morengi E, Bianchi P, Pellegrini C, Cordani N, Vaira V, Alloisio M, *et al*: *EGFR* overexpression in malignant pleural mesothelioma. An immunohistochemical and molecular study with clinico-pathological correlations. *Lung Cancer* 51: 207-215, 2006.
34. Pache JC, Janssen YM, Walsh ES, Quinlan TR, Zanella CL, Low RB, Taatjes DJ and Mossman BT: Increased epidermal growth factor-receptor protein in a human mesothelial cell line in response to long asbestos fibers. *Am J Pathol* 152: 333-340, 1998.
35. Cortese JF, Gowda AL, Wali A, Eliason JF, Pass HI and Everson RB: Common *EGFR* mutations conferring sensitivity to gefitinib in lung adenocarcinoma are not prevalent in human malignant mesothelioma. *Int J Cancer* 118: 521-522, 2006.
36. Velcheti V, Kasai Y, Viswanathan AK, Ritter J and Govindan R: Absence of mutations in the epidermal growth factor receptor (*EGFR*) kinase domain in patients with mesothelioma. *J Thorac Oncol* 4: 559, 2009.
37. Mezzapelle R, Miglio U, Rena O, Paganotti A, Allegrini S, Antona J, Molinari F, Frattini M, Monga G, Alabiso O, *et al*: Mutation analysis of the *EGFR* gene and downstream signalling pathway in histologic samples of malignant pleural mesothelioma. *Br J Cancer* 108: 1743-1749, 2013.
38. Tsao MS, Sakurada A, Cutz JC, Zhu CQ, Kamel-Reid S, Squire J, Lorimer I, Zhang T, Liu N, Daneshmand M, *et al*: Erlotinib in lung cancer - molecular and clinical predictors of outcome. *N Engl J Med* 353: 133-144, 2005.
39. Moroni M, Veronese S, Benvenuti S, Marrapese G, Sartore-Bianchi A, Di Nicolantonio F, Gambacorta M, Siena S and Bardelli A: Gene copy number for epidermal growth factor receptor (*EGFR*) and clinical response to anti-*EGFR* treatment in colorectal cancer: a cohort study. *Lancet Oncol* 6: 279-286, 2005.
40. Govindan R, Kratzke RA, Herndon JE, Niehans GA, Vollmer R, Watson D, Green MR and Kindler HL; Cancer and Leukemia Group B (CALGB 30101): Gefitinib in patients with malignant mesothelioma: A phase II study by the Cancer and Leukemia Group B. *Clin Cancer Res* 11: 2300-2304, 2005.
41. Garland LL, Rankin C, Gandara DR, Rivkin SE, Scott KM, Nagle RB, Klein-Szanto AJ, Testa JR, Altomare DA and Borden EC: Phase II study of erlotinib in patients with malignant pleural mesothelioma: A Southwest Oncology Group Study. *J Clin Oncol* 25: 2406-2413, 2007.





## Research Article

# Clinical Investigation of Benign Asbestos Pleural Effusion

**Nobukazu Fujimoto,<sup>1</sup> Kenichi Gemba,<sup>2,3</sup> Keisuke Aoe,<sup>4</sup>  
Katsuya Kato,<sup>5,6</sup> Takako Yokoyama,<sup>7</sup> Ikuji Usami,<sup>7</sup> Kazuo Onishi,<sup>8</sup>  
Keiichi Mizuhashi,<sup>9</sup> Toshikazu Yusa,<sup>10</sup> and Takumi Kishimoto<sup>11</sup>**

<sup>1</sup> Department of Medical Oncology, Okayama Rosai Hospital, 1-10-25 Chikkomidorimachi, Okayama 7028055, Japan

<sup>2</sup> Department of Respiratory Medicine, Okayama Rosai Hospital, 1-10-25 Chikkomidorimachi, Okayama 7028055, Japan

<sup>3</sup> Department of Respiratory Medicine, Chugoku Chuo Hospital, Fukuyama 7200001, Japan

<sup>4</sup> Department of Medical Oncology, Yamaguchi-Ube Medical Center, 685 Higashikiwa, Ube 7550241, Japan

<sup>5</sup> Department of Radiology, Okayama University Hospital, 2-5-1 Shikatacho, Okayama 7008558, Japan

<sup>6</sup> Department of Diagnostic Radiology 2, Kawasaki Medical School, Okayama 7008505, Japan

<sup>7</sup> Department of Respiratory Medicine, Asahi Rosai Hospital, 61 Hirakochokita, Owariasahi 4880875, Japan

<sup>8</sup> Department of Respiratory Medicine, Kobe Rosai Hospital, 4-1-23 Kagoikedori, Chuoku, Kobe 6510053, Japan

<sup>9</sup> Department of Respiratory Medicine, Toyama Rosai Hospital, 992 Rokuromaru, Uozu 9370042, Japan

<sup>10</sup> Department of Thoracic Surgery, Chiba Rosai Hospital, 2-16 Tatsumidaihigashi, Ichihara 2900003, Japan

<sup>11</sup> Department of Internal Medicine, Okayama Rosai Hospital, 1-10-25 Chikkomidorimachi, Okayama 7028055, Japan

Correspondence should be addressed to Nobukazu Fujimoto; [nfuj@okayamah.rofuku.go.jp](mailto:nfuj@okayamah.rofuku.go.jp)

Received 17 August 2015; Revised 29 October 2015; Accepted 9 November 2015

Academic Editor: Denis Caillaud

Copyright © 2015 Nobukazu Fujimoto et al. This is an open access article distributed under the Creative Commons Attribution License, which permits unrestricted use, distribution, and reproduction in any medium, provided the original work is properly cited.

There is no detailed information about benign asbestos pleural effusion (BAPE). The aim of the study was to clarify the clinical features of BAPE. The criteria of enrolled patients were as follows: (1) history of asbestos exposure; (2) presence of pleural effusion determined by chest X-ray, CT, and thoracentesis; and (3) the absence of other causes of effusion. Clinical information was retrospectively analysed and the radiological images were reviewed. There were 110 BAPE patients between 1991 and 2012. All were males and the median age at diagnosis was 74 years. The median duration of asbestos exposure and period of latency for disease onset of BAPE were 31 and 48 years, respectively. Mean values of hyaluronic acid, adenosine deaminase, and carcinoembryonic antigen in the pleural fluid were 39,840 ng/mL, 23.9 IU/L, and 1.8 ng/mL, respectively. Pleural plaques were detected in 98 cases (89.1%). Asbestosis was present in 6 (5.5%) cases, rounded atelectasis was detected in 41 (37.3%) cases, and diffuse pleural thickening (DPT) was detected in 30 (27.3%) cases. One case developed lung cancer (LC) before and after BAPE. None of the cases developed malignant pleural mesothelioma (MPM) during the follow-up.

## 1. Introduction

Asbestos-related pathological changes of the pleura include pleural plaques, malignant pleural mesothelioma (MPM), diffuse pleural thickening (DPT), and benign asbestos pleural effusion (BAPE). BAPE is a nonmalignant pleural disease initially described in 1964 [1]. It is also termed asbestos pleuritis. Once a patient is diagnosed with BAPE, he or she is compensated by workers' compensation in Japan. Epler et al. [2] advocated diagnostic criteria for BAPE, which

include (1) previous asbestos exposure, (2) determination of pleural effusion by chest X-ray or thoracentesis, and (3) the absence of other causes of effusion. They also stated that follow-up assessments for at least 3 years were essential to confirm the diagnosis and to exclude the development of malignant diseases such as MPM or lung carcinomatous pleuritis. Later, Hillerdal and Ozesmi [3] described that a 1-year follow-up would be sufficient based on a detailed exploration including computed tomographic (CT) scanning. Most of the previous studies included small numbers of

patients and were undertaken in the 1980s, so no detailed information is available about the disease.

In the current study, we retrospectively analysed the clinical features of BAPE in patients in Japan. The aim of the study was to clarify the clinical features of BAPE and to suggest more practical diagnostic standard for the disease.

## 2. Patients and Methods

**2.1. Subjects.** Enrolled patients were referred to Rosai Hospital and affiliated hospitals in Japan for an examination for pleural effusion and were finally diagnosed with BAPE. The criteria of enrolled patients were as follows: (1) previous history of asbestos exposure obtained by an in-person questionnaire or interview; (2) presence of pleural effusion determined by chest X-ray, CT, and thoracentesis; and (3) the absence of other causes of effusion. The pleural fluid was collected by thoracentesis or thoracoscopy, and information on cell classification, cytological analysis, and the biochemical examination was extracted from the medical records. Hyaluronic acid (HA), adenosine deaminase (ADA), and carcinoembryonic antigen (CEA) were included among the clinical laboratory tests. The HA concentration was determined using a latex agglutination turbidimetric immunoassay. ADA was measured using an enzymatic technique. CEA was measured using a chemiluminescent immunoassay.

**2.2. Data Collection and Analysis.** Clinical and demographic information was obtained from the medical records at each facility. The information included age, gender, smoking status, initial symptoms, and results of laboratory testing of the pleural effusion. The work histories, those of the family members, and residential histories were investigated to assess the patient's history of asbestos exposure.

The radiological images were sent to Okayama Rosai Hospital for review. Characteristic radiological findings associated with asbestos exposure were assessed as the presence of pleural effusion, asbestosis, rounded atelectasis, pleural plaques, and DPT. Asbestosis was classified on chest X-rays according to perfusion rate (PR) based on the International Labour Organization (ILO) criteria [4]. DPT was defined as pleural thickening of more than 5 mm on chest X-rays, extending for more than half of the lateral thoracic wall (LTW) in cases of unilateral DPT or more than quarter of the LTW in cases of bilateral DPT [5]. The presence of pleural effusion, rounded atelectasis, and pleural plaques was assessed on chest CT.

Survival data were determined from the day pleural effusion was detected to the day of death or last follow-up and analysed using the Kaplan-Meier method with SPSS 11.0 software (SPSS, Inc., Chicago, IL, USA).

This study was done according to the Ethical Guidelines for Epidemiological Research by the Japanese Ministry of Education, Culture, Sports, Science, and Technology and the Ministry of Health, Labour, and Welfare. This study was approved by Japan Labour Health and Welfare Organization and the institutional review boards of each institution. Patient confidentiality was strictly maintained. This study was carried

TABLE 1: Patient characteristics.

Age ( $n = 110$ )	
Median (range)	74 (36–90)
Gender ( $n = 110$ )	
Male/female	110/0
Smoking history ( $n = 63$ )	
Ever/current	56
Never	7
Symptoms ( $n = 65$ , multiple answers)	
Dyspnea	34
Cough	15
Chest pain	13
Fever	3
Palpitation	2
Sputum	1
Wheezing	1
Back pain	1
Weight loss	1
Fatigue	1

out according to the principles set out in the Declaration of Helsinki.

## 3. Results

**3.1. Patient Characteristics.** One hundred ten patients from 9 institutions fulfilled the enrolled criteria based on the descriptions in their medical records and review of the radiographs between 1991 and 2012. Characteristics of the patients are shown in Table 1. Smoking history was obtained in 63 cases including 56 ever/current smokers and 7 never smokers, with the median (range) pack-years of 34.5 (0–112). Pleural effusion was found in 56 cases in the right, 25 in the left, and 27 in both thoracis. Sixty-five patients visited the clinic for subjective symptoms, and pleural effusion was detected at the regular medical check-up in 35 cases without any symptoms. Pleural effusion was detected during the treatment of other diseases in another 15 cases. Thoracentesis was performed in all patients to collect pleural fluid. Thoracoscopic exploration was done in 78 patients to exclude carcinomatous pleuritis or MPM and to confirm the diagnosis of BAPE.

**3.2. Asbestos Exposure History.** A history of asbestos exposure was reported by 109 patients, with one patient whose detailed information of asbestos exposure was not obtained. Among the 109 patients, 108 patients had a history of occupational asbestos exposure and one patient had a history of environmental asbestos exposure. The occupational categories associated with asbestos exposure are shown in Table 2. The median (range) age of the first exposure to asbestos was 21.5 (14–58) years. The median (range) duration of asbestos exposure was 31 (0.75–50) years and the median (range) period of latency for disease onset of BAPE was 48 (17–76) years.

TABLE 2: Occupational category related to asbestos exposure.

Shipbuilding	25
Construction	20
Chemical facility	10
Asbestos products manufacturing	8
Electrical work	8
Plumbing	7
Asbestos transportation	5
Moisturizing work	4
Asbestos spraying	3
Steel production	3
Demolition work	2
Automobile manufacturing	2
Heat insulation	2
Firebrick manufacturing	2
Glasswork	1
Metallic product manufacture	1
Furnace installation	1
Coating industry	1
Shipman	1
Others	2
Total	108

**3.3. Characteristics of the Pleural Effusion.** Information regarding the pleural effusion was obtained in 104 cases. The gross impression of the pleural fluid was bloody in 75 cases, light yellow in 27, and light brown and dark red in 1 case each. The effusions were exudative in all cases. A cellular classification of the fluid was obtained in 57 cases and the median proportions of lymphocytes, macrophages, neutrophils, and eosinophils were 77.7%, 9.7%, 8.0%, and 8.0%, respectively. The HA concentration was determined in 106 cases and the mean (standard deviation) concentration was 39,840 (40,228) ng/mL. Mean (standard deviation) values of ADA and CEA were 23.9 (24.9) IU/L and 1.8 (1.3) ng/mL, respectively.

**3.4. Concomitant Asbestos-Related Findings.** As shown in Table 3, pleural plaques were detected in 98 cases (89.1%), among which 76 cases were calcified. Asbestosis was present in 6 cases, rounded atelectasis was detected in 41 cases (37.3%), and DPT was detected in 30 cases (27.3%). One of the cases developed lung cancer (LC) before and after diagnosis of BAPE. The patient had undergone right upper lobectomy for LC two years before his BAPE diagnosis and left partial lobectomy for another LC two years after his BAPE diagnosis.

**3.5. Clinical Course.** In most of the cases, thoracentesis and/or thoracotomy were done to collect the fluid and drain the pleural effusion. Oral steroids were prescribed in 5 cases and one of them demonstrated temporal decrease of the effusion. Survival data was obtained in 70 cases from Okayama Rosai Hospital. As shown in Figure 1, median overall survival was 104.2 months (95% confidence interval (CI), 67.3–141.0 months) after a median observation period of

TABLE 3: Concomitant asbestos-related radiological findings.

Findings	<i>n</i>	%
Pleural plaques	98	89.1
Calcified	76	
Asbestosis	6	5.7
	1	3
PR <sup>†</sup>	2	2
	3	1
Rounded atelectasis	41	37.3
DPT <sup>‡</sup>	30	27.3

<sup>†</sup> Perfusion rate, <sup>‡</sup> diffuse pleural thickening.

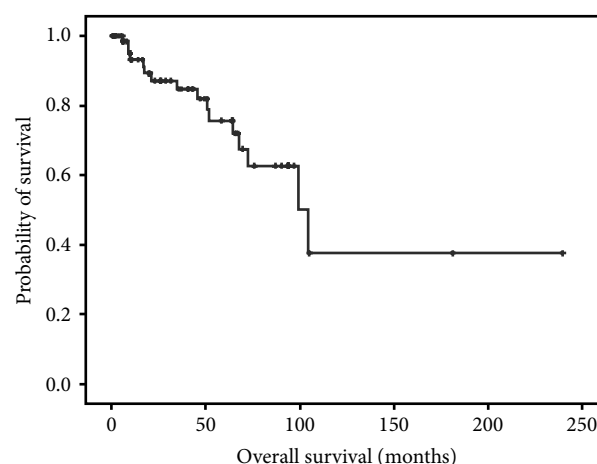


FIGURE 1: Overall survival of patients with benign asbestos-related pleural effusions at Okayama Rosai Hospital.

73.0 months (95% CI, 16.2–268.2 months). There were 17 dead cases out of 70 cases at the analysis. The causes of death were determined in 11 cases including 7 respiratory failure cases and each 1 of renal failure, suicide, septic shock due to urinary tract infection, and death of old age. There were 9 cases that developed DPT out of the 17 cases, including the 7 dead cases of respiratory failure. At the time of the analysis, none of the cases had developed MPM.

## 4. Discussion

In the current study, we examined the clinical features of BAPE and demonstrated that BAPE developed after long-term asbestos exposure. In a previous report, BAPE occurred 15–20 years after exposure and was more common in younger patients aged 21–40 years [6]. In another report, the interval between asbestos exposure and presentation of BAPE varied between 5 and more than 30 years, and early onset was correlated with higher asbestos exposure [7]. Wagner reported that BAPes were usually unilateral, and the most common manifestation of asbestos-related pleural disease occurred 10 to 20 years after exposure [8]. A limitation of these earlier studies is that the diagnosis criteria of BAPE were ambiguous in the studies. The median latency period between asbestos exposure and BAPE development in the current study was

TABLE 4: Proposed diagnostic criteria of benign asbestos pleural effusion.

Diagnostic criteria
(1) Asbestos exposure history.
(2) Exudative effusion.
(3) Exclusion of other pleuritis such as lung cancer, MPM <sup>†</sup> , and tuberculous pleuritis by radiological examination and pleural biopsy via thoracoscopy.
Additional diagnostic information
(1) In cases thoracoscopy could not be undergone, the diagnosis should be discussed based on the bacteriological examination and biochemical markers below.
(a) Elevated carcinoembryonic antigen (>5 ng/mL) suggests carcinomatous pleuritis.
(b) Elevated adenosine deaminase (>35 IU/L) suggests tuberculous pleuritis.
(c) Elevated hyaluronic acid (>100,000 ng/dL) suggests MPM.
(2) In cases with some concomitant medical problem such as autoimmune diseases, the activity of the disease should be carefully evaluated.

<sup>†</sup>Malignant pleural mesothelioma.

48 years, which was similar to that observed for MPM (41 years), LC (47 years), and asbestos-induced DPT (46 years) in our previous reports [4, 9, 10]. We consider that BAPE develops after a long latency period in those with a history of asbestos exposure. There is one point, however, that most of the patients of BAPE in the current study have associated with other asbestos-related lesions such as rounded atelectasis and/or diffuse pleural thickening. It is possible that BAPE might have been developed earlier in these cases, and this could be an explanation of the longer latency of BAPE than previously published. The current study suggests that BAPE can develop after moderate-to-high levels of exposure to asbestos, because the occupational category of the subjects in the current study included those of relatively high levels of asbestos exposure such as asbestos product manufacturing, construction, and shipbuilding, although the correlation between the exposure amount and development of BAPE is unclear. The subjects in the current study included substantial portion of those with smoking history. To our knowledge, the correlation between BAPE and smoking history has not been reported.

The diagnosis of BAPE should be based on a history of asbestos exposure and an exclusion of other causes of effusion such as tuberculous pleuritis, bacterial pleuritis, collagen diseases, heart failure, and malignant conditions such as MPM and LC. In our analysis, the gross impression of the pleural fluid was bloody in 72% of the cases, and cellular classification of the fluid demonstrated lymphocyte dominancy. These results are similar to those of a previous report showing that the effusion was exudative and could be hemorrhagic, as well as predominantly eosinophilic [11].

In cases of LC, tumor cells are detected in the fluid in more than 60% of cases [12]. In cases with MPM, tumor cells can be detected in the pleural fluid, but the detection rate has been reported as less than 30% [13]. Tuberculosis pleuritis or bacterial pleuritis could be diagnosed by staining for acid-fast bacteria, polymerase chain reaction detection, or bacterial culture, although the detection rate is usually low. These analyses may not always determine the diagnosis but should be undergone to exclude MPM, LC, and tuberculosis or bacterial pleuritis and to make the diagnosis of BAPE.

In addition, we analysed some markers such as HA concentration, ADA, and CEA. Recently, we reported the clinical usefulness of HA for the differential diagnosis of MPM and BAPE [14]. In cases with tuberculosis pleuritis, elevated values of ADA could help in the diagnosis [15]. However, elevated ADA may not be limited to tuberculous pleuritis, as it is also present in LC or MPM [16]. In cases with elevated CEA values, carcinomatous pleuritis is strongly suggested [17]. These markers should be determined to exclude these conditions and to confirm a diagnosis of BAPE. However, the differential diagnosis of MPM and BAPE is especially difficult, even when based on these markers. Especially in cases with exudative pleural effusions, thoracoscopic exploration and pleural biopsy should be performed to exclude MPM and confirm the diagnosis of BAPE [18].

Based on the findings in the current study and previous reports, we propose more practical diagnostic standard for the diagnosis of BAPE including (1) asbestos exposure history, (2) exudative effusion, and (3) exclusion of other pleuritis such as LC, MPM, and tuberculous pleuritis by radiological examination and pleural biopsy via thoracoscopy. Additional diagnostic information is as follows: (1) in cases thoracoscopy could not be undergone, the diagnosis should be discussed based on the bacteriological examination and biochemical markers such as CEA, ADA, and HA; in cases with elevated CEA (>5 ng/mL), ADA (>35 IU/L), or HA (>100,000 ng/dL), carcinomatous pleuritis, tuberculous pleuritis, or MPM is more likely, respectively; and (2) in cases with some concomitant medical problem such as autoimmune diseases, the activity of the disease should be carefully evaluated, because autoimmune diseases such as systemic lupus erythematosus or rheumatoid arthritis could involve the pleura and cause pleural effusion (Table 4).

“Benign” is meant to refer to a nonmalignant process, but these effusions can be associated with significant morbidity [19]. The effusion generally takes a long time to resolve. It may resolve spontaneously or be followed by DPT, which causes extrapulmonary restriction and may thereby ultimately become disabling. Previous studies reported that a considerable number of patients with BAPE subsequently developed DPT [2, 3]. Actually, in our previous study, half

the patients with asbestos-induced DPT had a history of BAPE [4]. Furthermore, in the current study one patient developed LC before and after being diagnosed with BAPE. The risks of developing MPM or LC in patients with BAPE are increased compared with those of the general population because of their past history of asbestos exposure. Particular attention should be paid to the management of patients with BAPE.

There are a few limitations to the current study. First, this was a retrospective study. Second, pathological analyses including immunohistochemistry were not reviewed. In addition, there are recent reports that increased uptake of fluorodeoxyglucose (FDG) by positron emission tomography (PET) may be a useful marker to distinguish MPM from benign pleural disease [20, 21]. In addition, recent reports revealed that biomarkers such as soluble mesothelin-related peptides (SMRP) are selectively elevated in patients with MPM [22, 23]. A clinical study to evaluate the utility of PET and/or SMRP for the differentiation between MPM and BAPE is warranted.

## 5. Conclusions

BAPE develops after a long latency period after past asbestos exposure. The diagnosis of BAPE should be based on the exclusion of other pleural diseases. A thorough evaluation, including diagnostic thoracentesis and cytological and bacterial analysis, must be performed. Clinical markers such as HA, ADA, and CEA might help with the differential diagnosis. However, thoroscopic exploration and pleural biopsy should be performed to confirm a diagnosis of BAPE.

## Disclosure

This study is a part of “the research and development and the dissemination projects related to the 9 fields of occupational injuries and illnesses” of Japan Labour Health and Welfare Organization. This organization had no involvement in the study design, collection, analysis, and interpretation of the data, writing of the paper, or decision to submit the paper for publication.

## Conflict of Interests

The authors declare that there is no conflict of interests in their submitted paper.

## References

- [1] H. B. Eisenstadt, “Asbestos pleurisy,” *Diseases of the Chest*, vol. 46, pp. 78–81, 1964.
- [2] G. R. Epler, T. C. McLoud, and E. A. Gaensler, “Prevalence and incidence of benign asbestos pleural effusion in a working population,” *The Journal of the American Medical Association*, vol. 247, no. 5, pp. 617–622, 1982.
- [3] G. Hillerdal and M. Ozesmi, “Benign asbestos pleural effusion: 73 exudates in 60 patients,” *European Journal of Respiratory Diseases*, vol. 71, no. 2, pp. 113–121, 1987.
- [4] N. Fujimoto, K. Kato, I. Usami et al., “Asbestos-related diffuse pleural thickening,” *Respiration*, vol. 88, no. 4, pp. 277–284, 2014.
- [5] American Thoracic Society, “Medical Section of the American Lung Association: the diagnosis of nonmalignant diseases related to asbestos,” *American Review of Respiratory Disease*, vol. 134, pp. 363–368, 1986.
- [6] P. Ernst and J. Zejda, “Pleural and airway diseases associated with mineral fibers,” in *Mineral Fibers and Health*, D. Liddell and K. Miller, Eds., pp. 121–134, CRC, Boca Raton, Fla, USA, 1991.
- [7] B. W. S. Robinson and A. W. Musk, “Benign asbestos pleural effusion: diagnosis and course,” *Thorax*, vol. 36, no. 12, pp. 896–900, 1981.
- [8] G. R. Wagner, “Asbestosis and silicosis,” *The Lancet*, vol. 349, no. 9061, pp. 1311–1315, 1997.
- [9] T. Kishimoto, K. Gemba, N. Fujimoto et al., “Clinical study on mesothelioma in Japan: relevance to occupational asbestos exposure,” *American Journal of Industrial Medicine*, vol. 53, no. 11, pp. 1081–1087, 2010.
- [10] T. Kishimoto, K. Gemba, N. Fujimoto et al., “Clinical study of asbestos-related lung cancer in Japan with special reference to occupational history,” *Cancer Science*, vol. 101, no. 5, pp. 1194–1198, 2010.
- [11] A. J. Ghio and V. L. Roggli, “Diagnosis and initial management of nonmalignant diseases related to asbestos,” *American Journal of Respiratory and Critical Care Medicine*, vol. 170, no. 6, pp. 691–715, 2004.
- [12] K. B. Sriram, V. Relan, B. E. Clarke et al., “Diagnostic molecular biomarkers for malignant pleural effusions,” *Future Oncology*, vol. 7, no. 6, pp. 737–752, 2011.
- [13] A. Medford and N. Maskell, “Pleural effusion,” *Postgraduate Medical Journal*, vol. 81, no. 961, pp. 702–710, 2005.
- [14] N. Fujimoto, K. Gemba, M. Asano et al., “Hyaluronic acid in the pleural fluid of patients with malignant pleural mesothelioma,” *Respiratory Investigation*, vol. 51, no. 2, pp. 92–97, 2013.
- [15] A. Gopi, S. M. Madhavan, S. K. Sharma, and S. A. Sahn, “Diagnosis and treatment of tuberculous pleural effusion in 2006,” *Chest*, vol. 131, no. 3, pp. 880–889, 2007.
- [16] Y. Ogata, K. Aoe, A. Hiraki et al., “Is adenosine deaminase in pleural fluid a useful marker for differentiating tuberculosis from lung cancer or mesothelioma in Japan, a country with intermediate incidence of tuberculosis?” *Acta Medica Okayama*, vol. 65, no. 4, pp. 259–263, 2011.
- [17] H.-Z. Shi, Q.-L. Liang, J. Jiang, X.-J. Qin, and H.-B. Yang, “Diagnostic value of carcinoembryonic antigen in malignant pleural effusion: a meta-analysis,” *Respirology*, vol. 13, no. 4, pp. 518–527, 2008.
- [18] A. Scherpereel, P. Astoul, P. Baas et al., “Guidelines of the European Respiratory Society and the European Society of Thoracic Surgeons for the management of malignant pleural mesothelioma,” *European Respiratory Journal*, vol. 35, no. 3, pp. 479–495, 2010.
- [19] R. Myers, “Asbestos-related pleural disease,” *Current Opinion in Pulmonary Medicine*, vol. 18, no. 4, pp. 377–381, 2012.
- [20] F. Bénard, D. Sterman, R. J. Smith, L. R. Kaiser, S. M. Albelda, and A. Alavi, “Metabolic imaging of malignant pleural mesothelioma with fluorodeoxyglucose positron emission tomography,” *Chest*, vol. 114, no. 3, pp. 713–722, 1998.
- [21] H. Yildirim, M. Metintas, E. Entok et al., “Clinical value of fluorodeoxyglucose-positron emission tomography/computed tomography in differentiation of malignant mesothelioma from


asbestos-related benign pleural disease: an observational pilot study,” *Journal of Thoracic Oncology*, vol. 4, no. 12, pp. 1480–1484, 2009.

- [22] A. Scherpereel, B. Grigoriu, M. Conti et al., “Soluble mesothelin-related peptides in the diagnosis of malignant pleural mesothelioma,” *American Journal of Respiratory and Critical Care Medicine*, vol. 173, no. 10, pp. 1155–1160, 2006.
- [23] N. Fujimoto, K. Gemba, M. Asano et al., “Soluble mesothelin-related protein in pleural effusion from patients with malignant pleural mesothelioma,” *Experimental and Therapeutic Medicine*, vol. 1, no. 2, pp. 313–317, 2010.



RESEARCH PAPER

# Brain metastases in malignant pleural mesothelioma

Tomoko Yamagishi<sup>1</sup> · Nobukazu Fujimoto<sup>2</sup>  · Yosuke Miyamoto<sup>1</sup> ·  
Michiko Asano<sup>1</sup> · Yasuko Fuchimoto<sup>1</sup> · Sae Wada<sup>1</sup> · Kenichi Kitamura<sup>1</sup> ·  
Shinji Ozaki<sup>1</sup> · Hideyuki Nishi<sup>3</sup> · Takumi Kishimoto<sup>4</sup>

Received: 1 September 2015 / Accepted: 25 November 2015  
© Springer Science+Business Media Dordrecht 2015

**Abstract** The brain is a rare site of metastasis in malignant pleural mesothelioma (MPM), and its clinical features and prognosis remain unclear. The aim of this study was to investigate the incidence, prognosis, and risk factors for brain metastases (BM) in MPM patients. Between July 1993 and October 2014, 150 patients with histologically proven MPM were included in this retrospective study. The cumulative incidence of BM was estimated with the Kaplan–Meier method, and differences between groups were analyzed by the log-rank test. Multivariate logistic regression analysis was applied to assess risk factors for BM. The median follow-up time was 11 months (range 0–154.0 months). A total of eight patients (5.3 %) developed BM during the course of their illness. Multivariate analysis identified age <65 years (odds ratio [OR] = 5.83,  $p = 0.038$ ) and International Mesothelioma Interest Group stage IV (OR = 1.69,  $p = 0.040$ ) as independent factors related to increased risk of developing BM. The 1- and 2-year cumulative rates of BM were 4.0 % (95 % confidence intervals [CI] 1.4–8.5 %) and 5.3 % (95 % CI 2.3–10.2 %), respectively. Our study showed that the overall survival (OS) of patients with BM was worse than

that of patients without BM (median OS 6.5 vs. 11.0 months,  $p = 0.037$ ). The prognosis for BM in MPM patients is poor. Clinicians should perform careful screening for BM, especially in patients with risk factors.

**Keywords** Asbestos · Malignant pleural mesothelioma · Brain metastases · Central nervous system · Brain

## Abbreviations

MPM	Malignant pleural mesothelioma
BM	Brain metastasis
ECOG	Eastern Cooperative Oncology Group
PS	Performance status
IMIG	International Mesothelioma Interest Group
EPS	European Organization for Research and Treatment of Cancer Prognostic Score
CALGB	Cancer and Leukemia Group B
MRI	Magnetic resonance imaging
CT	Computed tomography
OS	Overall survival

✉ Nobukazu Fujimoto  
nobufujimoto@gmail.com

<sup>1</sup> Department of Respiratory Medicine, Okayama Rosai Hospital, Okayama, Japan

<sup>2</sup> Department of Medical Oncology, Okayama Rosai Hospital, 1-10-25 Chikkomidorimachi, Minamiku, Okayama 702-8055, Japan

<sup>3</sup> Department of Surgery, Okayama Rosai Hospital, Okayama, Japan

<sup>4</sup> Department of Internal Medicine, Okayama Rosai Hospital, Okayama, Japan

## Introduction

Malignant pleural mesothelioma (MPM) is a rare but aggressive primary pleural neoplasm that is associated with asbestos exposure [1]. Its prognosis remains poor, as most patients have unresectable disease at the time of diagnosis. Although several treatment options are available to patients with MPM, the median survival time is approximately 12 months [2].

Brain metastasis (BM) is the most common type of intracerebral neoplasm and occurs in 10–30 % of adult

patients with systemic cancer [3]. The incidence of BM may be increasing, because of improved imaging techniques to detect BM and more effective systemic treatment that can prolong the tumor-bearing period of time, permitting the cancer to disseminate to the brain. Lung cancer, breast cancer, and malignant melanoma are the neoplasms most frequently associated with BM [4].

MPM typically spreads by local invasion or extension. Distant metastasis may occur; however, BM is quite rare and the majority of reported cases were identified by postmortem examination. The incidence of BM was reported to be only 3 % of MPM patients [5]. To date, there have been few reports on BM in patients with MPM. Recently, Chari et al. a case report and review of the literature on the topic [6], however, its clinical features and prognosis remain unclear. The aim of this single-institution retrospective study was to evaluate the incidence, risk factors, and survival outcome associated with BM in patients with MPM.

## Materials and methods

### Patient population

The study included 150 consecutive patients with histologically proven MPM who were seen between July 1993 and October 2014 at Okayama Rosai Hospital, Japan. Baseline demographic and clinicopathological variables were collected retrospectively from patients' medical records. These included age at initial diagnosis, gender, histological subtype, clinical stage, and baseline Eastern Cooperative Oncology Group (ECOG) performance status (PS). Clinical staging was determined according to the International Mesothelioma Interest Group (IMIG) staging system [7]. The European Organization for Research and Treatment of Cancer Prognostic Score (EPS) was used to subcategorize patients into low- or high-risk groups based on age, gender, histology, probability of diagnosis, and leukocyte count [8]. We also used the Cancer and Leukemia Group B (CALGB) score, which incorporates the presence of nonepithelial histology, weight loss, chest pain, high platelets and WBC, low hemoglobin, high serum lactate dehydrogenase, advanced age, and PS [9]. The patients were divided based on their CALGB score into three groups (i.e., groups 1/2, 3/4, or 5/6), because of the small numbers in the even-numbered groups [10].

Diagnosis of BM in MPM was based on magnetic resonance imaging (MRI) or contrast-enhanced computed tomography (CT) scans. Routine brain imaging was performed at the diagnosis but not during the follow-up period, unless BM was suspected. Leptomeningeal metastases

were not included in the actuarial incidence of BM in this study.

This study was approved by the Japan Labour, Health and Welfare Organization and the institutional review board of Okayama Rosai Hospital. Patient confidentiality was strictly maintained.

### Statistical analysis

A comparison of patient characteristics at diagnosis was performed by Fisher's exact test or Student's *t* test, as appropriate. Overall survival (OS) was calculated from the date of initial diagnosis to the date of last follow-up or death from any cause. OS was obtained by using Kaplan–Meier methods, and between-group differences were compared with the log-rank test. To determine risk factors associated with the development of BM, univariate and multivariate logistic regression models with a stepwise selection procedure were generated. A two-tailed *p* value of <0.05 was considered statistically significant. All statistical analysis was performed with STATA software (version 12.1; StataCorp, College Station, TX, USA).

## Results

### Patient characteristics

The median follow-up time for the 150 study participants was 11.0 months (range 0–154.0 months). Eight of the patients developed BM: three at diagnosis of MPM and five during the clinical course of MPM. Thus, the crude incidence rate of BM was 2.0 % (95 % confidence interval [CI] 0.4–5.7 %) at diagnosis and 5.3 % (95 % CI 2.3–10.2 %) overall. The median time from initial diagnosis to development of BM was 4.5 months (range 0–24.0 months); the 1- and 2-year cumulative rates for BM were 4.0 % (95 % CI 1.4–8.5 %) and 5.3 % (95 % CI 2.3–10.2 %), respectively.

In the cohort of patients with BM (*n* = 8), the median ( $\pm$ SD) age was 61.3 ( $\pm$ 6.3) years and all patients were men. The majority of the histological types were epithelioid (62.5 %) followed by sarcomatous (37.5 %). Three patients (37.5 %) had stage III disease, and five patients (62.5 %) had stage IV disease. Four patients (50 %) had symptoms of BM, such as ataxia (*n* = 2), headache (*n* = 1), and sensitivity disorders (*n* = 1). BM were in various locations including 5 in parietal lobe (62.5 %), 3 in frontal lobe (37.5 %), and each 2 in temporal lobe (25.0 %) and the cerebellum (25.0 %). The size of BM was 2 cm or less in all cases. At the time of detection of BM, four

**Table 1** Patients with brain metastases

Age/ gender	Histology	IMIG stage	Treatment for primary tumor	Interval to BM (months)	Metastatic site	Presence of other metastases	Treatment for BM	Clinical response to treatment for BM	Survival post BM (months)	OS (months)
64/M	Epithelioid	T3N0M0, stage III	Chemotherapy	24.0	Multiple	Lung, adrenals, lymph node	WBRT	No	3.0	27.0
70/M	Epithelioid	T3N0M1, stage IV	Chemotherapy	0.0	Right parietal lobe	–	Chemotherapy	No	2.0	2.0
63/M	Sarcomatous	T3N1M0, stage III	Surgery	2.0	Cerebellum	Lung, adrenals, liver, muscle, lymph node	Chemotherapy	No	1.0	3.0
54/M	Epithelioid	T2N0M1, stage IV	Chemotherapy	7.0	Multiple	Adrenals, bone	WBRT	No	1.0	8.0
64/M	Sarcomatous	T3N0M1, stage IV	Best supportive care	0.0	Multiple	Bone	WBRT	No	5.0	5.0
64/M	Epithelioid	T4N2M0, stage IV	Chemotherapy	15.0	Multiple	–	SRT + chemotherapy	Yes	5.0	20.0
49/M	Epithelioid	T3N0M0, stage III	Chemotherapy	7.0	Right frontal lobe	Adrenals, liver	SRT	No	5.0	12.0
66/M	Sarcomatous	T2N0M1, stage IV	Chemotherapy	0.0	Right parietal lobe	–	SRT	No	4.0	4.0

BM brain metastases, OS overall survival, IMIG International Mesothelioma Interest Group, WBRT whole brain radiation therapy, SRT stereotactic radiotherapy

patients (50 %) had developed other distant metastases, including adrenal gland ( $n = 3$ ), lung ( $n = 2$ ), lymph node ( $n = 2$ ), liver ( $n = 2$ ), muscle/soft tissue ( $n = 1$ ), and bone ( $n = 1$ ). The patients' baseline characteristics and therapies are presented in Table 1.

The clinicopathological characteristics of the patients with BM were compared with those of patients without BM (non-BM) (Table 2). Age at diagnosis was younger in BM than in non-BM patients ( $p = 0.034$ ), and there were more patients with pleural effusion at initial diagnosis in BM compared to non-BM patients ( $p = 0.044$ ). There was no difference between the two groups with respect to histological subtype.

## Treatment and survival

Of the three patients who presented BM at initial diagnosis, one patient underwent whole brain radiotherapy and one underwent radiosurgery. The remaining patient had asymptomatic BM and received systemic chemotherapy. Of the four patients who developed BM after initial systemic chemotherapy, two were treated with whole brain radiotherapy and two underwent radiosurgery. The final patient developed asymptomatic BM during the observation period after initial surgery and received systemic chemotherapy.

The median OS of the non-BM and BM groups was 11.0 months (range 0–154.0 months) and 6.5 months (range 2.0–27.0 months), respectively ( $p = 0.037$ ) (Fig. 1). All patients died of progressive disease, with a median survival of 3.5 months (range 1.0–5.0 months) after the development of BM.

## Risk factors

Univariate analysis revealed that age <65 years (odds ratio [OR] 6.06, 95 % CI 1.17–31.19,  $p = 0.031$ ), absence of pleural effusion (OR 4.56; 95 % CI 1.03–20.01,  $p = 0.044$ ), and IMIG stage IV (OR 1.72, 95 % CI 1.05–2.81,  $p = 0.031$ ) were potential risk factors for BM. In the multivariate analysis, age < 65 years (OR 5.83; 95 % CI 1.10–30.73,  $p = 0.038$ ) and IMIG stage IV (OR 1.69 95 % CI 1.02–2.80,  $p = 0.040$ ) remained associated with a high risk of BM (Table 3). Based on the results of multivariate analysis, we analyzed the effect of these two factors on the incidence of BM. For patients age  $\geq 65$  years and stage I–III, age <65 years and stage I–III, age  $\geq 65$  years and stage IV, and age <65 years and stage IV, the cumulative incidence rates of BM were 0, 8.1, 8.3, and 18.7 %, respectively ( $p = 0.003$ , Fisher's exact test) (Fig. 2).

**Table 2** Patient characteristics

Characteristic	Brain metastases ( <i>n</i> = 8)	No brain metastases ( <i>n</i> = 142)	<i>p</i> value
Median age, years (range)	61.3 ± 6.7	68.9 ± 9.9	0.034
Men	8 (100 %)	132 (93 %)	0.568
ECOG PS > 2	2 (25 %)	19 (13 %)	0.311
Pleural effusion at diagnosis			0.044
Yes	3 (38 %)	104 (73 %)	
No	5 (62 %)	38 (27 %)	
Histological subtype			0.584
Epithelioid subtype	5 (63 %)	92 (65 %)	
Nonepithelioid subtype	3 (37 %)	50 (35 %)	
Calretinin			0.07
Positive	5 (63 %)	121 (85 %)	
Negative	2 (25 %)	9 (6 %)	
Missing	1 (12 %)	12 (8 %)	
IMIG stage			0.051
I–II	0 (0 %)	54 (38 %)	
III–IV	8 (100 %)	88 (62 %)	
EORTC prognostic score			0.712
High risk	4 (50 %)	87 (61 %)	
Low risk	4 (50 %)	55 (39 %)	
CALGB score			0.076
1–2	0 (0 %)	49 (35 %)	
3–4	5 (63 %)	63 (44 %)	
5–6	3 (37 %)	30 (21 %)	
Treatment modality			0.630
Surgery	1 (12 %)	43 (30 %)	
Systemic chemotherapy alone	6 (75 %)	80 (56 %)	
Radiotherapy	0 (0 %)	3 (2 %)	
Best supportive care	1 (13 %)	16 (11 %)	

ECOG Eastern Cooperative Oncology Group, PS performance status, IMIG International Mesothelioma Interest Group, CALGB Cancer and Leukemia Group B, EORTC European Organisation for Research and Treatment of Cancer

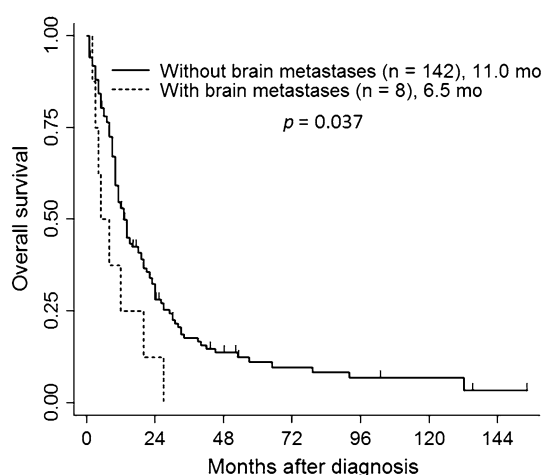


**Fig. 1** Overall survival in malignant pleural mesothelioma patients with and without brain metastases

## Discussion

MPM is an uncommon tumor of the thorax; typically, there is pernicious local invasion and extension into the pleural space and surrounding organs. The brain is a rare site for metastasis from MPM, and the majority of reported cases were identified in postmortem studies. To the best of our knowledge, this is the first report to have focused on the incidence, risk factors, and survival outcome associated with BM in patients with MPM.

In our patient cohort, eight out of 150 patients (5.3 %) developed BM. Falconieri et al. reviewed 171 cases of MPM at postmortem examination and discovered that 54 % of patients had distant metastases. The most frequently involved organs were the liver (55.9 %), adrenal glands (31.1 %), kidney (30.1 %), and contralateral lung (26.8 %). Intracranial (brain and meningeal) metastases

**Table 3** Cox regression model for factors associated with incidence of brain metastases

Variable	Univariate		Multivariate	
	Odds ratio (95 % CI)	<i>p</i> value	Odds ratio (95 % CI)	<i>p</i> value
Age at initial diagnosis				
≥65 years	1		1	
<65 years	6.06 (1.17–31.19)	0.031	5.83 (1.10–30.73)	0.038
ECOG PS				
≤1	1		NI	
>1	2.15 (0.40–11.48)	0.367		
Pleural effusion at diagnosis				
Yes	1		NI	
No	4.56 (1.03–20.01)	0.044		
Histological subtype				
Epithelioid	1		NI	
Nonepithelioid	1.10 (0.25–4.81)	0.895		
Calretinin				
Positive	1		NI	
Negative	5.02 (0.85–29.62)	0.075		
IMIG stage				
I–III	1		1	
IV	1.72 (1.05–2.81)	0.031	1.69 (1.02–2.80)	0.040
Surgery				
Yes	1		NI	
No	0.32 (0.03–2.75)	0.305		
CALGB score				
1–3	1		NI	
4–6	2.22 (0.53–9.31)	0.273		
EORTC prognostic score				
Low risk	1		NI	
High risk	1.58 (0.37–6.58)	0.529		

ECOG Eastern Cooperative Oncology Group, PS performance status, IMIG International Mesothelioma Interest Group; CALGB Cancer and Leukemia Group B, EORTC European Organisation for Research and Treatment of Cancer; NI not included

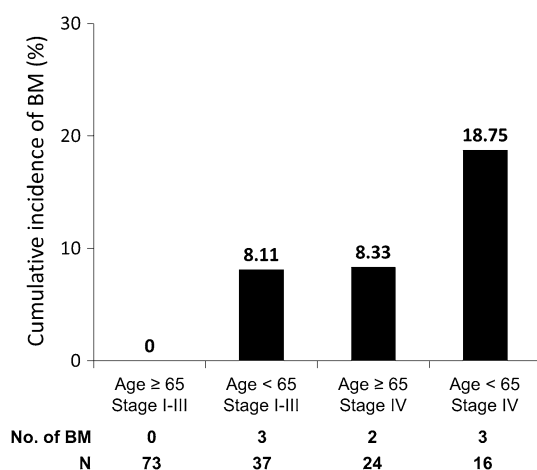


**Fig. 2** Cumulative incidence of brain metastases in malignant pleural mesothelioma patients characterized by identified risk factors. BM brain metastases

were found in only 3 % of cases [5]. Furthermore, pooling analysis of seven postmortem studies consisting of 655 patients revealed that the rate of intracranial metastases from malignant mesothelioma (including those of pleural, pericardial, and tunica vaginalis testis origin) was 2.7 % [11]. Our study demonstrated that the incidence of BM was approximately 5 %, which is higher than that in previous studies. The previous studies were limited to autopsy cases, and not all MPM patients were included. We believe that the true incidence of BM may be higher.

In our study, multivariate analysis showed that age <65 years and IMIG stage IV were independently associated with BM. An increased risk for BM in younger patients was reported in several studies on other malignancies [12–15]; however, the reason why younger patients are at a higher risk of BM is not well understood. Further

investigations are needed to determine the biological factors associated with BM in younger patients.

Among the clinicopathological features of MPM, histological subtype is one of the most important factors influencing survival and sarcomatous histology has the worst prognosis [16]. Miller et al. showed that the sarcomatous subtype predominates in patients with BM [11]; however, another study observed that the rate of extra thoracic dissemination does not differ among histology subtypes [17]. Our findings also demonstrated that histology was not a risk factor for BM.

The current study showed that outcomes for BM were equally poor regardless of treatment modalities. Surgery, stereotactic therapies, and systemic chemotherapy may play a role in selected situations; however, rapid recurrence after surgical excision [18] or after regression in response to systemic chemotherapy [19] has been reported. Clarification regarding the most appropriate treatment strategy for BM is urgently needed. The next best policy would be to identify patients with MPM who are at greater risk of developing BM. Based on our results, it may be reasonable to perform brain imaging on MPM patients with risk factors such as age <65 years and IMIG stage IV, even in the absence of neurological signs and symptoms.

There are a few limitations to the current study. First, this was a retrospective single-institution study. Second, due to the relatively small number of patients and events, statistical analysis was limited. Another limitation is that most BM were detected based on patients' symptoms. Therefore, asymptomatic BM may have been missed.

In conclusion, the prognosis for MPM patients with BM is poor. The incidence of MPM is predicted to reach a peak between 2015 and 2025 [20], and the development of BM has a severe effect on patients' quality of life and survival. Clinicians should perform careful screening for BM, especially in patients with risk factors.

**Acknowledgments** This study was supported by "The research and development and the dissemination projects related to the 9 fields of occupational injuries and illnesses" of the Japan Labour Health and Welfare Organization and by grants-in-aid from the Ministry of Health, Labor and Welfare, Japan (150401-02).

#### Compliance with ethical standards

**Conflict of interest** The authors declare that they have no conflict of interests.

**Ethical approval** All procedures performed in studies involving human participants were in accordance with the ethical standards of the institutional and/or national research committee and with the 1964 Helsinki declaration and its later amendments or comparable ethical standards. For this type of study (retrospective), formal consent is not required.

#### References

- Gemba K, Fujimoto N, Kato K, Aoe K, Takeshima Y, Inai K, Kishimoto T (2012) National survey of malignant mesothelioma and asbestos exposure in Japan. *Cancer Sci* 103:483–490
- Cao C, Tian D, Park J, Allan J, Pataky KA, Yan TD (2014) A systematic review and meta-analysis of surgical treatments for malignant pleural mesothelioma. *Lung Cancer* 83:240–245
- Wen P, Black P, Loeffler J (2001) Metastatic brain cancer. In: DeVita V, Hellman S, Rosenberg S (eds) *Cancer: principles and practice of oncology*, 6th edn. Lippincott, Williams & Wilkins, Philadelphia, pp 2655–2670
- Nayak L, Lee EQ, Wen PY (2012) Epidemiology of brain metastases. *Curr Oncol Rep* 14:48–54
- Falconieri G, Grandi G, DiBonito L, Bonifacio-Gori D, Giarelli L (1991) Intracranial metastases from malignant pleural mesothelioma. Report of three autopsy cases and review of the literature. *Arch Pathol Lab Med* 115:591–595
- Chari A, Kolias AG, Allinson K, Santarius T (2015) Cerebral metastasis of a malignant pleural mesothelioma: a case report and review of the literature. *Cureus* 7:e241. doi:10.7759/cureus.241
- Rusch VW (1995) A proposed new international TNM staging system for malignant pleural mesothelioma. From the International Mesothelioma Interest Group. *Chest* 108:1122–1128
- Fennell DA, Parmar A, Shamash J, Evans MT, Sheaff MT, Sylvester R, Dhaliwal K, Gower N, Steele J, Rudd R (2005) Statistical validation of the EORTC prognostic model for malignant pleural mesothelioma based on three consecutive phase II trials. *J Clin Oncol* 23:184–189
- Herndon JE, Green MR, Chahinian AP, Corson JM, Suzuki Y, Vogelzang NJ (1998) Factors predictive of survival among 337 patients with mesothelioma treated between 1984 and 1994 by the Cancer and Leukemia Group B. *Chest* 113:723–731
- Edwards J, Abrams K, Leverment J, Spyt T, Waller D, O'Byrne K (2000) Prognostic factors for malignant mesothelioma in 142 patients: validation of CALGB and EORTC prognostic scoring systems. *Thorax* 55:731–735
- Miller AC, Miettinen M, Schrupp DS, Hassan R (2014) Malignant mesothelioma and central nervous system metastases. Report of two cases, pooled analysis, and systematic review. *Ann Am Thorac Soc* 11:1075–1081
- Hubbs JL, Boyd JA, Hollis D, Chino JP, Saynak M, Kelsey CR (2010) Factors associated with the development of brain metastases: analysis of 975 patients with early stage nonsmall cell lung cancer. *Cancer* 116:5038–5046. doi:10.1002/cncr.25254
- Hsiao SH, Chung CL, Chou YT, Lee HL, Lin SE, Liu HE (2013) Identification of subgroup patients with stage IIIB/IV non-small cell lung cancer at higher risk for brain metastases. *Lung Cancer* 82:319–323. doi:10.1016/j.lungcan.2013.08.004
- Warren LE, Guo H, Regan MM, Nakhliis F, Yeh ED, Jacene HA, Hirshfield-Bartek J, Overmoyer BA, Bellon JR (2015) Inflammatory breast cancer and development of brain metastases: risk factors and outcomes. *Breast Cancer Res Treat* 151:225–232. doi:10.1007/s10549-015-3381-8
- Frankel TL, Bamboat ZM, Ariyan C, Coit D, Sabel MS, Brady MS (2014) Predicting the development of brain metastases in patients with local/regional melanoma. *J Surg Oncol* 109:770–774. doi:10.1002/jso.23574
- Mansfield AS, Symanowski JT, Peikert T (2014) Systematic review of response rates of sarcomatoid malignant pleural mesotheliomas in clinical trials. *Lung Cancer* 133–136. doi: 10.1016/j.lungcan.2014.08.017
- Finn RS, Brims FJ, Gandhi A, Olsen N, Musk AW, Maskell NA, Lee YC (2012) Postmortem findings of malignant pleural

- mesothelioma: a two-center study of 318 patients. *Chest* 142: 1267–1273
18. Ishikawa T, Wanifuchi H, Abe K, Kato K, Watanabe A, Okada Y (2010) Brain metastasis in malignant pleural mesothelioma presenting as intratumoral hemorrhage. *Neurol Med Chir (Tokyo)* 50:1027–1030
  19. Colleoni M, Liessi G, Avventi C, Pancheri F, Sgarbossa G, Vicario G, Manente P (1996) Response to chemotherapy of brain metastases from malignant pleural mesothelioma. *Tumori* 82:456–458
  20. Hooper CE, Morley AJ, Virgo P, Harvey JE, Kahan B, Maskell NA (2013) A prospective trial evaluating the role of mesothelin in undiagnosed pleural effusions. *Eur Respir J* 41:18–24



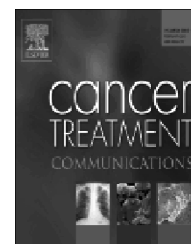




Available online at [www.sciencedirect.com](http://www.sciencedirect.com)

SciVerse ScienceDirect

[www.elsevier.com/locate/ctrc](http://www.elsevier.com/locate/ctrc)



# Lymphohistiocytoid mesothelioma with a response to cisplatin plus pemetrexed: A case report



Yosuke Miyamoto<sup>a</sup>, Nobukazu Fujimoto<sup>b,\*</sup>, Michiko Asano<sup>a</sup>,  
Takamasa Nakasuka<sup>a</sup>, Naofumi Hara<sup>a</sup>, Tomoko Yamagishi<sup>a</sup>,  
Yasuko Fuchimoto<sup>a</sup>, Sae Wada<sup>a</sup>, Kenichi Kitamura<sup>a</sup>, Shinji Ozaki<sup>a</sup>,  
Takumi Kishimoto<sup>c</sup>

<sup>a</sup>Department of Respiratory Medicine, Okayama Rosai Hospital, 1-10-25 Chikkomidorimachi, Okayama 7028055, Japan

<sup>b</sup>Department of Medical Oncology, Okayama Rosai Hospital, 1-10-25 Chikkomidorimachi, Okayama 7028055, Japan

<sup>c</sup>Department of Internal Medicine, Okayama Rosai Hospital, 1-10-25 Chikkomidorimachi, Okayama 7028055, Japan

Received 24 November 2014; received in revised form 4 February 2015; accepted 28 February 2015

## KEYWORDS

Malignant pleural mesothelioma;  
Lymphohistiocytoid mesothelioma;  
Asbestos;  
Systemic chemotherapy;  
Pemetrexed

## Abstract

We report the case of a patient with lymphohistiocytoid mesothelioma (LHM) with a response to systemic chemotherapy consisting of cisplatin and pemetrexed. A 72-year-old man was referred to our hospital because of abnormal shadows seen on chest X-rays. He had been exposed to asbestos at shipyards for 3 years. Computed tomography (CT) images of the chest showed multiple masses on the parietal pleura, diaphragm, and the interlobar pleura of the right. CT-guided percutaneous needle biopsy was performed and the biopsy specimen demonstrated fibrous thickening of the pleura with abundant lymphocyte infiltration. Immunohistochemical analyses revealed that the cells were positive for calretinin, WT-1, and CAM5.2, and negative for CEA, TTF-1, CK5/6, AE1/AE3, desmin, CD3, CD20, CD30, and CD68. Based on these findings, the diagnosis was confirmed as LHM. Systemic chemotherapy consisting of cisplatin (75 mg/m<sup>2</sup>) and pemetrexed (500 mg/m<sup>2</sup>) was delivered. After 6 courses of chemotherapy, multiple tumors had remarkably regressed, and the patient remains on maintenance treatment with pemetrexed. There are few reports of chemotherapy for LHM. The combination of cisplatin and pemetrexed could be a good treatment option for LHM.

© 2015 Elsevier Ltd. This is an open access article under the CC BY-NC-ND license (<http://creativecommons.org/licenses/by-nc-nd/4.0/>).

\*Corresponding author. Tel.: +81 86 2620131; fax: +81 86 2623391.

E-mail address: [nobufujimot@gmail.com](mailto:nobufujimot@gmail.com) (N. Fujimoto).

## 1. Introduction

Malignant pleural mesothelioma (MPM) is an aggressive malignancy arising from the mesothelial cells lining the pleura [1] and is generally associated with a history of asbestos exposure

[2]. Lymphohistiocytoid mesothelioma (LHM) is a rare subtype of MPM and there are few reports on the efficacy of systemic chemotherapy for this subtype. We report the case of a patient with LHM who had a response to systemic chemotherapy consisting of cisplatin and pemetrexed.

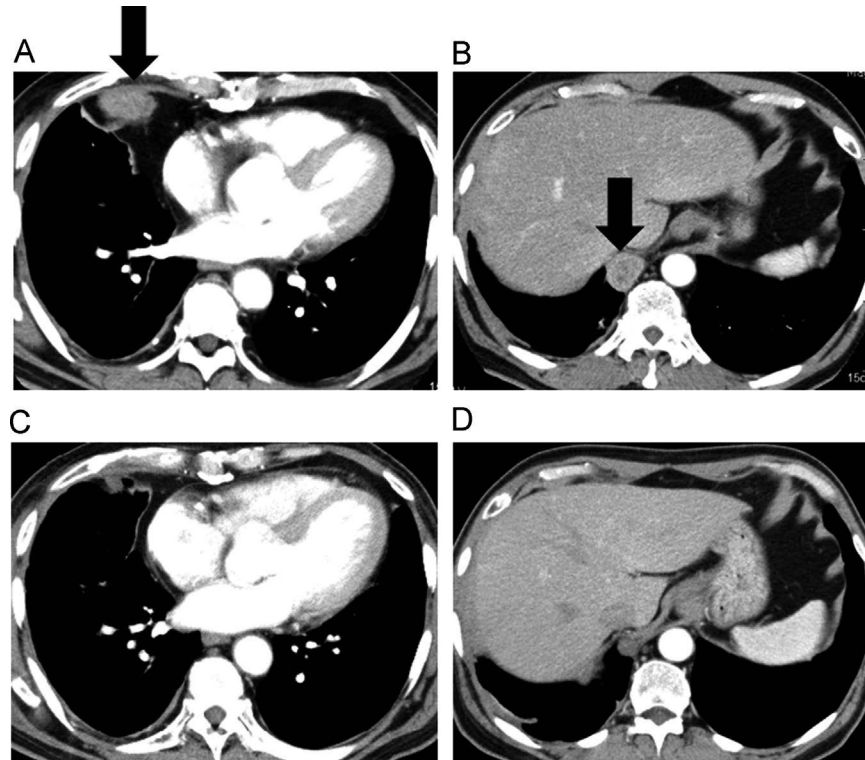


**Figure 1** Computed tomography images at diagnosis (A, B) and after the 6 cycles of systemic chemotherapy consisting of cisplatin and pemetrexed (C, D). Black arrows indicate the tumors on the pleura.

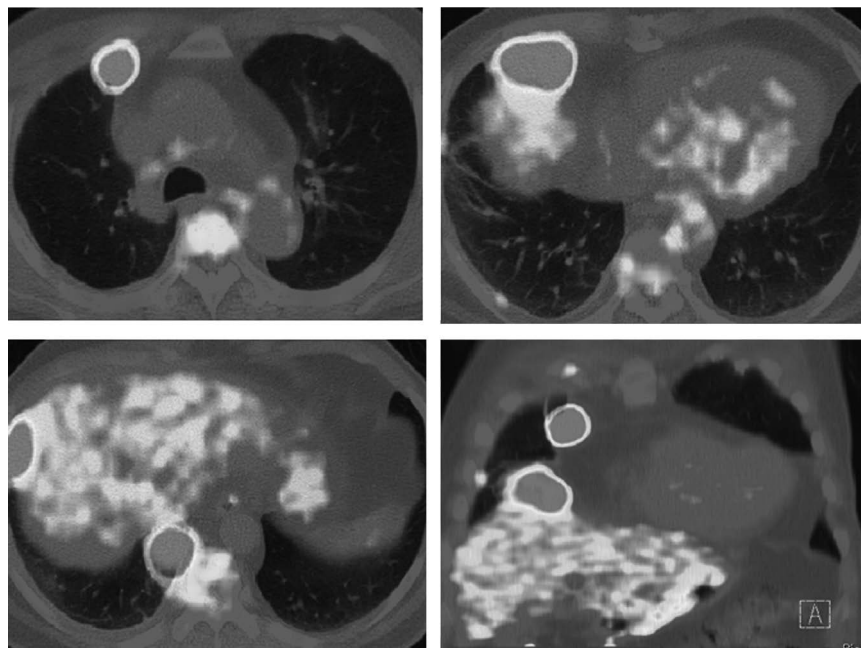


**Figure 2** Whole-body fluorine-18 2-fluoro-2-deoxy-D-glucose (FDG) positron emission tomography and CT images demonstrating abnormal FDG uptake (shown in red) in multiple masses on the pleura.

## 2. Case report

A 72-year-old man was referred to our hospital because of abnormal shadows seen on his chest X-ray determined at a regular medical checkup. He had a history of appendicitis and been diagnosed with type II diabetes mellitus. He had smoked between the ages of 18 and 35 years, and as a teenager had been exposed to asbestos at shipyards for 3 years. His physical examination revealed nothing specific and no superficial lymph nodes were palpable. Blood tests revealed a slight elevation in C-reactive protein and glucose levels. There were no increases in tumor markers. A chest X-ray revealed permeability decay in the right lower lung field, and computed tomography (CT) images of the chest showed multiple masses on the parietal pleura, diaphragm, and the interlobar pleura of the right (Figure 1A and B). Multiple masses on the pleura showed a contrast effect from the early stage of the arterial phase on enhanced CT images. Anterior mediastinal and gastric cardia lymphadenopathy were also detected and suspected to be lymph

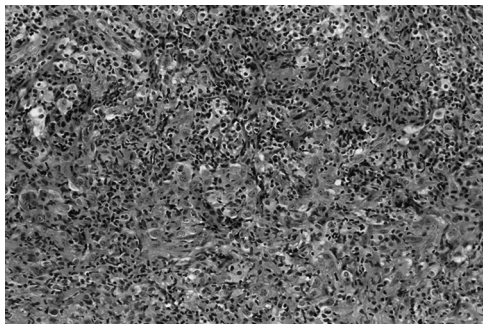


**Figure 3** Percutaneous needle biopsy specimen demonstrating fibrous thickening of the pleura with abundant lymphocyte infiltration.

node metastases. Whole-body fluorine-18 2-fluoro-2-deoxy-D-glucose (FDG) positron emission tomography and CT revealed abnormal FDG uptake in multiple masses and enlarged lymph nodes (Figure 2). CT-guided percutaneous needle biopsy was performed and the biopsy specimen demonstrated fibrous thickening of the pleura with an abundant lymphocyte infiltration (Figure 3). Among them were scattered polygonal cells with a nucleus containing clear oval nucleoli. Immunohistochemical analyses revealed that the cells were positive for calretinin, WT-1, and CAM5.2, and negative for CEA, TTF-1, CK5/6, AE1/AE3, desmin, CD3, CD20, CD30, and CD68 (Figure 4). Based on these findings, the diagnosis was confirmed as LHM. The patient's disease was diagnosed as stage IV (T1bN2M1) based on the International Mesothelioma Study Group staging system [3].

Systemic chemotherapy consisting of cisplatin (75 mg/m<sup>2</sup>) and pemetrexed (500 mg/m<sup>2</sup>) was delivered. After 6 courses of the chemotherapy, multiple tumors had remarkably regressed (Figure 1C and D). Mediastinal and intraperitoneal lymph nodes were also significantly diminished. The patient has been on maintenance treatment with pemetrexed and his disease remains stable.

## 3. Discussion

We report a case of LHM, which is a rare variant of MPM, in a patient who had a remarkable response to systemic chemotherapy consisting of cisplatin and pemetrexed. LHM was first identified in 1988 by Henderson et al. and characterized as having neoplastic cells with a histiocytoid appearance that are surrounded by a marked lymphocytic infiltration. LHM comprises less than 1% of mesotheliomas [4] and was categorized previously as a sarcomatous subtype of MPM [5]. However, in a recent report Galateau-Salle

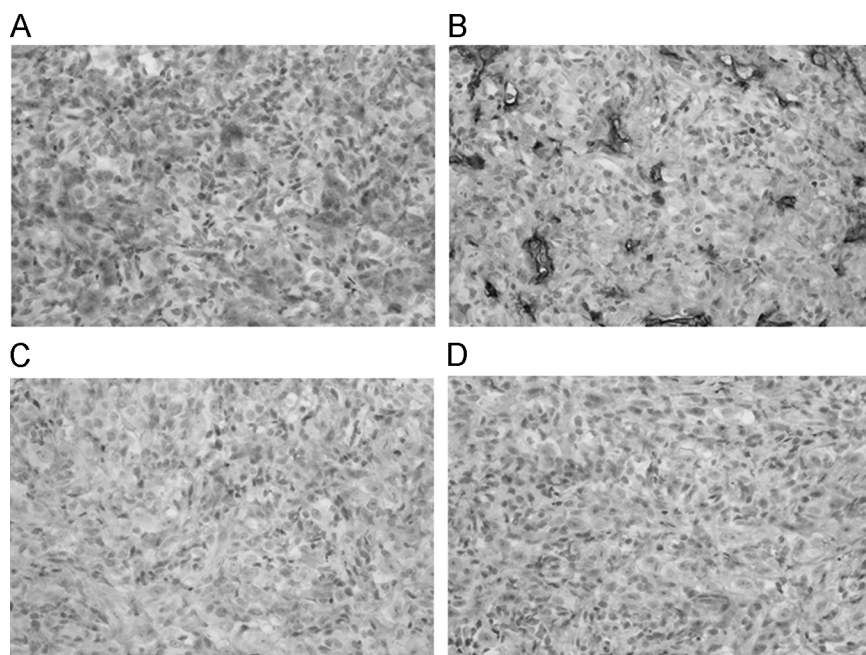


**Figure 4** Immunohistochemical analyses of the biopsy specimen revealed that the cells were positive for (A) calretinin and (B) D2-40 and negative for (C) CEA and (D) TTF-1.

**Table 1** Literature review of reported cases of lymphohistiocytoid mesothelioma.

Author	Year	Age/ sex	Asbestos exposure	Surgery	Radiotherapy	Chemotherapy	Pleurodesis	Survival (months)
Khalidi et al. [8]	2000	60/M	Unlikely	—	+	—	—	72
Khalidi et al. [8]	2000	74/F	Unknown	N.D.	N.D.	N.D.	N.D.	10
Khalidi et al. [8]	2000	67/M	Unlikely	N.D.	N.D.	N.D.	N.D.	3
Gallateau S et al. [6]	2007	56/F	Probably	—	+	—	+	12
Gallateau S et al. [6]	2007	78/M	Probably	—	—	—	+	3
Gallateau S et al. [6]	2007	62/M	Possibly	Pleurectomy	+	—	—	5
Gallateau S et al. [6]	2007	59/M	Probably	Pleurectomy	—	+	—	4
Gallateau S et al. [6]	2007	78/M	Unlikely	Palliative surgery	+	—	+	8
Gallateau S et al. [6]	2007	71/M	Unlikely	Palliative surgery	+	—	+	40
Gallateau S et al. [6]	2007	80/F	Probably	—	+	—	+	8
Gallateau S et al. [6]	2007	66/M	Probably	—	+	+	+	11
Gallateau S et al. [6]	2007	78/F	Unlikely	Palliative surgery	—	—	—	8
Gallateau S et al. [6]	2007	75/F	Unlikely	N.D.	N.D.	N.D.	N.D.	11
Gallateau S et al. [6]	2007	77/F	Unlikely	—	+	—	+	4
Gallateau S et al. [6]	2007	65/M	Probably	—	—	—	—	37
Gallateau S et al. [6]	2007	74/F	Unlikely	—	—	+	—	25
Gallateau S et al. [6]	2007	67/M	Possibly	Pleurectomy	—	—	—	32
Gallateau S et al. [6]	2007	58/M	Probably	Palliative surgery	+	+	—	7
Gallateau S et al. [6]	2007	82/M	Unknown	—	—	+	—	8
Gallateau S et al. [6]	2007	76/M	Probably	—	+	—	+	11
Gallateau S et al. [6]	2007	68/M	Probably	—	—	+	—	20
Gallateau S et al. [6]	2007	70/M	Probably	—	—	+	—	11
Gallateau S et al. [6]	2007	77/F	Probably	—	—	—	+	6
Gallateau S et al. [6]	2007	50/M	Possibly	—	—	—	+	
Gallateau S et al. [6]	2007	63/F	Probably	Palliative surgery	—	+	+	8
Kawai et al. [4]	2010	59/F	Unknown	Thoracotomy	N.D.	N.D.	N.D.	12
Kawai et al. [4]	2010	52/M	Unknown	Thoracotomy	N.D.	N.D.	N.D.	36
Kawai et al. [4]	2010	61/M	Unknown	—	N.D.	N.D.	N.D.	3
Kawai et al. [4]	2010	63/M	Probably	Extrapleural pneumonectomy	N.D.	N.D.	N.D.	19(alive)
Present case	2015	72/M	Probably	—	—	+	—	14(alive)

N.D.; not described.

et al. suggested that the survival of LHM was more similar to that of the epithelioid or biphasic subtype of MPM [6]. Whether LHM should be categorized as an epithelioid or sarcomatous subtype of MPM is still controversial.

Concerning chemotherapy for MPM, the combination of pemetrexed and cisplatin has shown significantly prolonged survival compared with cisplatin alone in a phase III study [7]. However, it was not clear whether or not LHM cases were included in the study. In fact, there are few reports of chemotherapy for LHM. We reviewed the reported cases of LHM particularly concerning the delivered treatment modalities in Table 1. These previous reports mainly discussed the pathological differentiation and there were few description of treatment. There were 8 cases those were delivered systemic chemotherapy, but the treatment regimen or the tumor responses to those chemotherapy was not described. To our knowledge, the current case might be the first case with a significant response to the treatment regimen. Cisplatin plus pemetrexed could therefore be a good treatment option for LHM.

In conclusion, we present a case of LHM, a rare variant of MPM, in a patient with a significant response to systemic chemotherapy.

### Conflict of interest statement

All authors have no conflict of interest to be declared.

### Acknowledgments

This study is a part of “the research and development and the dissemination projects related to the 13 fields of occupational injuries and illnesses” of the Japan Labour Health and Welfare Organization (Grant no. 14030101). This

sponsor had no involvement in the study design, collection, analysis and interpretation of the data, writing of the manuscript, or decision to submit the manuscript for publication.

### References

- [1] R. Ismail-Khan, L.A. Robinson, C.C. Williams Jr., C.R. Garrett, G. Bepler, G.R. Simon, Malignant pleural mesothelioma: a comprehensive review, *Cancer Control* 13 (2006) 255-263.
- [2] K. Gemba, N. Fujimoto, K. Kato, K. Aoe, Y. Takeshima, K. Inai, et al., National survey of malignant mesothelioma and asbestos exposure in Japan, *Cancer Sci.* 103 (2012) 483-490.
- [3] V.W. Rusch, A proposed new international TNM staging system for malignant pleural mesothelioma. From the International Mesothelioma Interest Group, *Chest* 108 (1995) 1122-1128.
- [4] T. Kawai, S. Hiroi, K. Nakanishi, K. Takagawa, R. Haba, K. Hayashi, et al., Lymphohistiocytoid mesothelioma of the pleura, *Pathol. Int.* 60 (2010) 566-574.
- [5] D.W. Henderson, H.D. Attwood, T.J. Constance, K.B. Shilkin, R.H. Steele, Lymphohistiocytoid mesothelioma: a rare lymphomatoid variant of predominantly sarcomatoid mesothelioma, *Ultrastruct. Pathol.* 12 (1988) 367-384.
- [6] F. Galateau-Salle, R. Attanoos, A.R. Gibbs, L. Burke, P. Astoul, P. Rolland, et al., Lymphohistiocytoid variant of malignant mesothelioma of the pleura: a series of 22 cases, *Am. J. Surg. Pathol.* 31 (2007) 711-716.
- [7] N.J. Vogelzang, J.J. Rusthoven, J. Symanowski, C. Denham, E. Kaukel, P. Ruffie, et al., Phase III study of pemetrexed in combination with cisplatin versus cisplatin alone in patients with malignant pleural mesothelioma, *J. Clin. Oncol.* 21 (2003) 2636-2644.
- [8] H.S. Khalidi, L.J. Medeiros, H. Battifora, Lymphohistiocytoid mesothelioma. An often misdiagnosed variant of sarcomatoid malignant mesothelioma, *Am. J. Clin. Pathol.* 113 (2000) 649-654.



## Endobronchial T-cell lymphoma in a patient with chronic pyothorax

Shinsaku Matsumoto<sup>1</sup>, Nobukazu Fujimoto<sup>2</sup>, Yasuko Fuchimoto<sup>3</sup>, Michiko Asano<sup>3</sup>, Tomofumi Yano<sup>1</sup> & Takumi Kishimoto<sup>1</sup>

<sup>1</sup>Department of Internal Medicine, Okayama Rosai Hospital, Okayama, Japan.

<sup>2</sup>Medical Oncology, Okayama Rosai Hospital, Okayama, Japan.

<sup>3</sup>Respiratory Medicine, Okayama Rosai Hospital, Okayama, Japan.

### Keywords

Bronchoscopy, endobronchial tumor, pulmonary lymphoma, pyothorax, T-cell lymphoma.

### Correspondence

Nobukazu Fujimoto, Department of Medical Oncology, Okayama Rosai Hospital, 1-10-25 Chikkomidorimachi, Okayama 7028055, Japan. E-mail: nobufujimot@gmail.com

Received: 18 March 2015; Revised: 30 March 2015; Accepted: 02 April 2015.

doi: 10.1002/rcr2.103

### Abstract

We report a very rare case of primary endobronchial peripheral T-cell lymphoma (PTCL) not otherwise specified (NOS), which presented as an endobronchial tumor obstructing the main airway. An 81-year-old man was referred to our hospital for a 1-month history of productive cough and wheeze. Computed tomography revealed chronic pyothorax with calcified foci in the right lung and a mass inside the bronchus intermedius. Flexible bronchoscopy identified an endobronchial tumor obstructing the bronchus intermedius. The biopsy specimen showed an infiltration composed predominantly of small atypical lymphocytes. Immunohistochemical analyses demonstrated that the proliferating cells were positive for CD3, CD4, and CD5 and negative for CD8 and CD20. Pathological tests confirmed that the case was PTCL-NOS. PTCL-NOS should be considered in the differential diagnosis of endobronchial tumors.

## Introduction

Peripheral T-cell lymphoma (PTCL) is one of the subtypes of T-cell lymphoma (TCL); it comprises a heterogeneous group of nodal and extranodal mature TCLs. Among the PTCLs, a subset is specifically defined as PTCL not otherwise specified (PTCL-NOS). PTCL-NOS do not correspond to any of the known T-cell entities. Primary pulmonary lymphoma (PPL) is a distinct entity that arises de novo in lung tissue [1]. We report an extremely rare case of primary endobronchial PTCL-NOS that presented as a tumor obstructing the main airway.

## Case Report

An 81-year-old Japanese man was referred to our hospital for a 1-month history of productive cough and wheeze. He was a smoker (approximately 56 packs per year) and had a

medical history of pulmonary tuberculosis at the age of 17 years. He had been diagnosed with chronic pyothorax and treated with intravenous injection of antibiotics 1 year prior to being seen at our facility. Upon examination, his body temperature was 37.2°C and a physical examination revealed wheeze and reduced air entry in the right mid-lung. No superficial lymph nodes were palpated. Blood assays revealed leukocytosis (12,500 leukocytes per microliter) and normal lactate dehydrogenase values (223 IU/L). Carcinoembryonic antigen and soluble interleukin-2 receptor values were slightly elevated to 5.8 ng/mL and 575 U/mL, respectively. A chest X-ray showed hypolucency of the right middle lung field, which suggested fluid accumulation. Computed tomography (CT) revealed chronic pyothorax with calcified foci in the right-hand portion of the right lung and a mass inside the bronchus intermedius (Fig. 1A). No mediastinal lymphadenopathy was detected. Flexible bronchoscopy



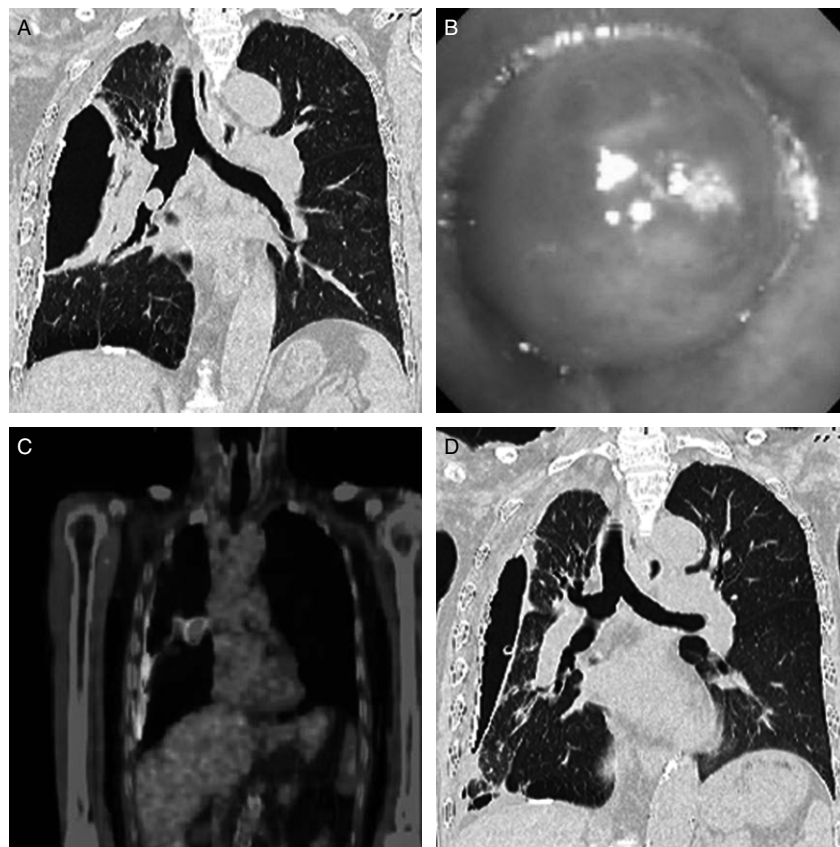


**Figure 1.** Imaging findings of the case. (A) Computed tomography (CT) revealed chronic pyothorax with calcified foci on the right and a mass inside the bronchus intermedius. (B) Flexible bronchoscopy identified an endobronchial tumor obstructing the bronchus intermedius. (C) Positron emission tomography with [18F] fluoro-2-deoxyglucose and CT revealed uptake at the endobronchial tumor. (D) CT after the chemotherapy demonstrated that the endobronchial tumor markedly diminished.

identified an endobronchial tumor obstructing the bronchus intermedius (Fig. 1B). The biopsy specimen showed an infiltration composed predominantly of small atypical lymphocytes (Fig. 2A). Immunohistochemical analyses demonstrated that the proliferating cells were positive for CD3 (Fig. 2B), CD4, CD5 (Fig. 2C), and CD7 and negative for CD8 (Fig. 2D), CD20 (Fig. 2E), and CD30. The Ki-67 labeling index was low. Based on these findings, we diagnosed the tumor as PTCL-NOS. Positron emission tomography (PET) with [18F] fluoro-2-deoxyglucose and CT revealed uptake at the endobronchial tumor, with a maximum standardized uptake value of 20.6 (Fig. 1C). There was no evidence of abnormal uptake at the pyothorax, mediastinal lymph node, or other extrathoracic organs. His disease was considered stage IE, and the patient was treated with systemic chemotherapy (pirarubicin, cyclophosphamide, vincristine, and prednisone). After the first course of the chemotherapy, the endobronchial tumor markedly diminished on chest CT (Fig. 1D) and bronchoscopy. However, because of complication with

refractory pyothorax, fenestration surgery was undertaken in a definitive fashion. Systemic chemotherapy was not delivered thereafter; however, the patient is free of recurrence 1 year after diagnosis.

## Discussion

PPL is defined as lymphomas that affect the lungs (parenchyma, bronchi, and/or trachea) with no evidence of extrapulmonary extension in 3-month follow-up [2]. It is a rare condition that comprises only 3–4% of extranodal non-Hodgkin lymphomas (NHL), less than 1% of all NHLs [2], and 0.5–1% of primary pulmonary malignancies [3]. The majority of the reported cases have been of the B-cell type, so-called mucosa-associated or bronchus-associated lymphoid tissue lymphomas [4]. The current patient presented with a solitary endobronchial tumor, which is an extremely rare manifestation of PPL. Solomonov *et al.* reported that in a series of 441 patients with newly diagnosed NHL over a 7-year period, eight patients presented

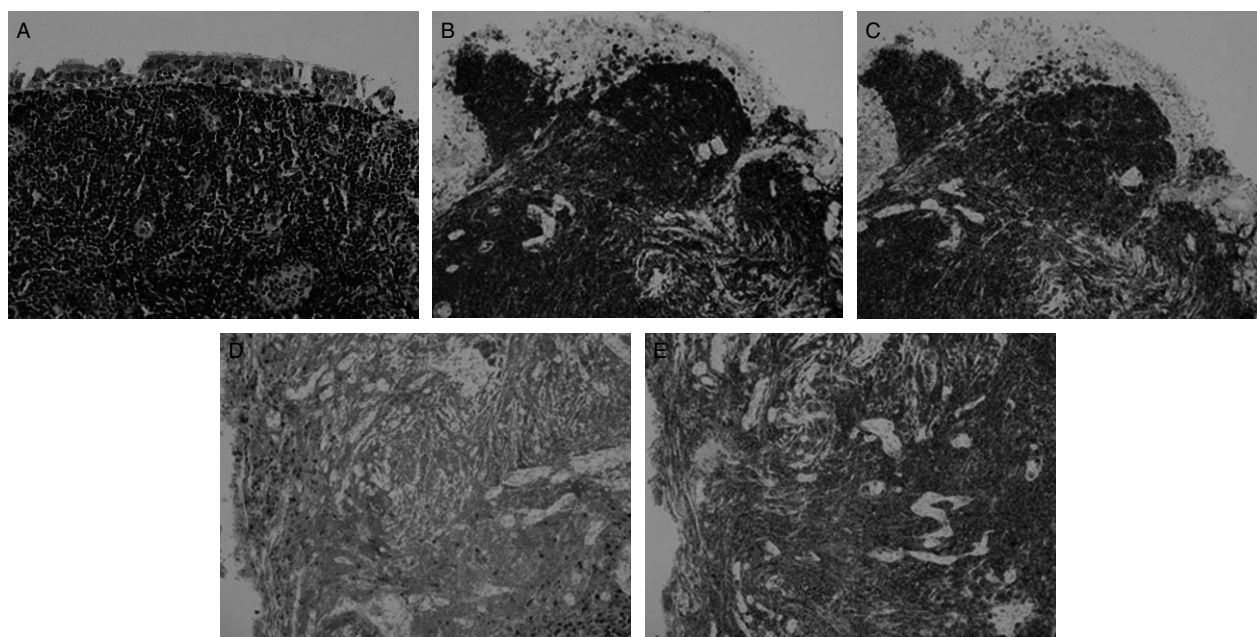


**Figure 2.** Biopsy specimen showed an infiltration comprised predominantly of small atypical lymphocytes (hematoxylin-eosin, 40 $\times$ ) (A). Immunohistochemical analyses demonstrated that the proliferating cells were positive for CD3 (B) and CD5 (C), and negative for CD8 (D) and CD20 (E).

with a primary endobronchial B-cell lymphoma [1]. To our knowledge, this is the first report of PTCL-NOS presenting as a primary endobronchial tumor. PTCL-NOS is a diagnosis made based on the results of a tissue biopsy that demonstrates evidence of a TCL that does not meet the criteria for other subtypes of TCL including anaplastic large-cell lymphoma, angioimmunoblastic TCL, extranodal NK/TCL, nasal type, subcutaneous panniculitis-like TCL, enteropathy-associated TCL, and hepatosplenic TCL. The differential diagnosis is based on histologic examination and immunophenotype evaluation such as immunohistochemical panel (CD20, CD3, CD10, BCL6, Ki-67, CD5, CD30, CD2, CD4, CD8, CD7, CD56, CD57, CD21, CD23, ALK) or cell surface marker analysis by flow cytometry (kappa/lambda, CD45, CD3, CD5, CD19, CD10, CD20, CD30, CD4, CD8, CD7, CD2), and in difficult or equivocal cases, polymerase chain reaction-based assay for molecular detection of a clonal T-cell receptor rearrangement. The limitation of the current case was that the pathological diagnosis was based on small specimen through flexible bronchoscopy, so not all these markers were examined. However, we are confident of the diagnosis based on multiple immunohistochemical analyses.

The current case was complicated by chronic pyothorax. Pyothorax-associated lymphoma is a category in which a lymphoproliferative disorder develops in the pleural cavity after a long-standing history of pyothorax; it represents an entity distinct from other malignant lymphomas [5]. In

our case, PET/CT revealed a hypermetabolic mass at the endobronchial tumor, but there was no abnormal uptake at the pyothorax. Endoscopic examination showed a smooth-surfaced, round tumor with a stalk; these features do not correspond to an outer parietal invasion. However, the coronal CT showed dense scar-like tissue between the wall of pyothorax and bronchus intermedius. These findings might suggest the relationship between the lymphoma and pyothorax. We think that the chronic inflammation could have contributed to the development of the disease.

In conclusion, we have reported upon what is, to the best of our knowledge, the first case of PTCL-NOS, which was confined to the bronchus. PTCL-NOS should be considered in the differential diagnosis of endobronchial tumor.

### Disclosure Statements

No conflict of interest declared.

Appropriate written informed consent was obtained for publication of this case report and accompanying images.

### Acknowledgments

We thank Drs. Kyotaro Ohno, Yasuharu Sato, and Prof. Tadashi Yoshino, Department of Pathology, Okayama University Graduate School of Medicine, Dentistry and Pharmaceutical Sciences, for detailed pathological analyses.

## References

1. Solomonov A, Zuckerman T, Goralnik L, et al. 2008. Non-Hodgkin's lymphoma presenting as an endobronchial tumor: report of eight cases and literature review. *Am. J. Hematol.* 83:416–419.
2. Chilosi M, Zinzani PL, and Poletti V. 2005. Lymphoproliferative lung disorders. *Semin. Respir. Crit. Care Med.* 26:490–501.
3. Cadranet J, Wislez M, and Antoine M. 2002. Primary pulmonary lymphoma. *Eur. Respir. J.* 20:750–762.
4. Cordier JF, Chailleux E, Lauque D, et al. 1993. Primary pulmonary lymphomas. A clinical study of 70 cases in nonimmunocompromised patients. *Chest* 103: 201–208.
5. Aozasa K, Takakuwa T, and Nakatsuka S. 2005. Pyothorax-associated lymphoma: a lymphoma developing in chronic inflammation. *Adv. Anat. Pathol.* 12:324–331.



## Case report

## Foreign body granuloma mimicking recurrence of malignant pleural mesothelioma



Takamasa Nakasuka <sup>a</sup>, Nobukazu Fujimoto <sup>b,\*</sup>, Naofumi Hara <sup>a</sup>, Yosuke Miyamoto <sup>a</sup>,  
Tomoko Yamagishi <sup>a</sup>, Michiko Asano <sup>a</sup>, Hideyuki Nishi <sup>c</sup>, Takumi Kishimoto <sup>d</sup>

<sup>a</sup> Department of Respiratory Medicine, Okayama Rosai Hospital, 1-10-25 Chikkomidorimachi, Okayama 7028055, Japan

<sup>b</sup> Department of Medical Oncology, Okayama Rosai Hospital, 1-10-25 Chikkomidorimachi, Okayama 7028055, Japan

<sup>c</sup> Department of Surgery, Okayama Rosai Hospital, 1-10-25 Chikkomidorimachi, Okayama 7028055, Japan

<sup>d</sup> Department of Internal Medicine, Okayama Rosai Hospital, 1-10-25 Chikkomidorimachi, Okayama 7028055, Japan

## ARTICLE INFO

## Article history:

Received 17 August 2015

Received in revised form

30 August 2015

Accepted 1 September 2015

## Keywords:

Asbestos

Foreign body granuloma

Mesothelioma

Pleura

Pneumonectomy

## ABSTRACT

A 72-year-old man visited our hospital due to right pleural effusion. He had worked as a welder at a shipbuilding company and had been exposed to asbestos. Cytological examination and thoracoscopic pleural biopsy yielded a diagnosis of epithelial malignant pleural mesothelioma (MPM); extrapleural pneumonectomy (EPP) was performed. Two years later, he became aware of right-back swelling that became a fist-sized mass over 2 months. Microscopy of a tissue specimen revealed no malignant cells, but did indicate foreign body granuloma. Subcutaneous lesions that develop after EPP do not necessarily result from the recurrence of MPM, but could have benign etiologies.

© 2015 The Authors. Published by Elsevier Ltd. This is an open access article under the CC BY-NC-ND license (<http://creativecommons.org/licenses/by-nc-nd/4.0/>).

## 1. Introduction

Malignant pleural mesothelioma (MPM) is an aggressive malignancy arising from the mesothelial cells lining the pleura and is generally associated with a history of asbestos exposure [1]. The clinical benefits of radical surgery for MPM remain controversial. Extrapleural pneumonectomy (EPP) has been performed for patients with earlier disease and good physical condition, but the disease often recurs at wide intervals. Here we report a case of foreign body granuloma (FBG) that mimicked a postoperative recurrence of MPM.

## 2. Case report

A 72-year-old man visited our hospital for examination of right pleural effusion. He had worked as a welder at a shipbuilding company and had been exposed to asbestos for 43 years. His pleural

effusion had been detected at a medical checkup for subjects with an occupational history of past asbestos exposure. Cytological examination of the effusion revealed the aggregated atypical mesothelial cells with nuclear enlargement and nucleus irregularity. Immunohistochemical analyses demonstrated that these cells were positive for calretinin, CAM5.2, CK5/6, AE1/AE3, WT-1, and EMA, and negative for CEA and TTF-1. These findings gave the diagnosis of epithelial subtype of MPM, and thoracoscopic pleural biopsy confirmed the diagnosis. EPP was performed; the pericardium and the diaphragm were also removed because the tumor had invaded the diaphragm. The pericardium and the diaphragm were reconstructed with Gore-Tex® mesh (1 mm in thickness, 20 cm × 15 cm, and 2 mm in thickness, 24 cm × 15 cm, respectively). The disease was categorized as T2N0M0, stage II, based on the staging system of the International Mesothelioma Study Group [2]; adjuvant chemotherapy consisting of carboplatin and pemetrexed was delivered. Talc was not used to treat the effusion during the course.

Two years later, the patient became aware that his right back was swelling. This swelling became a fist-sized mass over 2 months. Computed tomography (CT) of the chest visualized a tumor of soft-tissue density that expanded from the right pleural cavity into the subcutaneous tissue (Fig. 1A). Fluorine-18 2-fluoro-2-deoxy-D-glucose (18F-FDG) positron emission tomography (PET)-CT

Abbreviations: MPM, malignant pleural mesothelioma; EPP, extrapleural pneumonectomy; FBG, foreign body granuloma; CT, computed tomography; 18-F-FDG, fluorine-18 2-fluoro-2-deoxy-D-glucose; PET, positron emission tomography.

\* Corresponding author.

E-mail address: [nobufujimoto@gmail.com](mailto:nobufujimoto@gmail.com) (N. Fujimoto).

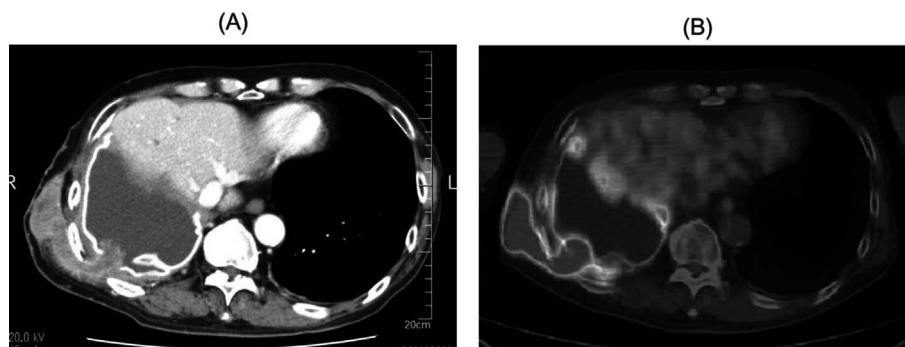


**Fig. 1.** Subcutaneous tumor on the right back of the patient. (A) CT of the chest revealed a tumor of soft-tissue density that expanded from the right pleural cavity into the subcutaneous tissue. (B) 18F-FDG PET-CT showed accumulation of 18F-FDG in the mass.

revealed an accumulation of 18F-FDG in the mass and along the pleura (Fig. 1B). It was near the chest tube site after the EPP. We suspected a recurrence of MPM, so we performed percutaneous needle biopsy. Microscopy of the tissue specimen showed no malignant cells; rather, we observed granulomas accompanied by giant cells, histiocytes, and inflammatory cells (Fig. 2). Immuno histochemical analyses revealed that these cells were negative for calretinin, CK AE1/3, or CAM5.2. Because the possibility of recurrence of MPM could not be ruled out with small specimen of needle biopsy, a tumorectomy was carried out. The tumor involved the Gore-Tex® mesh, so the mesh was removed with the tumor. Subsequent microscopy confirmed the diagnosis of FBG without evidence of MPM recurrence.

### 3. Discussion

A standard treatment for MPM has not yet been established. Patients exhibiting earlier stages of this disease have undergone EPP. However, a significant proportion of patients experience local recurrence as the first site of disease recurrence [3]. When patients who have undergone EPP display subcutaneous tumors, it is logical to suspect a recurrence of MPM.

FBG is a tumor-like mass or nodule of granulation tissue, with actively growing fibroblasts and capillary buds, consisting of a collection of modified macrophages resembling epithelial cells, surrounded by a rim of mononuclear cells, chiefly lymphocytes, and sometimes a center of giant multinucleate cells. It is due to a chronic inflammatory process associated with infectious disease or invasion by a foreign body such as surgical materials or pieces of stone or wood from a trauma. In the current case, we suspected that

the causative foreign material was the Gore-Tex® mesh that was used to reconstruct the patient's diaphragm. It is quite rare that Gore-Tex mesh induced inflammatory reactions, however, in the current case, the Gore-Tex mesh was involved in the tumor, so we considered that the granuloma was originated in the mesh.

Clinical diagnosis of FBG is challenging; it is difficult to identify FBG through physiological findings and CT. PET-CT is often applied to detect malignant lesions, but inflammatory lesions or granulomas (including FBG) would also accumulate 18F-FDG [4], rendering it difficult to diagnose FBG by imaging alone. The diagnosis should be confirmed through other means, such as percutaneous biopsy or surgery.

To our knowledge, this is the second report of FBG mimicking the recurrence of MPM; Shrestha et al. recently reported cases with pseudo-tumors that mimicked indwelling pleural catheter-tract metastases of MPM [5]. These cases remind physicians that subcutaneous lesions that develop after EPP do not necessarily result from the recurrence of MPM, but could have benign etiologies. Diagnostic procedures should be considered in such cases.

### Conflict of interest

I declare on behalf of my co-authors and myself that we do not have any conflict of interest to declare.

### Sources of funding

This study was supported by Research and Development and the Dissemination of Projects Related to the Nine Fields of Occupational Injuries and Illnesses of the Japan Labour Health and Welfare Organization. This work is also supported by grants-in-aid from the Ministry of Health, Labor and Welfare, Japan. These study sponsors had no involvement in study design, writing of the manuscript, the collection of data, and decision to submit the manuscript.

### References

- [1] K. Gemba, N. Fujimoto, K. Kato, K. Aoe, Y. Takeshima, K. Inai, et al., National survey of malignant mesothelioma and asbestos exposure in Japan, *Cancer Sci.* 103 (2012) 483–490.
- [2] V.W. Rusch, A proposed new international TNM staging system for malignant pleural mesothelioma. From the International Mesothelioma Interest Group, *Chest* 108 (1995) 1122–1128.
- [3] A.S. Tsao, I. Wistuba, J.A. Roth, H.L. Kindler, Malignant pleural mesothelioma, *J. Clin. Oncol.* 27 (2009) 2081–2090.
- [4] M. Hara, Y. Shibamoto, T. Tamaki, M. Nishio, A. Iida, N. Shiraki, The intermediate level of FDG-PET accumulation among various kinds of pulmonary and mediastinal diseases, *Radiology* 197 (Suppl.) (2003).
- [5] R.L. Shrestha, B.A. Wood, Y.C. Lee, Pseudo-tumor mimicking indwelling pleural catheter tract metastasis in mesothelioma, *J. Bronchol. Interv. Pulmonol.* 21 (2014) 350–352.

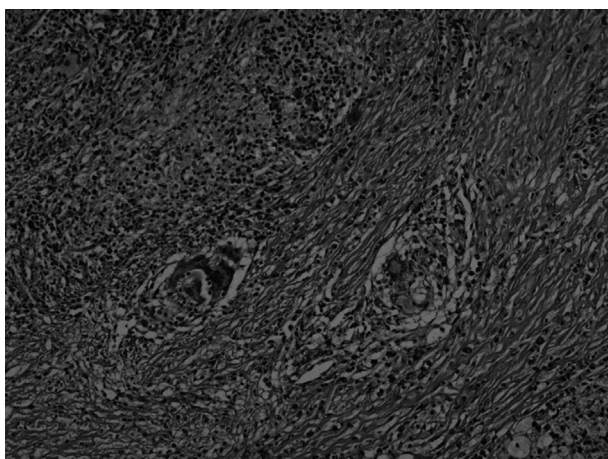


**Fig. 2.** Microscopy of the tissue specimen revealed a FBG accompanied by foreign-body giant cells, histiocytes, and inflammatory cells ( $\times 10$ ).

## The Rapid Appearance and Disappearance of Dendriform Pulmonary Ossification after Diffuse Alveolar Hemorrhage

Tomoko Yamagishi<sup>1</sup>, Nobukazu Fujimoto<sup>2</sup>, Yosuke Miyamoto<sup>1</sup>, Naofumi Hara<sup>1</sup>, Michiko Asano<sup>1</sup>, Yasuko Fuchimoto<sup>1</sup>, Sae Wada<sup>1</sup>, Kenichi Kitamura<sup>1</sup>, Shinji Ozaki<sup>1</sup>, Hideyuki Nishi<sup>3</sup>, and Takumi Kishimoto<sup>4</sup>

<sup>1</sup>Department of Respiratory Medicine, <sup>2</sup>Department of Medical Oncology, <sup>3</sup>Department of Surgery, and <sup>4</sup>Department of Internal Medicine, Okayama Rosai Hospital, Okayama, Japan

ORCID ID: 0000-0002-4516-0433 (N.F.).

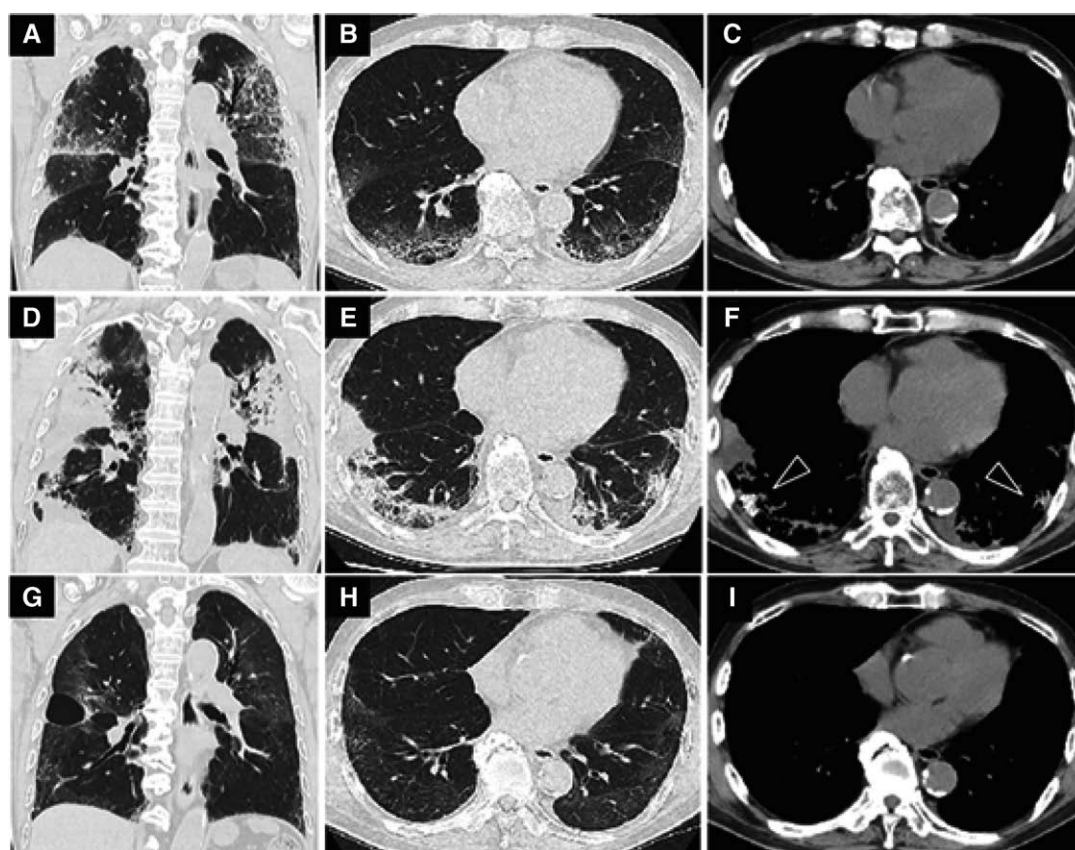


**Figure 1.** Coronal and axial chest computed tomography images of a 63-year-old man on admission showed diffuse bilateral ground-glass attenuation (A and B) without evidence of ossification (C). Chest computed tomography images 2 weeks after admission showed widespread areas of ground-glass attenuation and consolidation (D and E) with disseminated pulmonary ossification (*arrowheads*) in the subpleural zone (F). One month after administration of steroid therapy, bilateral consolidation and pulmonary ossification were dramatically decreased (G–I).

A 63-year-old man with a history of atrial fibrillation that had been treated with apixaban was admitted to our hospital for dyspnea and hemoptysis. Chest computed tomography showed diffuse bilateral ground-glass attenuation (Figures 1A–1C). Bronchoalveolar lavage fluid was bloody and contained hemosiderin-laden macrophages, suggesting apixaban-induced alveolar hemorrhage. Two weeks after cessation of the drug, acute respiratory failure occurred. Repeated chest computed tomography showed worsening

The authors are supported by the Ministry of Health, Labor and Welfare of Japan.

Am J Respir Crit Care Med Vol 193, Iss 3, pp 333–334, Feb 1, 2016

Copyright © 2016 by the American Thoracic Society

Originally published online as DOI: 10.1164/rccm.201506-1199IM on September 25, 2015

Internet address: [www.atsjournals.org](http://www.atsjournals.org)

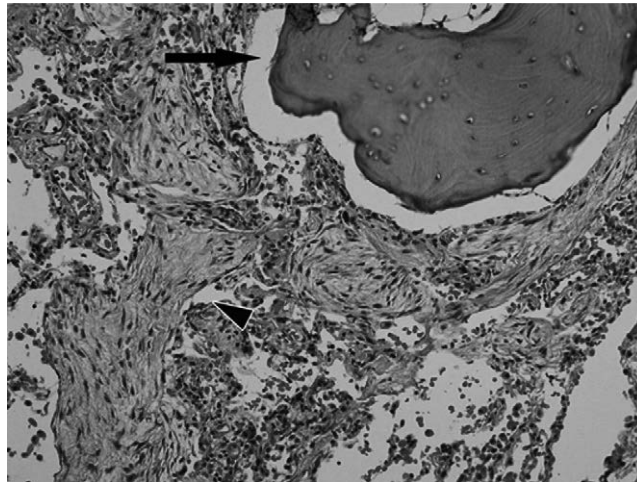


**Figure 2.** A surgical lung biopsy specimen shows dendriform mature bone formation within an area of scarring and widened alveolar septa (arrow). The background alveolar spaces are filled with numerous fibroblastic plugs (arrowhead) (hematoxylin and eosin,  $\times 200$ ).

bilateral airspace opacities with patchy diffuse sub-pleural pulmonary ossification (Figures 1D–1F). Surgical lung biopsy specimens revealed organizing pneumonia and branching bone within the fibrous stroma and alveolar spaces, typical of dendriform pulmonary ossification (DPO) (Figure 2). Daily prednisolone (1.0 mg/kg) was administered, and the bilateral consolidation and pulmonary ossification had markedly decreased 1 month later (Figures 1G–1I).

DPO is a rare condition, defined by the finding of branching lung in the air spaces of the distal lung. Patients are generally asymptomatic, and the condition is usually discovered after postmortem examination (1). Its pathogenesis is unclear, but DPO can occur after lung injuries such as pulmonary fibrosis and alveolar hemorrhage (2). There are no reports of DPO responding to steroids, and effective treatment for DPO has not yet been established (3, 4). However, this case suggests remission is possible with corticosteroid medications. ■

**Author disclosures** are available with the text of this article at [www.atsjournals.org](http://www.atsjournals.org).

## References

1. Peros-Golubicić T, Tekavec-Trkanjec J. Diffuse pulmonary ossification: an unusual interstitial lung disease. *Curr Opin Pulm Med* 2008;14:488–492.
2. Chan ED, Morales DV, Welsh CH, McDermott MT, Schwarz MI. Calcium deposition with or without bone formation in the lung. *Am J Respir Crit Care Med* 2002;165:1654–1669.
3. Martinez JB, Ramos SG. Dendriform pulmonary ossification. *Lancet* 2013;382:e22.
4. Mathai SK, Schwarz MI, Ellis JH Jr. Extensive diffuse pulmonary ossification after acute respiratory distress syndrome. *Am J Respir Crit Care Med* 2013;187:890.





## Case report

## Lymphoproliferative disorder in pleural effusion in a subject with past asbestos exposure



Naofumi Hara <sup>a</sup>, Nobukazu Fujimoto <sup>b,\*</sup>, Yosuke Miyamoto <sup>a</sup>, Tomoko Yamagishi <sup>a</sup>,  
Michiko Asano <sup>a</sup>, Yasuko Fuchimoto <sup>a</sup>, Sae Wada <sup>a</sup>, Shinji Ozaki <sup>a</sup>, Takumi Kishimoto <sup>c</sup>

<sup>a</sup> Department of Respiratory Medicine, Okayama Rosai Hospital, Okayama, Japan

<sup>b</sup> Department of Medical Oncology, Okayama Rosai Hospital, Okayama, Japan

<sup>c</sup> Department of Internal Medicine, Okayama Rosai Hospital, Okayama, Japan

## ARTICLE INFO

## Article history:

Received 14 October 2015

Received in revised form

2 November 2015

Accepted 8 November 2015

## Keywords:

Asbestos

Lymphoma

Mesothelioma

Pleural effusion

Thoracoscopy

## ABSTRACT

Primary effusion lymphoma (PEL) is a subtype of non-Hodgkin lymphoma that presents as serous effusions without detectable masses or organomegaly. Here we report a case of PEL-like lymphoma in a patient with past asbestos exposure. A 65-year-old man was referred to our hospital due to dyspnea upon exertion. He had been exposed to asbestos for three years in the construction industry. Chest X-ray and CT images demonstrated left pleural effusion. Cytological analysis of the pleural effusion revealed large atypical lymphocytes with distinct nuclear bodies and high nucleus-to-cytoplasm ratio. Immunohistochemical analyses showed that the cells were CD20<sup>+</sup>, CD3<sup>−</sup>, CD5<sup>−</sup>, and CD10<sup>−</sup>. These findings led to a diagnosis of diffuse large B-cell lymphoma. PEL or PEL-like lymphoma should be considered a potential cause of pleural effusion in subjects with past asbestos exposure.

© 2015 The Authors. Published by Elsevier Ltd. This is an open access article under the CC BY-NC-ND license (<http://creativecommons.org/licenses/by-nc-nd/4.0/>).

## 1. Introduction

Primary effusion lymphoma (PEL) is a subtype of non-Hodgkin lymphoma that presents as serous effusions without detectable masses or organomegaly. PEL usually occurs in the setting of immunodeficiency and is associated with human herpesvirus (HHV) - 8. Here we report a case of PEL-like lymphoma in a subject with a history of asbestos exposure.

## 2. Case report

A 65-year-old man was referred to our hospital due to dyspnea upon exertion. He was an occasional smoker and had been exposed to asbestos from 18 to 20 years old while employed in the construction industry, cutting asbestos-containing building material. Chest X-ray showed left pleural effusion (Fig. 1A), and computed tomographic (CT) images revealed left pleural effusion and calcified pleural plaques without pleural tumor (Fig. 1B). Thoracoscopic

exploration revealed red–brown pleural effusion and plaques, but no tumor was detected on the pleura. Culture of the pleural effusion was negative, and cytological examination revealed a cellular distribution of 1.0% macrophages, 1.5% neutrophils, and 97.5% lymphocytes. Other examinations of the fluid showed nonspecific findings. Pleural biopsy showed no evidence of malignancy.

During follow-up, the patient repeatedly exhibited accumulation of left pleural effusion, which was treated each time with thoracentesis. Four years after the first admission, analysis of pleural effusion from the fourth thoracentesis revealed large atypical lymphocytes with distinct nuclear bodies and a high nucleus-to-cytoplasm ratio (Fig. 2). Malignant lymphoma was suspected and thoracoscopic pleural biopsy was performed again, and the biopsy specimen from the fibrin tissues attached to the parietal pleura showed several groups of small round atypical lymphocytes. All of acid-fast bacteria stain, PCR analysis of tuberculosis, and culture for acid fast bacillus were negative. A culture test for standard plate count bacteria was also negative. Immunohistochemical analyses revealed that these cells were CD20<sup>+</sup> (Fig. 3), CD3<sup>−</sup>, CD5<sup>−</sup>, and CD10<sup>−</sup>. Based on these findings, the diagnosis was confirmed as diffuse large B-cell lymphoma (DLBCL). Contrast-enhanced CT imaging of whole body (neck to pelvis) revealed no lymphadenopathy or tumor. Serological tests for hepatitis-C virus, human T-cell lymphoma virus-1, and Epstein–Barr virus were negative, as was the

Abbreviations: PEL, primary effusion lymphoma; HHV, human herpesvirus; CT, computed tomography; DLBCL, diffuse large B-cell lymphoma.

\* Corresponding author. Department of Medical Oncology, Okayama Rosai Hospital, 1-10-25 Chikkomidorimachi, Okayama 7028055, Japan.

E-mail address: [nobufujimoto@gmail.com](mailto:nobufujimoto@gmail.com) (N. Fujimoto).

<http://dx.doi.org/10.1016/j.rmcr.2015.11.002>

2213-0071/© 2015 The Authors. Published by Elsevier Ltd. This is an open access article under the CC BY-NC-ND license (<http://creativecommons.org/licenses/by-nc-nd/4.0/>).



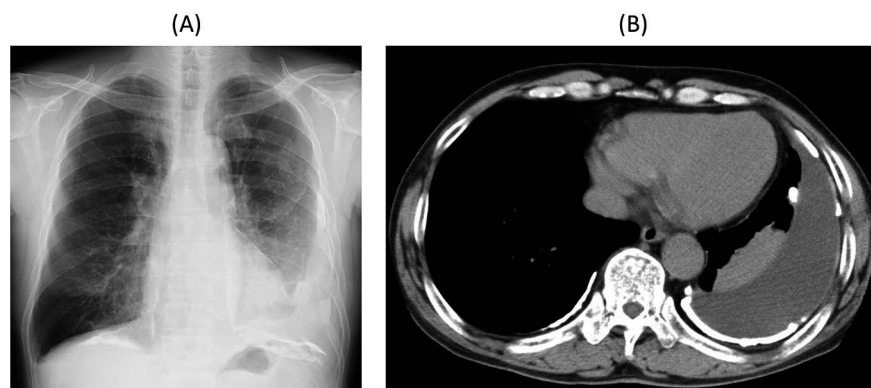


**Fig. 1.** Left pleural effusion and calcified pleural plaques visible on chest X-ray (A) and computed tomographic (B) images.

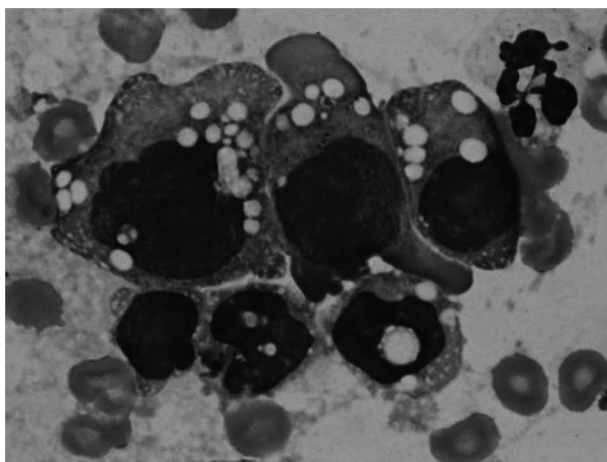


**Fig. 2.** Cytological analysis of pleural effusion revealed large atypical lymphocytes with distinct nuclear body and high nucleus-to-cytoplasm ratio ( $\times 40$ ).

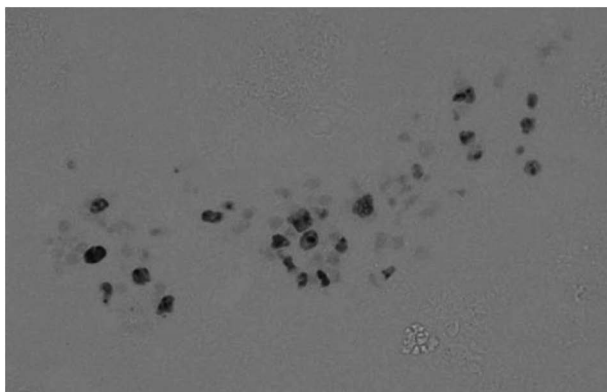


**Fig. 3.** Immunohistochemical analyses revealed that the cells were CD20<sup>+</sup> ( $\times 10$ ).

immunohistochemical analysis for HHV8. The patient has been followed-up, and has shown no disease progression for 3 years.

### 3. Discussion

The 2001 World Health Organization classification defines PEL as a disease entity representing a part of diffuse large B-cell lymphoma [1]. PEL is commonly associated with HHV8 infection [2]; however, PEL-like disease processes have recently been reported in

HHV8-negative patients. Those cases are considered a rare disease entity called HHV8-unrelated PEL-like lymphoma [3]. Advanced age [4] remains the only known risk factor for PEL-like lymphoma, and the pathogenic mechanisms remain unclear. It has been reported that patients with HHV8-unrelated PEL-like lymphoma show better outcomes than patients with PEL [5].

In our present case, the patient was elderly and had a past occupational history of asbestos exposure, but showed no immunological deterioration. To our knowledge, this is the first report of PEL-like lymphoma in a subject with past asbestos exposure. While no association has been established between lymphoproliferative disorder and asbestos exposure, it is possible that asbestos-induced chronic inflammation, in addition to advanced age, may have triggered lymphoproliferative disorder in the current case, though we cannot deny the possibility that the disease developed independently, considering relative short term of asbestos exposure.

In conclusion, here we report a rare manifestation of PEL-like lymphoma from a subject with past asbestos exposure. Subjects with past asbestos exposure sometimes develop pleural effusion, and suspected diagnoses include malignant pleural mesothelioma, lung cancer, benign asbestos pleural effusion, or tuberculous pleuritis. Our present case suggests that PEL or PEL-like lymphoma should also be considered as a potential cause of pleural effusion in subjects with past asbestos exposure.

### Conflict of interest

I declare on behalf of my co-authors and myself that we do not have any conflict of interest to declare.

### Source of funding

This study was supported by Research and Development and the Dissemination of Projects Related to the Nine Fields of Occupational Injuries and Illnesses of the Japan Labour Health and Welfare Organization. This work is also supported by grants-in-aid from the Ministry of Health, Labor and Welfare (grant number: 150401-02), Japan. These study sponsors had no involvement in study design, writing of the manuscript, the collection of data, and decision to submit the manuscript.

### References

- [1] P.M. Banks, R.A. Warnke, Primary effusion lymphoma, in: E.S. Jaffe, N.L. Harris, H. Stein, J.W. Verdman (Eds.), *World Health Organization Classification of Tumours. Pathology and Genetics of Tumours of Haematopoietic and Lymphoid Tissues*, IARC Press, Lyon, 2001.
- [2] D.S. Karcher, S. Alkan, Human herpesvirus-8-associated body cavity-based lymphoma in human immunodeficiency virus-infected patients: a unique B-

- cell neoplasm, *Hum. Pathol.* 28 (1997) 801–808.
- [3] A. Carbone, A. Gloghini, PEL and HHV8-unrelated effusion lymphomas: classification and diagnosis, *Cancer* 114 (2008) 225–227.
  - [4] F. Mohammad, M.N. Siddique, F. Siddiqui, M. Popalzai, M. Asgari, M. Odaimi, A unique case of malignant pleuropericardial effusion: HHV-8-unrelated PEL-like lymphoma—a case report and review of the literature, *Case Rep. Oncol. Med.* (2014) 436821.
  - [5] Y. Kobayashi, Y. Kamitsuji, J. Kuroda, S. Tsunoda, N. Uoshima, S. Kimura, et al., Comparison of human herpes virus 8 related primary effusion lymphoma with human herpes virus 8 unrelated primary effusion lymphoma-like lymphoma on the basis of HIV: report of 2 cases and review of 212 cases in the literature, *Acta Haematol.* 117 (2007) 132–144.



労災疾病臨床研究事業費補助金

悪性中皮腫に対するヒト化抗CD26抗体を基盤とする  
安全かつ有効な新規併用療法の確立

平成27年度～平成29年度

総合研究報告書

平成 30 年 3 月 31 日発行

発行：研究代表者 森本 幾夫

〒113-8421 東京都文京区本郷2-1-1

順天堂大学大学院医学研究科 免疫病・がん先端治療学講座

TEL：03-3868-2310

